BIOLOGY OF BRAIN DISORDERS – CELLULAR SUBSTRATES FOR DISRUPTED SYNAPTIC FUNCTION AND EXPERIENCE-DEPENDENT PLASTICITY

EDITED BY: Daniela Tropea, Abhishek Banerjee and Annalisa Scimemi
PUBLISHED IN: Frontiers in Cellular Neuroscience and
Frontiers in Molecular Neuroscience

frontiers Research Topics

frontiers

Frontiers eBook Copyright Statement

The copyright in the text of individual articles in this eBook is the property of their respective authors or their respective institutions or funders. The copyright in graphics and images within each article may be subject to copyright of other parties. In both cases this is subject to a license granted to Frontiers.

The compilation of articles constituting this eBook is the property of Frontiers.

Each article within this eBook, and the eBook itself, are published under the most recent version of the Creative Commons CC-BY licence. The version current at the date of publication of this eBook is CC-BY 4.0. If the CC-BY licence is updated, the licence granted by Frontiers is automatically updated to the new version.

When exercising any right under the CC-BY licence, Frontiers must be attributed as the original publisher of the article or eBook, as applicable.

Authors have the responsibility of ensuring that any graphics or other materials which are the property of others may be included in the CC-BY licence, but this should be checked before relying on the CC-BY licence to reproduce those materials. Any copyright notices relating to those materials must be complied with.

Copyright and source acknowledgement notices may not be removed and must be displayed in any copy, derivative work or partial copy which includes the elements in question.

All copyright, and all rights therein, are protected by national and international copyright laws. The above represents a summary only. For further information please read Frontiers' Conditions for Website Use and Copyright Statement, and the applicable CC-BY licence.

ISSN 1664-8714
ISBN 978-2-83250-072-9
DOI 10.3389/978-2-83250-072-9

About Frontiers

Frontiers is more than just an open-access publisher of scholarly articles: it is a pioneering approach to the world of academia, radically improving the way scholarly research is managed. The grand vision of Frontiers is a world where all people have an equal opportunity to seek, share and generate knowledge. Frontiers provides immediate and permanent online open access to all its publications, but this alone is not enough to realize our grand goals.

Frontiers Journal Series

The Frontiers Journal Series is a multi-tier and interdisciplinary set of open-access, online journals, promising a paradigm shift from the current review, selection and dissemination processes in academic publishing. All Frontiers journals are driven by researchers for researchers; therefore, they constitute a service to the scholarly community. At the same time, the Frontiers Journal Series operates on a revolutionary invention, the tiered publishing system, initially addressing specific communities of scholars, and gradually climbing up to broader public understanding, thus serving the interests of the lay society, too.

Dedication to Quality

Each Frontiers article is a landmark of the highest quality, thanks to genuinely collaborative interactions between authors and review editors, who include some of the world's best academicians. Research must be certified by peers before entering a stream of knowledge that may eventually reach the public - and shape society; therefore, Frontiers only applies the most rigorous and unbiased reviews.
Frontiers revolutionizes research publishing by freely delivering the most outstanding research, evaluated with no bias from both the academic and social point of view. By applying the most advanced information technologies, Frontiers is catapulting scholarly publishing into a new generation.

What are Frontiers Research Topics?

Frontiers Research Topics are very popular trademarks of the Frontiers Journals Series: they are collections of at least ten articles, all centered on a particular subject. With their unique mix of varied contributions from Original Research to Review Articles, Frontiers Research Topics unify the most influential researchers, the latest key findings and historical advances in a hot research area! Find out more on how to host your own Frontiers Research Topic or contribute to one as an author by contacting the Frontiers Editorial Office: frontiersin.org/about/contact

BIOLOGY OF BRAIN DISORDERS – CELLULAR SUBSTRATES FOR DISRUPTED SYNAPTIC FUNCTION AND EXPERIENCE-DEPENDENT PLASTICITY

Topic Editors:
Daniela Tropea, Trinity College Dublin, Ireland
Abhishek Banerjee, Newcastle University, United Kingdom
Annalisa Scimemi, University at Albany, United States

Citation: Tropea, D., Banerjee, A., Scimemi, A., eds. (2022). Biology of Brain Disorders – Cellular Substrates for Disrupted Synaptic Function and Experience-Dependent Plasticity. Lausanne: Frontiers Media SA.
doi: 10.3389/978-2-83250-072-9

Table of Contents

frontiers | Frontiers in Cellular Neuroscience

TYPE Editorial
PUBLISHED 10 August 2022
DOI 10.3389/fncel.2022.947926

Check for updates

OPEN ACCESS

EDITED AND REVIEWED BY
Dirk M. Hermann,
University of
Duisburg-Essen, Germany

*CORRESPONDENCE
Daniela Tropea
tropead@tcd.ie
Annalisa Scimemi
scimemia@gmail.com
Abhishek Banerjee
abhi.banerjee@newcastle.ac.uk

SPECIALTY SECTION
This article was submitted to Cellular Neuropathology, a section of the journal Frontiers in Cellular Neuroscience

RECEIVED 19 May 2022
ACCEPTED 15 June 2022
PUBLISHED 10 August 2022

CITATION
Tropea D, Scimemi A and Banerjee A (2022) Editorial: Biology of brain disorders—Cellular substrates for disrupted synaptic function and experience-dependent plasticity. *Front. Cell. Neurosci.* 16:947926. doi: 10.3389/fncel.2022.947926

COPYRIGHT
© 2022 Tropea, Scimemi and Banerjee. This is an open-access article distributed under the terms of the Creative Commons Attribution License (CC BY). The use, distribution or reproduction in other forums is permitted, provided the original author(s) and the copyright owner(s) are credited and that the original publication in this journal is cited, in accordance with accepted academic practice. No use, distribution or reproduction is permitted which does not comply with these terms.

Editorial: Biology of brain disorders—Cellular substrates for disrupted synaptic function and experience-dependent plasticity

Daniela Tropea[1,2,3,4]*, Annalisa Scimemi[5]* and Abhishek Banerjee[6]*

[1]Department of Psychiatry, Trinity College Dublin, Dublin, Ireland, [2]FutureNeuro Research Centre, Science Foundation Ireland, Dublin, Ireland, [3]Trinity College Institute for Neuroscience, Trinity College Dublin, Dublin, Ireland, [4]Trinity Translational Medicine Institute, Trinity College Dublin, Dublin, Ireland, [5]Department of Biology, University at Albany, Albany, NY, United States, [6]Biosciences Institute, Newcastle University, Newcastle upon Tyne, United Kingdom

KEYWORDS

synaptic plasticity, neurodevelopmental disorders, neurodegenerative disease, mouse models, brain function, molecular pathways

Editorial on the Research Topic
Biology of brain disorders—Cellular substrates for disrupted synaptic function and experience-dependent plasticity

This Research Topic on the "*Biology of Brain Disorders: Cellular Substrates for Disrupted Synaptic Function and Experience-Dependent Plasticity*" is a continuation of a series of topics and conferences on Brain Disorders that started in 2016. The topic aims to highlight the convergences and divergences between different types of brain disorders, including neuropsychiatric, neurological, and neurodegenerative. These pathologies remain one of the major problems in healthcare, and their incidence has continued to grow over the years. Consequently, one of the challenges that have captivated neuroscientists for decades is developing and exploiting sophisticated experimental approaches to understand how brain disorders arise and affect different features of brain function, including changes in synaptic transmission and plasticity. Indeed the field of neuroscience, among other areas of health sciences, has witnessed great technological advancements in the last several years, and has emerged as a positive circle of discovery and understanding: as new technologies are being developed, new mechanisms are discovered, and the need to understand the operating principle of such mechanisms in specific neuronal connections stimulates more research.

Aside from these technological advances, the use of animal models remains a classic approach to studying brain disorders. In this Research Topic, several disease models rely on genetically-engineered mice and models of brain injury. Pak et al. analyze how visual perception changes in a mouse model of the Fragile-X syndrome. Using a more classical approach, Cui et al. show how changes in Ca^{2+} channel subunit composition alter the synaptic plasticity of nociceptive pathways. In another study, Xu et al. present data collected from a rat model of chronic intermittent hypoxia. In brain injury, *in vitro* Ca^{2+} imaging reveals that the high-frequency head impact protocol (HFHIP) alters synaptic plasticity, resulting in a decreased coordination in the activity of neuronal ensembles (Chapman et al.). Further evidence of altered neuroplasticity due to brain injury is provided by Xu et al. and McDaid et al., using *in vivo* and *in vitro* studies.

While animal models have been extremely useful in advancing our understanding of brain function in health and disease, the translational potential of mouse models remains a general concern for applications in human patients. We acknowledge that this issue arises from the multiple failures of clinical trials at the advanced stage, despite the positive outcome of preclinical studies. Scientists are therefore discussing the validity of animals in studying the mechanisms of human disorders and recognizing the necessity to identify and focus on the specific endophenotypes that are present both in the animals and in patients. Often these endophenotypes are related to synaptic function and plasticity, as is the case for Huntington's disease and schizophrenia, which are linked to altered synaptic transmission in human and animal models (Barron et al.; Navarrete and Zhou). While the aforementioned works identify deficits in synaptic function that affect all cells, other disorders lead to patterned cell death only in specific cell types, as happens for Purkinje cells in patients and animal models of autosomal recessive spastic ataxia of Charlevoix-Saguenay (Toscano Márquez et al.).

To fill the gap between preclinical and clinical studies, and avoid differences among species, additional strategies have been developed for translational and clinical research. Cellular models consisting of patient-derived cells and organoids have been generated, and these preparations hold the promise of advancing our understanding of the molecular mechanisms disrupted in diseases, linking the clinical presentation to deficits in neurodevelopmental processes (de Paula Moreira et al.). This approach had several limitations initially, spanning from a lack of insights at the systems level to the limited molecular and cellular endophenotypes that can be measured. The field is growing fast, and these cellular models are now becoming an indispensable tool for translational research. In our view, animal models and patient-derived cellular preparations are complementary models for understanding the pathophysiology of brain disorders.

A theme that has emerged in recent years is the identification of convergences across disorders. Numerous genetic studies during the whole genomic sequencing era provided important contributions to understanding of the molecular basis of brain disorders, but they also showed that multiple common genes are associated with several pathologies. It is now clear that genetic studies alone are insufficient to identify molecular targets of intervention for specific brain disorders. The convergence of pathways across disorders is reported in this topic at a molecular and functional level. For example, RNA6 is involved in both epilepsy (Mathoux et al.) and Alzheimer's disease (Zhang et al.), while the review by Bach et al. examines the common mechanisms present at the circuitry level between Fragile-X and Rett syndrome. The overlap of genes and mechanisms suggests the possibility of ameliorating different disorders using similar therapeutic intervention strategies.

In the era of data science, we cannot ignore the contribution of big data in revealing the complexities of brain disorders. Indeed, in the paper by Chatterjee et al., computational analysis is used to process all existing functional data to generate predictions of alterations in autism spectrum disorders.

The articles and reviews featured in this Frontiers Research Topic confirm that the study of the genetic and synaptic mechanisms underlying brain disorders can shed light on the mechanisms of brain function. It provides insights on many of the molecular and cellular alterations that ultimately converge to modify the function and plasticity of single synapses and complex neuronal circuits.

Author contributions

All authors listed have made a substantial, direct, and intellectual contribution to the work and approved it for publication.

Funding

DT is an investigator in the FutureNeuro Research Centre supported by Science Foundation Ireland (SFI) under Grant Number 16/RC/3948 and co-funded under the European Regional Development Fund and by FutureNeuro industry partners. DT is also supported by Lejeune Foundation (1935–2020), International Rett Syndrome Foundation (IRSF- grant 3507-2017, Meath Foundation (2019 research grant -coPI). AS is supported by grant NSF 2011998, and AB is supported by a Wellcome Trust institutional strategic award and a Royal Society Research Grant.

Acknowledgments

We thank all the authors who contributed to this Research Topic.

Conflict of interest

The authors declare that the research was conducted in the absence of any commercial or financial relationships that could be construed as a potential conflict of interest.

Publisher's note

All claims expressed in this article are solely those of the authors and do not necessarily represent those of their affiliated organizations, or those of the publisher, the editors and the reviewers. Any product that may be evaluated in this article, or claim that may be made by its manufacturer, is not guaranteed or endorsed by the publisher.

frontiers in Cellular Neuroscience

ORIGINAL RESEARCH
published: 31 March 2021
doi: 10.3389/fncel.2021.652721

Sustained Hippocampal Synaptic Pathophysiology Following Single and Repeated Closed-Head Concussive Impacts

John McDaid[1], *Clark A. Briggs*[1], *Nikki M. Barrington*[1,2], *Daniel A. Peterson*[1,2,3], *Dorothy A. Kozlowski*[4] *and Grace E. Stutzmann*[1,2,3]*

[1]Center for Neurodegenerative Disease and Therapeutics, Rosalind Franklin University of Medicine and Science, North Chicago, IL, United States, [2]Chicago Medical School, Rosalind Franklin University of Medicine and Science, North Chicago, IL, United States, [3]Center for Stem Cell and Regenerative Medicine, Rosalind Franklin University of Medicine and Science, North Chicago, IL, United States, [4]Department of Biological Sciences and Neuroscience Program, DePaul University, Chicago, IL, United States

OPEN ACCESS

Edited by:
Annalisa Scimemi, University at Albany, United States

Reviewed by:
Terrance Kummer, Washington University School of Medicine in St. Louis, United States
Lauren Jantzie, Johns Hopkins University, United States

***Correspondence:**
Grace E. Stutzmann
grace.stutzmann@rosalindfranklin.edu

Specialty section:
This article was submitted to Cellular Neuropathology, a section of the journal Frontiers in Cellular Neuroscience

Received: *13 January 2021*
Accepted: *11 March 2021*
Published: *31 March 2021*

Citation:
McDaid J, Briggs CA, Barrington NM, Peterson DA, Kozlowski DA and Stutzmann GE (2021) Sustained Hippocampal Synaptic Pathophysiology Following Single and Repeated Closed-Head Concussive Impacts. Front. Cell. Neurosci. 15:652721. doi: 10.3389/fncel.2021.652721

Traumatic brain injury (TBI), and related diseases such as chronic traumatic encephalopathy (CTE) and Alzheimer's (AD), are of increasing concern in part due to enhanced awareness of their long-term neurological effects on memory and behavior. Repeated concussions, vs. single concussions, have been shown to result in worsened and sustained symptoms including impaired cognition and histopathology. To assess and compare the persistent effects of single or repeated concussive impacts on mediators of memory encoding such as synaptic transmission, plasticity, and cellular Ca^{2+} signaling, a closed-head controlled cortical impact (CCI) approach was used which closely replicates the mode of injury in clinical cases. Adult male rats received a sham procedure, a single impact, or three successive impacts at 48-hour intervals. After 30 days, hippocampal slices were prepared for electrophysiological recordings and 2-photon Ca^{2+} imaging, or fixed and immunostained for pathogenic phospho-tau species. In both concussion groups, hippocampal circuits showed hyper-excitable synaptic responsivity upon Schaffer collateral stimulation compared to sham animals, indicating sustained defects in hippocampal circuitry. This was not accompanied by sustained LTP deficits, but resting Ca^{2+} levels and voltage-gated Ca^{2+} signals were elevated in both concussion groups, while ryanodine receptor-evoked Ca^{2+} responses decreased with repeat concussions. Furthermore, pathogenic phospho-tau staining was progressively elevated in both concussion groups, with spreading beyond the hemisphere of injury, consistent with CTE. Thus, single and repeated concussions lead to a persistent upregulation of excitatory hippocampal synapses, possibly through changes in postsynaptic Ca^{2+} signaling/regulation, which may contribute to histopathology and detrimental long-term cognitive symptoms.

Keywords: Ca^{2+}, CTE, concussion, hippocampus, LTP, synaptic transmission, tau

INTRODUCTION

Traumatic brain injury (TBI) is a leading cause of death and disability in the US, affecting approximately 2.8 million people annually, resulting in a significant financial and human toll (Taylor et al., 2017). Numerous postmortem studies reveal a correlation between repeated concussion and chronic traumatic encephalopathy (CTE), a neurodegenerative condition characterized by cognitive impairment, mood swings, and depression, and disrupts vulnerable brain regions involved in memory processing such as the cortex and hippocampus (McKee et al., 2009, 2013; McKee and Robinson, 2014). While many high profile reports of TBI are associated with military and athletic events, a greater proportion of the general public is affected by concussions resulting primarily from falls and violence (CDC, 2014), with single or repeated concussions resulting in short-term memory loss (Mayer et al., 2017) or other symptoms of neurodegenerative disease (Fakhran et al., 2013). Indeed, TBI-related CTE bears many of the same pathophysiological hallmarks as Alzheimer's disease, including the buildup of hyperphosphorylated tau, a microtubule-associated protein involved in cytoskeletal function (Geddes et al., 1999; McKee and Robinson, 2014). Long-term effects of TBI also include increased likelihood of seizures (Annegers et al., 1998) and loss of balance/abnormal gait (Ellemberg et al., 2009), all of which further increase the likelihood of subsequent TBIs (Theadom et al., 2015). Although the long-term underlying physiology has not been well studied, the acute effects of a concussion are thought to result from several abnormal cellular processes occurring in the wake of a concussive impact. Upon impact, there is a rapid increase in extracellular glutamate (Hinzman et al., 2010), resulting in over-activation of postsynaptic Ca^{2+} channels including NMDA receptors (NMDARs; Geddes et al., 2003; Biegon et al., 2004) and voltage gated Ca^{2+} channels (VGCCs; Wolf et al., 2001). The consequences of increased neuronal Ca^{2+} may persist for hours or even days after impact (Sun et al., 2008) and are often accompanied by some form of cognitive impairment (Deshpande et al., 2008). The sustained alteration of Ca^{2+} homeostasis is a central feature of several neurological diseases including Alzheimer's and Huntington's diseases and may serve as a common underlying mechanism linking increased incidence of dementia in the years after a TBI (Giacomello et al., 2013; Schrank et al., 2020).

Ca^{2+} is a vitally important mediator of normal cellular and synaptic function. Neuronal Ca^{2+} is tightly regulated through several homeostatic mechanisms with disruption of these processes contributing to synaptic dysregulation, altered signaling cascades, and potential cell injury or death (Stutzmann, 2007; Chakroborty et al., 2009, 2019; Zhang et al., 2015). Postsynaptic ryanodine receptors (RyRs), which are high conductance Ca^{2+} channels on the endoplasmic reticulum (ER) membrane, are located close to NMDARs and VGCCs on dendritic spines of hippocampal pyramidal cells (Jaffe et al., 1994; Chavis et al., 1996; Thibault et al., 2007; Holbro et al., 2009). This relationship allows for the amplification of NMDAR and VGCC mediated Ca^{2+} influx through the process of Ca^{2+} induced Ca^{2+} release (CICR; Emptage et al., 1999; Borde et al., 2000; Holbro et al., 2009), and as such, RyRs are positioned to influence Ca^{2+}-dependent synaptic and plasticity processes (Chakroborty et al., 2009, 2019). Also, RyR expression is elevated in postmortem brain tissue from individuals with cognitive impairment, a feature of TBI (Bruno et al., 2012; McInnes et al., 2019). RyR sensitivity is altered by the processes of phosphorylation and oxidation which increase channel open probability, resulting in spontaneously "leaky" channels and increased Ca^{2+} release in the short term, but reduced ER store content and suppressed ER Ca^{2+} release if sustained (Liu et al., 2012; Lacampagne et al., 2017). Although the role of RyRs in the short-term effects of TBI is not well understood, TBI acutely results in an increased production of reactive oxygen species (ROS) which are known mediators of RyR hyperphosphorylation/oxidation (Görlach et al., 2015). As RyRs are also expressed presynaptically, increased presynaptic RyR sensitivity/Ca^{2+} may result in increased release of the excitatory neurotransmitter glutamate, resulting in feed-forward increased postsynaptic NMDAR and RyR-mediated Ca^{2+} release. Notably, stabilization of RyR-evoked Ca^{2+} release results in wide-ranging therapeutic effects, including reduced glutamate excitotoxicity (Frandsen and Schousboe, 1991; Niebauer and Gruenthal, 1999), normalized synaptic transmission and synaptic structure, reduced inflammatory markers, and improved behavioral outcomes (Chakroborty et al., 2012; Oules et al., 2012; Briggs et al., 2017). Thus, RyRs may emerge as a therapeutic target in the treatment of TBI and related disease conditions.

TBI generates several pathological features common to other neurological diseases, including abnormal protein aggregates and hyperphosphorylated tau. Under normal conditions, homeostasis of tau phosphorylation is maintained through a balance of kinase and phosphatase activity responsible for its phosphorylation and dephosphorylation, respectively (Geddes et al., 1999; McKee and Robinson, 2014). After TBI, multiple kinases are upregulated and result in a net increase of phosphorylated tau (Tran et al., 2012). Furthermore, increased neuronal Ca^{2+} following TBI, *via* NMDARs, VGCCs, and intracellular stores can upregulate specific Ca^{2+}-regulated kinases that phosphorylate tau, such as GSK3-β and Cdk5 (Avila et al., 2004; Dash et al., 2011; Zhao et al., 2012; Wilson et al., 2014). In turn, phosphorylated tau can increase intracellular Ca^{2+}, furthering tau phosphorylation (Gómez-Ramos et al., 2006; Stutzmann, 2007) and Ca^{2+}-related synaptic deficits. While acute excitotoxic Ca^{2+} events have been described in the minutes to hours following a TBI (Luo et al., 2011; Gurkoff et al., 2013; Arai et al., 2019), sustained intracellular Ca^{2+} dyshomeostasis, such as that seen in AD (Stutzmann, 2007), may also occur and underlie cognitive, histopathological, and synaptic defects that can arise weeks to months after injury (Deshpande et al., 2008; Sun et al., 2008).

Previous head injury is a significant risk factor for dementia-related diseases, with the delay from injury to onset of dementia-like symptoms ranging from months to years (Fleminger et al., 2003; Li et al., 2017). RyRs and

VGCCs each play an important role in Ca^{2+} homeostasis, synaptic transmission, and memory encoding, and despite the documented role of Ca^{2+} dysregulation in neurodegenerative diseases (Huang and Malenka, 1993; Huber et al., 1995; Chakroborty et al., 2012; Oules et al., 2012), their contribution to the sustained cellular and synaptic defects resulting from TBI has not been adequately studied. Here we investigate modes of sustained pathophysiology resulting from single or repeated TBI in a clinically-relevant rat model (Jamnia et al., 2017), and reveal key cellular signaling, synaptic circuit defects, and histopathological markers that are consistent with chronic neurological disease states.

MATERIALS AND METHODS

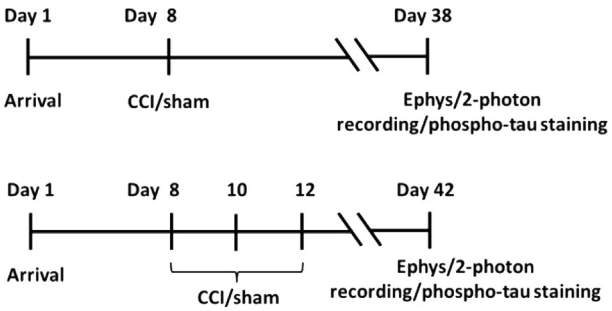

Timeline of the Experimental Procedure

Approximately 1 week after arrival, animals were subjected to sham surgery, or single or repeated closed-head controlled cortical impacts (CCI). Repeated CCI's were conducted using three successive impacts separated by 48-h intervals. Rats were examined 30 days after the last CCI to measure the extent of sustained synaptic and cellular effects; see the depiction below. Electrophysiology/2-photon recordings and phospho-tau staining were conducted using separate sets of animals.

Animals

Male hooded Long-Evans rats (Charles River Laboratory; 200–300g; P60-P80) were housed two per cage in the Rosalind Franklin University of Medicine and Science (RFUMS) Biological Resource Facility. While we acknowledge the importance of sex as a biological variable, the limited scale of the study, along with the much higher incidence of TBI in males (CDC, 2014) means we used only male rats in this study. Rats were kept on a 12:12 h light/dark cycle with food and water available *ad libitum*. Animals were handled daily for approximately 1 week before surgery. All experiments were performed following the National Institutes of Health Guide for the Care and Use of Animals and were approved by the RFUMS Institutional Animal Care and Use Committee.

Closed-Head Controlled Cortical Impact (CCI)

To inflict a closed-head TBI we used a modified CCI approach (Leica Impact One, Leica Microsystems Inc., Buffalo Grove, IL, USA) to model mild TBI (Jamnia et al., 2017). Rats were anesthetized using 2.0–3.0 ml/min isoflurane anesthesia and placed in a Kopf stereotaxic apparatus (Kopf, Tujunga, CA, USA), on a foam bed (5 cm thick) in a plexiglass frame; anesthesia was maintained through a nose cone. The frame consisted of a base (11.43 × 24.13 cm) and a side piece (9.52 × 22.86 cm) angled 11 degrees from the vertical. To allow for movement of the head, but to also provide stability to the rat during the impact, the lateral surface of the head was rested lightly against the plexiglass frame. The Impact One stereotactic device delivered the cortical impact at an angle 20 degrees from vertical, enabling the flat impactor tip to be perpendicular to the surface of the head; this was adjusted accordingly if necessary. All injuries were produced with a 5 mm flat tip at 6.5 m/s at a depth of 10 mm from the surface of the skin overlaying the right sensorimotor cortex for 300 ms. The depth measurement accounted for the amount of absorption in the foam (approximately 9 mm). This depth was previously tested to be the maximal level of impact that did not result in a skull fracture but produced behavioral impairment (Jamnia et al., 2017). All rats that received an impact received a topical analgesic, and body temperature was maintained at 37°C during recovery. Following recovery from anesthesia, rats were returned to their home cages and monitored daily. Repeated concussion animals had a total of three injuries 48 h apart; an additional group of rats with a single concussion were exposed to two subsequent anesthesia treatments 48 h apart. This group was placed in the anesthesia chamber for the duration of time that the repeated concussion animals were anesthetized for their subsequent injuries (approximately 20 min). This model of single or repeated TBI, previously used by us, does not result in any obvious tissue damage (Jamnia et al., 2017), and is considered a model of single or repeated mild TBI or concussion (Petraglia et al., 2014).

Brain Slice Preparation

Thirty days after the last CCI, animals were deeply anesthetized with isoflurane and coronal hippocampal slices (400 μm for field recording and 250 μm for whole-cell recording and Ca^{2+} imaging) were prepared as previously described (Stutzmann et al., 2004). Slices were perfused at 1.5–2 ml/min with standard artificial cerebrospinal fluid (aCSF) solution containing the following (in mM): 125 NaCl, 2.5 KCl, 2 $CaCl_2$, 1.2 $MgSO_4$, 1.25 NaH_2PO_4, 25.0 $NaHCO_3$, 10 D-dextrose equilibrated with 95% O_2 and 5% CO_2 (pH 7.3–7.4), at room temperature (22°C). Osmolarity was maintained at 310 mOsm. Patch pipettes (4–5 MΩ) were filled with intracellular solution containing the following substances (in mM): 135 K-gluconate, 10 HEPES, 10 Na-phosphocreatine, 2 $MgCl_2$, 4 NaATP, and 0.4 NaGTP, pH adjusted to 7.3–7.4 with KOH (Sigma). Hippocampal CA1 pyramidal neurons were identified visually *via* infrared differential interference contrast optics (IRDIC) on an Olympus BX51 upright microscope, through a 40× objective, and were identified electrophysiologically by their passive membrane properties and spike frequency adaptation in response to depolarizing current injection. Membrane potentials were obtained in current-clamp mode acquired at 10 kHz with a Digidata 1322 A-D converter and Multiclamp 700B amplifier

and were recorded and analyzed using pClamp 10.2 software (Molecular Devices).

Extracellular Field Potential Recordings

For extracellular field potential recording, 400 μm hippocampal slices were transferred to an interface chamber (Harvard Apparatus), perfused with oxygenated aCSF (1.5 ml/min) at room temperature, and covered with a continuous flow of humidified gas (95% O_2/5% CO_2). Data were acquired at 10 kHz using pClamp 10.2 software with an AxoClamp 2B amplifier and a DigiData 1322A board for digitization (Molecular Devices). Field excitatory postsynaptic potentials (fEPSPs) were recorded in the stratum radiatum of the CA1 subfield of the hippocampus using recording microelectrodes (2–6 MΩ) filled with aCSF. Microelectrodes were pulled from borosilicate glass capillaries (Harvard Apparatus) on a P-2000 pipette puller (Sutter Instruments, Novato, CA, USA). Synaptic fEPSP responses were evoked by stimulation of the Schaffer collateral/commissural pathway, using a bipolar stimulating electrode, with the fEPSP slope calculated as the change in potential (ΔV) of the initial fEPSP waveform over time (t), or ΔV/t (mV/ms; see **Figure 1A**). Input-stimulus/output-fEPSP slope (I-O) curves were generated by plotting the fEPSP slope vs. stimulus intensity, using stimulus intensities ranging from 100 to 1,000 μA. For induction of long-term potentiation (LTP), baseline fEPSPs were evoked at 50% of the maximum fEPSP slope, at 0.05 Hz for 20 min. LTP was induced at baseline intensity using a high-frequency stimulation (HFS) protocol consisting of two sets of 100 pulses at 100 Hz, with each set of pulses spaced 10 sapart. fEPSPs were recorded for a further 60 min at baseline frequency, after HFS. Immediately after HFS, we observed post-tetanic potentiation (PTP; 0–2 min after HFS), a Ca^{2+} dependent form of short-term synaptic plasticity (Zucker and Regehr, 2002). LTP was observed later and can be divided into a transient early phase that is mediated by modification of pre-existing proteins (E-LTP; 15–20 min after HFS), and a more persistent late phase that requires gene transcription and new protein synthesis (L-LTP; 50–60 min after HFS; Davies et al., 1989; Frey et al., 1993). Paired-pulse facilitation (PPF) was assessed after I-O recordings, using an interstimulus interval of 50 ms. Three successive response pairs were recorded at 0.05 Hz. All field recordings were performed on the hippocampal side ipsilateral to the impact site. Only one set of field recordings was carried out per slice, with typically two 400 μm hippocampal slices per rat used.

Ca^{2+} Imaging

Ca^{2+} imaging within individual CA1 pyramidal neurons was performed in hippocampal slices using a custom-built video-rate multiphoton-imaging system based on an upright Olympus BX51 microscope frame and Ti:Saph pulsed IR laser (Spectra-Physics, Santa Clara, CA, USA; Stutzmann and Parker, 2005). Individual neurons were filled with the Ca^{2+} indicator fura-2 (50 μM; ThermoFisher) *via* the patch pipette as described previously (Stutzmann et al., 2004). Laser excitation was provided by trains (80 MHz) of ∼100 frames/s pulses at 780 nm. At this wavelength, fura-2 excitation generates a bright signal at low Ca^{2+} levels, allowing us to see small compartments such as spines at resting levels; fluorescence proportionally decreases with increasing Ca^{2+} levels allowing for relative measurements of change from baseline. The femtosecond pulsed laser beam was scanned by a resonant galvanometer (General Scanning Lumonics), allowing rapid (7.9 kHz) bidirectional scanning in the *x*-axis and by a conventional linear galvanometer in the *y*-axis, to provide a full-frame scan rate of 30 frames/sec. The laser beam was focused onto the tissue through a 40× water-immersion objective (numerical aperture = 0.8). Emitted fluorescence light was detected by a wide-field photomultiplier (Electron Tubes) to derive a video signal that was captured and analyzed by Video Savant 5.0 software (IO Industries; London, ON). Further analysis of background-corrected images was performed off-line using MetaMorph software. For quantification of resting and changes in fura-2 fluorescence, we selected a region of the CA1 pyramidal cell soma (surrounding but excluding the nucleus), to obtain a measure of cytosolic Ca^{2+} (Stutzmann et al., 2003, 2004). An adjacent non-fluorescent area was selected for background subtraction. As fura-2 shows a decrease in fluorescence with increasing Ca^{2+}, using two-photon excitation at 780 nm, decreased basal F_0values represent increased basal Ca^{2+}. Relative percentage changes in Ca^{2+} were calculated as the percentage change in fluorescence intensity over baseline: $(F_0/\Delta F - 1) \times 100$ with values for F_0 and percentage change averaged across cells from each TBI group. After patching, fura-2 was allowed to equilibrate in the cell for 10–15 min, and after a fluorescent signal was attained, the positive current was injected into the cell while in current-clamp mode, resulting in depolarization of the cell membrane and triggering activation of voltage-gated Ca^{2+} channels (VGCCs). To ensure consistency between evoked responses within and between groups, the depolarization protocol was conducted first, before any drug exposure. Ca^{2+} measurements were acquired from the peak of the evoked response. Bath application of caffeine (10 mM) was used to trigger RyR-Ca^{2+} release from ER stores (Garaschuk et al., 1997; Sandler and Barbara, 1999). Each brain slice was exposed to only one application of caffeine. Typically on any recording day, two hippocampal slices were used for Ca^{2+} measurements with one CA1 pyramidal cell recording per slice. Minianalysis 6.0.7 (Synaptosoft; Fort Lee, NJ, USA) was used to detect and measure spontaneous excitatory postsynaptic potential (sEPSP) events with a minimal amplitude of 0.2 mV and minimal area of 3 mV×ms. The baseline was determined from a 1 ms average immediately before each event, or in the case of overlapping events, from the peak and decay kinetics of the preceding event using "complex peak detection" in Minianalysis. 6-Cyano-7-nitroquinoxaline-2, 3-dione (CNQX, Sigma-Aldrich), an AMPA antagonist, was used to confirm glutamatergic sEPSPs. sEPSP data was obtained in the sham and rTBI groups only, as we only observed effects of rTBI, but not sTBI, on the somatic RyR-Ca^{2+} response to caffeine (see **Figure 4**). All whole-cell/2-photon recordings were performed on the hippocampal side ipsilateral to the impact site. Multiple VGCC recordings were

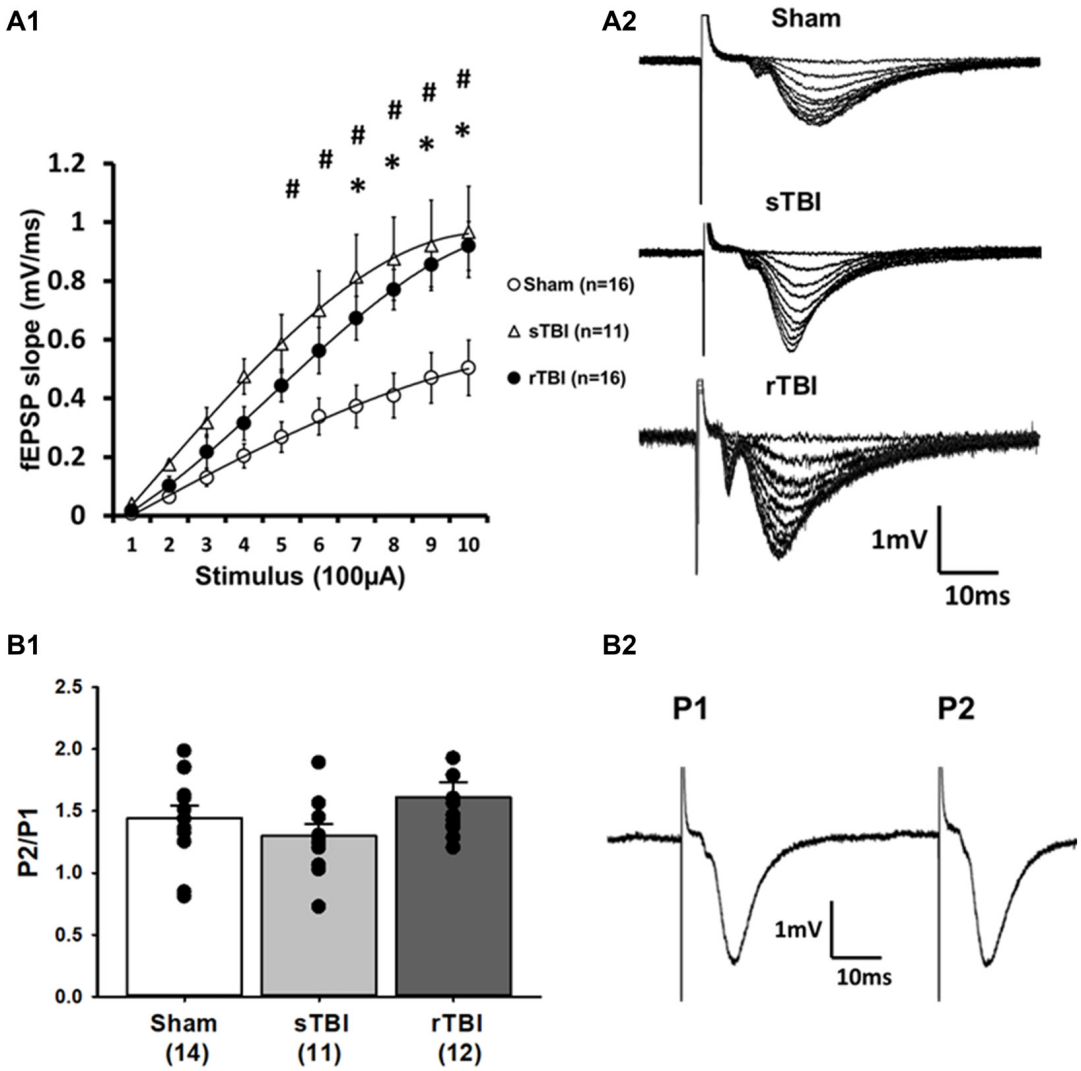

FIGURE 1 | Single or repeated traumatic brain injury (TBI) results in persistent hyperexcitability at CA3-CA1 synapses. Rats subjected to a single TBI (sTBI), or repeated TBI (rTBI), exhibited persistent upregulation at CA3-CA1 synapses, as revealed using extracellular field recordings (fEPSPs). **(A1)** fEPSP Input-output curves obtained from CA1 hippocampal field recordings using Schaffer collateral stimulation, 30 days after sham surgery, sTBI or rTBI, demonstrating increasing field potential (fEPSP) slopes resulting from increasing stimulus intensity ranging from 100 μA to 1,000 μA. fEPSPs from both the sTBI and rTBI groups showed a steeper slope at most stimulus intensities compared to the sham treatment group, with no significant difference between the sTBI and rTBI groups. **(A2)** Representative input-output fEPSP traces taken from sham, sTBI, and rTBI rats. **(B1)** sTBI and rTBI did not affect the paired-pulse ratio of fEPSPs, compared to sham, indicating that there was no significant difference in the presynaptic release probability of glutamate between groups. **(B2)** Representative traces showing paired fEPSPs evoked at a 50 ms interstimulus interval. All recordings were on the hippocampal side ipsilateral to the TBI impact site (over the right sensorimotor cortex). $^{\#}p < 0.05$ for sham vs. sTBI. $^{*}p < 0.05$.for sham vs. rTBI. Error bars represent the standard error of the mean.

carried out per slice, but only one RyR-Ca^{2+} response to caffeine per slice, with typically 2–3 250 μm hippocampal slices per rat used.

Immunohistochemistry

Rats were anesthetized with pentobarbital (200 mg/kg) and then transcardially perfused with ice-cold phosphate-buffered saline, immediately followed by 4% paraformaldehyde. Brains were removed and post-fixed for 24 h, then cut into sagittal sections on a Leica SM2000R microtome with a freezing stage at 40 μm thickness and stored in cryopreservation solution until immunostaining. Free-floating hippocampal sections were permeabilized with 0.1 M TBS 1.0% Triton-X (3 × 10 min) at room temperature on a platform rocker. Sections were blocked with 0.1 M TBS 0.1% Triton-X + 10% goat serum for 1 h at room temperature and subsequently incubated in primary antibody (phospho-Tau S262, 1:500, Invitrogen, catalog number 44-750G) diluted in 0.1 M TBS 0.1% Triton-X + 1% goat

serum for 24 h at 4°C on a platform rocker. The sections were washed with 0.1 M TBS 0.1% Triton-X (3 × 5 min) and incubated in secondary antibody (Alexa Fluor 488 conjugated to IgG goat anti-rabbit antibody, 1:1,000, Invitrogen, A-11008) diluted in 0.1 M TBS 0.1% Triton-X + 1% goat serum for one hour at room temperature on a platform rocker. Sections were rinsed in 0.1 M TBS 0.1% Triton-X (3 × 5 min) and stained with 1:10,000 DAPI diluted in 0.1 M TBS for 5 min. Sections were washed in 0.1 M TBS for 5 min and mounted with PVA-DABCO for microscopy. Control sections were obtained using the same procedure with primary antibody alone and secondary antibody alone, respectively, and imaged to ensure there was no off-target staining. Confocal images of the sections were obtained and analyzed using a 60× objective lens on an Olympus Fluoview Fv10i confocal microscope. Microscope settings were the same for all images. Several images were obtained of each hippocampal region as well as the cortex. MetaMorph software (Version 7) was used to quantify the percent staining density of fluorescently labeled phosphorylated tau over the threshold intensity level across the whole brain as well as in each hemisphere ipsilateral and contralateral to injury.

Statistical Analysis

Statistical differences among groups were determined using analysis of variance (one-way ANOVA or two-way repeated-measures ANOVA) with Tukey or Dunnett's *post hoc* tests where appropriate using SigmaPlot 12 data analysis software. Data are shown as mean ± standard error of the mean. Statistical significance was set at $p<0.05$.

RESULTS

In our previous study, repeated concussion/TBI resulted in more persistent memory deficits than a single concussion (Jamnia et al., 2017), with similar findings observed elsewhere (Meehan et al., 2012; Weil et al., 2014). Concussion-related memory deficits may result from persistent maladaptive pathophysiological effects in brain regions that play a role in learning and memory, such as the hippocampus. To this end, we tested for persistent hippocampal synaptic and neuronal Ca^{2+} signaling deficits, and tau pathology, in rats subjected to single or repeated TBI.

sTBI and rTBI Results in Hyperexcitable Synaptic Transmission in Hippocampal Circuits

Electrophysiological recordings in acute hippocampal brain slices were used to assess alterations in the local circuit and synaptic function resulting from either a single or repeated TBI. A total of 7, 6, and 8 rats were allocated to the sham, sTBI, and rTBI groups, respectively. Extracellular field potential recordings measured effects of Schaffer collateral CA3-CA1 stimulation on postsynaptic potentials (fEPSPs), using the initial slope function of the fEPSP as a measure of monosynaptic output. Assessment of the input-output function of fEPSPs revealed that both sTBI (11 recordings/11 slices/6 rats) and rTBI (18 recordings/18 slices/8 rats) resulted in significant potentiation at hippocampal synapses, across a range of stimulation intensities, when compared to the sham group (18 recordings/18 slices/8 rats). A two-way repeated-measures ANOVA was significant for effects of single and repeated TBI treatment ($F_{(2,40)} = 4.08$; $p = 0.024$), stimulation intensity ($F_{(9,40)} = 89.08$; $p < 0.001$) and treatment group vs. stimulation-intensity interaction ($F_{(2,9)} = 4.27$; $p < 0.001$). *Post hoc* analysis revealed a significant difference between the sTBI and sham groups at 500 μA ($p = 0.049$), 600 μA ($p = 0.02$), 700 μA ($p = 0.004$), 800 μA ($p = 0.002$), 900 μA ($p = 0.004$), and 1,000 μA ($p = 0.003$) stimulation intensities and between the rTBI and sham groups at 700 μA ($p = 0.025$), 800 μA ($p < 0.005$), 900 μA ($p < 0.004$), and 1,000 μA ($p < 0.002$) stimulation intensities (**Figure 1A**). To determine if the increased synaptic responses observed in the sTBI and rTBI groups reflect presynaptic alterations, we used the paired-pulse ratio, measured as the ratio of the slope of the second fEPSP to the slope of the first fEPSP of a pair of fEPSPs obtained at a 50 ms interval, as a relative measure of Ca^{2+}-dependent neurotransmitter release probability. A one-way ANOVA revealed no effect of either sTBI (11 recordings/11 slices/6 rats) or rTBI (12 recordings/12 slices/8 rats) on the paired-pulse ratio ($F_{(2,34)} = 1.44$; $p = 0.252$; **Figure 1B**), compared to sham (14 recordings/14 slices/8 rats), indicating that the probability of presynaptically-regulated vesicle release is not significantly different among these groups.

In addition to the measurement of basal synaptic transmission, we also examined long-term synaptic potentiation (LTP) at CA3-CA1 synapses. Using high-frequency stimulation (HFS, two 100 Hz pulse trains for 1 s each, spaced 10 s apart) of Schaffer collaterals, we observed a sequence of synaptic changes consisting of an initial short-term post-tetanic synaptic potentiation (PTP; 0–2 min after HFS; **Figure 2A**), followed by early LTP (E-LTP; 15–20 min after HFS) and late-phase LTP (L-LTP; 50–60 min after HFS; **Figure 2B**). PTP was not significantly altered by either single (sTBI; 8 recordings/8 slices/6 rats) or repeated TBI (rTBI; 10 recordings/10 slices/8 rats; one way ANOVA; $F_{(2,24)} = 2.34$; $p = 0.12$), compared to sham (7 recordings/7 slices/7 rats) and there was likewise no effect of sTBI or rTBI on the magnitude of E-LTP (one way ANOVA; $F_{(2,24)} = 0.57$; $p = 0.57$) or L-LTP (one way ANOVA; $F_{(2,24)} = 0.89$; $p = 0.43$; **Figure 2C**). Although our findings contrast with those from other studies showing a persistent attenuation of hippocampal LTP resulting from sTBI (Schwarzbach et al., 2006) or rTBI (Aungst et al., 2014), these studies used an open skull/exposed dura impact model, and not the closed-head model employed here. Indeed, while many studies have looked at hippocampal synaptic effects resulting from TBI using an open-head/exposed dura model at various time points post-injury (Miyazaki et al., 1992; D'Ambrosio et al., 1998; Atkins, 2011; Zhang B. et al., 2011; Zhang B.-L. et al., 2011; Titus et al., 2019), few studies have examined the persistent TBI effects on synaptic plasticity using a closed-head model of single (White et al., 2017) or repeated impacts (Logue et al., 2016). Also, other closed-head studies have employed a blast injury

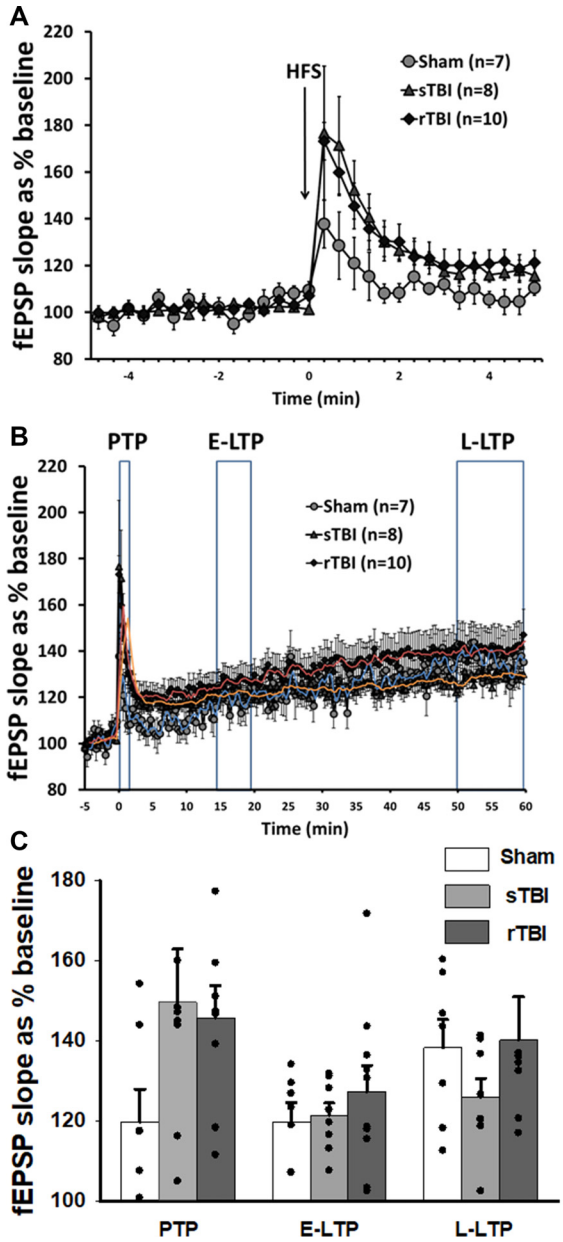

FIGURE 2 | Acute induction of hippocampal synaptic plasticity is unaffected by single or repeated TBI. **(A)** High-frequency stimulation (HFS) of CA3-CA1 Schaffer collaterals resulted in short-term post-tetanic synaptic potentiation (PTP), lasting for several minutes. Graph shows averaged time course of PTP in sham, single TBI (sTBI), and repeated TBI (rTBI) groups. **(B)** High-frequency stimulation (HFS) of CA3-CA1 Schaffer collaterals also resulted in long-term potentiation (LTP) lasting for 1 h. Graph shows averaged time course of early (E-LTP) and late-phase LTP (L-LTP) in sham, sTBI, and rTBI groups. Time of HFS indicated by the arrow. **(C)** Bar graph shows the percentage change in post-HFS response relative to baseline as PTP (0–2 min after HFS), E-LTP (15–20 min after HFS), and L-LTP (50–60 min after HFS). HFS consisted of two 100 Hz pulse trains of 1 s duration each, with a 10 s interval between pulse trains. There was no significant effect of sTBI or rTBI on the magnitude of PTP, E-LTP, or L-LTP. Superimposed trendlines represent mean data for sham (blue), sTBI (orange), and rTBI (red). All recordings were on the hippocampal side ipsilateral to the TBI impact site (over the right sensorimotor cortex). Error bars represent the standard error of the mean.

model (Beamer et al., 2016; Hernandez et al., 2018), with global physical effects that are less clinically relevant to mild TBI.

Ca^{2+} Dynamics and Membrane Properties in sTBI and rTBI

Neuronal Ca^{2+} dyshomeostasis due to changes in VGCC and RyR function can result in altered cellular signaling and synaptic function, as well as drive synaptic loss and neurodegeneration if sustained over time. Here we have assessed the persistent effects of single or repeated TBI on levels of resting Ca^{2+}, VGCC, and RyR function. The use of whole-cell patch recordings with 2-photon Ca^{2+} imaging allows for the simultaneous measurement of passive and active membrane properties, including input resistance and cell excitability, along with changes in Ca^{2+} handling during VGCC and RyR activation. Ca^{2+} influx through VGCCs was significantly increased in both the sTBI (16 recordings/12 slices/6 rats) and rTBI (19 recordings/12 slices/8 rats) groups compared to sham (10 recordings/6 slices/8 rats; $F_{(2,44)} = 7.89$; $p = 0.001$; **Figure 3A**). Basal Ca^{2+}, measured using the resting fura-2 fluorescence intensity (F_0) under identical laser power and recording conditions, was also significantly increased in the both the sTBI (15 recordings/15 slices/6 rats) and rTBI (18 recordings/18 slices/8 rats) groups relative to sham (8 recordings/8 slices/8 rats; $F_{(2,40)} = 5.0$; $p = 0.012$; **Figure 4A**). In contrast, RyR-evoked Ca^{2+} signals were significantly decreased in the rTBI group (18 recordings/18 slices/8 rats) only ($F_{(2,39)} = 4.57$; $p = 0.017$; **Figure 4A**), but not sTBI (15 recordings/15 slices/6 rats), compared to sham (8 recordings/8 slices/8 rats). Our findings are consistent with previous studies demonstrating sustained pathophysiological effects resulting from TBI, including increased cortical excitatory synaptic transmission (3–5 weeks post-injury; Koenig et al., 2019) and Ca^{2+} dyshomeostasis in hippocampal neurons at 30 days post-injury (Sun et al., 2008). Also, in both of these studies, the nature of the impact (open-head/exposed dura) was markedly different from the closed-head model used in our study, utilized only a single impact, and used Ca^{2+} imaging data obtained from acutely isolated CA3 hippocampal neurons and not in CA1 pyramidal neurons in a brain slice. Thus, although it is difficult to extrapolate directly across these studies, there is a clear precedent for synaptic defects and Ca^{2+} dyshomeostasis resulting from TBI in brain circuits critical for learning, memory, and cognition.

In addition to measurement of somatic RyR-evoked Ca^{2+} release, we also examined basal spontaneous synaptic transmission in the form of excitatory postsynaptic potentials (sEPSPs) and how RyR activation differentially affects sEPSC frequency and amplitude in the sham and rTBI groups. As the RyR-Ca^{2+} response was blunted in only the rTBI condition, we similarly tested for sEPSP effects of caffeine in the sham (9 recordings/9 slices/8 rats) and rTBI (17 recordings/17 slices/8 rats) groups. Prior to caffeine application, the baseline frequency of sEPSPs was similar in both groups (two-way repeated-measures ANOVA; $F_{(1,51)} = 0.295$; $p = 0.837$; **Figure 5A**) and the frequency of sEPSPs was similarly increased by caffeine (paired t-test; $t = -4.52$; $p < 0.001$;

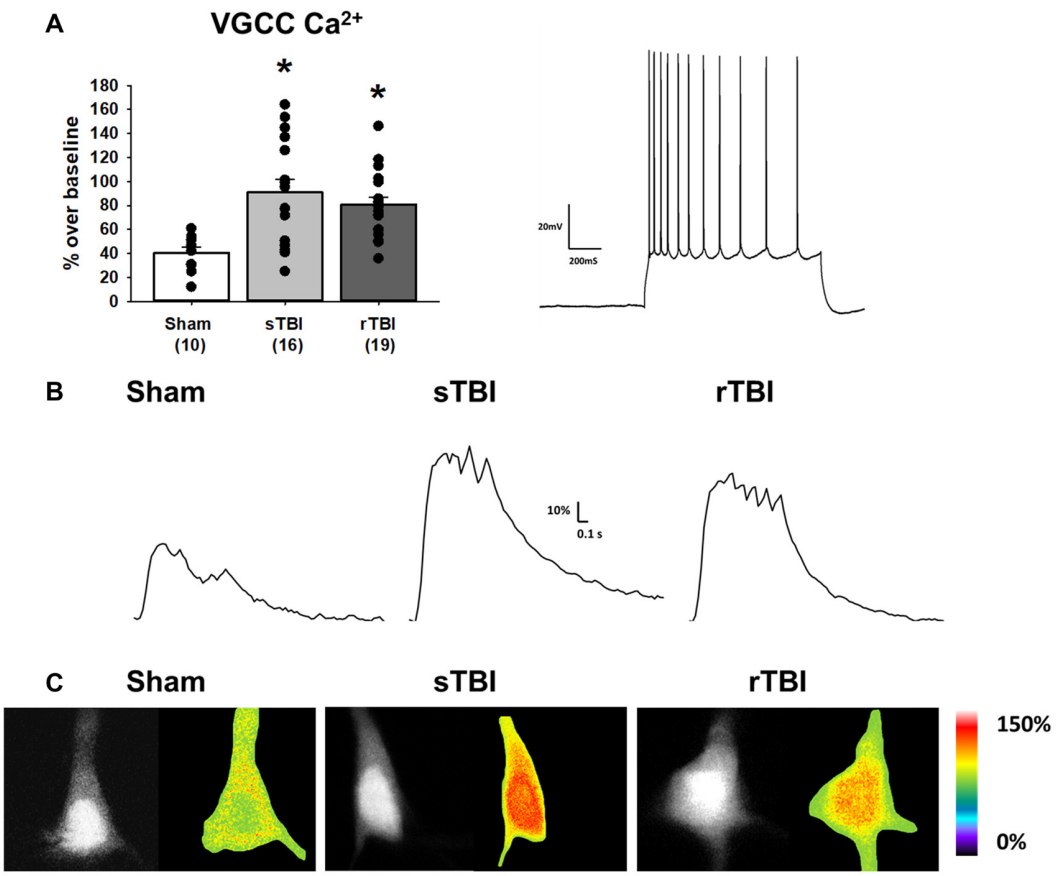

FIGURE 3 | TBI results in enhanced voltage-gated Ca^{2+} channel activity in hippocampal CA1 pyramidal neurons. **(A)** Left, bar graph summarizing peak Ca^{2+} effects of voltage-gated Ca^{2+} channel (VGCC) activation (using a depolarizing current injection in CA1 pyramidal neurons) 30 days after either a sham procedure, single TBI (sTBI), or repeated TBI (rTBI). Peak VGCC Ca^{2+} effects were larger in both the sTBI (gray bar) and rTBI (black bar) groups relative to sham (white bar). The number of recorded cells per group is in each bar. Right, action potential train in response to a depolarizing current injection in a CA1 pyramidal neuron (action potential characteristics were unchanged by either sTBI or rTBI, see **Table 1**). **(B)** Sample traces illustrating Ca^{2+} effects of VGCC activation in individual sham (left), sTBI (middle) or rTBI (right) CA1 pyramidal neurons. Calibration bars illustrate the % Ca^{2+} change over baseline. **(C)** Fluorescent (monochrome) and pseudocolored images of fura-2 loaded CA1 pyramidal neurons. Pseudocolored images illustrate relative Ca^{2+} responses to VGCC activation, from sham (left), sTBI (middle) and rTBI (right) groups. *$p < 0.05$. All recordings were on the hippocampal side ipsilateral to the TBI impact site (over the right sensorimotor cortex). Error bars represent the standard error of the mean.

Figure 5A). Prior to RyR activation, the baseline amplitude of sEPSPs was also similar in both the sham and rTBI groups ($F_{(1,51)} = 0.98$; $p = 0.47$; **Figure 5B**) and the amplitude of sEPSPs was similarly increased by caffeine (paired t-test; $t = -8.14$; $p < 0.05$; **Figure 5B**).

Increased Phosphorylated Tau Staining After TBI Is Sustained Throughout the Cortex and Hippocampus

The level of phosphorylated tau protein burden was examined in the hippocampus and overlying cortex in the sham, sTBI, and rTBI treatment groups, ipsilateral and contralateral to the injury site, using immunohistochemical labeling and imaged using confocal microscopy (**Figure 6**). The density of each fluorophore above the background threshold level was averaged across all images obtained for a given animal using Metamorph software (v.7). In the hippocampus, this analysis revealed increased phosphorylated tau staining in the rTBI group compared to the sham group (one-way ANOVA; $F_{(2,11)} = 7.242$; $p \leq 0.01$) and the sTBI group ($p \leq 0.05$). In the overlying sensorimotor cortex, significant increases in phosphorylated tau in the rTBI group compared to the sham group (one-way ANOVA; $F_{(2,11)} = 8.245$; $p \leq 0.01$) and the sTBI group ($p \leq 0.05$) were also observed. There were no significant differences in phosphorylated tau between the ipsilateral and contralateral hemispheres. This pattern suggests an active process that is generating phosphorylated tau long after the initial injury occurred, though other explanations are possible such as impairments in the clearance of pathogenic protein species. Furthermore, the tau pathology is not necessarily limited to the site or hemisphere of injury, but distributes across brain hemispheres over time regardless of the initial TBI site, with a higher phosphorylated tau burden associated with a repetitive injury.

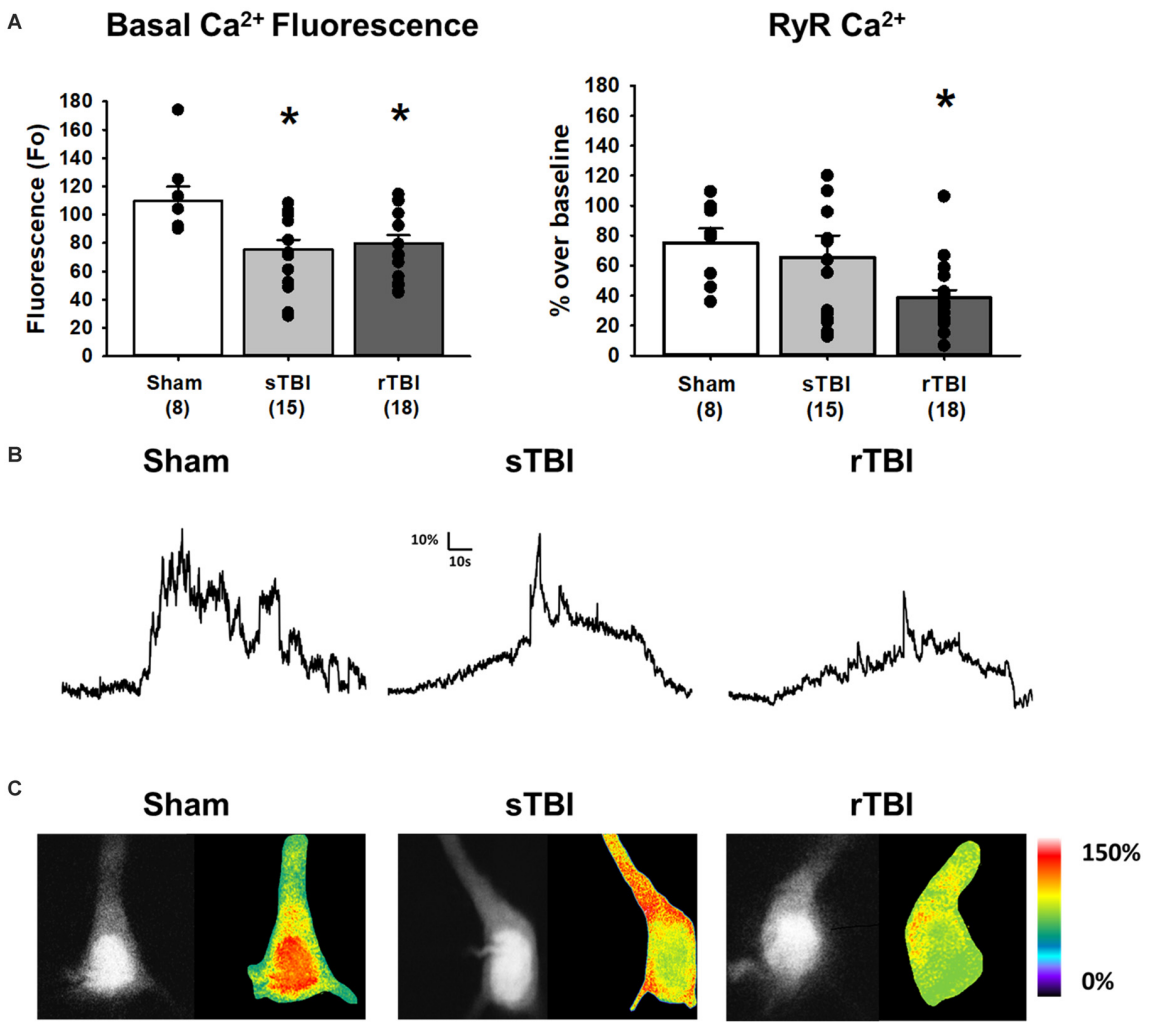

FIGURE 4 | TBI results in increased resting Ca^{2+} and blunted RyR-evoked Ca^{2+} release in hippocampal CA1 pyramidal neurons. **(A)** Left, bar graph summarizing averaged resting Ca^{2+}-based fluorescence (F_0) in CA1 pyramidal neurons 30 days after either a sham procedure (white bar), single TBI (sTBI, gray bar), or repeated TBI (rTBI, black bar). The decreased resting fluorescence (F_0) values of both TBI groups compared to the sham group are indicative of increased resting Ca^{2+}. Right, a bar graph illustrating that the averaged RyR-Ca^{2+} response to caffeine (20 mM) was decreased in the rTBI group (black bar) but not the sTBI group (gray bar), relative to sham (white bar). The number of recorded cells per group is in each bar. **(B)** Sample traces illustrating RyR-Ca^{2+} effects of caffeine (20 mM), in individual sham (left), sTBI (middle), and rTBI (right) CA1 pyramidal neurons. Calibration bars illustrate the % Ca^{2+} change over baseline. **(C)** Fluorescent (monochrome) and pseudocolored images of fura-2 loaded CA1 pyramidal neurons. Pseudocolored images illustrate relative RyR-Ca^{2+} effects of caffeine, from sham (left), sTBI (middle), and rTBI (right) groups. *$p < 0.05$. All recordings were on the hippocampal side ipsilateral to the TBI impact site (over the right sensorimotor cortex). Error bars represent the standard error of the mean.

Data Summary

Overall, our study reveals a cluster of resilient pathogenic or maladaptive features of mild TBI that persist long after the acute effects of the initial injury. These features may collectively impact memory encoding systems in the hippocampus and may contribute to the dementia symptoms that can emerge long after the injury. In particular, we show that sTBI and rTBI result in increased excitatory synaptic output, along with increased resting Ca^{2+} and VGCC activity, and reduced RyR function in the rTBI group. This combination of increased synaptic excitability and increased VGCC activity may play a role in the elevated basal Ca^{2+} observed (for a graphical summary see **Figure 7**). We also observed increased and graded levels of phosphorylated tau in the sTBI and rTBI groups, strengthening the idea of an association between increased neuronal excitation and tau pathology.

DISCUSSION

Mild TBI or concussion has received considerable attention in recent years, in part reflecting increased awareness of its pervasiveness in the general public and its role as a significant risk factor for AD-like dementia and other neurological diseases. Despite this, few studies have examined and compared the

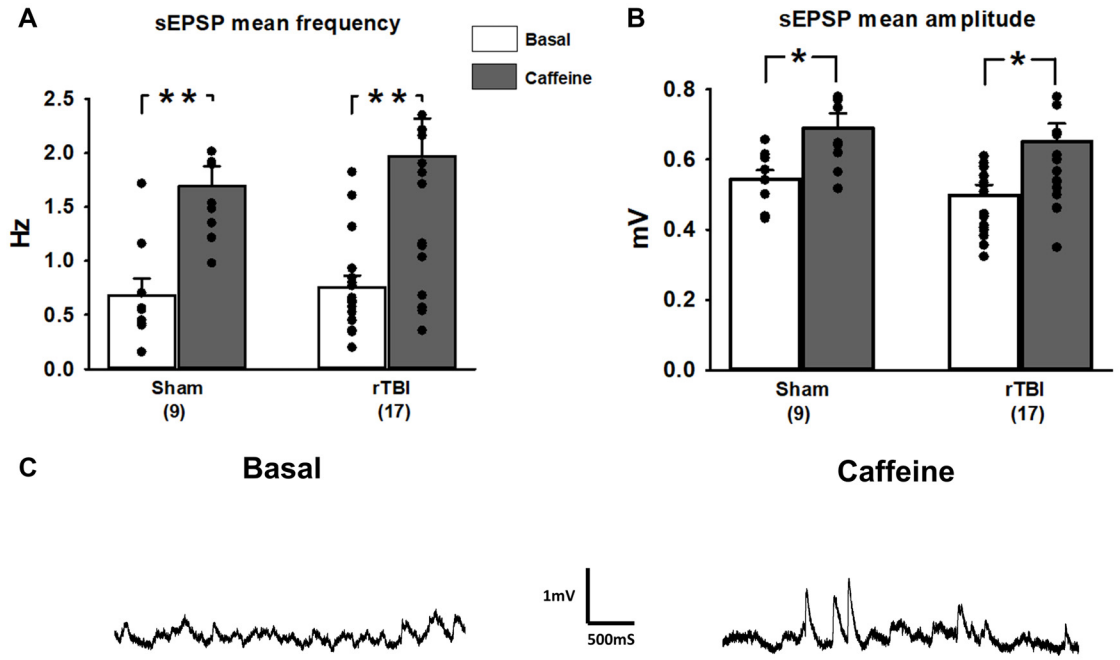

FIGURE 5 | Spontaneous synaptic events and contribution of RyR activation are unaffected by repeated TBI (rTBI). **(A)** The frequency of baseline spontaneous excitatory postsynaptic potentials (sEPSPs; gray bars) measured in hippocampal CA1 pyramidal neurons was not affected by rTBI at 30 days post-injury. sTBI neurons were not tested. In both the sham and rTBI groups, RyR activation by caffeine (20 mM; black bars) increased the frequency of sEPSPs similarly. **(B)** Baseline sEPSP amplitude (gray bars) was also unaffected by rTBI, but RyR activation by caffeine (20 mM; black bars) resulted in a significant increase in sEPSP amplitude in the rTBI group. **(C)** Representative traces illustrating effects of bath application of caffeine (20 mM) on the frequency and amplitude of sEPSPs during a whole-cell current-clamp recording in a CA1 pyramidal neuron from the rTBI group. $^{**}p < 0.001$, $^{*}p < 0.05$. All recordings were on the hippocampal side ipsilateral to the TBI impact site (over the right sensorimotor cortex). Error bars represent the standard error of the mean.

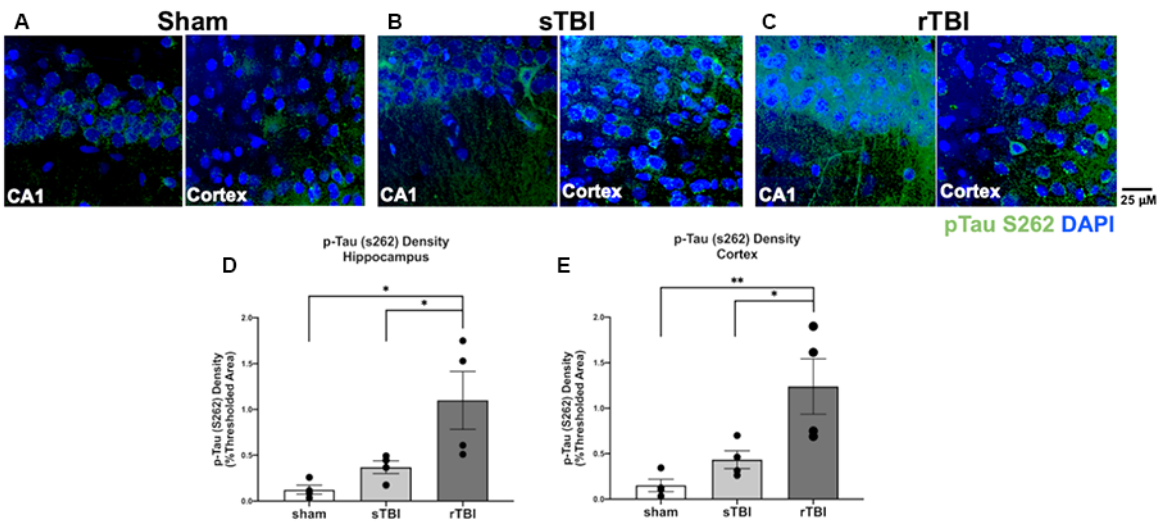

FIGURE 6 | Hippocampal and cortical phosphorylated tau is elevated after single (sTBI) or repeated TBI (rTBI). **(A–C)** Representative confocal images (63×, multi-plane) show immunolabeling of phosphorylated tau (pTau S262, green) within the CA1 region of the hippocampus (left) and Layer V of the cortex (right) ipsilateral to injury in sham **(A)**, sTBI **(B)**, and rTBI **(C)** animals. **(D)** Bar graphs show a significant increase in hippocampal phosphorylated tau burden in the rTBI group (black) relative to the sTBI (gray) and sham groups (white; $n = 16$ slices/4 rats for each treatment condition). **(E)** Bar graphs show a significant increase in cortical phosphorylated tau burden in the rTBI group (black) relative to the sTBI (gray) and sham groups (white; $n = 16$ slices/4 rats for each treatment condition). Representative images were obtained on a Leica Microsystems SP8 confocal microscope. The injury was over the right sensorimotor cortex. $^{*}p \leq 0.05$ and $^{**}p \leq 0.01$. Error bars represent the standard error of the mean.

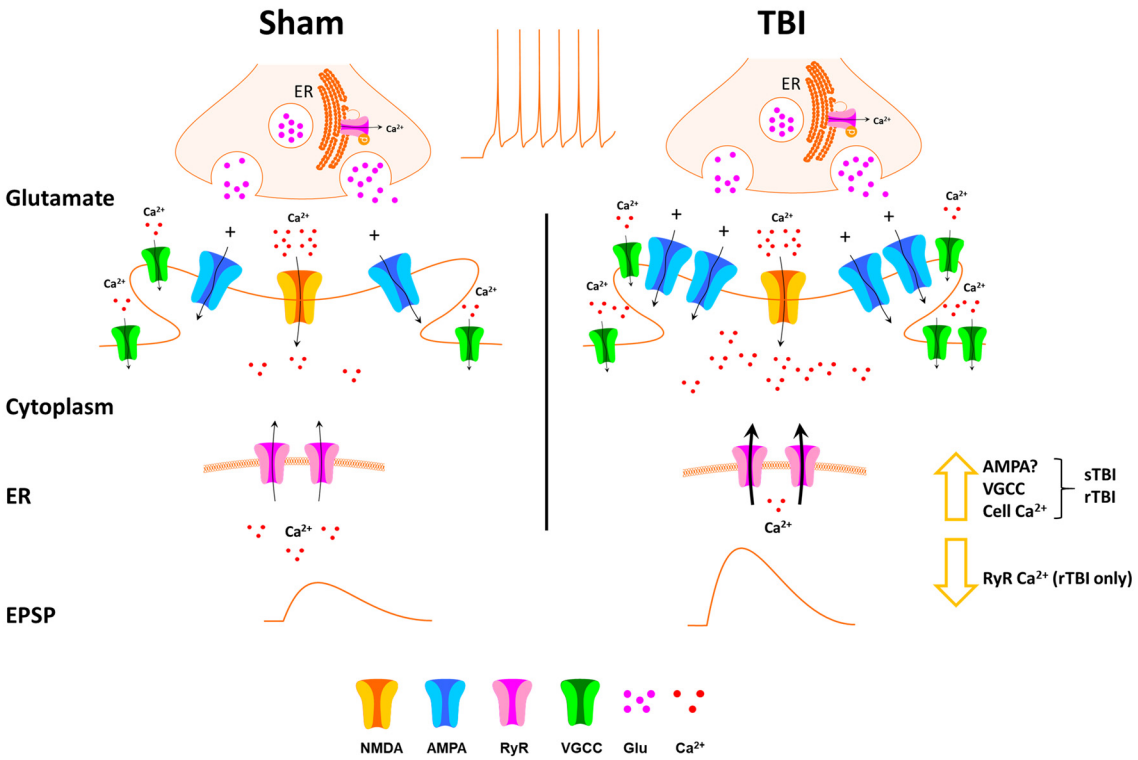

FIGURE 7 | Schematic of effects of TBI on hippocampal synaptic transmission and Ca^{2+} handling. Thirty days after single (sTBI) or repeated TBI (rTBI), we observed potentiation of evoked fEPSPs, indicating synaptic potentiation, possibly resulting from postsynaptic effects including increased AMPA receptor effects. VGCC function was also increased in the sTBI and rTBI groups, and this, combined with increased synaptic transmission, may play a role in the increased basal cytosolic Ca^{2+} observed in both TBI groups. RyR-mediated Ca^{2+} release was decreased, but only in the rTBI group, possibly due to depletion of endoplasmic reticulum (ER) Ca^{2+} stores.

persistent physiological and synaptic consequences of single or repeated, closed-head concussive events. To address the gaps in our understanding between brain injury and delayed cognitive deficits, we used a closed-head concussion model of single and repeated TBI that generates memory and performance deficits without overt hippocampal cell loss of detectable cell damage (Jamnia et al., 2017). One of the major limitations of most TBI studies to date has been the focus on measures of tissue damage or histopathology in fixed brain slices, a preparation in which active changes in real-time synaptic function cannot be detected. Here, we first employed extracellular field potential and whole-cell patch-clamp electrophysiological recordings to identify cellular and synaptic changes which may otherwise go undetected in fixed tissue. At the local circuit level in the hippocampus, we found a persistent upregulation of excitatory synaptic transmission at CA3-CA1 synapses which was present in both the single and repeated TBI groups 30 days after injury. Interestingly, these fundamental changes in synaptic responses did not result in altered expression of long-term synaptic plasticity; however, this does not preclude underlying LTP deficits in this injury model as the recruitment of compensatory mechanisms to sustain normal-appearing LTP has been demonstrated in compromised hippocampal networks (Chakroborty et al., 2012). There also were no explicit alterations in paired-pulse facilitation, which is generally accepted as an index of evoked presynaptic release probability (Regehr, 2012). Interestingly, rTBI also had no effect on the frequency of mEPSCs measured using whole-cell recordings, reinforcing the observation that TBI does not affect the presynaptic release probability weeks after injury. Although this does not rule out a presynaptic component due to an acute but transient increase in synaptic glutamate release in the wake of TBI (Huang et al., 1992).

As our data indicate that hippocampal synaptic transmission is similarly increased by either sTBI or rTBI, this suggests that even a single concussive event is sufficient to elicit long-term synaptic effects. Although the exact series of cellular events which lead to this potentiated synaptic state is still under investigation, our data suggest that it is a postsynaptic component of the fEPSP that is potentiated. As the fEPSP is typically mediated by activation of postsynaptic AMPA receptors (Davies and Collingridge, 1989; Tsien et al., 1996), upregulation of AMPA receptors may play a role in the synaptic potentiation observed. Additionally, as the resting membrane potential of CA1 pyramidal neurons was approximately −70 mV in all

TABLE 1 | Passive and active membrane properties are unchanged by single or repeated traumatic brain injury (TBI).

Passive and active membrane properties of CA1 Hippocampal Pyramidal Cells for sham, sTBI, and rTBI.

	Sham	sTBI	rTBI
Cell Potential (mV)	−70.8 ± 0.35 (*n* = 18)	−70.4 ± 0.17 (*n* = 18)	−70.6 ± 0.19 (*n* = 24)
Input Resistance (MΩ)	101 ± 5.23 (*n* = 18)	112 ± 5.77 (*n* = 18)	118 ± 7.71 (*n* = 24)
Sag (%)	24.8 ± 1.14 (*n* = 18)	25.1 ± 1.03 (*n* = 18)	27.2 ± 0.98 (*n* = 24)
Spike Threshold (mV)	−50.0 ± 1.41 (*n* = 11)	−46.1 ± 0.82 (*n* = 16)	−48.1 ± 1.00 (*n* = 19)
Spike Amplitude (mV)	102 ± 2.14 (*n* = 11)	97.1 ± 2.1 (*n* = 16)	99.4 ± 1.83 (*n* = 19)
Spike Half-Width (ms)	1.82 ± 0.04 (*n* = 11)	1.98 ± 0.06 (*n* = 16)	1.89 ± 0.05 (*n* = 19)

Passive and active membrane properties of hippocampal CA1 pyramidal neurons, including resting membrane potential, input resistance, and action potential characteristics were unchanged by either single TBI (sTBI) or repeated TBI (rTBI).

treatment groups (**Table 1**), it is unlikely that there is a substantial NMDAR fEPSP component due to the Mg^{2+} block of NMDARs at this hyperpolarized membrane potential. Circuit hyper-responsivity may also reflect decreased RyR function and downstream Ca^{2+}-regulated neuromodulators (Chakroborty et al., 2015), as well as pathological tau accumulation (Huijbers et al., 2019). Tau levels are associated with seizure incidence (DeVos et al., 2013), a well-documented consequence of TBI that may also occur as a result of hippocampal hyperactivity (Golarai et al., 2001). Another possible explanation for the hippocampal hyperexcitability observed is decreased CA1 hippocampal inhibitory neurotransmission, another feature shared in animal models of both TBI and Alzheimer's disease (Reeves et al., 1997; Hazra et al., 2013; Almeida-Suhett et al., 2015).

The decreased RyR-evoked Ca^{2+} release in the rTBI group is similar to the reported decreased RyR-Ca^{2+} response resulting from mechanical neuronal injury *in vitro* (Weber et al., 2002), an effect mediated by NMDAR mediated Ca^{2+} influx (Ahmed et al., 2002), subsequent increased CICR, and depletion of ER Ca^{2+} stores (Weber et al., 2002). Indeed, elevated basal cytosolic Ca^{2+} resulting from a single TBI event is prevented by pretreatment with the NMDAR antagonist MK801 (Deshpande et al., 2008). Although we did not observe decreased RyR-Ca^{2+} effects in the sTBI group, it is plausible that effects of repeated mechanical injury and repeated NMDAR Ca^{2+} influx are more persistent than those arising from a single injury (Slemmer et al., 2002; Weber, 2007), resulting in long-term modification of RyR-Ca^{2+} signaling as a result of rTBI. Notably, the sustained rTBI effect on RyR-Ca^{2+} correlates with persistent cognitive impairments resulting from rTBI, but not sTBI (Jamnia et al., 2017), further strengthening the association between RyR dysfunction, Ca^{2+} dyshomeostasis, and cognitive impairment after brain injury (Deshpande et al., 2008; Sun et al., 2008; Bruno et al., 2012; Liu et al., 2012).

While decreased RyR-Ca^{2+} was observed in the rTBI group only, increased VGCC activity was observed in both treatment groups, and may play a role in the elevated basal Ca^{2+} present in both TBI groups. The sustained upregulation of hippocampal synaptic transmission observed in both TBI groups may also be driven by the increased Ca^{2+} influx through VGCCs, and there is ample evidence that VGCCs play an important role in hippocampal synaptic potentiation (Huang and Malenka, 1993; Huber et al., 1995). As there was no significant effect of either sTBI or rTBI on the passive or active cell membrane properties measured 30 days post-injury (**Table 1**), the increased VGCC responses observed cannot be explained by changes in membrane resistance or postsynaptic action potential threshold.

Tau pathology is a well-documented feature of TBI and related conditions such as chronic traumatic encephalopathy (CTE) and Alzheimer's disease (McKee et al., 2013; McKee and Robinson, 2014; Albayram et al., 2016), yet the defined mechanisms by which tau phosphorylation is sustained after an injury have yet to be fully elucidated. Across TBI conditions, the uniformly distributed pathogenic tau seen 30 days post-injury is likely resulting from a feed-forward cascade, as the half-life of soluble tau is approximately 10 days (Yamada et al., 2015). A possible mechanism is the increased resting cytosolic Ca^{2+} levels following TBI, which can upregulate GSK3β and Cdk5 activity and phosphorylate tau at serine and threonine residues (Avila et al., 2004). This in turn can disrupt Ca^{2+} homeostasis, and sustain the pathogenic cycle (Gómez-Ramos et al., 2006). Consistent with this, GSK3β inhibitors have shown therapeutic potential for treating TBI beyond a reduction in phosphorylated tau, presumably by altering signaling *via* receptor tyrosine kinases (RTKs) and Wnt pathways, effects that would otherwise lead to the accumulation of pathological proteins, neuronal loss, and cognitive dysfunction (Shim and Stutzmann, 2016). In addition to altering Ca^{2+} homeostasis, abnormally phosphorylated tau disrupts microtubule assembly and axonal transport, leading to synaptic deficits and ultimately synaptic loss (Ial et al., 2005). Phosphorylated tau may also rapidly propagate and accumulate in brain regions distant from, but synaptically connected to, the site of injury following TBI (Edwards et al., 2020). Additional mechanisms of widespread histopathology may include contrecoup injury or generalized neuroinflammation (Edwards et al., 2020). The exact processes accounting for the propagation and distribution of tau pathology at this 30-day time point require further study.

Despite this evidence demonstrating alterations in synaptic physiology after TBI, much remains to be determined regarding the nature and source of sustained physiological changes in a closed-head injury model and how this relates to plasticity and memory deficits long after the initial components of the injury have healed. Ca^{2+} dyshomeostasis is a central pathogenic element and has been observed in TBI models at several time points (Deshpande et al., 2008; Sun et al., 2008; Weber, 2012). Ca^{2+} signaling is centrally involved in synaptic transmission, plasticity, and tau phosphorylation, and thus can generate a self-sustaining pathogenic cycle, as seen in chronic neurodegenerative disorders such as Alzheimer's

disease (Stutzmann, 2007; Chakroborty et al., 2009, 2012, 2019). In the rTBI group, the blunted RyR-Ca^{2+} response may reflect reduced ER Ca^{2+} stores resulting from leaky or sensitized RyRs; this leak may also contribute to the elevated resting cytosolic Ca^{2+} levels observed (Lacampagne et al., 2017). Furthermore, increased Ca^{2+} entry through VGCCs, coupled with increased synaptic excitation may also contribute to the elevated Ca^{2+} load. Elevated cell Ca^{2+} can subsequently increase PKA activity, which phosphorylates and subsequently sensitizes the RyR to leak excess ER Ca^{2+} into the cytosol (Morimoto et al., 2009; Liu et al., 2012; Lacampagne et al., 2017), thus lowering ER Ca^{2+} reserves and reducing evoked responses while contributing to increased cytosolic resting levels, as is observed in this study.

Several clinical studies have demonstrated positive effects of FDA-approved Ca^{2+} channel blockers such as nimodipine on improved cognitive function in TBI patients (Teasdale et al., 1990, 1992; Bailey et al., 1991), however, subsequent analyses have reported no effects on mortality rates (Langham et al., 2003; Vergouwen et al., 2007). Likewise, the RyR negative allosteric modulator dantrolene attenuates glutamate excitotoxicity *in vitro* (Frandsen and Schousboe, 1991) and *in vivo* (Niebauer and Gruenthal, 1999), and normalizes intracellular Ca^{2+} homeostasis in AD models (Chakroborty et al., 2012, 2019), thus raising the possibility that altered VGCC and RyR mediated Ca^{2+} signaling play a central role in the long term consequences of TBI. Given that VGCCs and RyRs may work in a feed-forward manner to sustain TBI pathophysiology, combined targeting of these channels may serve as an effective therapeutic strategy in the treatment of TBI.

Although our study extends 30 days after TBI, further investigation is warranted to determine whether these effects persist for longer periods, especially as hippocampal hyperactivity may precede synaptic depression and neurodegeneration (Huijbers et al., 2015). Also, human studies indicate cognitive effects lasting months to years (McInnes et al., 2019; Shen et al., 2020), indicating the need for animal studies of analogous duration.

CONCLUSIONS

Here, we demonstrated that both single and repeated mild TBI result in a similarly persistent upregulation of hippocampal synaptic transmission, effects accompanied by altered Ca^{2+} homeostasis and phosphorylated tau expression. These data strengthen the idea that a single concussive event can result in persistent brain pathophysiological effects that are similar in magnitude to those observed after repeated concussions, with future implications for behavior, learning, and memory.

DATA AVAILABILITY STATEMENT

The raw data supporting the conclusions of this article will be made available by the authors, without undue reservation.

ETHICS STATEMENT

The animal study was reviewed and approved by Rosalind Franklin University IACUC DePaul University IACUC.

AUTHOR CONTRIBUTIONS

JM, CB, and NB conducted the experiments and analyzed data, and contributed to the writing of manuscript. DP, DK, and GS contributed to the experimental design, oversight, execution of the study, and writing of the manuscript. All authors contributed to the article and approved the submitted version.

FUNDING

Funding was obtained from DePaul-RFUMS pilot awards to DP, DK, and GS.

ACKNOWLEDGMENTS

We thank Sarah Mustaly and Sean Schrank for editorial assistance.

REFERENCES

Ahmed, S. M., Weber, J. T., Liang, S., Willoughby, K. A., Sitterding, H. A., Rzigalinski, B. A., et al. (2002). NMDA receptor activation contributes to a portion of the decreased mitochondrial membrane potential and elevated intracellular free calcium in strain-injured neurons. *J. Neurotrauma* 19, 1619–1629. doi: 10.1089/089771502762300274

Albayram, O., Herbert, M. K., Kondo, A., Tsai, C. Y., Baxley, S., Lian, X., et al. (2016). Function and regulation of tau conformations in the development and treatment of traumatic brain injury and neurodegeneration. *Cell Biosci.* 6:59. doi: 10.1186/s13578-016-0124-4

Almeida-Suhett, C. P., Prager, E. M., Pidoplichko, V., Figueiredo, T. H., Marini, A. M., Li, Z., et al. (2015). GABAergic interneuronal loss and reduced inhibitory synaptic transmission in the hippocampal CA1 region after mild traumatic brain injury. *Exp. Neurol.* 273, 11–23. doi: 10.1016/j.expneurol.2015.07.028

Annegers, J. F., Hauser, W. A., Coan, S. P., and Rocca, W. A. (1998). A population-based study of seizures after traumatic brain injuries. *N. Engl. J. Med.* 338, 20–24. doi: 10.1056/NEJM199801013380104

Arai, M., Imamura, O., Kondoh, N., Dateki, M., and Takishima, K. (2019). Neuronal Ca^{2+} -dependent activator protein 1 (NCDAP1) induces neuronal cell death by activating p53 pathway following traumatic brain injury. *J. Neurochem.* 151, 795–809. doi: 10.1111/jnc.14803

Atkins, C. M. (2011). Decoding hippocampal signaling deficits after traumatic brain injury. *Transl. Stroke Res.* 2, 546–555. doi: 10.1007/s12975-011-0123-z

Aungst, S. L., Kabadi, S. V., Thompson, S. M., Stoica, B. A., and Faden, A. I. (2014). Repeated mild traumatic brain injury causes chronic neuroinflammation, changes in hippocampal synaptic plasticity, and associated cognitive deficits. *J. Cereb. Blood Flow Metab.* 34, 1223–1232. doi: 10.1038/jcbfm.2014.75

Avila, J., Pérez, M., Lim, F., Gómez-Ramos, A., Hernández, F., and Lucas, J. J. (2004). Tau in neurodegenerative diseases: tau phosphorylation and assembly. *Neurotox Res.* 6, 477–482. doi: 10.1007/BF03033284

Bailey, I., Bell, A., Gray, J., Gullan, R., Heiskanan, O., Marks, P. V., et al. (1991). A trial of the effect of nimodipine on outcome after head injury. *Acta Neurochir.* 110, 97–105. doi: 10.1007/BF01400674

Beamer, M., Tummala, S. R., Gullotti, D., Kopil, C., Gorka, S., Ted, A., et al. (2016). Primary blast injury causes cognitive impairments and hippocampal circuit alterations. *Exp. Neurol.* 283, 16–28. doi: 10.1016/j.expneurol.2016.05.025

Biegon, A., Fry, P. A., Paden, C. M., Alexandrovich, A., Tsenter, J., and Shohami, E. (2004). Dynamic changes in N-methyl-D-aspartate receptors after closed head injury in mice: implications for treatment of neurological and cognitive deficits. *Proc. Natl. Acad. Sci. U S A* 101, 5117–5122. doi: 10.1073/pnas.0305741101

Borde, M., Bonansco, C., Fernández de Sevilla, D., Le Ray, D., and Buño, W. (2000). Voltage-clamp analysis of the potentiation of the slow Ca^{2+}-activated K^+ current in hippocampal pyramidal neurons. *Hippocampus* 10, 198–206. doi: 10.1002/(SICI)1098-1063(2000)10:2<198::AID-HIPO9>3.0.CO;2-F

Briggs, C. A., Chakroborty, S., and Stutzmann, G. E. (2017). Emerging pathways driving early synaptic pathology in Alzheimer's disease. *Biochem. Biophys. Res. Commun.* 483, 988–997. doi: 10.1016/j.bbrc.2016.09.088

Bruno, A. M., Huang, J. Y., Bennett, D. A., Marr, R. A., Hastings, M. L., and Stutzmann, G. E. (2012). Altered ryanodine receptor expression in mild cognitive impairment and Alzheimer's disease. *Neurobiol. Aging* 33, 1001.e1–1001.e6. doi: 10.1016/j.neurobiolaging.2011.03.011

CDC, (2014). *Surveillance Report of Traumatic Brain Injury-Related Emergency Department Visits, Hospitalizations, and Deaths*. Available online at: https://www.cdc.gov/traumaticbraininjury/data/tbi-edhd.html.

Chakroborty, S., Briggs, C., Miller, M. B., Goussakov, I., Schneider, C., Kim, J., et al. (2012). Stabilizing ER Ca^{2+} channel function as an early preventative strategy for Alzheimer's disease. *PLoS One* 7:e52056. doi: 10.1371/journal.pone.0052056

Chakroborty, S., Goussakov, I., Miller, M. B., and Stutzmann, G. E. (2009). Deviant ryanodine receptor-mediated calcium release resets synaptic homeostasis in presymptomatic 3xTg-AD mice. *J. Neurosci.* 29, 9458–9470. doi: 10.1523/JNEUROSCI.2047-09.2009

Chakroborty, S., Hill, E. S., Christian, D. T., Helfrich, R., Riley, S., Schneider, C., et al. (2019). Reduced presynaptic vesicle stores mediate cellular and network plasticity defects in an early-stage mouse model of Alzheimer's disease. *Mol. Neurodegener.* 14:7. doi: 10.1186/s13024-019-0307-7

Chakroborty, S., Kim, J., Schneider, C., West, A. R., and Stutzmann, G. E. (2015). Nitric oxide signaling is recruited as a compensatory mechanism for sustaining synaptic plasticity in Alzheimer's disease mice. *J. Neurosci.* 35, 6893–6902. doi: 10.1523/JNEUROSCI.4002-14.2015

Chavis, P., Fagni, L., Lansman, J. B., and Bockaert, J. (1996). Functional coupling between ryanodine receptors and L-type calcium channels in neurons. *Nature* 382, 719–722. doi: 10.1038/382719a0

D'Ambrosio, R., Maris, D. O., Grady, M. S., Winn, H. R., and Janigro, D. (1998). Selective loss of hippocampal long-term potentiation, but not depression, following fluid percussion injury. *Brain Res.* 786, 64–79. doi: 10.1016/s0006-8993(97)01412-1

Dash, P. K., Johnson, D., Clark, J., Orsi, S. A., Zhang, M., Zhao, J., et al. (2011). Involvement of the glycogen synthase kinase-3 signaling pathway in TBI pathology and neurocognitive outcome. *PLoS One* 6:e24648. doi: 10.1371/journal.pone.0024648

Davies, S. N., and Collingridge, G. L. (1989). Role of excitatory amino acid receptors in synaptic transmission in area CA1 of rat hippocampus. *Proc. R. Soc. Lond. B Biol. Sci.* 236, 373–384. doi: 10.1098/rspb.1989.0028

Davies, S. N., Lester, R. A., Reymann, K. G., and Collingridge, G. L. (1989). Temporally distinct pre- and post-synaptic mechanisms maintain long-term potentiation. *Nature* 338, 500–503. doi: 10.1038/338500a0

Deshpande, L. S., Sun, D. A., Sombati, S., Baranova, A., Wilson, M. S., Attkisson, E., et al. (2008). Alterations in neuronal calcium levels are associated with cognitive deficits after traumatic brain injury. *Neurosci. Lett.* 441, 115–119. doi: 10.1016/j.neulet.2008.05.113

DeVos, S. L., Goncharoff, D. K., Chen, G., Kebodeaux, C. S., Yamada, K., Stewart, F. R., et al. (2013). Antisense reduction of tau in adult mice protects against seizures. *J. Neurosci.* 33, 12887–12897. doi: 10.1523/JNEUROSCI.2107-13.2013

Edwards, G. III., Zhao, J., Dash, P. K., Soto, C., and Moreno-Gonzalez, I. (2020). Traumatic brain injury induces tau aggregation and spreading. *J. Neurotrauma* 37, 80–92. doi: 10.1089/neu.2018.6348

Ellemberg, D., Henry, L. C., Macciocchi, S. N., Guskiewicz, K. M., and Broglio, S. P. (2009). Advances in sport concussion assessment: from behavioral to brain imaging measures. *J. Neurotrauma* 26, 2365–2382. doi: 10.1089/neu.2009.0906

Emptage, N., Bliss, T. V., and Fine, A. (1999). Single synaptic events evoke NMDA receptor-mediated release of calcium from internal stores in hippocampal dendritic spines. *Neuron* 22, 115–124. doi: 10.1016/s0896-6273(00)80683-2

Fakhran, S., Yaeger, K., and Alhilali, L. (2013). Symptomatic white matter changes in mild traumatic brain injury resemble pathologic features of early Alzheimer dementia. *Radiology* 269, 249–257. doi: 10.1148/radiol.13122343

Fleminger, S., Oliver, D. L., Lovestone, S., Rabe-Hesketh, S., and Giora, A. (2003). Head injury as a risk factor for Alzheimer's disease: the evidence 10 years on; a partial replication. *J. Neurol. Neurosurg. Psychiatry* 74, 857–862. doi: 10.1136/jnnp.74.7.857

Frandsen, A., and Schousboe, A. (1991). Dantrolene prevents glutamate cytotoxicity and Ca^{2+} release from intracellular stores in cultured cerebral cortical neurons. *J. Neurochem.* 56, 1075–1078. doi: 10.1111/j.1471-4159.1991.tb02031.x

Frey, U., Huang, Y. Y., and Kandel, E. R. (1993). Effects of cAMP simulate a late stage of LTP in hippocampal CA1 neurons. *Science* 260, 1661–1664. doi: 10.1126/science.8389057

Garaschuk, O., Yaari, Y., and Konnerth, A. (1997). Release and sequestration of calcium by ryanodine-sensitive stores in rat hippocampal neurones. *J. Physiol.* 502, 13–30. doi: 10.1111/j.1469-7793.1997.013bl.x

Geddes, D. M., LaPlaca, M. C., and Cargill, R. S. II. (2003). Susceptibility of hippocampal neurons to mechanically induced injury. *Exp. Neurol.* 184, 420–427. doi: 10.1016/s0014-4886(03)00254-1

Geddes, J. F., Vowles, G. H., Nicoll, J. A., and Révész, T. (1999). Neuronal cytoskeletal changes are an early consequence of repetitive head injury. *Acta Neuropathol.* 98, 171–178. doi: 10.1007/s004010051066

Giacomello, M., Oliveros, J. C., Naranjo, J. R., and Carafoli, E. (2013). Neuronal Ca^{2+} dyshomeostasis in Huntington disease. *Prion* 7, 76–84. doi: 10.4161/pri.23581

Golarai, G., Greenwood, A. C., Feeney, D. M., and Connor, J. A. (2001). Physiological and structural evidence for hippocampal involvement in persistent seizure susceptibility after traumatic brain injury. *J. Neurosci.* 21, 8523–8537. doi: 10.1523/JNEUROSCI.21-21-08523.2001

Gómez-Ramos, A., Díaz-Hernandez, M., Cuadros, R., Hernández, F., and Avila, J. (2006). Extracellular tau is toxic to neuronal cells. *FEBS Lett.* 580, 4842–4850. doi: 10.1016/j.febslet.2006.07.078

Görlach, A., Bertram, K., Hudecova, S., and Krizanova, O. (2015). Calcium and ROS: a mutual interplay. *Redox Biol.* 6, 260–271. doi: 10.1016/j.redox.2015.08.010

Gurkoff, G. G., Feng, J.-F., Van, K. C., Izadi, A., Ghiasvand, R., Shahlaie, K., et al. (2013). NAAG peptidase inhibitor improves motor function and reduces cognitive dysfunction in a model of TBI with secondary hypoxia. *Brain Res.* 1515, 98–107. doi: 10.1016/j.brainres.2013.03.043

Hazra, A., Gu, F., Aulakh, A., Berridge, C., Eriksen, J. L., and Ziburkus, J. (2013). Inhibitory neuron and hippocampal circuit dysfunction in an aged mouse model of Alzheimer's disease. *PLoS One* 8:e64318. doi: 10.1371/journal.pone.0064318

Hernandez, A., Tan, C., Plattner, F., Logsdon, A. F., Pozo, K., Yousuf, M. A., et al. (2018). Exposure to mild blast forces induces neuropathological effects, neurophysiological deficits and biochemical changes. *Mol. Brain* 11:64. doi: 10.1186/s13041-018-0408-1

Hinzman, J. M., Thomas, T. C., Burmeister, J. J., Quintero, J. E., Huettl, P., Pomerleau, F., et al. (2010). Diffuse brain injury elevates tonic glutamate levels and potassium-evoked glutamate release in discrete brain regions at two days post-injury: an enzyme-based microelectrode array study. *J. Neurotrauma* 27, 889–899. doi: 10.1089/neu.2009.1238

Holbro, N., Grunditz, A., and Oertner, T. G. (2009). Differential distribution of endoplasmic reticulum controls metabotropic signaling and plasticity at hippocampal synapses. *Proc. Natl. Acad. Sci. U S A* 106, 15055–15060. doi: 10.1073/pnas.0905110106

Huang, Y. Y., Colino, A., Selig, D. K., and Malenka, R. C. (1992). The influence of prior synaptic activity on the induction of long-term potentiation. *Science* 255, 730–733. doi: 10.1126/science.1346729

Huang, Y. Y., and Malenka, R. C. (1993). Examination of TEA-induced synaptic enhancement in area CA1 of the hippocampus: the role of voltage-dependent Ca^{2+} channels in the induction of LTP. *J. Neurosci.* 13, 568–576. doi: 10.1523/JNEUROSCI.13-02-00568.1993

Huber, K. M., Mauk, M. D., and Kelly, P. T. (1995). LTP induced by activation of voltage-dependent Ca^{2+} channels requires protein kinase activity. *Neuroreport* 6, 1281–1284. doi: 10.1097/00001756-199506090-00013

Huijbers, W., Mormino, E. C., Schultz, A. P., Wigman, S., Ward, A. M., Larvie, M., et al. (2015). Amyloid-β deposition in mild cognitive impairment is associated with increased hippocampal activity, atrophy and clinical progression. *Brain* 138, 1023–1035. doi: 10.1093/brain/awv007

Huijbers, W., Schultz, A. P., Papp, K. V., LaPoint, M. R., Hanseeuw, B., Chhatwal, J. P., et al. (2019). Tau accumulation in clinically normal older adults is associated with hippocampal hyperactivity. *J. Neurosci.* 39, 548–556. doi: 10.1523/JNEUROSCI.1397-18.2018

Ial, K., Alonso Adel, C., Chen, S., Chohan, M. O., El-Akkad, E., Gong, C. X., et al. (2005). Tau pathology in Alzheimer disease and other tauopathies. *Biochim. Biophys. Acta* 1739, 198–210. doi: 10.1016/j.bbadis.2004.09.008

Jaffe, D. B., Fisher, S. A., and Brown, T. H. (1994). Confocal laser scanning microscopy reveals voltage-gated calcium signals within hippocampal dendritic spines. *J. Neurobiol.* 25, 220–233. doi: 10.1002/neu.480250303

Jamnia, N., Urban, J. H., Stutzmann, G. E., Chiren, S. G., Reisenbigler, E., Marr, R., et al. (2017). A clinically relevant closed-head model of single and repeat concussive injury in the adult rat using a controlled cortical impact device. *J. Neurotrauma* 34, 1351–1363. doi: 10.1089/neu.2016.4517

Koenig, J. B., Cantu, D., Low, C., Sommer, M., Noubary, F., Croker, D., et al. (2019). Glycolytic inhibitor 2-deoxyglucose prevents cortical hyperexcitability after traumatic brain injury. *JCI Insight* 5:e126506. doi: 10.1172/jci.insight.126506

Lacampagne, A., Liu, X., Reiken, S., Bussiere, R., Meli, A. C., Lauritzen, I., et al. (2017). Post-translational remodeling of ryanodine receptor induces calcium leak leading to Alzheimer's disease-like pathologies and cognitive deficits. *Acta Neuropathol.* 134, 749–767. doi: 10.1007/s00401-017-1733-7

Langham, J., Goldfrad, C., Teasdale, G., Shaw, D., and Rowan, K. (2003). Calcium channel blockers for acute traumatic brain injury. *Cochrane Database Syst. Rev.* 4:CD000565. doi: 10.1002/14651858.CD000565

Li, Y., Li, Y., Li, X., Zhang, S., Zhao, J., Zhu, X., et al. (2017). Head injury as a risk factor for dementia and Alzheimer's disease: a systematic review and meta-analysis of 32 observational studies. *PLoS One* 12:e0169650. doi: 10.1371/journal.pone.0169650

Liu, X., Betzenhauser, M. J., Reiken, S., Meli, A. C., Xie, W., Chen, B. X., et al. (2012). Role of leaky neuronal ryanodine receptors in stress-induced cognitive dysfunction. *Cell* 150, 1055–1067. doi: 10.1016/j.cell.2012.06.052

Logue, O. C., Cramer, N. P., Xu, X., Perl, D. P., and Galdzicki, Z. (2016). Alterations of functional properties of hippocampal networks following repetitive closed-head injury. *Exp. Neurol.* 277, 227–243. doi: 10.1016/j.expneurol.2015.12.019

Luo, P., Fei, F., Zhang, L., Qu, Y., and Fei, Z. (2011). The role of glutamate receptors in traumatic brain injury: implications for postsynaptic density in pathophysiology. *Brain Res. Bull.* 85, 313–320. doi: 10.1016/j.brainresbull.2011.05.004

Mayer, A. R., Quinn, D. K., and Master, C. L. (2017). The spectrum of mild traumatic brain injury: a review. *Neurology* 89, 623–632. doi: 10.1212/WNL.0000000000004214

McInnes, K., Friesen, C. L., MacKenzie, D. E., Westwood, D. A., and Boe, S. G. (2019). Mild Traumatic Brain Injury (mTBI) and chronic cognitive impairment: a scoping review. *PLoS One* 14:e0218423. doi: 10.1371/journal.pone.0218423

McKee, A. C., Cantu, R. C., Nowinski, C. J., Hedley-Whyte, E. T., Gavett, B. E., Budson, A. E., et al. (2009). Chronic traumatic encephalopathy in athletes: progressive tauopathy after repetitive head injury. *J. Neuropathol. Exp. Neurol.* 68, 709–735. doi: 10.1097/NEN.0b013e3181a9d503

McKee, A. C., and Robinson, M. E. (2014). Military-related traumatic brain injury and neurodegeneration. *Alzheimers Dement.* 10, S242–S253. doi: 10.1016/j.jalz.2014.04.003

McKee, A. C., Stern, R. A., Nowinski, C. J., Stein, T. D., Alvarez, V. E., Daneshvar, D. H., et al. (2013). The spectrum of disease in chronic traumatic encephalopathy. *Brain* 136, 43–64. doi: 10.1093/brain/aws307

Meehan, W. P. III., Zhang, J., Mannix, R., and Whalen, M. J. (2012). Increasing recovery time between injuries improves cognitive outcome after repetitive mild concussive brain injuries in mice. *Neurosurgery* 71, 885–891. doi: 10.1227/NEU.0b013e318265a439

Miyazaki, S., Katayama, Y., Lyeth, B. G., Jenkins, L. W., DeWitt, D. S., Goldberg, S. J., et al. (1992). Enduring suppression of hippocampal long-term potentiation following traumatic brain injury in rat. *Brain Res.* 585, 335–339. doi: 10.1016/0006-8993(92)91232-4

Morimoto, S., J, O. U., Kawai, M., Hoshina, T., Kusakari, Y., Komukai, K., et al. (2009). Protein kinase A-dependent phosphorylation of ryanodine receptors increases Ca^{2+} leak in mouse heart. *Biochem. Biophys. Res. Commun.* 390, 87–92. doi: 10.1016/j.bbrc.2009.09.071

Niebauer, M., and Gruenthal, M. (1999). Neuroprotective effects of early vs. late administration of dantrolene in experimental status epilepticus. *Neuropharmacology* 38, 1343–1348. doi: 10.1016/s0028-3908(99)00059-3

Oules, B., Del Prete, D., Greco, B., Zhang, X., Lauritzen, I., Sevalle, J., et al. (2012). Ryanodine receptor blockade reduces amyloid-β load and memory impairments in Tg2576 mouse model of Alzheimer disease. *J. Neurosci.* 32, 11820–11834. doi: 10.1523/JNEUROSCI.0875-12.2012

Petraglia, A. L., Dashnaw, M. L., Turner, R. C., and Bailes, J. E. (2014). Models of mild traumatic brain injury: translation of physiological and anatomic injury. *Neurosurgery* 75, S34–S49. doi: 10.1227/NEU.0000000000000472

Reeves, T. M., Lyeth, B. G., Phillips, L. L., Hamm, R. J., and Povlishock, J. T. (1997). The effects of traumatic brain injury on inhibition in the hippocampus and dentate gyrus. *Brain Res.* 757, 119–132. doi: 10.1016/s0006-8993(97)00170-4

Regehr, W. G. (2012). Short-term presynaptic plasticity. *Cold Spring Harb. Perspect. Biol.* 4:a005702. doi: 10.1101/cshperspect.a005702

Sandler, V. M., and Barbara, J. G. (1999). Calcium-induced calcium release contributes to action potential-evoked calcium transients in hippocampal CA1 pyramidal neurons. *J. Neurosci.* 19, 4325–4336. doi: 10.1523/JNEUROSCI.19-11-04325.1999

Schrank, S., Barrington, N., and Stutzmann, G. E. (2020). Calcium-handling defects and neurodegenerative disease. *Cold Spring Harb. Perspect. Biol.* 12:a035212. doi: 10.1101/cshperspect.a035212

Schwarzbach, E., Bonislawski, D. P., Xiong, G., and Cohen, A. S. (2006). Mechanisms underlying the inability to induce area CA1 LTP in the mouse after traumatic brain injury. *Hippocampus* 16, 541–550. doi: 10.1002/hipo.20183

Shen, I. H., Lin, Y.-J., Chen, C.-L., and Liao, C.-C. (2020). Neural correlates of response inhibition and error processing in individuals with mild traumatic brain injury: an event-related potential study. *J. Neurotrauma* 37, 115–124. doi: 10.1089/neu.2018.6122

Shim, S. S., and Stutzmann, G. E. (2016). Inhibition of glycogen synthase kinase-3: an emerging target in the treatment of traumatic brain injury. *J. Neurotrauma* 33, 2065–2076. doi: 10.1089/neu.2015.4177

Slemmer, J. E., Matser, E. J., De Zeeuw, C. I., and Weber, J. T. (2002). Repeated mild injury causes cumulative damage to hippocampal cells. *Brain* 125, 2699–2709. doi: 10.1093/brain/awf271

Stutzmann, G. E. (2007). The pathogenesis of Alzheimers disease is it a lifelong "calciumopathy"? *Neuroscientist* 13, 546–559. doi: 10.1177/1073858407299730

Stutzmann, G. E., Caccamo, A., LaFerla, F. M., and Parker, I. (2004). Dysregulated IP3 signaling in cortical neurons of knock-in mice expressing an Alzheimer's-linked mutation in presenilin1 results in exaggerated Ca2+ signals and altered membrane excitability. *J. Neurosci.* 24, 508–513. doi: 10.1523/JNEUROSCI.4386-03.2004

Stutzmann, G. E., LaFerla, F. M., and Parker, I. (2003). Ca^{2+} signaling in mouse cortical neurons studied by two-photon imaging and photoreleased inositol triphosphate. *J. Neurosci.* 23, 758–765. doi: 10.1523/JNEUROSCI.23-03-00758.2003

Stutzmann, G. E., and Parker, I. (2005). Dynamic multiphoton imaging: a live view from cells to systems. *Physiology* 20, 15–21. doi: 10.1152/physiol.00028.2004

Sun, D. A., Deshpande, L. S., Sombati, S., Baranova, A., Wilson, M. S., Hamm, R. J., et al. (2008). Traumatic brain injury causes a long-lasting calcium (Ca^{2+})-plateau of elevated intracellular Ca levels and altered Ca^{2+} homeostatic mechanisms in hippocampal neurons surviving brain injury. *Eur. J. Neurosci.* 27, 1659–1672. doi: 10.1111/j.1460-9568.2008.06156.x

Taylor, C. A., Bell, J. M., Breiding, M. J., and Xu, L. (2017). Traumatic brain injury-related emergency department visits, hospitalizations, and deaths—united

states, 2007 and 2013. *MMWR Surveill. Summ.* 66, 1–16. doi: 10.15585/mmwr.ss6609a1

Teasdale, G., Bailey, I., Bell, A., Gray, J., Gullan, R., Heiskanan, O., et al. (1992). A randomized trial of nimodipine in severe head injury: HIT I. British/Finnish Co-operative Head Injury Trial Group. *J. Neurotrauma* 9, S545–S550.

Teasdale, G., Bailey, I., Bell, A., Gray, J., Gullan, R., Heiskanan, U., et al. (1990). The effect of nimodipine on outcome after head injury: a prospective randomized control trial. The British/Finnish Co-operative Head Injury Trial Group. *Acta Neurochir. Suppl.* 51, 315–316. doi: 10.1007/978-3-7091-9115-6_106

Theadom, A., Parmar, P., Jones, K., Barker-Collo, S., Starkey, N. J., McPherson, K. M., et al. (2015). Frequency and impact of recurrent traumatic brain injury in a population-based sample. *J. Neurotrauma* 32, 674–681. doi: 10.1089/neu.2014.3579

Thibault, O., Gant, J. C., and Landfield, P. W. (2007). Expansion of the calcium hypothesis of brain aging and Alzheimer's disease: minding the store. *Aging Cell* 6, 307–317. doi: 10.1111/j.1474-9726.2007.00295.x

Titus, D. J., Johnstone, T., Johnson, N. H., London, S. H., Chapalamadugu, M., Hogenkamp, D., et al. (2019). Positive allosteric modulation of the α7 nicotinic acetylcholine receptor as a treatment for cognitive deficits after traumatic brain injury. *PLoS One* 14:e0223180. doi: 10.1371/journal.pone.0223180

Tran, H. T., Sanchez, L., and Brody, D. L. (2012). Inhibition of JNK by a peptide inhibitor reduces traumatic brain injury-induced tauopathy in transgenic mice. *J. Neuropathol. Exp. Neurol.* 71, 116–129. doi: 10.1097/NEN.0b013e3182456aed

Tsien, J. Z., Huerta, P. T., and Tonegawa, S. (1996). The essential role of hippocampal CA1 NMDA receptor-dependent synaptic plasticity in spatial memory. *Cell* 87, 1327–1338. doi: 10.1016/s0092-8674(00)81827-9

Vergouwen, M. D., Vermeulen, M., de Haan, R. J., Levi, M., and Roos, Y. B. (2007). Dihydropyridine calcium antagonists increase fibrinolytic activity: a systematic review. *J. Cereb. Blood Flow Metab.* 27, 1293–1308. doi: 10.1038/sj.jcbfm.9600431

Weber, J. T. (2007). Experimental models of repetitive brain injuries. *Prog. Brain Res.* 161, 253–261. doi: 10.1016/S0079-6123(06)61018-2

Weber, J. T. (2012). Altered calcium signaling following traumatic brain injury. *Front. Pharmacol.* 3:60. doi: 10.3389/fphar.2012.00060

Weber, J. T., Rzigalinski, B. A., and Ellis, E. F. (2002). Calcium responses to caffeine and muscarinic receptor agonists are altered in traumatically injured neurons. *J. Neurotrauma* 19, 1433–1443. doi: 10.1089/089771502320914660

Weil, Z. M., Gaier, K. R., and Karelina, K. (2014). Injury timing alters metabolic, inflammatory and functional outcomes following repeated mild traumatic brain injury. *Neurobiol. Dis.* 70, 108–116. doi: 10.1016/j.nbd.2014.06.016

White, E. R., Pinar, C., Bostrom, C. A., Meconi, A., and Christie, B. R. (2017). Mild traumatic brain injury produces long-lasting deficits in synaptic plasticity in the female juvenile hippocampus. *J. Neurotrauma* 34, 1111–1123. doi: 10.1089/neu.2016.4638

Wilson, S. M., Ki Yeon, S., Yang, X.-F., Park, K. D., and Khanna, R. (2014). Differential regulation of collapsin response mediator protein 2 (CRMP2) phosphorylation by GSK3ss and CDK5 following traumatic brain injury. *Front. Cell. Neurosci.* 8:135. doi: 10.3389/fncel.2014.00135

Wolf, J. A., Stys, P. K., Lusardi, T., Meaney, D., and Smith, D. H. (2001). Traumatic axonal injury induces calcium influx modulated by tetrodotoxin-sensitive sodium channels. *J. Neurosci.* 21, 1923–1930. doi: 10.1523/JNEUROSCI.21-06-01923.2001

Yamada, K., Patel, T. K., Hochgräfe, K., Mahan, T. E., Jiang, H., Stewart, F. R., et al. (2015). Analysis of *in vivo* turnover of tau in a mouse model of tauopathy. *Mol. Neurodegener.* 10:55. doi: 10.1186/s13024-015-0052-5

Zhang, B., Chen, X., Lin, Y., Tan, T., Yang, Z., Dayao, C., et al. (2011). Impairment of synaptic plasticity in hippocampus is exacerbated by methylprednisolone in a rat model of traumatic brain injury. *Brain Res.* 1382, 165–172. doi: 10.1016/j.brainres.2011.01.065

Zhang, B.-L., Chen, X., Tan, T., Yang, Z., Carlos, D., Jiang, R.-C., et al. (2011). Traumatic brain injury impairs synaptic plasticity in hippocampus in rats. *Chin. Med. J.* 124, 740–745.

Zhang, H., Liu, J., Sun, S., Pchitskaya, E., Popugaeva, E., and Bezprozvanny, I. (2015). Calcium signaling, excitability, and synaptic plasticity defects in a mouse model of Alzheimer's disease. *J. Alzheimers Dis.* 45, 561–580. doi: 10.3233/JAD-142427

Zhao, S., Fu, J., Liu, X., Wang, T., Zhang, J., and Zhao, Y. (2012). Activation of Akt/GSK-3β/β-catenin signaling pathway is involved in survival of neurons after traumatic brain injury in rats. *Neurol. Res.* 34, 400–407. doi: 10.1179/1743132812Y.0000000025

Zucker, R. S., and Regehr, W. G. (2002). Short-term synaptic plasticity. *Annu. Rev. Physiol.* 64, 355–405. doi: 10.1146/annurev.physiol.64.092501.114547

Conflict of Interest: The authors declare that the research was conducted in the absence of any commercial or financial relationships that could be construed as a potential conflict of interest.

Copyright © 2021 McDaid, Briggs, Barrington, Peterson, Kozlowski and Stutzmann. This is an open-access article distributed under the terms of the Creative Commons Attribution License (CC BY). The use, distribution or reproduction in other forums is permitted, provided the original author(s) and the copyright owner(s) are credited and that the original publication in this journal is cited, in accordance with accepted academic practice. No use, distribution or reproduction is permitted which does not comply with these terms.

frontiers in Cellular Neuroscience

REVIEW
published: 19 May 2021
doi: 10.3389/fncel.2021.671932

Regulatory Mechanisms of the RNA Modification m^{6}A and Significance in Brain Function in Health and Disease

Justine Mathoux[1,2], *David C. Henshall*[1,2] *and Gary P. Brennan*[2,3]*

[1] Department of Physiology and Medical Physics, RCSI, University of Medicine and Health Sciences, Dublin, Ireland, [2] FutureNeuro SFI Research Centre, RCSI, University of Medicine and Health Sciences, Dublin, Ireland, [3] UCD School of Biomolecular and Biomedical Science, UCD Conway Institute, University College Dublin, Dublin, Ireland

RNA modifications have emerged as an additional layer of regulatory complexity governing the function of almost all species of RNA. N^6-methyladenosine (m^{6}A), the addition of methyl groups to adenine residues, is the most abundant and well understood RNA modification. The current review discusses the regulatory mechanisms governing m^{6}A, how this influences neuronal development and function and how aberrant m^{6}A signaling may contribute to neurological disease. M^{6}A is known to regulate the stability of mRNA, the processing of microRNAs and function/processing of tRNAs among other roles. The development of antibodies against m^{6}A has facilitated the application of next generation sequencing to profile methylated RNAs in both health and disease contexts, revealing the extent of this transcriptomic modification. The mechanisms by which m^{6}A is deposited, processed, and potentially removed are increasingly understood. Writer enzymes include METTL3 and METTL14 while YTHDC1 and YTHDF1 are key reader proteins, which recognize and bind the m^{6}A mark. Finally, FTO and ALKBH5 have been identified as potential erasers of m^{6}A, although there *in vivo* activity and the dynamic nature of this modification requires further study. M^{6}A is enriched in the brain and has emerged as a key regulator of neuronal activity and function in processes including neurodevelopment, learning and memory, synaptic plasticity, and the stress response. Changes to m^{6}A have recently been linked with Schizophrenia and Alzheimer disease. Elucidating the functional consequences of m^{6}A changes in these and other brain diseases may lead to novel insight into disease pathomechanisms, molecular biomarkers and novel therapeutic targets.

Keywords: m6A (N6-methyladenosine), brain function and brain diseases, brain development, epitranscriptomics, METTL3

OPEN ACCESS

Edited by:
Daniela Tropea,
Trinity College Dublin, Ireland

Reviewed by:
Francesca Ruberti,
Institute of Biochemistry and Cell Biology, National Research Council, Consiglio Nazionale delle Ricerche, Italy
Christina Gross,
Cincinnati Children's Hospital Medical Center, United States

***Correspondence:**
Gary P. Brennan
gary.brennan@ucd.ie

Specialty section:
This article was submitted to Cellular Neuropathology, a section of the journal Frontiers in Cellular Neuroscience

Received: *24 February 2021*
Accepted: *19 April 2021*
Published: *19 May 2021*

Citation:
Mathoux J, Henshall DC and Brennan GP (2021) Regulatory Mechanisms of the RNA Modification m^{6}A and Significance in Brain Function in Health and Disease. Front. Cell. Neurosci. 15:671932. doi: 10.3389/fncel.2021.671932

INTRODUCTION

The brain is the most complex and cellularly diverse organ in the body. Higher order brain functions, and those functions critical to sustain life are facilitated by the concerted activity of different cell types, each functionally driven by distinct, context dependent gene expression and gene expression regulation patterns (Hawrylycz et al., 2012; Mitra et al., 2021). Recently, the application of single cell RNA-sequencing technologies has begun to reveal at single cell resolution

this dynamic and distinct gene expression patterns and how they respond to stimulus or activity (Agarwal et al., 2020; Pfisterer et al., 2020; Joglekar et al., 2021; Song et al., 2021).

Appropriate spatiotemporal gene expression in the brain involves several tightly monitored layers of regulation. Broad effector transcription factors direct transcription of genes via canonical binding sites throughout the genome, a process known to be critical for learning and memory and memory consolidation (Kaldun and Sprecher, 2019). Epigenetic mechanisms (DNA methylation, histone modifications etc.), often in response to transcription factor signals, modify DNA and associated histone structure to enhance or repress transcription (Kim et al., 2009; Conboy et al., 2021). Post-transcriptional mechanisms, including microRNAs, are also known to profoundly influence gene expression (or rather mRNA translation) in the brain adding an additional layer of regulatory complexity and fine-tuning of gene output (Bartel, 2018; Brennan and Henshall, 2020). The proteome is also tightly regulated and post-translational modifications such as phosphorylation, ubiquitylation and sumoylation dictate the efficacy or function of the resulting protein according to the needs of a given cell (Zhang et al., 2016; Czuba et al., 2018). These processes are not independent of each other and function cohesively, cumulatively forming a complex control over gene output.

RNA is now widely recognized to undergo complex post-transcriptional editing and modification (in addition to alternative splicing and polyadenylation) which confer additional information carrying capacity and profoundly influence its fate (Jain et al., 2019; Zaccara et al., 2019; He and He, 2021). Among the most well studied involves adenosine to inosine (A-to-I) conversion which is mediated by both ADAR I and II enzymes (Eisenberg and Levanon, 2018; Christofi and Zaravinos, 2019). A-I editing involves the hydrolytic deamination of adenosine to inosine. This recoding can result in non-synonymous amino acid substitutions, resulting in altered protein-coding sequences and potentially altered protein structure (Eisenberg and Levanon, 2018). Additionally, recoding of the RNA sequence within the 3′-UTR may alter mRNA-translational efficiency as it may affect microRNA-mediated targeting (Brummer et al., 2017; van der Kwast et al., 2020). Other modifications are more subtle than overt structural modification of bases, involving covalent modification of RNA such as the addition of methyl groups to specific nucleotides. Various forms of RNA were known to undergo extensive methylation as far back as the 1970s (Munns et al., 1977; Wei and Moss, 1977; Burke and Joh, 1982). However, recent advances in transcriptomic technologies and the development of antibodies, which specifically target these modifications have made it possible to reveal the extent and identity of these novel RNA modifications (Dominissini et al., 2012; Meyer et al., 2012; Dominissini et al., 2013). Critically, many of these modifications may be dynamic in nature undergoing context-dependent addition and removal.

The addition of methyl groups to the N6 position of adenosine [N6-methyladenosine (m^6A)] is the most abundant internal modification in RNA and is prevalent in brain tissue. However, the function of m^6A in brain is only beginning to emerge. In this review, we provide an overview of the mechanisms by which m^6A is regulated and try to define its overall contribution to the gene expression landscape in brain cells. We also discuss recent reports, which detail the involvement of m^6A in neurological diseases.

M^6A RNA METHYLATION

It was identified in the 1970s that certain forms of RNA such as rRNA undergo extensive methylation (Munns et al., 1977; Wei and Moss, 1977). However, it was thought to be mainly structural and further interrogation was limited by the technology at this time (Furuichi et al., 1975). The development of an antibody which recognizes the m^6A mark prompted transcriptome-wide investigations of N6-methyladenosine. This modification was found to be widespread and enriched near stop codons, the 5′ and 3′ UTR and internal long exons of mRNA, as well as rRNA, tRNA, snoRNA and lncRNA (Meyer et al., 2012; Berulava et al., 2015). A canonical m^6A motif was identified and consists of RRACH with R =G/A and H =A/C/U (Balacco and Soller, 2019; Dominissini et al., 2012). The methyl group is catalyzed from a donor substrate S-adenosylmethionine (SAM) to an adenosine residue of an RNA moiety along a specific sequence as stated above (Bokar et al., 1997). The m6A modification plays a role in several diverse RNA mechanisms, most notably RNA stability and translational efficiency (Meyer et al., 2015; Chen X.Y. et al., 2019). Other studies have implicated m6A in the control of mRNA dynamics including alternative splicing (although there is considerable debate regarding this Ke et al., 2017) and subcellular localization. Moreover, the role of m^6A may be dictated by the subcellular localization of the m^6A-tagged RNA. In the nucleus, m^6A deposited on nascent pre-mRNA may influence alternative splicing (Dominissini et al., 2012), and microRNA biogenesis (Alarcon et al., 2015), while in the cytoplasm, it is thought to regulate RNA stability (Batista et al., 2014; Wang X. et al., 2014), translational efficiency and RNA decay (Wang et al., 2015).

M^6A MACHINERY

M^6A is a dynamic modification, catalyzed by a distinct enzymatic complex (writers), identified and processed by several "reader" proteins and potentially removed by "eraser" proteins. In the following sections, we summarize what is known about the proteins associated with the deposition, identification, and removal of m^6A (**Figure 1**).

M^6A WRITERS

The methyltransferase complex which catalyzes m^6A addition is composed of two distinct sub-complexes (Knuckles et al., 2018): the m^6A-methyltransferase-like (METTL) complex (MAC) which is composed of METTL3 and METTL14 and the m^6A-METTL associated complex (MACOM) which consists of RBM15, ZC3H13, WTAP, and VIRMA (Meyer and Jaffrey, 2014; Cao et al., 2016; Lence et al., 2019). Together MAC and MACOM function to catalyze the addition of methyl groups to adenosine.

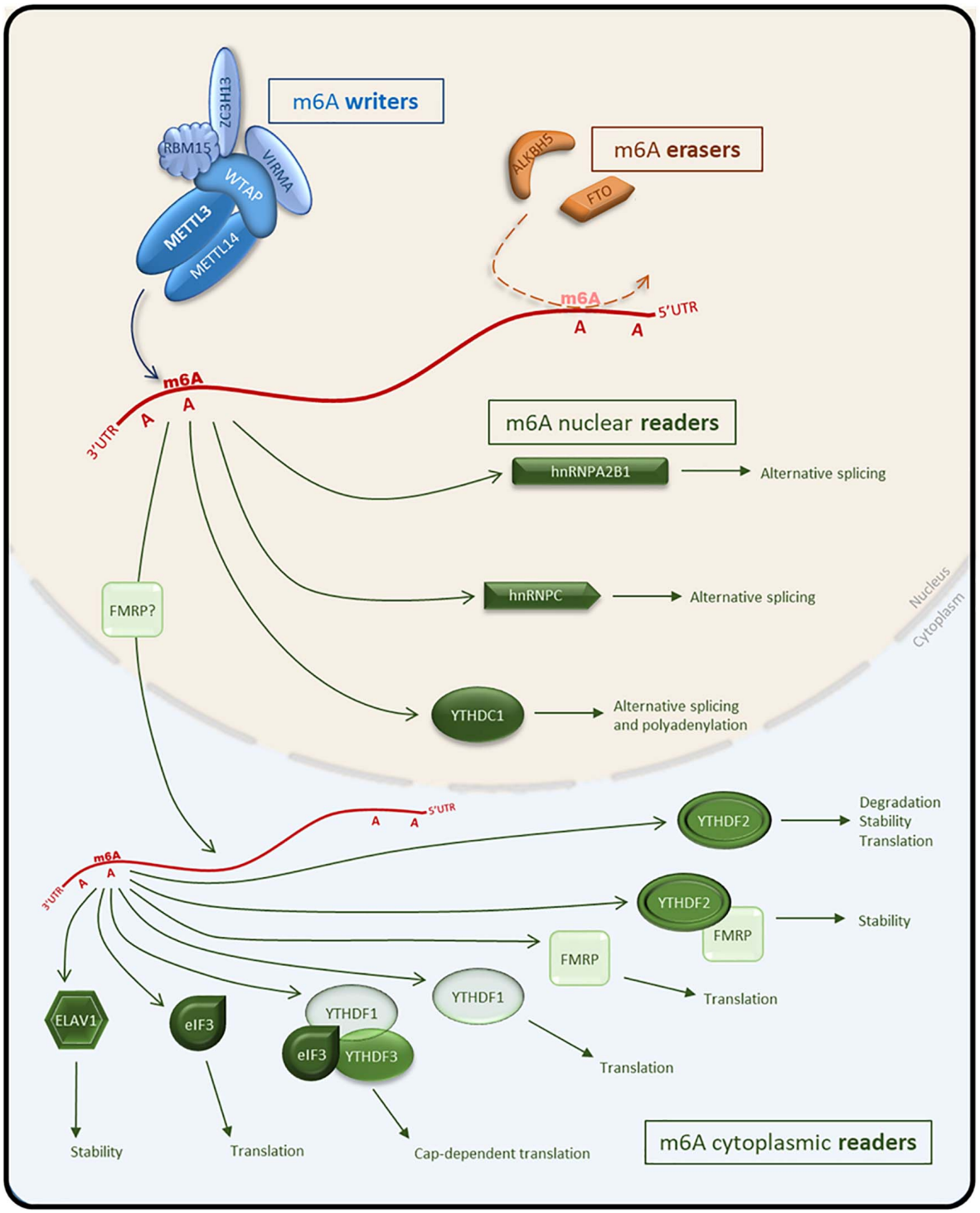

FIGURE 1 | Schematic representation of the m^{6}A pathway and effectors on mRNA. The MACOM complex composed of m^{6}A writers (METTL3, METTL14, WTAP, VIRMA, ZC3H13, and RBM15) deposits m^{6}A on target RNAs. M^{6}A erasers (FTO and ALKBH5) remove the m^{6}A mark. M^{6}A nuclear readers (hnRNPC, hnRNPA2B1, and YTHDC1) facilitate alternative splicing or polyadenylation following recognition of m^{6}A-tagged RNA. M^{6}A-tagged RNA can be exported to the cytoplasm and bound by cytoplasmic readers (elf3, ELAVL1, YTHDF1,2,3) to modulate stability, translational efficiency or the degradation of RNA. Blue, m^{6}A writers; Orange, m^{6}A erasers; Green, m^{6}A readers.

MAC Complex

The MAC-associated proteins comprise the catalytic components of the methyltransferase complex, which co-transcriptionally deposit m^{6}A on target mRNAs (Liu et al., 2014). There are two essential components of the MAC complex, METTL3 and METTL14 which form a conserved heterodimeric core. This dimerization is essential for their methylation function and provides a synergistic effect on the catalytic activity of the complex (Liu et al., 2014; Balacco and Soller, 2019). Crystallographic studies of the MAC complex have shed light on the mechanisms of m^{6}A deposition on target mRNA molecules (Sledz and Jinek, 2016). Additionally, transcriptome-wide profiling of m^{6}A has identified a specific sequence motif known as a RRACH with R = G/A and H = A/C/U sequence within which m^{6}A is usually confined. This RRACH sequence is highly conserved and restricts m^{6}A to a selection of conserved transcripts (Dominissini et al., 2012). In some species, such as *C. elegans*, the dimer is replaced by a prologue, METTL4. Furthermore, METTL16, which is not a prologue, can also methylate mRNA but its mechanism of action remains to be elucidated (Balacco and Soller, 2019).

METTL3 is the primary catalytic component of the MAC complex. Knockout of METTL3 has been reported to result in a significant reduction in global m^{6}A levels (Batista et al., 2014; Wang Y. et al., 2014). METTL3 selectively targets mRNAs, depositing m^{6}A on nascent RNA via its zinc-finger motifs (Batista et al., 2014; Sledz and Jinek, 2016). A mechanistic study in acute myeloid leukemia (AML) found that METTL3 is recruited by the transcription factor CHOP (CEBPζ) and methylates CHOP-regulated transcripts (Barbieri et al., 2017). METTL3 levels influence the expression of other m^{6}A-associated writers. Indeed, both elevated and reduced levels of METTL3 lead to increased amounts of WTAP mRNA translation and promote the stabilization of the protein (Sorci et al., 2018). Furthermore, METTL3 can reportedly switch from writer to reader by translocating to the cytoplasm where it may regulate the translation of specific mRNAs by direct binding to RNA and recruitment of eIF3 (Lin et al., 2016).

METTL14 has a functional role in structural stabilization and RNA substrate recognition (Sledz and Jinek, 2016). METTL14 enhances METTL3 methyltransferase activity by binding the mRNA and orientating the SAM methyl group for the reaction (Schwartz et al., 2014; Balacco and Soller, 2019). In the brain, METTL14 also plays an important role in maintaining neuronal populations via targeting transcripts of transcription factors of cell cycle to promote their decay (Yoon et al., 2017; Balacco and Soller, 2019). While it does not possess catalytic activity, the depletion of METTL14 causes profound reduction in m^{6}A levels in embryonic stem cells, is embryonic lethal in mice and affects cortical development suggesting a critical role in development and highlighting its necessity for normal MAC activity (Wang Y. et al., 2014; Yoon et al., 2017).

MACOM Complex

MACOM is an m^{6}A-associated complex (Meyer and Jaffrey, 2014; Cao et al., 2016; Lence et al., 2019). It is thought that the proteins associated with the MACOM complex may regulate m^{6}A deposition by integrating cellular signaling pathways and stimuli, dictating the repertoire of transcripts which undergo m^{6}A-tagging (Livneh et al., 2020). The function of the MACOM is under intense investigation.

WTAP (Wilms' tumor 1-associated protein) is a ubiquitously expressed protein and a regulatory subunit required for formation of a functional and stable MACOM complex (Ping et al., 2014). WTAP also modulates RNA processing, translation, and alternative splicing (Horiuchi et al., 2013). It was through the mass-spectrometric analysis of WTAP binding partners that several other methyltransferase enzymes were identified including METTL3-METTL14, RBM15 and VIRMA (Ping et al., 2014).

VIRMA (vir like m^{6}A methyltransferase associated), also named KIAA1429, recruits the WTAP-METTL3-METTL14 complex via its binding to WTAP (Yue et al., 2018; Balacco and Soller, 2019). VIRMA may also interact with polyadenylation cleavage factors linking the machineries of m^{6}A methylation and polyadenylation during mRNA processing (Yue et al., 2018).

RBM15 (RNA-binding motif protein 15) interacts with METTL3 via WTAP. It is particularly associated with the regulation of m^{6}A levels on lncRNAs (Patil et al., 2016; Balacco and Soller, 2019). RBM15 acts as an adaptor protein recruiting the m^{6}A methylosome to U-rich regions.

ZC3H13 (Zinc Finger CCCH-type containing 13), also named Flacc (Fl(2)d-associated complex component) (Wen et al., 2018; Balacco and Soller, 2019) may have a scaffolding function in the m^{6}A methylosome. In Wen et al. (2018) found that ZC3H13 promotes pluripotency-associated gene expression and suppresses differentiation-associated genes in mESCs. Loss of ZC3H13 impairs WTAP-dependent 3′UTR m^{6}A events. Moreover, Knuckles et al. have shown that ZC3H13 binds RBM15 and regulates the m^{6}A pathway via the stabilization of the interaction between WTAP and RBM15 (Knuckles et al., 2018).

M^{6}A ERASERS

Two proteins have been shown to possess m^{6}A-demethylase activity. FTO (Fat mass and obesity-associated protein) and ALKBH5 (AlkB homologue 5 protein). These proteins are [(α-ketoglutarate (α-KG)-dependent dioxygenases which are inhibited by D2-hydroxyglutarate (D2-HG)] (Fedeles et al., 2015; Chen X.Y. et al., 2019).

FTO is an AlkB-like 2-oxoglutarate-dependent nucleic acid demethylase (Gerken et al., 2007), initially identified for its role in diabetes and obesity (Lindgren and McCarthy, 2008; Loos and Bouchard, 2008). Since then it has been shown that, in the nucleus, FTO catalyzes the removal of m^{6}A and m^{6}Am (N^6, 2'-O-dimethyladenosine) marks from mRNA although importantly shows a 100-fold greater affinity for m^{6}Am than m^{6}A (Mauer et al., 2017; Mauer and Jaffrey, 2018; Balacco and Soller, 2019). The m^{6}Am mark is a terminal modification distinct from the internal m^{6}A mark and follows the m^{7}G (N^7-methylguanosine) cap at the N^6 position (Wei et al., 1975), where A or m^{6}A are not found (Wei et al., 1976). Some studies have identified

FTO as an important regulator of m^{6}A-tagged transcripts, important for mRNA alternative splicing and gene expression, contributing to the regulation of adipogenesis (Zhao et al., 2014; Bartosovic et al., 2017; Chen X.Y. et al., 2019). However, some recent emerging data does not support the role of FTO as an m^{6}A eraser and suggests that FTO under normal physiological conditions does not remove m^{6}A and solely functions on m^{6}Am (Mauer et al., 2017). Indeed, FTO is present almost exclusively in the nucleus, which suggests it is unlikely to dynamically regulate cytosolic mRNAs. Furthermore, studies by the Darnell group have shown that the levels of m^{6}A are perhaps stable once deposited. Together, this calls into question the extent of m^{6}A demethylation *in vivo,* at least under normal physiological conditions (Mauer et al., 2017; Mauer and Jaffrey, 2018). M^{6}A removal by FTO or others may therefore be context and cell-type specific and/or developmentally regulated and this warrants further investigation.

ALKBH5 is an α-ketoglutarate dependent oxidase and nuclear demethylase only found in vertebrates which can bind single stranded nucleic acids (Zheng et al., 2013; Balacco and Soller, 2019). In Ensfelder et al. (2018) identified ALKBH5 as a ribosomal RNA m^{6}A eraser. It has since been shown that ALKBH5 is also required for correct splicing and production of transcripts in spermatocytes via selective removal of m^{6}A (Tang et al., 2018). Moreover, ALKBH5 is involved in glioblastoma to repress tumorigenesis (Zhang et al., 2017), in spermatogenesis and in male fertility (Zheng et al., 2013). Again, the relevance of ALKBH5 as an m^{6}A eraser in somatic cells remains unclear. The study by Darnell did note that there was loss of m^{6}A on a minority of transcripts suggesting a small amount of selective demethylation may occur under normal physiological conditions (Ke et al., 2017).

M^{6}A READERS

M^{6}A readers elicit different actions upon recognition and binding of the methylated RNA transcripts. Several reader proteins have now been identified.

HNRNPC & HNRNPA2B1 (Heterogeneous Nuclear Ribonucleoprotein C & A2B1) are both nuclear-confined m^{6}A readers and are particularly involved in pre-mRNA processing and in maturation of pri-miRNA to pre-miRNA (Cao et al., 2016). HNRNPA2B1 promotes processing of METTL3-dependent microRNAs and plays a role in the regulation of the alternative splicing of exons (Alarcon et al., 2015).

YTH domain containing proteins (YTHDC1 and YTHDC2) and **YTH domain-containing family proteins** (YTHDF1, YTHDF2 and YTHDF3), a highly conserved family of proteins, have been shown to detect and bind m^{6}A (Berlivet et al., 2019). The DC proteins are usually confined to the nucleus (Balacco and Soller, 2019) while the DF proteins are found primarily in the cytoplasm. The structure of m^{6}A-bound by YTH-domain containing proteins was elucidated several years ago. The YTH domain is critical for this binding and is involved in the development of a tryptophan cage around the m^{6}A mark (Theler et al., 2014; Xu et al., 2014). Recent iCLIP data from the Jaffrey lab, identified the binding sites for all YTH proteins. They found that DC1 binds m^{6}A sites in mRNA and nuclear non-coding RNAs, while all three DF proteins bind most m^{6}A sites (Patil et al., 2018). It has been found that DC1 contributes to extensive alternative polyadenylation and 3′UTR length alteration (Chen X.Y. et al., 2019) while DC2 is primarily localized in the testes where it has been found to have weak m^{6}A affinity (Wojtas et al., 2017). In the mouse hippocampus, upon binding, YTHDF1 promotes the translation of m^{6}A-tagged transcripts via interaction with a translation initiation factor (Wang et al., 2015) and the help of YTHDF3 (Shi et al., 2017) and of eIF1 (Chen X.Y. et al., 2019) to facilitate learning and memory (Shi et al., 2018). YTHDF2 recognition of m^{6}A sites, contrarily, was reported to regulate the degradation of specific mRNAs via the recruitment of CCR4-NOT (Alarcon et al., 2015; Cao et al., 2016; Du et al., 2016; Chen X.Y. et al., 2019). This protein may also play a role in mRNA stability and translation (Wang X. et al., 2014; Chen X.Y. et al., 2019), targeting stop codon regions, 3′UTR and coding regions (Wang X. et al., 2014). Recent studies however, including iCLIP-sequencing datasets suggest that all three DF proteins do not selectively bind to m^{6}A-tagged transcripts and all likely lead to degradation of bound transcripts. It is possible that context dependence is critical toward understanding the function of m^{6}A-recognition by YTH-domain containing proteins.

METTL16, usually a writer enzyme, may also function as a reader when SAM levels are low, in order to stimulate the SAM synthetase MAT2A mRNA translation to increase the level of SAM. In contrast, when SAM levels are high, METTL16 methylates MAT2A mRNA, which promotes nuclear mRNA decay (Pendleton et al., 2017; Balacco and Soller, 2019).

eIF3 (eukaryotic initiation Factor 3) is a component of the 43s translation pre-initiation complex. It has been found that this protein is an m^{6}A reader, which promotes translation via two mechanisms. First, eIF3 can directly bind the 5′UTR-localised m^{6}A to allow the recruitment of the 43s complex (Meyer et al., 2015; Cao et al., 2016). The second method is via its interaction with YTHDF1 which facilitates cap-dependent translation (Wang et al., 2015).

FMRP (Fragile X mental retardation protein) is an RNA-binding protein, loss of which is implicated in the neurodevelopmental condition Fragile X syndrome (FXS). It has been shown to be important for the stability of m^{6}A-tagged mRNA (Zhang et al., 2018) and for their nuclear export (Hsu et al., 2019). FMRP has been found to interact with WTAP and recently suggested to bind m^{6}A sites by competing with YTHDF2 to regulate specific mRNA turnover (Horiuchi et al., 2013; Balacco and Soller, 2019). Indeed, another study found that FMRP modulates the stability of its target through YTHDF2 (Zhang et al., 2018). FMRP was recently shown to directly bind to m^{6}A-marked mRNA (Westmark et al., 2020) and negatively regulate their translation (Edupuganti et al., 2017). How m^{6}A processing in FXS is affected has yet to be analyzed.

ELAVL1 (Drosophila homologue-like 1), also known as human antigen R (HuR), and IGF2BPs (Insulin-like growth factor 2 mRNA-binding proteins) has been identified as

an m^{6}A reader (Balacco and Soller, 2019). Several studies show that ELAVL1 increases the stability of transcripts via m^{6}A-mRNA-binding. Indeed, in prostatic carcinoma cells, ELAVL1 plays a role in stabilizing integrin β1 mRNA (Li et al., 2020). It may also promote SOX2 mRNA stabilization to stimulate the maintenance of glioma stem-like cells (Visvanathan et al., 2018) as well as DRG1 in osteosarcoma human tissue (Ling et al., 2020).

M^{6}A IN THE BRAIN

The m^{6}A mark influences the behavior of RNA in several biological pathways and subsequently biological processes like cell differentiation and proliferation, development, sex determination and circadian rhythms (Chen et al., 2017). Here, we review the most important and studied cerebral processes impacted by m^{6}A methylation such as learning and memory as well as neurogenesis, neurodevelopment, the stress response, myelination, and axon plasticity (**Table 1**).

Learning and Memory

In Widagdo et al. (2016) performed the first exploration of m^{6}A in synaptic plasticity and memory processes. To assess whether m^{6}A was regulated by experience, they used a cued-fear conditioning model in mice and found extensive experience-induced m^{6}A changes using meRIP-Seq. Additionally, they found an increase in m^{6}A marks on mRNA in the medial prefrontal cortex (mPFC) following the cued-fear conditioning paradigm as well as increased levels of METTL3 suggesting a critical role for m^{6}A in behavioral adaptation. A subsequent study also using a fear-conditioning paradigm, found decreased levels of FTO in dorsal CA1 hippocampal neurons following fear-conditioning (Walters et al., 2017). Subsequent knock-down of FTO, in mPFC or in the CA1 increased m^{6}A levels (Walters et al., 2017) and enhanced memory retention suggesting m^{6}A plays a critical role in memory formation and consolidation (Widagdo et al., 2016; Walters et al., 2017). Zhang et al. found that conditional postnatal depletion of *METTL3* in hippocampus of mice prolonged the process of memory consolidation but did not alter short-term plasticity. Furthermore, restitution of *METTL3* improved learning while the overexpression of *METTL3* with a mutated methyltransferase domain had no effect (Zhang et al., 2018). Together this suggests that METTL3 participates in the enhancement of long-term memory consolidation via its m^{6}A methyltransferase function (Zhang et al., 2018). Moreover, another study showed that m^{6}A methylation promotes learning and memory through YTHDF1, which boosts translation of memory-associated transcripts. Indeed, the depletion of YTHDF1 impairs long-term potentiation of hippocampal synapses leading to impairment of memory formation (Shi et al., 2018). The METTL3/YTHDF pathway is also required for memory formation in *Drosophila*. *METTL3* knockdown in the mushroom body, impaired memory as assessed using an aversive conditioning paradigm to assess short-term memory. They further identified that YTHDF hemizygotes exhibited age-related memory impairments similar to *METTL3* knockdown flies. Furthermore, METTL14 deletion in striatal neurons induces a decrease of m^{6}A methylation and impairs learning in mice (Koranda et al., 2018).

Local supply of mRNA, microRNAs and translational machinery facilitate rapid synaptic alterations required for learning and memory. Recently, Merkurjev et al. (2018) demonstrated synaptic enrichment of several m^{6}A-associated enzymes including METTL14, and YTHDF1-3 as well as m^{6}A-tagged polyA RNA. The authors isolated and profiled synaptosomal m^{6}A-tagged RNA using a low-input meRIP-Seq approach to reveal that the most significant biological processes represented by synaptic m^{6}A-tagged RNAs were those critical for neuronal integrity and function, suggesting m^{6}A-tagged synaptic RNAs critically modulate neuronal function. Furthermore, disruption of m^{6}A-processing via knockdown of reader proteins YTHDF1 or YTHDF3 resulted in significant morphological disruptions including increased spine neck length and decreased spine head width, reduced PSD-95 clustering, and reduced surface expression of AMPA receptors (Merkurjev et al., 2018).

Other studies have also revealed a potential role for m^{6}A-tagged RNAs in synaptic function. Indeed, several experimental paradigms have been shown to alter methylation of synapse associated RNAs including cocaine exposure, depression, and deep brain stimulation (Madugalle et al., 2020; Song et al., 2020; Xue et al., 2021).

Although further studies are required, these initial data suggest that m^{6}A may represent a critical mechanism of mRNA translational priming and enable rapid sorting of mRNAs required for synaptic function.

Neurogenesis/Neuronal Development

Neurogenesis, the process by which new neurons are formed, is critical for correct neurodevelopment, function and repair. Furthermore, aberrant neurogenesis is associated with several neurological diseases including epilepsy (Danzer, 2008; Livneh et al., 2020). Selective deletion of M*ETTL14* in embryonic mouse brains expands cortical neurogenesis into the postnatal stage, extends the cell cycle progression in neuronal progenitor cells and prolongs maintenance of radial glia cells (Yoon et al., 2017). This suggests m^{6}A has an important role during brain development. During pre-natal cortical development m^{6}A-tagging of developmental transcription factors Pax6, Sox2 and Neurogenin2 is enriched and promotes turnover allowing rapid and complex temporal regulation of gene expression critical for development (Donega et al., 2018). M^{6}A levels and deposition are dynamically regulated during post-natal cerebellum development which correlates with spatiotemporal regulation of m^{6}A-associated enzymes including METTL3, 14, and FTO (Ma et al., 2018). Importantly, transcripts essential for development in post-natal cerebellum were continuously and consistently methylated whereas time-specific processes were temporarily methylated inducing proper cerebellar development as disruption of either METTL3 or FTO caused developmental deficits. Furthermore, it has been shown that FTO deficiency reduces the proliferation and differentiation of adult

TABLE 1 | m^6A machinery proteins associated in Neurological functions.

Neurological function	Related proteins	Explication	References
Learning and memory	METTL3	Increased METTL3 after cued fear conditioning in mPFC. Knockdown of METTL3 increases the time of memory consolidation process.	Widagdo et al., 2016; Zhang et al., 2018
	METTL14	Knockdown of METTL14 in striatal neurons decreases m6A levels and impairs learning in mice.	Koranda et al., 2018
	FTO	Decreased FTO following cued fear conditioning in CA1 of hippocampus. Knockdown of FTO increased m^6A levels and enhanced memory retention.	Walters et al., 2017
	YTHDF1	YTHDF1 promotes translation of memory association transcripts. Knockdown of YTHDF1 impairs memory formation.	Shi et al., 2018
Neurogenesis, neurodevelopment and plasticity	METTL14	Knockdown of METTL14 extends cortical neurogenesis in post natal stage. Ablation of METTL14 decreases the maturation of oligodendrocyte and causes abnormal myelination.	Donega et al., 2018; Xu H. et al., 2020
	FTO	FTO depletion reduces proliferation and differentiation of aNSCs. FTO regulates m^6A in axonal GAP-43 mRNA.	Li et al., 2017; Yu et al., 2018
	YTHDF2	Loss of YTHDF2 reduces basal progenitor cells and impairs neuronal differentiation.	Li et al., 2018
	YTHDF1	YTHDF1 allows synthesis of proteins for axonal regeneration by enhancing mRNA translation.	Weng et al., 2018
Stress response regulation	METTL3	Knockout of METTL3 disrupts stress behavior.	Engel et al., 2018
	FTO	Knockout of FTO disrupts stress behavior.	Engel et al., 2018
	YTHDF2	After heat shock stress, YTHDF2 limits m^6Ademethylation by FTO.	Zhou et al., 2015

mPFC, medial PreFrontal Cortex; CA1, Cornus Ammonis1; aNSCs, adult Neural Stem Cells. Blue, m^6A writers; Orange, m^6A erasers; Green, m^6A readers.

neural stem cells (aNSCs) leading to a smaller brain in mice (Li et al., 2017). While m^6A writers have emerged as important mediators of neuronal development, the role of m^6A readers is less clear. Recently, Li and colleagues demonstrated that loss of YTHDF2 is embryonic lethal and found that neuronal development dysfunction resulting from YTHDF2 loss prevented viability. Analysis of embryonic brains from E12.5 to E14.5 mice identified that YTHDF2 loss resulted in reduced cortical layering and reduced cortical development. Further analysis revealed reduced basal progenitor cells and impaired neural differentiation (Li et al., 2018).

M^6A methylation has been found to be essential for the maturation of oligodendrocytes and for central nervous system myelination. In mice, in the early postnatal stage, METTL14 ablation leads to a decrease of oligodendrocyte maturation and causes abnormal myelination. *In vitro*, METTL14 depletion induced a diminution of oligodendrocyte differentiation and a prolongation of the cell cycle progression. This indicates a role for m^6A methylation in neuronal development, transmission and plasticity (Xu H. et al., 2020).

In addition to a role in neuronal development, m^6A may also play a crucial role in neuronal repair and in axonal regeneration. In peripheral nerves, it was shown that m^6A allows the translation of retrograde signaling molecule mRNAs which enables rapid axonal regeneration. Following axonal injury, m^6A levels are increased, which promotes the synthesis of proteins involved in axon regeneration and recovery, through YTHDF1, to enhance mRNA translation (Weng et al., 2018). Moreover, FTO is enriched in axons leading to a regulation of m^6A in axonal *GAP-43* mRNA, which is required for axon elongation (Yu et al., 2018). Further research is now required to determine whether the m^6A pathway may be exploited to improve nerve regeneration following physical injury.

Stress Response Regulation

Physical and emotional stressors are known to influence transcriptional and translational output and significantly impact cognitive function long-term (Short and Baram, 2019). Recently, studies have also shown that m^6A-mediated gene regulation is significantly affected by stress. The dynamic nature of the stress response was recently demonstrated by Engel and colleagues, using a restraint stressor, a stressful stimulus for rodents. This elicited large-scale changes in the RNA methylome in a temporospatial manner (Engel et al., 2018). Restraint stress led to an increase in global methylation levels in amygdala and a decrease in prefrontal cortex. Mice deficient in METTL3 and FTO from excitatory hippocampal cells displayed lower resilience to stressful stimuli suggesting m^6A-mediated mRNA regulation may improve adaptation to stress. These results highlight a role of m^6A in stress response.

Heat Shock Stress Response

Zhou et al. found that m^6A levels change in response to heat shock stress in both mouse embryonic fibroblasts (MEFs) and HeLa cells. They detected more m^6A deposition in the 5′UTR of mRNAs, which promotes cap-independent translational initiation, allowing selective translation of heat-shock response proteins. YTHDF2 plays a key role in maintaining this 5′UTR methylation by preventing FTO-mediated demethylation (Zhou et al., 2015).

M^{6}A IN BRAIN DISORDERS

As described above, m^{6}A RNA methylation is involved in many essential cerebral processes, so, unsurprisingly, this process is found to be altered in many brain disorders. Here we describe neurological disorders in which m^{6}A, or m^{6}A-associated proteins are affected such as Alzheimer's disease, Parkinson's disease, glioblastoma, schizophrenia, depression, transient focal ischemia, and traumatic brain injury (**Table 2**).

Neurodegenerative Diseases

Several studies in recent years have linked m^{6}A involvement with neurodegenerative processes. Keller found that FTO is associated with dementia-like Alzheimer's disease (AD) risk, suggesting that FTO may interact with the AD-risk factor gene APOE (Keller et al., 2011). Follow up studies have found that m^{6}A is indeed dysregulated in AD. M^{6}A levels were found to be disrupted in the cortex of APP/PS1 AD mice (Han et al., 2020), specifically they found gross changes in the RNA methylome with enhanced m^{6}A levels on 659 gene transcripts and depleted m^{6}A on 991 gene transcripts. Additionally, they found increased METTL3 expression in AD mice while FTO expression was decreased (Han et al., 2020). Aberrant METTL3 expression has been shown in human post-mortem brain of AD patients compared to non-AD autopsy tissue, further confirming mouse model data and strengthening the potential involvement of m^{6}A-associated gene expression dysregulation in AD (Huang et al., 2020). Further investigations are needed however to determine whether aberrant m^{6}A is a causal factor in AD development and progression or a consequence of altered physiological processes in the diseased brain.

M^{6}A levels were reduced in the striatum of rats with 6-OHDA-induced Parkinson's disease (PD) potentially due to an upregulation of ALKBH5. This reduction in m^{6}A may promote the expression of N-methyl-D-aspartate receptor 1 (NMDA) and a subsequent elevation of oxidative stress and Ca^{2+} influx. This molecular cascade may then promote excitotoxic cell death of dopaminergic neurons (Chen X. et al., 2019). Since then, five Parkinson's Disease-associated m^{6}A-SNPs were identified in PD patients which perturbed this pathway, three of these SNPs were identified in the *ALKBH5* gene (Qiu et al., 2020).

Together these data highlight the complex interplay amongst m^{6}A associated proteins and suggest that further research investigating how m^{6}A may actively contribute to perturbed gene expression regulation in neurodegenerative diseases is required.

CNS Tumors

M^{6}A has been found to regulate glioblastoma stem cell tumorigenesis by controlling the expression of cancer-associated genes and processes. As in several other forms of cancer, m^{6}A is thought to regulate the growth and self-renewal of cells via the methyltransferase catalytic activity of METTL3 (Cui et al., 2017). M^{6}A readers may also play a critical role in glioblastoma tumorigenesis, indeed HNRNPC, YTHDF1 and YTHDF2 are all expressed at elevated levels in glioblastoma (Wang L.C. et al., 2020). YTHDF2 has been found to regulate glucose metabolism via the stabilization of the proto-oncogene *MYC* in glioblastoma stem cells (Dixit et al., 2020). Elevated YTHDF1 was associated with poor prognosis as it is thought to promote the proliferation and migration of glioblastoma cells (Yarmishyn et al., 2020). HNRNPC contributes to glioma progression although the mechanisms underlying this association are not yet known (Wang L.C. et al., 2020). The m^{6}A-demethylase *ALKBH5* has been shown to be overexpressed in patient-derived glioblastoma stem cells and may influence radio-resistance via regulation of DNA damage response genes including Chk1 (Kowalski-Chauvel et al., 2020).

M^{6}A RNA modification has also been associated with other brain cancers such as neuroblastoma. Zhuo et al. identified several SNPs in the gene encoding *METTL14*, which may be associated with a predisposition to neuroblastoma development in a Chinese population (Zhuo et al., 2020). Moreover, m^{6}A and associated proteins may also represent potential biomarkers of various brain cancers including neuroblastoma. High expression of *METTL14* was correlated with low survival of neuroblastoma patients along with reduced expression of *WTAP* or a high expression of *YTHDF1* (Wang Z. et al., 2020).

Brain Injury

Ischemic stroke resulting from blood vessel occlusion deprives neurons and brain cells of oxygen and nutrients and causes pronounced neuronal damage in affected tissues. Recently, Chokkalla et al. found using immunoprecipitation of m^{6}A followed by microarray analysis that following ischemic stroke in mice, there is an increase in m^{6}A levels in the brain and levels are perturbed particularly on inflammation, apoptosis and transcription-associated transcripts suggesting involvement of m^{6}A in the regulation of the molecular milieu initiated by stroke. Elevated levels of m^{6}A following stroke may be explained by decreased expression of FTO levels (Chokkalla et al., 2019; Xu K. et al., 2020).

Using the middle cerebral artery occlusion (MCAO) model of ischemic stroke in rats, Si and colleagues found that METTL3-mediated methylation promoted maturation of miR-355 which then promoted stress granule formation which was neuroprotective (Si et al., 2020). A role for m^{6}A readers as regulators of the brain response to stroke has also been proposed. YTHDC1 levels increased following ischemia in rats while YTHDF1, 2, and 3 levels were repressed (Zhang et al., 2020). Elevated YTHDC1 levels may support post-ischemic neuronal survival via the modulation of the Akt/PTEN pathway (Zhang et al., 2020). YTHDF1 reduction may be a protective or adaptive mechanism by limiting post-stroke inflammation (Zheng et al., 2020).

Following traumatic brain injury (TBI) in rats, *METTL3, METTL14* and *FTO* expression are all downregulated in the cortex. m^{6}A methylation levels are also significantly changed with upregulated m^{6}A-tagging of some mRNA (370 transcripts) and a downregulation of others (552 transcripts) as detected using meRIP-Seq (Wang et al., 2019; Yu et al., 2020). The exact role of m^{6}A following TBI has yet to be fully elucidated but initial reports suggest these investigations are warranted.

TABLE 2 | m^6A machinery proteins in neurological diseases.

Neurological diseases	Related proteins	Explication	References
Alzheimer's disease	METTL3	Increased METTL3 levels in AD mice. Aberrant METTL3 expression in human post-mortem brain of AD patient.	Han et al., 2020; Huang et al., 2020
	FTO	Genetic variation in *FTO* associated with AD risk.	Reitz et al., 2012
	Unknown	Variation of m^6A levels in cortex and hippocampi of AD mice.	Han et al., 2020
Glioblastoma	METTL3	METTL3, via m^6A methylation, regulates the growth and renewal of cancer cells.	Cui et al., 2017
	ALKBH5	Overexpression of ALBKH5 in patient-derived glioblastoma stem cells.	Kowalski-Chauvel et al., 2020; Yarmishyn et al., 2020
	YTHDF1	Overexpression of YTHDF1 to promote proliferation of glioblastoma cells.	Dixit et al., 2020
	YTHDF2	Overexpression of YTHDF2 to regulate glucose metabolism in glioblastoma stem cells.	Wang L.C. et al., 2020
	HNRNPC	Overexpression of HNRNPC to promote glioma progression.	
Neuroblastoma	METTL14	SNPs in METTL14 gene associated with predisposition to neuroblastoma. High expression of METTL14 associated with low survival of patient.	Wang Z. et al., 2020; Zhuo et al., 2020
	WTAP	Low expression of WTAP associated with low survival of patient.	Wang Z. et al., 2020
	YTHDF1	High expression of YTHDF1 associated with low survival of patient	Wang Z. et al., 2020
Parkinson's disease	FTO	Increased FTO in midbrain of PD rat model.	Chen X. et al., 2019
	ALKBH5	SNPs identified in ALKBH5 gene in PD patients.	Qiu et al., 2020
Transient focal ischemia	METTL3	METTL3 promotes stress granule formation (neuroprotective).	Si et al., 2020
	FTO	Decreased FTO after stoke.	Chokkalla et al., 2019
	YTHDC1	Increase of YTHDC1 following ischemia in rat supports neuronal survival.	Zhang et al., 2020
	YTHDF1	Decreased YTHDFL following ischemia in rat limits inflammation.	Zhang et al., 2020
Traumatic brain injury	METTL3	Decreased METTL3 in TBI rat model.	Yu et al., 2020
	METTL14	Decreased METTL14 levels in TBI rat model.	Yu et al., 2020
	FTO	Decreased FTO levels in TBI rat model.	Yu et al., 2020

AD, Alzheimer's disease; PD, Parkinson's disease; TBI, Traumatic Brain Injury. Blue, m^6A writers; Orange, m^6A erasers; Green, m^6A readers.

ENABLING TECHNOLOGIES

As discussed, m^6A was identified as a prevalent RNA modification as far back as the 1970s yet was largely ignored until recently due to a lack of resources available to profile and probe its function (Munns et al., 1977; Wei and Moss, 1977; Burke and Joh, 1982). The development of an m^6A specific antibody coupled with the growing use of next generation sequencing in the last decade led to the development of methylated RNA immunoprecipitation sequencing (meRIP-Seq/m^6A-Seq) approaches (Dominissini et al., 2013). This technology is an adaptation of a standard RIP-Seq approach whereby RNA is isolated from a sample and sheared to a specific length. RNA is ribosome depleted and/or polyA-selected and then subjected to immunoprecipitation to isolate m^6A-tagged mRNAs. The resulting isolated m^6A-tagged RNA is then used to prepare RNA-Seq libraries and subjected to next generation sequencing and whole transcriptome analysis. The development of this technique enabled widespread analysis of this modification in various tissues, organisms and disease settings and highlighted the extent of the epitranscriptomic modification as well as identify how it may contribute to disease. Certain limitations existed however including high RNA input requirements (300 (μg total RNA) and it also suffers from limited resolution although bioinformatic predictions do help to identify exact sites of m6A. These limitations have been overcome to some degree and meRIP-seq can now be performed with as little as 3 (μg starting material (Zeng et al., 2018). Furthermore, single base resolution of m6A can now be mapped using crosslinking and immunoprecipitation (miCLIP) approaches (Linder et al., 2015).

M^6A can now be mapped in native full length RNA moieties without the need for reverse transcription, shearing or immunoprecipitation steps using nanopore long read sequencing technologies (Liu et al., 2019; McIntyre et al., 2019; Jenjaroenpun et al., 2021). Several robust bioinformatic pipelines to identify methylated bases from long sequencing reads have now also been established.

FUTURE DIRECTIONS

The complex functions of the mammalian brain are dependent upon precise control of gene expression and regulation in a temporospatial fashion. M^6A represents an additional layer of gene regulation, which has now been shown to critically regulate neuronal development and function. Technically difficult to study, tools are now available to analyze m^6A RNA methylation at a global level and at single base resolution and there is huge scientific interest in this modification at present (Dominissini et al., 2012; Linder and Jaffrey, 2019). The next hurdle lies in developing and adapting current applications to profile m^6A profiles in discrete cell types and populations/brain regions to

understand how it contributes to neurodevelopment at the single cell level as well as specific brain functions such as learning and memory. Further challenges lie in understanding the precise function of m^{6}A-eraser proteins in a context-dependent manner as well as probing the regulatory mechanisms governing m^{6}A-associated protein expression and function.

Understanding the role of m^{6}A in physiological homeostasis and disease is critical as components of these pathways may represent therapeutic targets for the treatment of neurological disease including many underserved conditions like TBI and stroke. The development of specific pharmacological inhibitors and antisense oligonucleotide approaches will also enable more precise interrogation of transient manipulations of m^{6}A-associated proteins and therapeutic viability.

AUTHOR CONTRIBUTIONS

JM, DH, and GB researched and wrote the article. All authors contributed to the article and approved the submitted version.

FUNDING

This publication has emanated from research supported in part by a research grant from Science Foundation Ireland (SFI) under Grant nos. 18/SIRG/5646 (GPB) and 16/RC/3948 (DH) and co-funded under the European Regional Development Fund and by FutureNeuro industry partners.

REFERENCES

Agarwal, D., Sandor, C., Volpato, V., Caffrey, T. M., Monzon-Sandoval, J., Bowden, R., et al. (2020). A single-cell atlas of the human substantia nigra reveals cell-specific pathways associated with neurological disorders. *Nat. Commun.* 11:4183.

Alarcon, C. R., Lee, H., Goodarzi, H., Halberg, N., and Tavazoie, S. F. (2015). N6-methyladenosine marks primary microRNAs for processing. *Nature* 519, 482–485. doi: 10.1038/nature14281

Balacco, D. L., and Soller, M. (2019). The m(6)A writer: rise of a machine for growing tasks. *Biochemistry* 58, 363–378. doi: 10.1021/acs.biochem.8b01166

Barbieri, I., Tzelepis, K., Pandolfini, L., Shi, J., Millan-Zambrano, G., Robson, S. C., et al. (2017). Promoter-bound METTL3 maintains myeloid leukaemia by m(6)A-dependent translation control. *Nature* 552, 126–131. doi: 10.1038/nature24678

Bartel, D. P. (2018). Metazoan MicroRNAs. *Cell* 173, 20–51. doi: 10.1016/j.cell.2018.03.006

Bartosovic, M., Molares, H. C., Gregorova, P., Hrossova, D., Kudla, G., and Vanacova, S. (2017). N6-methyladenosine demethylase FTO targets pre-mRNAs and regulates alternative splicing and 3′-end processing. *Nucleic Acids Res.* 45, 11356–11370. doi: 10.1093/nar/gkx778

Batista, P. J., Molinie, B., Wang, J., Qu, K., Zhang, J., Li, L., et al. (2014). m(6)A RNA modification controls cell fate transition in mammalian embryonic stem cells. *Cell Stem Cell* 15, 707–719. doi: 10.1016/j.stem.2014.09.019

Berlivet, S., Scutenaire, J., Deragon, J. M., and Bousquet-Antonelli, C. (2019). Readers of the m(6)A epitranscriptomic code. *Biochim. Biophys. Acta Gene Regul. Mech.* 1862, 329–342. doi: 10.1016/j.bbagrm.2018.12.008

Berulava, T., Rahmann, S., Rademacher, K., Klein-Hitpass, L., and Horsthemke, B. (2015). N6-adenosine methylation in MiRNAs. *PLoS One* 10:e0118438. doi: 10.1371/journal.pone.0118438

Bokar, J. A., Shambaugh, M. E., Polayes, D., Matera, A. G., and Rottman, F. M. (1997). Purification and cDNA cloning of the AdoMet-binding subunit of the human mRNA (N6-adenosine)-methyltransferase. *RNA* 3, 1233–1247.

Brennan, G. P., and Henshall, D. C. (2020). MicroRNAs as regulators of brain function and targets for treatment of epilepsy. *Nat. Rev. Neurol.* 16, 506–519. doi: 10.1038/s41582-020-0369-8

Brummer, A., Yang, Y., Chan, T. W., and Xiao, X. (2017). Structure-mediated modulation of mRNA abundance by A-to-I editing. *Nat. Commun.* 8:1255.

Burke, W. J., and Joh, T. H. (1982). Effects of N6-methyladenosine on the synthesis of phenylethanolamine N-methyltransferase in cultured explants of rat adrenal medulla. *J. Neurochem.* 39, 92–96. doi: 10.1111/j.1471-4159.1982.tb04705.x

Cao, G., Li, H. B., Yin, Z., and Flavell, R. A. (2016). Recent advances in dynamic m6A RNA modification. *Open Biol.* 6:160003. doi: 10.1098/rsob.160003

Chen, X., Sun, Y. Z., Liu, H., Zhang, L., Li, J. Q., and Meng, J. (2017). RNA methylation and diseases: experimental results, databases, Web servers and computational models. *Brief. Bioinform.* 20, 896–917. doi: 10.1093/bib/bbx142

Chen, X., Yu, C., Guo, M., Zheng, X., Ali, S., Huang, H., et al. (2019). Down-regulation of m6A mRNA methylation is involved in dopaminergic neuronal death. *ACS Chem. Neurosci.* 10, 2355–2363. doi: 10.1021/acschemneuro.8b00657

Chen, X. Y., Zhang, J., and Zhu, J. S. (2019). The role of m(6)A RNA methylation in human cancer. *Mol. Cancer* 18:103.

Chokkalla, A. K., Mehta, S. L., Kim, T., Chelluboina, B., Kim, J., and Vemuganti, R. (2019). Transient focal ischemia significantly alters the m(6)A epitranscriptomic tagging of RNAs in the brain. *Stroke* 50, 2912–2921. doi: 10.1161/strokeaha.119.026433

Christofi, T., and Zaravinos, A. (2019). RNA editing in the forefront of epitranscriptomics and human health. *J. Transl. Med.* 17:319.

Conboy, K., Henshall, D. C., and Brennan, G. P. (2021). Epigenetic principles underlying epileptogenesis and epilepsy syndromes. *Neurobiol. Dis.* 148:105179. doi: 10.1016/j.nbd.2020.105179

Cui, Q., Shi, H., Ye, P., Li, L., Qu, Q., Sun, G., et al. (2017). m(6)A RNA methylation regulates the self-renewal and tumorigenesis of glioblastoma stem cells. *Cell Rep.* 18, 2622–2634. doi: 10.1016/j.celrep.2017.02.059

Czuba, L. C., Hillgren, K. M., and Swaan, P. W. (2018). Post-translational modifications of transporters. *Pharmacol. Ther.* 192, 88–99. doi: 10.1016/j.pharmthera.2018.06.013

Danzer, S. C. (2008). Postnatal and adult neurogenesis in the development of human disease. *Neuroscientist* 14, 446–458. doi: 10.1177/1073858408317008

Dixit, D., Prager, B. C., Gimple, R. C., Poh, H. X., Wang, Y., Wu, Q., et al. (2020). The RNA m6A reader YTHDF2 maintains oncogene expression and is a targetable dependency in glioblastoma stem cells. *Cancer Discov.* 11, 480–499. doi: 10.1158/2159-8290.cd-20-0331

Dominissini, D., Moshitch-Moshkovitz, S., Salmon-Divon, M., Amariglio, N., and Rechavi, G. (2013). Transcriptome-wide mapping of N(6)-methyladenosine by m(6)A-seq based on immunocapturing and massively parallel sequencing. *Nat. Protoc.* 8, 176–189. doi: 10.1038/nprot.2012.148

Dominissini, D., Moshitch-Moshkovitz, S., Schwartz, S., Salmon-Divon, M., Ungar, L., Osenberg, S., et al. (2012). Topology of the human and mouse m6A RNA methylomes revealed by m6A-seq. *Nature* 485, 201–206. doi: 10.1038/nature11112

Donega, V., Marcy, G., Lo Giudice, Q., Zweifel, S., Angonin, D., Fiorelli, R., et al. (2018). Transcriptional dysregulation in postnatal glutamatergic progenitors contributes to closure of the cortical neurogenic period. *Cell. Rep.* 22, 2567–2574. doi: 10.1016/j.celrep.2018.02.030

Du, H., Zhao, Y., He, J., Zhang, Y., Xi, H., Liu, M., et al. (2016). YTHDF2 destabilizes m(6)A-containing RNA through direct recruitment of the CCR4-NOT deadenylase complex. *Nat. Commun.* 7:12626.

Edupuganti, R. R., Geiger, S., Lindeboom, R. G. H., Shi, H., Hsu, P. J., Lu, Z., et al. (2017). N(6)-methyladenosine (m(6)A) recruits and repels proteins to regulate mRNA homeostasis. *Nat. Struct. Mol. Biol.* 24, 870–878. doi: 10.1038/nsmb.3462

Eisenberg, E., and Levanon, E. Y. (2018). A-to-I RNA editing - immune protector and transcriptome diversifier. *Nat. Rev. Genet.* 19, 473–490. doi: 10.1038/s41576-018-0006-1

Engel, M., Eggert, C., Kaplick, P. M., Eder, M., Roh, S., Tietze, L., et al. (2018). The Role of m(6)A/m-RNA methylation in stress response regulation. *Neuron* 99, 389.e9–403.e9.

Ensfelder, T. T., Kurz, M. Q., Iwan, K., Geiger, S., Matheisl, S., Muller, M., et al. (2018). ALKBH5-induced demethylation of mono- and dimethylated adenosine. *Chem. Commun.* 54, 8591–8593. doi: 10.1039/c8cc03980a

Fedeles, B. I., Singh, V., Delaney, J. C., Li, D., and Essigmann, J. M. (2015). The AlkB family of Fe(II)/alpha-ketoglutarate-dependent dioxygenases: repairing nucleic acid alkylation damage and beyond. *J. Biol. Chem.* 290, 20734–20742. doi: 10.1074/jbc.r115.656462

Furuichi, Y., Morgan, M., Shatkin, A. J., Jelinek, W., Salditt-Georgieff, M., and Darnell, J. E. (1975). Methylated, blocked 5 termini in HeLa cell mRNA. *Proc. Natl. Acad. Sci. U.S.A.* 72, 1904–1908. doi: 10.1073/pnas.72.5.1904

Gerken, T., Girard, C. A., Tung, Y. C., Webby, C. J., Saudek, V., Hewitson, K. S., et al. (2007). The obesity-associated FTO gene encodes a 2-oxoglutarate-dependent nucleic acid demethylase. *Science* 318, 1469–1472. doi: 10.1126/science.1151710

Han, M., Liu, Z., Xu, Y., Liu, X., Wang, D., Li, F., et al. (2020). Abnormality of m6A mRNA methylation is involved in Alzheimer's disease. *Front. Neurosci.* 14:98. doi: 10.3389/fnins.2020.00098

Hawrylycz, M. J., Lein, E. S., Guillozet-Bongaarts, A. L., Shen, E. H., Ng, L., Miller, J. A., et al. (2012). An anatomically comprehensive atlas of the adult human brain transcriptome. *Nature* 489, 391–399.

He, P. C., and He, C. (2021). m(6) A RNA methylation: from mechanisms to therapeutic potential. *EMBO J.* 40:e105977.

Horiuchi, K., Kawamura, T., Iwanari, H., Ohashi, R., Naito, M., Kodama, T., et al. (2013). Identification of Wilms' tumor 1-associating protein complex and its role in alternative splicing and the cell cycle. *J. Biol. Chem.* 288, 33292–33302. doi: 10.1074/jbc.m113.500397

Hsu, P. J., Shi, H., Zhu, A. C., Lu, Z., Miller, N., Edens, B. M., et al. (2019). The RNA-binding protein FMRP facilitates the nuclear export of N^6-methyladenosine-containing mRNAs. *J. Biol. Chem.* 294, 19889–19895. doi: 10.1074/jbc.AC119.010078

Huang, H., Camats-Perna, J., Medeiros, R., Anggono, V., and Widagdo, J. (2020). Altered expression of the m6A methyltransferase METTL3 in Alzheimer's disease. *eNeuro* 7:ENEURO.0125-20.2020.

Jain, M., Jantsch, M. F., and Licht, K. (2019). The Editor's I on disease development. *Trends Genet.* 35, 903–913.

Jenjaroenpun, P., Wongsurawat, T., Wadley, T. D., Wassenaar, T. M., Liu, J., Dai, Q., et al. (2021). Decoding the epitranscriptional landscape from native RNA sequences. *Nucleic Acids Res.* 49:e7. doi: 10.1093/nar/gkaa620

Joglekar, A., Prjibelski, A., Mahfouz, A., Collier, P., Lin, S., Schlusche, A. K., et al. (2021). A spatially resolved brain region- and cell type-specific isoform atlas of the postnatal mouse brain. *Nat. Commun.* 12:463.

Kaldun, J. C., and Sprecher, S. G. (2019). Initiated by CREB: resolving gene regulatory programs in learning and memory: switch in cofactors and transcription regulators between memory consolidation and maintenance network. *Bioessays* 41:e1900045.

Ke, S., Pandya-Jones, A., Saito, Y., Fak, J. J., Vagbo, C. B., Geula, S., et al. (2017). m(6)A mRNA modifications are deposited in nascent pre-mRNA and are not required for splicing but do specify cytoplasmic turnover. *Genes Dev.* 31, 990–1006. doi: 10.1101/gad.301036.117

Keller, L., Xu, W., Wang, H. X., Winblad, B., Fratiglioni, L., and Graff, C. (2011). The obesity related gene, FTO, interacts with APOE, and is associated with Alzheimer's disease risk: a prospective cohort study. *J. Alzheimers Dis.* 23, 461–469. doi: 10.3233/jad-2010-101068

Kim, J. K., Samaranayake, M., and Pradhan, S. (2009). Epigenetic mechanisms in mammals. *Cell Mol. Life Sci.* 66, 596–612.

Knuckles, P., Lence, T., Haussmann, I. U., Jacob, D., Kreim, N., Carl, S. H., et al. (2018). Zc3h13/Flacc is required for adenosine methylation by bridging the mRNA-binding factor Rbm15/Spenito to the m(6)A machinery component Wtap/Fl(2)d. *Genes Dev.* 32, 415–429. doi: 10.1101/gad.309146.117

Koranda, J. L., Dore, L., Shi, H., Patel, M. J., Vaasjo, L. O., Rao, M. N., et al. (2018). Mettl14 is essential for epitranscriptomic regulation of striatal function and learning. *Neuron* 99, 283.e5–292.e5.

Kowalski-Chauvel, A., Lacore, M. G., Arnauduc, F., Delmas, C., Toulas, C., Cohen-Jonathan-Moyal, E., et al. (2020). The m6A RNA demethylase ALKBH5 promotes radioresistance and invasion capability of glioma stem cells. *Cancers* 13:40. doi: 10.3390/cancers13010040

Lence, T., Paolantoni, C., Worpenberg, L., and Roignant, J. Y. (2019). Mechanistic insights into m(6)A RNA enzymes. *Biochim. Biophys. Acta Gene Regul. Mech.* 1862, 222–229. doi: 10.1016/j.bbagrm.2018.10.014

Li, E., Wei, B., Wang, X., and Kang, R. (2020). METTL3 enhances cell adhesion through stabilizing integrin beta1 mRNA via an m6A-HuR-dependent mechanism in prostatic carcinoma. *Am. J. Cancer Res.* 10, 1012–1025.

Li, L., Zang, L., Zhang, F., Chen, J., Shen, H., Shu, L., et al. (2017). Fat mass and obesity-associated (FTO) protein regulates adult neurogenesis. *Hum. Mol. Genet.* 26, 2398–2411. doi: 10.1093/hmg/ddx128

Li, M., Zhao, X., Wang, W., Shi, H., Pan, Q., Lu, Z., et al. (2018). Ythdf2-mediated m(6)A mRNA clearance modulates neural development in mice. *Genome Biol.* 19:69.

Lin, S., Choe, J., Du, P., Triboulet, R., and Gregory, R. I. (2016). The m(6)A methyltransferase METTL3 promotes translation in human cancer cells. *Mol. Cell* 62, 335–345. doi: 10.1016/j.molcel.2016.03.021

Linder, B., Grozhik, A. V., Olarerin-George, A. O., Meydan, C., Mason, C. E., and Jaffrey, S. R. (2015). Single-nucleotide-resolution mapping of m6A and m6Am throughout the transcriptome. *Nat. Methods* 12, 767–772. doi: 10.1038/nmeth.3453

Linder, B., and Jaffrey, S. R. (2019). Discovering and mapping the modified nucleotides that comprise the epitranscriptome of mRNA. *Cold Spring Harb. Perspect. Biol.* 11:a032201. doi: 10.1101/cshperspect.a032201

Lindgren, C. M., and McCarthy, M. I. (2008). Mechanisms of disease: genetic insights into the etiology of type 2 diabetes and obesity. *Nat. Clin. Pract. Endocrinol. Metab.* 4, 156–163. doi: 10.1038/ncpendmet0723

Ling, Z., Chen, L., and Zhao, J. (2020). m6A-dependent up-regulation of DRG1 by METTL3 and ELAVL1 promotes growth, migration, and colony formation in osteosarcoma. *Biosci. Rep.* 40:BSR20200282.

Liu, H., Begik, O., Lucas, M. C., Ramirez, J. M., Mason, C. E., Wiener, D., et al. (2019). Accurate detection of m(6)A RNA modifications in native RNA sequences. *Nat. Commun.* 10:4079.

Liu, J., Yue, Y., Han, D., Wang, X., Fu, Y., Zhang, L., et al. (2014). A METTL3-METTL14 complex mediates mammalian nuclear RNA N6-adenosine methylation. *Nat. Chem. Biol.* 10, 93–95. doi: 10.1038/nchembio.1432

Livneh, I., Moshitch-Moshkovitz, S., Amariglio, N., Rechavi, G., and Dominissini, D. (2020). The m(6)A epitranscriptome: transcriptome plasticity in brain development and function. *Nat. Rev. Neurosci.* 21, 36–51. doi: 10.1038/s41583-019-0244-z

Loos, R. J., and Bouchard, C. (2008). FTO: the first gene contributing to common forms of human obesity. *Obes. Rev.* 9, 246–250.

Ma, C., Chang, M., Lv, H., Zhang, Z. W., Zhang, W., He, X., et al. (2018). RNA m(6)A methylation participates in regulation of postnatal development of the mouse cerebellum. *Genome Biol.* 19:68.

Madugalle, S. U., Meyer, K., Wang, D. O., and Bredy, T. W. (2020). RNA N(6)-methyladenosine and the regulation of RNA localization and function in the brain. *Trends Neurosci.* 43, 1011–1023. doi: 10.1016/j.tins.2020.09.005

Mauer, J., and Jaffrey, S. R. (2018). FTO, m(6) Am, and the hypothesis of reversible epitranscriptomic mRNA modifications. *FEBS Lett.* 592, 2012–2022. doi: 10.1002/1873-3468.13092

Mauer, J., Luo, X., Blanjoie, A., Jiao, X., Grozhik, A. V., Patil, D. P., et al. (2017). Reversible methylation of m(6)Am in the 5′ cap controls mRNA stability. *Nature* 541, 371–375. doi: 10.1038/nature21022

McIntyre, A. B. R., Alexander, N., Grigorev, K., Bezdan, D., Sichtig, H., Chiu, C. Y., et al. (2019). Single-molecule sequencing detection of N6-methyladenine in microbial reference materials. *Nat. Commun.* 10:579.

Merkurjev, D., Hong, W. T., Iida, K., Oomoto, I., Goldie, B. J., Yamaguti, H., et al. (2018). Synaptic N(6)-methyladenosine (m(6)A) epitranscriptome reveals functional partitioning of localized transcripts. *Nat. Neurosci.* 21, 1004–1014. doi: 10.1038/s41593-018-0173-6

Meyer, K. D., and Jaffrey, S. R. (2014). The dynamic epitranscriptome: N6-methyladenosine and gene expression control. *Nat. Rev. Mol. Cell Biol.* 15, 313–326. doi: 10.1038/nrm3785

Meyer, K. D., Patil, D. P., Zhou, J., Zinoviev, A., Skabkin, M. A., Elemento, O., et al. (2015). 5′ UTR m(6)A promotes cap-independent translation. *Cell* 163, 999–1010. doi: 10.1016/j.cell.2015.10.012

Meyer, K. D., Saletore, Y., Zumbo, P., Elemento, O., Mason, C. E., and Jaffrey, S. R. (2012). Comprehensive analysis of mRNA methylation reveals enrichment in 3′ UTRs and near stop codons. *Cell* 149, 1635–1646. doi: 10.1016/j.cell.2012.05.003

Mitra, S., Lee, W., Hayashi, K., Boyd, J., Milloy, M. J., Dong, H., et al. (2021). A gender comparative analysis of post-traumatic stress disorder among a community-based cohort of people who use drugs in Vancouver, Canada. *Addict. Behav.* 115:106793. doi: 10.1016/j.addbeh.2020.106793

Munns, T. W., Liszewski, M. K., and Sims, H. F. (1977). Characterization of antibodies specific for N6-methyladenosine and for 7-methylguanosine. *Biochemistry* 16, 2163–2168. doi: 10.1021/bi00629a019

Patil, D. P., Chen, C. K., Pickering, B. F., Chow, A., Jackson, C., Guttman, M., et al. (2016). m(6)A RNA methylation promotes XIST-mediated transcriptional repression. *Nature* 537, 369–373. doi: 10.1038/nature19342

Patil, D. P., Pickering, B. F., and Jaffrey, S. R. (2018). Reading m(6)A in the transcriptome: m(6)A-binding proteins. *Trends Cell Biol.* 28, 113–127. doi: 10.1016/j.tcb.2017.10.001

Pendleton, K. E., Chen, B., Liu, K., Hunter, O. V., Xie, Y., Tu, B. P., et al. (2017). The U6 snRNA m(6)A methyltransferase METTL16 regulates SAM synthetase intron retention. *Cell* 169, 824.e14–835.e14.

Pfisterer, U., Petukhov, V., Demharter, S., Meichsner, J., Thompson, J. J., Batiuk, M. Y., et al. (2020). Identification of epilepsy-associated neuronal subtypes and gene expression underlying epileptogenesis. *Nat. Commun.* 11:5038.

Ping, X. L., Sun, B. F., Wang, L., Xiao, W., Yang, X., Wang, W. J., et al. (2014). Mammalian WTAP is a regulatory subunit of the RNA N6-methyladenosine methyltransferase. *Cell Res.* 24, 177–189. doi: 10.1038/cr.2014.3

Qiu, X., He, H., Huang, Y., Wang, J., and Xiao, Y. (2020). Genome-wide identification of m(6)A-associated single-nucleotide polymorphisms in Parkinson's disease. *Neurosci. Lett.* 737:135315. doi: 10.1016/j.neulet.2020.135315

Reitz, C., Tosto, G., Mayeux, R., Luchsinger, J. A., Group, N.-L. N. F. S., and Alzheimer's Disease Neuroimaging, I. (2012). Genetic variants in the Fat and Obesity Associated (FTO) gene and risk of Alzheimer's disease. *PLoS One* 7:e50354. doi: 10.1371/journal.pone.0050354.

Schwartz, S., Mumbach, M. R., Jovanovic, M., Wang, T., Maciag, K., Bushkin, G. G., et al. (2014). Perturbation of m6A writers reveals two distinct classes of mRNA methylation at internal and 5′ sites. *Cell. Rep.* 8, 284–296. doi: 10.1016/j.celrep.2014.05.048

Shi, H., Wang, X., Lu, Z., Zhao, B. S., Ma, H., Hsu, P. J., et al. (2017). YTHDF3 facilitates translation and decay of N(6)-methyladenosine-modified RNA. *Cell Res.* 27, 315–328. doi: 10.1038/cr.2017.15

Shi, H., Zhang, X., Weng, Y. L., Lu, Z., Liu, Y., Lu, Z., et al. (2018). m(6)A facilitates hippocampus-dependent learning and memory through YTHDF1. *Nature* 563, 249–253. doi: 10.1038/s41586-018-0666-1

Short, A. K., and Baram, T. Z. (2019). Early-life adversity and neurological disease: age-old questions and novel answers. *Nat. Rev. Neurol.* 15, 657–669. doi: 10.1038/s41582-019-0246-5

Si, W., Li, Y., Ye, S., Li, Z., Liu, Y., Kuang, W., et al. (2020). Methyltransferase 3 mediated miRNA m6A methylation promotes stress granule formation in the early stage of acute ischemic stroke. *Front. Mol. Neurosci.* 13:103. doi: 10.3389/fnmol.2020.00103

Sledz, P., and Jinek, M. (2016). Structural insights into the molecular mechanism of the m(6)A writer complex. *eLife* 5:e18434.

Song, L., Pan, S., Zhang, Z., Jia, L., Chen, W. H., and Zhao, X. M. (2021). STAB: a spatio-temporal cell atlas of the human brain. *Nucleic Acids Res.* 49, D1029–D1037.

Song, N., Du, J., Gao, Y., and Yang, S. (2020). Epitranscriptome of the ventral tegmental area in a deep brain-stimulated chronic unpredictable mild stress mouse model. *Transl. Neurosci.* 11, 402–418. doi: 10.1515/tnsci-2020-0146

Sorci, M., Ianniello, Z., Cruciani, S., Larivera, S., Ginistrelli, L. C., Capuano, E., et al. (2018). METTL3 regulates WTAP protein homeostasis. *Cell Death Dis.* 9:796.

Tang, C., Klukovich, R., Peng, H., Wang, Z., Yu, T., Zhang, Y., et al. (2018). ALKBH5-dependent m6A demethylation controls splicing and stability of long 3′-UTR mRNAs in male germ cells. *Proc. Natl. Acad. Sci. U.S.A.* 115, E325–E333.

Theler, D., Dominguez, C. Blatter, M., Boudet, J., and Allain, F. H. (2014). Solution structure of the YTH domain in complex with N6-methyladenosine RNA: a reader of methylated RNA. *Nucleic Acids Res.* 42, 13911–13919. doi: 1093/nar/gku1116

van der Kwast, R., Parma, L., van der Bent, M. L., van Ingen, E., Baganha, F., Peters, H. A. B., et al. (2020). Adenosine-to-inosine editing of vasoactive MicroRNAs alters their targetome and function in ischemia. *Mol. Ther. Nucleic Acids* 21, 932–953. doi: 10.1016/j.omtn.2020.07.020

Visvanathan, A., Patil, V., Arora, A., Hegde, A. S., Arivazhagan, A., Santosh, V., et al. (2018). Essential role of METTL3-mediated m(6)A modification in glioma stem-like cells maintenance and radioresistance. *Oncogene* 37, 522–533. doi: 10.1038/onc.2017.351

Walters, B. J., Mercaldo, V., Gillon, C. J., Yip, M., Neve, R. L., Boyce, F. M., et al. (2017). The role of The RNA demethylase FTO (fat mass and obesity-associated) and mRNA methylation in hippocampal memory formation. *Neuropsychopharmacology* 42, 1502–1510. doi: 10.1038/npp.2017.31

Wang, L. C., Chen, S. H., Shen, X. L., Li, D. C., Liu, H. Y., Ji, Y. L., et al. (2020). M6A RNA methylation regulator HNRNPC contributes to tumorigenesis and predicts prognosis in glioblastoma multiforme. *Front. Oncol.* 10:536875. doi: 10.3389/fonc.2020.536875

Wang, X., Lu, Z., Gomez, A., Hon, G. C., Yue, Y., Han, D., et al. (2014). N6-methyladenosine-dependent regulation of messenger RNA stability. *Nature* 505, 117–120. doi: 10.1038/nature12730

Wang, X., Zhao, B. S., Roundtree, I. A., Lu, Z., Han, D., Ma, H., et al. (2015). N(6)-methyladenosine modulates messenger RNA translation efficiency. *Cell* 161, 1388–1399. doi: 10.1016/j.cell.2015.05.014

Wang, Y., Li, Y., Toth, J. I., Petroski, M. D., Zhang, Z., and Zhao, J. C. (2014). N6-methyladenosine modification destabilizes developmental regulators in embryonic stem cells. *Nat. Cell Biol.* 16, 191–198. doi: 10.1038/ncb2902

Wang, Y., Mao, J., Wang, X., Lin, Y., Hou, G., Zhu, J., et al. (2019). Genome-wide screening of altered m6A-tagged transcript profiles in the hippocampus after traumatic brain injury in mice. *Epigenomics* 11, 805–819. doi: 10.2217/epi-2019-0002

Wang, Z., Cheng, H., Xu, H., Yu, X., and Sui, D. (2020). A five-gene signature derived from m6A regulators to improve prognosis prediction of neuroblastoma. *Cancer Biomark.* 28, 275–284. doi: 10.3233/cbm-191196

Wei, C., Gershowitz, A., and Moss, B. (1975). N6, O2'-dimethyladenosine a novel methylated ribonucleoside next to the 5′ terminal of animal cell and virus mRNAs. *Nature* 257, 251–253. doi: 10.1038/257251a0

Wei, C. M., Gershowitz, A., and Moss, B. (1976). 5′-Terminal and internal methylated nucleotide sequences in HeLa cell mRNA. *Biochemistry* 15, 397–401. doi: 10.1021/bi00647a024

Wei, C. M., and Moss, B. (1977). Nucleotide sequences at the N6-methyladenosine sites of HeLa cell messenger ribonucleic acid. *Biochemistry* 16, 1672–1676. doi: 10.1021/bi00627a023

Wen, J., Lv, R., Ma, H., Shen, H., He, C., Wang, J., et al. (2018). Zc3h13 regulates nuclear RNA m(6)A methylation and mouse embryonic stem cell self-renewal. *Mol. Cell.* 69, 1028.e6–1038.e6.

Weng, Y. L., Wang, X., An, R., Cassin, J., Vissers, C., Liu, Y., et al. (2018). Epitranscriptomic m(6)A regulation of axon regeneration in the adult mammalian nervous system. *Neuron* 97, 313.e6–325.e6.

Westmark, C. J., Maloney, B., Alisch, R. S., Sokol, D. K., and Lahiri, D. K. (2020). FMRP regulates the nuclear export of *Adam9* and *Psen1* mRNAs: secondary Analysis of an N^6-methyladenosine dataset. *Sci. Rep.* 10:10781. doi: 10.1038/s41598-020-66394-y

Widagdo, J., Zhao, Q. Y., Kempen, M. J., Tan, M. C., Ratnu, V. S., Wei, W., et al. (2016). Experience-dependent accumulation of N^6-methyladenosine in the prefrontal cortex is associated with memory processes in mice. *J. Neurosci.* 36, 6771–6777. doi: 10.1523/JNEUROSCI.4053-15.2016

Wojtas, M. N., Pandey, R. R., Mendel, M., Homolka, D., Sachidanandam, R., and Pillai, R. S. (2017). Regulation of m(6)A transcripts by the 3′–>5′ RNA helicase YTHDC2 is essential for a successful meiotic program in the mammalian germline. *Mol. Cell.* 68, 374.e12–387.e12.

Xu, C., Wang, X., Liu, K., Roundtree, I. A., Tempel, W., Li, Y., et al. (2014). Structural basis for selective binding of m^{6}A RNA by the YTHDC1 YTH domain. *Nat. Chem. Biol.* 10, 927–929. doi: 10.1038/nchembio.1654

Xu, H., Dzhashiashvili, Y., Shah, A., Kunjamma, R. B., Weng, Y. L., Elbaz, B., et al. (2020). m(6)A mRNA methylation is essential for oligodendrocyte maturation and CNS myelination. *Neuron* 105, 293.e5–309.e5.

Xu, K., Mo, Y., Li, D., Yu, Q., Wang, L., Lin, F., et al. (2020). N(6)-methyladenosine demethylases Alkbh5/Fto regulate cerebral ischemia-reperfusion injury. *Ther. Adv. Chronic Dis.* 11:2040622320916024.

Xue, A., Huang, Y., Li, M., Wei, Q., and Bu, Q. (2021). Comprehensive analysis of differential m6A RNA methylomes in the hippocampus of cocaine-conditioned mice. *Mol. Neurobiol.* [Epub ahead of print].

Yarmishyn, A. A., Yang, Y. P., Lu, K. H., Chen, Y. C., Chien, Y., Chou, S. J., et al. (2020). Musashi-1 promotes cancer stem cell properties of glioblastoma cells via upregulation of YTHDF1. *Cancer Cell. Int.* 20:597.

Yoon, K. J., Ringeling, F. R., Vissers, C., Jacob, F., Pokrass, M., Jimenez-Cyrus, D., et al. (2017). Temporal control of mammalian cortical neurogenesis by m(6)A methylation. *Cell* 171, 877.e17–889.e17.

Yu, J., Chen, M., Huang, H., Zhu, J., Song, H., Zhu, J., et al. (2018). Dynamic m6A modification regulates local translation of mRNA in axons. *Nucleic Acids Res.* 46, 1412–1423. doi: 10.1093/nar/gkx1182

Yu, J., Zhang, Y., Ma, H., Zeng, R., Liu, R., Wang, P., et al. (2020). Epitranscriptomic profiling of N6-methyladenosine-related RNA methylation in rat cerebral cortex following traumatic brain injury. *Mol. Brain* 13:11.

Yue, Y., Liu, J., Cui, X., Cao, J., Luo, G., Zhang, Z., et al. (2018). VIRMA mediates preferential m(6)A mRNA methylation in 3′UTR and near stop codon and associates with alternative polyadenylation. *Cell Discov.* 4:10.

Zaccara, S., Ries, R. J., and Jaffrey, S. R. (2019). Reading, writing and erasing mRNA methylation. *Nat. Rev. Mol. Cell Biol.* 20, 608–624.

Zeng, Y., Wang, S., Gao, S., Soares, F., Ahmed, M., Guo, H., et al. (2018). Refined RIP-seq protocol for epitranscriptome analysis with low input materials. *PLoS Biol.* 16:e2006092. doi: 10.1371/journal.pbio.2006092

Zhang, P., Torres, K., Liu, X., Liu, C. G., and Pollock, R. E. (2016). An overview of chromatin-regulating proteins in cells. *Curr. Protein Pept. Sci.* 17, 401–410.

Zhang, S., Zhao, B. S., Zhou, A., Lin, K., Zheng, S., Lu, Z., et al. (2017). m(6)A demethylase ALKBH5 maintains tumorigenicity of glioblastoma stem-like cells by sustaining FOXM1 expression and cell proliferation program. *Cancer Cell* 31, 591.e6–606.e6.

Zhang, Z., Wang, M., Xie, D., Huang, Z., Zhang, L., Yang, Y., et al. (2018). METTL3-mediated N(6)-methyladenosine mRNA modification enhances long-term memory consolidation. *Cell Res.* 28, 1050–1061.

Zhang, Z., Wang, Q., Zhao, X., Shao, L., Liu, G., Zheng, X., et al. (2020). YTHDC1 mitigates ischemic stroke by promoting Akt phosphorylation through destabilizing PTEN mRNA. *Cell Death Dis.* 11:977.

Zhao, X., Yang, Y., Sun, B. F., Shi, Y., Yang, X., Xiao, W., et al. (2014). FTO-dependent demethylation of N6-methyladenosine regulates mRNA splicing and is required for adipogenesis. *Cell Res.* 24, 1403–1419.

Zheng, G., Dahl, J. A., Niu, Y., Fedorcsak, P., Huang, C. M., Li, C. J., et al. (2013). ALKBH5 is a mammalian RNA demethylase that impacts RNA metabolism and mouse fertility. *Mol. Cell.* 49, 18–29.

Zheng, L., Tang, X., Lu, M., Sun, S., Xie, S., Cai, J., et al. (2020). microRNA-421-3p prevents inflammatory response in cerebral ischemia/reperfusion injury through targeting m6A Reader YTHDF1 to inhibit p65 mRNA translation. *Int. Immunopharmacol.* 88:106937.

Zhou, J., Wan, J., Gao, X., Zhang, X., Jaffrey, S. R., and Qian, S. B. (2015). Dynamic m(6)A mRNA methylation directs translational control of heat shock response. *Nature* 526, 591–594.

Zhuo, Z., Lu, H., Zhu, J., Hua, R. X., Li, Y., Yang, Z., et al. (2020). METTL14 gene polymorphisms confer neuroblastoma susceptibility: an eight-center case-control study. *Mol. Ther. Nucleic Acids* 22, 17–26.

Conflict of Interest: The authors declare that the research was conducted in the absence of any commercial or financial relationships that could be construed as a potential conflict of interest.

Copyright © 2021 Mathoux, Henshall and Brennan. This is an open-access article distributed under the terms of the Creative Commons Attribution License (CC BY). The use, distribution or reproduction in other forums is permitted, provided the original author(s) and the copyright owner(s) are credited and that the original publication in this journal is cited, in accordance with accepted academic practice. No use, distribution or reproduction is permitted which does not comply with these terms.

frontiers in Cellular Neuroscience

ORIGINAL RESEARCH
published: 19 May 2021
doi: 10.3389/fncel.2021.668230

Impaired Adaptation and Laminar Processing of the Oddball Paradigm in the Primary Visual Cortex of Fmr1 KO Mouse

*Alexandr Pak, Samuel T. Kissinger and Alexander A. Chubykin**

Department of Biological Sciences, College of Science, Purdue Institute for Integrative Neuroscience, Purdue University, West Lafayette, IN, United States

Both adaptation and novelty detection are an integral part of sensory processing. Recent animal oddball studies have advanced our understanding of circuitry underlying contextual processing in early sensory areas. However, it is unclear how adaptation and mismatch (MM) responses depend on the tuning properties of neurons and their laminar position. Furthermore, given that reduced habituation and sensory overload are among the hallmarks of altered sensory perception in autism, we investigated how oddball processing might be altered in a mouse model of fragile X syndrome (FX). Using silicon probe recordings and a novel spatial frequency (SF) oddball paradigm, we discovered that FX mice show reduced adaptation and enhanced MM responses compared to control animals. Specifically, we found that adaptation is primarily restricted to neurons with preferred oddball SF in FX compared to WT mice. Mismatch responses, on the other hand, are enriched in the superficial layers of WT animals but are present throughout lamina in FX animals. Last, we observed altered neural dynamics in FX mice in response to stimulus omissions. Taken together, we demonstrated that reduced feature adaptation coexists with impaired laminar processing of oddball responses, which might contribute to altered sensory perception in FX syndrome and autism.

Keywords: adaptation, Fmr1 KO, mismatch, oddball, spatial frequency, V1

OPEN ACCESS

Edited by:
Abhishek Banerjee, Newcastle University, United Kingdom

Reviewed by:
Tommaso Pizzorusso, University of Florence, Italy
Dennis Kätzel, University of Ulm, Germany

****Correspondence:***
Alexander A. Chubykin
chubykin@purdue.edu

Specialty section:
This article was submitted to Cellular Neuropathology, a section of the journal Frontiers in Cellular Neuroscience

Received: *15 February 2021*
Accepted: *19 April 2021*
Published: *19 May 2021*

Citation:
Pak A, Kissinger ST and Chubykin AA (2021) Impaired Adaptation and Laminar Processing of the Oddball Paradigm in the Primary Visual Cortex of Fmr1 KO Mouse. Front. Cell. Neurosci. 15:668230. doi: 10.3389/fncel.2021.668230

INTRODUCTION

Fragile X Syndrome (FX) is the most common cause of intellectual disability and the inherited form of autism. Nearly 1 in 4,000 males and half as many females are affected by this condition. It is associated with social communication deficits, hyperactivity, and sensory hypersensitivity (Freund and Reiss, 1991). Given the comorbidity of FX and autism, *Fmr1* KO mice (FX mice) represent a well-defined genetic model that can provide neural circuit-level insights into autism, especially considering the vast diversity of phenotypes and manifestations observed in autism spectrum disorders (ASDs). Such diverse alterations posit a challenge to develop effective diagnostic and treatment tools. FX mice have been shown to exhibit cellular, circuit, and behavioral alterations that recapitulate some of the manifestations observed in human individuals with FX. Prior autism research has been mostly focused on social-cognitive and behavioral impairments (Robertson and Baron-Cohen, 2017). However, a recent revision of diagnostic criteria for autism

recognized sensory processing as an important factor to be considered (American Psychiatric Association, 2013). Previous research in humans suggests that sensory alterations may be predictive of social communication deficits later in life in autism (Boyd et al., 2010; Turner-Brown et al., 2012).

Both human and animal studies provide evidence that there is impaired information processing in early sensory areas in both FX and autism (Goel et al., 2018; Rais et al., 2018). Sensory hypersensitivity and reduced adaptation to sensory stimuli are some of the hallmark perceptual impairments in autism. An increase in visual detail processing is often reported in this condition. Visual oddball paradigm studies revealed reduced habituation to repeated stimuli and novel distractors in autistic patients (Sokhadze et al., 2017). Similarly, alterations in the event-related potentials during the auditory and visual oddball tasks were found in FX patients (Van Der Molen et al., 2012). Recent work in FX mice found circuit-level impairments in early visual processing, including reduced orientation tuning and functional output from fast-spiking neurons in V1. Reduced orientation tuning of the neurons in the visual cortex correlated with the decreased ability to resolve different orientations of sinusoidal grating stimuli in both mice and human individuals with FX (Goel et al., 2018). Furthermore, altered dendritic spine function and integration were found in layer 4 of the somatosensory cortex in FX mice (Booker et al., 2019). Structural and functional imaging studies of FX mice revealed local hyperconnectivity and long-range hypoconnectivity in V1 (Haberl et al., 2015). Our group has recently shown that there are impaired visual experience-dependent oscillations and altered functional laminar connectivity in V1 of FX mice (Kissinger et al., 2020). Overall, these studies suggest that there may be circuit-level impairments in early sensory processing in FX.

To shed light on the neural basis of atypical visual perception in FX, we investigated how statistical context influences visual information processing by testing both basic and contextual processing of spatial frequencies (SF) in V1 of FX mice. We measured visually evoked potentials (VEPs) and unit responses in an SF oddball paradigm (Ulanovsky et al., 2003; Hamm and Yuste, 2016). Two stimuli were presented at different probabilities so that one was a standard stimulus (STD) (STD, frequent, redundant), which builds a statistical context. Another one was rare and violated the expectations of the STD stimulus leading to a mismatch (MM) response. This response is hypothesized to reflect a perceptual deviance or change detection. First observed in EEG studies in humans as a delayed negative deflection in event-related potentials, later called mismatch negativity (MMN; Naatanen et al., 1978), it has been replicated in different species and sensory modalities (Chen et al., 2015; Musall et al., 2015; Parras et al., 2017). A decrease in the neural response to the standard stimulus (STD), termed stimulus-specific adaptation (SSA), may be attributed to the predictability of the stimulus because the incoming sensory input matches prediction. Alternatively, it may also be explained by the presynaptic short-term plasticity mechanisms. We computed SSA as the difference between control (CTR) and STD (Hamm and Yuste, 2016; Parras et al., 2017). Given that STD and deviant (DEV) stimuli share the same SF, mismatch (MM) response reports moment-to-moment change detection under the high adaptation level in the local microcircuit, so that any response enhancement can be attributed to change detection. MM, similarly to human MMN, was quantified as the difference between DEV and STD stimuli.

Our SF oddball paradigm is different from the prior oddball studies because both STD and DEV stimuli are of the same low-level feature, a spatial frequency (SF) so that they only differ in the global pattern. Prior studies used two stimuli that differed in low-level features (e.g., orientation, frequency) and thus needed a reverse sequence (flip-flop), in which low and high probability stimuli switch to control for feature preference of the neurons. Our oddball paradigm allowed us to investigate how contextual processing depended on neuronal tuning. Specifically, we investigated how oddball responses changed as a function of the neuron's preferred SF. Furthermore, we investigated how oddball responses are represented by different cortical layers and neuronal types (regular vs. fast-spiking) neurons in WT vs. FX mice.

Here, we performed silicon probe recordings in WT and FX mouse V1 during the SF oddball paradigm. First, we report excessive processing of high SF stimuli in late neural responses. Second, we demonstrate that adaptation is mostly confined to neurons preferring the SF within one octave of the oddball SF in FX, but not in WT mice, in which it spreads beyond that range. Third, mismatch responses were differentially modulated by cortical layers in WT but not in FX mice. Last, we observed altered neural dynamics during the omission paradigm in FX animals.

MATERIALS AND METHODS

Experimental Animals

All animal experiments were approved by the Purdue University Animal Care and Use Committee. The following strains were used to generate mice for this study: B6.129P2-Fmr1tm1Cgr/J (Fmr1 KO, JAX Stock No. 003025), B6.Cg-453 Tg(Thy1-COP4/EYFP)18Gfng/J (Thy1-ChR2-YFP, JAX Stock No. 007612), and wild type (WT) C57/BL6. We used 10 male Fmr1 KO and seven littermate controls. We also bred Thy1-ChR2 with Fmr1 KO mice to generate Thy1-Fmr1 KO mice. We used four male Thy1-Fmr1 KO and four littermate controls. Additionally, we had six male WT mice. In total, we used 14 Fmr1 KO and 17 control animals for physiology experiments. Animals were group-housed on a 12 h light/dark cycle with full water and food access.

Surgical Procedures

Animal surgeries were performed as previously described (Pak et al., 2020). Briefly, about 2-month-old animals were induced with 5% isoflurane and secured to a motorized stereotaxic apparatus (Neurostar). Their body temperature was controlled using a heating pad, and they were maintained at 1.5–2% isoflurane anesthesia. The scull was exposed to install a small head post and a reference pin. The binocular V1 coordinates (from lambda AP 0.8 mm, LM: ±3.2 mm) were labeled using a Neurostar software with an integrated mouse brain atlas. Medical

grade Metabond™ was then used to seal all exposed areas and form a head cap. After surgery, all animals were monitored for 3 days for any signs of distress or infection. Mice were then habituated to a head-fixation apparatus for at least 4 days 90 min per day. They were positioned in front of the monitor that displayed a gray screen. On the recording day, a small craniotomy was made above V1 on one of the hemispheres under 1.5% isoflurane anesthesia. They were then moved to the recording room and head-fixed to the apparatus in front of the monitor screen.

Electrophysiology

All recordings were performed in awake head-fixed mice. After mice were transferred to the recording room, we inserted a 64-channel silicon probe (Shobe et al., 2015a; channel separation: vertical 25 μm, horizontal 20 μm, three columns, 1.05 mm in length) to perform acute extracellular electrophysiology. Thirty minutes was allowed after insertion for the probe to settle down. Each mouse underwent a maximum of two recording sessions (one per hemisphere). We acquired data at 30 kHz using OpenEphys hardware and software. We used an Arduino board to synchronize recordings and visual stimulus presentations using TTL communication. Custom written Python scripts using PsychoPy and pyserial were used to present visual stimuli and send TTL signals. Trypsin (2.5%) was used to clean the probe after recording sessions.

Histology

Animals were anesthetized with 100 mg/kg ketamine and 16 mg/kg xylazine solution. Mice were then perfused transcardially with a 1×PBS followed by a 4% paraformaldehyde. After decapitation, their brain was extracted and stored in PFA in the fridge. After 24 h, the brain was sliced in 0.1 mm sections in PBS using a vibratome. Coronal slices were mounted on slides using n-propyl-gallate media and sealed with transparent nail polish. Slices were imaged using light microscopy (VWR) to verify the probe placement in V1.

Visual Stimulation

We used a PsychoPy, an open-source Python software, to create and present all visual stimulations (Peirce, 2009). A gamma calibrated LCD monitor (22" ViewSonic VX2252, 60 Hz) was used to present visual stimuli. The mean luminance of the monitor was 30 cd/m^2. The monitor was placed 17 cm in front of the mouse to binocularly present stimuli. To generate visual stimulations for a spatial frequency tuning and an oddball paradigm, we performed a spatial frequency filtering of random noise. Specifically, we bandpass filtered random noise in different non-overlapping SF bands. This was done by performing the following steps. First, we randomly generated noise and converted it to a frequency domain using FFT (numpy FFT). Second, we created a spatial frequency bandpass filter using the Psychopy Butterworth filter with an order of 10. Third, we multiplied the white noise in the frequency domain by our bandpass filter. This step filtered all the frequencies but the desired SF band. Fourth, we took the inverse Fourier transform of our altered frequency domain. The procedure and a Python code for spatial frequency filtering were adapted from http://www.djmannion.net/psych_programming/vision/sf_filt/sf_filt.html. We modified the above code to generate SF filtered noise. Overall, we used six different spatial frequencies for SF tuning: 7.5E-3, 0.015, 0.03, 0.06, 0.12, and 0.24 cycles/degrees. We chose these frequencies based on previous studies and known spatial frequency tuning of mouse V1 neurons. We verified that we could obtain reliable SF tuning similarly to our previous study (Kissinger et al., 2018). SF tuning sequence contained six different SF stimuli presented in a pseudorandom order at equal probability. Each SF was repeated 20 times so that the experiment had 120 trials in total. We used an inter-trial interval of at least 4 s to prevent any adaptation. Furthermore, SF filtered stimuli were randomly generated on each trial to uniformly sample different receptive fields. This was mainly important for lower spatial frequencies. For the oddball paradigm, we used two stimuli of the same SF but different overall patterns. The first stimulus was a standard (STD) with a probability of 0.875. Its texture did not change across trials. The second one was a deviant (DEV) with a probability of 0.125, its overall pattern changed across trials. This was done to maximize the surprise response. Inter stimulus interval was 0.5 s plus a random delay chosen from the range of 0.5 and 1.2 s. The stimulus was presented for 0.5 s. In total, 200 trials were presented during the oddball paradigm. For the omission paradigm, every eighth stimulus was omitted to investigate omission responses. Inter stimulus interval was set to 1.7 s, and 200 trials were presented. Overall, a maximum of 520 trials was presented to a mouse during a single recording session.

LFP Analysis

Raw electrophysiology traces were first downsampled to 1 kHz. We then used a symmetric linear-phase FIR filter (default parameters) from the mne Python library to remove 60 Hz noise. Next, we identified Layer 4 by finding a channel with the strongest negative deflection in the first 100 ms after stimulus onset. Time-frequency analysis was done using a complex wavelet convolution. Forty different wavelets were designed across a logarithmic range of 2–80 Hz, with cycles ranging from 3 to 10. This gave us an optimal time-frequency precision tradeoff. We convolved these wavelets with averaged LFP traces and then averaged the resulting power spectra across different conditions. For heatmaps, power was dB baseline normalized. To quantify a mean power within a particular band, we averaged responses within a 0.05–0.5 s time window. We used six different frequency bands: theta (4–8 Hz), alpha (8–12 Hz), beta (12–30 Hz), low gamma (30–50 Hz), and high gamma (50–80 Hz).

Single Unit Analysis

Clustering and manual curation of units were performed as previously described (Pak et al., 2020). Kilosort was used for spike detection and sorting. It uses a template matching algorithm and allows a GPU acceleration (Pachitariu et al., 2016). Default configuration parameters were used for clustering, but a threshold for spike detection was changed from −4 to −6. SD. Templates were initialized from the data. Kilosort was run using MATLAB (Mathworks) on Windows 10 running

computer. For clustering purposes, all the different recording blocks were concatenated together. This allowed us to track single neurons across different recording sessions. After clustering, we visualized and verified clustering results using Klusta/Phy GUI. It speeds up the process of manually removing, splitting, and merging units (Rossant et al., 2016). We used several criteria to only include well-isolated units: (1) had more than 10 spikes for each experimental block; (2) less than 5% of spikes violated an absolute refractory period; (3) clean template shape; and (4) templates were localized within a small channel group. To merge and split units, we followed the guidelines available online (https://github.com/kwikteam/phy-contrib/blob/master/docs/template-gui.md). Peristimulus time histograms (PSTHs) of single units were constructed by binning spike times across trials with 10 ms bins and convolving the obtained histogram with a Gaussian Kernel (width = 100 ms). *Z*-score was calculated by the following formula:

$$z = \frac{R - mean(baseFR)}{sd(baseFR)}$$

where, FR is a firing rate at each time point, and base refers to the baseline activity over 0–0.3 s.

For spatial frequency analysis, we averaged the firing rate within 0.05–0.2 s for tuning analysis and 0.2–0.5 s to investigate later responses. Population tuning curves were constructed using baseline-subtracted firing rates across different neurons. We fitted a difference of Gaussian function to SF tuning curves (Hawken and Parker, 1987):

$$R(SF) = R_0 + K_e e^{\frac{-(SF-\mu_e)^2}{2\sigma_e^2}} - K_i e^{\frac{-(SF-\mu_i)^2}{2\sigma_i^2}}$$

This function has seven free parameters: baseline firing rate R_0, amplitude K_e, K_i, center μ_e and μ_i, width σ_e and σ_i of the excitatory and inhibitory components, respectively.

$$\text{fit error} = \frac{\sum(y_i - f_i)^2}{\sum(y_i - \bar{y})^2}$$

where, y_i is the observed value, $\bar{y}$ is the mean of observed data, and f_i is the fitted value. The fitting procedure was performed using curve_fit from Python. Initial value for each parameter was set to 0.01. Bounds were set to [0, 1] for width and [0, max firing*2] for other parameters. Tuning sharpness was quantified using the quality factor (Q):

$$Q = \frac{SF_{\text{peak}}}{SF_{\text{high}} - SF_{\text{low}}}$$

where SF_{peak} is the preferred SF of the unit, SF_{high} and SF_{low} are the high and low SF cut-offs at which the tuning curve drops below peak $\sqrt{2}$ (Bredfeldt and Ringach, 2002).

To investigate oddball responses, we focused on neurons that upregulate their firing in response to visual stimuli. We used Wilcoxon signed-rank test to identify these neurons by comparing baseline firing rate −0.25–0.05 s vs. stimulus window 0.05–0.35 s. The response to the SF0.03 was used as the control for the oddball paradigm. To equalize the number of trials between STD and DEV stimuli, we only used pre-DEV trials for STD. We computed modulation indices for mismatch response (MM) and stimulus-specific adaptation (SSA) using the following formulas.

$$iSSA = \frac{CTR - STD}{CTR + STD}; \quad iMM = \frac{DEV_{\text{late}} - STD_{\text{late}}}{Dev_{\text{late}} + STD_{\text{late}}}$$

where STD/CTR represents baseline-corrected mean firing rate within 0.05–0.5 s, and STD_{late}/DEV_{late} 0.2–0.5 s relative to the stimulus onset.

To investigate how SSA and MM change as a function of preferred SF of the units, we split neurons into three groups: tuned_in, tuned_out, and untuned units. Tuned_in group included units with preferred SF that lies within 1 octave of oddball SF, 0.03 cpd (0.015 < pref SF < 0.06). The tuned_out group included units with preferred SF that lies outside the 1 octave of the oddball SF (pref SF < 0.015 or pref SF > 0.06). The untuned group included units that did not show any SF tuning properties; the fitting procedure was not successful, or the fitting error exceeded 0.9. These units were then further split by the cortical depth. The layer of each neuron was assigned based on the depth of the channel with the strongest negative deflection of the template. We used Kilosort template waveform features to split units into putative regular or fast-spiking (RS vs. FS) neurons. FS units were defined as those with trough-to-peak times less than 0.45 and spike width less than 1.2. RS units, on the other hand, had trough-to-peak times more than 0.45 and spike width larger than 1.2. Units that fall in between were defined as unclassified.

The omission paradigm was analyzed in two different ways. First, we decided to investigate the laminar processing of omission responses. Omission-responsive units were defined as those with significant neural responses during omission (expected stimulus timing vs. baseline 0.05–0.35 vs. −0.25–0.05). Neurons with significant responses were further subdivided into omis-excited and omis-inhibited depending on whether their mean response exceeds 0 or not. Overall, 122 WT and 95 FX units were omis-excited, 93 and 92 omis-inhibited, and 230 WT and 134 FX units did not have a significant omission response. The second approach employed an unsupervised clustering algorithm, *k*-means. The input was omission responses (0.05–0.5 s) from both genotypes. We used scikit-learn implementation of *k*-means and initialized it with PCA for consistency. The number of clusters was determined using an "elbow method," in which distortion and inertia can be plotted against the number of clusters. It is challenging to find an optimal number of groups for *k*-means with neurophysiology data; however, we observed that $k = 4$ is the point at which a slope changes in the inertia and distortion plots. In addition, we qualitatively observed that four groups captured the diversity of omission responses. Given that genotype of units is independent of the clustering process, we compared omission responses within each *k*-means group.

SF neural decoding was performed using Linear Discriminant Analysis in Python scikit-learn package (default parameters; Virtanen et al., 2020). Population spike counts from different time windows were used to train classifiers. We used 4-fold cross-validation with five repeats. The number of folds was chosen

so that the test size was not below 30 samples. We also trained logistic regression (multinomial) and SVM (with RBF kernel) classifiers (data not shown), but LDA gave better performance given the number of parameters to specify. The number of units used for training was comparable in both groups. For example, decoding from the 0.35 to 0.45 s interval was performed using 1,324 units from WT and 1,226 units from FX.

Statistical Analysis

We used scipy.stats Python library to perform statistical analysis. Data were not tested for normality of residuals, and only non-parametric tests were used. Mann–Whitney *U* test was used to compare two independent populations. It was used to compare a trial-averaged LFP and neuronal firing rate in response. *P*-values were adjusted using a Benjamini–Hochberg procedure that controls for a false discovery rate. Kolmogorov–Smirnov 2 sample test was used to compare distributions of iSSA and iMM indices between WT and FX mice in different layers.

RESULTS

Enhanced Oddball Responses in LFP of FX Mice

Using 64 channel silicon probes that span the cortical depth of V1 (Shobe et al., 2015b), we investigated visual processing of spatial frequencies (SF) during tuning (many standards control) and oddball paradigm in awake head-fixed WT and FX mice (**Figures 1A,B**). For SF tuning, we presented animals with SF filtered visual noise stimuli using six different non-overlapping SF bands (**Figures 1C,D**). Stimuli of the same band have the same spatial frequency but a different overall global pattern. These stimuli have been previously validated for tuning measurements. Furthermore, there was no significant difference between WT and FX mice in neural response variability to the same SF band with different overall patterns (**Supplementary Figure 1**). Oddball responses were analyzed by comparing responses to standard (STD) and control (CTR) stimuli for SSA and delayed part of STD and deviant (DEV) responses for calculating the mismatch (MM) response (**Figures 1E,F**). In contrast to previous animal oddball studies, our STD and DEV have the same low-level features (SF), so that increased delayed part of the DEV response can be attributed to change detection.

We first focused on oddball responses in local field potential (LFP), which represents local population subthreshold activities. We found adaptation and mismatch responses in layer 4 LFP of both genotypes (**Figures 2A,C**). Interestingly, MM responses but not SSA were stronger in FX animals [**Figures 2B,D**, SSA: STD vs. CTR WT (P = 0.0057), FX (0.002); WT vs. FX STD (P = 0.440), CTR (P = 0.105); MM: STD vs. DEV WT (P = 0.0016), FX (P = 0.0002), WT vs. FX STD (0.075), DEV (P = 0.015), n = 17 and 15 mice, Mann–Whitney *U* test, *p*-values were adjusted for multiple comparisons using the Benjamini–Hochberg method]. Time-frequency analysis was then performed on L4 LFP to investigate whether any frequency bands are modulated by oddball responses (**Figure 2E**). Entire duration of DEV response was used, so that the window is big enough to quantify low frequency oscillations. We found that only theta oscillations were modulated by the oddball responses in both genotypes [**Figure 2F**, STD vs. DEV: theta WT (P = 0.021) and FX (P = 0.0006); alpha WT (P = 0.089) and FX (P = 0.089); beta WT (P = 0.45) and FX (P = 0.45); low gamma WT (P = 0.21 and FX (P = 0.40), high gamma WT (P = 0.05) and FX (P = 0.05); WT vs. FX STD and DEV all bands ($P > 0.05$), n = 17 WT and 15 FX mice, Mann–Whitney *U* test, *p*-values were adjusted for multiple comparisons within each frequency band using the Benjamini–Hochberg method].

Excessive Processing of High Spatial Frequencies in V1 of FX Mice in Late Unit Responses

We next focused on single-unit activity during tuning (control) and oddball sequence. The time course heatmap of SF tuning revealed enhanced activity in late unit responses in all layers of FX animals, especially at higher SF (**Figure 3A**). To obtain a preferred SF for each unit, we fitted a Difference-of-Gaussian model to tuning curves, which were obtained by averaging the firing rate within 0.05–0.2 s relative to the stimulus onset (**Figure 3B**). We did not observe any differences in the distribution of preferred SF or Q-factor (tuning sharpness) between genotypes (**Figure 3C**) WT vs. FX pref SF (P = 0.357), n = 949 and 705 units; Q-factor (P = 0.404), n = 192 and 126 units, Kolmogorov–Smirnov 2 sample test). The population mean responses to different SF stimuli revealed enhanced activity in late unit responses at high SF (**Figure 3D**). To quantify these differences, we averaged firing rates within different time windows: 0.05–0.2 s for early and 0.2–0.5 s for late visual responses. We found a significantly stronger response at higher SF (>0.06 cpd) in late visual responses [**Figure 3D** right, WT vs. FX 0.05–0.2 s all stimuli ($P > 0.05$), 0.2–0.5 s: SF 7.5e-3–0.06 ($P > 0.05$), SF 0.12 (P = 0.014), and SF 0.24 (P = 0.035), n = 1,057 and 820 units, Mann–Whitney *U* test, *p*-values were adjusted for multiple comparisons using the Benjamini–Hochberg method].

Next, SF neural decoding was performed using population spike counts (**Figure 3E**). We reasoned that enhanced processing of higher SF might lead to enhanced detection of these stimuli in FX mice. Classifiers were trained on spike counts from different time windows of WT and FX mice using a linear discriminant analysis with 4-fold cross-validation with five repeats. Classifiers trained on spike counts from 0.05–0.5 s performed similarly (SF classification mean ± SEM % error WT vs. FX: 9.1 ± 0.9 vs. 12.0 ± 1). WT classifiers performed slightly better in early time windows (SF classification mean ± SEM % error WT vs. FX 0.05–0.15 s: 16.3 ± 1.1 vs. 23.1 ± 1.8; 0.15–0.25 s: 6.7 ± 0.9 vs 10.7 ± 1.1). However, classifiers trained on the intervals after 0.25 s show a reduced error in FX vs. WT mice (SF classification mean ± SEM % error WT vs. FX 0.25–0.35 s: 22.5 ± 1.4 vs. 16.3 ± 1.7; 0.35–0.45 s: 26.0 ± 1.6 vs. 15.0 ± 1.6), suggesting enhanced processing in late neural responses.

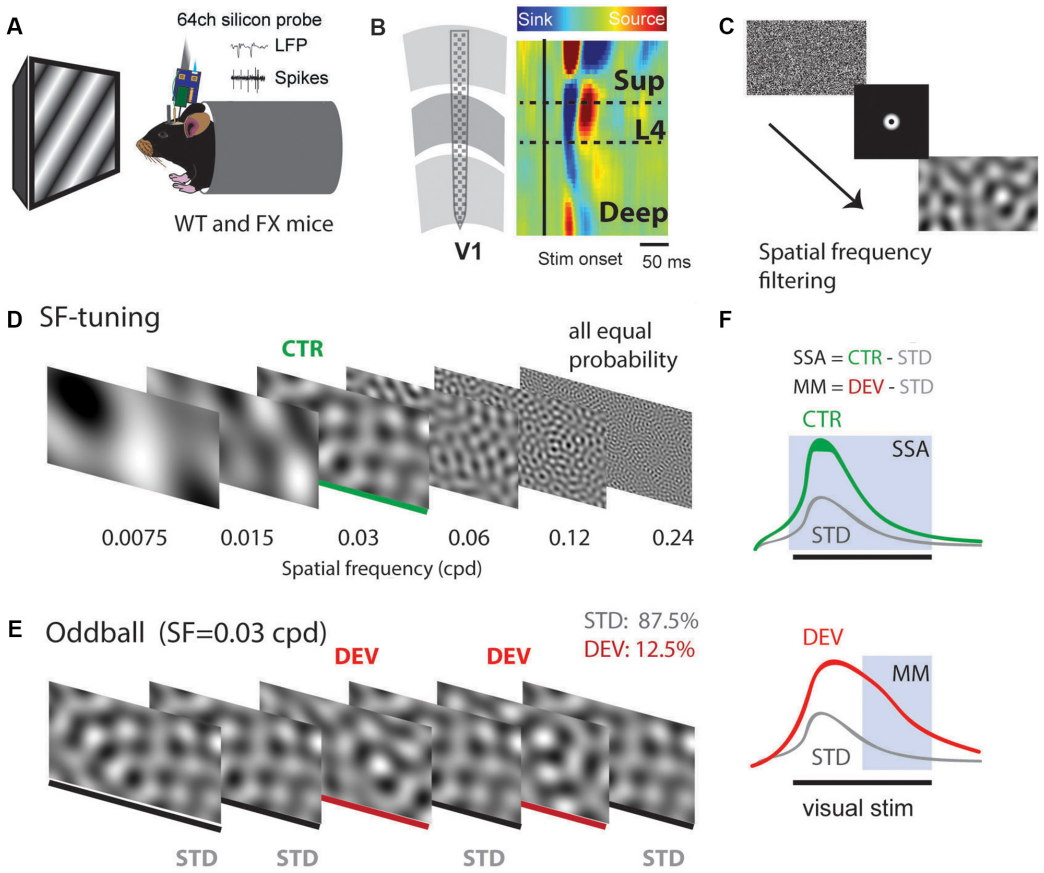

FIGURE 1 | A visual oddball paradigm with all the stimuli containing the same low-level features [spatial frequency (SF)] but different global SF patterns and expectancy. **(A)** *In vivo* extracellular silicon probe recordings in V1 of head-fixed mice. **(B)** Schematic of a 64-channel silicon probe spanning the whole cortical depth and an example of current source density (CSD) heatmap. **(C)** To generate visual stimuli, we performed SF filtering of white noise. **(D)** We used six different non-overlapping SF bands from 7.5E-3 to 0.24 cpd for spatial frequency tuning (many standards control). Stimuli were presented in a pseudorandom order and had equal probability. **(E)** The oddball sequence contained stimuli of the same SF (0.03 cpd) that only differ in their probability and overall texture. Standard (STD) and deviant (DEV) stimuli were presented with a probability of 0.875 and 0.125, respectively. **(F)** Given that STD and DEV have the same low-level features (SF), we computed a neuronal mismatch (MM) response by comparing late (0.3–0.5 s) responses of STD and DEV. Stimulus-specific adaptation (SSA) was obtained by comparing STD and CTR. Since both STD and DEV had the same SF, neural population activity is expected to be adapted during the oddball.

Together, these findings suggest an enhancement of processing in late neural responses in FX vs. WT mice, especially at high spatial frequencies.

Both SSA and MM Are Present in SF Tuned Units

To investigate whether adaptation and change detection depend on the tuning properties of the units, we split neurons based on their preferred SF. It was defined as a peak (maximum) of the fitted tuning curve of the unit. Based on preferred SF, we then split units into three groups: tuned_in group included neurons with preferred SF that was within ±1 octave of the oddball SF, 0.03 cpd (0.015 < pref SF < 0.06; **Figure 4A**, gray shaded region); tuned_out group included units with preferred SF that was outside the ± 1 octave of the oddball SF (pref SF < 0.015 or pref SF > 0.06; **Figure 4G**, gray shaded region); the untuned group included units that did not show any SF tuning, so that curve fitting was not successful or fitting error was larger than 0.9 ("Materials and Methods" section).

We first focused on oddball responses of tuned_in units (**Figures 4A–F**). iSSA and iMM modulation indices [−1, +1] quantify how strong a given unit is adapted and report MM response correspondingly (positive values indicate stronger modulation). We observed that the majority of tuned_in neurons show both SSA and MM in both genotypes [**Figure 4B**, note marginal distributions). Direct comparison of iSSA and iMM distributions did not reveal any differences between WT and FX mice (**Figure 4C**, WT vs. FX iSSA (P = 0.803) and iMM (P = 0.325), n = 201 and 147 units, Kolmogorov–Smirnov 2 sample test]. Unit population responses revealed an overall strong adaptation in both genotypes, which is not surprising given that the preferred SF of these units was close to the oddball SF. Interestingly, tuned_in units also show strong MM responses [**Figure 4F**, STD vs. CTR WT (P = 1.04e-10) and FX (P = 1.58e-7); STD vs. DEV WT (P = 0.0003) and FX (P = 0.0002),

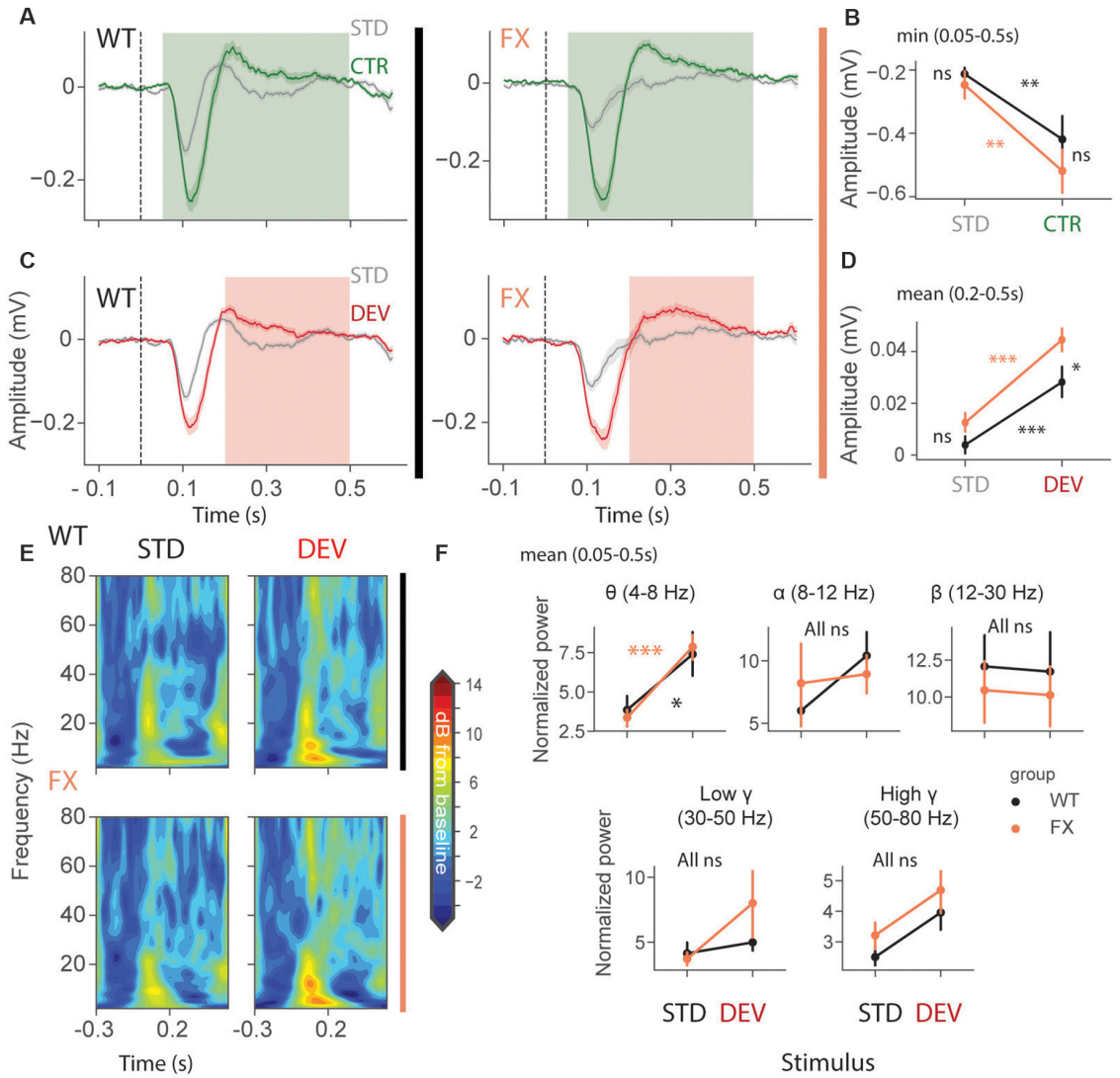

FIGURE 2 | Enhanced late responses in L4 of FX mice during a visual oddball paradigm. **(A)** Averaged layer 4 LFP traces in response to STD and CTR stimuli for WT (left) and FX (right) from cortical layer 4. **(B)** The point plots show the mean and s.e.m. of the strongest negative deflection within 0.05–0.5 s relative to the stimulus onset. **(C)** Same as in **(A)** but comparing STD vs. DEV. **(D)** Same as in **(B)**, but responses were averaged within 0.2–0.5 s. **(E)** Time-frequency spectra of the L4 LFP traces of WT (top) and FX (bottom). **(F)** Point plots show the mean power within 0.05–0.5 s relative to the stimulus onset across different frequency bands. $^{*}p < 0.05$, $^{**}p < 0.01$, $^{***}p < 0.001$, ns = not significant.

n = 249 and 184 units, Mann–Whitney U test]. This diverges from theories suggesting that enhancement of DEV response is primarily due to the non-adapted units in the local microcircuit (Ross and Hamm, 2020). The proportion of tuned_in units was comparable between genotypes (**Supplementary Figure 2**). Tuned_out units also showed both SSA and MM at the single-unit level (**Figure 4H**). Distribution of iMM but not iSSA was significantly different between groups [**Figure 4I**, WT vs. FX iSSA (P = 0.102) and iMM (P = 0.019), n = 235 and 193 units, Kolmogorov–Smirnov 2 sample test]. There was a significant adaptation at the population level in both genotypes, which suggests that adaptation spreads to the units preferring distant SFs (**Figures 4J,K**). Strong MM responses were also present in both genotypes [**Figure 4L**, STD vs. CTR WT (P = 9.04e-8) and FX (P = 0.014); STD vs. DEV WT (P = 2.58e-7) and FX (P = 0.0006), n = 341 and 278 units, Mann–Whitney U test].

Altered Oddball Responses in Untuned and Inhibited Units of FX Mice

An identical analysis was performed for untuned and inhibited unit oddball responses (**Figure 5**). Untuned units are not tuned to a particular SF (**Figure 5A**), and the inhibited group was suppressed by visual stimuli. Oddball responses in the untuned group were diverse in both genotypes (**Figure 5B**). We found a significant difference in iMM distribution between genotypes [**Figure 5C**, WT vs. FX iSSA (P = 0.061) and iMM (P = 0.023),

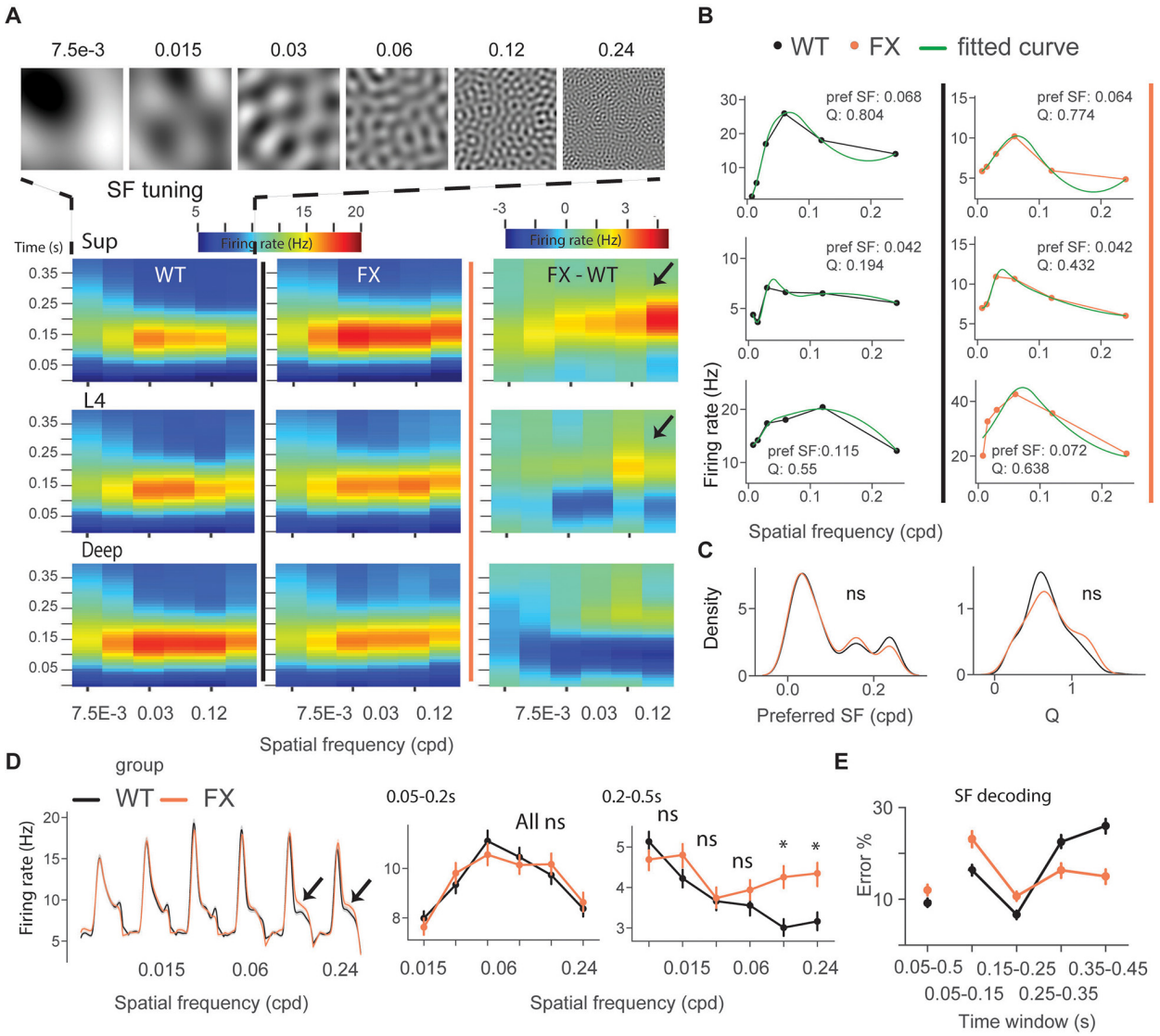

FIGURE 3 | Excessive processing of high SF stimuli in late responses of single units in FX mice. **(A)** Time-course analysis of SF tuning across the cortical layers. Unit responses for different SF stimuli were plotted for each time step to create the heatmaps for WT (left), FX (middle), and FX-WT (right). **(B)** SF tuning curves were computed by averaging responses within 0.05–0.2 s relative to the stimulus onset and fitted using Difference-of-Gaussians. Example plots are shown for WT (left) and FX mice (right). **(C)** Distribution of preferred SF (left) and Q-factor (right) for both groups. The larger Q values indicate sharper tuning. **(D)** Population average firing rates of all units in response to the SF tuning sequence. Note enhanced late part responses at higher SF. The population mean SF tuning responses were averaged for different time intervals. 0.05–0.2 (left) and 0.2–0.5 s (right). **(E)** Population spike counts from different time windows were used for SF neural decoding. The classifiers that were trained on responses after 0.25 s relative to stimulus onset had a lower error in FX vs. WT mice. *$p < 0.05$, ns = not significant.

n = 178 and 145 units, Kolmogorov–Smirnov 2 sample test]. Unit population responses showed adaptation in both genotypes, whereas MM was not present in WT animals, the latter part of the STD response was slightly stronger than DEV [**Figures 5D–F**, STD vs. CTR WT (P = 1.52–5) and FX (P = 0.0011); STD vs. DEV WT (P = 0.023) and FX (P = 0.0003), n = 257 and 177 units, Mann–Whitney U test]. Interestingly, DEV and CTR evoked significantly stronger inhibition in FX, but not in WT mice [**Figures 5G–I**, STD vs. CTR WT (P = 0.226) and FX (P = 0.011); STD vs. DEV WT (P = 0.065) and FX (P = 0.005), n = 94 and 61 units, Mann–Whitney U test]. Contextual modulation of inhibited units in FX but not in WT mice might suggest an altered coupling of regular and fast-spiking (RS and FS) neurons.

Adaptation Depends on the Spatial Frequency Tuning of the Units and Is Reduced in FX Animals

We next directly compared iSSA and iMM magnitude across different tuning groups and genotypes (**Figure 6A**). First, we observed that iSSA was significantly larger in tuned_in compared to other groups in both genotypes. Interestingly, tuned_out units show stronger adaptation than untuned in WT, but

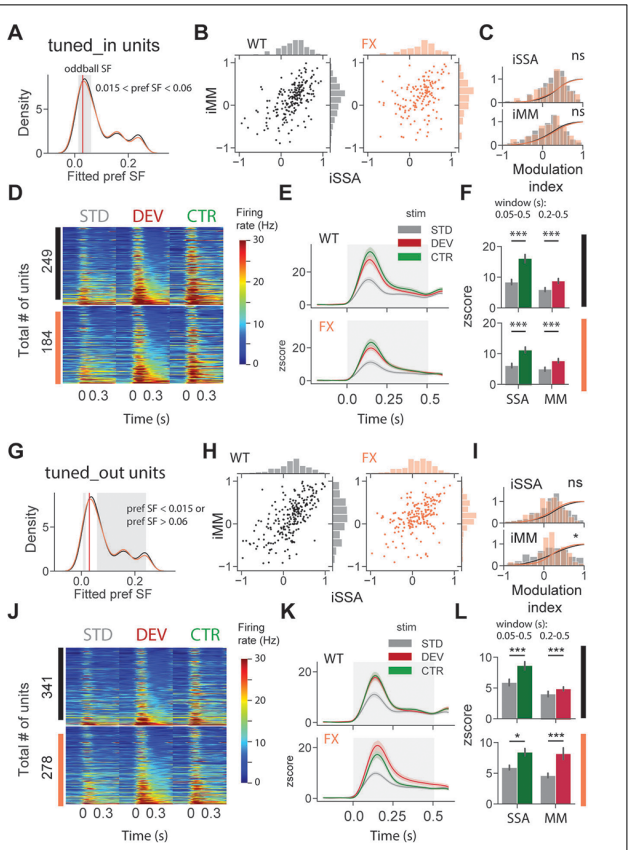

FIGURE 4 | SSA and MM are present in single units tuned to various spatial frequencies of both genotypes. **(A)** Distribution of preferred SF of two different genotypes. Gray shaded area represents tuned_in group, which included units with preferred SF that lies ±1 octave of oddball SF (0.03, red vertical line). **(B)** Distribution of iSSA and iMM modulation indices for WT and FX mice (each point is a single unit). **(C)** Superimposed distributions of iSSA and iMM with KDE. **(D)** The heatmaps show single-unit firing rates in response to STD, DEV, and CTR stimuli across different genotypes. (**E**) The line plots show the mean *z*-scored responses of the units from the heatmaps. **(F)** The point plots show the mean ± SEM of the *z*-scored firing rate between 0.05 and 0.5 s for SSA and 0.2–0.5 s for MM relative to the stimulus onset. **(G–L)** Same as in **(A–F)** but for units which preferred SF was outside 1 octave of the oddball SF. $^{*}p < 0.05$, $^{***}p < 0.001$, ns = not significant.

not in FX animals. Furthermore, iSSA was significantly larger in WT vs. FX tuned_out units [**Figure 6A** top, iSSA: WT tuned_in vs. tuned_out (P = 0.005), tuned_in vs. untuned (P = 1.45e-8), tuned_out vs. untuned (P = 0.005); FX tuned_in vs. tuned_out (P = 0.0003), tuned_in vs. untuned (P = 0.002), tuned_out vs. untuned (P = 0.465); WT vs. FX tuned_in (P = 0.419), tuned_out (P = 0.041), and untuned (P = 0.252), n = 201, 235 and 178 WT units, 147, 193, and 145 FX units, Mann–Whitney U test, p-values were adjusted for multiple comparisons using the Benjamini–Hochberg method]. MM responses, on the other hand, were not significantly modulated by tuning properties of neurons [**Figure 6A** top, all comparisons (P > 0.05)]. We did not observe any systematic patterns between iSSA/iMM and preferred SF at the single unit level (**Supplementary Figure 4**).

It has been recently reported that FS neurons are differentially modulated in V1 of FX mice. Thus, we investigated whether oddball processing is altered in FS units (**Supplementary Figure 3**). SSA and MM responses were observed in FS of both genotypes (**Supplementary Figure 3**). We thus decided to investigate how iSSA and iMM are represented in RS and FS units. We observed that difference in RS rather than FS units mostly accounted for the differences observed across different tuning groups and genotypes [**Figures 6B,C** top, RS: WT tuned_in vs. tuned_out (P = 0.041), tuned_in vs. untuned (P = 7.0e-5), tuned_out vs. untuned (P = 0.013); FX tuned_in vs. tuned_out (P = 0.008), tuned_in vs. untuned (P = 0.011), tuned_out vs. untuned (P = 0.438); WT vs. FX tuned_in (P = 0.335), tuned_out (P = 0.036), and untuned (P = 0.461), n = 150, 175, and 141 WT units, 109, 148, and 101 FX units; **FS**: WT tuned_in vs. untuned (P = 0.003), all other comparisons (P > 0.05), Mann–Whitney U test, p-values were adjusted for multiple comparisons using the Benjamini–Hochberg method]. MM responses were not significantly modulated by tuning properties in RS and FS units [**Figures 6B,C** top, all comparisons (P > 0.05)]. The proportion of units in each subgroup was comparable between genotypes (**Supplementary Figure 2**). Overall, our results suggest that adaptation depends on the tuning properties of units but not their laminar position along with reduced feature co-adaptation in FX animals.

Impaired Laminar Processing of MM Responses in FX Mice

To gain insight into laminar processing of oddball responses, we quantified population level iSSA and iMM modulation indices across different cortical layers (**Figure 7**). Adaptation was similarly represented across the cortical column in both genotypes, however, there was a trend towards stronger iSSA in superficial layers of WT mice [**Figures 7A–C** top, all comparisons (P > 0.05)]. iMM responses, on other hand, were significantly modulated by cortical layers. They were significantly stronger in L2/3 vs. L4 and L5/6 in WT, however, there was not any laminar preference for MM responses in FX mice. Furthermore, L4 MM responses were significantly stronger in FX vs. WT mice [**Figure 7A** top, iMM: WT tuned_in vs. tuned_out (P = 0.0018), tuned_in vs. untuned (P = 0.04), tuned_out vs. untuned (P = 0.242); FX tuned_in vs. tuned_out (P = 0.281), tuned_in vs. untuned (P = 0.431), tuned_out vs. untuned (P = 0.319); WT vs. FX tuned_in (P = 0.431), tuned_out (P = 0.042), and untuned (P = 0.068), n = 208, 191 and 215 WT units, 154, 153, and 1,178 FX units, Mann–Whitney U test, p-values were adjusted for multiple comparisons using the Benjamini–Hochberg method]. RS units showed similar oddball responses [**Figure 7B**, iMM RS: WT tuned_in vs. tuned_out (P = 0.005), tuned_in vs. untuned (P = 0.04), tuned_out vs. untuned (P = 0.237); FX tuned_in vs. tuned_out (P = 0.281), tuned_in vs. untuned (P = 0.321), tuned_out vs. untuned (P = 0.148); WT vs. FX tuned_in (P = 0.237), tuned_out (P = 0.189), and untuned (P = 0.085), n = 129, 154 and 183 WT units, 87, 122, and 149 FX units; **FS**: all comparisons (P > 0.05), Mann–Whitney U test, p-values were adjusted for multiple comparisons using the Benjamini–Hochberg method]. iSSA and iMM responses in FS

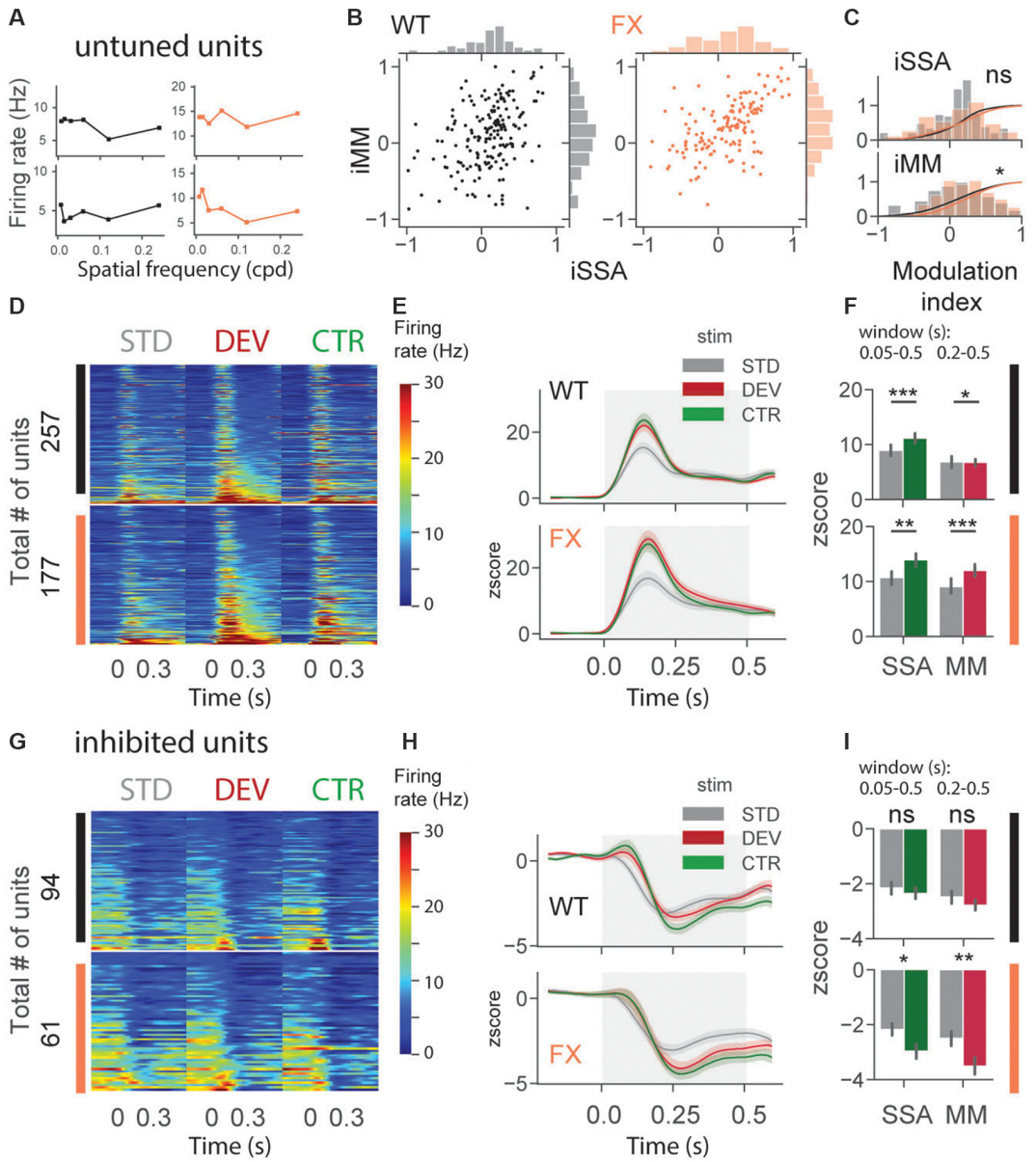

FIGURE 5 | Altered oddball responses in untuned and inhibited units of FX mice. **(A)** Example SF tuning curves of untuned neurons. Two criteria were used to identify those units: (1) failure of DOG model fitting or (2) high fitting error (>0.9). **(B)** Distribution of iSSA and iMM modulation indices for WT and FX mice (each point is a single unit). **(C)** Superimposed distributions of iSSA and iMM with KDE. **(D)** The heatmaps show single-unit firing rates in response to STD, DEV, and CTR stimuli across different genotypes. **(E)** The line plots represent mean *z*-scored responses of the units from the heatmaps. **(F)** The point plots show the mean ± SEM of the *z*-scored firing rate between 0.05–0.5 s for SSA and 0.2–0.5 s for MM relative to the stimulus onset. **(G–I)** Same as in **(D–F)** but for inhibited units. $^{*}p < 0.05$, $^{**}p < 0.01$, $^{***}p < 0.001$, ns = not significant.

units were not significantly modulated by cortical layers, though there was a trend towards stronger adaptation in L4 of FX mice (**Figure 7C**). It is unlikely that tuning properties of neurons can explain these observations because there is no difference in cortical distribution of different tuning groups between WT and FX animals (**Supplementary Figure 5**). Taken together, these findings suggest that there is a laminar specialization for MM responses in WT but not in FX animals.

Altered Representation of Omission Responses in FX Mice

In a subset of animals, we performed omission experiments, in which every eighth stimulus was omitted (**Figure 8A**). Omission responsive neurons were defined as those with significantly different stimulus (0.05–0.35 s) vs. baseline (−0.25–0.05 s) responses (both excited and inhibited see **Supplementary Figures 6B–D**). Laminar analysis of omission

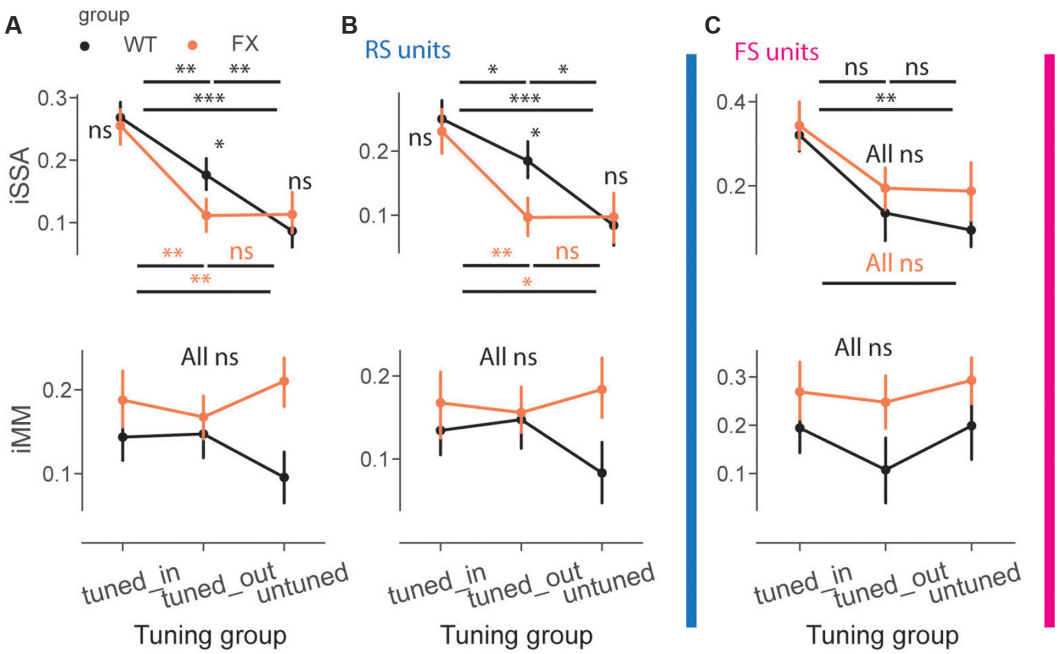

FIGURE 6 | Adaptation depends on the preferred SF of the units. **(A)** The point plots show iSSA and iMM magnitude for tuned_in, tuned_out, and untuned group for WT and FX for all units. **(B)** Same as in **(A)**, but for RS units. **(C)** Same as in **(A)**, but for FS units. *$p < 0.05$, **$p < 0.01$, ***$p < 0.001$, ns = not significant.

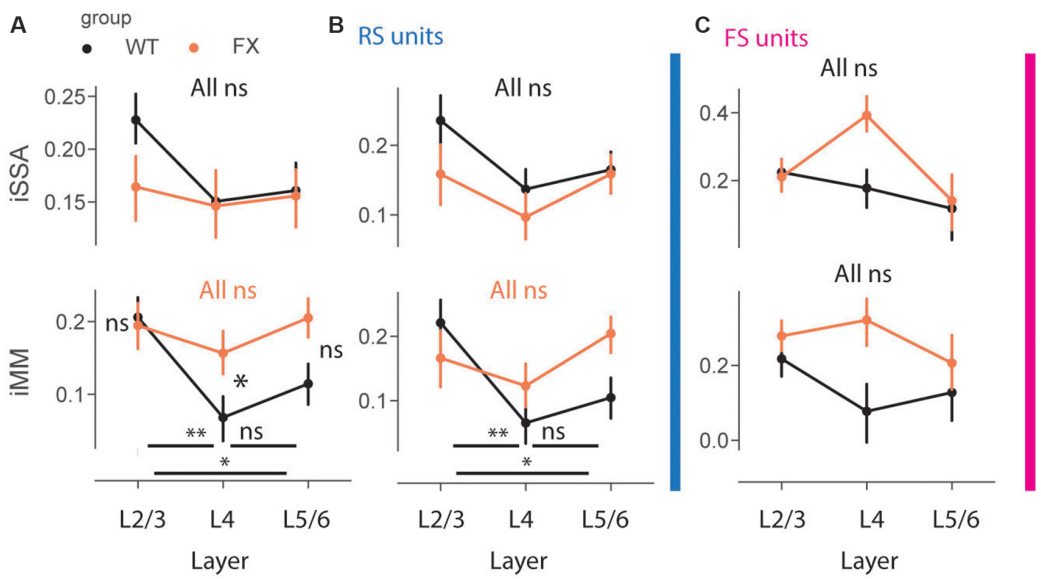

FIGURE 7 | Impaired laminar processing of MM responses in FX mice. **(A)** The point plots show iSSA and iMM magnitude for L2/3, L4, and L5/6 for WT vs. FX for all units. **(B)** Same as in **(A)**, but for RS units. **(C)** Same as in **(A)**, but for FS units. *$p < 0.05$, **$p < 0.01$, ns = not significant.

responses did not reveal any differences between WT and FX mice (**Supplementary Figure 6E**). We then decided to use an unsupervised clustering algorithm, *k*-means, to reveal neural dynamics during omissions of the stimulus. Clustering was performed on neural responses within 0.05–0.5 s relative to the stimulus onset from both genotypes. Using an elbow method, we determined that $k = 4$ was an optimal number of groups (**Figure 8B**). Given that genotype was independent of clustering, we were able to compare responses between WT and FX within each *k*-means group. Clustering revealed four different types of

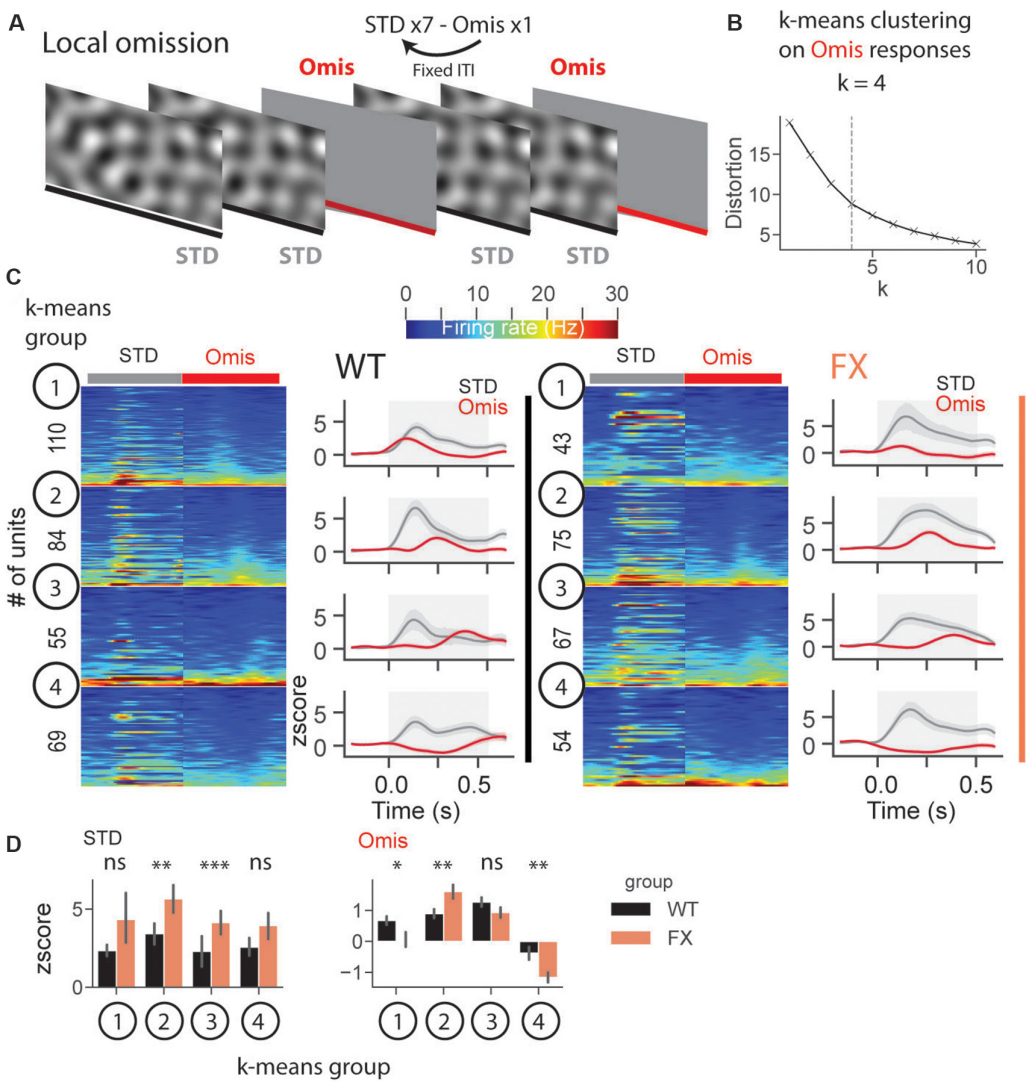

FIGURE 8 | Altered representation of omission responses in FX mice. **(A)** During the omission paradigm every eighth stimulus was not presented (omission). **(B)** The number of groups for *k*-means was determined using the elbow method. Clustering was performed on omission responses (0.05–0.5 s) from units of both genotypes. Given that genotype is independent of clustering, we compared neural responses between WT and FX within each *k*-means group. **(C)** The heatmaps of unit firing rate responses across different *k*-means groups and genotypes (left = STD, right = Omis). The line plots show the mean *z* score firing rate responses of units shown in the heatmaps. 1st *k*-means group shows early, 2nd group mid, and 3rd group late omission responses, and 4th group was inhibited by Omis. **(D)** The point plots show the mean ± SEM *z* score firing rate for STD (left) and Omis (right) responses for WT and FX. $^{*}p < 0.05$, $^{**}p < 0.01$, $^{***}p < 0.001$, ns = not significant.

responses: *k*-means group 1—early, group 2—mid, group 3—late omission responses, and group 4 was inhibited by the omission [**Figure 8C**). Direct comparison of STD between WT and FX revealed stronger responses in FX groups 2 (mid) and 3 (late), which might indicate reduced adaptation during the omission paradigm. Omission responses were stronger in *k*-means group 1 (early) in WT, whereas group 2 (mid), and group 4 (inhibited) were stronger in FX mice [**Figure 8D**, WT vs. FX *k*-means group 1 STD ($P = 0.436$), $n = 110$ and 43 units, Omis ($P = 0.042$), $n = 120$ and 45 units; group 2 STD ($P = 0.004$), $n = 84$ and 75 units, Omis ($P = 0.009$), $n = 85$ and 77 units; group 3 STD ($P = 0.0001$), $n = 55$ and 67 units, Omis ($P = 0.052$), $n = 58$ and 70 units, group 4 STD ($P = 0.200$), $n = 69$ and 54 units, Omis ($P = 0.005$), $n = 73$ and 59 units, Mann–Whitney U test]. Overall, we found the altered processing of omission responses in FX animals.

DISCUSSION

The lack of a common framework to explain the disparate sensory and social-cognitive deficits in FX and autism is a major roadblock to scientific progress and designing effective diagnostic and intervention tools. Atypical sensory processing has recently been recognized to be an important diagnostic

criterion for autism (American Psychiatric Association, 2013). Furthermore, early sensory alterations are predictive of social communication deficits later in life (Robertson and Baron-Cohen, 2017). Investigating the reproducible sensory perception paradigms in well-defined genetic models of autism provides a great opportunity to shed light on the neural basis of atypical sensory experience and its possible interaction with social-cognitive domains in ASD.

Here, we used a novel visual oddball paradigm and silicon probe recordings in V1 to investigate the neural basis of altered sensory perception in FX. Using SF tuning, we first demonstrated that high SF bands are excessively processed in the late stages of visual responses in FX mice. Increased firing rate and lower SF decoding errors at late stages of processing are indicative of over-processing of details. This finding is consistent with previous psychophysical and physiology studies showing altered spatiotemporal processing of high SF information in autism (Kéïta et al., 2014; Caplette et al., 2016). Interestingly, we didn't observe any difference in SF tuning between genotypes while focusing on peak responses.

Using SF oddball paradigm, we then showed that there was a differential contextual processing in V1 of FX mice across different cortical layers and unit types (**Table 1**). To investigate the feature specificity of SSA and MM responses, we split neurons into three groups based on their SF preference. We discovered that adaptation was more dependent on the tuning preferences rather than the laminar position of the units. SSA was strongest in tuned_in units in both genotypes, which is not surprising given that their preferred SF was close to the oddball SF (Chen et al., 2015). We observed comparable adaptation levels in tuned_in and tuned_out group in WT but not in FX animals (**Table 1**). Interestingly, RS but not FS units were mostly responsible for the observed differences. Analysis of SSA across different cortical layers revealed the strongest adaptation in L2/3 in WT, but it did not reach significant after adjustment for multiple comparisons. Overall, SSA was dependent on the preferred SF of the units and covered a narrower range of spatial frequencies in FX compared to WT animals. This observation might be explained by the reduced spread of adaptation (co-adaptation to neighboring SF) in FX. Our results may provide a mechanism for the reduced habituation and sensory hypersensitivity in FX and autism.

Mismatch responses, on the other hand, were more dependent on the laminar position rather than the tuning preference of units. MM responses were present in the adapted units, suggesting that single units might report mismatch despite strong adaptation levels (Ross and Hamm, 2020). L2/3 had the strongest MM responses in WT, but not in FX, where they were equally represented across the cortical column. Furthermore, L4 MM responses were significantly stronger in FX mice (**Table 1**). These observations might be explained by the altered intrinsic properties of L4 neurons similar to the previously reported observations in the somatosensory cortex (Booker et al., 2019). The lack of laminar specialization for MM in FX might also be linked to the altered information processing in L4 barrel cortex (Domanski et al., 2019). It is important to note that RS units were mostly responsible for the observed differences in MM. This observation is consistent with the previous studies of the reduced excitatory drive onto FS units, which may potentially explain the altered dynamics of FS interneurons (Gibson et al., 2008; Goel et al., 2018).

Lastly, we observed the altered neural dynamics in FX animals during the omission paradigm. Interestingly, STD responses were weaker in WT vs. FX animals, which might be indicative of reduced adaptation in FX animals. Our unsupervised clustering revealed four different types of responses to stimulus omissions. Interestingly, these groups had different temporal patterns covering the whole omission duration with early, mid, late peak responses and inhibition. Early omission responses were stronger in WT, whereas mid and inhibition ones were enhanced in FX animals. We also observed increased delayed responses during SF tuning, oddball, and omission paradigms, which suggests that it might be a common pattern in FX circuits (**Table 1**). Given the regularity of omission responses (every eighth stimulus) and fixed inter-trial-interval, we expected the animals to be entrained by the sequence. Overall, reduced STD responses and stimulus timing-locked omission responses suggest that WT but not FX animals were able to learn the regularity of the sequence of stimuli.

In conclusion, we extend prior oddball studies by showing how tuning properties, laminar position, and spiking profile of the neurons influence the contextual processing of visual information. Our discovery of reduced adaptation and altered laminar processing in FX mice provides the mechanistic circuit-level understanding of the impaired sensory perception in FX and might lead to potential diagnostic and therapeutic advances.

TABLE 1 | Summary of differences in oddball and omission responses between WT and FX animals.

Oddball/pref SF	**Tuned_in**	**Tuned_out**	**Untuned**	
iSSA	ns	↑*	ns	
iMM	ns	ns	ns	
Oddball/Layer	**L2/3**	**L4**	**L5/6**	
iSSA	ns	ns	ns	
iMM	ns	↓*	ns	
Omission/*k*-means	**Group 1**	**Group 2**	**Group 3**	**Group 4**
STD	ns	↓**	↓***	ns
Omis	↑*	↓**	ns	↓**

*↑ stronger in WT and weaker in FX; ↓ weaker in WT and stronger in FX; *p < 0.05, **p < 0.01, ***p < 0.001, ns = not significant.*

DATA AVAILABILITY STATEMENT

The raw data supporting the conclusions of this article will be made available by the authors, without undue reservation.

ETHICS STATEMENT

The animal study was reviewed and approved by PACUC.

AUTHOR CONTRIBUTIONS

AP and AC designed the study. AP and SK performed the experiments. AP analyzed the data. AP, SK, and AC wrote the manuscript. All authors contributed to the article and approved the submitted version.

FUNDING

This work was funded by the National Institute of Mental Health (R01 MH116500) to AC.

ACKNOWLEDGMENTS

We thank Sotiris Masmanidis for providing silicon probes, Maria Dadarlat for feedback on the manuscript, and Chubykin lab members for useful discussions.

SUPPLEMENTARY MATERIAL

The Supplementary Material for this article can be found online at: https://www.frontiersin.org/articles/10.3389/fncel.2021.668230/full#supplementary-material.

REFERENCES

American Psychiatric Association (2013). *Diagnostic and Statistical Manual of Mental Disorders*, 5th edition Washington, DC: American Psychiatric Press Inc.

Booker, S. A., Domanski, A. P. F., Dando, O. R., Jackson, A. D., Isaac, J. T. R., Hardingham, G. E., et al. (2019). Altered dendritic spine function and integration in a mouse model of fragile X syndrome. *Nat Commun.* 10:4813. doi: 10.1038/s41467-019-11891-6

Boyd, B. A., Baranek, G. T., Sideris, J., Poe, M. D., Watson, L. R., Patten, E., et al. (2010). Sensory features and repetitive behaviors in children with autism and developmental delays. *Autism Res.* 3, 78–87. doi: 10.1002/aur.124

Bredfeldt, C. E., and Ringach, D. L. (2002). Dynamics of spatial frequency tuning in macaque V1. *J. Neurosci.* 22, 1976–1984. doi: 10.1523/JNEUROSCI.22-05-01976.2002

Caplette, L., Wicker, B., and Gosselin, F. (2016). Atypical time curse of object recognition in autism spectrum disorder. *Sci. Rep.* 6:35494. doi: 10.1038/srep35494

Chen, I. -W., Helmchen, F., and Lütcke, H. (2015). Specific early and late oddball-evoked responses in excitatory and inhibitory neurons of mouse auditory cortex. *J. Neurosci.* 35, 12560–12573. doi: 10.1523/JNEUROSCI.2240-15.2015

Domanski, A. P. F., Booker, S. A., Wyllie, D. J. A., Isaac, J. T. R., and Kind, P. C. (2019). Cellular and synaptic phenotypes lead to disrupted information processing in Fmr1-KO mouse layer 4 barrel cortex. *Nat. Commun.* 10:4814. doi: 10.1038/s41467-019-12736-y

Freund, L. S., and Reiss, A. L. (1991). Cognitive profiles associated with the fra(X) syndrome in males and females. *Am. J. Med. Genet.* 38, 542–547. doi: 10.1002/ajmg.1320380409

Gibson, J. R., Bartley, A. F., Hays, S. A., and Huber, K. M. (2008). Imbalance of neocortical excitation and inhibition and altered UP states reflect network hyperexcitability in the mouse model of fragile X syndrome. *J. Neurophysiol.* 100, 2615–2626. doi: 10.1152/jn.90752.2008

Goel, A., Cantu, D. A., Guilfoyle, J., Chaudhari, G. R., Newadkar, A., Todisco, B., et al. (2018). Impaired perceptual learning in a mouse model of Fragile X syndrome is mediated by parvalbumin neuron dysfunction and is reversible. *Nat. Neurosci.* 21, 1404–1411. doi: 10.1038/s41593-018-0231-0

Haberl, M. G., Zerbi, V., Veltien, A., Ginger, M., Heerschap, A., and Frick, A. (2015). Structural-functional connectivity deficits of neocortical circuits in the Fmr1$^{(-/y)}$ mouse model of autism. *Sci. Adv.* 1:e1500775. doi: 10.1126/sciadv.1500775

Hamm, J. P., and Yuste, R. (2016). Somatostatin interneurons control a key component of mismatch negativity in mouse visual cortex. *Cell Rep.* 16, 597–604. doi: 10.1016/j.celrep.2016.06.037

Hawken, M. J., and Parker, A. J. (1987). Spatial properties of neurons in the monkey striate cortex. *Proc. R Soc. Lond. B Biol. Sci.* 231, 251–288. doi: 10.1098/rspb.1987.0044

Kéïta, L., Guy, J., Berthiaume, C., Mottron, L., and Bertone, A. (2014). An early origin for detailed perception in autism spectrum disorder: biased sensitivity for high-spatial frequency information. *Sci. Rep.* 4;5475. doi: 10.1038/srep05475

Kissinger, S. T., Pak, A., Tang, Y., Masmanidis, S. C., and Chubykin, A. A. (2018). Oscillatory encoding of visual stimulus familiarity. *J. Neurosci.* 38, 6223–6240. doi: 10.1523/JNEUROSCI.3646-17.2018

Kissinger, S. T., Wu, Q., Quinn, C. J., Anderson, A. K., Pak, A., and Chubykin, A. A. (2020). Visual experience-dependent oscillations and underlying circuit connectivity changes are impaired in Fmr1 KO mice. *Cell Rep.* 31:107486. doi: 10.1016/j.celrep.2020.03.050

Musall, S., Haiss, F., Weber, B., and Von Der Behrens, W. (2015). Deviant processing in the primary somatosensory cortex. *Cereb. Cortex* 27, 863–876. doi: 10.1093/cercor/bhv283

Naatanen, R., Gaillard, A. W., and Mantysalo, S. (1978). Early selective-attention effect on evoked potential reinterpreted. *Acta Psychol.* 42, 313–329. doi: 10.1016/0001-6918(78)90006-9

Pachitariu, M., Steinmetz, N., Kadir, S., Carandini, M., and Harris, K. D. (2016). Kilosort: realtime spike-sorting for extracellular electrophysiology with hundreds of channels. *bioRxiv* [Preprint]. doi: 10.1101/061481

Pak, A., Ryu, E., Li, C., and Chubykin, A. A. (2020). Top-down feedback controls the cortical representation of illusory contours in mouse primary visual cortex. *J. Neurosci.* 40, 648–660. doi: 10.1523/JNEUROSCI.1998-19.2019

Parras, G. G., Nieto-Diego, J., Carbajal, G. V., Valdés-Baizabal, C., Escera, C., and Malmierca, M. S. (2017). Neurons along the auditory pathway exhibit a hierarchical organization of prediction error. *Nat. Commun.* 8:2148. doi: 10.1038/s41467-017-02038-6

Peirce, J. (2009). Generating stimuli for neuroscience using PsychoPy. *Front. Neuroinform.* 2:10. doi: 10.3389/neuro.11.010.2008

Rais, M., Binder, D. K., Razak, K. A., and Ethell, I. M. (2018). Sensory processing phenotypes in fragile X syndrome. *ASN Neuro* 10:1759091418801092. doi: 10.1177/1759091418801092

Robertson, C. E., and Baron-Cohen, S. (2017). Sensory perception in autism. *Nat. Rev. Neurosci.* 18, 671–684. doi: 10.1038/nrn.2017.112

Ross, J. M., and Hamm, J. P. (2020). Cortical microcircuit mechanisms of mismatch negativity and its underlying subcomponents. *Front. Neural Circuits* 14:13. doi: 10.3389/fncir.2020.00013

Rossant, C., Kadir, S. N., Goodman, D. F. M., Schulman, J., Hunter, M. L. D., Saleem, A. B., et al. (2016). Spike sorting for large, dense electrode arrays. *Nat. Neurosci.* 19:634. doi: 10.1038/nn.4268

Shobe, J. L., Claar, L. D., Parhami, S., Bakhurin, K. I., and Masmanidis, S. C. (2015a). Brain activity mapping at multiple scales with silicon microprobes

containing 1,024 electrodes. *J. Neurophysiol.* 114, 2043–2052. doi: 10.1152/jn.00464.2015

Shobe, J. L., Claar, L. D., Parhami, S., Bakhurin, K. I., and Masmanidis, S. C. (2015b). Brain activity mapping at multiple scales with silicon microprobes containing 1,024 electrodes. *J. Neurophysiol.* 114, 2043–2052. doi: 10.1152/jn.00464.2015

Sokhadze, E., Lamina, E., Casanova, E., Kelly, D., Opris, I., Khachidze, I., et al. (2017). Atypical processing of novel distracters in a visual oddball task in autism spectrum disorder. *Behav. Sci.* 7:79. doi: 10.3390/bs7040079

Turner-Brown, L. M., Baranek, G. T., Reznick, J. S., Watson, L. R., and Crais, E. R. (2012). The first year inventory: a longitudinal follow-up of 12-month-old to 3-year-old children. *Autism* 17, 527–540. doi: 10.1177/1362361312439633

Ulanovsky, N., Las, L., and Nelken, I. (2003). Processing of low-probability sounds by cortical neurons. *Nat. Neurosci.* 6, 391–398. doi: 10.1038/nn1032

Van Der Molen, M. J., Van Der Molen, M. W., Ridderinkhof, K. R., Hamel, B. C., Curfs, L. M., and Ramakers, G. J. (2012). Auditory and visual cortical activity during selective attention in fragile X syndrome: a cascade of processing deficiencies. *Clin. Neurophysiol.* 123, 720–729. doi: 10.1016/j.clinph.2011.08.023

Virtanen, P., Gommers, R., Oliphant, T. E., Haberland, M., Reddy, T., Cournapeau, D., et al. (2020). SciPy 1.0: fundamental algorithms for scientific computing in Python. *Nat. Methods* 17, 261–272. doi: 10.1038/s41592-019-0686-2

Conflict of Interest: The authors declare that the research was conducted in the absence of any commercial or financial relationships that could be construed as a potential conflict of interest.

Copyright © 2021 Pak, Kissinger and Chubykin. This is an open-access article distributed under the terms of the Creative Commons Attribution License (CC BY). The use, distribution or reproduction in other forums is permitted, provided the original author(s) and the copyright owner(s) are credited and that the original publication in this journal is cited, in accordance with accepted academic practice. No use, distribution or reproduction is permitted which does not comply with these terms.

frontiers in Cellular Neuroscience

REVIEW
published: 15 June 2021
doi: 10.3389/fncel.2021.689332

Huntingtin and the Synapse

*Jessica C. Barron, Emily P. Hurley and Matthew P. Parsons**

Division of Biomedical Sciences, Faculty of Medicine, Memorial University, St. John's, NL, Canada

Huntington disease (HD) is a monogenic disease that results in a combination of motor, psychiatric and cognitive symptoms. HD is caused by a CAG trinucleotide repeat expansion in the huntingtin (*HTT*) gene, which results in the production of a pathogenic mutant HTT protein (mHTT). Although there is no cure at present for HD, a number of RNA-targeting therapies have recently entered clinical trials which aim to lower mHTT production through the use of antisense oligonucleotides (ASOs) and RNAi. However, many of these treatment strategies are non-selective in that they cannot differentiate between non-pathogenic wild type HTT (wtHTT) and the mHTT variant. As HD patients are already born with decreased levels of wtHTT, these genetic therapies may result in critically low levels of wtHTT. The consequence of wtHTT reduction in the adult brain is currently under debate, and here we argue that wtHTT loss is not well-tolerated at the synaptic level. Synaptic dysfunction is an extremely sensitive measure of subsequent cell death, and is known to precede neurodegeneration in numerous brain diseases including HD. The present review focuses on the prominent role of wtHTT at the synapse and considers the consequences of wtHTT loss on both pre- and postsynaptic function. We discuss how wtHTT is implicated in virtually all major facets of synaptic neurotransmission including anterograde and retrograde transport of proteins to/from terminal buttons and dendrites, neurotransmitter release, endocytic vesicle recycling, and postsynaptic receptor localization and recycling. We conclude that wtHTT presence is essential for proper synaptic function.

Keywords: Huntington disease, Huntingtin, synaptic plastcity, endocytosis, exocytosis, intracellular tranport, autophagy, excitotoxicity

OPEN ACCESS

Edited by:
Annalisa Scimemi, University at Albany, United States

Reviewed by:
Ioannis Dragatsis, University of Tennessee Health Science Center(UTHSC), United States
Maggie Panning Pearce, University of the Sciences, United States

***Correspondence:**
Matthew P. Parsons
matthew.parsons@med.mun.ca

Specialty section:
This article was submitted to Cellular Neuropathology, a section of the journal Frontiers in Cellular Neuroscience

Received: *31 March 2021*
Accepted: *24 May 2021*
Published: *15 June 2021*

Citation:
Barron JC, Hurley EP and Parsons MP (2021) Huntingtin and the Synapse. Front. Cell. Neurosci. 15:689332. doi: 10.3389/fncel.2021.689332

HUNTINGTON DISEASE: AN OVERVIEW

Huntington disease (HD) is an autosomal dominant neurodegenerative disease that results in a triad of motor, psychiatric and cognitive symptoms, and has an estimated prevalence of 13.7 per 100,000 in the general population (Fisher and Hayden, 2014). Although HD is considered a brain-wide disease, neuronal degeneration primarily targets spiny projection neurons (SPNs) of the striatum, a brain area essential for regulating voluntary and involuntary movement. HD symptoms typically appear during middle age in most patients; however, disease onset can occur anytime between 1 and 80 years of age. HD is fatal, and life expectancy after diagnosis is estimated to be 15-20 years (Walker, 2007). Symptoms pertaining to the motor system include chorea, dystonia, motor impersistence and motor incoordination. In terms of cognition, HD patients often have problems with tasks involving executive function, such as planning and organizing, and impaired procedural memory (Walker, 2007). Common psychiatric symptoms associated with HD include depression, apathy, aggression and disinhibition, and suicide rates of HD patients are four times higher than

that of the general population (Di Maio et al., 1993). Notably, cognitive deficits manifest as many as 20 years earlier than the onset of motor symptoms, and cognitive and behavioral-related issues are reported as the most burdensome for patients (Hamilton et al., 2003; Paulsen, 2011). In HD, these early cognitive abnormalities have mostly been associated with disruption in frontostriatal neural pathways, although multiple other brain areas including the hippocampus also show significant volume loss in the early stages of disease (Rosas et al., 2003). Currently, there is no cure for HD.

Huntington disease is a monogenic disease that is caused by a CAG trinucleotide repeat expansion in exon 1 of the *HTT* gene (also known as the *IT15* gene), which encodes the large, 348 kDa protein huntingtin (HTT) (MacDonald et al., 1993). CAG repeat lengths of 40 or more result in the production of a mutated huntingtin protein (mHTT) while healthy individuals typically have less than 36 repeats. Intermediate CAG repeat lengths of 36-39 result in incomplete penetrance of the HD phenotype (Rubinsztein et al., 1996). Longer CAG repeat expansions are correlated with earlier disease onset (Penney et al., 1997). Wild-type huntingtin (wtHTT; herein used to refer to the non-pathogenic HTT protein) is ubiquitously expressed throughout the body. Within the brain, wtHTT is largely present in nuclei, cell somas, dendrites and terminal buttons, while mHTT has a tendency to accumulate in intranuclear inclusions and dystrophic neurites (DiFiglia et al., 1997). The N-terminal region of wtHTT contains the polyglutamine stretch encoded by the CAG repeat expansion and for this reason has been the most extensively studied portion of the protein, despite accounting for only about 2% of HTT's structure. In addition, wtHTT contains several HEAT repeats that are important for its numerous protein-protein interactions (Saudou and Humbert, 2016). An essential role of wtHTT is well-documented by the fact that homozygous wtHTT knockout is embryonic lethal at day E8.5 (Duyao et al., 1995; Nasir et al., 1995; Zeitlin et al., 1995). Heterozygous knockout of wtHTT from birth has been shown to result in hyperactivity, deficits in cognitive flexibility and decreased overall volume and neuronal density in the subthalamic nucleus (Nasir et al., 1995). Additionally, wt*HTT* deletion in the forebrain and testis of adult mice results in neurodegeneration, motor impairments and a shortened lifespan (Dragatsis et al., 2000). The essentiality of wtHTT is further supported by its role in numerous fundamental cellular functions due to its extensive number of interaction partners. A few hundred interacting partners had previously been identified using *ex vivo* methods such as yeast two-hybrid and affinity pulldown assays; however, most of these experiments used only small N-terminal fragments of wtHTT, neglecting a large part of its full-length structure (summarized in Table 1 of Harjes and Wanker, 2003). In Shirasaki et al. (2012), the authors used a novel methodological approach to identifying wtHTT interacting partners, which incorporated the use of a high-affinity mass spectrometer. This study was highly successful, identifying 747 candidate proteins from various brain regions that interact with wtHTT. Among the top ranked functional groups for the wtHTT interactors were presynaptic function and postsynaptic function, highlighting a role for wtHTT in synaptic homeostasis. The role that wtHTT plays at both pre- and postsynaptic sites is the main focus of the present review and will be discussed in detail in the following sections.

Wild type HTT has been shown to act as a scaffolding protein, functioning to stabilize intracellular cargo onto molecular motors to streamline fast axonal transport and to assist in anchoring receptors at the plasma membrane (Saudou and Humbert, 2016). As we will discuss throughout this review, wtHTT has been heavily implicated in almost all major facets of synaptic neurotransmission including anterograde and retrograde transport of proteins to/from terminal buttons and dendrites, neurotransmitter release, endocytic vesicle recycling and postsynaptic receptor localization and recycling. Additionally, wtHTT has been shown to influence autophagy, which has been highlighted in recent years as an important regulator of synaptic homeostasis (Vijayan and Verstreken, 2017; Liang and Sigrist, 2018; Nikoletopoulou and Tavernarakis, 2018; Birdsall and Waites, 2019), and synapse-to-nuclear communication via its regulation of transcription factors such as CREB, REST/NRSF and NF-κB (Steffan et al., 2000; Zuccato et al., 2003; Marcora and Kennedy, 2010). In HD, synaptic dysfunction occurs prior to cell death and predicts subsequent neuronal degeneration and symptom onset (Milnerwood and Raymond, 2010; Milnerwood et al., 2010; Parsons and Raymond, 2014; Ravalia et al., 2021). As HD is originally a disease of the synapse, this review will summarize research from the last two decades that provide fundamental evidence for wtHTT as a major regulator of synaptic function and will consider potential and identified consequences of wtHTT depletion at the synapse. It is imperative that we increase our understanding of wtHTT's function in the developed brain, as many novel therapeutic strategies — discussed in the following section — aim to treat HD by reducing both wtHTT and mHTT expression.

TARGETING THE ROOT CAUSE: HUNTINGTIN-LOWERING THERAPEUTICS

Genetic therapy for HD has shown great promise as a treatment for this crippling disease, with significant recent advancements in the development of both DNA- and RNA-targeting therapies. As HD is a monogenic disease, DNA- and RNA-targeting therapies can target the root cause of the disease itself. Therapies targeting RNA include antisense oligonucleotides (ASOs), RNAi and small molecules, while those targeting DNA include zinc finger nucleases (ZFNs), transcription activator-like effector nucleases (TALENs) and CRISPR-Cas9. Each of the various strategies have specific benefits as well as drawbacks which have been reviewed recently (Tabrizi et al., 2019a). As an example, therapies targeting *HTT* mRNA aim to reduce the production of the mutant protein variant; however, many of these options will also decrease the production of wtHTT. Furthermore, there is evidence that pathogenic exon 1 fragments can result from incomplete splicing at the pre-mRNA level, thereby evading the mRNA-targeting approaches (Sathasivam et al., 2013).

Antisense oligonucleotides target the pre-mRNA stage of mHTT for degradation by RNase H. The delivery and dispersal

of ASOs within the central nervous system (CNS) also make these therapeutics particularly desirable. ASOs can penetrate cell membranes without the need for an accompanying viral vector and can be delivered to the brain through intrathecal injections into the spinal cord. The Roche GENERATION HD1 clinical trial using the non-selective ASO tominersen (previously known as HTT_{RX} or RG6042) was recently halted early in phase III. Unfortunately, tominersen was no more effective than placebo when administered every 16 weeks, and actually worsened motor and cognitive symptoms when administered every eight weeks (Kwon, 2021). The recent news to terminate this clinical trial is particularly disappointing considering that cerebral spinal fluid (CSF) levels of two established HD biomarkers, mHTT and neurofilament light chain (NfL), showed a dose-dependent decrease after tominersen administration (Tabrizi et al., 2019b).

In terms of selective mHTT lowering therapeutics, Wave Life Sciences initiated their parallel stage I/IIa clinical trials in 2017, PRECISION HD1 and PRECISION HD2, which aim to selectively lower levels of mHTT while leaving wtHTT levels unchanged (Hersch et al., 2017). These selective ASOs are designed to specifically lower mHTT (leaving wtHTT intact) by targeting single nucleotide polymorphisms (SNPs) located exclusively on the mutant allele. Allele-specific ASOs have recently shown promising results in a preclinical study that used humanized HD mice (Southwell et al., 2013); selective mHTT ASOs reduced mHTT expression by approximately 70% while having no effect on wtHTT expression. Furthermore, selective mHTT silencing reduced many of the cognitive and behavioral deficits in these mice (Southwell et al., 2018). Unfortunately, both PRECISION HD1 and PRECISION HD2 trials were recently discontinued as they did not significantly reduce CSF levels of mHTT. Further complicating the SNP-based ASO approach is the fact that HD mutation carriers express different SNPs and some don't express any heterozygous SNPs at all; therefore this selective strategy is not applicable to the entire HD population (Skotte et al., 2014). Nonetheless, allele-specific ASOs have tremendous promise in the treatment of HD and will continue to be pursued in future clinical trials with similar ASOs that incorporate various chemical modifications designed to improve their efficacy. Another strategy to achieve selective mHTT knockdown is to target the CAG tract itself, although many genes in the human genome also contain consecutive CAG repeats and a number of these genes code for transcription factors. Therefore, targeting the CAG trinucleotide repeat for degradation may result in significant off-target effects. RNAi are another group of RNA-targeting therapies that employ micro RNAs (miRNAs), short interfering RNAs (siRNAs) or short hairpin RNAs (shRNAs) to target mRNA for degradation by RNA-induced silencing complex (RISC) machinery (Aguiar et al., 2017). In contrast to ASOs, RNAi therapies act further downstream and can only target within the intron-lacking mature mRNA. Therefore, RNAi drugs have more limitations in terms of sequence targets (Tabrizi et al., 2019a). As well, these therapies require the use of a viral vector and a more direct injection into the brain. However, a potentially attractive feature of these drugs is their permanence. Whereas patients undergoing clinical trials for ASO therapeutics must receive intrathecal injections every few months, RNAi treatments may only require a single dose. On the other hand, the less reversible nature of these drugs can quickly turn into to a disadvantage if unwanted side-effects are observed. In June 2020, UniQure announced the launch of their phase I/II clinical trial where early manifest HD patients will receive a single intra-striatal administration of AMT-130, a non-selective rAAV5-miRNA (Reilmann et al., 2020). Another type of RNA-targeting therapeutics currently in development for HD are bioavailable small molecules. These drugs are ideal in terms of delivery as they can be taken orally, and positive results have been observed in rodent models of spinal muscular atrophy (SMA) that were treated with small molecules that target and degrade SMN2 RNA (Naryshkin et al., 2014). Gene-editing therapies for the treatment of HD are currently in preclinical development. These drugs target the absolute root cause of HD: the *HTT* (*IT15)* gene. Precise silencing of the mutant allele using gene-editing techniques such as CRISPR-Cas9 would halt m*HTT* transcription at its source; however, gene editing therapies require invasive delivery systems and are largely irreversible. Human clinical trials for DNA-targeting HD therapies are yet to be announced, although initial rodent studies have shown promising results (Yang et al., 2017).

In sum, a plethora of HTT-lowering strategies exist, and all can target the root cause of HD by lowering mHTT expression. However, it is important to note that non-selective HTT silencing is much easier to achieve that allele-selective silencing, and many of the therapeutic options are indeed non-selective therapies that will further reduce wtHTT expression. Therefore, we now turn our attention to the role of wtHTT and the potential consequences of its loss in adulthood.

HUNTINGTIN AND THE SYNAPSE

Given the clinical importance and immediate relevance of HTT-lowering therapies for the treatment of HD — many of which are not selective for mHTT over wtHTT — it is of paramount importance to increase our understanding of the function of wtHTT and the consequences of its loss in adulthood. As HD mutation carriers are born with reduced expression of wtHTT, it is also essential to fully understand how wtHTT reduction affects CNS development. In mouse models of HD, one must keep in mind that CAG repeat lengths must be greatly exaggerated before a HD-like phenotype can be observed within the lifespan of a mouse; in that regard, the lack of any obvious consequences of wtHTT loss — particularly at the behavioral level — following a relatively short period of wtHTT reduction is insufficient to conclude that wtHTT loss is well-tolerated. Similarly, while HTT-lowering strategies in the clinic are unlikely to eliminate 100% of the wtHTT and mHTT in the brain, cellular and animal studies that observe deleterious effects only after the complete depletion of wtHTT should not be viewed as lacking physiological relevance; like exaggerated CAG repeat lengths, perhaps complete wtHTT knockdown is the best way to observe the consequences of wtHTT loss within the lifespan of a mouse. In this review, we discuss how wtHTT regulates synaptic function in numerous ways. We chose to focus on wtHTT's role at

the synapse, as synaptic dysfunction is observed prior to cell death and HD behavioral signs, and therefore represents one of the most sensitive measures of disease pathogenesis (Li et al., 2003; Milnerwood and Raymond, 2010; Raymond et al., 2011; Tyebji and Hannan, 2017; Ravalia et al., 2021). In reviewing the multidimensional roles that wtHTT plays at both pre- and postsynaptic sites, we conclude that wtHTT reduction is not well-tolerated at the synaptic level.

HUNTINGTIN AND THE PRESYNAPSE

Numerous mechanisms regulating presynaptic neurotransmitter release have been identified to date, though our understanding is far from complete. Presynaptic release is complex and can occur in different modes — including synchronous, asynchronous or spontaneous — depending on whether release is tightly coupled with action potential (AP) firing, exhibits poor temporal coordination with AP firing, or occurs independently of AP firing, respectively. The different modes of presynaptic release are associated with overlapping but distinct underlying mechanisms, and research is ongoing to fully understand how presynaptic release is regulated and maintained at different synapses throughout the healthy brain (Chanaday and Kavalali, 2018). The complexity of presynaptic neurotransmission extends well beyond the successful release of neurotransmitters into the extracellular space. The maintenance of high-fidelity synaptic neurotransmission is a multifaceted process that relies on highly coordinated intracellular mechanisms. For example, presynaptic function relies on the ability to rapidly recycle synaptic vesicles (SVs) (Marx et al., 2015), to ship new SVs from the cell body to the terminal (Okada et al., 1995; Goldstein et al., 2008), to rapidly refill SVs with neurotransmitter (Nakakubo et al., 2020), and to remove damaged proteins from presynaptic sites (Vijayan and Verstreken, 2017). As a result of this complexity, presynaptic function is not only reliant on exocytic release machinery, but also on clathrin-mediated endocytosis, axonal trafficking and autophagy, to name a few. In this section, we will discuss how wtHTT's role in endocytosis, exocytosis, intracellular transport and autophagy positions wtHTT as a critical mediator of presynaptic neurotransmission. Some of ways in which wtHTT can influence presynaptic function are depicted schematically in **Figure 1**.

Huntingtin and the Presynapse: Endocytosis

A finite number of SVs exist at presynaptic release sites. During neural activity, SVs release their contents by fusing with the plasma membrane, and the pool of SVs available within a presynaptic neuron can be rapidly depleted during sustained neural activity. For example, at the CA3-CA1 synapse in the hippocampus, it is estimated that approximately 30 seconds of neural activity at a physiologically relevant firing rate of four hertz is sufficient to completely deplete the presynaptic supply of glutamate SVs (Marx et al., 2015). To maintain neurotransmission in the face of sustained neural activity, numerous mechanisms are in place to help ensure a rapid recovery and replenishment of the SV pool. Often, the rate of SV fusion with the membrane during neural activity far exceeds the rate at which new SVs can be delivered via anterograde transport from the cell body; thus, an essential method of SV replenishment during activity is through local clathrin-mediated endocytosis at the terminal itself.

A role for wtHTT in presynaptic neurotransmission was suggested by its association with SVs (DiFiglia et al., 1995; Yao et al., 2014). Recently, it was demonstrated that a key wtHTT interactor, ADAM10, is heavily involved in presynaptic homeostasis. ADAM10 is a transmembrane protease that is well-established as an alpha-secretase which cleaves amyloid precursor protein (APP) in a non-amyloidogenic fashion (Kuhn et al., 2010). ADAM10 localizes presynaptically with SVs, suggesting a role in presynaptic regulation (Lundgren et al., 2020). While Alzheimer disease (AD) is associated with reduced ADAM10 levels (Kuhn et al., 2010), thereby resulting in excess amyloidogenic processing of amyloid precursor protein, ADAM10 is hyperactive in the HD brain at both pre- and postsynaptic localizations (Cozzolino et al., 2021). Using immunoprecipitation followed by mass spectrometry and gene ontology analysis, it was found that the ADAM10 interactome exhibits substantial overlap with the wtHTT interactome; many of the shared interactors were identified as proteins essential for presynaptic function, thereby highlighting a putative functional role for both wtHTT and ADAM10 at the presynaptic active zone. For example, both ADAM10 (Cozzolino et al., 2021) and wtHTT (Yao et al., 2014) bind to piccolo, a large cytomatrix protein that is critical for SV maintenance and efficient SV recycling (Ackermann et al., 2019). Hyperactive ADAM10, which can be induced either by pathogenic polyQ expansion of HTT or by wtHTT loss (Lo Sardo et al., 2012), disrupts the ADAM10/piccolo complex, resulting in depleted SVs at the readily releasable and reserve vesicle pools. Restoring ADAM10 activity to control levels in HD mice, achieved by crossing R6/2 mice with heterozygous conditional ADAM10 knockout mice (CaMKIIα-Cre:Adam10$^{Flox/+}$), restored the ADAM10/piccolo interaction and replenished SV stores (Cozzolino et al., 2021). Thus, wtHTT loss may have detrimental effects on presynaptic homeostasis by interrupting the HTT/ADAM10/piccolo complex. In addition to complexing with ADAM10/piccolo and other presynaptic regulatory proteins including bassoon (Yao et al., 2014), wtHTT and ADAM10 both interact with the clathrin adaptor protein AP-2 (Borgonovo et al., 2013; Marcello et al., 2013), and wtHTT serves as a docking protein that helps recruit AP-2 to the membrane. Interestingly, polyQ expansion of HTT results in a loss of wtHTT's docking function, thereby reducing AP-2 presence at the membrane and impairing clathrin-mediated endocytosis (Borgonovo et al., 2013).

Wild type HTT's interactions with huntingtin interacting protein 1 (HIP1) also position wtHTT to influence presynaptic transmission. When the wtHTT/HIP1 interaction was first described, it was recognized that disrupting this interaction could negatively impact the integrity of the cytoskeleton (Kalchman et al., 1997). A few years later, HIP1 was implicated in endocytosis through interactions with both clathrin and the AP-2 adaptor complex (Metzler et al., 2001; Mishra et al., 2001;

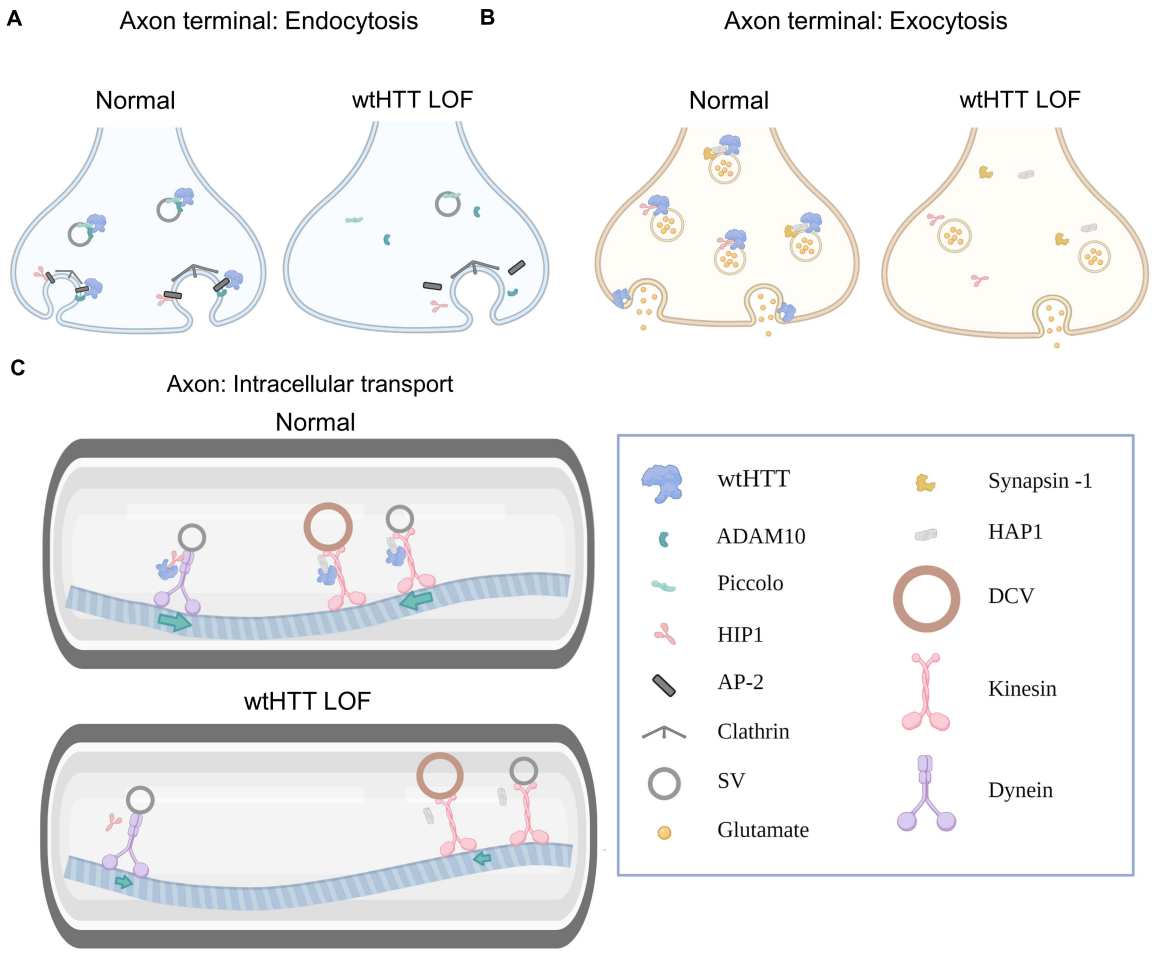

FIGURE 1 | Huntingtin and the presynapse. **(A)** Select examples demonstrating how wtHTT positively regulates endocytosis (left). Through associations with ADAM10 and piccolo, wtHTT regulates SV density at the readily releasable and reserve vesicle pools. Through associations with HIP1, AP-2 and ADAM10, wtHTT regulates clathrin-mediated endocytosis. wtHTT loss impairs endocytosis by disrupting the function of complexes with the aforementioned proteins (right). wtHTT LOF decreases SV density at the readily releasable and reserve vesicle pools and impairs clathrin-mediated endocytosis. **(B)** Select examples demonstrating how wtHTT positively regulates exocytosis. Through its associations with synapsin-1, HAP1 and HIP1, wtHTT can regulate the rate of SV exocytosis and the amount of neurotransmitter release. wtHTT loss disrupts exocytosis (right). **(C)** Select examples demonstrating how wtHTT positively regulates axonal transport (top). Through its associations with HAP1 and HIP1, as well as molecular motors, wtHTT maintains proper anterograde and retrograde transport of cellular cargoes including SVs and DCVs. wtHTT loss impairs axonal transport (bottom). Due to its associations with HAP1 and HIP1, as well as molecular motors, wtHTT loss interferes with anterograde and retrograde transport of cellular cargoes including SVs and DCVs. Abbreviations: LOF, loss of function; ADAM10, A disintegrin and metalloproteinase domain-containing protein 10; HIP1, huntingtin-interacting protein 1; AP-2, adaptor protein complex 2; SV, synaptic vesicle; HAP1, huntingtin-associated protein 1; DCV, dense-core vesicle. Figure created using Biorender.com.

Waelter et al., 2001). Consistent with a role in synaptic vesicle recycling through endocytosis, HIP1 knockout mice exhibit a slower recovery from synaptic depression (Parker et al., 2007).

Together, the aforementioned studies suggest that wtHTT loss of function (LOF) may disrupt presynaptic homeostasis by impairing clathrin-mediated SV recycling. A direct role of wtHTT in SV endocytosis was demonstrated recently when self-deliverable, cholesterol-conjugated siRNAs were used to knock down wtHTT expression in cultured neurons (McAdam et al., 2020). In this study, wtHTT levels were reduced to approximately 20% of that observed in control neurons, and the fluorescent reporter synaptophysin-pHluorin (syp-pH) was used to quantify the rate of SV recycling. Syp-pH fluorescence is quenched when in the acidic environment inside SVs, and SV exocytosis during neural activity increases syp-pH fluorescence. In striatal cultures with reduced wtHTT expression, the rate of SV recovery — quantified by the decay of the evoked syp-pH transient — was slower in striatal cultures with reduced wtHTT expression. SV recycling was also impaired in cells cultured from knock-in HD mice and this deficit could be fully rescued by the overexpression of wtHTT. Together, these data demonstrate a clear role for wtHTT as a positive regulator of SV recycling. Interestingly, the recycling rate was unaffected in cultured hippocampal neurons following wtHTT knockdown, suggesting that the consequences of wtHTT reduction on synaptic function varies in a region-dependent manner (McAdam et al., 2020).

In sum, wtHTT interacts with key presynaptic proteins that regulate SV endocytosis, and wtHTT LOF slows the rate of SV recycling following a period of evoked neural activity. It will be of interest for future studies to further pinpoint the mechanisms underlying wtHTT's role in SV recycling and to determine how much wtHTT reduction in the adult brain can be safely tolerated before SV replenishment rates are negatively impacted.

Huntingtin and the Presynapse: Exocytosis

The effects of wtHTT loss on SV exocytosis are not fully understood, though mHTT expression was shown to inhibit exocytosis by depleting complexin II (Edwardson et al., 2003). Many of the proteins that complex together with wtHTT have been shown to play a clear role in exocytic neurotransmitter release, and wtHTT lowering can interfere with the normal functions of these protein complexes. For example, the wtHTT binding partner huntingtin associated protein 1 (HAP1) (Li et al., 1995), interacts with the presynaptic protein synapsin-I, and HAP1 depletion was shown to reduce both the rate of SV exocytosis and the amount of evoked glutamate release in excitatory neurons (Mackenzie et al., 2016). Similarly, HIP1 knockout increases the paired-pulse ratio measured at hippocampal CA3-CA1 synapses, indicative of a decrease in neurotransmitter release probability (Parker et al., 2007). Another major wtHTT interactor, huntingtin interacting protein 14 (HIP14), has also been shown to facilitate presynaptic neurotransmitter release. HIP14 is a palmitoyl acyltransferase that palmitoylates target substrates including a variety of presynaptic proteins such as cysteine string protein and SNAP25. wtHTT is a positive regulator of HIP14 (Huang et al., 2011), and HIP14 depletion impairs activity-dependent SV exocytosis at the neuromuscular junction in *Drosophila* (Ohyama et al., 2007) and reduces electrophysiological measures of release probability at glutamatergic synapses within the striatum (Milnerwood et al., 2013). When HIP14 knockdown is initiated in adulthood, reduced release probability and mEPSC frequency is observed in SPNs, and the mice exhibit motor deficits and increased anxiety-like behaviors (Sanders et al., 2016). In HeLa cells, wtHTT itself is directly involved in secretory vesicle fusion with the plasma membrane during exocytosis (Brandstaetter et al., 2014). Presynaptic wtHTT expression has also been implicated in long-term synaptic plasticity, as long-term facilitation of the sensory-to-motor neuron synapse was impaired when the Aplysia wtHTT homolog was silenced by ASO injection into the presynaptic sensory neuron (Choi et al., 2014). While additional questions remain regarding wtHTT's precise role in exocytosis, multiple lines of evidence indicate that wtHTT and its interactome are essential components of the presynaptic machinery regulating exocytic neurotransmitter release.

Huntingtin and the Presynapse: Axonal Transport

One particularly well-acknowledged function of wtHTT is its role intracellular transport. The wtHTT/HAP1 complex influences intracellular trafficking by forming larger complexes with kinesin and dynein molecular motors, which are responsible for anterograde (away from the cell body) and retrograde (toward the cell body) transport of various molecular cargoes, respectively (Engelender et al., 1997; Li et al., 1998; McGuire et al., 2006; Saudou and Humbert, 2016; Vitet et al., 2020). Both pathogenic polyQ expansion of HTT (Li et al., 1995) and wtHTT loss have been shown to impair axonal trafficking by interfering with the known functions of the HTT/HAP1 complex (Gunawardena et al., 2003; Gauthier et al., 2004; Zala et al., 2013). Perhaps the most acknowledged functional outcome of wtHTT's trafficking role is in the anterograde delivery of BDNF to the striatum from presynaptic cortical neurons. The striatum produces low amounts of this trophic factor on its own and striatal neurons require BDNF delivery from cortical terminals for long-term survival (Baquet et al., 2004). Through associations with HAP1 and the $p150^{Glued}$ subunit of dynactin, an essential co-factor of the dynein molecular motor, wtHTT facilitates both anterograde and retrograde BDNF transport along microtubules, and loss of wtHTT is sufficient to slow BDNF transport (Gauthier et al., 2004). In addition to facilitating BDNF transport, wtHTT also enhances BDNF synthesis by sequestering REST, a transcription factor that normally acts in the nucleus to silence BDNF expression (Zuccato et al., 2001, 2003). Thus, by increasing synthesis and accelerating the intracellular transport of BDNF, wtHTT plays a critical role in delivering presynaptic trophic support to the striatum. BDNF is important not only for survival but is also essential for synaptic plasticity (Harward et al., 2016), and BDNF deficiencies may in fact underlie synaptic plasticity deficits observed in mouse models of HD (Lynch et al., 2007; Simmons et al., 2009). Interestingly, synaptic plasticity deficits occur earlier and are more severe in homozygous knock-in HD mice (which completely lack wtHTT) compared to heterozygous knock-in HD mice, although it is not known whether this accelerated plasticity deficit results from a higher expression of mHTT or the lack of wtHTT in the homozygous HD mice (Quirion and Parsons, 2019).

Numerous post-translational modifications (PTMs) of wtHTT have been shown to be essential to its role in vesicular transport. For example, serine 421 (S421) on wtHTT has been identified as an important phosphorylation site that mediates axonal trafficking; phosphorylation of wtHTT at S421 recruits kinesin-1 and promotes anterograde transport of BDNF-containing vesicles whereas S421 dephosphorylation favors retrograde transport following kinesin-1 detachment (Colin et al., 2008). On the other hand, dephosphorylation at S1181 and S1201 strengthens molecular motor attachment to microtubules and enhances the transport of BDNF (Ben et al., 2013). In addition to phosphorylation, the arginine methyltransferase PRMT6 was recently shown to methylate arginine R118 of wtHTT, increasing wtHTT's association with vesicles and facilitating vesicular trafficking (Migazzi et al., 2021). Knocking down PRMT6 or transfecting neurons with a methylation-resistant wtHTT (R118K) reduced both the number and speed of vesicles traveling in the anterograde direction. Increasing methylation was able to rescue axonal transport deficits in mHTT-expressing neurons and was protective in a fly model of HD, highlighting methylation

and the restoration of wtHTT's trafficking function as a potential therapeutic strategy for HD (Migazzi et al., 2021).

Impaired axonal trafficking can have profound functional consequences that extend well beyond the aforementioned reduction in BDNF delivery to the striatum. Efficient trafficking of a variety of cargo both to and from synaptic compartments is essential for the maintenance of synaptic homeostasis. For example, wtHTT loss interferes with the delivery of large dense core vesicles (DCV), which carry neurotrophins and neuropeptides, to release sites (Weiss and Littleton, 2016; Bulgari et al., 2017). Growing evidence supports a key role of APP in regulating synaptic structure and function (Priller et al., 2006; Tyan et al., 2012; Müller et al., 2017), and wtHTT also facilitates the transport of APP to the presynapse (Colin et al., 2008; Her and Goldstein, 2008; Bruyère et al., 2020). Either silencing wtHTT (Her and Goldstein, 2008) or preventing wtHTT phosphorylation at S421 (Bruyère et al., 2020) impairs APP axonal transport. Thus, wtHTT dephosphorylation reduces the amount of APP at presynaptic compartments (Bruyère et al., 2020). By reducing APP at presynaptic sites, wtHTT dephosphorylation increases synapse density in CA1 stratum radiatum. As well, the excessive synaptic connectivity induced by wtHTT dephosphorylation can be restored by APP overexpression (Bruyère et al., 2020). The finding that wtHTT dephosphorylation increased the volume of the cortex and hippocampus but not the striatum suggests that regional sensitivities to the consequence of wtHTT LOF do not necessarily mimic the known regional sensitivities to mHTT toxicity (Bruyère et al., 2020).

Anterograde axonal transport of SV precursors (SVPs) is required to bring the proper release machinery to the presynapse. Newly synthesized SVP delivery works together with endocytosis, albeit at a slower rate, to contribute to the maintenance of presynaptic SV supply (Guedes-Dias and Holzbaur, 2019). SVPs are vesicles containing essential presynaptic proteins that are required to fill, dock and release SVs at terminal buttons. These SVPs travel from the cell body to axon terminals by kinesin-mediated anterograde transport. Fluorescence recovery after photobleaching demonstrates that HAP1 facilitates the axonal trafficking of synapsin-I-positive SVs to axon terminals. In neurons cultured from HAP1 knockout mice, the transport rate of synapsin-I was reduced by approximately 50% (Mackenzie et al., 2016). While the authors did not investigate wtHTT in this study, it is conceivable that wtHTT LOF may produce similar effects by interfering with the efficiency of the HTT/HAP1 complex. Indeed, in *Drosophila*, knocking out the *Drosophila* homolog of wtHTT was found to slow axonal trafficking of synaptotagmin-containing SVs (Zala et al., 2013). More recent evidence demonstrates that wtHTT moves along the axon together with $Rab4^+$ SVs that also contain synaptic SNARE proteins synaptotagmin and synaptobrevin (White et al., 2020). Rab4 is a Rab GTPase that plays a key role synaptic homeostasis by controlling the recycling and degradation of synaptic vesicles (Dey et al., 2017). The bidirectional movement of these $Rab4^+$ vesicles was mediated by interactions with HIP1, rather than HAP1, and the molecular motors kinesin-1 and dynein. RNAi-mediated wtHTT reduction reduced the axonal mobility of $Rab4^+$ vesicles (White et al., 2020). Together, wtHTT appears to facilitate the axonal trafficking of a variety of cargos, many of which have essential roles in presynaptic fidelity and SV maintenance.

HTT and the Presynapse: Autophagy

In recent years, it has become clear that autophagy is more than a simple housekeeping process that rids the cell of unwanted materials. In fact, autophagy is being increasingly recognized as a major contributor to synaptic function, which has been recently reviewed elsewhere and will not be extensively covered in the present review (Vijayan and Verstreken, 2017; Liang and Sigrist, 2018; Nikoletopoulou and Tavernarakis, 2018; Birdsall and Waites, 2019). Synapses are particularly sensitive to proteostatic disruption, and at presynaptic sites, autophagy is not only essential for removing defective proteins but can also influence neurotransmitter release. For example, enhancing presynaptic autophagy reduced the size of dopamine (DA) terminals, the number of synaptic vesicles found at DA terminals and the magnitude of evoked DA release (Hernandez et al., 2012). In contrast, when Atg7 — an essential protein for autophagic vesicle formation — was deleted in DA neurons, the opposite effects were observed; in these autophagy-deficient mice, DA axon profiles were larger, evoked DA release was enhanced, and presynaptic recovery following evoked DA release was accelerated (Hernandez et al., 2012). In HD, mHTT can increase the number of autophagosomes by sequestering mTOR, which normally functions to inhibit phagophore formation (Ravikumar et al., 2004). However, these autophagosomes that accumulate in HD cells are largely devoid of cargo due to cargo recognition failure (Martinez-Vicente et al., 2010). wtHTT has been shown to be an important scaffold protein that facilitates selective autophagy — the removal of specific cytoplasmic materials rather than bulk degradation. Through physical interactions with the cargo adaptor p62 and the autophagy initiation kinase ULK1 proteins, wtHTT plays an essential role in both selective autophagy cargo recognition and autophagy initiation (Rui et al., 2015). Post-translational myristylation of wtHTT at Gly553 promotes the formation of autophagosomes (Martin et al., 2014, 2015), and autophagy dysfunction was observed in wtHTT conditional knockout mice where wtHTT loss was driven by the nestin promoter (Ochaba et al., 2014). Consistent with a wtHTT role in intracellular trafficking, both wtHTT and HAP1 also contribute to autophagosome content degradation by facilitating autophagosome transport to the lysosome. wtHTT and HAP1 were identified in autosome-enriched fractions, and siRNA-mediated wtHTT knockdown decreased the number and speed of autophagosomes traveling in the retrograde direction while increasing the number of stationary autophagosomes (Wong and Holzbaur, 2014). In sum, wtHTT serves as a positive regulator of autophagy, autophagic deficits are observed following wtHTT loss, and autophagy is now recognized to play an essential role in presynaptic neurotransmission and synaptic homeostasis. It will be of interest for future studies to determine the precise extent of synaptic dysfunction caused by wtHTT loss, and how much of that impairment can be attributed to defective autophagic mechanisms.

HUNTINGTIN AND THE POSTSYNAPSE

In addition to the myriad ways in which wtHTT positively influences presynaptic neurotransmission as discussed above, ample evidence exists to suggest that wtHTT is equally as important to proper postsynaptic function. In this section, we discuss how wtHTT is involved in the bidirectional transport of essential synaptic cargoes between the soma and dendritic tree, postsynaptic receptor clustering and subcellular localization, as well as spine stabilization and synaptic plasticity. Some of ways in which wtHTT can influence postsynaptic function are depicted schematically in **Figure 2**.

Huntingtin and the Postsynapse: Dendritic Transport

Like the presynapse, bidirectional transport of a variety of cargoes between the cell body and postsynaptic sites is critical for proper synapse formation and function. The wtHTT/HAP1 complex, through an interaction with kinesin family motor protein 5 (KIF5), assists the delivery of $GABA_A$ receptors to postsynaptic sites at inhibitory synapses (Twelvetrees et al., 2010). Disrupting the HAP1/KIF5 interaction reduced the surface expression of $GABA_A$ receptors and decreased the amplitude of miniature inhibitory postsynaptic currents (mIPSCs). Interestingly, wtHTT/HAP1/KIF5 protein complexes also deliver AMPA receptors to postsynaptic sites at excitatory synapses. In cultured neurons, wtHTT increased the strength of the interaction between HAP1 and KIF5 motors, promoting the transport GluA2-containing vesicles along microtubules to reach postsynaptic sites. Interfering with the protein complex, either through mHTT presence or by knocking down HAP1 or KIF5, reduced AMPA receptor trafficking and decreased mEPSC amplitude. Overexpressing wtHTT had the opposite effect, increasing mEPSC amplitude at excitatory synapses (Mandal et al., 2011). In addition to delivering GABA and glutamate receptors to postsynaptic sites, wtHTT also promotes soma-to-dendrite transport of RNA granules, which allows localized protein translation to occur at dendric sites (Savas et al., 2010). For example, via interactions with HAP1 and KIF5 motors, wtHTT helps bring β-actin mRNA to dendrites. Local dendritic translation of β-actin is important for dendritic growth and plasticity (Eom et al., 2003), and it was shown that shRNA-mediated knockdown of either wtHTT, HAP1 or KIF5 reduced the amount of β-actin mRNA in dendrites (Ma et al., 2011).

Wild type HTT also colocalizes with the BDNF receptor TrkB at postsynaptic sites. As mentioned above, wtHTT depletion can negatively impact BDNF production and its anterograde delivery to synaptic sites (Zuccato et al., 2001; Gauthier et al., 2004). At the postsynapse, siRNA-mediated wtHTT knockdown was shown to impair the anterograde transport of BDNF TrkB receptors to striatal dendrites (Liot et al., 2013), in agreement with reports of reduced TrkB expression in the context of HD (Ginés et al., 2006). Once activated by BDNF, TrkB receptors internalize and are transported to the cell body where they can exert pro-growth and survival effects in the postsynaptic neuron (Zheng et al., 2008), and wtHTT reduction also slows TrkB receptor retrograde transport in dendrites (Liot et al., 2013). Furthermore, it was recently demonstrated that autophagosomes are responsible for the retrograde transport of BDNF-activated TrkB receptors via associations between the $p150^{Glued}$ subunit of dynactin and the adaptor protein AP-2. The AP-2-mediated retrograde transport of BDNF/TrkB autophagosomes was shown to bring active TrkB to the soma where it promoted neuronal complexity and protected against neurodegeneration (Kononenko et al., 2017). As discussed above, wtHTT loss impairs autophagosome transport (Wong and Holzbaur, 2014), which may help explain why TrkB retrograde transport is reduced following wtHTT knockdown (Liot et al., 2013). Thus, in addition to decreasing BDNF production and axonal trafficking to presynaptic cortico-striatal terminals (Zuccato et al., 2001; Gauthier et al., 2004), wtHTT loss can also interfere with the delivery of TrkB receptors to the postsynapse, as well as the transport of activated TrkB receptors from the dendrite to the soma, thereby interfering with BDNF/TrkB's normal pro-survival and pro-growth effects at multiple levels. Similarly, the wtHTT/HAP1 complex has also been implicated in TrkA internalization and trafficking, which is required to promote neurite outgrowth (Rong et al., 2006). In agreement with a role of wtHTT in promoting postsynaptic growth and survival, wtHTT knockdown in adulthood reduces the survival of newly born neurons in the dentate gyrus and diminishes dendritic complexity (Pla et al., 2013).

Transcriptional dysregulation is a major component of HD pathogenesis (Kumar et al., 2014), and previous literature suggests that the transcriptional dysregulation observed in HD may be partially recapitulated by wtHTT reduction. For example, NF-κB is a ubiquitous transcription factor that controls the expression of numerous genes with wide ranging functions including cell survival and synaptic plasticity among many others (Kaltschmidt and Kaltschmidt, 2015). NF-κB translocates to the nucleus to activate target genes, and this translocation occurs in an activity-dependent manner that relies on retrograde transport via dynein motors (Mikenberg et al., 2007). In the postsynaptic density, wtHTT co-localizes with NF-κB, and in cultured neurons from conditional wtHTT knockout mice — mice lacking wtHTT in cortical neurons — the activity-dependent transport of NF-κB out of dendritic spines was slowed two-fold. Similarly, wtHTT loss reduced NF-κB activity in the nucleus, demonstrating that wtHTT LOF impairs the movement of NF-κB from synaptic sites to the nucleus, thereby inhibiting its actions on target genes (Marcora and Kennedy, 2010). While NF-κB has myriad effects on gene expression when in the nucleus, it is thought that the ongoing synaptic activity that drives the tonic level of nuclear NF-κB is neuroprotective (Bhakar et al., 2002; Fridmacher et al., 2003). Thus, wtHTT reduction may decrease neuronal survival by reducing the activity-dependent dendrite-to-nucleus transport of this ubiquitous transcription factor. Overall, wtHTT plays a clear role in both axonal and dendritic transport, and many of the identified cargoes trafficked with wtHTT's assistance play essential roles in both pre- and postsynaptic function. As more and more huntingtin-lowering strategies enter the clinic, we desperately need to increase our understanding of how wtHTT loss in adulthood impacts the delivery efficiency of essential proteins to pre- and postsynaptic sites.

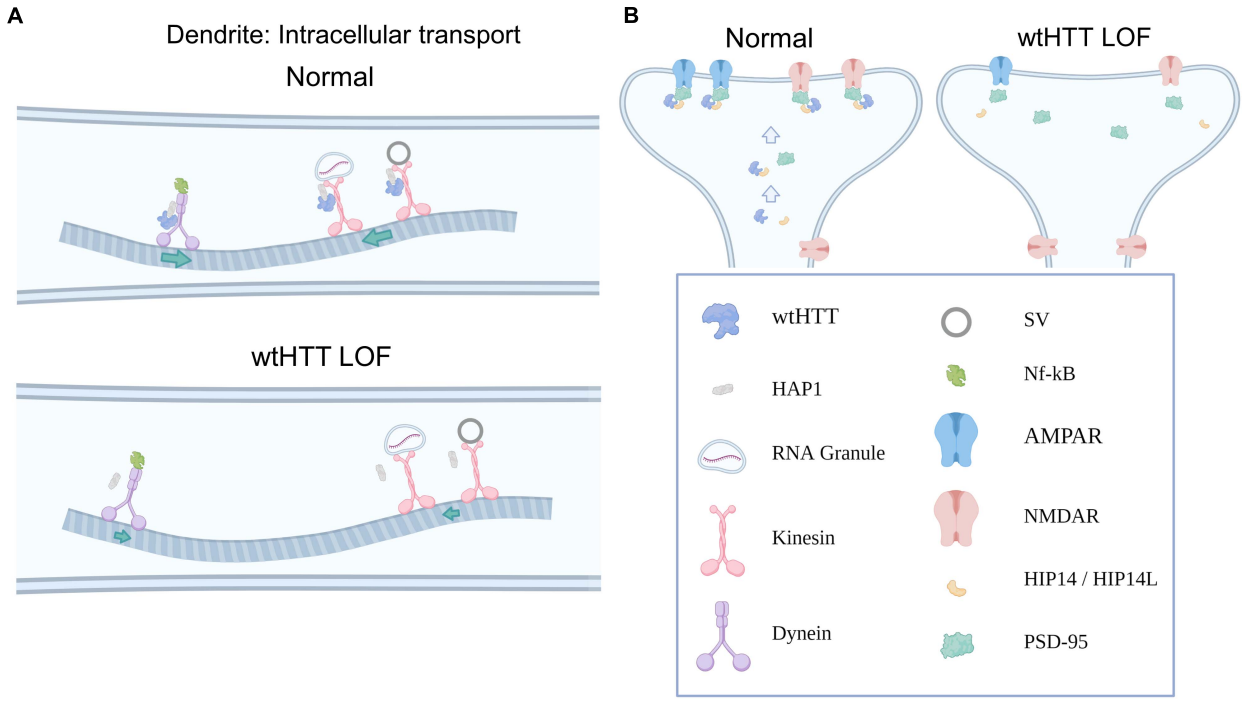

FIGURE 2 | Huntingtin and the postsynapse. **(A)** Select examples demonstrating how wtHTT positively regulates dendritic transport (top). Through its associations with HAP1, as well as molecular motors, wtHTT regulates anterograde and retrograde transport of synaptic receptors and other cargo in dendrites (left). wtHTT LOF disrupts this transport and slows delivery of synaptic cargo to their respective anterograde or retrograde targets (bottom). **(B)** Select examples demonstrating how wtHTT positively regulates receptor localization (left). Through its associations with HIP14 and PSD-95, wtHTT regulates synaptic receptor stabilization at the PSD in a healthy postsynaptic neuron. wtHTT LOF disrupts postsynaptic protein clustering and receptor localization (right). Abbreviations: LOF, loss of function; HAP1, huntingtin-associated protein 1; SV, synaptic vesicle; NF-κB, nuclear factor kappa B; AMPAR, α-Amino-3-hydroxy-5-methyl-4-isoxazolepropionic acid receptor; NMDAR, N-Methyl-D-aspartate receptor; HIP14/HIP14L, huntingtin-interacting protein 14/huntingtin-interacting protein 14-like; PSD-95, postsynaptic density protein 95. Figure created using Biorender.com.

Huntingtin and the Postsynapse: Receptor Localization and Cellular Toxicity

Through interactions with palmitoyl acyltransferases HIP14 and HIP14-like (HIP-14L), wtHTT acts as a positive modulator of palmitoylation, a PTM known to affect the subcellular localization and clustering of numerous synaptic proteins. For example, palmitoylation of PSD-95 targets this important postsynaptic scaffold to synaptic sites, and thereby regulates glutamate receptor clustering and activity-dependent synaptic plasticity (Craven et al., 1999; El-Husseini et al., 2002). Direct palmitoylation of AMPA and NMDA receptor subunits also regulates their trafficking and localization at synaptic sites (Hayashi et al., 2005, 2009). wtHTT has been identified as a positive modulator of HIP14, as either mHTT presence or wtHTT loss can reduce the enzymatic activity of HIP14 (Huang et al., 2011). Disrupting the function of these PATs has serious consequences at both the synaptic and behavioral levels. Behaviorally, HIP14 knockout mice, as well as HIP14L knockout mice, recapitulate many of the motor and cognitive impairments observed in HD mouse models (Singaraja et al., 2011; Milnerwood et al., 2013; Sutton et al., 2013). At the postsynaptic level, HIP14 knockout mice exhibit enhanced excitability of striatal SPNs, as well as decreased spine density and impaired synaptic plasticity in the hippocampus; the latter likely contributing to the observed spatial memory deficits in HIP14 knockout mice (Milnerwood et al., 2013). Consistent with a role for wtHTT as a positive modulator of synaptic protein palmitoylation, wtHTT overexpression was also shown to increase the palmitoylation and clustering of PSD-95 at synaptic sites, while ASO-mediated knockdown of wtHTT reduced PSD-95 cluster size (Parsons et al., 2014). Recently, it was shown that HIP14L, which also interacts with HTT (Sutton et al., 2013), palmitoylates cluster II of the GluN2B NMDA receptor subunit, and reducing cluster II palmitoylation on GluN2B increases GluN2B-containing NMDA receptor presence at extrasynaptic sites (Kang et al., 2019). Based on structural similarities to HIP14, it is likely that wtHTT also enhances the enzymatic activity of HIP14L (Sanders et al., 2014), as it does for HIP14 (Huang et al., 2011). As one of the earliest identified synaptic abnormalities to occur in HD mice is the overexpression of GluN2B-containing extrasynaptic NMDARs that are preferentially coupled to cell-death pathways (Okamoto et al., 2009; Milnerwood and Raymond, 2010; Milnerwood et al., 2010; Parsons and Raymond, 2014), reduced GluN2B cluster II palmitoylation and subsequent NMDAR mislocalization may

play a key role in early HD synaptic dysfunction. Together, these data suggest that by facilitating palmitoylation, wtHTT plays an important role in synaptic protein organization, particularly at the postsynaptic density.

Through interaction with PSD-95, wtHTT forms a complex with NMDA and kainate receptors, and decreasing the interaction between HTT and PSD-95 can sensitize NMDARs (Sun et al., 2001). Thus, it is suggested that wtHTT normally functions to limit NMDAR toxicity through strong interactions with PSD-95. Indeed, overexpression of wtHTT protects against excitotoxicity (Leavitt et al., 2006) and can even limit the toxicity caused by mHTT presence (Leavitt et al., 2001). Furthermore, wtHTT also interacts with caspase-3 and inhibits this pro-apoptotic executioner caspase. siRNA-mediated wtHTT knockdown increases the level of active caspase-3, and hippocampal levels of caspase-3 are significantly elevated in wtHTT-depleted cells in chimeric mice that contain populations of wtHTT-lacking neurons (Zhang et al., 2006). In addition, HAP1 and wtHTT interact with IP3 receptors, which module calcium release from internal stores, to form a ternary complex. While it remains to be determined how wtHTT loss affects the function of these IP3 receptors, it was shown that mHTT presence increases the sensitivity of IP3 receptors to IP3, thereby contributing to toxicity through the excessive release of intracellular calcium stores (Tang et al., 2003). Thus, while receptor mislocalization and enhanced excitotoxicity are well-accepted as major pathogenic mechanisms in the neurobiology of HD, there are numerous routes through which wtHTT reduction could result in similar outcomes.

In addition to palmitoylation discussed above, both wtHTT and mHTT are subject to numerous other PTMs including proteolysis, phosphorylation and myristoylation, to name a few (Ehrnhoefer et al., 2011; Saudou and Humbert, 2016). Considering the large size of the HTT protein and that most research has focused on its N-terminal region, it is unlikely that all HTT PTMs have been characterized. However, many PTMs discovered thus far have direct implications in the toxicity of HTT, some of which can even turn non-pathogenic wtHTT into a toxic protein. After translation, HTT is subject to various proteolysis events by proteases such as caspases and calpains. Notably, caspase cleavage of mHTT, particularly at the caspase-6 cleavage site, is an essential contributor to mHTT toxicity (Wellington et al., 2000; Graham et al., 2006), and the presence of N-terminal mHTT fragments alone is sufficient to produce a robust HD-like phenotype in animal models (Mangiarini et al., 1996). Interestingly, there is evidence to suggest that the C-terminal fragments produced by HTT cleavage — fragments that do not contain the mutant-defining polyQ stretch — can cause endoplasmic reticulum stress and cellular toxicity. This C-terminal fragment toxicity was due to the interaction with and inactivation of dynamin-1, which inhibited endocytosis at the plasma membrane and increased endoplasmic reticulum vacuolation (El-Daher et al., 2015). The surprising finding that protease-mediated cleavage may convert the protective wtHTT protein into a toxic protein fragment highlights the need to further understand the toxic and protective mechanisms of relevant HTT fragments, not just those at the N-terminal region containing the glutamine repeat. Phosphorylation is another PTM that can directly influence HTT's contribution to cellular toxicity. For example, wtHTT is phosphorylated at S1181 and S1201 by cyclin-dependant kinase 5, and this PTM directly impacts striatal neuron survival. While phosphorylation at these sites was found to protect against mHTT toxicity, dephosphorylation at S1181 and S1201 in wtHTT increased cell death in striatal neurons (Anne et al., 2007). Recently, a single nucleotide polymorphism (SNP) was identified that inhibits post translational myristoylation of wtHTT, which results in impaired cell health due to caspase cleavage at D513 (Martin et al., 2018). Thus, in addition to the effects of PTMs on wtHTT's role in vesicular trafficking described earlier in this review, numerous PTMs have been identified that can abolish the protective properties of wtHTT or even convert it to a toxic protein itself.

Huntingtin and the Postsynapse: Synaptic Stability and Plasticity

In addition to the previously discussed role of ADAM10 in presynaptic SV regulation, this metalloproteinase is also found in dendrites and spines and is known to play a major role in postsynaptic function. wtHTT inhibits ADAM10, and hyperactive ADAM10 can result from mHTT presence or from wtHTT loss (Lo Sardo et al., 2012). Hyperactive ADAM10 leads to excessive cleavage of N-cadherin which decreases synapse stability by reducing post- and presynaptic membrane adhesion. In the context of HD, inhibiting ADAM10 can partially rescue the reduced EPSC frequency recorded from SPNs in R6/2 and zQ175 mice (Vezzoli et al., 2019). As wtHTT loss also increases ADAM10 activity (Lo Sardo et al., 2012), it can be predicted that wtHTT loss would have similar effects on N-cadherin processing and synaptic dysregulation. Interestingly, when wtHTT is knocked out in developing cortical neurons, the excessive synaptic connections that are formed early cannot be maintained (McKinstry et al., 2014). While the McKinstry 2014 study did not investigate ADAM10 activity, their finding of decreased spine stability following wtHTT loss is consistent with wtHTT's regulatory role over ADAM10 and the cleavage of its substrates like N-cadherin.

Synaptic plasticity deficits have been observed in numerous mouse models of HD (Usdin et al., 1999; Murphy et al., 2000; Lynch et al., 2007; Simmons et al., 2009; Brito et al., 2014; Giralt et al., 2017; Quirion and Parsons, 2019) as well as in HD patients (Orth et al., 2010). While it is unknown to what extent wtHTT LOF contributes to the observed plasticity deficits in the context of HD, there are numerous mechanisms by which wtHTT reduction could negatively impact synaptic plasticity in the brain. For example, hippocampal long-term potentiation (LTP) is heavily reliant on BDNF (Lu et al., 2014), and we have already discussed how wtHTT upregulates the synthesis and trafficking of this essential neurotrophin (Zuccato et al., 2001; Gauthier et al., 2004). Therefore, it can be speculated that a decrease in BDNF synthesis and/or delivery to synaptic sites following wtHTT loss may impair hippocampal LTP. In HD mice, exogenous BDNF application is sufficient to restore LTP to control levels (Lynch et al., 2007). CREB binding protein (CBP),

a histone acetyltransferase and CREB co-activator that helps regulate the expression of a number of plasticity-related genes, is a known wtHTT interactor and its transcriptional activity is disrupted in HD mouse models (Steffan et al., 2000; Cong et al., 2005; Jiang et al., 2006). Furthermore, by reducing the clustering of PSD-95 at postsynaptic sites (Parsons et al., 2014), wtHTT loss may reduce the number of trapping slots available for AMPA receptor insertion during LTP (Opazo et al., 2012). It is also conceivable that wtHTT loss can impact long-term depression (LTD) by interfering with the normal function of the wtHTT/HIP1 complex. In addition to a role for this complex in the presynapse as discussed above, HIP1 is also known to be particularly enriched in dendrites and at postsynaptic sites (Metzler et al., 2003; Okano et al., 2003; Yao et al., 2006), where it colocalizes and interacts with GluA1. Activity-dependent AMPA receptor internalization is absent in HIP1 knockout mice, with attenuated internalization observed in heterozygous mice (Metzler et al., 2003). Excess unbound HIP1, which may arise either through mHTT presence (Kalchman et al., 1997) or loss of wtHTT, increases the activation of proapoptotic caspases including caspase-3 and caspase-8 (Hackam et al., 2000; Gervais et al., 2002; Zhang et al., 2006). In addition to its well-accepted role as an executioner caspase, transient caspase-3 activation is required for NMDA receptor-dependent LTD (Li et al., 2010). In sum, while largely speculative at present, numerous possibilities exist in which a reduction in wtHTT can negatively impact synaptic plasticity. Indeed, it has been demonstrated that postsynaptic expression of the wtHTT homolog in Aplysia is required for long-term facilitation of excitatory responses at the sensory-to-motor neuron synapse (Choi et al., 2014). More recently, shRNA-mediated wtHTT knockdown in the hippocampus was found to prevent novel location learning (Shen et al., 2019). It is important for future studies to determine how wtHTT reductions impact different forms of synaptic plasticity in different brain regions, as cognitive disturbances can emerge early in HD-mutation carriers and are often reported to be the most debilitating aspect of the disease (Paulsen, 2011).

HTT LOSS *in vivo* DURING DEVELOPMENT

It is indisputable that wtHTT is essential for development, as its knockout is embryonic lethal (Duyao et al., 1995; Nasir et al., 1995; Zeitlin et al., 1995). Furthermore, heterozygous wtHTT knockout mice exhibit motor and cognitive deficits, as well as substantial neuronal loss (up to 50%) in the globus pallidus and the subthalamic nucleus (Nasir et al., 1995; O'Kusky et al., 1999). However, no cell death is observed in the striatum of these heterozygous mice, again demonstrating that the regional sensitivities to wtHTT loss do not necessarily mirror the regional sensitivities of mHTT toxicity.

Conditional wtHTT models also clearly demonstrate that wtHTT is necessary for proper synapse development, function, and stability. Interestingly, early hyperexcitability that cannot be maintained has been reported in HD (Joshi et al., 2009). In the YAC128 mouse model of HD, increased glutamate release and excitatory currents are observed in the striatum at one month of age — well in advance of a detectable HD-like behavioral phenotype. However, reduced excitatory synaptic activity is observed in the stratum in later disease stages when a behavioral phenotype is present (Joshi et al., 2009). Synapse instability leading to synapse loss is well documented in HD, particularly in later disease stages (Murmu et al., 2013, 2015; Smith-Dijak et al., 2019). Interestingly, a similar bidirectional alteration in excitatory synaptic activity was observed in a conditional wtHTT knockout model (McKinstry et al., 2014). By crossing Emx1-Cre mice with wtHTT floxed mice, the authors generated mice with wtHTT depleted in the developing cortex. In these mice, excitatory synaptic connections developed in an accelerated manner in both the cortex and the striatum, although the accelerated synaptogenesis could not be maintained in the cortex and by 5 weeks of age, a reduction of synaptic contacts was observed. Thus, evidence for early hyperexcitability followed by synapse loss has been observed for both HD and wtHTT loss. A separate study observed axonal degeneration when wtHTT was deleted from forebrain neurons (Dragatsis et al., 2000). A similar approach was used more recently to deplete wtHTT in striatal SPNs during development (Burrus et al., 2020). By crossing A2A-Cre or D1-Cre mice with wtHTT floxed mice, the authors generated mice that lack wtHTT in either direct pathway SPNs (dSPNs) or indirect pathway SPNs (iSPNs). When they examined key projection targets of SPNs, namely the globus pallidum external segment (GPe) and the substantia nigra pars reticulata (SNR), they found that wtHTT was required for the proper development of inhibitory synaptic connections. Knocking out wtHTT in iSPNs decreased the number of inhibitory synapses and reduced mIPSC frequency in the GPe. Knocking out wtHTT in dSPNs increased the number of inhibitory synapses in the GPe (but was without effect on mIPSC frequency) and increased mIPSC frequency in the SNR (but was without an effect on inhibitory synapse number). In addition to altering inhibitory synapse development in key SPN target regions, wtHTT knockdown in either dSPNs or iSPNs was sufficient to impair motor function. Together, these studies clearly indicate that wtHTT plays a key role in proper synapse development. As HD mutation carriers are born with low levels of wtHTT in addition to the presence of mHTT, it is possible that the low wtHTT expression, or dominant-negative functions of mHTT presence, may alter the normal course of synapse development. Whether similar alterations in synaptic connectivity are observed following wtHTT reduction in adulthood remains to be seen, though particular attention must be paid in future studies to assess whether synapse loss can result from long-term HTT reduction therapies.

HUNTINGTIN LOSS IN ADULTHOOD: IS IT SAFE?

One particularly pressing question that remains to be answered is whether or not wtHTT loss in adulthood is safe. Although many *in vivo* studies have been performed that reduce wtHTT to varying amounts in the brain, a clear consensus has yet to

be reached (for a detailed recent review on HTT-lowering, also see Grondin and Kaemmerer, 2019). Methodological differences make it extremely challenging to directly compare the results of independent studies, as the magnitude, spread and duration of wtHTT loss can vary considerably from one study to the next. Furthermore, the readout of tolerability can range from survival to rotarod performance to western blot and immunohistochemical quantification of markers of neuronal density and gliosis. Based on our review of the literature, it is clear to us that wtHTT loss is not well-tolerated at the synaptic level, which is known to precede neurodegeneration in not just HD but also in many other neurodegenerative diseases (Selkoe, 2002; Milnerwood and Raymond, 2010; Mandolesi et al., 2015; Tyebji and Hannan, 2017). While the present review focused on wtHTT's role at the pre- and postsynapse, it is well-established that many synapses exist in a tripartite configuration with astrocytes playing an essential role in synaptic function. For example, perisynaptic astrocytic processes dictate the spatial spread and temporal profile of extracellular glutamate transients following synaptic release (for a recent review, see Brymer et al., 2021). Astrocyte dysfunction has been well-documented in HD (Khakh et al., 2017), and expressing mHTT specifically in astrocytes can impair astrocytic BDNF release (Hong et al., 2016) and recapitulate many key features of the HD-like phenotype in mice (Bradford et al., 2009). Conversely, reducing mHTT in astrocytes can ameliorate behavioral, electrophysiological and neuropathological measures of disease progression in HD mice (Wood et al., 2019). At present, very little is known regarding how wtHTT loss affects essential astrocytic functions; however, given that mHTT inhibits astrocytic BDNF release by reducing BDNF vesicle docking, and given the known roles of wtHTT in vesicular regulation described earlier in this review, it would not be surprising if wtHTT loss in astrocytes exerted a similar effect. Given the strong link between astrocyte dysfunction and HD pathogenesis, and the non-selective nature of many HTT-lowering therapeutics, it is important that we better understand the role of wtHTT in not just neurons, but glial cells as well.

Numerous studies in both rodents and Rhesus moneys have reported that partial reduction of wtHTT (ranging from approximately 40 to 75% loss) does not negatively impact motor function nor does it cause any obvious signs of neurodegeneration, gliosis or inflammation (McBride et al., 2011; Grondin et al., 2012; Kordasiewicz et al., 2012). In the HD-171-82Q mouse model of HD, reducing both wtHTT and mHTT significantly improved the motor phenotype in these mice (Boudreau et al., 2009). Similarly, a study using tamoxifen-induced Cre recombinase demonstrated that wtHTT depletion in the adult brain had no effect on motor performance on the rotarod 7-8 months after tamoxifen injection (Wang et al., 2016). In this same study, 3 months of wtHTT knockdown had no effect on brain size nor did it affect the expression of markers of neurons, astrocytes, apoptosis or autophagy. On the other hand, RNAi-mediated wtHTT reductions in the striatum have been shown to alter the expression of numerous genes; genes that are up- or downregulated by wtHTT loss in adulthood play key roles in many of the functions described above in the present review, including axonal transport and secretion, LTP and LTD, glutamate and calcium signaling, and synaptic neurotransmission (Boudreau et al., 2009; Drouet et al., 2009).

Huntington disease mutation carriers almost always carry one copy of each the mutant allele and the wild-type allele. As a result, wtHTT levels are reduced throughout development and will be reduced further with any of the non-selective HTT reduction strategies. wtHTT reduction during development is likely to exert a negative effect on its own, as wtHTT heterozygous mice exhibit motor and cognitive deficits as well as neurodegeneration (Nasir et al., 1995; O'Kusky et al., 1999). Interestingly, in HD mutation carriers, a SNP on the wt*HTT* allele that reduces its expression is associated with an earlier disease onset (Bećanović et al., 2015). Recently, Dietrich and colleagues (2017) used a tamoxifen-inducible Cre-recombinase model to deplete wtHTT. However, in their study, one allele of wt*HTT* was floxed while the other was knocked out. In other words, these mice developed with half the normal levels of wtHTT before wtHTT was depleted by tamoxifen injection in adulthood at 3, 6, and 9 months of age. When wtHTT was depleted in adulthood in these mice, the authors observed a significantly reduced lifespan, impaired motor performance on the rotarod, various behavioral abnormalities (as assessed by the SHIRPA scale described previously Glynn et al., 2003), reduced brain weight, reactive gliosis, and impaired iron metabolism leading to calcification in the thalamus (Dietrich et al., 2017). Despite all these observed consequences of wtHTT loss, they found no clear evidence of pathology in the striatum or cortex, again suggesting that the regional sensitivities of wtHTT LOF do not necessarily mimic those of mHTT gain of function.

CONCLUSION

Many of the studies discussed in this review demonstrate a clear role for wtHTT in synaptic function; for example, by complexing with essential synaptic proteins or by facilitating the delivery of synaptic cargoes from the cell body to pre- and postsynaptic compartments. In studies that reduce wtHTT *in vivo*, many putative emerging synaptic deficits are likely to go unnoticed in behavioral assessments that occur within a few months of wtHTT knockdown. After all, an excessive number of CAG repeats — only seen in the most severe cases of juvenile HD — is required to produce a HD-like phenotype within the lifespan of a rodent. In HD, synaptic deficits emerge before cells die and before a behavioral phenotype is evident (Li et al., 2003; Milnerwood and Raymond, 2010; Raymond et al., 2011; Tyebji and Hannan, 2017; Ravalia et al., 2021). Here, we argue that many core synaptic functions are at risk with non-selective HTT reduction strategies, and that if those synaptic functions are indeed compromised following wtHTT knockdown, then it is only a question of how long it will take before overt consequences are observed at the behavioral level. While we are not arguing against the belief that the net benefit of combined wtHTT and mHTT lowering may outweigh the continued presence of high levels of mHTT in HD individuals, we do argue that longer durations of wtHTT loss coupled with more sensitive tests of CNS dysfunction are required before a consensus can be reached

regarding the relative tolerability of wtHTT loss in adulthood. Lastly, we emphasize the importance of acknowledging that the most sensitive regions in HD, such as the striatum and cortex, are not necessarily the regions that will be impacted the most by wtHTT reduction. For example, the thalamus is rarely discussed as a major brain region of particular susceptibility in HD yet shows striking calcification following wtHTT loss (Dietrich et al., 2017). Iron homeostasis is altered in the thalamus and the cerebellum following wtHTT loss (Dietrich et al., 2017), even though the cerebellum is often relatively spared in HD mouse models (Zhang et al., 2010; Carroll et al., 2011; Brooks et al., 2012). Similarly, the regional cell death patterns observed in heterozygous wtHTT knockout mice do not match the patterns of cell death observed in HD (Nasir et al., 1995; O'Kusky et al., 1999). Thus, when assessing the consequences of wtHTT loss, it is of utmost importance to consider extrastriatal brain regions as well as non-motor behavioral signs, as the non-motor symptoms of HD can oftentimes become the most burdensome aspect of the disease. Interestingly, there is evidence to suggest that wtHTT function can modulate depression and anxiety, two debilitating non-motor symptoms associated with HD. Specifically, reduced phosphorylation of wtHTT at S1181 and S1201 can increase hippocampal neurogenesis and reduce anxiety and depression-like behaviors in mice (Ben et al., 2013). By obtaining a more thorough understanding of the consequences of wtHTT loss, it will be possible to determine whether wtHTT can be safely lowered in HD patients, and if not, what essential functions of wtHTT must be restored following non-selective HTT reduction.

AUTHOR CONTRIBUTIONS

JB, EH, and MP wrote the manuscript. All authors contributed to the article and approved the submitted version.

FUNDING

This study was funded by the Canadian Institutes of Health Research.

REFERENCES

Ackermann, F., Schink, K. O., Bruns, C., Izsvák, Z., Hamra, F. K., Rosenmund, C., et al. (2019). Critical role for piccolo in synaptic vesicle retrieval. *eLife* 8:e46629. doi: 10.7554/eLife.46629

Aguiar, S., van der Gaag, B., and Cortese, F. A. B. (2017). RNAi mechanisms in Huntington's disease therapy: SiRNA versus shRNA. *Transl. Neurodegener.* 6:30. doi: 10.1186/s40035-017-0101-9

Anne, S. L., Saudou, F., and Humbert, S. (2007). Phosphorylation of huntingtin by cyclin-dependent kinase 5 is induced by DNA damage and regulates wild-type and mutant huntingtin toxicity in neurons. *J. Neurosci.* 27, 7318–7328. doi: 10.1523/JNEUROSCI.1831-07.2007

Baquet, Z. C., Gorski, J. A., and Jones, K. R. (2004). Early striatal dendrite deficits followed by neuron loss with advanced age in the absence of anterograde cortical brain-derived neurotrophic factor. *J. Neurosci.* 24, 4250–4258. doi: 10.1523/JNEUROSCI.3920-03.2004

Bećanović, K., Nørremølle, A., Neal, S. J., Kay, C., Collins, J. A., Arenillas, D., et al. (2015). A SNP in the HTT promoter alters NF-κB binding and is a bidirectional genetic modifier of Huntington disease. *Nat. Neurosci.* 18, 807–816. doi: 10.1038/nn.4014

Ben, M., Barek, K., Pla, P., Orvoen, S., Benstaali, C., Godin, J. D., et al. (2013). Huntingtin mediates anxiety/depression-related behaviors and hippocampal neurogenesis. *J. Neurosci.* 33, 8608–8620. doi: 10.1523/JNEUROSCI.5110-12.2013

Bhakar, A. L., Tannis, L. L., Zeindler, C., Russo, M. P., Jobin, C., Park, D. S., et al. (2002). Constitutive nuclear factor-κB activity is required for central neuron survival. *J. Neurosci.* 22, 8466–8475. doi: 10.1523/jneurosci.22-19-08466.2002

Birdsall, V., and Waites, C. L. (2019). Autophagy at the synapse. *Neurosci. Lett.* 697, 24–28. doi: 10.1016/j.neulet.2018.05.033

Borgonovo, J. E., Troncoso, M., Lucas, J. J., and Sosa, M. A. (2013). Mutant huntingtin affects endocytosis in striatal cells by altering the binding of AP-2 to membranes. *Exp. Neurol.* 241, 75–83. doi: 10.1016/j.expneurol.2012.11.025

Boudreau, R. L., McBride, J. L., Martins, I., Shen, S., Xing, Y., Carter, B. J., et al. (2009). Nonallele-specific silencing of mutant and wild-type huntingtin demonstrates therapeutic efficacy in Huntington's disease mice. *Mol. Ther.* 17, 1053–1063. doi: 10.1038/mt.2009.17

Bradford, J., Shin, J. Y., Roberts, M., Wang, C. E., Li, X. J., and Li, S. (2009). Expression of mutant huntingtin in mouse brain astrocytes causes age-dependent neurological symptoms. *Proc. Natl. Acad. Sci. U.S.A.* 106, 22480–22485. doi: 10.1073/pnas.0911503106

Brandstaetter, H., Kruppa, A. J., and Buss, F. (2014). Huntingtin is required for ER-to-Golgi transport and for secretory vesicle fusion at the plasma membrane. *Dis. Model. Mech.* 7, 1335–1340. doi: 10.1242/dmm.017368

Brito, V., Giralt, A., Enriquez-barreto, L., Puigdellívol, M., Suelves, N., Zamora-moratalla, A., et al. (2014). Neurotrophin receptor p75 NTR mediates Huntington's disease-associated synaptic and memory dysfunction. *J. Clin. Invest.* 124, 4411–4428. doi: 10.1172/JCI74809.long-term

Brooks, S. P., Jones, L., and Dunnett, S. B. (2012). Comparative analysis of pathology and behavioural phenotypes in mouse models of Huntington's disease. *Brain Res. Bull.* 88, 81–93. doi: 10.1016/j.brainresbull.2011.10.002

Bruyère, J., Abada, Y. S., Vitet, H., Fontaine, G., Deloulme, J. C., Cès, A., et al. (2020). Presynaptic APP levels and synaptic homeostasis are regulated by Akt phosphorylation of Huntingtin. *eLife* 9:e56371. doi: 10.1101/2020.04.21.052506

Brymer, K. J., Barnes, J. R., and Parsons, M. P. (2021). Entering a new era of quantifying glutamate clearance in health and disease. *J. Neurosci. Res.* 99, 1598–1617. doi: 10.1002/jnr.24810

Bulgari, D., Deitcher, D. L., and Levitan, E. S. (2017). Loss of Huntingtin stimulates capture of retrograde dense-core vesicles to increase synaptic neuropeptide stores. *Eur. J. Cell Biol.* 96, 402–406. doi: 10.1016/j.ejcb.2017.01.001

Burrus, C. J., McKinstry, S. U., Kim, N., Ozlu, M. I., Santoki, A. V., Fang, F. Y., et al. (2020). Striatal projection neurons require huntingtin for synaptic connectivity and survival. *Cell Rep.* 30, 642–657.e6. doi: 10.1016/j.celrep.2019.12.069

Carroll, J. B., Lerch, J. P., Franciosi, S., Spreeuw, A., Bissada, N., Henkelman, R. M., et al. (2011). Natural history of disease in the YAC128 mouse reveals a discrete signature of pathology in Huntington disease. *Neurobiol. Dis.* 43, 257–265. doi: 10.1016/j.nbd.2011.03.018

Chanaday, N. L., and Kavalali, E. T. (2018). Presynaptic origins of distinct modes of neurotransmitter release. *Curr. Opin. Neurobiol.* 51, 119–126. doi: 10.1016/j.conb.2018.03.005

Choi, Y. B., Kadakkuzha, B. M., Liu, X. A., Akhmedov, K., Kandel, E. R., and Puthanveettil, S. V. (2014). Huntingtin is critical both pre- and postsynaptically for long-term learning-related synaptic plasticity in Aplysia. *PLoS One* 9:e103004. doi: 10.1371/journal.pone.0103004

Colin, E., Zala, D., Liot, G., Rangone, H., Borrell-Pagès, M., Li, X. J., et al. (2008). Huntingtin phosphorylation acts as a molecular switch for anterograde/retrograde transport in neurons. *EMBO J.* 27, 2124–2134. doi: 10.1038/emboj.2008.133

Cong, S. Y., Pepers, B. A., Evert, B. O., Rubinsztein, D. C., Roos, R. A. C., Van Ommen, G. J. B., et al. (2005). Mutant huntingtin represses CBP, but not p300, by binding and protein degradation. *Mol. Cell. Neurosci.* 30, 12–23. doi: 10.1016/j.mcn.2005.05.003

Cozzolino, F., Vezzoli, E., Cheroni, C., Besusso, D., Conforti, P., Valenza, M., et al. (2021). ADAM10 hyperactivation acts on piccolo to deplete synaptic vesicle stores in Huntington's disease. *Hum. Mol. Genet.* doi: 10.1093/hmg/ddab047 [Epub ahead of print].

Craven, S. E., El-Husseini, A. E., and Bredt, D. S. (1999). Synaptic targeting of the postsynaptic density protein PSD-95 mediated by lipid and protein motifs. *Neuron* 22, 497–509. doi: 10.1016/S0896-6273(00)80705-9

Dey, S., Banker, G., and Ray, K. (2017). Anterograde transport of Rab4-associated vesicles regulates synapse organization in *Drosophila*. *Cell Rep.* 18, 2452–2463. doi: 10.1016/j.celrep.2017.02.034

Di Maio, L., Squitieri, F., Napolitano, G., Campanella, G., Trofatter, J. A., and Conneally, P. M. (1993). Suicide risk in Huntington's disease. *J. Med. Genet.* 30, 293–295.

Dietrich, P., Johnson, I. M., Alli, S., and Dragatsis, I. (2017). Elimination of huntingtin in the adult mouse leads to progressive behavioral deficits, bilateral thalamic calcification, and altered brain iron homeostasis. *PLoS Genet.* 13:e1006846. doi: 10.1371/journal.pgen.1006846

DiFiglia, M., Sapp, E., Chase, K. O., Davies, S. W., Bates, G. P., Vonsattel, J. P., et al. (1997). Aggregation of huntingtin in neuronal intranuclear inclusions and dystrophic neurites in brain. *Science* 277, 1990–1993. doi: 10.1126/science.277.5334.1990

DiFiglia, M., Sapp, E., Chase, K., Schwarz, C., Meloni, A., Young, C., et al. (1995). Huntingtin is a cytoplasmic protein associated with vesicles in human and rat brain neurons. *Neuron* 14, 1075–1081. doi: 10.1016/0896-6273(95)90346-1

Dragatsis, I., Levine, M. S., and Zeitlin, S. (2000). Inactivation of Hdh in the brain and testis results in progressive neurodegeneration and sterility in mice. *Nat. Genet.* 26, 300–306. doi: 10.1038/81593

Drouet, V., Perrin, V., Hassig, R., Dufour, N., Auregan, G., Alves, S., et al. (2009). Sustained effects of nonallele-specific huntingtin silencing. *Ann. Neurol.* 65, 276–285. doi: 10.1002/ana.21569

Duyao, M. P., Auerbach, A. B., Ryan, A., Persichetti, F., Barnes, G. T., McNeil, S. M., et al. (1995). Inactivation of the mouse huntington's disease gene homolog Hdh. *Science* 269, 407–410. doi: 10.1126/science.7618107

Edwardson, J. M., Wang, C. T., Gong, B., Wyttenbach, A., Bai, J., Jackson, M. B., et al. (2003). Expression of mutant huntingtin blocks exocytosis in PC12 cells by depletion of complexin II. *J. Biol. Chem.* 278, 30849–30853. doi: 10.1074/jbc.M304615200

Ehrnhoefer, D. E., Sutton, L., and Hayden, M. R. (2011). Small changes, big impact: posttranslational modifications and function of huntingtin in huntington disease. *Neuroscientist* 17, 475–492. doi: 10.1177/1073858410390378

El-Husseini, A. E. D., Schnell, E., Dakoji, S., Sweeney, N., Zhou, Q., Prange, O., et al. (2002). Synaptic strength regulated by palmitate cycling on PSD-95. *Cell* 108, 849–863. doi: 10.1016/S0092-8674(02)00683-9

El-Daher, M., Hangen, E., Bruyère, J., Poizat, G., Al-Ramahi, I., Pardo, R., et al. (2015). Huntingtin proteolysis releases non−polyQ fragments that cause toxicity through dynamin 1 dysregulation. *EMBO J.* 34, 2255–2271. doi: 10.15252/embj.201490808

Engelender, S., Sharp, A. H., Colomer, V., Tokito, M. K., Lanahan, A., Worley, P., et al. (1997). Huntingtin-associated protein 1 (HAP1) interacts with the p150(Glued) subunit of dynactin. *Hum. Mol. Genet.* 6, 2205–2212. doi: 10.1093/hmg/6.13.2205

Eom, T., Antar, L. N., Singer, R. H., and Bassell, G. J. (2003). Localization of a B-actin messenger ribonucleoprotein complex with Zipcode-binding protein modulates the density of dendritic filopodia and filopodial synapses. *J. Neurosci.* 23, 10433–10444. doi: 10.1523/jneurosci.23-32-10433.2003

Fisher, E. R., and Hayden, M. R. (2014). Multisource ascertainment of Huntington disease in Canada: prevalence and population at risk. *Mov. Disord.* 29, 105–114. doi: 10.1002/mds.25717

Fridmacher, V., Kaltschmidt, B., Goudeau, B., Ndiaye, D., Rossi, F. M., Pfeiffer, J., et al. (2003). Forebrain-specific neuronal inhibition of nuclear factor-κB activity leads to loss of neuroprotection. *J. Neurosci.* 23, 9403–9408. doi: 10.1523/jneurosci.23-28-09403.2003

Gauthier, L. R., Charrin, B. C., Borrell-Pagès, M., Dompierre, J. P., Rangone, H., Cordelières, F. P., et al. (2004). Huntingtin controls neurotrophic support and survival of neurons by enhancing BDNF vesicular transport along microtubules. *Cell* 118, 127–138. doi: 10.1016/j.cell.2004.06.018

Gervais, F. G., Singaraja, R., Xanthoudakis, S., Gutekunst, C. A., Leavitt, B. R., Metzler, M., et al. (2002). Recruitment and activation of caspase-8 by the Huntingtin-interacting protein Hip-1 and a novel partner Hippi. *Nat. Cell Biol.* 4, 95–105. doi: 10.1038/ncb735

Ginés, S., Bosch, M., Marco, S., Gavaldà, N., Díaz-Hernández, M., Lucas, J. J., et al. (2006). Reduced expression of the TrkB receptor in Huntington's disease mouse models and in human brain. *Eur. J. Neurosci.* 23, 649–658. doi: 10.1111/j.1460-9568.2006.04590.x

Giralt, A., Brito, V., Chevy, Q., Simonnet, C., Otsu, Y., Cifuentes-Díaz, C., et al. (2017). Pyk2 modulates hippocampal excitatory synapses and contributes to cognitive deficits in a Huntington's disease model. *Nat. Commun.* 8:15592. doi: 10.1038/ncomms15592

Glynn, D., Bortnick, R. A., and Morton, A. J. (2003). Complexin II is essential for normal neurological function in mice. *Hum. Mol. Genet.* 12, 2431–2448. doi: 10.1093/hmg/ddg249

Goldstein, A. Y., Wang, X., and Schwarz, T. L. (2008). Axonal transport and the delivery of pre-synaptic components. *Curr. Opin. Neurobiol.* 18, 495–503. doi: 10.1016/j.conb.2008.10.003

Graham, R. K., Deng, Y., Slow, E. J., Haigh, B., Bissada, N., Lu, G., et al. (2006). Cleavage at the Caspase-6 site is required for neuronal dysfunction and degeneration due to mutant Huntingtin. *Cell* 125, 1179–1191. doi: 10.1016/j.cell.2006.04.026

Grondin, R. C., and Kaemmerer, W. F. (2019). The effects of Huntingtin-lowering?: What do we know so far? *Degener. Neurol. Neuromuscul. Dis.* 9, 3–17.

Grondin, R., Kaytor, M. D., Ai, Y., Nelson, P. T., Thakker, D. R., Heisel, J., et al. (2012). Six-month partial suppression of Huntingtin is well tolerated in the adult rhesus striatum. *Brain* 135, 1197–1209. doi: 10.1093/brain/awr333

Guedes-Dias, P., and Holzbaur, E. L. F. (2019). Axonal transport: driving synaptic function. *Science* 366:eaaw9997. doi: 10.1126/science.aaw9997

Gunawardena, S., Her, L. S., Brusch, R. G., Laymon, R. A., Niesman, I. R., Gordesky-Gold, B., et al. (2003). Disruption of axonal transport by loss of huntingtin or expression of pathogenic polyQ proteins in *Drosophila*. *Neuron* 40, 25–40. doi: 10.1016/S0896-6273(03)00594-4

Hackam, A. S., Yassa, A. S., Singaraja, R., Metzler, M., Gutekunst, C. A., Gan, L., et al. (2000). Huntingtin interacting protein 1 induces apoptosis via a novel caspase-dependent death effector domain. *J. Biol. Chem.* 275, 41299–41308. doi: 10.1074/jbc.M008408200

Hamilton, J. M., Salmon, D. P., Corey-Bloom, J., Gamst, A., Paulsen, J. S., Jerkins, S., et al. (2003). Behavioural abnormalities contribute to functional decline in Huntington's disease. *J. Neurol. Neurosurg. Psychiatry* 74, 120–122. doi: 10.1136/jnnp.74.1.120

Harjes, P., and Wanker, E. E. (2003). The hunt for huntingtin function: interaction partners tell many different stories. *Trends Biochem. Sci.* 28, 425–433. doi: 10.1016/S0968-0004(03)00168-3

Harward, S. C., Hedrick, N. G., Hall, C. E., Parra-Bueno, P., Milner, T. A., Pan, E., et al. (2016). Autocrine BDNF-TrkB signalling within a single dendritic spine. *Nature* 538, 99–103. doi: 10.1038/nature19766

Hayashi, T., Rumbaugh, G., and Huganir, R. L. (2005). Differential regulation of AMPA receptor subunit trafficking by palmitoylation of two distinct sites. *Neuron* 47, 709–723. doi: 10.1016/j.neuron.2005.06.035

Hayashi, T., Thomas, G. M., and Huganir, R. L. (2009). Dual palmitoylation of NR2 subunits regulates NMDA receptor trafficking. *Neuron* 64, 213–226. doi: 10.1016/j.neuron.2009.08.017

Her, L. S., and Goldstein, L. S. B. (2008). Enhanced sensitivity of striatal neurons to axonal transport defects induced by mutant huntingtin. *J. Neurosci.* 28, 13662–13672. doi: 10.1523/JNEUROSCI.4144-08.2008

Hernandez, D., Torres, C. A., Setlik, W., Cebrián, C., Mosharov, E. V., Tang, G., et al. (2012). Regulation of presynaptic neurotransmission by macroautophagy. *Neuron* 74, 277–284. doi: 10.1016/j.neuron.2012.02.020

Hersch, S., Claassen, D., Edmondson, M., Wild, E., Guerciolini, R., and Panzara, M. (2017). Multicenter, randomized, double-blind, placebo-controlled Phase 1b/2a Studies of WVE-120101 and WVE-120102 in Patients with Huntington's disease (P2.006). *Neurology* 88:P2.006.

Hong, Y., Zhao, T., Li, X.-J., and Li, S. (2016). Mutant Huntingtin impairs BDNF release from astrocytes by disrupting conversion of Rab3a-GTP into Rab3a-GDP. *J. Neurosci.* 36, 8790–8801. doi: 10.1523/JNEUROSCI.0168-16.2016

Huang, K., Sanders, S. S., Kang, R., Carroll, J. B., Sutton, L., Wan, J., et al. (2011). Wild-type HTT modulates the enzymatic activity of the neuronal palmitoyl transferase HIP14. *Hum. Mol. Genet.* 20, 3356–3365. doi: 10.1093/hmg/ddr242

Jiang, H., Poirier, M. A., Liang, Y., Pei, Z., Weiskittel, C. E., Smith, W. W., et al. (2006). Depletion of CBP is directly linked with cellular toxicity caused by mutant huntingtin. *Neurobiol. Dis.* 23, 543–551. doi: 10.1016/j.nbd.2006.04.011

Joshi, P. R., Wu, N. P., André, V. M., Cummings, D. M., Cepeda, C., Joyce, J. A., et al. (2009). Age-dependent alterations of corticostriatal activity in the YAC128 mouse model of Huntington disease. *J. Neurosci.* 29, 2414–2427. doi: 10.1523/JNEUROSCI.5687-08.2009

Kalchman, M. A., Koide, H. B., McCutcheon, K., Graham, R. K., Nichol, K., Nishiyama, K., et al. (1997). HIP1, a human homologue of S. *cerevisiae* Sla2p, interacts with membrane- associated huntingtin in the brain. *Nat. Genet.* 16, 44–53. doi: 10.1038/ng0597-44

Kaltschmidt, B., and Kaltschmidt, C. (2015). NF-KappaB in long-term memory and structural plasticity in the adult mammalian brain. *Front. Mol. Neurosci.* 8:69. doi: 10.3389/fnmol.2015.00069

Kang, R., Wang, L., Sanders, S. S., Zuo, K., Hayden, M. R., and Raymond, L. A. (2019). Altered regulation of striatal neuronal N-methyl-D-aspartate receptor trafficking by palmitoylation in Huntington disease mouse model. *Front. Synaptic Neurosci.* 11:3. doi: 10.3389/fnsyn.2019.00003

Khakh, B. S., Beaumont, V., Cachope, R., Munoz-Sanjuan, I., Goldman, S. A., and Grantyn, R. (2017). Unravelling and exploiting astrocyte dysfunction in Huntington's disease. *Trends Neurosci.* 40, 422–437. doi: 10.1016/j.tins.2017.05.002

Kononenko, N. L., Claßen, G. A., Kuijpers, M., Puchkov, D., Maritzen, T., Tempes, A., et al. (2017). Retrograde transport of TrkB-containing autophagosomes via the adaptor AP-2 mediates neuronal complexity and prevents neurodegeneration. *Nat. Commun.* 8:14819. doi: 10.1038/ncomms14819

Kordasiewicz, H. B., Stanek, L. M., Wancewicz, E. V., Mazur, C., McAlonis, M. M., Pytel, K. A., et al. (2012). Sustained therapeutic reversal of Huntington's disease by transient repression of huntingtin synthesis. *Neuron* 74, 1031–1044.

Kuhn, P. H., Wang, H., Dislich, B., Colombo, A., Zeitschel, U., Ellwart, J. W., et al. (2010). ADAM10 is the physiologically relevant, constitutive α-secretase of the amyloid precursor protein in primary neurons. *EMBO J.* 29, 3020–3032. doi: 10.1038/emboj.2010.167

Kumar, A., Vaish, M., and Ratan, R. R. (2014). Transcriptional dysregulation in Huntington's disease: a failure of adaptive transcriptional homeostasis. *Drug Discov. Today* 19, 956–962. doi: 10.1016/j.drudis.2014.03.016

Kwon, D. (2021). Failure of genetic therapies for Huntington's devastates community. *Nature* 593:180. doi: 10.1038/d41586-021-01177-7

Leavitt, B. R., Guttman, J. A., Hodgson, J. G., Kimel, G. H., Singaraja, R., Vogl, A. W., et al. (2001). Wild-type Huntingtin reduces the cellular toxicity of mutant Huntingtin *in vivo*. *Am. J. Hum. Genet.* 68, 313–324. doi: 10.1086/318207

Leavitt, B. R., Van Raamsdonk, J. M., Shehadeh, J., Fernandes, H., Murphy, Z., Graham, R. K., et al. (2006). Wild-type huntingtin protects neurons from excitotoxicity. *J. Neurochem.* 96, 1121–1129. doi: 10.1111/j.1471-4159.2005.03605.x

Li, J. Y., Plomann, M., and Brundin, P. (2003). Huntington's disease: A synaptopathy? *Trends Mol. Med.* 9, 414–420. doi: 10.1016/j.molmed.2003.08.006

Li, S. H., Gutekunst, C. A., Hersch, S. M., and Li, X. J. (1998). Interaction of Huntingtin-associated protein with dynactin P150Glued. *J. Neurosci.* 18, 1261–1269. doi: 10.1523/jneurosci.18-04-01261.1998

Li, X. J., Li, S. H., Sharp, A. H., Nucifora, F. C., Schilling, G., Lanahan, A., et al. (1995). A huntingtin-associated protein enriched in brain with implications for pathology. *Nature* 378, 398–402. doi: 10.1038/378398a0

Li, Z., Jo, J., Jia, J. M., Lo, S. C., Whitcomb, D. J., Jiao, S., et al. (2010). Caspase-3 activation via mitochondria is required for long-term depression and AMPA receptor internalization. *Cell* 141, 859–871. doi: 10.1016/j.cell.2010.03.053

Liang, Y. T., and Sigrist, S. (2018). Autophagy and proteostasis in the control of synapse aging and disease. *Curr. Opin. Neurobiol.* 48, 113–121. doi: 10.1016/j.conb.2017.12.006

Liot, G., Zala, D., Pla, P., Mottet, G., Piel, M., and Saudou, F. (2013). Mutant Huntingtin alters retrograde transport of TrkB receptors in striatal dendrites. *J. Neurosci.* 33, 6298–6309. doi: 10.1523/JNEUROSCI.2033-12.2013

Lo Sardo, V., Zuccato, C., Gaudenzi, G., Vitali, B., Ramos, C., Tartari, M., et al. (2012). An evolutionary recent neuroepithelial cell adhesion function of huntingtin implicates ADAM10-Ncadherin. *Nat. Neurosci.* 15, 713–721. doi: 10.1038/nn.3080

Lu, B., Nagappan, G., and Lu, Y. (2014). "BDNF and synaptic plasticity, cognitive function, and dysfunction," in *Neurotrophic Factors*, eds G. R. Lewin and B. D. Carter (Berlin: Springer), 223–250. doi: 10.1007/978-3-642-45106-5_9

Lundgren, J. L., Vandermeulen, L., Sandebring-Matton, A., Ahmed, S., Winblad, B., Di Luca, M., et al. (2020). Proximity ligation assay reveals both pre- and postsynaptic localization of the APP-processing enzymes ADAM10 and BACE1 in rat and human adult brain. *BMC Neurosci.* 21:6. doi: 10.1186/s12868-020-0554-0

Lynch, G., Kramar, E. A., Rex, C. S., Jia, Y., Chappas, D., Gall, C. M., et al. (2007). Brain-derived neurotrophic factor restores synaptic plasticity in a knock-in mouse model of Huntington's disease. *J. Neurosci.* 27, 4424–4434. doi: 10.1523/JNEUROSCI.5113-06.2007

Ma, B., Savas, J. N., Yu, M. S., Culver, B. P., Chao, M. V., and Tanese, N. (2011). Huntingtin mediates dendritic transport of β-actin mRNA in rat neurons. *Sci. Rep.* 1:140. doi: 10.1038/srep00140

MacDonald, M. E., Ambrose, C. M., Duyao, M. P., Myers, R. H., Lin, C., Srinidhi, L., et al. (1993). A novel gene containing a trinucleotide repeat that is expanded and unstable on Huntington's disease chromosomes. *Cell* 72, 971–983. doi: 10.1016/0092-8674(93)90585-E

Mackenzie, K. D., Lumsden, A. L., Guo, F., Duffield, M. D., Chataway, T., Lim, Y., et al. (2016). Huntingtin-associated protein-1 is a synapsin I-binding protein regulating synaptic vesicle exocytosis and synapsin I trafficking. *J. Neurochem.* 138, 710–721. doi: 10.1111/jnc.13703

Mandal, M., Wei, J., Zhong, P., Cheng, J., Duffney, L. J., Liu, W., et al. (2011). Impaired α-amino-3-hydroxy-5-methyl-4-isoxazolepropionic acid (AMPA) receptor trafficking and function by mutant Huntingtin. *J. Biol. Chem.* 286, 33719–33728. doi: 10.1074/jbc.M111.236521

Mandolesi, G., Gentile, A., Musella, A., Fresegna, D., De Vito, F., Bullitta, S., et al. (2015). Synaptopathy connects inflammation and neurodegeneration in multiple sclerosis. *Nat. Rev. Neurol.* 11, 711–724. doi: 10.1038/nrneurol.2015.222

Mangiarini, L., Sathasivam, K., Seller, M., Cozens, B., Harper, A., Hetherington, C., et al. (1996). Exon I of the HD gene with an expanded CAG repeat is sufficient to cause a progressive neurological phenotype in transgenic mice. *Cell* 87, 493–506. doi: 10.1016/S0092-8674(00)81369-0

Marcello, E., Saraceno, C., Musardo, S., Vara, H., De La Fuente, A. G., Pelucchi, S., et al. (2013). Endocytosis of synaptic ADAM10 in neuronal plasticity and Alzheimer's disease. *J. Clin. Invest.* 123, 2523–2538. doi: 10.1172/JCI65401

Marcora, E., and Kennedy, M. B. (2010). The Huntington's disease mutation impairs Huntingtin's role in the transport of NF-κB from the synapse to the nucleus. *Hum. Mol. Genet.* 19, 4373–4384. doi: 10.1093/hmg/ddq358

Martin, D. D. O., Heit, R. J., Yap, M. C., Davidson, M. W., Hayden, M. R., and Berthiaume, L. G. (2014). Identification of a post-translationally myristoylated autophagy-inducing domain released by caspase cleavage of huntingtin. *Hum. Mol. Genet.* 23, 3166–3179. doi: 10.1093/hmg/ddu027

Martin, D. D. O., Kay, C., Collins, J. A., Nguyen, Y. T., Slama, R. A., and Hayden, M. R. (2018). A human huntingtin SNP alters post-Translational modification and pathogenic proteolysis of the protein causing Huntington disease. *Sci. Rep.* 8:8096. doi: 10.1038/s41598-018-25903-w

Martin, D. D. O., Ladha, S., Ehrnhoefer, D. E., and Hayden, M. R. (2015). Autophagy in Huntington disease and huntingtin in autophagy. *Trends Neurosci.* 38, 26–35. doi: 10.1016/j.tins.2014.09.003

Martinez-Vicente, M., Talloczy, Z., Wong, E., Tang, G., Koga, H., Kaushik, S., et al. (2010). Cargo recognition failure is responsible for inefficient autophagy in Huntington's disease. *Nat. Neurosci.* 13, 567–576. doi: 10.1038/nn.2528

Marx, M. C., Billups, D., and Billups, B. (2015). Maintaining the presynaptic glutamate supply for excitatory neurotransmission. *J. Neurosci. Res.* 93, 1031–1044. doi: 10.1002/jnr.23561

McAdam, R. L., Morton, A., Gordon, S. L., Alterman, J. F., Khvorova, A., Cousin, M. A., et al. (2020). Loss of huntingtin function slows synaptic vesicle endocytosis in striatal neurons from the httQ140/Q140 mouse model of Huntington's disease. *Neurobiol. Dis.* 134:104637. doi: 10.1016/j.nbd.2019.104637

McBride, J. L., Pitzer, M. R., Boudreau, R. L., Dufour, B., Hobbs, T., Ojeda, S. R., et al. (2011). Preclinical safety of RNAi-mediated HTT suppression in the rhesus macaque as a potential therapy for Huntington's disease. *Mol. Ther.* 19, 2152–2162. doi: 10.1038/mt.2011.219

McGuire, J. R., Rong, J., Li, S. H., and Li, X. J. (2006). Interaction of Huntingtin-associated protein-1 with kinesin light chain: implications in intracellular trafficking in neurons. *J. Biol. Chem.* 281, 3552–3559. doi: 10.1074/jbc.M509806200

McKinstry, S. U., Karadeniz, Y. B., Worthington, A. K., Hayrapetyan, V. Y., Ozlu, M. I., Serafin-Molina, K., et al. (2014). Huntingtin is required for normal excitatory synapse development in cortical and striatal circuits. *J. Neurosci.* 34, 9455–9472. doi: 10.1523/JNEUROSCI.4699-13.2014

Metzler, M., Legendre-Guillemin, V., Gan, L., Chopra, V., Kwok, A., McPherson, P. S., et al. (2001). HIP1 functions in Clathrin-mediated endocytosis through binding to Clathrin and adaptor protein 2. *J. Biol. Chem.* 276, 39271–39276. doi: 10.1074/jbc.C100401200

Metzler, M., Li, B., Gan, L., Georgiou, J., Gutekunst, C. A., Wang, Y., et al. (2003). Disruption of the endocytic protein HIP1 results in neurological deficits and decreased AMPA receptor trafficking. *EMBO J.* 22, 3254–3266. doi: 10.1093/emboj/cdg334

Migazzi, A., Scaramuzzino, C., Anderson, E., Tripathy, D., Hernandez, I., Virlogeux, A., et al. (2021). Huntingtin-mediated axonal transport requires arginine methylation by PRMT6. *Cell Rep.* 35:108980. doi: 10.2139/ssrn.3520100

Mikenberg, I., Widera, D., Kaus, A., Kaltschmidt, B., and Kaltschmidt, C. (2007). Transcription factor NF-κB is transported to the nucleus via cytoplasmic dynein/dynactin motor complex in hippocampal neurons. *PLoS One* 2:e589. doi: 10.1371/journal.pone.0000589

Milnerwood, A. J., Gladding, C. M., Pouladi, M. A., Kaufman, A. M., Hines, R. M., Boyd, J. D., et al. (2010). Early increase in extrasynaptic NMDA receptor signaling and expression contributes to phenotype onset in Huntington's disease mice. *Neuron* 65, 178–190. doi: 10.1016/j.neuron.2010.01.008

Milnerwood, A. J., Parsons, M. P., Young, F. B., Singaraja, R. R., Franciosi, S., Volta, M., et al. (2013). Memory and synaptic deficits in Hip14/DHHC17 knockout mice. *Proc. Natl. Acad. Sci. U.S.A.* 110, 20296–20301. doi: 10.1073/pnas.1222384110

Milnerwood, A. J., and Raymond, L. A. (2010). Early synaptic pathophysiology in neurodegeneration: insights from Huntington's disease. *Trends Neurosci.* 33, 513–523. doi: 10.1016/j.tins.2010.08.002

Mishra, S. K., Agostinelli, N. R., Brett, T. J., Mizukami, I., Ross, T. S., and Traub, L. M. (2001). Clathrin- and AP-2-binding sites in HIP1 uncover a general assembly role for endocytic accessory proteins. *J. Biol. Chem.* 276, 46230–46236. doi: 10.1074/jbc.M108177200

Müller, U. C., Deller, T., and Korte, M. (2017). Not just amyloid: physiological functions of the amyloid precursor protein family. *Nat. Rev. Neurosci.* 18, 281–298. doi: 10.1038/nrn.2017.29

Murmu, R. P., Li, W., Holtmaat, A., and Li, J. Y. (2013). Dendritic spine instability leads to progressive neocortical spine loss in a mouse model of Huntington's disease. *J. Neurosci.* 33, 12997–13009. doi: 10.1523/JNEUROSCI.5284-12.2013

Murmu, R. P., Li, W., Szepesi, Z., and Li, J.-Y. (2015). Altered sensory experience exacerbates stable dendritic spine and synapse loss in a mouse model of Huntington's disease. *J. Neurosci.* 35, 287–298. doi: 10.1523/JNEUROSCI.0244-14.2015

Murphy, K. P., Carter, R. J., Lione, L. A., Mangiarini, L., Mahal, A., Bates, G. P., et al. (2000). Abnormal synaptic plasticity and impaired spatial cognition in mice transgenic for exon 1 of the human Huntington's disease mutation. *J. Neurosci.* 20, 5115–5123.

Nakakubo, Y., Abe, S., Yoshida, T., Takami, C., Isa, M., Wojcik, S. M., et al. (2020). Vesicular glutamate transporter expression ensures high-fidelity synaptic transmission at the calyx of held synapses. *Cell Rep.* 32:108040. doi: 10.1016/j.celrep.2020.108040

Naryshkin, N. A., Weetall, M., Dakka, A., Narasimhan, J., Zhao, X., Feng, Z., et al. (2014). SMN2 splicing modifiers improve motor function and longevity in mice with spinal muscular atrophy. *Science* 345, 688–693. doi: 10.1126/science.1250127

Nasir, J., Floresco, S. B., O'Kusky, J. R., Diewert, V. M., Richman, J. M., Zeisler, J., et al. (1995). Targeted disruption of the Huntington's disease gene results in embryonic lethality and behavioral and morphological changes in heterozygotes. *Cell* 81, 811–823. doi: 10.1016/0092-8674(95)90542-1

Nikoletopoulou, V., and Tavernarakis, N. (2018). Regulation and roles of autophagy at synapses. *Trends Cell Biol.* 28, 646–661. doi: 10.1016/j.tcb.2018.03.006

O'Kusky, J. R., Nasir, J., Cicchetti, F., Parent, A., and Hayden, M. R. (1999). Neuronal degeneration in the basal ganglia and loss of pallido- subthalamic synapses in mice with targeted disruption of the Huntington's disease gene. *Brain Res.* 818, 468–479. doi: 10.1016/S0006-8993(98)01312-2

Ochaba, J., Lukacsovich, T., Csikos, G., Zheng, S., Margulis, J., Salazar, L., et al. (2014). Potential function for the Huntingtin protein as a scaffold for selective autophagy. *Proc. Natl. Acad. Sci. U.S.A.* 111, 16889–16894. doi: 10.1073/pnas.1420103111

Ohyama, T., Verstreken, P., Ly, C. V., Rosenmund, T., Rajan, A., Tien, A. C., et al. (2007). Huntingtin-interacting protein 14, a palmitoyl transferase required for exocytosis and targeting of CSP to synaptic vesicles. *J. Cell Biol.* 179, 1481–1496. doi: 10.1083/jcb.200710061

Okada, Y., Yamazaki, H., Sekine-Aizawa, Y., and Hirokawa, N. (1995). The neuron-specific kinesin superfamily protein KIF1A is a uniqye monomeric motor for anterograde axonal transport of synaptic vesicle precursors. *Cell* 81, 769–780. doi: 10.1016/0092-8674(95)90538-3

Okamoto, S., Pouladi, M. A., Talantova, M., Yao, D., Xia, P., Ehrnhoefer, D. E., et al. (2009). Balance between synaptic versus extrasynaptic NMDA receptor activity influences inclusions and neurotoxicity of mutant huntingtin. *Nat. Med.* 15, 1407–1413. doi: 10.1038/nm.2056

Okano, A., Usuda, N., Furihata, K., Nakayama, K., Tian, Q. B., Okamoto, T., et al. (2003). Huntingtin-interacting protein-1-related protein of rat (rHIP1R) is localized in the postsynaptic regions. *Brain Res.* 967, 210–225. doi: 10.1016/S0006-8993(03)02236-4

Opazo, P., Sainlos, M., and Choquet, D. (2012). Regulation of AMPA receptor surface diffusion by PSD-95 slots. *Curr. Opin. Neurobiol.* 22, 453–460. doi: 10.1016/j.conb.2011.10.010

Orth, M., Schippling, S., Schneider, S. A., Bhatia, K. P., Talelli, P., Tabrizi, S. J., et al. (2010). Abnormal motor cortex plasticity in premanifest and very early manifest Huntington disease. *J. Neurol. Neurosurg. Psychiatry* 81, 267–270. doi: 10.1136/jnnp.2009.171926

Parker, J. A., Metzler, M., Georgiou, J., Mage, M., Roder, J. C., Rose, A. M., et al. (2007). Huntingtin-interacting protein 1 influences worm and mouse presynaptic function and protects *Caenorhabditis elegans* neurons against mutant polyglutamine toxicity. *J. Neurosci.* 27, 11056–11064. doi: 10.1523/JNEUROSCI.1941-07.2007

Parsons, M. P., Kang, R., Buren, C., Dau, A., Southwell, A. L., Doty, C. N., et al. (2014). Bidirectional control of Postsynaptic Density-95 (PSD-95) clustering by Huntingtin. *J. Biol. Chem.* 289, 3518–3528. doi: 10.1074/jbc.M113.513945

Parsons, M. P., and Raymond, L. A. (2014). Extrasynaptic NMDA receptor involvement in central nervous system disorders. *Neuron* 82, 279–293. doi: 10.1016/j.neuron.2014.03.030

Paulsen, J. S. (2011). Cognitive impairment in Huntington disease: diagnosis and treatment. *Curr. Neurol. Neurosci. Rep.* 11, 474–483. doi: 10.1007/s11910-011-0215-x

Penney, J. B., Vonsattel, J. P., MacDonald, M. E., Gusella, J. F., and Myers, R. H. (1997). CAG repeat number governs the development rate of pathology in huntington's disease. *Ann. Neurol.* 41, 689–692. doi: 10.1002/ana.410410521

Pla, P., Orvoen, S., Benstaali, C., Dodier, S., Gardier, A. M., David, D. J., et al. (2013). Huntingtin acts non cell-autonomously on hippocampal neurogenesis and controls anxiety-related behaviors in adult mouse. *PLoS One* 8:e73902. doi: 10.1371/journal.pone.0073902

Priller, C., Bauer, T., Mitteregger, G., Krebs, B., Kretzschmar, H. A., and Herms, J. (2006). Synapse formation and function is modulated by the amyloid precursor protein. *J. Neurosci.* 26, 7212–7221. doi: 10.1523/JNEUROSCI.1450-06.2006

Quirion, J. G., and Parsons, M. P. (2019). The onset and progression of hippocampal synaptic plasticity deficits in the Q175FDN mouse model of Huntington disease. *Front. Cell. Neurosci.* 13:326. doi: 10.3389/fncel.2019.00326

Ravalia, A. S., Lau, J., Barron, J., Purchase, S., Southwell, A. L., Hayden, M. R., et al. (2021). Super-resolution imaging reveals extrastriatal synaptic dysfunction in presymptomatic Huntington disease mice. *Neurobiol. Dis.* 152:105293. doi: 10.1016/j.nbd.2021.105293

Ravikumar, B., Vacher, C., Berger, Z., Davies, J. E., Luo, S., Oroz, L. G., et al. (2004). Inhibition of mTOR induces autophagy and reduces toxicity of polyglutamine expansions in fly and mouse models of Huntington disease. *Nat. Genet.* 36, 585–595. doi: 10.1038/ng1362

Raymond, L. A., André, V. M., Cepeda, C., Gladding, C. M., Milnerwood, A. J., and Levine, M. S. (2011). Pathophysiology of Huntington's disease: time-dependent alterations in synaptic and receptor function. *Neuroscience* 198, 252–273. doi: 10.1016/j.neuroscience.2011.08.052

Reilmann, R., Ross, C., Testa, C., Frank, S., Evers, M., de Haan, M., et al. (2020). Translation of AMT-130 preclinical data to inform the design of the first FDA-approved human AAV gene therapy clinical trial in adults with early manifest Huntington's disease (4531). *Neurology* 94:4531.

Rong, J., McGuire, J. R., Fang, Z. H., Sheng, G., Shin, J. Y., Li, S. H., et al. (2006). Regulation of intracellular trafficking of huntingtin-associated protein-1 is critical for TrkA protein levels and neurite outgrowth. *J. Neurosci.* 26, 6019–6030. doi: 10.1523/JNEUROSCI.1251-06.2006

Rosas, H. D., Koroshetz, W. J., Chen, Y. I., Skeuse, C., Vangel, M., Cudkowicz, M. E., et al. (2003). Evidence for more widespread cerebral pathology in early HD: an MRI-based morphometric analysis. *Neurology* 60, 1615–1620. doi: 10.1212/01.WNL.0000065888.88988.6E

Rubinsztein, D. C., Leggo, J., Coles, R., Almqvist, E., Biancalana, V. V., Cassiman, J. J., et al. (1996). Phenotypic characterization of individuals with 30-40 CAG repeats in the Huntington disease (HD) gene reveals HD cases with 36 repeats and apparently normal elderly individuals with 36-39 repeats. *Am. J. Hum. Genet.* 59, 16–22.

Rui, Y. N., Xu, Z., Patel, B., Chen, Z., Chen, D., Tito, A., et al. (2015). Huntingtin functions as a scaffold for selective macroautophagy. *Nat. Cell Biol.* 17, 262–275. doi: 10.1038/ncb3101

Sanders, S. S., Mui, K. K. N., Sutton, L. M., and Hayden, M. R. (2014). Identification of binding sites in huntingtin for the huntingtin interacting proteins HIP14 and HIP14L. *PLoS One* 9:e90669. doi: 10.1371/journal.pone.0090669

Sanders, S. S., Parsons, M. P., Mui, K. K. N., Southwell, A. L., Franciosi, S., Cheung, D., et al. (2016). Sudden death due to paralysis and synaptic and behavioral deficits when Hip14/Zdhhc17 is deleted in adult mice. *BMC Biol.* 14:108. doi: 10.1186/s12915-016-0333-7

Sathasivam, K., Neueder, A., Gipson, T. A., Landles, C., Benjamin, A. C., Bondulich, M. K., et al. (2013). Aberrant splicing of HTT generates the pathogenic exon 1 protein in Huntington disease. *Proc. Natl. Acad. Sci. U.S.A.* 110, 2366–2370. doi: 10.1073/pnas.1221891110

Saudou, F., and Humbert, S. (2016). The biology of Huntingtin. *Neuron* 89, 910–926. doi: 10.1016/j.neuron.2016.02.003

Savas, J. N., Ma, B., Deinhardt, K., Culver, B. P., Restituito, S., Wu, L., et al. (2010). A role for Huntington disease protein in dendritic RNA granules. *J. Biol. Chem.* 285, 13142–13153. doi: 10.1074/jbc.M110.114561

Selkoe, D. J. (2002). Alzheimer's disease is a synaptic failure. *Science* 298, 789–791. doi: 10.1126/science.1074069

Shen, M., Wang, F., Li, M., Sah, N., Stockton, M. E., Tidei, J. J., et al. (2019). Reduced mitochondrial fusion and Huntingtin levels contribute to impaired dendritic maturation and behavioral deficits in Fmr1-mutant mice. *Nat. Neurosci.* 22, 386–400. doi: 10.1038/s41593-019-0338-y

Shirasaki, D. I., Greiner, E. R., Al-Ramahi, I., Gray, M., Boontheung, P., Geschwind, D. H., et al. (2012). Network organization of the huntingtin proteomic interactome in mammalian brain. *Neuron* 75, 41–57. doi: 10.1016/j.neuron.2012.05.024

Simmons, D. A., Rex, C. S., Palmer, L., Pandyarajan, V., Fedulov, V., Gall, C. M., et al. (2009). Up-regulating BDNF with an ampakine rescues synaptic plasticity and memory in Huntington's disease knockin mice. *Proc. Natl. Acad. Sci. U.S.A.* 106, 4906–4911. doi: 10.1073/pnas.0811228106

Singaraja, R. R., Huang, K., Sanders, S. S., Milnerwood, A. J., Hines, R., Lerch, J. P., et al. (2011). Altered palmitoylation and neuropathological deficits in mice lacking HIP14. *Hum. Mol. Genet.* 20, 3899–3909. doi: 10.1093/hmg/ddr308

Skotte, N. H., Southwell, A. L., Østergaard, M. E., Carroll, J. B., Warby, S. C., Doty, C. N., et al. (2014). Allele-specific suppression of mutant huntingtin using antisense oligonucleotides: providing a therapeutic option for all Huntington disease patients. *PLoS One* 9:e107434. doi: 10.1371/journal.pone.0107434

Smith-Dijak, A. I., Sepers, M. D., and Raymond, L. A. (2019). Alterations in synaptic function and plasticity in Huntington disease. *J. Neurochem.* 150, 346–365. doi: 10.1111/jnc.14723

Southwell, A. L., Kordasiewicz, H. B., Langbehn, D., Skotte, N. H., Parsons, M. P., Villanueva, E. B., et al. (2018). Huntingtin suppression restores cognitive function in a mouse model of Huntington's disease. *Sci. Transl. Med.* 10:eaar3959. doi: 10.1126/scitranslmed.aar3959

Southwell, A. L., Warby, S. C., Carroll, J. B., Doty, C. N., Skotte, N. H., Zhang, W., et al. (2013). A fully humanized transgenic mouse model of Huntington disease. *Hum. Mol. Genet.* 22, 18–34. doi: 10.1093/hmg/dds397

Steffan, J. S., Kazantsev, A., Spasic-Boskovic, O., Greenwald, M., Zhu, Y. Z., Gohler, H., et al. (2000). The Huntington's disease protein interacts with p53 and CREB-binding protein and represses transcription. *Proc. Natl. Acad. Sci. U.S.A.* 97, 6763–6768. doi: 10.1073/pnas.100110097

Sun, Y., Savanenin, A., Reddy, P. H., and Liu, Y. F. (2001). Polyglutamine-expanded Huntingtin promotes sensitization of N-Methyl-D-aspartate Receptors via Post-synaptic Density 95. *J. Biol. Chem.* 276, 24713–24718. doi: 10.1074/jbc.M103501200

Sutton, L. M., Sanders, S. S., Butland, S. L., Singaraja, R. R., Franciosi, S., Southwell, A. L., et al. (2013). Hip14l-deficient mice develop neuropathological and behavioural features of Huntington disease. *Hum. Mol. Genet.* 22, 452–465. doi: 10.1093/hmg/dds441

Tabrizi, S. J., Ghosh, R., and Leavitt, B. R. (2019a). Huntingtin lowering strategies for disease modification in Huntington's disease. *Neuron* 101, 801–819. doi: 10.1016/j.neuron.2019.01.039

Tabrizi, S. J., Leavitt, B. R., Landwehrmeyer, G. B., Wild, E. J., Saft, C., Barker, R. A., et al. (2019b). Targeting Huntingtin expression in patients with Huntington's disease. *N. Engl. J. Med.* 380, 2307–2316. doi: 10.1056/nejmoa1900907

Tang, T. S., Tu, H., Chan, E. Y. W., Maximov, A., Wang, Z., Wellington, C. L., et al. (2003). Huntingtin and huntingtin-associated protein 1 influence neuronal calcium signaling mediated by inositol-(1,4,5) triphosphate receptor type 1. *Neuron* 39, 227–239. doi: 10.1016/S0896-6273(03)00366-0

Twelvetrees, A. E., Yuen, E. Y., Arancibia-Carcamo, I. L., MacAskill, A. F., Rostaing, P., Lumb, M. J., et al. (2010). Delivery of GABAARs to synapses is mediated by HAP1-KIF5 and Disrupted by Mutant Huntingtin. *Neuron* 65, 53–65. doi: 10.1016/j.neuron.2009.12.007

Tyan, S. H., Shih, A. Y. J., Walsh, J. J., Maruyama, H., Sarsoza, F., Ku, L., et al. (2012). Amyloid precursor protein (APP) regulates synaptic structure and function. *Mol. Cell. Neurosci.* 51, 43–52. doi: 10.1016/j.mcn.2012.07.009

Tyebji, S., and Hannan, A. J. (2017). Synaptopathic mechanisms of neurodegeneration and dementia: insights from Huntington's disease. *Prog. Neurobiol.* 153, 18–45. doi: 10.1016/j.pneurobio.2017.03.008

Usdin, M. T., Shelbourne, P. F., Myers, R. M., and Madison, D. V. (1999). Impaired synaptic plasticity in mice carrying the Huntington's disease mutation. *Hum. Mol. Genet.* 8, 839–846. doi: 10.1093/hmg/8.5.839

Vezzoli, E., Caron, I., Talpo, F., Besusso, D., Conforti, P., Battaglia, E., et al. (2019). Inhibiting pathologically active ADAM10 rescues synaptic and cognitive decline in Huntington's disease. *J. Clin. Invest.* 129, 2390–2403. doi: 10.1172/JCI120616

Vijayan, V., and Verstreken, P. (2017). Autophagy in the presynaptic compartment in health and disease. *J. Cell Biol.* 216, 1895–1906. doi: 10.1083/jcb.201611113

Vitet, H., Brandt, V., and Saudou, F. (2020). Traffic signaling: new functions of huntingtin and axonal transport in neurological disease. *Curr. Opin. Neurobiol.* 63, 122–130. doi: 10.1016/j.conb.2020.04.001

Waelter, S., Scherzinger, E., Hasenbank, R., Nordhoff, E., Lurz, R., Goehler, H., et al. (2001). The huntingtin interacting protein HIP1 is a clathrin and α-adaptin-binding protein involved in receptor-mediated endocytosis. *Hum. Mol. Genet.* 10, 1807–1817. doi: 10.1093/hmg/10.17.1807

Walker, F. O. (2007). Huntington's disease. *Lancet* 369, 218–228. doi: 10.1016/S0140-6736(07)60111-1

Wang, G., Liu, X., Gaertig, M. A., Li, S., and Li, X.-J. (2016). Ablation of huntingtin in adult neurons is nondeleterious but its depletion in young mice causes acute pancreatitis. *Proc. Natl. Acad. Sci. U.S.A.* 113, 3359–3364. doi: 10.1073/pnas.1524575113

Weiss, K. R., and Littleton, J. T. (2016). Characterization of axonal transport defects in Drosophila Huntingtin mutants. *J. Neurogenet.* 30, 212–221. doi: 10.1080/01677063.2016.1202950

Wellington, C. L., Singaraja, R., Ellerby, L., Savill, J., Roy, S., Leavitt, B., et al. (2000). Inhibiting caspase cleavage of huntingtin reduces toxicity and aggregate formation in neuronal and nonneuronal cells. *J. Biol. Chem.* 275, 19831–19838. doi: 10.1074/jbc.M001475200

White, J. A., Krzystek, T. J., Hoffmar-Glennon, H., Thant, C., Zimmerman, K., Iacobucci, G., et al. (2020). Excess Rab4 rescues synaptic and behavioral dysfunction caused by defective HTT-Rab4 axonal transport in Huntington's disease. *Acta Neuropathol. Commun.* 8:97. doi: 10.1186/s40478-020-00964-z

Wong, Y. C., and Holzbaur, E. L. F. (2014). The regulation of autophagosome dynamics by huntingtin and HAP1 is disrupted by expression of mutant huntingtin, leading to defective cargo degradation. *J. Neurosci.* 34, 1293–1305. doi: 10.1523/JNEUROSCI.1870-13.2014

Wood, T. E., Barry, J., Yang, Z., Cepeda, C., Levine, M. S., and Gray, M. (2019). Mutant huntingtin reduction in astrocytes slows disease progression in the BACHD conditional Huntington's disease mouse model. *Hum. Mol. Genet.* 28, 487–500. doi: 10.1093/hmg/ddy363

Yang, S., Chang, R., Yang, H., Zhao, T., Hong, Y., Kong, H. E., et al. (2017). CRISPR/Cas9-mediated gene editing ameliorates neurotoxicity in mouse model of Huntington's disease. *J. Clin. Invest.* 127, 2719–2724. doi: 10.1172/JCI92087

Yao, J., Ong, S. E., and Bajjalieh, S. (2014). Huntingtin is associated with cytomatrix proteins at the presynaptic terminal. *Mol. Cell. Neurosci.* 63, 96–100. doi: 10.1016/j.mcn.2014.10.003

Yao, P. J., Bushlin, I., and Petralia, R. S. (2006). Partially overlapping distribution of Epsin1 and HIP1 at the synapse: analysis by immunoelectron microscopy. *J. Comp. Neurol.* 494, 368–379. doi: 10.1002/cne.20810

Zala, D., Hinckelmann, M. V., and Saudou, F. (2013). Huntingtin's function in axonal transport is conserved in *Drosophila melanogaster*. *PLoS One* 8:e60162. doi: 10.1371/journal.pone.0060162

Zeitlin, S., Liu, J.-P., Chapman, D. L., Papaioannou, V. E., and Efstratiadis, A. (1995). Increased apoptosis and early embryonic lethality in mice nullizygous for the Huntington's disease gene homologue. *Nat. Genet.* 11, 155–163. doi: 10.1038/ng0595-111

Zhang, J., Peng, Q., Li, Q., Jahanshad, N., Hou, Z., Jiang, M., et al. (2010). Longitudinal characterization of brain atrophy of a Huntington's disease mouse model by automated morphological analyses of magnetic resonance images. *Neuroimage* 49, 2340–2351. doi: 10.1016/j.neuroimage.2009.10.027

Zhang, Y., Leavitt, B. R., Van Raamsdonk, J. M., Dragatsis, I., Goldowitz, D., MacDonald, M. E., et al. (2006). Huntingtin inhibits caspase-3 activation. *EMBO J.* 25, 5896–5906. doi: 10.1038/sj.emboj.7601445

Zheng, J., Shen, W. H., Lu, T. J., Zhou, Y., Chen, Q., Wang, Z., et al. (2008). Clathrin-dependent endocytosis is required for TrkB-dependent Akt-mediated neuronal protection and dendritic growth. *J. Biol. Chem.* 283, 13280–13288. doi: 10.1074/jbc.M709930200

Zuccato, C., Ciammola, A., Rigamonti, D., Leavitt, B. R., Goffredo, D., Conti, L., et al. (2001). Loss of huntingtin-mediated BDNF gene transcription in Huntington's disease. *Science* 293, 493–498. doi: 10.1126/science.1059581

Zuccato, C., Tartari, M., Crotti, A., Goffredo, D., Valenza, M., Conti, L., et al. (2003). Huntingtin interacts with REST/NRSF to modulate the transcription of NRSE-controlled neuronal genes. *Nat. Genet.* 35, 76–83. doi: 10.1038/ng1219

Conflict of Interest: The authors declare that the research was conducted in the absence of any commercial or financial relationships that could be construed as a potential conflict of interest.

Copyright © 2021 Barron, Hurley and Parsons. This is an open-access article distributed under the terms of the Creative Commons Attribution License (CC BY). The use, distribution or reproduction in other forums is permitted, provided the original author(s) and the copyright owner(s) are credited and that the original publication in this journal is cited, in accordance with accepted academic practice. No use, distribution or reproduction is permitted which does not comply with these terms.

frontiers in Cellular Neuroscience

ORIGINAL RESEARCH
published: 20 July 2021
doi: 10.3389/fncel.2021.674030

SyNC, a Computationally Extensive and Realistic Neural Net to Identify Relative Impacts of Synaptopathy Mechanisms on Glutamatergic Neurons and Their Networks in Autism and Complex Neurological Disorders

Rounak Chatterjee[1], *Janet L. Paluh*[2]*, *Souradeep Chowdhury*[1], *Soham Mondal*[3], *Arnab Raha*[4] *and Amitava Mukherjee*[5]

[1] Department of Electronics and Telecommunication Engineering, Jadavpur University, Kolkata, India, [2] SUNY Polytechnic Institute, College of Nanoscale Science and Engineering, Nanobioscience, Albany, NY, United States, [3] Flash Controller Team, Memory Solutions, Samsung Semiconductor India Research, Samsung Electronics Co., Ltd., Bangalore, India, [4] Advanced Architecture Research, Intel Intelligent Systems Group, Intel Edge AI, Intel Corporation, Santa Clara, CA, United States, [5] Independent Researcher, Kolkata, India

OPEN ACCESS

Edited by:
Daniela Tropea,
Trinity College Dublin, Ireland

Reviewed by:
Antonio Marcos Batista,
Universidade Estadual de Ponta Grossa, Brazil
Stanislava Pankratova,
University of Copenhagen, Denmark

***Correspondence:**
Janet L. Paluh
jpaluh@sunypoly.edu

Specialty section:
This article was submitted to Cellular Neuropathology, a section of the journal Frontiers in Cellular Neuroscience

Received: *28 February 2021*
Accepted: *25 May 2021*
Published: *20 July 2021*

Citation:
Chatterjee R, Paluh JL, Chowdhury S, Mondal S, Raha A and Mukherjee A (2021) SyNC, a Computationally Extensive and Realistic Neural Net to Identify Relative Impacts of Synaptopathy Mechanisms on Glutamatergic Neurons and Their Networks in Autism and Complex Neurological Disorders. Front. Cell. Neurosci. 15:674030. doi: 10.3389/fncel.2021.674030

Synaptic function and experience-dependent plasticity across multiple synapses are dependent on the types of neurons interacting as well as the intricate mechanisms that operate at the molecular level of the synapse. To understand the complexity of information processing at synaptic networks will rely in part on effective computational models. Such models should also evaluate disruptions to synaptic function by multiple mechanisms. By co-development of algorithms alongside hardware, real time analysis metrics can be co-prioritized along with biological complexity. The hippocampus is implicated in autism spectrum disorders (ASD) and within this region glutamatergic neurons constitute 90% of the neurons integral to the functioning of neuronal networks. Here we generate a computational model referred to as ASD interrogator (ASDint) and corresponding hardware to enable in silicon analysis of multiple ASD mechanisms affecting glutamatergic neuron synapses. The hardware architecture Synaptic Neuronal Circuit, SyNC, is a novel GPU accelerator or neural net, that extends discovery by acting as a biologically relevant realistic neuron synapse in real time. Co-developed ASDint and SyNC expand spiking neural network models of plasticity to comparative analysis of retrograde messengers. The SyNC model is realized in an ASIC architecture, which enables the ability to compute increasingly complex scenarios without sacrificing area efficiency of the model. Here we apply the ASDint model to analyse neuronal circuitry dysfunctions associated with autism spectral disorder (ASD) synaptopathies and their effects on the synaptic learning parameter and demonstrate SyNC on an ideal ASDint scenario. Our work highlights the value of secondary pathways in regard to evaluating complex ASD synaptopathy mechanisms. By comparing the degree of variation in the synaptic learning parameter to the response obtained from simulations of the ideal

scenario we determine the potency and time of the effect of a particular evaluated mechanism. Hence simulations of such scenarios in even a small neuronal network now allows us to identify relative impacts of changed parameters and their effect on synaptic function. Based on this, we can estimate the minimum fraction of a neuron exhibiting a particular dysfunction scenario required to lead to complete failure of a neural network to coordinate pre-synaptic and post-synaptic outputs.

Keywords: synaptic plasticity, software, hardware, synaptopathy, ASIC, computational neuroscience, accelerator

1. INTRODUCTION

The exceptional computational power of the brain in memory and learning is accomplished by conversion of an electrical signal into the interneuronal transmission of chemical neurotransmitter information at synapses (Hebb, 1949; Burns and Augustine, 1995; Südhof and Malenka, 2008). As the complexity of synapses continues to evolve, so must the evolution of computational and hardware tools to evaluate such models. The events are non-spontaneous and dependent on input intensity and frequency and the measured electrophysiological response is an action potential that brings into play the complex physiology of neuron dendritic, cell body, axonal hillock, and axonal compartments. The largest contribution of information passing in neural circuits occurs at synapses (Di Maio, 2008) and is regulated by a diversity of synaptic plasticity mechanisms (Citri and Malenka, 2008; Choquet and Triller, 2013) that must operate over timescales (Abbott and Regehr, 2004). In 1949, Hebb described activity-dependent synaptic modulation (Hebb, 1949) that forms the basis of current models of neuronal plasticity. Long-term changes impact learning and memory and short-term changes support synaptic computations (Tetzlaff et al., 2012). This can be described in terms of spike timing dependent plasticity (STDP) that relates changes in synaptic strength, or synaptic weights, to the timing of pre- and post-synaptic spikes, a key mechanism in memory formation. When linked to synaptic stability it can be used to describe flexible or stable memories (Park et al., 2017) and complex topologies of neural networks (Borges et al., 2017; Lameu et al., 2021). Less investigated in regard to learning and memory is the relative impact of altered biological mechanisms on synaptic strength, owing to lack of generalized computational models as well as scalable hardware architectures that can process such complexity.

As the main information transfer between neurons, neurotransmitter release is a highly regulated yet probabilistic process (Benfenati, 2007; Regehr, 2012). Indeed in short term plasticity to modify neuronal circuits, synapses are viewed as active filters of information, not just conveyers, reducing noise and enhancing relevant information (Klyachko and Stevens, 2006). An important mechanism to dynamically fine tune the probability of neurotransmitter release is through local feedback regulation (Branco and Staras, 2009; Minneci et al., 2012). Intermediate initial release dynamics behave as band pass filters. These events and others allow adaptive regulation to changes in network activity and enables neurons to respond to prolonged alterations. How relative changes to this homeostatic mechanism arising from synaptopathies affect synaptic plasticity has not been previously examined. Here we consider the glutamatergic synapse, that is a low pass filter type. Glutamatergic neurons encompass most of the synapses in the central nervous system (CNS) and are relevant to cognitive decline (Volk et al., 2015). We generate a neuron model that is adapted to study the implications to synaptic strength and efficiency when stochastic variations occur in underlying mechanisms and that can also be implemented into hardware.

Spiking Neural Networks (SNNs) are used to model synapses to reflect action potential spikes and a large number of SNN software and hardware models have been proposed for mimicking neurological behavior. The software based SNN neural analysis methods that have been developed include NEURON (Hines and Carnevale, 1997), Brain (Goodman and Brette, 2009), NeMo (Fidjeland et al., 2009), PyNN (Davison et al., 2008), and more. Although providing biological accuracy, these software based simulations encounter extraordinarily high computational costs for subsequent hardware development while performing numerical simulations. Hence modern computers fail to obtain real-time performance when scaled to simulate large neural networks. As a case in point, a 1 s simulation of a network composed of 8 million neurons that includes 4 billion integrate-and-fire synapses when analyzed on the Gene rack supercomputer using 2,048 processors, takes ∼80 min. By co-development of software and hardware implementation jointly, considerations of compactness, power-efficiency, and ease of implementation of circuits can be optimized. In this regard, circuits involving feedback mechanisms are desired and has led to analog circuit designs of SNNs. The relative efficiency of an analog vs. digital implementation varies dependent on the required signal-to-noise ratio. In neural dynamics challenging temporal features are present, such as high and nonuniform pulse latency and activity dependent synaptic plasticity that results in long-lasting long-term potentiation (LTP) processing. This creates a need for capacitors of value >0.1 F, that imposes physical constraints. This challenge is significant and nullifies much of the advantage offered by analog circuits in terms of a smaller number of transistors. Analog circuits also suffer from transistor mismatch, process variation and model size limitations owing to a process termed gate fan-out that relates the number of gate inputs to a single original logic gate. Another challenge is in reliable analog memory, that has not yet been robustly achieved in regard to storage of significant processing values. This includes synaptic weight whose subtle variations have significant importance to the accuracy of the entire system.

Hence, owing to essential needs in user capabilities, including resource management and real-time speed, we employ a digital solution for large-scale simulation of neural networks. Our approach emulates neuron spiking with minimum possible error and also importantly without sacrificing speed of processivity of the digital system implemented as hardware.

A number of synaptic models have been developed for digital implementation including the Time Machine approach, SpinNaker (Furber et al., 2014), Neurogrid (Benjamin et al., 2014), and BrainScales (Pfeil et al., 2013), among others. BrainScales is a wafer-scale neuromorphic system, in which each wafer contains 48 reticles with eight High-Count Analog Neural Network (HiCANN) dice. Each such HiCANN die has the capability to emulate 512 adaptive exponential neuron models. SpiNNaker is a one-million-core supercomputer, developed exclusively for massively-parallel real-time simulation of large-scale neural networks, making it one of the largest digital neuromorphic platforms to date. Neurogrid is a real-time system consisting of over one million quadratic integrate-and-fire neurons, in which neuron and synapse dynamics are emulated using analog circuits and communications are performed by digital means, for simulation of over a billion synapses. However, since these models have been developed with the intention of utilization in Spiking Neural Network (SNN) architectures, they only approximate the effect of the numerous parameters in a neuron.

In current large scale neuromorphic platforms that rely on SNN architectures, the exclusive abstraction of intracellular dynamics of a neuron that ignores other biologically modulated parameters is severely restricted in applications to understand and modulate plasticity. Our jointly developed software and hardware solutions are designed instead to be able to retain computational speed while also simulating the effect of a broader range of individual biologically relevant parameters in the neuronal synapse and its networks relevant to normal function and synaptopathies. Glutamate is known to be the main excitatory neurotransmitter in the CNS and accounts for 90% of the total neurotransmitter usage in the CNS. Glutamate provides us with the most fundamental form of a neuron and is ideal for extension to other models. In developing the hardware architecture Synaptic Neuronal Circuit, SyNC, we focus on the design of the excitatory glutamatergic neuron communication network. Synaptic plasticity and multiple brain functions rely on glutamate that is the most abundant excitatory neurotransmitter in the brain. Glutamate and glutamatergic neurotransmission dysfunction is central to ASD (reviewed in Rojas, 2014) and to broader impacts on neurodegeneration (Lewerenz and Maher, 2015) as well as psychiatric disorders (Li et al., 2018). To capture the speed of the network we use a retrograde messenger mediated plasticity (RMMP) model as opposed to a glial cell-mediated model (Postnov et al., 2007). In the RMMP bipartite neuron system there are no intermediary dynamics considered in the synaptic cleft and hence the synaptic current from the pre-synaptic region is the same as the synaptic current entering the post-synaptic region. We consider the dynamics of retrograde messengers that travel across the synapse via diffusion to be the feedback initiator in our model. These considerations allow us to expand biological detail in a digital framework to address multiple pre- and post-synaptic interacting molecular mechanisms found in synaptopathies and to cross-evaluate dysfunction by a rapid multi-classification comparison. Expanded detail includes receptor inhibitors and activators, including allosteric regulation, as well as receptor type ratios, synaptic cell adhesion molecules, and calcium signaling and organelle stores.

In our model, we consider Hebbian plasticity parameter Δ which records the activity at pre-synaptic and post-synaptic boutons and evaluates the gain in synaptic potential in the form of synaptic weight. While many different mechanisms have been suggested in the literature to explain LTP, we have approached it from a rather simplistic model such that it can be adapted for utility in other models as well. To our knowledge this is the first work to co-develop and implement a diverse and highly adaptable design of a neuron in detail in software and hardware and we demonstrate its effectiveness in complex and scaled neuronal networks applied to Autism Spectrum Disorders (ASD) (**Figure 1**). We mapped and synthesized our SyNC hardware designs in 45 nm technology. Our simulation results show that differential forms of these equations reproduce the expected characteristics of the pre-synaptic region of a neuron, while conveniently transformed into discretized form. Application of ASDint over the SyNC core demonstrates an ability to effectively reproduce phenotypes for each synaptopathy. Synthesis results show that using a posit operation core gives us PPA performance that is slightly better than the IEEE 754 double precision while having higher accuracy than the IEEE single precision operation core. This outcome affirms the use of posit as a valid replacement of floats. In relation to biological discovery, the SyNC platform for the first time, allows us to examine complex individual and combined impacts of synaptopathies on synaptic plasticity in real time.

2. BACKGROUND

2.1. System Description

2.1.1. The Dynamic Synapse as a Lipid-Derived Retrograde Signaling Model

How to best incorporate the interplay between synapse dynamics that is generated by multiple underlying interacting mechanisms (Choquet and Triller, 2013) and which defines plasticity remains a challenge. In **Figure 2**, we describe the key elements in our proposed synaptic dynamics model. Two primary components in our software for synapse dynamics are retrograde signaling and post-synaptic receptor type. Retrograde signaling (Brenman and Bredt, 1997; Regehr et al., 2009) systems integrate the post-synaptic response with regulation of pre-synaptic output generating rapid changes in synaptic strength. Although diverse chemical messengers exist, retrograde models share many basic steps. Firstly, the production and release of retrograde messengers from post-synaptic cells are regulated by post-synaptic calcium, and triggered by post-synaptic metabotropic receptors and second messenger. Secondly, the entirety of the concentration of retrograde messenger produced at the post-synaptic region is assumed to be transmitted to the pre-synaptic

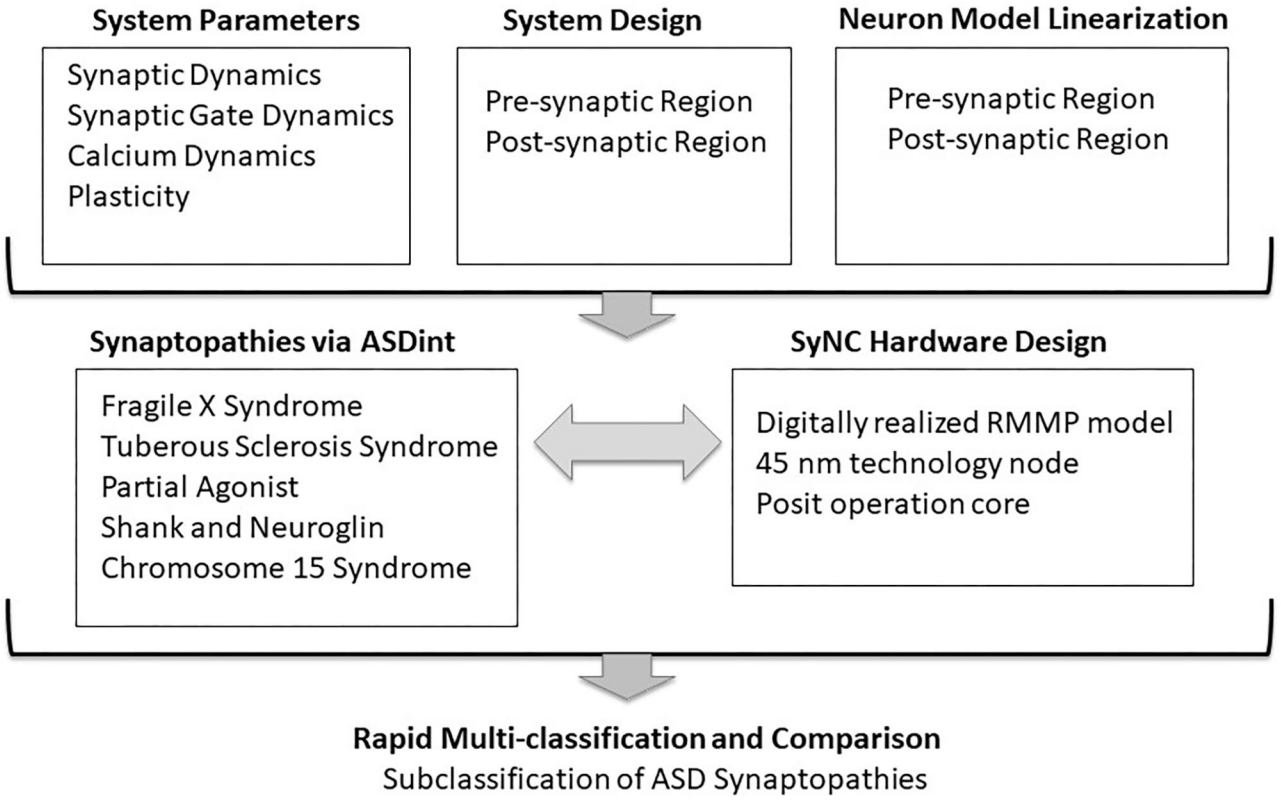

FIGURE 1 | Co-development of SyNC with neural algorithms to relay ASD complexity. The goal of this study was to advance algorithms of neuronal synapse modeling in the context of a complex neural disorder, such as ASD, while obtaining high (1 GHz) optimal frequency in hardware. The diagram outlines general considerations in codevelopment. mGluR, metabatropic glutamate Receptor; NMDAR, N-methyl-D-aspartate Receptor.

receptors with no losses in transmission or within the synaptic cavity. While such an assumption might feel out of place, we consider that such losses if they happen initially would eventually saturate to a point in which no loss occurs. The retrograde messenger acts on the pre-synaptic target to modulate the plasticity parameter and activity spike strength in the pre-synaptic region.

The duration and latency of a retrograde signal is controlled by parameters of uptake and degradation of the molecules at a cellular level. As a result, the nonlinear relationship between the release of a retrograde signal and the magnitude and duration of the retrograde signal available to activate pre-synaptic receptors must be considered in the ultimate effect on synaptic strength. A final consideration is the extent to which the release of the retrograde messenger can be sustained. Many cells contain few vesicles and dense core secretory granules in their dendrites, which suggest that it would be possible to deplete the release of conventional neurotransmitters, peptides, and growth factors. The low density of vesicles suggests that the dendritic release may be much more prone to depletion. The ability to recover from depletion would then depend crucially on endocytosis and vesicle and granule refilling. Alternately, some lipid-derived messengers are produced on demand (Piomelli, 2003; Chevaleyre et al., 2006), and as a result the release of these messengers may be sustained. To describe the regulated release of neurotransmitter at the synapse, we consider the lipophilic (lipid-derived) retrograde signaling model (Chevaleyre et al., 2006). The output of our model for observing effects of plasticity is calcium dynamics in the pre-synaptic region and therefore we can determine the impact of all the processes in the model that impact that parameter. Plasticity is achieved in the system by increasing the latency of calcium signals, which in turn can lower the peak calcium levels. Activation of Gq-coupled receptors such as mGluR1 in the post-synaptic region can promote release of inhibitory factors in the pre-synaptic region by increasing the production of retrograde messenger 2-AG that in turn reduces calcium levels.

2.1.2. Synaptic Gate Dynamics and Glutamatergic Receptors

Amongst the six main neurotransmitters in the human body, the main excitatory neurotransmitter in the brain is glutamate, which activates several postsynaptic receptors. Two primary types of receptors encountered in a glutamatergic neuron are ionotropic Glutamate Receptors (iGluR) and metabotropic Glutamate Receptors (mGluR). The mGluRs bind glutamate within a large extracellular domain and transmit signals through the receptor protein to intracellular secondary messenger signals. The receptors primarily involved in this process are the group I mGluRs: mGluR1 and mGluR5. Ionotropic glutamate receptors

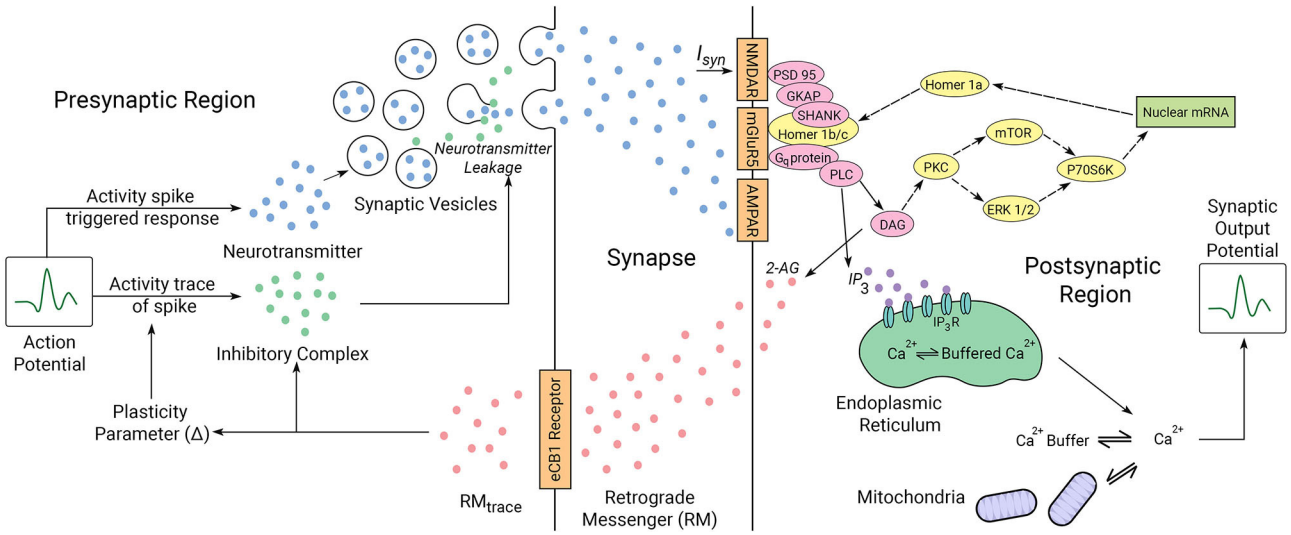

FIGURE 2 | Illustrated mechanics of the neuron system model. The pre-synaptic and post-synaptic region dynamics are described for the model. The synaptic cleft acts as a lossless channel, and is not involved in any dynamic processes involving neuronal communication. Proteins expressed in yellow are involved in the interactions between the locally transcribed mRNA and the synaptic gate receptors as indicated by dotted arrows. Proteins represented in pink are bridge proteins involved in inter-receptor dynamics. The parameters involved in synaptic activity are linked by solid arrows. The roles of the proteins in synaptic activity diagrammed here are described in the text in regard to ASD mechanisms we have considered.

(iGluRs) are faster responding and the two major types of iGluRs: α-amino-3-hydroxy-5-methyl-4-isoxazolepropionic acid (AMPA) and N-methyl D-aspartate (NMDA) have central roles in hippocampal synaptic plasticity. Both are ligand-gated ion channels and have unique properties that subserve different phases of synaptic plasticity. Glutamate released from the pre-synaptic neuron opens AMPA receptors to depolarize the post-synaptic cell. Each AMPA receptor has four sites to which an agonist (such as glutamate) can bind, one for each subunit. The channel opens when two sites become occupied, and current increases with subsequent binding. The AMPA receptor's permeability to calcium, and other cations such as sodium and potassium, is governed by the presence of the GluA2 subunit in the AMPARs. The presence of GluA2 renders the channel impermeable to calcium and is proposed to guard against excitotoxicity.

2.1.3. Calcium-Mediated Synaptic Events Including Organelle Stores

Calcium mediated synaptic events have been proposed to sustain temporary holding of information as in working memory (Mongillo et al., 2008) and is considered in our model. To enable the flow of synaptic current through the post-synaptic receptors, mGluR1-type receptors coupled to the G protein (Gq) are activated. Together calcium and Gq activate phospholipase C beta (PLC), which cleaves the lipid phosphatidylinositol bisphosphate (PIP2) into diacylglycerol (DAG) and inositol trisphosphate (IP3). DAG is converted into the endocannabinoid 2-arachidonoylglycerol (2-AG). The rate-limiting and Ca2+-sensitive step in 2-AG production is the formation DAG. IP3 and DAG are free to diffuse through the cell cytoplasm and their impacts can be described computationally. In our model we consider the role of mitochondria and the endoplasmic reticulum (ER) in calcium dynamics. Mitochondria are important for numerous roles related to synaptic transmission and neurodegeneration (Lee et al., 2018) including calcium regulation in neurons (Gunter and Gunter, 1994; Gunter et al., 2004) along with the ER (Karagas and Venkatachalam, 2019). Calcium mobilization from mitochondria is controlled by neurotransmitter release (Rizzuto et al., 2003) as well as more complex proposed buffering roles (Matthews and Dietrich, 2015).

When IP3 binds to an IP3 receptor (IPR) on the ER membrane it causes the release of Ca^{2+} from the ER. Five pathways have been considered in the modulation of Ca^{2+} influx, which we describe in a pair of dynamic equations. Thus, we efficiently incorporate abstractions of several terms in our model (**Figure 2**) to describe these dynamics. Ca^{2+} taken up into (Juni), or released from (Jmito) mitochondria, and that bound to (Jon), or released from (Joff), Ca^{2+} buffers are considered to create a constant Ca^{2+} flow that does not vary with instigation of cell membrane receptors. 2-AG then regulates pre-synaptic pathways to affect synaptic transmission by decreasing the probability of neurotransmitter release from the pre-synaptic terminal. In the model, the common cell structures act as an impedance and the calcium buffers in the cytoplasm provide capacitance and are not a part of the signaling circuit, hence acting as a channel to drain higher frequencies away.

2.2. Application of Anti-symmetric Hebbian Plasticity

Synaptic strength is influenced by pre- and post-synaptic activity in activity-dependent synaptic plasticity processes such as long-term potentiation LTP and LTD (Lee et al., 2013). Hebbian

plasticity is used to define these features in synaptic plasticity (Hebb, 1949). The N-methyl-D-aspartate receptors (NMDARs) are calcium permeable and when activated, allow an influx of calcium needed for the induction of LTP. However, NMDARs require both pre-synaptic transmitter release and post-synaptic depolarization for activation. Enhancement in the amplitude of action potential takes place when both the pre-synaptic and post-synaptic regions are active, resulting in potentiation of synaptic output potential. However, when either region is selectively active, the amplitude of action potential is attenuated, resulting in depression of synaptic output potential. These two processes together constitute the synaptic plasticity mechanism and hence act as substrates for fundamental brain function. LTP is a process involving such persistent enhancement of synaptic gain resulting in a long-lasting increase in synaptic transmission gain between the neurons. It is an important process in the context of synaptic plasticity. LTP recording is widely considered to be the cellular model for storage of information in the brain. LTD is an opposite process that modulates and controls the effect of LTP in the brain. Full opening of the NMDAR channel and the consequent influx of calcium requires both the binding of glutamate to the receptor and post-synaptic depolarization. The induction of potentiation is dependent on activation of NMDARs and a rise in post-synaptic calcium. The NMDAR dependence provides a ready explanation for the associativity and asymmetry of Hebbian learning rule. The binding of glutamate follows the release of a transmitter by the pre-synaptic spike, and the post-synaptic depolarization is provided by the post-synaptic spike. Thus, neither the release of glutamate alone nor the post-synaptic spike alone will result in the opening of the receptor. Both must occur at the same time. In the frog optic tectum (Zhang et al., 1998) and in cultured hippocampal cells (Bi and Poo, 1998), no potentiation was observed when the pre-synaptic spike preceded the post-synaptic spike by more than 20 ms and no depression was observed when the pre-synaptic spike followed the post-synaptic spike by more than 20ms. LTD is induced at a lower concentration of calcium than required for induction of LTP, however the parameters of the timing window for depression are not fully predicted by the expected calcium concentration alone. In layer V/VI of the neocortex of the developing frog optic tectum (Zhang et al., 1998) and cultured hippocampal cells (Bi and Poo, 1998), the depression, like the potentiation, depended on the activation of NMDARs, but the depression found in layer II/III pyramidal cells of the somatosensory cortex did not. It is observed for layer II/III pyramidal cells that the interval for depression is considerably larger than the interval for potentiation. All of these learning rules are asymmetric, in that positive actions have different effects than negative delays. Tsodyks and Markram (1997) proposed an anti-symmetric form of Hebbian plasticity where the time interval of potentiation and depression are comparably similar. This is the form of plasticity we have used in our system.

2.3. Modeling Neuronal Damage Scenarios Associated With Autism Spectrum Disorder

ASDs form a group of diverse neurodevelopmental conditions defined by two core symptoms: social deficits that include communication and interaction impairments; and stereotypical, repetitive, and restricted behaviors. One of the main features of ASD is the high level of heterogeneity resulting in complexity both when considering symptoms and causative factors. It is in fact possible that every single disorder within the group has its unique mechanisms and consequences, with environmental and genetic factors playing roles in the etiology of ASD. In that regard, computational models will be imperative to help compare and categorize ASD effects on synaptic function. We consider multiple ASD mechanisms. It is in fact possible that every single disorder within the group has its unique mechanisms and consequences, with environmental and genetic factors playing roles in the etiology of ASD. We consider multiple ASD mechanisms in mathematical descriptions that incorporate various regions of the synapse (**Figure 3**).

2.3.1. Fragile X Syndrome

For our model, we consider the role of Fragile X protein, FMRP, in mRNA translation regulation and binding, which is decisive in determining the quality of synaptic communication between the pre-synaptic and post-synaptic regions (Davis and Broadie, 2017). It has been recently demonstrated that alterations in signaling, expression, and function of group I mGluRs are related to neurodevelopmental disorders (Wang et al., 2018). Group I mGluRs comprising mGluR1 and mGluR5 have been proposed as key regulators of syndromic and non-syndromic forms of ASD, making them possible therapeutic targets. There are two distinct groups of mGluRs. Some groups of mGluR couple with Gq proteins and are involved in excitatory neural communication, like mGluR1 and mGluR5. The rest of the mGluR groups are involved in non-excitatory neural communication without assistance from Gq proteins. mGluR5 signaling was shown to be affected in opposing directions in both Fragile X Syndrome (FXS) and Tuberous Sclerosis Complex (TSC). We observe the response of these variations onto secondary mediator dynamics in our model, which is directly related to mGluR5 dynamics. Activation of group 1 mGluR mediates the release of Ca^{2+} in the postsynaptic region through the activation of kinases such as mTOR and ERK. These kinases are involved in the modulation of Homer 1a protein generation in the nucleus, which in turn modulates the mGluR5 receptor dynamics through its companion protein Homer 1 b/c. FMRP in this mechanism plays the role of a inhibitor responsible for attenuating the production of Homer 1a. However, in the absence of FMRP, there is an abnormal increase in mGluR5 receptor dynamics. The consequent excessive mGluR-LTD constitutes the aberrations observed in FXS.

FXS is the most common monogenic form of inherited intellectual disability. In a majority of the cases observed, the cause of hampered FMRP dynamics is the expansion of the CGG trinucleotide, repeating in the five untranslated region of the Fragile X FMR1 gene. When the repetition of CGG is as high as more than 1,000 times, this segment of the FMR1 gene undergoes methylation, effectively silencing gene activity and consequently, the generation of FMRP protein. FMRP suppresses mGluR5 receptor dynamics in the post-synaptic region and absence of FMRP leads to exaggerated synthesis of proteins required for mGluR dependent LTP, thereby enhancing its magnitude.

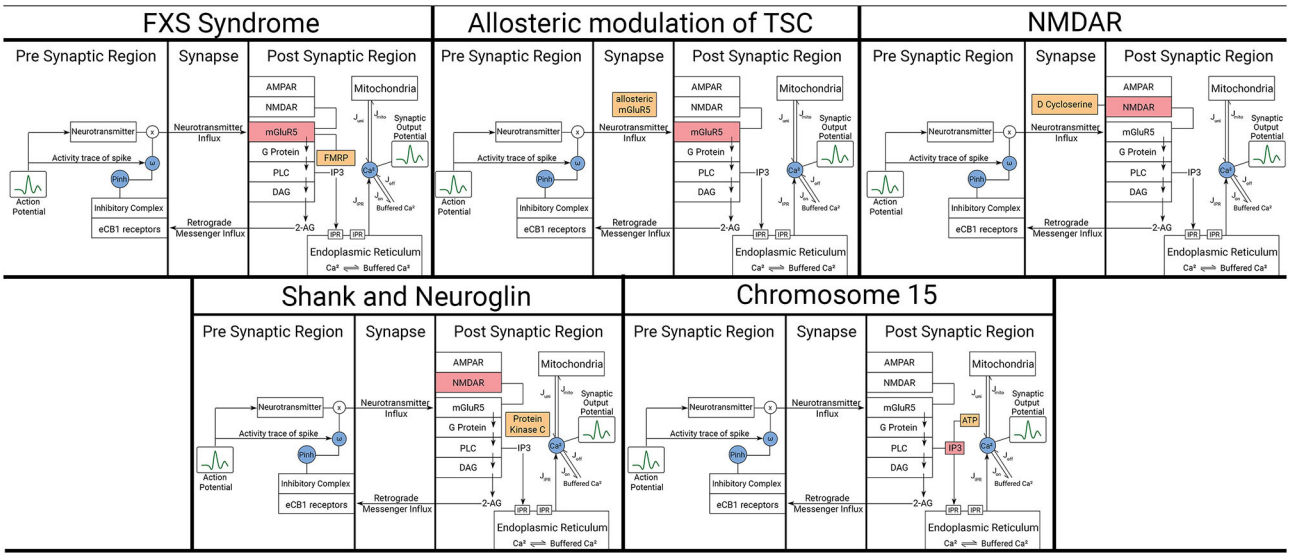

FIGURE 3 | Representation of affected components and modulators in the model for each considered ASD scenario. The five scenarios here are described in detail in the text. Orange boxes represent the modulating variables and red boxes represent the components being affected by those variables. Blue circles represent mathematical variables describing certain phenomenon in those pathways.

2.3.2. Tuberous Sclerosis Syndrome

Another inherited intellectual disability associated with ASD is Tuberous Sclerosis Syndrome (TSC). The syndrome is caused by heterozygous mutations in genes of the TSC1/2 complex involved in mTOR mediated signaling that couples cell surface receptors to protein synthesis (Kelly et al., 2018). Several studies of mouse models of TSC in mouse models have exhibited reduction in decreased mGluR5-mediated LTD caused by impaired protein synthesis. Consistently, treatment with an allosteric mGluR5 agonist was able to restore mGluR5-mediated LTD (Auerbach et al., 2011). Both positive and negative allosteric modulation of mGluR5 have been proposed as a therapeutic intervention in neurodevelopmental disorders. Negative allosteric modulators (NAMs) of mGluR5 have been shown to alleviate long-term memory deficits, excessive repetitive behaviors, motor stereotypes and social interaction abnormalities in various models of autism (Silverman et al., 2012; Tian et al., 2015). The mGluR5 positive allosteric modulator (PAM) was reported to ameliorate deficits in learning and memory and chemically induced hippocampal LTD in Tsc2+/mice.

2.3.3. NMDAR and the Partial Agonist D-Cycloserine

The NMDAR is a glutamate channel protein and ion receptor at the synapse. The implication of NMDARs in the etiology of ASD has been supported by both clinical and non-clinical studies. Clinical studies have identified genetic variants in the GRIN2A and GRIN2B genes encoding the GluN2A and GluN2B subunits of the NMDAR, respectively. It is highly plausible that differences in subunit composition affect functional properties of NMDARs and/or NMDAR-dependent plasticity. A role for NMDARs in ASD is supported by the fact that social withdrawal and repetitive behavior in individuals with ASD can be alleviated by the NMDAR co-agonist D-cycloserine. By contrast, NMDAR antagonists memantine and amantadine improve ASD-related symptoms. Thus, ASD could result, at least in part, from deviations in hormetic NMDAR responses. D-cycloserine is considered to be a partial agonist of NMDAR i.e., it acts like an agonist when it is the primary neurotransmitter involved but has antagonistic features when it is abundant in the system. This seems to be due to its different receptor subtype selectivity and intrinsic action, which depends on various NR2 subunits (NR2A, NR2B, NR2C), which happen to be the location of glutamate binding. One of the most prevalent hypotheses suggested is that the effects seen *in vivo* at low doses of D-cycloserine reflect its agonistic action at the NR1/NR2C receptors, for which it has a high affinity, while at high doses the effects might be due to antagonistic inhibition of NR1/NR2A and NR1/NR2B receptors, for which D-cycloserine has a lower affinity. It is observed that this effects the glutamate binding and hence does not affect the plasticity from its own path. The resultant glutamate binding is inhibited at NR2A, NR2B once all sites of NR2C are occupied by either of the agonist. It must be noted that D-cycloserine in natural state is not an activated pathway, hence making it the noise source in the system.

2.3.4. Shank and Neuroglin

Shank proteins are master scaffold proteins within the post-synaptic density of glutamatergic neurons important for synaptogenesis and function (Sala et al., 2015) but have also recently been described to have a pre-synaptic role in Drosophila (Wu et al., 2017). Mutations in human Shank genes are also found in ASD (Durand et al., 2007; Berkel et al., 2010; Sato et al., 2012) and expected to relate to their role in activity-dependent formation and remodeling of synaptic function. Analysis in a

mouse model of Shank2, lacking exons 6 and 7, showed reduced hippocampal NMDAR function, whereas mice lacking only exon 7 show up-regulation of NMDARs in synaptosomes, increased NMDAR/AMPAR ratio, and enhanced NMDAR dependent LTP (Wegener et al., 2018). We can model this condition by varying the equilibrium constant value of k or kNMDAR. Hence, the synaptic weight limit is increased as the limit of excitation current is increased. Due to higher NMDAR/AMPAR value, we adopt a working assumption that synaptic vesicle release is unbounded. However, two Shank2 deletion mouse models resulted in very similar social deficits, which support the notion that deviation in NMDAR function in either direction can result in ASD like phenotypes. Interestingly, aberrant NMDAR function and behavioral deficits observed in those mice could be normalized with systemic D-cycloserine and administration of the positive modulator of mGluR5 3-Cyano-N-1, 3-diphenyl-1H-pyrazol-5-ylbenzamide (CDPPB) (Jiang and Ehlers, 2013). Shank1 similarly has been associated with ASD-like behavior in mice, including increased anxiety and deficits in contextual fear learning, but with improvements in spatial learning. This corresponds well with the cognitive changes observed in many individuals with ASD. Shank1 mice additionally show smaller dendritic spines in CA1 pyramidal hippocampal neurons and weaker synaptic transmission (Hung et al., 2008), supporting recent evidence that dendritic spine abnormalities are associated with ASD. We also consider Neuroglins that are synaptic cell adhesion molecules (Dean and Dresbach, 2006; Craig and Kang, 2007) in which several mutations have been found associated with ASD (Südhof, 2008). Knocking-in the ASD-associated R451C substitution into the endogenous Neuroglins NLGN3 locus caused a prominent decrease in Neuroglin levels that resulted in impaired social behaviors, enhanced spatial learning, and increased synaptic inhibition in the mouse somatosensory cortex. Its effects are complementary to Shank, as in the ratio of AMPAR/NMDAR becomes lower. We model the Shank and Neuroglin mechanisms on the effective change in synaptic current and the impacted changes can be observed in the secondary mediator dynamics.

2.3.5. Chromosomal Defects

2.3.5.1. Chromosome 15 Syndrome

A "chromosome 15 phenotype" characterized by ataxia, language delay, intellectual disability, repetitive movement disorders and facial dysmorphic features has been described in individuals with chromosome 15 duplications (Muhle et al., 2004). Within the 15q11–15q13 locus. We model the chromosome 15 inhibitory receptor action on neuronal dynamics onto the synaptic mediator dynamics and observe their effect on the calcium dynamics in the post-synaptic region of the neuron as a consequence of ITP3K enzyme and ATP on IP3 dynamics.

3. METHODS FOR IMPLEMENTATION OF SOFTWARE AND HARDWARE MODELS

3.1. Algorithm Design

3.1.1. Pre-synaptic Region

We consider the neuron model proposed by Faghini-Moustafa (Faghihi and Moustafa, 2015) that describes the processes involved in synaptic plasticity in a synapse mediated by retrograde messengers (RMs). The model, described in **Figure 2**, demonstrates the synaptic current release from the pre-synaptic region when activity spike and retrograde messenger are provided to it. The amount of RM that diffuses into the pre-synaptic neuron consists of RMtrace. Activity trace of input spike considers the effect of plasticity and assigns the effect of latency to the input impulse train. RMtrace along with the activity trace of input spike decide the amount of inhibitory complex released. This inhibitory complex decides the effective release of synaptic vesicles from the pre-synaptic region. Thus, inhibitory complex concentration along with the concentration of neurotransmitter release and the activity trace of input spike decide the magnitude associated with the released synaptic current. This value is the synaptic weight and its rate of change gives the synaptic efficacy, a parameter that describes the strength of plasticity.

The equilibrium point of inhibitory complex is adjusted because the value considered in Faghihi and Moustafa (2015) has a very high threshold and is impractical, to a value where the effects of the impulses can be observed distinctly.

The state variables of the pre-synaptic region: effective strength of feedback of Retrograde Messenger (RMtrace), Inhibitory complex concentration (Inh), and activity trace of spike (C), and the concentration of neurotransmitter (D) are defined using the Tsodyks Markram Model as:

$$\frac{d}{dt}RMtrace = -\frac{RMtrace}{\tau_r} + RM \tag{1}$$

$$\frac{d}{dt}Inh = -\frac{Inh}{\tau_{inh}} + RMtrace.C \tag{2}$$

$$\frac{d}{dt}C = -\frac{1}{\tau_c}[C + \Delta\delta(t - t_p)] \tag{3}$$

$$\frac{d}{dt}D = -\frac{1}{\tau_d}[D + \sum \delta(t - t_d)] \tag{4}$$

where, τ_r is the time constant associated with the influx of RMs, τ_{inh} is the time constant associated with inhibition of release of neurotransmitters, t_p is the time when an impulse is received at the pre-synaptic neuron, RM is the concentration of retrograde messenger present in the post-synaptic region and τ_c and τ_d are the time constants associated with the biological latency in activity spike and neurotransmitter release, respectively. Equations (1)–(3) give the resulting effect of the action potential on the concentration of the inhibitory complex. Equation (4) gives the concentration of neurotransmitter released from the pre-synaptic neuron which depends on the rate at which impulses enter. Δ is the parameter for Hebbian plasticity and is calculated according to **Table 1**.

The probability of inhibition and release of neurotransmitter, concentration of neurotransmitter and synaptic current are written as:

$$P_{inh} = e^{e^{-\frac{0.0000001}{Inh}} - 1} \tag{5}$$

TABLE 1 | Specific values of timescales, threshold values, and control parameters in neuron model.

u[n]	*sgn(RMtrace − RMrest)*	Δ
1	1	1
1	0	−1
0	1	−1
0	0	0

$$P_{rel} = P_{init}(1 - P_{inh}) \tag{6}$$

Here, the probability of inhibition is a function dependent only on the concentration of the inhibitory complex. The probabilities considered here decide the synaptic weight of a neuron i.e., the amount by which the transmission of an impulse through the synapse is magnified. The rate of change of synaptic weight is called synaptic efficacy and is calculated as:

$$\frac{d}{dt}\omega = P_{rel}.C.D \tag{7}$$

Hence, the resulting synaptic current transmitted can be written as:

$$Isyn(t) = \omega \sum \frac{t - t_p}{\tau} e^{\frac{t-t_p}{\tau}} \delta(t - t_p) \tag{8}$$

3.1.2. Post-synaptic Region

At the post-synaptic RM, the RM depends on the calcium concentration due to endoplasmic reticulum and secondary mediator. Calcium effects due to endoplasmic reticulum and secondary mediator can be written as:

$$\tau_{C_c}\frac{dC_c}{dt} = -C_c - C_4.f(C_c, C_e) + [r + \alpha(W_{post} - W_{post_{rest}}) + \beta S_m] + k.\frac{dm}{dt} \tag{9}$$

$$\tau_{C_c}.e_{C_c}\frac{dC_e}{dt} = f(C_c, C_e) \tag{10}$$

$$f(C_c, C_e) = C_1\frac{C_c^2}{1 + C_c^2} - \frac{C_e^2}{1 + C_e^2}.\frac{C_c^4}{C_2^4 + C_c^4} - C_3C_e \tag{11}$$

$$\frac{dm}{dt} = \nu_{1_{max}}\frac{C_c^2}{K_d^2 + C_c^2} - \nu_{2_{max}}\frac{[Na^{2+}]^2}{K_{Na^{2+}}^2 + [Na^{2+}]^2}.\frac{m}{1 + m} \tag{12}$$

$$\tau_{Sm}\frac{dSm}{dt} = (1 + tanh(S_{Sm}(I_{syn} - I_{Sm})))(1 - Sm) - \frac{Sm}{d_{Sm}} \tag{13}$$

Here, in these equations, c1, c2, c3, and c4 are the fixed control parameters of the function f(cc,ce), cc describes the calcium concentration in the cytoplasm, ce represents the calcium concentration in the internal store (endoplasmic reticulum ER), Wpost is the recovery variable for the post-synaptic current in FHN model, Sm is the generation of IP3 in response to the influx of calcium current. The term $[r + \alpha(Wpost - Wpostrest) + \beta.Sm]$ represents the calcium influx from the external space. Also, interaction between the cytoplasmic calcium (cc) and endoplasmic calcium (ce) is described with a two-variable function f(cc,ce). There is threshold value for the Sm production that is triggered by the synaptic current. Threshold parameter ISm is hence selected to distinguish between activated and inactivated states of the variable.

The plasticity of the system is decided by the retrograde messenger. The concentration of retrograde messenger is only dependent on the post-synaptic calcium concentration. The concentration of post-synaptic retrograde messenger is written as:

$$RM = e^{-e^{-e\sqrt{3}log(C_c)+25.4146}} \tag{14}$$

By FHN model, a simplified version of the Hodgkin-Huxley model, for post-synaptic site, we get:-

$$\begin{aligned}\frac{dW_{post}}{dt} &= V_{post} + I_{post} - I_{syn}\\ \frac{dV_{post}}{dt} &= V_{post} - \frac{V_{post}^3}{3} - W_{post}\end{aligned} \tag{15}$$

3.2. Linearization of Neuron Model

The equations are optimized to improve the computational efficiency of the model and reduce its implementation cost by implementing polynomial expansion of functions to reduce complex and lengthy functions. While this does mean that the hardware will be easier to design, the approximations are taken such that they resemble the curve closely in the domain the functions shall be operating in.

3.2.1. Pre-synaptic Region

In the 1st order Tsodyks Markram differential Equations (14)–(4), since all the equations are linear, there is no requirement to make any adjustments to them.

For determining the probability of inhibition, we encounter the implementation of exponential function. On using CORDIC algorithm to implement the same, the area of the hardware is increased by a large amount. Also since the CORDIC algorithm operates on convergence, this would lead to an increase in time taken per process for computation. Hence, we solve by using an rectangular hyperbolic function that closely resembles the curve in the region of operation.

$$P_{inh} = \frac{-0.00007}{Inh - 0.00001} + 1.1 \tag{16}$$

For synaptic current, we consider the summation segment as a reset enabled function. Thus, we obtain a pair of equations Y and Z, which generate the form of unweighted synaptic current.

$$\begin{aligned}Y &= \frac{t - t_p}{\tau}e^{\frac{t-t_p}{\tau}}\\ Z &= \tau e^{\frac{t-t_p}{\tau}}\end{aligned} \tag{17}$$

For a pre-fixed frequency of t_{p0} interval, the summation symbol in (8) is removed without any loss of accuracy by considering the summation of each power for a finite number of terms. However, for SyNC model to function for any form of t_p provided, we needed to make some approximations. Adoption of a piece-wise approach leads to a trade-off between area efficiency and error efficiency. Also the properties of the curve are lost at every new impulse completely, which leads to significant error in output, unless more functions are added to compensate the loss. But this almost doubles the area. Hence, the alternative is to go for differential form of these equations. As such the impulse driven activation can be enabled, without removing the value of Y completely before the activation. For this particular set of equations, activation conditions can be met simply by adding 1 to Z, when an impulse arrives in each cycle. Such a form is more robust in error handling for discretized calculations. Based on above technique, Isyn is calculated as follows:

$$\begin{aligned} \frac{dY}{dt} &= \frac{Z-Y}{\tau} \\ \frac{dZ}{dt} &= \frac{-Z}{\tau} + u[n] \end{aligned} \tag{18}$$

$$Isyn = \omega.Y \tag{19}$$

3.2.2. Post-synaptic Region

It is observed that the value of f(c_c, c_e) is in the order of 10–12, hence making the detection of this potential via instruments impossible. Moreover, the value of the function is much lower than the noise threshold, due to which the noise parameter will be the primary contributor to the value of this function. Hence, we consider f(c,E)=0. This in turn gives us E=0 (from Equation 12). Hence, the changed calcium dynamics equations are:

$$\tau_{C_c}\frac{dC_c}{dt} = -C_c + [r + \alpha(W_{post} - W_{post_{rest}}) + \beta S_m] + k.\frac{dm}{dt} \tag{20}$$

$$\begin{aligned} \frac{dm}{dt} &= \nu_{1_{max}} C_c^2 K_d^2 (1 - \frac{C_c^2}{K_d^2} + \frac{C_c^4}{K_d^4}) - \nu_{2_{max}}.k1.(1 - m + m^2) \\ k1 &= \frac{[Na^{2+}]^2}{K_{Na^{2+}}^2 + [Na^{2+}]^2} \end{aligned} \tag{21}$$

For secondary mediator, polynomial expansion of tanh is implemented to reduce the complexity of the equation:

$$\begin{aligned} \tau_{Sm}\frac{dSm}{dt} &= (1 + k_s - \frac{k_s}{3})(1 - Sm) - \frac{Sm}{d_{Sm}} \\ k_s &= S_{Sm}(I_{syn} - I_{Sm}) \end{aligned} \tag{22}$$

For concentration of retrograde messenger, we implement polynomial expansion of exponential function:

$$RM = 1 - (k2.c^{k1}) + \frac{(k2.c^{k1})^2}{2} - \frac{(k2.c^{k1})^3}{6} \tag{23}$$

where k1 = 2.0447, k2 = $9.1799x10^{-12}$.

We modify the original FHN model such that the nonlinear terms are eliminated. Unlike the other equations, where we have allowed powers of a variable in expansion, we avoid this scenario here since we are able to reduce power taken in this particular variable description with no noticeable precision loss. This enables us to approximately solve both linearized FHN equations for the power cost of one. So, the nonlinear term from equation:

$$f(V_{post}) = V_{post} - \frac{V_{post}^3}{3} \tag{24}$$

can be rewritten into the closest fitting linear curve (Hayati et al., 2016). The curve we chose here is:

$$f(V_{post}) = 1 - \frac{|V_{post}|}{2} \tag{25}$$

4. RESULTS

4.1. Hardware Design

This section provides a detailed description of the hardware realization of the proposed discretized SyNC model. The computation core has been developed to work with IEEE-754 single precision floating point number system. The pathways of information flow in the hardware realization of SyNC are described in **Figure 4**. **Figure 5** describes the different stages of pipelining in terms of registers or flip-flops in each arithmetic unit used in the model. The design has been pipelined extensively and even arithmetic operators have been pipelined for mantissa operations by using custom-made, non-compressed, tree structured, pipelined, moderately large sized and power consuming high speed, wallace tree multipliers. The largest combinational unit floating point multiplier architecture is a mantissa multiplication of respective mantissa widths, whereas the largest one in division is the iterative Newton-Raphson division method which consists of three mantissa width multiplications for both posit and float. All of these multiplications are done using custom implemented wallace tree unsigned multipliers for gaining greater speed and to meet acceptable operating frequency.

Design has been pipelined with basic pipeline registers and clock speed has been achieved as high as 1 GhZ in 45 nm technology node. The hardware design of the SyNC model, with exact same input configurations, are simulated in Questasim 10.0b Simulator by simulation scripts and output results are functionally verified by self-developed utility scripts in C++ v.11 and Python 3.8. For simulation as well as the hardware design for the given system of equations, we consider a constant input of retrograde messenger from the pre-synaptic region such that it is always just above the threshold for activation of synaptic plasticity parameter. We have implemented SyNC in RTL which are then mapped and synthesized using Synopsys Design Compiler on 45 nm OpenNangate technology. The power consumption is derived using Synopsys Power Compiler. Standard operating frequencies of almost 1 GHz is met for all the designs in 45 nm ASIC.

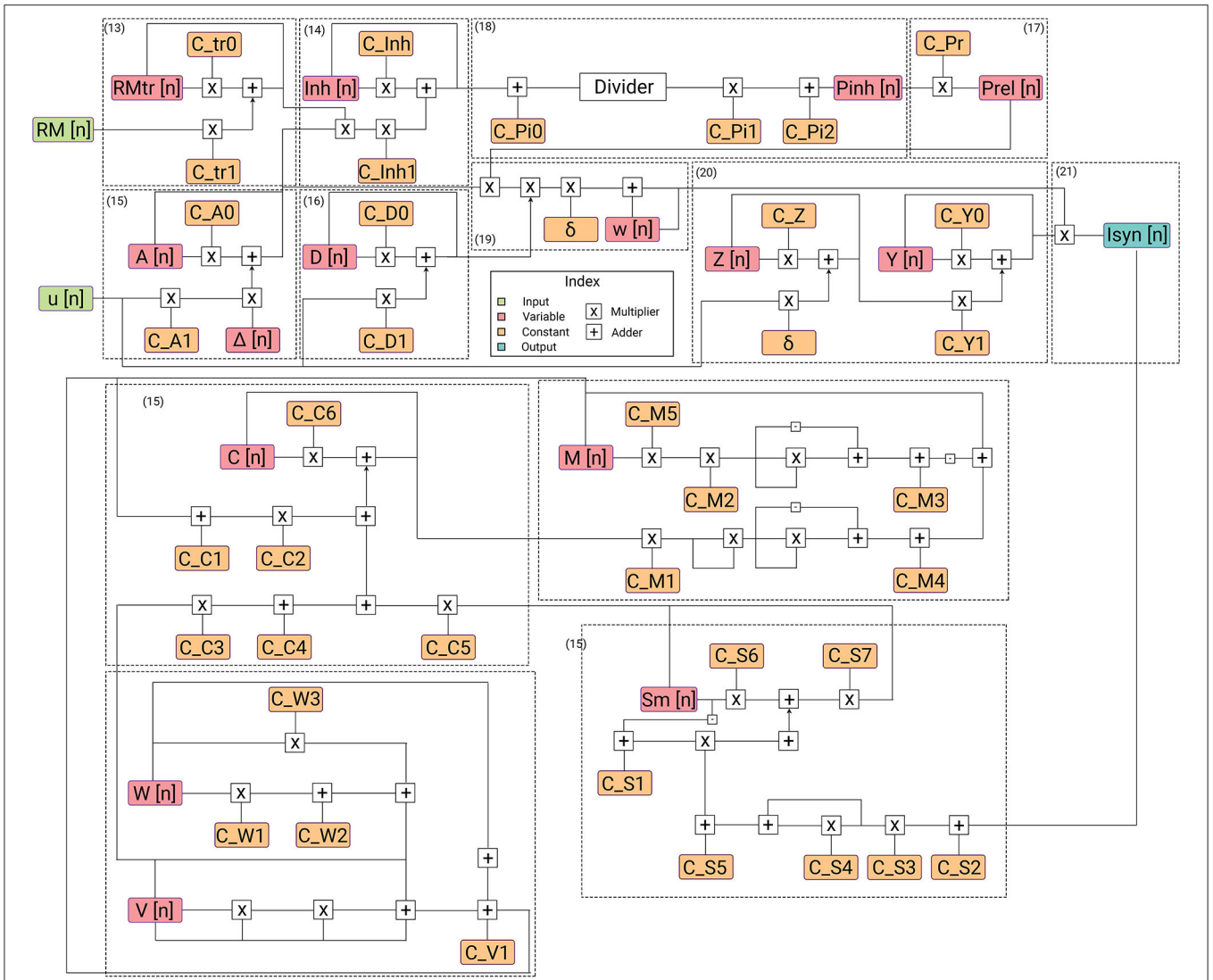

FIGURE 4 | Description of flow of data in hardware architecture. Each submodule for its corresponding equation is highlighted. The architecture has the lowest power requirements for the complexity of the designed model.

For low power, economical and optimized implementation of most widely used single precision float, we have made use of reduced complexity hardware of base arithmetic units. Complexity of other numerous subunits are also significantly reduced. This brought down the power and area footprints by orders of magnitude than the base version to 2.135 W and 1.877 mm^2, respectively, by reduction of the number of intermediate registers and less frequent switching of intermediate variables. Through extensive pipelining, single precision floating point optimized version is able to meet acceptable operating frequency of 1,030 MHz. The operation parameters are described in **Table 2**.

One of the key features of our mathematical design is that an endocannabinoid feedback mechanism is involved. While this is a staple in analog designs, for hardware implementation, an inadvertent delay is obtained in the system. This is observed to be equivalent to 25 clock cycles in the hardware domain. Here, instead of resorting to Verilog AMS, we control the accuracy to the model and minimize this delay to negligible extent by varying δ. The role of δ in our model is defining the relationship between

TABLE 2 | Operation parameters of SyNC architecture.

Sl.No.	Parameter	Value	Units
1.	Area	1.877	mm^2
2.	Dynamic power	2.135	Watt
3.	Cell leakage power	32.1054	mW
4.	Total cell power	2.167	Watt
5.	Total no. of gates	2.35	Million
6.	Total no. of transistors	9.4	Million
7.	Speed-up by pipelining	3.88	N/A

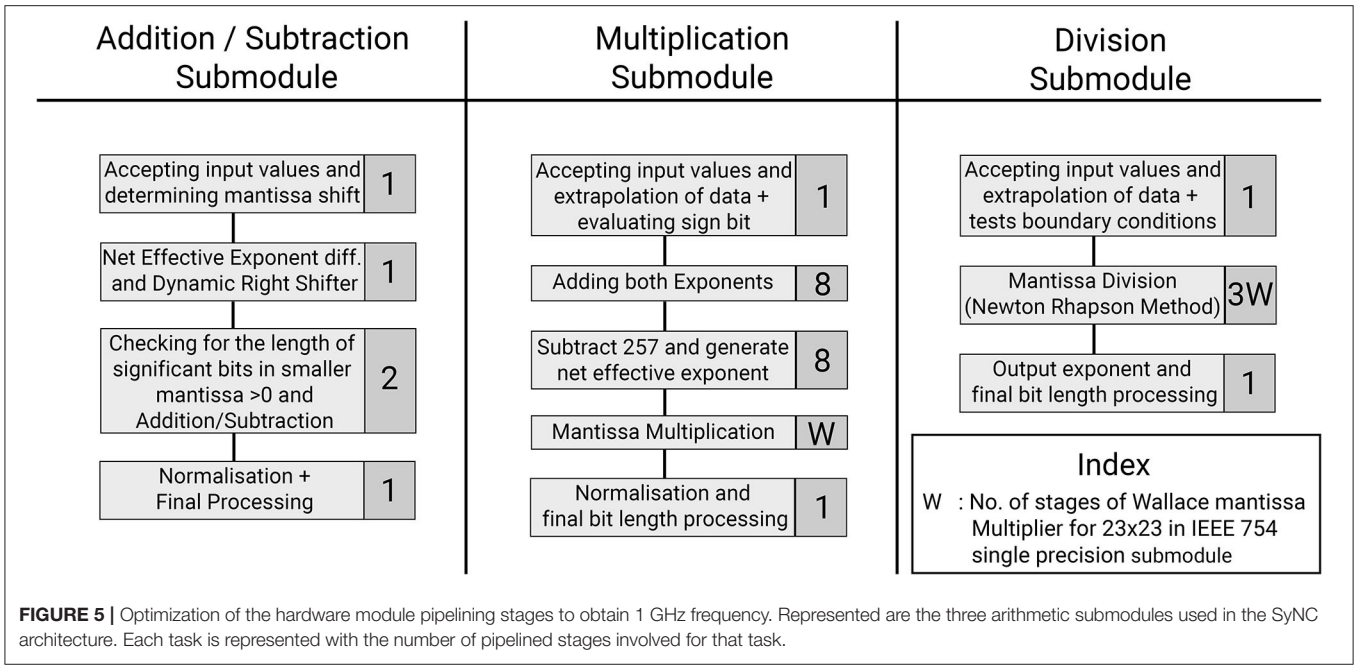

FIGURE 5 | Optimization of the hardware module pipelining stages to obtain 1 GHz frequency. Represented are the three arithmetic submodules used in the SyNC architecture. Each task is represented with the number of pipelined stages involved for that task.

the clock timing and the actual timeframe of operation. Hence by increasing δ, we decrease the effective influence of the delay in the timeframe of operation of the synapse.

4.1.1. Considerations for Error vs. Complexity in Architectural Design

The primary focus for development of a hardware model is for future use in large scale hardware implementations. Such applications necessitate low power consumption designs. Solutions such as linearization have been applied to obtain the required level of biological complexity but with reduced mathematical complexity. In the variable outputs obtained from the hardware realization of the SyNC neuron model, a latency in the results is observed. The net latency across all variables is 0.031 s, which is an effect of pipelining as well as the delay in feedback of retrograde messenger to the pre-synaptic region. As can be observed from the equations, while other equations have some garbage value output before the system stabilized for accepting action potential input, the only variable that does not always return to rest and which impacts the variables that come after it is synaptic weight, ω. For this very reason, the first values obtained just during the initialization of the model within this period must be rejected and the value of ω is fixed at 0, to remove the effect of default values of ω from influencing the nature of the curve. The error is $<1\%$ for architectures designed, which are sufficiently low and the output is barely affected and hence acceptable.

4.1.2. Device Sensitivity Compared to Mathematical Model

For our hardware design with precision mode IEEE-754 Single Precision floating point, we observe that the amplitudes of the variables are higher in the hardware realization of our models than that of our software results. This is a result of using differential forms of the equations to develop the SyNC hardware realization. The response of the variables in the current curves is a consequence of the choice of value of δ for model implementation. The smoothness and root mean square (RMS) accuracy of all obtained curves are directly proportional to δ. Hence, we designed our hardware model with such considerations in mind. We can't increase the value of δ in our model because such an adjustment will reduce the speed-up achieved by the system.

However, for a biological system, the currency of communication is not entirely the form of the curve, but also the concentration of calcium influx associated with it. Rather, after RMS error reaches a particular range, it is this concentration influx which is more important to replicate. This can be evaluated by obtaining the error in area under the curve in the form of Area Average Error (AAE). Since for the SyNC neuron model, the conservation of molecules involved is of higher importance from a biological perspective, we disregard the amplitude error in favor of lower AAE after RMS error is within 1%.

4.2. Software Analysis of Autism Spectral Disorders

4.2.1. Designing Mathematical Modules for ASD Scenarios in Extended Model

4.2.1.1. FXS Syndrome

For modeling the effect of FMRP in FXS syndrome in a synaptic device, we consider its impact on mGluR5 LTD. We define the equilibrium dynamics for the mGluR5 due to accelerated generation of Homer 1a. The synaptic current influx in the postsynaptic region can be considered a directly proportional to mGluR5 activity. Since the increased sensitivity in dynamics is observed, the gain achieved can be expressed as:

$$\frac{dInflux}{dt} = -k_{fmrp}.k_t.[Isyn] \qquad Isyn' = Isyn + Influx \tag{26}$$

Here, the dynamic parameter k_{fmrp} is the outcome of molecular stochastic process. Therefore, it behaves as the source of noisy behavior in this model for FMRP concentration. The variations in FXS are expressed first in secondary mediator in our model.

4.2.1.2. Tuberous Sclerosis Complex

To understand and model TSC, we approach it from the perspective of the solutions that have been suggested in the literature. Allosteric modulation has been one of the most promising solutions that have been studied extensively in the recent times. Due to lack of an exact model of how both enhancement and inhibition of mGluR5 activity improves synaptic output in allosteric modulation of TSC (**Figure 6**), we hypothesize a mathematical form for the same that can duplicate such behavior successfully. Hence in our model, we consider the behavior of the NAM akin to lowering the threshold of mGluR5 activation, leading to easier activation of the post-synaptic region and improving mGluR-LTP. We consider the equivalent mechanism of the action of PAM by considering the impact of impaired protein function behavior onto the output dynamics of the synapse.

As observed from numerous studies, the activity of TSC is essentially centered around the activity of mGluR5. This is consistent with mGluR5 PAM alleviation of LTP by compensating for reduced mGluR5. However, mGluR5 must also be the primary carrier of distortion in this system because reduction of mGluR5 activity by NAM is also beneficial for the plasticity of the system. Hence, we hypothesize that the impaired protein synthesis is the generator of distortion in the process. We develop the equilibrium constructs of the system as follows:

$$\frac{dk_{mGluR5}}{dt} = +k_{mGluR5} - k_{namGluR5} \qquad \frac{dk_{mGluR5}}{dt} = +k_{mGluR5} + k_{pamGluR5} \qquad k_{namGluR5} > k_{mGluR5} > k_{pamGluR5} \tag{27}$$

4.2.1.3. NMDAR and Partial Agonist

D-cycloserine's activity as a partial agonist can be best described as a competitive process at NMDAR. Electrodynamically, in the concerned scenarios, the concentration of D-cycloserine is more than the concentration of NMDAR, hence the molecules unable to bind with NR1/NR2C receptors act as agonists. However, it is also observed that this effects the glutamate binding and hence does not affect the plasticity from its own path. The resultant glutamate binding is inhibited at NR2A, NR2B once all sites of NR2C are occupied by either of the agonist. It must be noted that D-cycloserine in natural state is not an action potential activated pathway involved in synaptic transmission dynamics, hence making it the noise source in the system. To demonstrate the role of D-cycloserine, we model its role in synaptic transmission dynamics via the competitive concentration dynamics process. The effect of such dynamics can be first observed in our model at the secondary mediator, the first state variable evaluated at the post-synaptic region and is directly dependent to mGluR5 activity. To better understand the process dynamics, the distortion for this specific case is evaluated by comparison between the simulated outputs to a noisy signal for the case where D-cycloserine is acting passively along with primary neurotransmitter (glutamate).

For the scenario involving D-cycloserine along with glutamate:

$$\frac{dIsyn}{dt} = [+\frac{Isyn}{k_{Glutamate}} - \frac{N}{k_{D-cycloserine}} + \frac{1}{k_{adjust}}] \tag{28}$$

4.2.1.4. Shank and Neuroglin

The role of Shank proteins in synaptogenesis and function (Sala et al., 2015) while understood to a certain extent, have not been successfully generalized due to the numerous ways Shank proteins can impact the synaptic function. Many experimental studies have been made to understand its role, but the highly diverse and often contentious conclusions from these studies have been an impediment. Here, we seek to reduce the core properties of the Shank such that all such scenarios can be simulated successfully. The core properties of Shank protein can be reduced to variations in NMDAR activity, NMDAR mediated LTP and NMDAR/AMPAR ratio at the postsynaptic region. We can model this condition by varying the equilibrium constant value of k or kNMDAR. To be able to model a wide range of NMDAR/AMPAR values, we adopt a working assumption that synaptic vesicle release is unbounded. We also consider the action of Neuroglins, synaptic cell adhesion molecules, which have effects complementary to that of Shank, as in the ratio of AMPAR/NMDAR becomes lower. We can hence develop a composite model that can effectively demonstrate the impact of Shank and Neuroglin dynamics on the effective change in synaptic current and the impacted changes can be observed in the secondary mediator dynamics.

$$\frac{Isyn'}{Isyn} = \frac{k_{Shank}}{.k_{Neuroglin}}.k_{adjust} \tag{29}$$

4.2.1.5. Chromosome 15 Syndrome

A "chromosome 15 phenotype" is characterized by ataxia, language delay, epilepsy, intellectual disability, repetitive movement disorders, and facial dysmorphic features and has been described in individuals with chromosome 15 duplications (Muhle et al., 2004). We model the chromosome 15 inhibitory receptor action on neuronal dynamics onto the synaptic mediator and observe the effects on calcium dynamics in the post-synaptic region of the neuron.

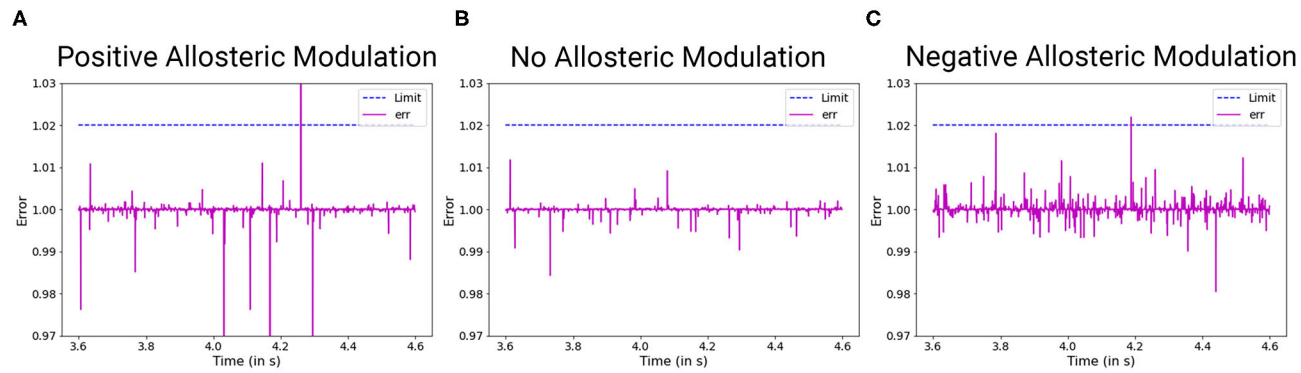

FIGURE 6 | The effect of allosteric modulation in TSC. The limitations for positive allosteric modulation **(A)** and negative allosteric modulation **(C)** are compared with an unperturbed scenario **(B)** in which no allosteric modulation agents were introduced into the system. **(A)** Positive allosteric modulation results in higher amplitude and low frequency filter. **(C)** Negative allosteric modulation results in lower amplitude threshold and high frequency filter.

4.2.2. Classification of Noise Response to Steady Synaptic Output Potential for ASD Scenarios

Here, we observe the normalized impact of an identical noisy input to the synaptic potential output at the post-synaptic region of the neuron. The effective distortion observed in the synaptic output potential can be classified into three primary types (**Figure 7**). Type A shows the least amount of distortions. The impact on one synapse can be considered unobservable by experimental methods. Hence, we can say that to have observable impact on the neuronal circuit, multiple synapses and neural networks with them must be affected by these particular synaptopathies. Type B events show considerable distortions whose impact can be considered observable via high precision experimentations. To have observable impact on the neuronal circuit, a small collective of such affected synapses and networks are sufficient. Type C shows abruptly high distortions whose impact on a single synapse can be considered observable by experimental methods. Few such altered synapses for neurons in key processing regions of the brain will lead to observable variations in the neuronal circuit.

5. DISCUSSION

In this work, we realize a biologically descriptive synaptic model for neural communication, with primary focus on modeling the complexity of a synapse in a way that can translate into competent hardware models. Large scale implementation of such models is aimed at utility in designing biologically extensive neuronal circuits. We focus on Autism Spectrum Disorders in which a variety of synaptopathy mechanisms operate in various syndromes. By generating a set of ASD interrogation algorithms (ASDint) we modeled changes to synaptic dynamics in regard to corresponding disease variables and observed the spread of their impact in larger neural circuits. This is the first demonstration of algorithms designed specifically to address complex synaptopathies of ASD. Co-development of ASDint over the SyNC core algorithm provides a powerful new computational and hardware approach to benefit ASD experimental analysis and to help predict manifestation of symptoms for ASD. This is accomplished by abstraction of neuronal behavior at the synapse while describing the complexity involved in the interactions of the implicated primary state variables. Importantly, such an approach is not restricted to ASD and the SYNC algorithmic core can be used to design network models for any such synaptopathies with complex dynamics.

Most of the synapses in the CNS are low pass filters. While the synaptic communication properties are not ideal, the attenuation is not significant. For a large network of neurons consisting of many synaptic nodes, it is important that the signal amplitude is not attenuated to a large degree or else distant synaptic nodes in the neural communication framework won't be able to communicate with each other. Synapses modulate not only the amplitude of the action potential but also the selectivity and accuracy of the synaptic output response. The filter form of synapses has decisive implications on their noise response (Voglis and Tavernarakis, 2006; Faghihi and Moustafa, 2015). Synapses as such can be widely classified into three such classes: high pass, low pass and band pass filters. Those synapses with release probability below 0.3 act as high pass filters (Goda and Südhof, 1997). Such synapses have very high selectivity and noise resistance to environmental procedures. However, the attenuation to synaptic output potential is also very significant in such synapses. Synapses with initial probability of neurotransmitter release greater than 0.7 act as low pass filters (Murphy et al., 2004). Such synapses have very low selectivity, while attenuation to synaptic output potential is also rather insignificant in such synapses. However, the resulting synaptic transmission is affected by noise generated by environmental procedures to an observable degree. Synapses with intermediate initial release probability, between 0.3 and 0.7, act as band pass filters (Rose et al., 2013). In our models, we consider the initial neurotransmitter release probability of 0.5, which adequately describes a low pass filter glutamatergic synapse.

Synaptopathies can be described in the form of distortions observed in the system compared to normal conditions.

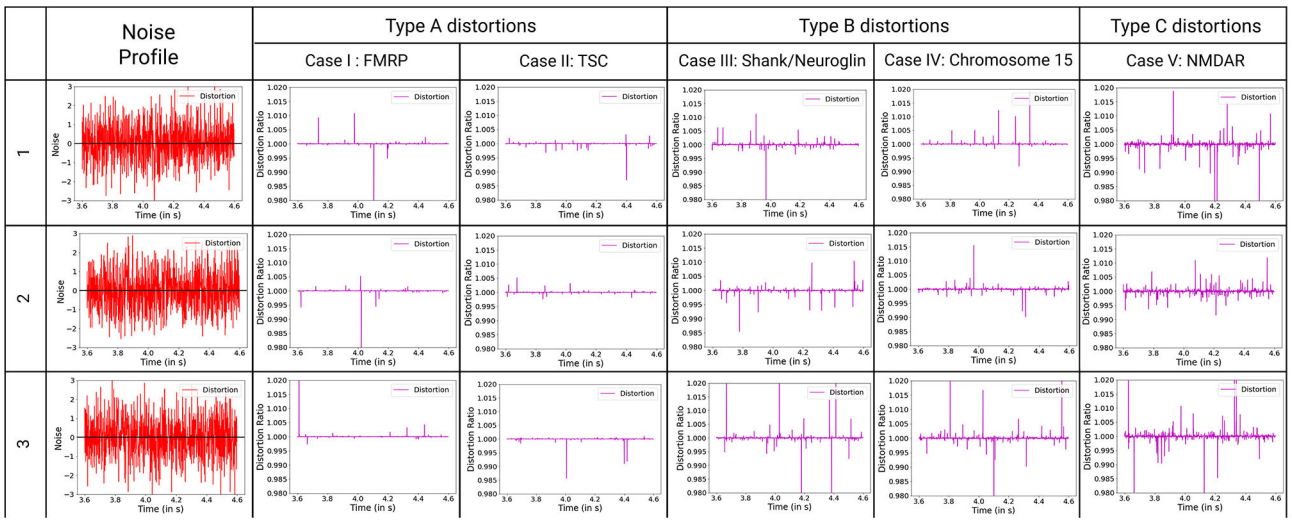

FIGURE 7 | Classification of ASD mechanisms considered based on distortion from the ideal synaptic output potential, with ideal distortion response set at 1. Noise describes the variations in variables that are considered for these synaptopathies, with baseline for no noise input set at zero. The baseline for noise is added to the plots for reference. D-cycloserine here acts as partial agonist on NMDAR. Type A synaptopathies are categorized as the least amount of distortions. Multiple neurons must be affected by these particular synaptopathies to be observable. Type B synaptopathies have observable impact on the neuronal circuit even when occurring in a small collective of such affected neurons. Type C synaptopathies show abruptly high distortions that can lead to easily observable variations in the neuronal circuit.

The distortion obtained from the ASDint simulations show consistency with the conditions underlying those specific synaptopathies. Two primary ways to look at a noise response is the gain in potential strength they provide and the number of spikes in the resultant output that are at a threshold to impact the system dynamics. Gain in potential results in stronger and more sensitive LTP dynamics, reducing the threshold of action potential spike input and frequency required to activate it. Such an output response implies improved LTP dynamics and lower LTD threshold, resulting in greater sensitivity of the model as well as lower duration of information retention of the synapse. Greater noise spikes result in false activation of the region and can result in faulty activation of the boutons. Such impulses can result in variations in synaptic weight and lead to repetitive behaviors. In analysis of the ASD mechanisms different resulting distortions occurred.

Evaluation of distortions provides insights into phenotypes observed in ASD synaptopathies. For TSC under the impact of negative allosteric modulation, the noise spikes in the distorted curve, although of lower amplitude threshold, are greater than the general scenario. This can manifest itself in the form of false activation of the post-synaptic region, which can be considered a trigger for repetitive behaviors. When positive allosteric modulation occurs, we observe the distortion curve to have higher noisy spikes as well as lower attenuation of action potential. Hence, it has better LTP characteristics and LTD threshold that can be associated with obstructions in learning and lower attention span. Modeling the FXS syndrome in ASDint module, we observe that LTP is very easily activated here and can be observed in the form of lower LTP threshold. Thus, it can be associated with difficulty in learning process as well as increased sensitivity to noisy inputs in the neural circuitry. The interactions of partial agonist with NMDAR show us the output of competition in the synaptic channel manifested at the synaptic gate. Social withdrawal and repetitive behavior are associated with this particular synaptopathy. On observing the noise response of the ASDint module, we see that the noise-induced variations are the highest when compared to the other three scenarios and can be considered a trigger for repetitive behavior. For Shank, NG activity variations, the NMDAR induced LTP is affected and results in higher required amplitude of LTD, which we can see from the noise plots resembles the expected activity variations. Chromosome 15 syndrome is associated with repetitive movements which as observed from the distortion curve, could be a consequence of false activation of post-synaptic regions.

Large scale hardware usage is key for further understanding the impact of plasticity and synaptopathy mechanisms on larger circuits. In our hardware modeling, use of the IEEE 754 single precision floating point has accuracy within tolerable error ranges. It is also remarkably small and efficient in terms of PPA (power, performance, area) vs. ARM core implementations. It has been a prevalent practice of late to use floating point numerals in 16 bit widths or lower order custom width floats to optimize computational resources specifically for edge computing use-cases. Such practices give us higher power efficiency which increases the scalability of the neuronal circuit model. We were unable to consider them without decisive loss in accuracy within the neuron ASDint model. Due to such considerations, IEEE 754 single precision floating point is noticeably the most suitable bit width for our application. For comparison of our neural network, one of the well known state-of-the-art SNN architectures, IBM TrueNorth (Akopyan et al., 2015) and Intel Loihi (Davies et al., 2018) has been considered. IBM TrueNorth uses a smaller

technology node of 28 nm and consumes about 100 mW of power. It has a power density of 20 mW/cm^2 consisting of 5.4 billion transistors. Intel Loihi has used a further smaller node of 14 nm processor with a 2 billion transistor size or 60 mm^2 in chip area. The proposed SyNC architecture is designed on a technology node of 45 nm and consists of 9.4 million transistors over an area of 1.877 mm^2. Hence, we can observe that we are able to bypass the requirements of programmability to model diverse descriptive synaptic models by design of a minimalist ASIC synaptic core that describes every state variable in a synapse. On utilization of lower technology nodes, we expect performance of our device to be at par with state of the art SNN architectures. For future studies a programmable Application Specific Processor like the former chips are being targeted for better flexibility and programmability and to have a one chip for all solutions.

Models built in equivalent Posit numeral representation, such as Jaiswal and So (2019) and Chatterjee et al. (2021) have demonstrated highly flexible and fast convergence in specific format scientific functions. Such models have shown accuracy comparable to IEEE 754 double precision floating point, using much lesser resources than the latter. However, due to complications in evaluations that result from dynamic power owing to higher switching of states, the net power requirement is significantly high on account of deep pipeline and conversion of FPGA fabric optimized design to general ASIC.

CONCLUSION

The SyNC model provides us with an elaborate and accurate neuron model. It is one of the only hardware models that has efficiently used posit in highly sensitive systems, while achieving low error percentages. Its low power and low error margins make it optimal for large scale digital implementations. Finally, ASDint and SyNC can be used to process and test data obtained from experiments and hypothesize neuron network possibilities and hence identify key variables and areas for experimental verification. Hence, when used in large scale network models, SyNC accelerates our understanding of the roles of synapses, synaptic plasticity and neuronal circuits in brain function.

DATA AVAILABILITY STATEMENT

The datasets presented in this study can be found in online repositories. The name of the repository and accession number are found at this link: https://github.com/RnkC/SyNC.

AUTHOR CONTRIBUTIONS

AM and JP conceived of the project and experimental design and helped to generate algorithms and analyzed the data, and wrote the manuscript. AR supervised all aspects of the hardware design and realization. RC generated the software algorithms, performed the ASD analysis, and developed ASDint algorithms for case study. SC and SM developed and deep pipelined the SyNC model in relation to the algorithms with assistance from RC. RC wrote the initial manuscript and generated figures and tables. All authors contributed to the article and approved the submitted version.

FUNDING

This work was supported by a multi-university and university-industry collaborative effort.

REFERENCES

Abbott, L. F., and Regehr, W. G. (2004). Synaptic computation. *Nature* 431, 796–803. doi: 10.1038/nature03010

Akopyan, F., Sawada, J., Cassidy, A., Alvarez-Icaza, R., Arthur, J., Merolla, P., et al. (2015). Truenorth: design and tool flow of a 65 mw 1 million neuron programmable neurosynaptic chip. *IEEE Trans. Comput. Aided Des. Integr. Circuits Syst.* 34, 1537–1557. doi: 10.1109/TCAD.2015.2474396

Auerbach, B. D., Osterweil, E. K., and Bear, M. F. (2011). Mutations causing syndromic autism define an axis of synaptic pathophysiology. *Nature* 480, 63–68. doi: 10.1038/nature10658

Benfenati, F. (2007). Synaptic plasticity and the neurobiology of learning and memory. *Acta Biomed.* 78(Suppl. 1), 58–66.

Benjamin, B., Gao, P., McQuinn, E., Choudhary, S., Chan-drasekaran, A. R., Bussat, J., et al. (2014). "Neurogrid: a mixed-analog-digital multichip system for large-scale neural simulation," in *Proceedings of the IEEE*, Vol. 102, 699–716. doi: 10.1109/JPROC.2014.2313565

Berkel, S., Marshall, C. R., Weiss, B., Howe, J., Roeth, R., Moog, U., et al. (2010). Mutations in the SHANK2 synaptic scaffolding gene in autism spectrum disorder and mental retardation. *Nat. Genet.* 42, 489–491. doi: 10.1038/ng.589

Bi, G. Q., and Poo, M. M. (1998). Synaptic modifications in cultured hippocampal neurons: dependence on spike timing, synaptic strength, and postsynaptic cell type. *J. Neurosci.* 18, 10464–10472. doi: 10.1523/JNEUROSCI.18-24-10464.1998

Borges, R., Borges, F., Lameu, E., Batista, A., Iarosz, K., Caldas, I., et al. (2017). Spike timing-dependent plasticity induces non-trivial topology in the brain. *Neural Netw.* 88, 58–64. doi: 10.1016/j.neunet.2017.01.010

Branco, T., and Staras, K. (2009). The probability of neurotransmitter release: variability and feedback control at single synapses. *Nat. Rev. Neurosci.* 10, 373–383. doi: 10.1038/nrn2634

Brenman, J. E., and Bredt, D. S. (1997). Synaptic signaling by nitric oxide. *Curr. Opin. Neurobiol.* 7, 374–378. doi: 10.1016/S0959-4388(97)80065-7

Burns, M. E., and Augustine, G. J. (1995). Synaptic structure and function: dynamic organization yields architectural precision. *Cell* 83, 187–194. doi: 10.1016/0092-8674(95)90160-4

Chatterjee, R., Chowdhury, S., Mondal, S., Raha, A., Paluh, J., and Mukherjee, A. (2021). "Presync: Hardware realization of the presynaptic region of a biologically extensive neuronal circuitry," in *2021 34th International Conference on VLSI Design and 2021 20th International Conference on Embedded Systems (VLSID)*, 228–233. doi: 10.1109/VLSID51830.2021.00044

Chevaleyre, V., Takahashi, K. A., and Castillo, P. E. (2006). Endocannabinoid-mediated synaptic plasticity in the CNS. *Annu. Rev. Neurosci.* 29, 37–76. doi: 10.1146/annurev.neuro.29.051605.112834

Choquet, D., and Triller, A. (2013). The dynamic synapse. *Neuron* 80, 691–703. doi: 10.1016/j.neuron.2013.10.013

Citri, A., and Malenka, R. C. (2008). Synaptic plasticity: multiple forms, functions, and mechanisms. *Neuropsychopharmacology* 33, 18–41. doi: 10.1038/sj.npp.1301559

Craig, A. M., and Kang, Y. (2007). Neurexin-neuroligin signaling in synapse development. *Curr. Opin. Neurobiol.* 17, 43–52. doi: 10.1016/j.conb.2007.01.011

Davies, M., Srinivasa, N., Lin, T., Chinya, G., Cao, Y., Choday, S. H., et al. (2018). Loihi: a neuromorphic manycore processor with on-chip learning. *IEEE Micro* 38, 82–99. doi: 10.1109/MM.2018.112130359

Davis, J. K., and Broadie, K. (2017). Multifarious functions of the fragile X mental retardation protein. *Trends Genet*. 33, 703–714. doi: 10.1016/j.tig.2017.07.008

Davison, A. P., Brüderle, D., Eppler, J., Kremkow, J., Muller, E., Pecevski, D., et al. (2008). PyNN: a common interface for neuronal network simulators. *Front. Neuroinform*. 2:11. doi: 10.3389/neuro.11.011.2008

Dean, C., and Dresbach, T. (2006). Neuroligins and neurexins: linking cell adhesion, synapse formation and cognitive function. *Trends Neurosci*. 29, 21–29. doi: 10.1016/j.tins.2005.11.003

Di Maio, V. (2008). Regulation of information passing by synaptic transmission: a short review. *Brain Res*. 1225, 26–38. doi: 10.1016/j.brainres.2008.06.016

Durand, K., Gallay, M., Seigneuric, A., Robichon, F., and Baudouin, J. Y. (2007). The development of facial emotion recognition: the role of configural information. *J. Exp. Child Psychol*. 97, 14–27. doi: 10.1016/j.jecp.2006.12.001

Faghihi, F., and Moustafa, A. A. (2015). A computational model of pattern separation efficiency in the dentate gyrus with implications in schizophrenia. *Front. Syst. Neurosci*. 9:42. doi: 10.3389/fnsys.2015.00042

Fidjeland, K., Roesch, E. B., Shanahan, M. P., and Luk, W. (2009). "Nemo: a platform for neural modelling of spiking neurons using GPUs," in *2009 20th IEEE International Conference on Application-specific Systems, Architectures and Processors*, 137–144. doi: 10.1109/ASAP.2009.24

Furber, S. B., Galluppi, F., Temple, S., and Plana, L. A. (2014). The spinnaker project. *Proc. IEEE* 102, 652–665. doi: 10.1109/JPROC.2014.2304638

Goda, Y., and Südhof, T. C. (1997). Calcium regulation of neurotransmitter release: reliably unreliable? *Curr. Opin. Cell Biol.* 9, 513–518. doi: 10.1016/s0955-0674(97)80027-0

Goodman, D. F., and Brette, R. (2009). The brian simulator. *Front. Neurosci*. 3, 192–197. doi: 10.3389/neuro.01.026.2009

Gunter, K. K., and Gunter, T. E. (1994). Transport of calcium by mitochondria. *J. Bioenerg. Biomembr*. 26, 471–485. doi: 10.1007/BF00762732

Gunter, T. E., Yule, D. I., Gunter, K. K., Eliseev, R. A., and Salter, J. D. (2004). Calcium and mitochondria. *FEBS Lett*. 567, 96–102. doi: 10.1016/j.febslet.2004.03.071

Hayati, M., Nouri, M., Haghiri, S., and Abbott, D. (2016). A digital realization of astrocyte and neural glial interactions. *IEEE Trans. Biomed. Circuits Syst*. 10, 518–529. doi: 10.1109/TBCAS.2015.2450837

Hebb, D. O. (1949). *Organization of Behavior: A Neuropsychological Theory*. New York, NY: Wiley.

Hines, M. L., and Carnevale, N. T. (1997). The NEURON simulation environment. *Neural. Comput*. 9, 1179–1209. doi: 10.1162/neco.1997.9.6.1179

Hung, A. Y., Futai, K., Sala, C., Valtschanoff, J. G., Ryu, J., Woodworth, M. A., et al. (2008). Smaller dendritic spines, weaker synaptic transmission, but enhanced spatial learning in mice lacking Shank1. *J. Neurosci*. 28, 1697–1708. doi: 10.1523/JNEUROSCI.3032-07.2008

Jaiswal, M. K., and So, H. K. (2019). Pacogen: a hardware posit arithmetic core generator. *IEEE Access* 7, 74586–74601. doi: 10.1109/ACCESS.2019.2920936

Jiang, Y. H., and Ehlers, M. D. (2013). Modeling autism by SHANK gene mutations in mice. *Neuron* 78, 8–27. doi: 10.1016/j.neuron.2013.03.016

Karagas, N. E., and Venkatachalam, K. (2019). Roles for the endoplasmic reticulum in regulation of neuronal calcium homeostasis. *Cells* 8:1232. doi: 10.3390/cells8101232

Kelly, E., Schaeffer, S. M., Dhamne, S. C., Lipton, J. O., Lindemann, L., Honer, M., et al. (2018). mGluR5 modulation of behavioral and epileptic phenotypes in a mouse model of tuberous sclerosis complex. *Neuropsychopharmacology* 43, 1457–1465. doi: 10.1038/npp.2017.295

Klyachko, V. A., and Stevens, C. F. (2006). Excitatory and feed-forward inhibitory hippocampal synapses work synergistically as an adaptive filter of natural spike trains. *PLoS Biol*. 4:e207. doi: 10.1371/journal.pbio.0040207

Lameu, E. L., Borges, F. S., Iarosz, K. C., Protachevicz, P. R., Antonopoulos, C. G., Macau, E. E., et al. (2021). Short-term and spike-timing-dependent plasticity facilitate the formation of modular neural networks. *Commun. Nonlin. Sci. Numer. Simul*. 96:105689. doi: 10.1016/j.cnsns.2020.105689

Lee, K.-S., Huh, S., Lee, S., Wu, Z., Kim, A.-K., Kang, H.-Y., et al. (2018). Altered ER?mitochondria contact impacts mitochondria calcium homeostasis and contributes to neurodegeneration *in vivo* in disease models. *Proc. Natl. Acad. Sci. U.S.A*. 115, E8844?-E8853. doi: 10.1073/pnas.1721136115

Lee, K. J., Park, I. S., Kim, H., Greenough, W. T., Pak, D. T., and Rhyu, I. J. (2013). Motor skill training induces coordinated strengthening and weakening between neighboring synapses. *J. Neurosci*. 33, 9794–9799. doi: 10.1523/JNEUROSCI.0848-12.2013

Lewerenz, J., and Maher, P. (2015). Chronic glutamate toxicity in neurodegenerative diseases-what is the evidence? *Front. Neurosci*. 9:469. doi: 10.3389/fnins.2015.00469

Li, C. T., Yang, K. C., and Lin, W. C. (2018). Glutamatergic dysfunction and glutamatergic compounds for major psychiatric disorders: evidence from clinical neuroimaging studies. *Front. Psychiatry* 9:767. doi: 10.3389/fpsyt.2018.00767

Matthews, E. A., and Dietrich, D. (2015). Buffer mobility and the regulation of neuronal calcium domains. *Front. Cell. Neurosci*. 9:48. doi: 10.3389/fncel.2015.00048

Minneci, F., Kanichay, R. T., and Silver, R. A. (2012). Estimation of the time course of neurotransmitter release at central synapses from the first latency of postsynaptic currents. *J. Neurosci. Methods* 205, 49–64. doi: 10.1016/j.jneumeth.2011.12.015

Mongillo, G., Barak, O., and Tsodyks, M. (2008). Synaptic theory of working memory. *Science* 319, 1543–1546. doi: 10.1126/science.1150769

Muhle, R., Trentacoste, S. V., and Rapin, I. (2004). The genetics of autism. *Pediatrics* 113, e472–e486. doi: 10.1542/peds.113.5.e472

Murphy, G. J., Glickfeld, L. L., Balsen, Z., and Isaacson, J. S. (2004). Sensory neuron signaling to the brain: properties of transmitter release from olfactory nerve terminals. *J. Neurosci*. 24, 3023–3030. doi: 10.1523/JNEUROSCI.5745-03.2004

Park, H., Rhee, J., Park, K., Han, J. S., Malinow, R., and Chung, C. (2017). Exposure to stressors facilitates long-term synaptic potentiation in the lateral habenula. *J. Neurosci*. 37, 6021–6030. doi: 10.1523/JNEUROSCI.2281-16.2017

Pfeil, T., Grübl, A., Jeltsch, S., Müller, E., Müller, P., Petrovici, M. A., et al. (2013). Six networks on a universal neuromorphic computing substrate. *Front. Neurosci*. 7:11. doi: 10.3389/fnins.2013.00011

Piomelli, D. (2003). The molecular logic of endocannabinoid signalling. *Nat. Rev. Neurosci*. 4, 873–884. doi: 10.1038/nrn1247

Postnov, D. E., Ryazanova, L. S., and Sosnovtseva, O. V. (2007). Functional modeling of neural-glial interaction. *Biosystems* 89, 84–91. doi: 10.1016/j.biosystems.2006.04.012

Regehr, W. G. (2012). Short-term presynaptic plasticity. *Cold Spring Harb. Perspect. Biol*. 4:a005702. doi: 10.1101/cshperspect.a005702

Regehr, W. G., Carey, M. R., and Best, A. R. (2009). Activity-dependent regulation of synapses by retrograde messengers. *Neuron* 63, 154–170. doi: 10.1016/j.neuron.2009.06.021

Rizzuto, R., Pinton, P., Ferrari, D., Chami, M., Szabadkai, G., Magalhães, P. J., et al. (2003). Calcium and apoptosis: facts and hypotheses. *Oncogene* 22, 8619–8627. doi: 10.1038/sj.onc.1207105

Rojas, D. C. (2014). The role of glutamate and its receptors in autism and the use of glutamate receptor antagonists in treatment. *J. Neural Transm*. 121, 891–905. doi: 10.1007/s00702-014-1216-0

Rose, T., Schoenenberger, P., Jezek, K., and Oertner T. G. (2013). Developmental refinement of vesicle cycling at Schaffer collateral synapses. *Neuron*. 77, 1109–1121. doi: 10.1016/j.neuron.2013.01.021

Sala, C., Vicidomini, C., Bigi, I., Mossa, A., and Verpelli, C. (2015). Shank synaptic scaffold proteins: keys to understanding the pathogenesis of autism and other synaptic disorders. *J. Neurochem*. 135, 849–858. doi: 10.1111/jnc.13232

Sato, D., Lionel, A. C., Leblond, C. S., Prasad, A., Pinto, D., Walker, S., et al. (2012). SHANK1 deletions in males with autism spectrum disorder. *Am. J. Hum. Genet*. 90, 879–887. doi: 10.1016/j.ajhg.2012.03.017

Silverman, J. L., Smith, D. G., Rizzo, S. J., Karras, M. N., Turner, S. M., Tolu, S. S., et al. (2012). Negative allosteric modulation of the mGluR5 receptor reduces repetitive behaviors and rescues social deficits in mouse models of autism. *Sci. Transl. Med*. 4:131ra51. doi: 10.1126/scitranslmed.3003501

Südhof, T. C. (2008). Neuroligins and neurexins link synaptic function to cognitive disease. *Nature* 455, 903–911. doi: 10.1038/nature07456

Südhof, T. C., and Malenka, R. C. (2008). Understanding synapses: past, present, and future. *Neuron* 60, 469–476. doi: 10.1016/j.neuron.2008.10.011

Tetzlaff, T., Helias, M., Einevoll, G. T., and Diesmann, M. (2012). Decorrelation of neural-network activity by inhibitory feedback. *PLoS Comput. Biol*. 8:e1002596. doi: 10.1371/journal.pcbi.1002596

Tian, D., Stoppel, L. J., Heynen, A. J., Lindemann, L., Jaeschke, G., Mills, A. A., et al. (2015). Contribution of mGluR5 to pathophysiology in a mouse model

of human chromosome 16p11.2 microdeletion. *Nat. Neurosci.* 18, 182–184. doi: 10.1038/nn.3911

Tsodyks, M. V., and Markram, H. (1997). The neural code between neocortical pyramidal neurons depends on neurotransmitter release probability. *Proc. Natl. Acad. Sci. U.S.A.* 94, 719–723. doi: 10.1073/pnas.94.2.719

Voglis, G., and Tavernarakis, N. (2006). The role of synaptic ion channels in synaptic plasticity. *EMBO Rep.* 7, 1104–1110. doi: 10.1038/sj.embor.7400830

Volk, L., Chiu, S. L., Sharma, K., and Huganir, R. L. (2015). Glutamate synapses in human cognitive disorders. *Annu. Rev. Neurosci.* 38, 127–149. doi: 10.1146/annurev-neuro-071714-033821

Wang, X., Zorio, D. A. R., Schecterson, L., Lu, Y., and Wang, Y. (2018). Postsynaptic FMRP regulates synaptogenesis *in vivo* in the developing cochlear nucleus. *J. Neurosci.* 38, 6445–6460. doi: 10.1523/JNEUROSCI.0665-18.2018

Wegener, S., Buschler, A., Stempel, A. V., Kang, S. J., Lim, C. S., Kaang, B. K., et al. (2018). Defective synapse maturation and enhanced synaptic plasticity in Shank2 ex7-/- Mice. *eNeuro* 5:ENEURO.0398-17.2018. doi: 10.1523/ENEURO.0398-17.2018

Wu, S., Gan, G., Zhang, Z., Sun, J., Wang, Q., Gao, Z., et al. (2017). A presynaptic function of shank protein in drosophila. *J. Neurosci.* 37, 11592–11604. doi: 10.1523/JNEUROSCI.0893-17.2017

Zhang, L. I., Tao, H. W., Holt, C. E., Harris, W. A., and Poo, M. (1998). A critical window for cooperation and competition among developing retinotectal synapses. *Nature* 395, 37–44. doi: 10.1038/25665

Disclaimer: The views and opinions expressed in this paper are those of the authors and do not necessarily reflect the official policy or position of either Samsung Electronics or Intel Corporation.

Conflict of Interest: SM is employed by the company Samsung Electronic. AR is employed by the company Intel Corporation.

All authors have a patent pending for software/hardware related to this study.

Copyright © 2021 Chatterjee, Paluh, Chowdhury, Mondal, Raha and Mukherjee. This is an open-access article distributed under the terms of the Creative Commons Attribution License (CC BY). The use, distribution or reproduction in other forums is permitted, provided the original author(s) and the copyright owner(s) are credited and that the original publication in this journal is cited, in accordance with accepted academic practice. No use, distribution or reproduction is permitted which does not comply with these terms.

frontiers in Cellular Neuroscience

REVIEW
published: 30 September 2021
doi: 10.3389/fncel.2021.699731

The Calcium Channel α2δ1 Subunit: Interactional Targets in Primary Sensory Neurons and Role in Neuropathic Pain

Wenqiang Cui[1†], Hongyun Wu[1†], Xiaowen Yu[1], Ting Song[1], Xiangqing Xu[1] and Fei Xu[2*]*

[1] *Department of Neurology, Affiliated Hospital of Shandong University of Traditional Chinese Medicine, Jinan, China,*
[2] *Department of Geriatric Medicine, Affiliated Hospital of Shandong University of Traditional Chinese Medicine, Jinan, China*

Neuropathic pain is mainly triggered after nerve injury and associated with plasticity of the nociceptive pathway in primary sensory neurons. Currently, the treatment remains a challenge. In order to identify specific therapeutic targets, it is necessary to clarify the underlying mechanisms of neuropathic pain. It is well established that primary sensory neuron sensitization (peripheral sensitization) is one of the main components of neuropathic pain. Calcium channels act as key mediators in peripheral sensitization. As the target of gabapentin, the calcium channel subunit α2δ1 (Cavα2δ1) is a potential entry point in neuropathic pain research. Numerous studies have demonstrated that the upstream and downstream targets of Cavα2δ1 of the peripheral primary neurons, including thrombospondins, *N*-methyl-D-aspartate receptors, transient receptor potential ankyrin 1 (TRPA1), transient receptor potential vanilloid family 1 (TRPV1), and protein kinase C (PKC), are involved in neuropathic pain. Thus, we reviewed and discussed the role of Cavα2δ1 and the associated signaling axis in neuropathic pain conditions.

Keywords: neuropathic pain, primary sensory neuron, Cavα2δ1, molecular target, peripheral sensitization

OPEN ACCESS

Edited by:
Daniela Tropea,
Trinity College Dublin, Ireland

Reviewed by:
Zheyu Chen,
Shandong University, China
Hsien-Yu Peng,
Mackay Medical College, Taiwan

***Correspondence:**
Xiangqing Xu
happyxiangqing@163.com
Fei Xu
Fei_Xu1012@126.com

[†] These authors have contributed equally to this work

Specialty section:
This article was submitted to Cellular Neuropathology, a section of the journal Frontiers in Cellular Neuroscience

Received: *24 April 2021*
Accepted: *10 September 2021*
Published: *30 September 2021*

Citation:
Cui W, Wu H, Yu X, Song T, Xu X and Xu F (2021) The Calcium Channel α2δ1 Subunit: Interactional Targets in Primary Sensory Neurons and Role in Neuropathic Pain. Front. Cell. Neurosci. 15:699731. doi: 10.3389/fncel.2021.699731

INTRODUCTION

Neuropathic pain is a chronic pain triggered by peripheral nerve injury, postherpetic neuralgia, diabetic neuropathy, and chemotherapeutic agents, such as cisplatin (Colleoni and Sacerdote, 2010). Its prominent symptoms are spontaneous pain, hyperalgesia (increased pain sensitivity from a painful stimulus), and allodynia (pain in response to a non-painful stimulus) (Kim et al., 2014). These symptoms lead to prolonged discomfort in patients. It is calculated that 9.8% of the population in the United States experiences neuropathic pain (Yawn et al., 2009). Because the molecular mechanisms of neuropathic pain have not been fully elucidated, the management of neuropathic pain remains challenging.

Currently, the commonly used drugs for neuropathic pain include antiepileptics, antidepressants, anticonvulsants, opioid analgesics, and *N*-methyl-D-aspartate receptor (NMDAR) antagonists (Amato et al., 2019). Gabapentin (GBP), a second-generation antiepileptic drug, is one of the first-choice drugs for the treatment of neuropathic pain (Moore and Gaines, 2019). It has good curative effect on diabetic neuralgia, postherpetic neuralgia, trigeminal neuralgia, and sciatica neuralgia. However, the adverse effects of gabapentin are significant, and its precise mechanism of action is uncertain. Many lines of evidence have

demonstrated that voltage-gated Ca^{2+} channels were directly blocked by GBP binding to its α2δ1 subunit (Grice and Mertens, 2008; Skubatz, 2019). That leaded to the reduction of presynaptic Ca^{2+} influx and the decreased synaptic release of glutamate, which is the major excitatory neurotransmitter of the brain (Grice and Mertens, 2008; Skubatz, 2019). Thus, the calcium channel α2δ1 subunit is a potential target for the treatment of neuropathic pain. To develop novel effective anti-neuropathic pain agents with fewer side effects, it is promising to understand the α2δ1-related mechanisms and reveal new mechanism-specific treatment targets.

The calcium channel α2δ subunits were first described as accessory subunits of voltage-gated calcium channels (VGCCs) (Gurnett and Campbell, 1996). Four α2δ subunits have been cloned: α2δ1, α2δ2, α2δ3, and α2δ4. The α2δ1 subunit is the receptor of GBP and certain thrombospondins (TSPs). It is expressed in neurons and their axonal terminals and dendrites throughout the central and peripheral nervous system (CNS and PNS) (Eroglu et al., 2009). The TSPs secreted by astrocytes exert their synaptogenic effects by binding to their neuronal receptor α2δ1 (Wang et al., 2020). TSP–α2δ1 interactions participate in synaptic development and neuropathic pain (Risher et al., 2018). Due to its very short cytoplasmic tail, α2δ1 is not able to active intracellular signaling by itself, while its extracellular domain almost could functionally mimic the full-length α2δ1 during synapse formation (Eroglu et al., 2009). Thus, Cavα2δ1 is linked to intracellular signaling via other membrane proteins and is involved in the occurrence and development of neuropathic pain by interacting with several molecules.

This review will cover several novel findings concerning the calcium channel α2δ1 subunit and α2δ1-related proteins of the PNS, particularly their roles in neuropathic pain. This review will aid in the better understanding of the peripheral mechanisms of neuropathic pain and develop novel effective anti-neuropathic pain agents with fewer side effects.

THE α2δ1 SUBUNIT AND ITS ROLE IN NEUROPATHIC PAIN

In the human genome, four α2δ proteins (α2δ1–α2δ4) are encoded by four genes (*CACNA2D1–CACNA2D4*), respectively (Dolphin, 2012). Four different α2δ isoforms have selective effects on the level of functional expression and the voltage dependence of different α1 subunits (Davies et al., 2007). Among the genes encoded for α2δ, the *CACNA2D1* may be appropriate for drug development to alleviate neuropathic pain. The upregulated expression of *CACNA2D1* contributed to chronically maintain neuropathic pain by enhancing VGCCs activation, neuronal excitability, and neurotransmission (Yusaf et al., 2001; Gribkoff, 2006; Li et al., 2006, 2014). Moreover, *CACNA2D1* could modulate CGRP and AC-PKA/protein kinase C (PKC)/MAPK signaling pathways in the dorsal root ganglion (DRG) in chronic pain process (Sun et al., 2020). Fundamentally, *CACNA2D1* gene performs these functions by the genetic translation product—the α2δ1 protein. In addition, the expression of α2δ1 is also regulated by epigenetic factors. The histone deacetylase inhibitors—JNJ-26481585—significantly upregulated the expression of α2δ1 subunit in spinal cord and induced mechanical hypersensitivity in mice (Capasso et al., 2015). MicroRNA-183 cluster (miR-183/96/182) controlled more than 80% of neuropathic pain-regulated genes and scaled mechanical pain sensitivity in mice by regulating the expression of α2δ1 and α2δ2 (Peng et al., 2017). Meanwhile, human *CACNA2D1* and *CACNA2D2* genes of DRG are predictive targets of miR-183 cluster. Bioinformatic analysis revealed that miR-107 had a potential binding site for the α2δ1 encoding gene *CACNA2D1*. In laryngeal cancer cells, miR-107 decreased the expression levels of *CACNA2D1* (Huang C. et al., 2020). Thus, epigenetic mechanisms, such as histone posttranslational modification and microRNA, may play an important role in mediating the expression of α2δ1 and chronic neuropathic pain, as they are instructive for transcription, and potentially long lasting.

The α2δ1 subunit is strongly expressed in the cardiac and smooth muscles, and is likely to be the main α2δ subunit associated with calcium channels in these tissues (Bikbaev et al., 2020). In addition, the α2δ1, a structural subunit of the VGCCs, is strongly expressed in the nervous system. The core complex of neuronal VGCCs consists of an α1 subunit, which contains the ion-conducting pore, and the auxiliary β and α2δ subunits. The α1 subunit is a transmembrane protein linking α2δ and β. It consists of four transmembrane regions (I–IV) that have the same transmembrane structure. Each transmembrane structure has six transmembrane helices (S1–S6). The vast majority of the α2δ segment is extracellular and most likely linked to the plasma membrane via glycosyl-phosphatidylinositol (GPI) anchors. The β subunit is the intracellular component and binds the intracellular I-II linker of α1 subunits at the so-called α-interaction domain (**Figure 1**; De Waard et al., 1995; Davies et al., 2010; Catterall, 2011; Geisler et al., 2015).

In the CNS, α2δ1 is present in neurons, axonal terminals (Marais et al., 2001), and dendrites (Eroglu et al., 2009). α2δ1 is correlated with excitatory rather than inhibitory neurons (Bikbaev et al., 2020). It is mainly present in presynaptic terminals and, to a much lower extent, in the cell bodies of neurons in many brain regions under physiological conditions (Alles and Smith, 2018; Bikbaev et al., 2020). In the PNS, α2δ1 is strongly expressed in all neuronal cell types of DRG and trigeminal ganglion (TG), such as $IB4^+$, $CGRP^+$, and $NF200^+$ neurons (Tachiya et al., 2018; Cui et al., 2020). It was found that α2δ1 was expressed in most neurons of different sizes after nerve injuries, predominantly in small (less 20 μm) and medium (20–50 μm) neurons in animal models of sciatica neuralgia and trigeminal neuralgia (Tachiya et al., 2018; Cui et al., 2020). In addition, studies using rat models of chronic constriction injury to the infraorbital nerve (CCI-ION) have shown that the number of α2δ1-immunoreactive neurons over 25 μm in diameter was obviously increased (Li et al., 2014). The α2δ1 subunit was increased in the neurons of the DRG and TG and was mainly associated with terminal fields, rather than cell bodies, after nerve injury (Bauer et al., 2010). Research has shown that α2δ1 was synthesized in the neuron cell bodies

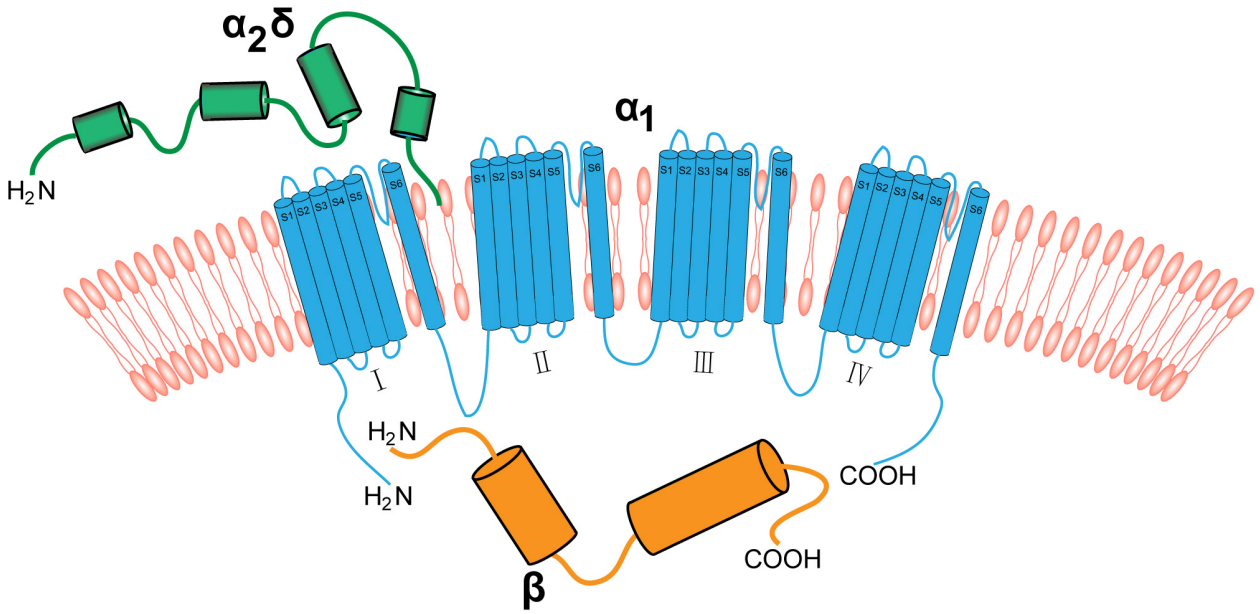

FIGURE 1 | The neuronal voltage-gated calcium channel complex. Voltage-gated calcium channels include the transmembrane pore-forming α1 subunit (red), extracellular α2δ (green), and cytoplasmic β (blue) subunits. The α1 subunit is a transmembrane protein linking the α2δ subunit and β subunit. The α2δ subunit is mainly extracellular and binds to the membrane via GPI anchors. The β subunit binds to α1 subunit via the intracellular I–II linker.

and then trafficked to the plasma membrane of the DRG presynaptic terminals that terminate in the spinal cord dorsal horn (Bauer et al., 2009). Meanwhile, the ipsilateral myelinated and non-myelinated DRG axons were increased after partial sciatic nerve ligation and the α2δ1 accumulated at the ligation site (Bennett et al., 2003). In a rat model of CCI-ION, the α2δ1 and $Vglut_2$-positive ($Vglut_2^+$) puncta (excitatory presynaptic glutamatergic terminal) were increased in the superficial dorsal horn of the cervical spinal cord, and all increased terminals were $\alpha2\delta1^+$ (Li et al., 2014). These studies indicated that α2δ1, which was trafficked and accumulated in the superficial dorsal horn of the spinal cord, regulated the excitatory synaptogenesis. However, the mechanisms of trafficking and accumulation of α2δ1 in neuropathic pain remain unclear. If the key target is found to block α2δ1's transmission and accumulation at the terminal and prevent the generation of abnormal excitatory synapses, the occurrence and development of neuropathic pain will be attenuated.

Several studies have demonstrated that the expression level of α2δ1 was elevated in the TG after partial transection of the infraorbital nerve (pT-ION) (Cui et al., 2020) and CCI-ION (Li et al., 2014). The mechanical and cold hyperalgesia induced by nerve injury could be mimicked by injecting the Cavα2δ1 overexpression adeno-associated virus (AAV) and be reversed by injecting the AAV of Cavα2δ1 downregulation in TG neurons (Cui et al., 2020). These results indicated that the Cavα2δ1 of primary afferent neurons play a vital role in neuropathic pain and that is mainly related to its regulation of Ca^{2+} inflow.

However, the regulation of Ca^{2+} influx of α2δ1 is different from that of the well-studied TRP channels and NMDA receptors in neuropathic pain. TRPs and NMDA receptors can directly mediate the Ca^{2+} influx when they are activated, but α2δ1 indirectly. α2δ1, an accessory subunit of VGCCs, is fully exposed to the extracellular environment and anchored outside the plasma membrane by a phosphatidylinositol. For one thing, nociceptive stimuli induced the upregulation of the expression of α2δ subunit. That regulated the transport, localization, and biophysical properties of α1 subunit and induced the fast assembly of VGCCs (Gurnett et al., 1997; Brodbeck et al., 2002). These processes triggered the influx of Ca^{2+} and the increased excitability of neurons. For another, α2δ1 can bind to other calcium channels through the binding site and then induce the Ca^{2+} inflow. Thus, the study of α2δ1-related targets is important to understand the role of α2δ1 in neuropathic pain.

THE α2δ1 SUBUNIT IS THE NEURONAL THROMBOSPONDINS RECEPTOR RESPONSIBLE FOR SYNAPTOGENESIS

Thrombospondins are expressed in various cell types and play various roles in cell signaling; these consist of extracellular, oligomeric, multi-domain, and calcium-binding glycoproteins (Adams and Lawler, 2011). They are present in various tissues and consist of five members, TSP 1–5 (Sipes et al., 2018). For example, platelets, endothelial cells, skeletal muscles, fibroblasts, neurons, and astrocytes each express one or more TSP isoforms (Christopherson et al., 2005; Sipes et al., 2018). In mammals, TSPs have many functions, such as wound healing, angiogenesis, and synaptogenesis (Adams and Lawler, 2011; Ponticelli and Anders, 2017).

Studies have demonstrated that the expression levels of TSPs were thoroughly altered in pathophysiological conditions (Chen et al., 2000; Adams and Lawler, 2011). Particularly, the expression of TSP4 was increased in the DRG after peripheral nerve injury (Pan et al., 2015; Risher et al., 2018). Thus, TSP4 of PNS is the protein of focus in neuropathic pain research. Risher et al. showed that elevated targeting of α2δ1 by TSP4 contributed to hypersensitivity of the peripheral sensory systems by decreasing the activation of high-voltage calcium currents while increasing low voltage-activated calcium currents in DRG neurons (Risher et al., 2018). TSP4 promotes the assembly of excitatory glutamatergic synapses by binding to α2δ1 in the CNS (Crosby et al., 2015; El-Awaad et al., 2019). GBP antagonizes the binding of TSPs to α2δ1 and powerfully inhibits excitatory synapse formation *in vitro* and *in vivo* (Eroglu et al., 2009; Lana et al., 2016). Once α2δ1 is activated by TSP, the inter- and intracellular signaling events subsequently occur, which trigger the gathering of synaptic adhesion and scaffolding molecules at nascent synaptic sites. Overexpression of α2δ1 in the absence of TSPs enhances calcium channel surface expression, but does not lead to any changes in the number of synapses (Eroglu et al., 2009). Overexpression of TSPs increases synapse formation but is blocked in α2δ1 knockout mice (Eroglu et al., 2009). There is an interaction between the VWF-A domain of α2δ1 and the epidermal growth factor of all TSPs (**Figure 2**; Eroglu et al., 2009). Drugs directed toward the VWF-A domain of α2δ1 exert the synaptogenic function of TSPs (Eroglu et al., 2009). This indicates that the binding of TSPs and α2δ1 is the key to synapse formation. Kim et al. (2012) showed that nerve ligation induces upregulation of TSP4 in spinal astrocytes and the enhancement of excitatory synaptic transmission in the dorsal horn, whereas spinal TSP1 and TSP2 exhibit no changes following injury. According to this study, we can assume that increased α2δ1 subunits in the peripheral ganglion transfer from cell bodies to the central terminal and accumulate at the central terminal spinal region when under the influence of elevated TSP4 levels after nerve injury. This progress would promote synaptogenesis between neurons themselves and between neurons and glial cells. Although it has been reported that α2δ1 interacts with TSP to trigger synaptogenesis (Eroglu et al., 2009), a study demonstrated that α2δ1 and thrombospondin had a weak interaction at the membrane surface (Lana et al., 2016). Thus, more work remains to be carried out to improve our knowledge of the role of TSP4-α2δ1 signaling in synaptogenesis in neuropathic pain, particularly in the PNS.

THE α2δ1-*N*-METHYL-D-ASPARTATE RECEPTOR COMPLEX IS ESSENTIAL FOR THE ACTIVATION OF PRESYNAPTIC *N*-METHYL-D-ASPARTATE RECEPTOR IN NEUROPATHIC PAIN

Although NMDARs are conventionally expressed in postsynaptic neurons (Zhou et al., 2011), they are also expressed presynaptically, particularly in primary sensory neurons of the TG and DRG and in their central terminals in the spinal dorsal horn (SDH) (Li et al., 2016; Xie et al., 2016). Pre- and postsynaptic NMDARs play an indispensable role in many physiological and pathological processes, such as the release of neurotransmitters, synaptic plasticity, and neuropathic pain (Li et al., 2016; Xie et al., 2016; Deng et al., 2019; Huang Y. et al., 2020). The reason for this is that NMDARs are essential for the coordinated activity of pre- and postsynaptic neurons (Mayer et al., 1984). In the physiological state, the NMDARs of the TG and DRG are functionally inactive and do not facilitate the release of neurotransmitters (Yan et al., 2013; Deng et al., 2019). However, NMDARs of the central terminals of primary sensory neurons become tonically active in chronic neuropathic pain conditions (Yan et al., 2013). Activation of presynaptic NMDARs induces calcium influx and vesicle exocytosis, causing neuronal depolarization and neurotransmitter release into the SDH (in particular, glutamate) (Yan et al., 2013; Vandresen-Filho et al., 2015). Increased glutamate release from primary afferent terminals to SDH neurons is essential for the synaptic plasticity in neuropathic pain induced by nerve injury and chemotherapy (Yan et al., 2013). Meanwhile, the activation of NMDARs induces activity-dependent DNA double-strand breaks and the following transcription of several neuronal immediate-early genes (Madabhushi et al., 2015; Hagenston et al., 2020). That is important for synaptic plasticity and sensitization of neurons in chronically maintained neuropathic pain.

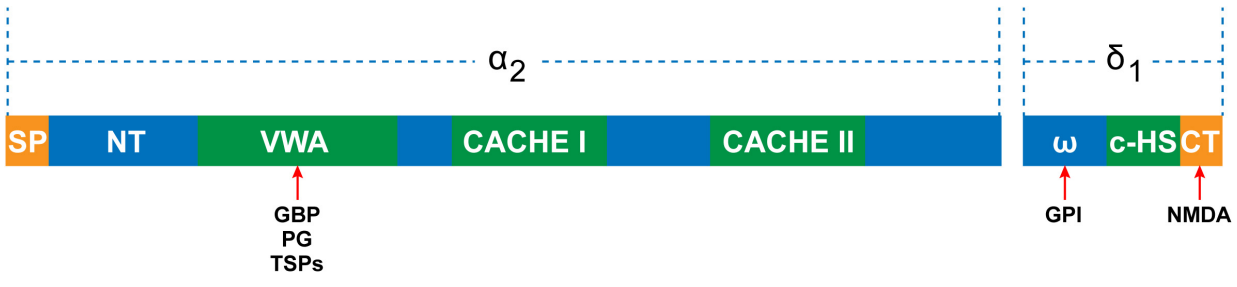

FIGURE 2 | The domain structure of the α2δ1 subunit. The α2 peptide contains N-terminal domain, VWA domain, and two extracellular domains (CACHE I and II). The VWA domain is the potential binding site for gabapentin (GBP), pregabalin (PG), and thrombospondins (TSPs). The δ peptide contains ω amino acids, to which the glycosyl-phosphatidylinositol (GPI) anchor can attach, C-terminal hydrophobic sequence (c-HS), and C-terminal, which is the NMDA binding site.

The activity of NMDARs is regulated mainly by their own phosphorylation status and/or the phosphorylation status of their interacting targets. The α2δ1 subunit directly interacts with NMDARs and forms a heteromeric complex through its C-terminal domain (**Figure 2**). This induces the activation of presynaptic NMDARs by facilitating synaptic targeting and trafficking of α2δ1–NMDAR complexes at primary afferent terminals in neuropathic pain caused by nerve injury and chemotherapy (Chen et al., 2018, 2019; Deng et al., 2019). The α2δ1–NMDAR complex in the SDH was significantly increased in rats with spinal nerve ligation (SNL) (Chen et al., 2018). The α2δ1 subunit knockout and intrathecal injection of α2δ1 C termini-interfering peptides or pregabalin reversed the synaptic NMDAR hyperactivity associated with neuropathic pain by interrupting the α2δ1–NMDAR interaction and complex formation (Deng et al., 2019). Thus, increased synaptic expression of the α2δ1–NMDAR complex is essential for the enhancement of the activity of synaptic NMDARs in neuropathic pain.

Chemotherapeutic drugs, such as paclitaxel, are known to potentiate nociceptive input by inducing the tonic activation of presynaptic NMDARs, but not postsynaptic NMDARs in the SDH (Xie et al., 2016; Chen et al., 2019; Deng et al., 2019). Given that α2δ1 is involved in surface trafficking as a highly glycosylated protein, the chemotherapy or nerve injury induced excess of α2δ1 protein at primary afferent terminals may facilitate its interaction with NMDARs and promote synaptic expression of α2δ1–NMDAR complexes (Chen et al., 2018; Deng et al., 2019). Chemotherapy induces the assembly of α2δ1 and causes increases in α2δ1–NMDAR complexes at central terminals, causing persistent increases in glutamatergic nociceptive input to postsynaptic SDH neurons, thereby incurring chronic neuropathic pain (Chen et al., 2019). α2δ1 knockout and the inhibition of α2δ1 trafficking by pregabalin or by disrupting α2δ1–NMDAR interactions with α2δ1 C-termini-interfering peptides completely normalized the paclitaxel-induced NMDAR-dependent glutamate release from primary afferent terminals to postsynaptic SDH neurons and significantly attenuated neuropathic pain (Chen et al., 2019). Overexpression of α2δ1 in neurons results in an increased frequency (but not amplitude) of mEPSCs that were induced by NMDA receptors upon depolarization. In addition, selective blocking of the GluN2A subunits of NMDARs decreases the frequency of mEPSCs evoked from SDH neurons in paclitaxel-induced neuropathic pain rats (Xie et al., 2016). Paclitaxel failed to increase the frequency of mEPSCs by dorsal root stimulation in α2δ1 knockout mice (Chen et al., 2019). These results indicated that a transition from being α2δ1-free to α2δ1-bound NMDAR is essential for the activation of presynaptic NMDARs in the SDH and the increase in glutamate release from the central terminals of presynaptic neurons. Targeting α2δ1-bound NMDARs (not the physiological α2δ1–free NMDARs) may be a new promising strategy for treating neuropathic pain. Unlike VGCCs, the NMDARs is also permeable to Na^+ and K^+ except for Ca^{2+} (Zhou et al., 2011). Thus, whether the α2δ1–NMDAR interactions can regulate NMDA-dependent cation inflow is also the focus of neuropathic pain research.

TRANSIENT RECEPTOR POTENTIAL VANILLOID FAMILY 1 AND TRANSIENT RECEPTOR POTENTIAL ANKYRIN 1 ARE INTERACTIONAL TARGETS OF THE α2δ1 SUBUNIT IN PRIMARY SENSORY NEURONS

The transient receptor potential (TRP) channel family was first discovered in Drosophila and proposed as a Ca^{2+} permeable channel/transporter (Bloomquist et al., 1988). This discovery led investigators to focus on the study of Ca^{2+} signaling in TRP channels (Zhu et al., 1996; Minke and Parnas, 2006). The high Ca^{2+} selectivity of TRP channels is due to their crucial amino acid residues (Hardie and Minke, 1992). Thus, TRP channels play an important role in the understanding of sensory nerve function in pain conditions (Silverman et al., 2020; Aleixandre-Carrera et al., 2021). TRP channels contribute to many processes, such as the activation of neurons, the release of neurotransmitters from presynaptic central terminals to postsynaptic SDH neurons, and the release of inflammatory mediators (Hung and Tan, 2018; Silverman et al., 2020). Among all TRP channels, transient receptor potential ankyrin 1 (TRPA1) and transient receptor potential vanilloid family 1 (TRPV1) are generally considered to be expressed in nociception-specific neurons (Patil et al., 2020). Thus, they are the two most frequently reported members of pain research.

TRPA1, a cold-sensing channel, is expressed mostly in small-diameter DRG neurons and activated by temperatures lower than 17°C (Peier et al., 2002; Kobayashi et al., 2005; Chukyo et al., 2018). It is a non-selective channel permeable to Ca^{2+}, Na^+, and K^+, with a much higher permeability to Ca^{2+} compared to other TRPs (Souza et al., 2020). In human, the methylation of a CpG dinucleotide in the promoter of TRPA1 was negatively correlated with the thermal and mechanical pain sensitivity (Gombert et al., 2017). Some studies reported that pharmacological antagonizing and channel silencing of TRPA1 in the peripheral nerves significantly reduced mechanical allodynia as well as chemical and thermal hyperalgesia in different pain models (Honda et al., 2017; Marone et al., 2018). One study indicated that the increased expression of TRPA1 in the cell bodies of TG neurons contributed to migraines induced by glyceryl trinitrate (Marone et al., 2018). Moreover, the TRPA1 receptor antagonist HC-030031 significantly attenuated mechanical allodynia and cold hyperalgesia in a mouse migraine model (Marone et al., 2018). In our research, the expression of TRPA1 was found to be increased in the TG after trigeminal nerve injury and was inhibited by Cavα2δ1 downregulation in the TG (Cui et al., 2020). Importantly, adenovirus-mediated Cavα2δ1 overexpression in TG neurons induced an increase in the expression of TRPA1 in the TG (Cui et al., 2020). These results indicate that TRPA1 in the peripheral nerves contributes to cold, thermal, and mechanical hyperalgesia in neuropathic pain models and that Cavα2δ1 could potentially be an upstream target of TRPA1. A study suggested that the expression of TRPA1 was increased in models of inflammatory and nerve injuries; TRPA1 knockdown reduced

cold hyperalgesia but had little effect on mechanical allodynia and thermal hyperalgesia in these models (Obata et al., 2005). Although these data indicated that TRPA1 was involved in cold sensing, the results from TRPA1 knockout mice were confusing; further experimental studies by the authors also failed to clarify the relationship between TRPA1 and cold-sensitive neurons (Obata et al., 2005). Therefore, the role of TRPA1 in the occurrence and development of cold hyperalgesia remains controversial.

Although TRPA1 and α2δ1 are co-involved in the occurrence and development of neuropathic pain, TRPA1 has different cellular localization and functional characteristics. Glial TRPA1 becomes a new focus of neuropathic pain research. Activated Schwann cells TRPA1 induced the generation of reactive oxygen species (ROS) and 4-HNE involved in alcohol-evoked neuropathic pain (De Logu et al., 2019). It suggests that Schwann cells' TRPA1 is closely related to oxidative stress in neuropathic pain. TRPA1 is activated not only by external stimuli but also by intracellular calcium released by the endoplasmic reticulum (Zurborg et al., 2007; Cavanaugh et al., 2008). Certainly, TRPA1 is important for neuronal calcium homeostasis in both physiological and pathological states. Interestingly, several lines of evidence support that a compensatory expression of TRPA1 could occur after nerve injury; the expression of TRPA1 was downregulated in L5/DRG and upregulated in L4/DRG (Obata et al., 2005; Katsura et al., 2006; Staaf et al., 2009). However, the mechanism of this expression mode is unclear. Further studies are recommended to illuminate the physiological and pathological actions of TRPA1 in sensory transduction and the interaction between TRPA1 and Cavα2δ1.

TRPV1 is predominantly expressed in primary afferent terminals as well as in the cell bodies of DRG and TG neurons. Immunofluorescence results demonstrated that 85% of α2δ1 immunoreactive neurons co-expressed TRPV1, and 64% of neurons that were positive for TRPV1 immunoreactivity also co-expressed α2δ1 (**Figure 3**; Li et al., 2014; Cakici et al., 2016; Bikbaev et al., 2020). These findings suggest a functional relationship between TRPV1 and α2δ1 in primary sensory neurons. One study demonstrated that gabapentin regulated mosquito allergens induced itching by acting on the voltage-dependent calcium channels' α2δ1 subunits, which were located in the TRPV1-positive sensory neurons in the peripheral nerve system (Akiyama et al., 2018). Although TRPA1 channels occupy advantageous positions to allow gabapentin to infiltrate primary afferent terminals, it is still unclear whether the activation and opening of TRPV1 channels in peripheral nerve endings effectively transport GBP to its presumed position of action in primary afferent terminals. Future investigations are required to verify this question.

Like VGCCs, TRPV1 activation also mediates Ca^{2+} influx. However, TRPV1 is also subject to calcium-dependent desensitization (Tominaga et al., 1998), which may involve interaction between Ca^{2+}-calmodulin and one or more cytoplasmic regions at the N and C termini of the channel (Numazaki et al., 2003; Rosenbaum et al., 2004; Lau et al., 2012). In addition, TRPV1 is mainly expressed in unmyelinated, slowly conducting primary neurons (C-fibers) (Tominaga et al., 1998; Kobayashi et al., 2005). Activation of these fibers promotes the release of proinflammatory factors. Indeed, TRPV1 has come to represent the preeminent molecular marker for defining the nociceptor subpopulation that accounts for sensitivity to thermal stimulation, neurogenic inflammation, and low pH environment (Julius, 2013). Remarkably, 30–50% of TRPV1-expressing neurons also express TRPA1 and TRPV1 interacts with TRPA1 to form a heteromeric channel (Kobayashi et al., 2005; Fischer et al., 2014). In human, neuropathic pain was associated with the specific single-nucleotide polymorphism of TRPV1 and TRPA1 channels (Binder et al., 2011). Rare genetic variants in the genes coding for TRPA1 and TRPV1 had also been found in patients with erythromelalgia (Zhang et al., 2014). Therefore, TRPV1 may be involved in many physiological and pathological processes by interacting with TRPA1. Of course, more research is needed to confirm these.

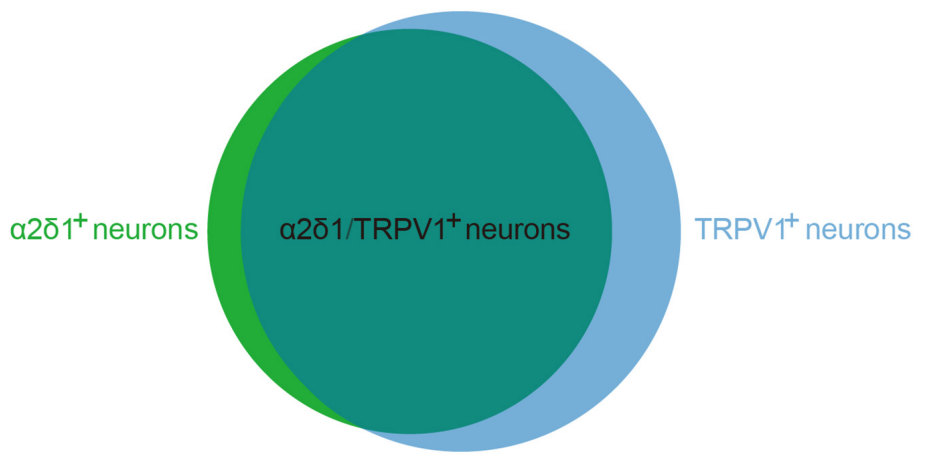

FIGURE 3 | The co-expression proportion of α2δ1 and TRPV1 in primary sensory neurons. α2δ1 and TRPV1 co-expression neurons occupy 85% of α2δ1 immunoreactive neurons (α2δ1^{+}) and 64% of neurons that were positive for TRPV1 immunoreactivity (TRPV1^{+}).

CAVα2δ1 CONTRIBUTES TO NEUROPATHIC PAIN BY ACTIVATING ITS DOWNSTREAM PROTEIN KINASE C TARGET

PKC, the family of serine/threonine kinases, is composed of 11 different isoenzymes and divided into many subtypes (Nishizuka, 1988). This family is calcium-dependent and activated by phosphatidylserine (PS), diacylglycerol (DAG), and protein–protein interactions (Newton, 2010). Different PKC isoforms exist in different tissue and cell locations. For instance, PKCα is expressed at the outer surface of pre- and postsynaptic vessels, while PKCγ is mainly found in the perikaryal cytoplasm and postsynaptic dendrites in adult rats (Hirai, 2018). Interestingly, PKCs are mainly located in the cell bodies and presynaptic central terminals of DRG-nociceptive neurons with small and medium diameters in the SDH (Ase et al., 1988). All PKC subtypes have an identical carboxyterminal that is highly conserved and linked to a divergent amino-terminal regulatory domain by a hinge region (Hirai, 2018; He and Wang, 2019). Normally, PKCs are self-inhibited by a pseudo-substrate sequence that appears at the regulatory domain and occupies the substrate binding site (Hirai, 2018). The self-inhibition of PKCs is disturbed when the regulatory domain is transported to the plasma membrane under the effects of second messengers and allosteric effectors, where its phosphorylation domain is then exposed to the target substrates (He and Wang, 2019).

In cultured DRG neurons separated from adult rats, PKCδ, a PKC isoform, was activated by paclitaxel in a dose- and

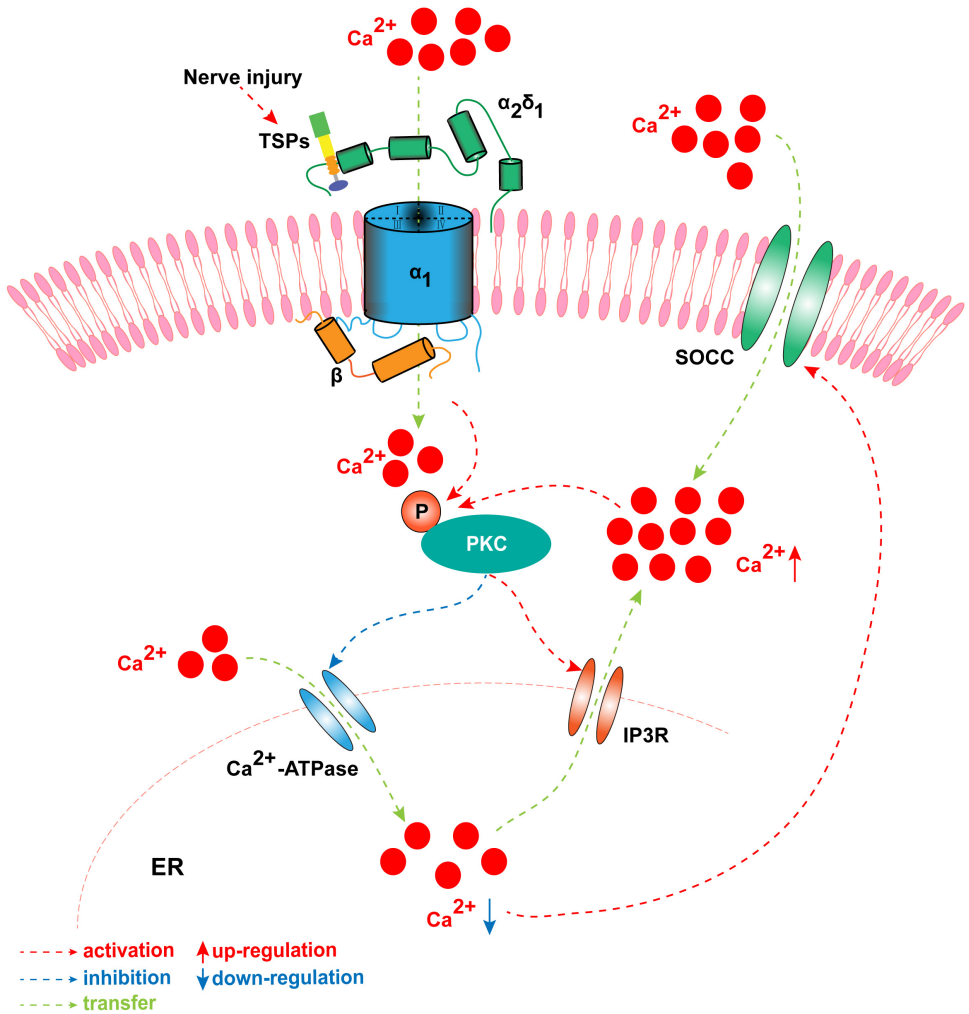

FIGURE 4 | The concentration of intracellular Ca^{2+} is elevated by TSP4 via binding to Cavα2δ1 and activating the downstream PKC signaling pathway when nerve is injured. Once nerve is damaged, TSP4 first binds with the Cavα2δ1 and mediates Ca^{2+} influx, and then induces the phosphorylation of PKC. The p-PKC decreases the function of endoplasmic reticulum (ER) Ca^{2+}-ATPase and inhibits Ca^{2+} entering into ER. Meanwhile, p-PKC activates IP3R and allows Ca^{2+} flowing out of ER. It results in the downregulation of ER Ca^{2+} concentration which induces the opening of store-operated calcium channel. These processes successfully cause the influx of Ca^{2+} and the upregulation of intracytoplasmic Ca^{2+}. Finally, the intracellular Ca^{2+} further activates primary sensory neurons, which leads to the formation of peripheral sensitization.

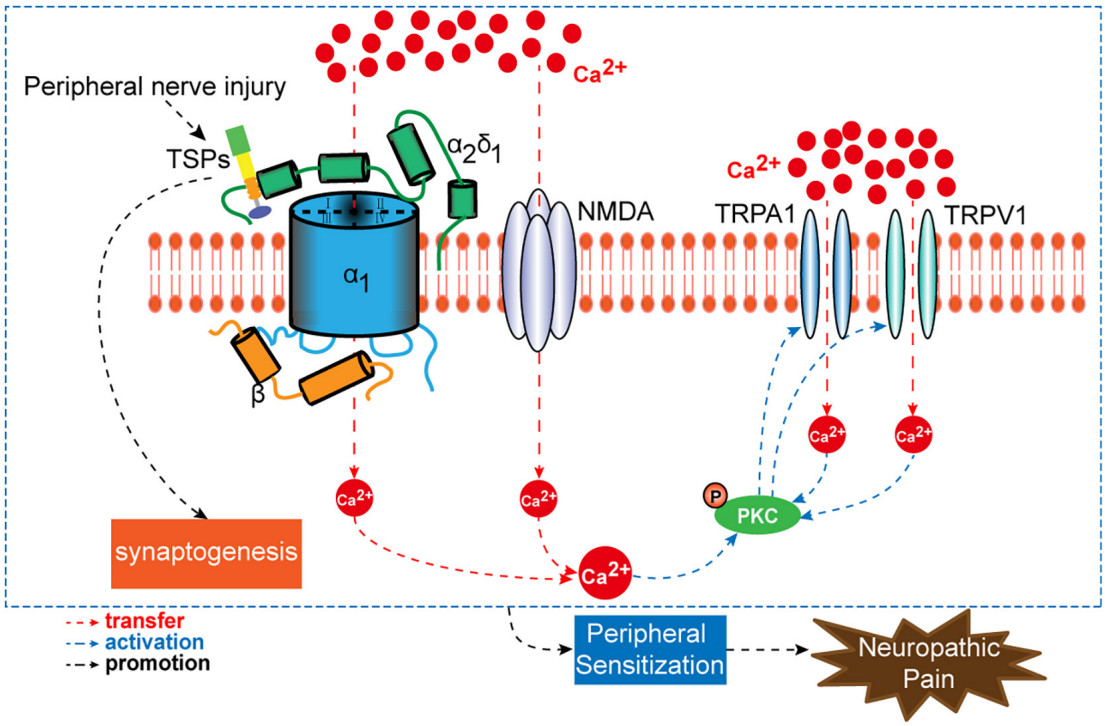

FIGURE 5 | A schematic overview of presynaptic Cavα2δ1 and its interactional targets (TSPs, NMDAR, PKC, TRPA1, and TRPV1) in the process of neuropathic pain.

time-dependent manner (He and Wang, 2015). PKC_δ inhibitors administered intrathecally reduced the excitability of DRG neurons and relieved neuropathic pain in a paclitaxel-induced peripheral neuropathy mouse model (Chen et al., 2011). In response to inflammatory mediators such as bradykinin and substance P (SP), PKCε from primary sensory neurons was transported from afferent nerve terminals to the plasma membrane of nociceptors in neuropathic pain and inflammatory pain models (Zhang et al., 2007; Penniyaynen et al., 2019). It is verified that PKCε regulates nociception through the modulation of the function of TRPV1 (Chen et al., 2011; Liu et al., 2020). The activation of PKCε can phosphorylate the Ser502 and Ser800 sites of TRPV1, which mediate the increase of capsaicin-induced excitability in afferent neurons (Minke and Parnas, 2006; Chen et al., 2011; Liu et al., 2020). Thus, PKC may have significant implications for neuropathic pain. However, it has not yet been determined which proteins PKC interacts with, or if these proteins are being phosphorylated by PKC.

TSP4 modulates intracellular Ca^{2+} homeostasis in primary sensory neurons of the TG and DRG by activating PKC signaling and subsequently regulating Ca^{2+} influx and buffering. This process involves the Ca^{2+}-ATPase of the sarco-endoplasmic reticulum and plasma membrane after binding to the α2δ1 subunit (**Figure 4**; Guo et al., 2017). The regulating action of TSP4 on intracellular Ca^{2+} signaling is weakened in conditional knockout Cavα2δ1 mice and is also dependent on the PKC signaling pathway (Guo et al., 2017). These findings indicate that TSP4 contributes to the process of neuropathic pain by increasing the concentration of intracellular Ca^{2+} via binding to Cavα2δ1 and activating the downstream PKC signaling pathway (**Figure 4**). Cavα2δ1 contributes to the occurrence and development of neuropathic pain by modulating the PKA/PKC/MAPK signaling pathways in the DRG (Sun et al., 2020). GBP significantly attenuates neuropathic pain by binding to Cavα2δ1 and regulating the intracellular PKC signaling pathway in the SDH of rats (Sun et al., 2020). Moreover, our recent study showed that the phosphorylation of PKC was increased in the TG after pT-ION, and the PKC inhibitor GF109203X (0.2 mg/kg) significantly attenuated the mechanical allodynia and cold hyperalgesia induced by trigeminal nerve injury (Cui et al., 2020). The p-PKC elevation induced by nerve injury was inhibited by Cavα2δ1 downregulation in the TG (Cui et al., 2020). Adenovirus-mediated Cavα2δ1 overexpression in TG neurons induced the increased expression of p-PKC in the TG (Cui et al., 2020). Meanwhile, TRPA1 and gap junctions (CX26, CX36, and CX43) are regulated by PKC, the downstream target of Cavα2δ1 (Cui et al., 2020). In the aforementioned study, the amount of Cavα2δ1 bound to either TSP4 or NMDARs increased after pT-ION. The increased binding induces the activation and opening of these channels and then increases the amount of Ca^{2+} flowing into the neurons, and thus triggers a downstream signaling cascade reaction, such as the phosphorylation of PKC. However, the mechanisms of Cavα2δ1/PKC signaling in primary sensory neurons in neuropathic pain remain unclear. The targets of Cavα2δ1/PKC signaling in primary sensory neurons in neuropathic pain have yet to be determined.

CONCLUSION AND IMPLICATION

Neuropathic pain is induced and maintained by the activation of molecular targets that trigger primary sensory neuron sensitization. Current therapies for neuropathic pain are intractable, and these are limited by unclear mechanisms. In clinical practice, many patients with neuropathic pain do not achieve satisfactory pain relief using analgesic drugs. Moreover, the side effects of analgesic drugs are unbearable. Cavα2δ1 is described as an accessory subunit of VGCCs. It contributes to the activation of primary sensory neurons by regulating the entry of Ca^{2+}. As discussed above, nerve injury promotes the binding of Cavα2δ1 to either TSP4 or NMDA receptors in primary sensory neurons, which upon activation will increase the influx of Ca^{2+} into the neurons and thus stimulate PKC and the downstream signaling of TRPA1 and TRPV1 channels (**Figure 5**). These molecules have emerged as alternative targets for the treatment of neuropathic pain. Despite progress being made in terms of understanding the mechanisms of presynaptic Cavα2δ1, our knowledge on its roles and interactions with target sites in the development of neuropathic pain is inadequate. Extensive research is required to further elucidate the genetics and epigenetic mechanisms of Cavα2δ1 in long-lasting neuropathic pain. In addition, the specific intraganglionic administration method requires further validation and subsequent inclusion to clinical practice.

Cavα2δ1 is the important target of gabapentin and pregabalin that are clinically used to treat neuropathic pain (Grice and Mertens, 2008; Chen et al., 2019; Deng et al., 2019; Huang Y. et al., 2020). Recently, mirogabalin, a novel selective ligand for the calcium channel α2δ subunit, is approved for the treatment of neuralgia (Deeks, 2019; Tetsunaga et al., 2020; Zajaczkowska et al., 2021). Drugs targeting α2δ1 for neuralgia are constantly being updated. It will contribute to the development of the more effective drugs to accurately research the mechanisms of α2δ1 and its interactional targets in neuropathic pain via using specific gene interference and genetic methods.

Recent studies demonstrated that calcium channel α2δ1 is a specific candidate marker and therapeutic target for tumor-initiating cells in gastric cancer, hepatocellular carcinoma, and non-small cell lung cancer (Amhimmid et al., 2018; Zhang et al., 2019; Ma et al., 2021). Meanwhile, one study showed that α2δ1 signaling drove cell death, synaptogenesis, circuit reorganization, and gabapentin-mediated neuroprotection in a model of insult-induced cortical malformation (Lau et al., 2017). Therefore, the roles of the calcium channel α2δ1 subunit and its interactional targets are worth investigating in other diseases rather than neuropathic pain.

AUTHOR CONTRIBUTIONS

WC and HW wrote the manuscript. XY reviewed the literature. TS modified the language. FX and XX made equal contributions to the drawing of the figures and the revision of the manuscript. All authors contributed to the article and approved the submitted version.

FUNDING

This work was supported by the National Natural Science Foundation of China (No. 82001190), Science and Technology Foundation of Shandong Traditional Chinese Medicine (No. 2020Q035), and Natural Science Foundation of Shandong Province (No. ZR2020MH348).

REFERENCES

Adams, J. C., and Lawler, J. (2011). The thrombospondins. *Cold Spring Harb. Perspect Biol.* 3:a009712. doi: 10.1101/cshperspect.a009712

Akiyama, T., Andoh, T., Ohtsuka, E., Nojima, H., Ouchi, H., Takahata, H., et al. (2018). Peripheral gabapentin regulates mosquito allergy-induced itch in mice. *Eur. J. Pharmacol.* 833, 44–49. doi: 10.1016/j.ejphar.2018.05.037

Aleixandre-Carrera, F., Engelmayer, N., Ares-Suárez, D., Acosta, M., Belmonte, C., Gallar, J., et al. (2021). Optical assessment of nociceptive TRP channel function at the peripheral nerve terminal. *Int. J. Mol. Sci.* 22:481. doi: 10.3390/ijms22020481

Alles, S., and Smith, P. A. (2018). Etiology and pharmacology of neuropathic pain. *Pharmacol. Rev.* 70, 315–347. doi: 10.1124/pr.117.014399

Amato, N. S., Sharma, R., Waldfogel, J. M., Zhang, A., Bennett, W. L., Yeh, H. C., et al. (2019). Non-pharmacologic treatments for symptoms of diabetic peripheral neuropathy: a systematic review. *Curr. Med. Res. Opin.* 35, 15–25. doi: 10.1080/03007995.2018.1497958

Amhimmid, B. S., Waheeb, F. M., Mahmoud, N. M., and Mohammad, E. M. (2018). Calcium channel alpha2delta1 subunit as a novel biomarker for diagnosis of hepatocellular carcinoma. *Cancer Biol. Med.* 15, 52–60. doi: 10.20892/j.issn.2095-3941.2017.0167

Ase, K., Saito, N., Shearman, M. S., Kikkawa, U., Ono, Y., Igarashi, K., et al. (1988). Distinct cellular expression of beta I- and beta II-subspecies of protein kinase C in rat cerebellum. *J. Neurosci.* 8, 3850–3856.

Bauer, C. S., Nieto-Rostro, M., Rahman, W., Tran-Van-Minh, A., Ferron, L., Douglas, L., et al. (2009). The increased trafficking of the calcium channel subunit alpha2delta-1 to presynaptic terminals in neuropathic pain is inhibited by the alpha2delta ligand pregabalin. *J. Neurosci.* 29, 4076–4088. doi: 10.1523/JNEUROSCI.0356-09.2009

Bauer, C. S., Tran-Van-Minh, A., Kadurin, I., and Dolphin, A. C. (2010). A new look at calcium channel alpha2delta subunits. *Curr. Opin. Neurobiol.* 20, 563–571. doi: 10.1016/j.conb.2010.05.007

Bennett, G. J., Chung, J. M., Honore, M., and Seltzer, Z. (2003). Models of neuropathic pain in the rat. *Curr. Protoc. Neurosci.* Chapter 9, 9–14. doi: 10.1002/0471142301.ns0914s22

Bikbaev, A., Ciuraszkiewicz-Wojciech, A., Heck, J., Klatt, O., Freund, R., Mitlohner, J., et al. (2020). Auxiliary alpha2delta1 and alpha2delta3 subunits of calcium channels drive excitatory and inhibitory neuronal network development. *J. Neurosci.* 40, 4824–4841. doi: 10.1523/JNEUROSCI.1707-19.2020

Binder, A., May, D., Baron, R., Maier, C., Tolle, T. R., Treede, R. D., et al. (2011). Transient receptor potential channel polymorphisms are associated with the somatosensory function in neuropathic pain patients. *PLoS One* 6:e17387. doi: 10.1371/journal.pone.0017387

Bloomquist, B. T., Shortridge, R. D., Schneuwly, S., Perdew, M., Montell, C., Steller, H., et al. (1988). Isolation of a putative phospholipase C gene of Drosophila, norpA, and its role in phototransduction. *Cell* 54, 723–733. doi: 10.1016/s0092-8674(88)80017-5

Brodbeck, J., Davies, A., Courtney, J. M., Meir, A., Balaguero, N., Canti, C., et al. (2002). The ducky mutation in Cacna2d2 results in altered Purkinje cell morphology and is associated with the expression of a truncated alpha 2 delta-2 protein with abnormal function. *J. Biol. Chem.* 277, 7684–7693. doi: 10.1074/jbc.M109404200

Cakici, N., Fakkel, T. M., van Neck, J. W., Verhagen, A. P., and Coert, J. H. (2016). Systematic review of treatments for diabetic peripheral neuropathy. *Diabet. Med.* 33, 1466–1476. doi: 10.1111/dme.13083

Capasso, K. E., Manners, M. T., Quershi, R. A., Tian, Y., Gao, R., Hu, H., et al. (2015). Effect of histone deacetylase inhibitor JNJ-26481585 in pain. *J. Mol. Neurosci.* 55, 570–578. doi: 10.1007/s12031-014-0391-7

Catterall, W. A. (2011). Voltage-gated calcium channels. *Cold Spring Harb. Perspect. Biol.* 3:a003947. doi: 10.1101/cshperspect.a003947

Cavanaugh, E. J., Simkin, D., and Kim, D. (2008). Activation of transient receptor potential A1 channels by mustard oil, tetrahydrocannabinol and Ca2+ reveals different functional channel states. *Neuroscience* 154, 1467–1476. doi: 10.1016/j.neuroscience.2008.04.048

Chen, J., Li, L., Chen, S. R., Chen, H., Xie, J. D., Sirrieh, R. E., et al. (2018). The alpha2delta-1-NMDA receptor complex is critically involved in neuropathic pain development and gabapentin therapeutic actions. *Cell Rep.* 22, 2307–2321. doi: 10.1016/j.celrep.2018.02.021

Chen, Y., Chen, S. R., Chen, H., Zhang, J., and Pan, H. L. (2019). Increased alpha2delta-1-NMDA receptor coupling potentiates glutamatergic input to spinal dorsal horn neurons in chemotherapy-induced neuropathic pain. *J. Neurochem.* 148, 252–274. doi: 10.1111/jnc.14627

Chen, Y., Yang, C., and Wang, Z. J. (2011). Proteinase-activated receptor 2 sensitizes transient receptor potential vanilloid 1, transient receptor potential vanilloid 4, and transient receptor potential ankyrin 1 in paclitaxel-induced neuropathic pain. *Neuroscience* 193, 440–451. doi: 10.1016/j.neuroscience.2011.06.085

Chen, Y. W., Zhao, P., Borup, R., and Hoffman, E. P. (2000). Expression profiling in the muscular dystrophies: identification of novel aspects of molecular pathophysiology. *J. Cell Biol.* 151, 1321–1336. doi: 10.1083/jcb.151.6.1321

Christopherson, K. S., Ullian, E. M., Stokes, C. C. A., Mullowney, C. E., Hell, J. W., Agah, A., et al. (2005). Thrombospondins are astrocyte-secreted proteins that promote CNS synaptogenesis. *Cell* 120, 421–433. doi: 10.1016/j.cell.2004.12.020

Chukyo, A., Chiba, T., Kambe, T., Yamamoto, K., Kawakami, K., Taguchi, K., et al. (2018). Oxaliplatin-induced changes in expression of transient receptor potential channels in the dorsal root ganglion as a neuropathic mechanism for cold hypersensitivity. *Neuropeptides* 67, 95–101. doi: 10.1016/j.npep.2017.12.002

Colleoni, M., and Sacerdote, P. (2010). Murine models of human neuropathic pain. *Biochim. Biophys. Acta* 1802, 924–933. doi: 10.1016/j.bbadis.2009.10.012

Crosby, N. D., Zaucke, F., Kras, J. V., Dong, L., Luo, Z. D., and Winkelstein, B. A. (2015). Thrombospondin-4 and excitatory synaptogenesis promote spinal sensitization after painful mechanical joint injury. *Exp. Neurol.* 264, 111–120. doi: 10.1016/j.expneurol.2014.11.015

Cui, W. Q., Chu, Y. X., Xu, F., Chen, T., Gao, L., Feng, Y., et al. (2020). Calcium channel alpha2delta1 subunit mediates secondary orofacial hyperalgesia through PKC-TRPA1/Gap junction signaling. *J. Pain* 21, 238–257. doi: 10.1016/j.jpain.2019.08.012

Davies, A., Hendrich, J., Van Minh, A. T., Wratten, J., Douglas, L., and Dolphin, A. C. (2007). Functional biology of the alpha(2)delta subunits of voltage-gated calcium channels. *Trends Pharmacol. Sci.* 28, 220–228. doi: 10.1016/j.tips.2007.03.005

Davies, A., Kadurin, I., Alvarez-Laviada, A., Douglas, L., Nieto-Rostro, M., Bauer, C. S., et al. (2010). The alpha2delta subunits of voltage-gated calcium channels form GPI-anchored proteins, a posttranslational modification essential for function. *Proc. Natl. Acad. Sci. U.S.A.* 107, 1654–1659. doi: 10.1073/pnas.0908735107

De Logu, F., Li, P. S., Landini, L., Portelli, F., Innocenti, A., de Araujo, D., et al. (2019). Schwann cells expressing nociceptive channel TRPA1 orchestrate ethanol-evoked neuropathic pain in mice. *J. Clin. Invest.* 129, 5424–5441. doi: 10.1172/JCI128022

De Waard, M., Witcher, D. R., Pragnell, M., Liu, H., and Campbell, K. P. (1995). Properties of the alpha 1-beta anchoring site in voltage-dependent Ca2+ channels. *J. Biol. Chem.* 270, 12056–12064. doi: 10.1074/jbc.270.20.12056

Deeks, E. D. (2019). Mirogabalin: first global approval. *Drugs* 79, 463–468. doi: 10.1007/s40265-019-01070-8

Deng, M., Chen, S. R., and Pan, H. L. (2019). Presynaptic NMDA receptors control nociceptive transmission at the spinal cord level in neuropathic pain. *Cell. Mol. Life Sci.* 76, 1889–1899. doi: 10.1007/s00018-019-03047-y

Dolphin, A. C. (2012). Calcium channel auxiliary alpha2delta and beta subunits: trafficking and one step beyond. *Nat. Rev. Neurosci.* 13, 542–555. doi: 10.1038/nrn3311

El-Awaad, E., Pryymachuk, G., Fried, C., Matthes, J., Isensee, J., Hucho, T., et al. (2019). Direct, gabapentin-insensitive interaction of a soluble form of the calcium channel subunit α(2)δ-1 with thrombospondin-4. *Sci. Rep.* 9:16272. doi: 10.1038/s41598-019-52655-y

Eroglu, C., Allen, N. J., Susman, M. W., O'Rourke, N. A., Park, C. Y., Ozkan, E., et al. (2009). Gabapentin receptor alpha2delta-1 is a neuronal thrombospondin receptor responsible for excitatory CNS synaptogenesis. *Cell* 139, 380–392. doi: 10.1016/j.cell.2009.09.025

Fischer, M. J., Balasuriya, D., Jeggle, P., Goetze, T. A., Mcnaughton, P. A., Reeh, P. W., et al. (2014). Direct evidence for functional TRPV1/TRPA1 heteromers. *Pflugers Arch.* 466, 2229–2241. doi: 10.1007/s00424-014-1497-z

Geisler, S., Schopf, C. L., and Obermair, G. J. (2015). Emerging evidence for specific neuronal functions of auxiliary calcium channel alpha(2)delta subunits. *Gen. Physiol. Biophys.* 34, 105–118. doi: 10.4149/gpb_2014037

Gombert, S., Rhein, M., Eberhardt, M., Munster, T., Bleich, S., Leffler, A., et al. (2017). Epigenetic divergence in the TRPA1 promoter correlates with pressure pain thresholds in healthy individuals. *Pain* 158, 698–704. doi: 10.1097/j.pain.0000000000000815

Gribkoff, V. K. (2006). The role of voltage-gated calcium channels in pain and nociception. *Semin. Cell Dev. Biol.* 17, 555–564. doi: 10.1016/j.semcdb.2006.09.002

Grice, G. R., and Mertens, M. K. (2008). Gabapentin as a potential option for treatment of sciatica. *Pharmacotherapy.* 28, 397–402. doi: 10.1592/phco.28.3.397

Guo, Y., Zhang, Z., Wu, H. E., Luo, Z. D., Hogan, Q. H., and Pan, B. (2017). Increased thrombospondin-4 after nerve injury mediates disruption of intracellular calcium signaling in primary sensory neurons. *Neuropharmacology* 117, 292–304. doi: 10.1016/j.neuropharm.2017.02.019

Gurnett, C. A., and Campbell, K. P. (1996). Transmembrane auxiliary subunits of voltage-dependent ion channels. *J. Biol. Chem.* 271, 27975–27978. doi: 10.1074/jbc.271.45.27975

Gurnett, C. A., Felix, R., and Campbell, K. P. (1997). Extracellular interaction of the voltage-dependent Ca^{2+} channel alpha2 delta and alpha1 subunits. *J. Biol. Chem.* 272, 18508–18512. doi: 10.1074/jbc.272.29.18508

Hagenston, A. M., Bading, H., and Bas-Orth, C. (2020). Functional consequences of calcium-dependent synapse-to-nucleus communication: focus on transcription-dependent metabolic plasticity. *Cold Spring Harb. Perspect. Biol.* 12:a035287. doi: 10.1101/cshperspect.a035287

Hardie, R. C., and Minke, B. (1992). The trp gene is essential for a light-activated Ca2+ channel in Drosophila photoreceptors. *Neuron* 8, 643–651. doi: 10.1016/0896-6273(92)90086-s

He, Y., and Wang, Z. J. (2015). Nociceptor beta II, delta, and epsilon isoforms of PKC differentially mediate paclitaxel-induced spontaneous and evoked pain. *J. Neurosci.* 35, 4614–4625. doi: 10.1523/JNEUROSCI.1580-14.2015

He, Y., and Wang, Z. J. (2019). Spinal and afferent PKC signaling mechanisms that mediate chronic pain in sickle cell disease. *Neurosci. Lett.* 706, 56–60. doi: 10.1016/j.neulet.2019.04.055

Hirai, H. (2018). Protein Kinase C in the cerebellum: its significance and remaining conundrums. *Cerebellum* 17, 23–27. doi: 10.1007/s12311-017-0898-x

Honda, K., Shinoda, M., Kondo, M., Shimizu, K., Yonemoto, H., Otsuki, K., et al. (2017). Sensitization of TRPV1 and TRPA1 via peripheral mGluR5 signaling contributes to thermal and mechanical hypersensitivity. *Pain* 158, 1754–1764. doi: 10.1097/j.pain.0000000000000973

Huang, C., Wang, Z., Zhang, K., Dong, Y., Zhang, A., Lu, C., et al. (2020). MicroRNA-107 inhibits proliferation and invasion of laryngeal squamous cell carcinoma cells by targeting CACNA2D1 in vitro. *Anticancer Drugs* 31, 260–271. doi: 10.1097/CAD.0000000000000865

Huang, Y., Chen, S. R., Chen, H., Luo, Y., and Pan, H. L. (2020). Calcineurin Inhibition causes α2δ-1-Mediated tonic activation of synaptic NMDA receptors and pain hypersensitivity. *J. Neurosci.* 40, 3707–3719. doi: 10.1523/JNEUROSCI.0282-20.2020

Hung, C. Y., and Tan, C. H. (2018). TRP channels in nociception and pathological pain. *Adv. Exp. Med. Biol.* 1099, 13–27. doi: 10.1007/978-981-13-1756-9_2

Julius, D. (2013). TRP channels and pain. *Annu. Rev. Cell Dev. Biol.* 29, 355–384.

Katsura, H., Obata, K., Mizushima, T., Yamanaka, H., Kobayashi, K., Dai, Y., et al. (2006). Antisense knock down of TRPA1, but not TRPM8, alleviates cold hyperalgesia after spinal nerve ligation in rats. *Exp. Neurol.* 200, 112–123. doi: 10.1016/j.expneurol.2006.01.031

Kim, D. S., Li, K. W., Boroujerdi, A., Peter, Y. Y., Zhou, C. Y., Deng, P., et al. (2012). Thrombospondin-4 contributes to spinal sensitization and neuropathic pain states. *J. Neurosci.* 32, 8977–8987. doi: 10.1523/JNEUROSCI.6494-11.2012

Kim, Y. S., Chu, Y., Han, L., Li, M., Li, Z., Lavinka, P. C., et al. (2014). Central terminal sensitization of TRPV1 by descending serotonergic facilitation modulates chronic pain. *Neuron* 81, 873–887. doi: 10.1016/j.neuron.2013.12.011

Kobayashi, K., Fukuoka, T., Obata, K., Yamanaka, H., Dai, Y., Tokunaga, A., et al. (2005). Distinct expression of TRPM8, TRPA1, and TRPV1 mRNAs in rat primary afferent neurons with adelta/c-fibers and colocalization with trk receptors. *J. Comp. Neurol.* 493, 596–606. doi: 10.1002/cne.20794

Lana, B., Page, K. M., Kadurin, I., Ho, S., Nieto-Rostro, M., and Dolphin, A. C. (2016). Thrombospondin-4 reduces binding affinity of [3H]-gabapentin to calcium-channel α2δ-1-subunit but does not interact with α2δ-1 on the cell-surface when co-expressed. *Sci. Rep.* 6:24531. doi: 10.1038/srep24531

Lau, L. A., Noubary, F., Wang, D., and Dulla, C. G. (2017). alpha2delta-1 signaling drives cell death, synaptogenesis, circuit reorganization, and gabapentin-mediated neuroprotection in a model of insult-induced cortical malformation. *eNeuro* 4:ENEURO.316–ENEURO.317. doi: 10.1523/ENEURO.0316-17.2017

Lau, S. Y., Procko, E., and Gaudet, R. (2012). Distinct properties of Ca2+-calmodulin binding to N- and C-terminal regulatory regions of the TRPV1 channel. *J. Gen. Physiol.* 140, 541–555.

Li, C. Y., Zhang, X. L., Matthews, E. A., Li, K. W., Kurwa, A., Boroujerdi, A., et al. (2006). Calcium channel alpha2delta1 subunit mediates spinal hyperexcitability in pain modulation. *Pain* 125, 20–34. doi: 10.1016/j.pain.2006.04.022

Li, K. W., Yu, Y. P., Zhou, C., Kim, D. S., Lin, B., Sharp, K., et al. (2014). Calcium channel alpha2delta1 proteins mediate trigeminal neuropathic pain states associated with aberrant excitatory synaptogenesis. *J. Biol. Chem.* 289, 7025–7037. doi: 10.1074/jbc.M114.548990

Li, L., Chen, S. R., Chen, H., Wen, L., Hittelman, W. N., Xie, J. D., et al. (2016). Chloride homeostasis critically regulates synaptic NMDA receptor activity in neuropathic pain. *Cell Rep.* 15, 1376–1383. doi: 10.1016/j.celrep.2016.04.039

Liu, L., Yudin, Y., and Rohacs, T. (2020). Diacylglycerol kinases regulate TRPV1 channel activity. *J. Biol. Chem.* 295, 8174–8185. doi: 10.1074/jbc.RA119.012505

Ma, Y., Yang, X., Zhao, W., Yang, Y., and Zhang, Z. (2021). Calcium channel alpha2delta1 subunit is a functional marker and therapeutic target for tumor-initiating cells in non-small cell lung cancer. *Cell Death Dis.* 12:257. doi: 10.1038/s41419-021-03522-0

Madabhushi, R., Gao, F., Pfenning, A. R., Pan, L., Yamakawa, S., Seo, J., et al. (2015). Activity-Induced DNA breaks govern the expression of neuronal early-response genes. *Cell* 161, 1592–1605. doi: 10.1016/j.cell.2015.05.032

Marais, E., Klugbauer, N., and Hofmann, F. (2001). Calcium channel alpha(2)delta subunits-structure and Gabapentin binding. *Mol. Pharmacol.* 59, 1243–1248. doi: 10.1124/mol.59.5.1243

Marone, I. M., De Logu, F., Nassini, R., De Carvalho, G. M., Benemei, S., Ferreira, J., et al. (2018). TRPA1/NOX in the soma of trigeminal ganglion neurons mediates migraine-related pain of glyceryl trinitrate in mice. *Brain* 141, 2312–2328. doi: 10.1093/brain/awy177

Mayer, M. L., Westbrook, G. L., and Guthrie, P. B. (1984). Voltage-dependent block by Mg2+ of NMDA responses in spinal cord neurones. *Nature* 309, 261–263. doi: 10.1038/309261a0

Minke, B., and Parnas, M. (2006). Insights on TRP channels from in vivo studies in Drosophila. *Annu. Rev. Physiol.* 68, 649–684. doi: 10.1146/annurev.physiol.68.040204.100939

Moore, J., and Gaines, C. (2019). Gabapentin for chronic neuropathic pain in adults. *Br. J. Commun. Nurs.* 24, 608–609. doi: 10.12968/bjcn.2019.24.12.608

Newton, A. C. (2010). Protein kinase C: poised to signal. *Am. J. Physiol. Endocrinol. Metab.* 298, E395–E402. doi: 10.1152/ajpendo.00477.2009

Nishizuka, Y. (1988). The molecular heterogeneity of protein kinase C and its implications for cellular regulation. *Nature* 334, 661–665. doi: 10.1038/334661a0

Numazaki, M., Tominaga, T., Takeuchi, K., Murayama, N., Toyooka, H., and Tominaga, M. (2003). Structural determinant of TRPV1 desensitization interacts with calmodulin. *Proc. Natl. Acad. Sci. U.S.A.* 100, 8002–8006. doi: 10.1073/pnas.1337252100

Obata, K., Katsura, H., Mizushima, T., Yamanaka, H., Kobayashi, K., Dai, Y., et al. (2005). TRPA1 induced in sensory neurons contributes to cold hyperalgesia after inflammation and nerve injury. *J. Clin. Invest.* 115, 2393–2401. doi: 10.1172/JCI25437

Pan, B., Yu, H., Park, J., Yu, Y. P., Luo, Z. D., and Hogan, Q. H. (2015). Painful nerve injury upregulates thrombospondin-4 expression in dorsal root ganglia. *J. Neurosci. Res.* 93, 443–453. doi: 10.1002/jnr.23498

Patil, M. J., Salas, M., Bialuhin, S., Boyd, J. T., Jeske, N. A., and Akopian, A. N. (2020). Sensitization of small-diameter sensory neurons is controlled by TRPV1 and TRPA1 association. *FASEB J.* 34, 287–302. doi: 10.1096/fj.201902026R

Peier, A. M., Moqrich, A., Hergarden, A. C., Reeve, A. J., Andersson, D. A., Story, G. M., et al. (2002). A TRP channel that senses cold stimuli and menthol. *Cell* 108, 705–715. doi: 10.1016/s0092-8674(02)00652-9

Peng, C., Li, L., Zhang, M. D., Bengtsson, G. C., Parisien, M., Belfer, I., et al. (2017). miR-183 cluster scales mechanical pain sensitivity by regulating basal and neuropathic pain genes. *Science* 356, 1168–1171. doi: 10.1126/science.aam7671

Penniyaynen, V. A., Plakhova, V. B., Rogachevskii, I. V., Terekhin, S. G., Podzorova, S. A., and Krylov, B. V. (2019). Molecular mechanisms and signaling by comenic acid in nociceptive neurons influence the pathophysiology of neuropathic pain. *Pathophysiology* 26, 245–252. doi: 10.1016/j.pathophys.2019.06.003

Ponticelli, C., and Anders, H. J. (2017). Thrombospondin immune regulation and the kidney. *Nephrol. Dial. Transplant.* 32, 1084–1089. doi: 10.1093/ndt/gfw431

Risher, W. C., Kim, N., Koh, S., Choi, J. E., Mitev, P., Spence, E. F., et al. (2018). Thrombospondin receptor alpha2delta-1 promotes synaptogenesis and spinogenesis via postsynaptic Rac1. *J. Cell Biol.* 217, 3747–3765. doi: 10.1083/jcb.201802057

Rosenbaum, T., Gordon-Shaag, A., Munari, M., and Gordon, S. E. (2004). Ca2+/calmodulin modulates TRPV1 activation by capsaicin. *J. Gen. Physiol.* 123, 53–62. doi: 10.1085/jgp.200308906

Silverman, H. A., Chen, A., Kravatz, N. L., Chavan, S. S., and Chang, E. H. (2020). Involvement of neural transient receptor potential channels in peripheral inflammation. *Front. Immunol.* 11:590261. doi: 10.3389/fimmu.2020.590261

Sipes, J. M., Murphy-Ullrich, J. E., and Roberts, D. D. (2018). Thrombospondins: purification of human platelet thrombospondin-1. *Methods Cell Biol.* 143, 347–369. doi: 10.1016/bs.mcb.2017.08.021

Skubatz, H. (2019). Neuropeptide FF (FLFQPQRF-NH2) and its fragments bind to α2δ subunit of voltage-gated calcium channels. *J. Pharm. Pharm. Sci.* 22, 292–300. doi: 10.18433/jpps30358

Souza, M. D. A. D., Nassini, R., Geppetti, P., and De Logu, F. (2020). TRPA1 as a therapeutic target for nociceptive pain. *Expert Opin. Ther. Targets* 24, 997–1008.

Staaf, S., Oerther, S., Lucas, G., Mattsson, J. P., and Ernfors, P. (2009). Differential regulation of TRP channels in a rat model of neuropathic pain. *Pain* 144, 187–199. doi: 10.1016/j.pain.2009.04.013

Sun, L., Wang, G., He, M., Mei, Z., Zhang, F., and Liu, P. (2020). Effect and mechanism of the CACNA2D1-CGRP pathway in osteoarthritis-induced ongoing pain. *Biomed. Pharmacother.* 129:110374. doi: 10.1016/j.biopha.2020.110374

Tachiya, D., Sato, T., and Ichikawa, H. (2018). Nerve injury increases the expression of Alpha-2/Delta-1 subunit of L-Type calcium channel in sensory neurons of rat spinal and trigeminal nerves. *Ann. Neurosci.* 24, 191–200. doi: 10.1159/000477604

Tetsunaga, T., Tetsunaga, T., Nishida, K., Misawa, H., Takigawa, T., Yamane, K., et al. (2020). Short-term outcomes of mirogabalin in patients with peripheral neuropathic pain: a retrospective study. *J. Orthop. Surg. Res.* 15:191. doi: 10.1186/s13018-020-01709-3

Tominaga, M., Caterina, M. J., Malmberg, A. B., Rosen, T. A., Gilbert, H., Skinner, K., et al. (1998). The cloned capsaicin receptor integrates multiple

pain-producing stimuli. *Neuron* 21, 531–543. doi: 10.1016/s0896-6273(00)80564-4

Vandresen-Filho, S., Severino, P. C., Constantino, L. C., Martins, W. C., Molz, S., Dal-Cim, T., et al. (2015). N-methyl-D-aspartate preconditioning prevents quinolinic acid-induced deregulation of glutamate and calcium homeostasis in mice hippocampus. *Neurotox. Res.* 27, 118–128. doi: 10.1007/s12640-014-9496-6

Wang, J., Li, K. L., Shukla, A., Beroun, A., Ishikawa, M., Huang, X., et al. (2020). Cocaine triggers astrocyte-mediated synaptogenesis. *Biol. Psychiatry* 89, 386–397. doi: 10.1016/j.biopsych.2020.08.012

Xie, J. D., Chen, S. R., Chen, H., Zeng, W. A., and Pan, H. L. (2016). Presynaptic N-Methyl-d-aspartate (n.d.) receptor activity is increased through protein kinase C in paclitaxel-induced neuropathic pain. *J. Biol. Chem.* 291, 19364–19373. doi: 10.1074/jbc.M116.732347

Yan, X., Jiang, E., Gao, M., and Weng, H. R. (2013). Endogenous activation of presynaptic NMDA receptors enhances glutamate release from the primary afferents in the spinal dorsal horn in a rat model of neuropathic pain. *J. Physiol.* 591, 2001–2019. doi: 10.1113/jphysiol.2012.250522

Yawn, B. P., Wollan, P. C., Weingarten, T. N., Watson, J. C., Hooten, W. M., and Melton, L. R. (2009). The prevalence of neuropathic pain: clinical evaluation compared with screening tools in a community population. *Pain Med.* 10, 586–593. doi: 10.1111/j.1526-4637.2009.00588.x

Yusaf, S. P., Goodman, J., Gonzalez, I. M., Bramwell, S., Pinnock, R. D., Dixon, A. K., et al. (2001). Streptozocin-induced neuropathy is associated with altered expression of voltage-gated calcium channel subunit mRNAs in rat dorsal root ganglion neurones. *Biochem. Biophys. Res. Commun.* 289, 402–406. doi: 10.1006/bbrc.2001.5943

Zajaczkowska, R., Mika, J., Leppert, W., Kocot-Kepska, M., Malec-Milewska, M., and Wordliczek, J. (2021). Mirogabalin-A novel selective ligand for the alpha2delta calcium channel subunit. *Pharmaceuticals (Basel)* 14:112. doi: 10.3390/ph14020112

Zhang, H., Cang, C. L., Kawasaki, Y., Liang, L. L., Zhang, Y. Q., Ji, R. R., et al. (2007). Neurokinin-1 receptor enhances TRPV1 activity in primary sensory neurons via PKCepsilon: a novel pathway for heat hyperalgesia. *J. Neurosci.* 27, 12067–12077. doi: 10.1523/JNEUROSCI.0496-07.2007

Zhang, Z., Schmelz, M., Segerdahl, M., Quiding, H., Centerholt, C., Jureus, A., et al. (2014). Exonic mutations in SCN9A (NaV1.7) are found in a minority of patients with erythromelalgia. *Scand. J. Pain* 5, 217–225. doi: 10.1016/j.sjpain.2014.09.002

Zhang, Z., Zhao, W., Lin, X., Gao, J., Zhang, Z., and Shen, L. (2019). Voltage-dependent calcium channel alpha2delta1 subunit is a specific candidate marker for identifying gastric cancer stem cells. *Cancer Manag. Res.* 11, 4707–4718. doi: 10.2147/CMAR.S199329

Zhou, H. Y., Chen, S. R., and Pan, H. L. (2011). Targeting N-methyl-D-aspartate receptors for treatment of neuropathic pain. *Expert. Rev. Clin. Pharmacol.* 4, 379–388. doi: 10.1586/ecp.11.17

Zhu, X., Jiang, M., Peyton, M., Boulay, G., Hurst, R., Stefani, E., et al. (1996). trp, a novel mammalian gene family essential for agonist-activated capacitative Ca2+ entry. *Cell* 85, 661–671. doi: 10.1016/s0092-8674(00)81233-7

Zurborg, S., Yurgionas, B., Jira, J. A., Caspani, O., and Heppenstall, P. A. (2007). Direct activation of the ion channel TRPA1 by Ca2+. *Nat. Neurosci.* 10, 277–279. doi: 10.1038/nn1843

Conflict of Interest: The authors declare that the research was conducted in the absence of any commercial or financial relationships that could be construed as a potential conflict of interest.

Publisher's Note: All claims expressed in this article are solely those of the authors and do not necessarily represent those of their affiliated organizations, or those of the publisher, the editors and the reviewers. Any product that may be evaluated in this article, or claim that may be made by its manufacturer, is not guaranteed or endorsed by the publisher.

Copyright © 2021 Cui, Wu, Yu, Song, Xu and Xu. This is an open-access article distributed under the terms of the Creative Commons Attribution License (CC BY). The use, distribution or reproduction in other forums is permitted, provided the original author(s) and the copyright owner(s) are credited and that the original publication in this journal is cited, in accordance with accepted academic practice. No use, distribution or reproduction is permitted which does not comply with these terms.

frontiers in Cellular Neuroscience

REVIEW
published: 19 November 2021
doi: 10.3389/fncel.2021.764761

Rett Syndrome and Fragile X Syndrome: Different Etiology With Common Molecular Dysfunctions

Snow Bach[1,2†], Stephen Shovlin[2†], Michael Moriarty[3], Barbara Bardoni[4] and Daniela Tropea[2,5,6]*

[1] School of Mathematical Sciences, Dublin City University, Dublin, Ireland, [2] Neuropsychiatric Genetics, Department of Psychiatry, School of Medicine, Trinity College Dublin, Trinity Translational Medicine Institute, St James's Hospital, Dublin, Ireland, [3] School of Medicine, Trinity College Dublin, Dublin, Ireland, [4] Inserm, CNRS UMR 7275, Institute of Molecular and Cellular Pharmacology, Université Côte d'Azur, Valbonne, France, [5] Trinity College Institute of Neuroscience, Trinity College Dublin, Dublin, Ireland, [6] FutureNeuro, The SFI Research Centre for Chronic and Rare Neurological Diseases, Dublin, Ireland

OPEN ACCESS

Edited by:
Shuxin Li,
Temple University, United States

Reviewed by:
Michael Telias,
University of California, Berkeley, United States
Christina Gross,
Cincinnati Children's Hospital Medical Center, United States

***Correspondence:**
Daniela Tropea
tropead@tcd.ie

[†] These authors have contributed equally to this work

Specialty section:
This article was submitted to Cellular Neuropathology, a section of the journal Frontiers in Cellular Neuroscience

Received: 25 August 2021
Accepted: 27 October 2021
Published: 19 November 2021

Citation:
Bach S, Shovlin S, Moriarty M, Bardoni B and Tropea D (2021) Rett Syndrome and Fragile X Syndrome: Different Etiology With Common Molecular Dysfunctions. Front. Cell. Neurosci. 15:764761. doi: 10.3389/fncel.2021.764761

Rett syndrome (RTT) and Fragile X syndrome (FXS) are two monogenetic neurodevelopmental disorders with complex clinical presentations. RTT is caused by mutations in the Methyl-CpG binding protein 2 gene (*MECP2*) altering the function of its protein product MeCP2. MeCP2 modulates gene expression by binding methylated CpG dinucleotides, and by interacting with transcription factors. FXS is caused by the silencing of the *FMR1* gene encoding the Fragile X Mental Retardation Protein (FMRP), a RNA binding protein involved in multiple steps of RNA metabolism, and modulating the translation of thousands of proteins including a large set of synaptic proteins. Despite differences in genetic etiology, there are overlapping features in RTT and FXS, possibly due to interactions between MeCP2 and FMRP, and to the regulation of pathways resulting in dysregulation of common molecular signaling. Furthermore, basic physiological mechanisms are regulated by these proteins and might concur to the pathophysiology of both syndromes. Considering that RTT and FXS are disorders affecting brain development, and that most of the common targets of MeCP2 and FMRP are involved in brain activity, we discuss the mechanisms of synaptic function and plasticity altered in RTT and FXS, and we consider the similarities and the differences between these two disorders.

Keywords: Rett syndrome, Fragile X syndrome, synaptic plasticity, FMRP, MeCP2, neurodevelopmental disorders

INTRODUCTION

Rett syndrome (RTT) and Fragile X syndrome (FXS) are neurodevelopmental disorders associated with mutations in genes located on the X chromosome. Hence, in both RTT and FXS, the presentation is more severe in male patients, and the reduced severity in females is to be attributed to the presence of two copies of the genes, although X-inactivation influences the number of copies that remain active.

Patients with RTT show apparent normal development up until 18 months, after which there is a regression in motor and language skills accompanied to behavioral and autonomic

deficits. Diagnosis of RTT in males is rare as patients do not often survive past infancy (Reichow et al., 2015), except for rare cases reported beyond early childhood (Pitzianti et al., 2019; Takeguchi et al., 2020). Consequently, the majority of patients with RTT are females with a prevalence of one in every 10,000 births. RTT is caused by mutations in the *MECP2* gene (Amir et al., 1999) which codes for Methyl-CpG binding protein 2 (MeCP2), a protein that binds to methylated DNA to regulate transcription. MeCP2 also interacts with other important molecules by regulating microRNA (miRNA) (Wu et al., 2010). Although ubiquitously present, MeCP2 is expressed mostly in the brain, and it is an important regulator in brain development. Its altered functionality leads to neurodevelopmental deficits including impaired modulation of brain cell connectivity.

Fragile X syndrome affects one in every 4000 males, and one in every 7000 females. The symptoms in male patients with FXS are more severe than in females, and include developmental delays, behavioral and social deficits. FXS patients may show some degree of intellectual disabilities, while females may have normal intelligence to mild intellectual disability (Maurin et al., 2014; Dahlhaus, 2018).

Fragile X syndrome is caused by the silencing of the Fragile X Mental Retardation gene 1 (*FMR1*), which is associated to CGG repeat expansion in its 5′UTR region (Pieretti et al., 1991; Verkerk et al., 1991; Dahlhaus, 2018). As result of the expansion, the 5'UTR and the promoter of the *FMR1* gene are hypermethylated, *FMR1* expression is silenced and its encoded protein, the Fragile X Mental Retardation Protein (FMRP) is not expressed. FMRP is an RNA-binding protein and a component of ribonucleoprotein complexes involved in shuttling between nucleus and cytoplasm, transport along dendrites and association to polyribosomes (Maurin et al., 2014; Richter and Zhao, 2021). Indeed, FMRP modulates the subcellular localization (Xing and Bassell, 2013) and expression of thousands of its target mRNAs (Maurin and Bardoni, 2018; Richter and Zhao, 2021). The role of FMRP in translational regulation - being both repressor and enhancer of translation – is to date its most studied function (Bechara et al., 2009; Darnell et al., 2011; Maurin and Bardoni, 2018; Richter and Zhao, 2021).

Because of their monogenic origin, it has been possible for researchers to develop animal models to study RTT (Na et al., 2012; Pietri et al., 2013; Ezeonwuka and Rastegar, 2014; Cortelazzo et al., 2020) and FXS (Dahlhaus, 2018). These models provide the necessary framework to study the function of MeCP2 and FMRP and extrapolate mechanisms of action and putative targets. In addition, these animal models allow pre-clinical testing to set up therapeutic approaches. Many animal models are now available to study RTT, and several of them have the same mutation present in patients. Additionally, *Mecp2* mutant models can also be generated for studying MeCP2 overexpression or *MECP2* duplication syndrome (Collins et al., 2004; Na et al., 2012; Bodda et al., 2013). *Mecp2* duplication syndrome is marked by features of autism and it is distinct from typical RTT (Ramocki et al., 2009, 2010).

Multiple models for FXS have been generated in flies (Drozd et al., 2018), zebrafish (Vaz et al., 2019), rat (Kulkarni and Sevilimedu, 2020), and mice (Bakker et al., 1994; Mientjes et al., 2006; Dahlhaus, 2018). The mouse model is the most used, as it recapitulates the main phenotype of the disorder. The similarities are present even if silencing of the gene was obtained by a classical knockout (KO) approach and not by CGG expansion: the KO-1 (Bakker et al., 1994) with the neomycin cassette in the exon 5 of the *Fmr1*-gene and the KO-2 (Mientjes et al., 2006) that was generated from a conditional *Fmr1* KO by flanking the promoter and first exon of *Fmr1* with lox P site. In addition, two *Fmr1* knockin (KI) model mice have been generated and they reproduced sporadic missense mutations identified in the *FMR1* gene in FXS patients (Zang et al., 2009; Prieto et al., 2021).

Despite different molecular etiology and severity of clinical presentation, there are several overlapping symptoms between the disorders: intellectual disabilities, seizures, communication deficits, attention deficits, and defects in the skeletal apparatus. At the cellular level, the impairment of synaptic function and plasticity is recognized in both diseases.

These commonalities can be explained by the interplay between MeCP2 and FMRP, and by the common targets between both molecules. Recently, it was reported that MeCP2 expression is elevated in *Fmr1* KO mice cerebral cortex, while FMRP levels are reduced in mice mutants for *Mecp2* (Arsenault et al., 2020). This reciprocal relationship was confirmed using MeCP2 knockdown mouse N2A, and human HEK-293 cells lines (Arsenault et al., 2020). MeCP2 association with *FMR1* gene has been shown *in silico* (Bach et al., 2020). Moreover, MeCP2 and FMRP influence the expression of brain derived neurotrophic factor (BDNF), and, on the other hand, alteration in BDNF signaling affects the expression of *Fmr1* (Castrén and Castrén, 2014; Vicario et al., 2015).

Several authors, to clarify the neurobiology of RTT and FXS, investigated the molecular targets of MeCP2 and of FMRP (Skene et al., 2010; Darnell et al., 2011; Baubec et al., 2013; Maxwell et al., 2013; Gabel et al., 2015; Rube et al., 2016; Maurin et al., 2018; Sawicka et al., 2019). These studies show that many of the targets are involved in neurodevelopment and modulate brain function. With this premise, here we discuss the similarities and differences between mechanisms of synaptic function and plasticity in RTT and FXS as well as common molecular factors modulated in both disorders.

ALTERED SYNAPTIC FUNCTIONING IN RETT SYNDROME AND FRAGILE X SYNDROME

Alterations in synaptic function have been reported in both RTT and FXS (Sidorov et al., 2013; Bagni and Zukin, 2019; Banerjee et al., 2019) with functional consequences on the balance between excitation and inhibition (E/I ratio) and the mechanisms of synaptic plasticity (**Table 1**). The E/I ratio has been found to be altered in several neuropsychiatric disorders. While it represents a change in the extent of excitatory and inhibitory transmission, the underlying activity is complicated and multifaceted (Sohal and Rubenstein, 2019). Several sources report a shift in the E-I ratio in both RTT and FXS, however the alterations may differ depending on the brain region or cell-type investigated.

TABLE 1 | Altered synaptic function in Rett syndrome and Fragile X syndrome.

Source	Cell type (Age)	Finding	References
Mecp2$^{Null/y}$, Mecp2^{Tg1}	Hippocampal neurons (7–14 DIV)	MeCP2 regulates glutamatergic synapse number and synapse strength	Chao et al., 2007
Mecp2$^{-/Y}$	L5 neurons in S1 (P28–P35)	Reduced Cortical Activity: ↓mEPSC	Dani et al., 2005
Mecp2$^{-/Y}$	L2/3 neurons of M1 (P21–28)	↓Local Excitatory input; No Change to Local Inhibitory input	Wood and Shepherd, 2010
Mecp2$^{-/Y}$	L2/3 neurons of V1 (P∼45)	↓ Excitatory and ↓ inhibitory conductance; Altered GABA reversal potential	Banerjee et al., 2016
Mecp2$^{-/Y}$	Pyramidal Neurons of the Hippocampus (P1, DIV 11–14)	↓ mEPSC; No change in mIPSC	Nelson et al., 2006
Mecp2$^{-/Y}$	Layer 2/3 pyramidal neurons of S1 (P25–35). Primary culture of striatal neurons (P1, newborn)	↓ mIPSC	Chao et al., 2010
Mecp2$^{tm1.1Jae}$	Pyramidal CA3 Hippocampal Neurons (P40–60)	↑ mEPSC ↓mIPSC	Calfa et al., 2015
Mecp2$^{-/Y}$	Layer 4 pyramidal and paravalbumin neurons of V1 (P28–30 and P50)	Selective ↓ excitatory input; No change in inhibitory or thalamo-cortical input	He et al., 2014
Mecp2$^{-/Y}$	PV + and SOM + neurons	Specific RTT-like symptoms: ↓ Motor coordination and learning/memory (PV + *Mecp2*$^{-/Y}$), seizures and ↑ Stereotypes (SOM + *Mecp2*$^{-/Y}$)	Ito-Ishida et al., 2015
Mecp2$^{tm1.1Jae}$	Layer 5 pyramidal neurons of mPFC (p32–42)	↓ E/I Ratio and sEPSC; No change sIPSC, mEPSC, mIPSC	Sceniak et al., 2016
Mecp2$^{-/Y}$	Layer 2/3 and layers 5/6 of V1 (P60–240)	↓ E/I Ratio; ↓ Excitatory input	Durand et al., 2012
Mecp2$^{30/}$ heterozygous iPSCs	IPSCs differentiated into glutamatergic neurons	↓ Sodium and potassium currents ↓ sEPSC frequency	Farra et al., 2012
Fmr1$^{-/Y}$	Layer 2/3 neurons of S1 (P19–31)	↓ Inhibitory control on pyramidal output	Paluszkiewicz et al., 2011
Fmr1$^{-/Y}$	Principal excitatory neurons of Basolateral amygdala (P21–30)	↓ Tonic GABAergic capacity; No change in E/I ratio	Martin et al., 2014
Fmr1$^{-/y}$, *Fmr1*$^{-/HET}$	Pyramidal neurons of CA1 (P18–23)	↑ E/I ratio; ↓GABA release (TA inhibitory synapses)	Wahlstrom-Helgren and Klyachko, 2015
Fmr1$^{-/Y}$	Layer 2/3 and layer 4 fast-spiking inhibitory and excitatory (mostly spiny stellate), Neurons of somatosensory cortex	↓ Excitatory input onto fast spiking Inhibitory neurons and onto excitatory neurons	Gibson et al., 2008
Fmr1$^{-/Y}$	CA1 pyramidal layer of dorsal hippocampus	↑ Theta oscillation power; ↑ Slow gamma band coherence; ↓ Spike count of specific interneurons	Arbab et al., 2018
Fmr1$^{-/Y}$	Layer 4 fast-spiking neurons, layer 5 fast-spiking and layer 4 excitatory neurons in the somatosensory cortex	↓ Excitatory input on fast-spiking inhibitory neurons	Patel et al., 2013

Main findings of studies reporting on synaptic function in Rett syndrome and Fragile X syndrome. Mecp2, methyl-CpG binding protein 2 gene; S1, primary somatosensory cortex; M1, primary motor cortex; V1, primary visual cortex; mEPSC, miniature excitatory postsynaptic currents; mIPSC, miniature inhibitory postsynaptic currents; DIV, days in vitro; PV+, parvalbumin-positive neurons; SOM+, somatostatin-positive neurons; mPFC, medial prefrontal cortex; sEPSC, spontaneous excitatory postsynaptic currents; sIPSC, spontaneous excitatory postsynaptic currents; iPSC, induced pluripotent stem cells; Fmr1, fragile X mental retardation 1 gene; TA, temporoammonic.

In symptomatic *Mecp2* KO mice there is a shift in E/I ratio in favor of inhibition present in a number of brain regions including S1, V1, and mPFC (Dani et al., 2005; Durand et al., 2012; Sceniak et al., 2016). However, at birth *Mecp2* mutant mice show an increased glutamatergic transmission, due to the altered shift in GABA function, which is excitatory during the first phases of development, but reverses during the first weeks of postnatal development. In *Mecp2* KO mice the GABA shift is postponed, and treatment with bumetanide, an inhibitor of the chloride channel NKCC1 reduces the effects of the delay. When bumetanide is administered prenatally, some of the symptoms of RTT are decreased, but the respiratory dysfunction and the mortality remain (Lozovaya et al., 2019). Symptomatic *Mecp2* KO mice display decreased dendritic spine density (Kishi and Macklis, 2004; Tropea et al., 2009; Castro et al., 2014) and MeCP2 deficit has been found to decrease glutamatergic synapse number and strength (Chao et al., 2007).

Deletion of *Mecp2* in particular cell neuronal subtypes in mice, reveal the complicated nature of shifts in E/I ratio. Conditional deletion of *Mecp2* in parvalbuminergic (PV) neurons removes the experience dependent critical period of plasticity in the visual cortex, and produces only a partial Rett-like phenotype, specifically motor dysfunction (He et al., 2014; Ito-Ishida et al., 2015). A more general effect of GABAergic neurons has been observed in the brainstem, with a reduction in the number of GABAergic synapses. In patients with RTT, abnormality of inhibitory transmission is associated with respiratory dysfunction, and blockade of GABA reuptake decreased the breathing dysfunction in Mecp2 KO mice (Abdala et al., 2016).

Studies in patients-derived cells confirm the decrease excitatory synaptic transmission in iPS cells derived from mice. These results were also observed in mouse preparations *in vivo* and *in vitro* (Farra et al., 2012).

In FXS mouse models changes to E/I ratio appear to be more specific compared to the *Mecp2* KO mice. Increased intrinsic excitability is observed in FXS at cellular, circuit and behavioral level. The cellular excitability stays with altered ion channels activity, dependent both on the translational activity of FMRP, but also on the direct interaction between FMRP and ion channels (Contractor et al., 2015). In FXS, one aspect of hyperexcitability is linked to the delayed switch in GABA polarity. As for RTT, this timeline is delayed in FXS, where the GABA transmission remains excitatory for longer. The overall increased excitability of the circuits influences also synaptic excitability and spike-timing dependent plasticity, and it is dependent on the chloride transporter NKCC1.

Another aspect of the increased excitability in FXS is due to a reduced expression of GABAA receptors' subunits, with reduced frequency of IPSCs, but not amplitude of GABA currents. The general imbalance in favor of excitation in FXS reflects on the hyper-reactivity to stimuli, anxiety, and seizures in animal models and patients.

Studies in human-derived cells confirmed the morphological findings in FMRP deprived cultures, but they not always confirmed the altered excitability, especially at early stages of development (Telias et al., 2015). This discrepancy can be due to an un-matched decrease in FMRP expression during the *in vitro* development (Linda et al., 2018).

The frequency of the brain waves is also affected in FXS. In *Fmr1* KO mice, increased synchronization of local field potentials occurs and may underlie deficits to information processing in hippocampal circuitry. This hyper-synchronization was characterized in a freely moving mouse, as increased theta power and coherence of slow gamma oscillations (Sohal et al., 2009; Arbab et al., 2018). More recently, the single-cell analyses of a subpopulation of interneurons in *Fmr1*-KO brain at Post-natal day (PND) 18 highlighted the increased levels of inhibitory markers in the absence of FMRP (Castagnola et al., 2020).

Morphological Correlates of Synaptic Functions

Alterations in synaptic functions are reflected also in morphological differences between the two disorders. Reduced neuronal cell size and numbers of dendrites have been observed in patients with RTT alongside short dendrites and a decrease in dendritic spines (Armstrong, 2005; Belichenko et al., 2008). In RTT, there is an overall decrease in brain volume differences and altered brain structures that are also present in mice studies (Chen et al., 2001; Ballas et al., 2009; Xu et al., 2014).

In contrast to RTT and MeCP2 deficiency, a lack of FRMP is associated with increases spine density in human patients and mice models (Levenga et al., 2011; Hodges et al., 2017). Both in *Fmr1* KO mice, and in brain from patients, it has been reported an increase in the number of elongated spines (filopodia) in absence of functional FMRP (Comery et al., 1997), suggesting a reduction in the pruning of spines (Irwin et al., 2000). However, recent studies on spine functionality (Thomazeau et al., 2020) and spine compartmentalization over time (Wijetunge et al., 2014), find that the altered morphology does not correlate with abnormal function between *Fmr1* KO mice and controls. These findings challenge the view of immature status of connections in FXS (He and Portera-Cailliau, 2013), and even the turnover of the spines seems to be invariant to that of matched controls. However, all these measures can be dependent on the brain area and on the stage of development (He and Portera-Cailliau, 2013).

In fact, the presence of the filopodia is dependent on the stage of development and on the preparation. Nimchinsky et al. (2001) analyzed mutant and control mice at several developmental stages and showed that differences in spine morphology and density decreased between 1 and 4 weeks of age. The closing of these phenotypic gaps originally suggested that FMRP played a role in coordinating synaptogenesis in a time-dependant manner. Different cell populations of the hippocampus also show that long and irregular spines are also present in juvenile and adult *Fmr1* KO mice, while *in vitro* and *in vivo* studies show discrepancies for spine densities as with LTP and LTD function (as reviewed by Bostrom et al., 2016). A summary of the studies investigating morphological correlates of synaptic functions in RTT and FXS is reported in **Table 2**.

COMMON FORMS OF SYNAPTIC PLASTICITY DISRUPTED IN RETT SYNDROME AND FRAGILE X SYNDROME

The long-term activity-dependent variation in synaptic connectivity and the associated molecular changes are defined as synaptic plasticity (Citri and Malenka, 2008). Several forms of synaptic plasticity have been reported to be disrupted in RTT and FXS (Huber et al., 2002; Blackman et al., 2012; Wang et al., 2012; Na et al., 2013; Wondolowski and Dickman, 2013).

Alterations in Long-Term Potentiation and Long-Term Depression in Rett Syndrome and Fragile X Syndrome

Both RTT and FXS display endophenotypes that signal aberrant Long-term potentiation (LTP) and long-term depression (LTD), which are Hebbian Forms of plasticity.

In RTT, deficits have been reported in excitatory synapses and LTP. Hippocampal slices show reduced LTP in *Mecp2* KO (Asaka et al., 2006) and *Mecp2*$^{308/Y}$ mice (Moretti et al., 2006). Reduced potentiation is present around onset of symptoms while pre-symptomatic mice maintain the same level of activity observed in matching controls, suggesting that synaptic dysfunction and decline in plasticity is an early event in RTT. Pyramidal neuron synapses in the hippocampus are indeed potentiated in *Mecp2* KO mice, however there is a failure to regulate AMPA receptors post-activation and an overall deficit in LTP (Li et al., 2016). *Mecp2* KO mice display a lack of structural plasticity, and enlarged spines are observed regardless of stimulation or sham (Li et al., 2016). AMPA receptor-related transmission is enhanced at hippocampal synapses and over time, the decrease in internalization fails to counterbalance excessive accumulation. In addition, the lack of receptor trafficking

TABLE 2 | Morphological correlates in Rett syndrome and Fragile X syndrome.

Source	Region/Sample	Experiment	Findings	References
Mecp2$^{tm1.1Jae}$, *Mecp2*$^{308/Y}$, *Mecp2*$^{tm1.1Bird}$, *Patients with RTT*	Hippocampus, cortex, cerebellum	Imaging studies	↓ Neuronal size; ↓ Dendrite numbers; ↓ Dendrite length; ↓ Dendrite spines	Armstrong, 2005; Belichenko et al., 2008
Mecp2$^{-/y}$, *Patients with RTT*	Cerebral cortex, total brain	Imaging studies	↓ Volume	Chen et al., 2001; Armstrong, 2005
Fmr1$^{-/Y}$	Hippocampus (25 weeks)	Immunohistochemistry, imaging studies	↑ Spine density	Levenga et al., 2011; Hodges et al., 2017
Fmr1$^{-/Y}$, *Patients with FXS*	Cortex (16 weeks), temporal cortex	Immunohistochemistry, imaging studies	↑ Filopodia; ↑ Dendrite length; ↑ Dendrite spines	Comery et al., 1997; Irwin et al., 2000
Fmr1$^{-/Y}$	CA1 and layer 5 neurons (P14-P37), hippocampal slices (P25-P35)	Imaging studies	Altered morphology may not correlate with abnormal function	Wijetunge et al., 2014; Thomazeau et al., 2020
Fmr1$^{-/Y}$	Layer 5 neurons (P7-P28)	Imaging studies	Synaptogenesis is mediated by FMRP in a time-dependant manner	Nimchinsky et al., 2001

Main findings of studies reporting on morphological phenotypes in Rett syndrome and Fragile X syndrome. Mecp2, methyl-CpG binding protein 2 gene; RTT, Rett syndrome; Fmr1, fragile X mental retardation 1 gene, FXS, Fragile X syndrome.

prevents activated synapses from becoming plastic, affecting both LTP and LTD.

Long-term depression is also altered in RTT, however to a lesser extent than LTP. Moretti et al. (2006) induced LTD with two different stimulus paradygms in the hippocampus of *Mecp2*$^{308/Y}$ mice and show that when LTD was induced by administration of the mGluR agonist 3,5-dihydroxyphenylglycine (DHPG), the response was comparable in mutant and wildtype mice. However, when paired pulse stimulation was applied, LTD was observed in wild type mice, but not in *Mecp2*$^{308/Y}$ mice. Since both stimulation paradigms affect the post-synaptic sites, but only the paired pulse stimulation protocol is dependent on the presynaptic site, the authors conclude that the impairments in plasticity are due to altered presynaptic terminals, while there is some preservation of LTD. It has also been shown that hippocampal slices of symptomatic mice with an *Mecp2* KO show no NMDAR-dependent LTD by low frequency stimulation (Asaka et al., 2006). More recently, in younger P15 *Mecp2* KO mice, LTD has been induced by DHPG at two different stages: early and late (Lozovaya et al., 2019). Only early induced LTD displays a significant decrease in the amplitude of the response, implicating even earlier synaptic impairment onset in RTT mice.

In FXS LTP was reported to be reduced in several brain regions (Desai et al., 2006; Lauterborn et al., 2007; Suvrathan and Chattarji, 2011; Seese et al., 2012), however, the main form of plasticity studied in FXS is LTD.

The first to show alterations in synaptic plasticity in the absence of FMRP were Huber and colleagues (Huber et al., 2002), who showed an increase in mGluR-dependent LTD in the hippocampus of *Fmr1* KO mice. The dysregulation of mGluR signaling was further confirmed by other authors (Weiler et al., 1997; Gross et al., 2012; Tian et al., 2017), and all the data support the theory that FMRP controls the translation of specific proteins involved in synaptic function, including glutamatergic receptors.

Similarly to what reported in RTT, AMPA aberrant receptors trafficking is driven by a lack of FMRP and consequently associated with cognitive deficits (Nakamoto et al., 2007). PSD-95 synthesis increases in response to DHPG-activation of mGluR, and is co-translated with FMRP (Todd et al., 2003). Further studies in other brain areas showed that LTD in enhanced in multiple cell populations, including cerebellum, where it controls abnormal motor behavior and development of synaptic circuitry in the somatosensory cortex (Greenough et al., 2001; Huber et al., 2002; Koekkoek et al., 2005).

Overall, LTP deficits have been shown in RTT and to a lesser extent in FXS. On the other hand, FXS tends to display enhanced LTD, while RTT shows some LTD preservation.

A summary of the experiments exploring Hebbian forms of plasticity in RTT and FXS is reported in **Table 3**. Beside LTP and LTD, other forms of plasticity are affected in RTT and FXS.

Alterations in Homeostatic Plasticity in Rett Syndrome and Fragile X Syndrome

Homeostatic plasticity controls the changes in synaptic strength that individual neurons operate in response to prolonged changes of neuronal stimulation, and it also mediates the balance of excitation and inhibition. Both RTT and FXS have shown alterations in mechanisms of homeostatic plasticity, and these alterations may explain the general changes in neuronal activity in patients and animal models with RTT and FXS (**Table 4**).

One of the main mechanisms controlling homeostatic changes is synaptic scaling, and it relies on the synthesis, trafficking, and function of AMPA receptors.

Defects in functional levels of *Mecp2* alter homeostatic plasticity. Hence, in RTT, where there is a loss of function of MeCP2, there is impaired ability to respond to homeostatic changes (Na et al., 2013). One of the first studies of homeostatic plasticity in RTT was performed in neuronal cultures. In this study, stimulation with bicuculline produced an increase in neuronal activity, with a sequential decrease in the expression

TABLE 3 | Alteration of long-term potentiation and long-term depression in Rett syndrome and Fragile X syndrome.

Source	Region/Sample	Experiment	Findings	References
Mecp2$^{-/Y}$ established by crossing two lines (Chen et al., 2001; Guy et al., 2001)	Hippocampal slices	Tetanic stimulation, theta-burst stimulation, low frequency stimulation	↓ NMDA- dependant LTP; ↓ NMDA- dependant LTD in symptomatic mice; No difference in presymptomatic mice	Asaka et al., 2006
Mecp2$^{308/Y}$	Hippocampal slices	DHPG LTD conduction, theta-burst stimulation, paired-pulse facilitation	↑ STP; ↓ LTP; No changes in LTD	Moretti et al., 2006
Mecp2$^{-/Y}$	Hippocampal slices (P20–P22, P45–P65)	Theta-burst stimulation, forskolin-induced chemical LTP	↓ LTP	Li et al., 2016
Mecp2$^{-/Y}$	CA3 pyramidal layer (P14–P16)	DHPG LTD Induction, maternal pretreatment of bumetanide	↓ Early-LTD; No difference in late-LTD; Bumetanide improves early-LTD	Lozovaya et al., 2019
Fmr1$^{exon8-KO}$ by CRISPR/Cas9	Rat hippocampi (8–12 weeks)	Theta-burst stimulation, DHPG LTD Induction, low frequency stimulation	↑ LTD by DHPG LTD induction; ↓ LTD by low frequency stimulation; ↓ LTP	Tian et al., 2017
Fmr1$^{-/Y}$	Hippocampal slices (P21–30)	Paired-pulse low-frequency stimulation, NMDAR-LTD induction	↑ mGluR-dependant LTD; No difference in NMDAR-LTD or LTP	Huber et al., 2002
Fmr1$^{-/Y}$ and Purkinje cell-specific *L7-Fmr1*$^{-/Y}$	Cerebellar slices	Low frequency stimulation	↑ LTD	Koekkoek et al., 2005
Fmr1$^{-/Y}$	Hippocampal slices	High frequency stimulation	No difference in LTP	Godfraind et al., 1996
Fmr1$^{-/Y}$	Hippocampal slices (P35–P56)	Paired-pulse facilitation, theta-burst stimulation	No difference in LTP	Paradee et al., 1999
Fmr1$^{-/Y}$	Somatosensory cortex (P5–P11)	LTP stimulation, bumetanide treatment	↑ LTP which is corrected by bumetanide	He et al., 2019

Main findings of studies reporting on long-term potentiation and long-term depression in Rett syndrome and Fragile X syndrome. Mecp2, methyl-CpG binding protein 2 gene; NMDA, N-methyl-D-aspartate; LTP, long-term potentiation; LTD, long-term depression; DHPG, 3,5-dihydroxyphenylglycine; STP, short-term potentiation; Fmr1, fragile X mental retardation 1 gene; NMDAR, N-methyl-D-aspartate receptor.

TABLE 4 | Altered homeostatic plasticity in Rett syndrome and Fragile X syndrome.

Source	Region/Sample	Experiment	Findings	References
Mecp2$^{-/y}$ by shRNA	Hippocampus	Whole cell voltage clamp	*Mecp2* downregulation prevents activity-dependent synaptic scaling	Qiu et al., 2012
Mecp2 knockdown by shRNA	Rat visual cortex neurons	Whole cell patch clamp	MeCP2 is necessary for cell-autonomous scaling up	Blackman et al., 2012
Mecp2$^{tm1.1Jae}$	Hippocampal neurons	Whole cell patch clamp and molecular analysis	↑ EEA1 expression re-establishes synaptic scaling in *Mecp2* mutant mice	Xu and Pozzo-Miller, 2017
Mecp2$^{S421A;S424A/y}$ and Mecp2$^{-/y}$	Hippocampal neurons	Whole cell patch clamp and molecular analysis	MeCP2 phosphorylation is necessary for synaptic scaling	Zhong et al., 2012
Fmr1$^{-/Y}$	Hippocampal slice/cultures	Patch Clamp	FMRP is necessary postsynaptically to mediate the RA mediated synaptic scaling	Soden and Chen, 2010
Fmr1$^{-/Y}$	Hippocampal neurons	Patch Clamp	GluA1 ubiquitination synaptic downscaling is prevented in *Fmr1* knockout mice	Lee et al., 2018

Main findings of studies reporting homeostatic plasticity in Rett syndrome and Fragile X syndrome. Mecp2, methyl-CpG binding protein 2 gene; Fmr1, fragile X mental retardation 1 gene, FRMP, fragile X mental retardation protein EEA1, early endosome antigen 1, RA, retinoic acid.

of the AMPA receptors subunit GluR2 and a reduction of mEPSC amplitude. However, the expression of GluR2 is under the control of the transcriptional repressor MeCP2, whose levels also increase during bicuculline stimulation. As a result, the bicuculline treatment in *Mecp2* KO neurons, does not lead to the expected decrease of the GluR2 receptor subunit at the synapse. These experiments were among the first to show the importance of Mecp2 in the control of synaptic scaling (Qiu et al., 2012), and they were confirmed by Blackman et al. (2012), who showed that reduced neuronal drive in *Mecp2* KO preparations does not produce the expected increase in synaptic scaling as observed in WT controls. One of the factors controlling

homeostatic plasticity in RTT is the Early Endosome Antigen 1 (EEA1), which regulates AMPA receptor endocytosis. EEA1 expression is reduced in *Mecp2* KO mice, where the synaptic scaling is reduced. However, the increased expression of EEA1 in *Mecp2* KO cultures, reinstates the ability to scale the synapses in response to changes in activity (Xu and Pozzo-Miller, 2017). It is important to remember that not only *Mecp2* expression, but also its activation, is important for the proper functioning of the protein. Indeed, post translational modifications of MeCP2 have also been found to be implicated in synaptic function and homeostasis (Bellini et al., 2014) and the phosphorylated MeCP2 modulates synaptic scaling -down through mGluR5 (Zhong et al., 2012).

Fragile X mental retardation protein has been involved in synaptic scaling in response to both increased and decreased activity- as observed in *Fmr1* KO mice and in neuronal cultures derived from patients with FXS. The increased activity of AMPA receptors consequent to a decrease in activity, is mediated by the Retinoic Acid (RA), which is produced in response to the altered activity, and promotes the synthesis of new AMPA receptors. However, in FXS, while the transcription of the AMPA receptor remains unchanged, the RA- mediated translation of AMPA is reduced, and only restoration of the proper full length functional FMRP re-establishes synaptic scaling in primary cultures derived from *Fmr1KO* mice (Soden and Chen, 2010). These results suggest that FMRP is essential for the postsynaptic response in RA-mediated synaptic scaling. However, RA is required for the combined action of TTX and NMDA blockade- as there are no changes in scaling with TTX alone. In this regard it is interesting to note that the RA does not affect spine morphology and number. Zhang and colleagues confirmed the impaired synaptic scaling in neuronal cultures derived from patients with FXS (Zhang et al., 2018) and the role of RA as mediator of synaptic scaling. The RA action is effective both on excitatory and inhibitory synapses. Interestingly, RA is one of the mediators of the post- to presynaptic communication and could be involved in linking the post-synaptic events to pre-synaptic adjustments. In FXS, the imbalance in protein synthesis determines a dysregulation in RA which is important at postsynaptic level, but also at the presynaptic level with the regulation of EPSC frequencies (Wang et al., 2011; McCarthy et al., 2012).

Synaptic downscaling – the scaling down in response to increased synaptic activity- is also altered in *Fmr1* KO mice. One of the mechanisms of downscaling is the degradation of AMPA receptor through ubiquitination (Lee et al., 2018). The ubiquitination of AMPA receptors is mediated by a complex cascade of molecules, which includes cell-cycle molecules and phosphatases, and FMRP interferes with the mechanism that leads to homeostatic-dependent ubiquitination.

It is worth of note that the Neuroligin-Neurexin complexes, involved in circuitry development and function is also essential for presynaptic homeostatic plasticity (Sons et al., 2006). Several molecular studies in RTT and FXS report that these molecules are targets of FMRP and MeCP2 (Darnell et al., 2011; Gulmez Karaca et al., 2018; Maurin et al., 2018; Raman et al., 2018), suggesting that impaired homeostatic plasticity in these syndromes may be mediated by deficits in Neuroligin or Neurexin.

MOLECULES AND PATHWAYS CONTROLLING CHANGES IN SYNAPTIC STRENGTH AND CONNECTIVITY IN RETT SYNDROME AND FRAGILE X SYNDROME

The alteration in several forms of plasticity observed in RTT and FXS can be explained considering that many molecular targets of MeCP2 and FMRP are involved in the regulation of synaptic function. The identification of these molecular regulators can shed light on the neurobiology of RTT and FXS and can suggest strategies for treatment. In this section we will examine several of these molecules and pathways (**Table 5**).

Brain derived neurotrophic factor (BDNF) controls brain development and function, and it is involved in activity dependent plasticity. Its expression is highly specific and functionally defined in the mammalian brain (Kowiański et al., 2018). BDNF expression is dependent on the neurodevelopmental stage, and it is present in several different forms that bind different receptors. Pre-Pro-BDNF is concentrated at the endoplasmic reticulum before becoming pro-BDNF at the Golgi apparatus (Foltran and Diaz, 2016). Pro-BDNF is highly expressed during early postnatal development and binds p75 Neurotrophin Receptor (p75NTR) and Sortilin receptor, with a particular polymorphism Val66Met dictating the receptor binding properties (Anastasia et al., 2013). Meanwhile the mature BDNF protein (mBDNF) is present more during adulthood and binds the tyrosine kinase B receptor (TrkB) (Reichardt, 2006).

All these receptors are located on the membranes and in intracellular compartments. The complex resulting from pro-BDNF, Sortilin receptor, and p75NTR signals to RhoA, NFKB and JNK related pathways. These pathways have roles in neurodevelopment, survival and apoptosis respectively (Reichardt, 2006). mBDNF binding to TrkB results in receptor dimerization and phosphorylation on membrane lipid rafts. This complex is also associated with a number of downstream signaling pathways including PI3K, mitogen-activated protein kinase (MAPK), PLC-gamma and GTPases of the Rho family all with a range of neuronal functions (Suzuki et al., 2004). The amount of neuronal cellular processes that BDNF effects means that its expression is highly relevant to synaptic plasticity and functioning. Indeed decrease in BDNF concentration inhibits synaptogenesis and dendritic arborization (Wang et al., 2015).

Brain derived neurotrophic factor administration in control mice increases the synaptic localization of PSD95. This effect is suppressed in *Fmr1* KO mice, but it can be retrieved by inhibition of mTORC-S6K1 signaling (Yang et al., 2019). PSD95 is one of the core postsynaptic proteins that functions by regulating activity of excitatory neurotransmitter receptors (Keith and El-Husseini, 2008), and its expression is modulated by FMRP (Muddashetty et al., 2011; Xing and Bassell, 2013; Ifrim et al., 2015).

Brain derived neurotrophic factor level is deficient in *Mecp2* KO mouse brain and, consistently, its overexpression has been shown to reverse some RTT phenotypes (Chang et al., 2006). In patients with RTT, BDNF serum and cerebrospinal fluid (CSF)

TABLE 5 | Pathways implicated in Rett syndrome and Fragile X syndrome.

Source	Region/Sample	Experiment	Findings	References
Brain-derived neurotrophic factor signaling pathway				
Mecp2$^{-/Y-}$, Conditional BDNF-over-expression	CA2 neurons	Behavioral assessment, electrophysiology, immunohistochemistry	BDNF overexpression reverses some RTT phenotypes	Chang et al., 2006
Patients with RTT	Serum and CSF	Patient studies	No changes in BDNF expression in patients with RTT vs. healthy controls	Vanhala et al., 1998
Mecp2$^{-/y}$, *patients with RTT*	Cerebrum, frontal cortex, whole brains (mice)	Chromatin immunoprecipitation, qPCR	↓BDNF expression↑; TrkB	Abuhatzira et al., 2007; Deng et al., 2007
Mecp2$^{-/y}$	Hippocampal glutamatergic neurons, CA1	Immunofluorescence	↓PSD95; (1–3)IGF1 restores PSD95 levels	Chao et al., 2007; Tropea et al., 2009
Fmr1$^{-/y}$	Hippocampal neurons (P0)	Western blotting	↓PSD95 localization; restored by inhibition of mTORC-S6K1 signaling	Yang et al., 2019
Fmr1$^{-/y}$	Primary cortical cultures (14–15DIV; E15), hippocampal neuronal cultures (E19)	Immunofluorescence, western blotting, mRNA stability assay	↓PSD95; FMRP binds to and stabilize Psd95 mRNA	Todd et al., 2003; Zalfa et al., 2007
Insulin-like growth factor 1 signaling pathway				
Mecp2$^{-/y}$	CSF	Patient studies	No changes in IGF1 expression	Riikonen, 2003
Mecp2$^{-/y}$, *Mecp2*$^{-/+}$	Motor cortex, cortical slices	Behavioral assessment, immunocytochemistry, electrophysiology	IGF1 improves several RTT symptoms incl. cortical plasticity	Tropea et al., 2009; Castro et al., 2014; Khwaja et al., 2014; O'Leary et al., 2018
Fmr1$^{-/y}$	Testes	Western blot, *Igf1r* knockout	Correcting IGF1R levels reduces macro-orchidism	Wise, 2017
Fmr1$^{-/y}$, *Patients with FXS*	Mice (14 weeks), primary hippocampal cell cultures (17 DIV)	Clinical trials, behavioral assessment, kinase assays	NNZ-2566 administration improves patients' symptom scoring	Deacon et al., 2015; Berry-Kravis et al., 2020
Cyclic adenosine monophosphate (cAMP) response element binding protein signaling pathway				
MECP2T$^{158M/T158M}$ *hESC, MECP2-V247fs-MT iPSC, Mecp2*$^{-/+}$	hESC differentiated into forebrain neurons, iPSC	Electrophysiology, western blotting, behavioral assessment	↓CREB; Correcting CREB levels improves some RTT phenotypes	Bu et al., 2017
SWR/J mice, dfmr1$^{3/+}$ Drosophila	SWR/J mice (15–25 weeks,	qPCR, western blotting, immunofluorescence, behavioral assessment	*Fmr1* is bound by CREB	Kanellopoulos et al., 2012; Rani and Prasad, 2015
Phosphatidylinositol-3-kinases signaling pathway				
Mecp2^{308}, *Mecp2*^{tm1Jae}	Male (*Mecp2*^{308}, 5 months), cortical neurons (P1)	Behavioral assessment, qPCR, western blotting, immune-histochemistry	↓PI3K pathway activation	Ricciardi et al., 2011; Yuan et al., 2020
Fmr1$^{-/y}$	Primary hippocampal neurons (E17)	Western blotting, immune-histochemistry, kinase assays	↑PI3K pathway activation	Gross et al., 2010
Fmr1$^{-/y}$	Cortex, cerebellum (P11–13), hippocampus (P28–32) Hippocampal slices (4–6 weeks)	Immuno-histochemistry, bioinformatics, qPCR, electrophysiology	↑mTOR phosphorylation	Sharma et al., 2010; Casingal et al., 2020
Mitogen-activated protein kinase signaling pathway				
Mecp2$^{-/y}$	Motor cortex, cortical slices	Behavioral assessment, immuno-cytochemistry, electrophysiology	↓MAPK activation; rhIGF1 increases activation	Castro et al., 2014
Fmr1$^{-/y}$	Mice (14 weeks), primary hippocampal cell cultures (17 DIV)	Behavioral assessment, kinase assays	↑MAPK activation; Corrected by NNZ-2566	Deacon et al., 2015
Bioenergetics				
Patients with RTT	34 patients with RTT, 37 healthy controls	Metabolomic analysis	Metabolic dysfunction, oxidative stress.	Neul et al., 2020
Mecp2$^{tm1.1Bird}$, *Patients with RTT*	Isolated microglia, primary hippocampal cell cultures, fibroblasts isolated from patients with RTT	Immunofluorescence, qPCR, imaging studies, western blotting, bioenergetic assays	↓Microglial viability; ↓Microglia numbers; ↑ROS; ↓ATP production; ↑Glutamate	Jin et al., 2015; Crivellari et al., 2021

(Continued)

TABLE 5 | (Continued)

Source	Region/Sample	Experiment	Findings	References
Fmr1$^{-/y}$	Fibroblasts cell lines, synaptosomes, primary hippocampal (E19) and cortical cell cultures (P0–P2)	Behavioral assessment, immune-precipitation, western blotting, qPCR, bioenergetic assay	Mitochondrial proton leak	Licznerski et al., 2020
Fmr1$^{-/y}$	Brain slices, macrophages, total brain; (2–6 months)	Bioenergetic assay,	↑ROS; ↑Lipid peroxidation; ↑Protein oxidation; ↑NADPH oxidase activity	El Bekay et al., 2007
Fmr1$^{-/y}$	Various	Review	↑Metabolites from superoxide attack on lipids ↑ROS	Maurin et al., 2014

Main findings of studies reporting signaling and pathway dysfunctions in Rett syndrome and Fragile X syndrome. Mecp2, methyl-CpG binding protein 2 gene; BDNF, brain-derived neurotrophic factor; RTT, Rett syndrome; CSF, cerebrospinal fluid; TrkB, tropomycin receptor kinase B; Fmr1, fragile X mental retardation 1 gene, PSD95, postsynaptic density protein 95; DIV, days in vitro; FRMP, fragile X mental retardation protein; IGF1, insulin-like growth factor 1; Igf1r/IGF1R, insulin-like growth factor 1 receptor; NNZ-2566, (1–3)IGF1 tripeptide; CREB, cAMP response element binding protein; hESC, human embryonic stem cells; iPSC, induced pluripotent stem cells; PI3K, phosphatidylinositol-3-kinase; mTOR, mammalian target of rapamycin; MAPK, mitogen-activated protein kinase; rhIGF1, recombinant human insulin-like growth factor 1; ROS, reactive oxygen species.

protein levels have been found to be no different from healthy controls (Vanhala et al., 1998), while in the brain the BDNF level is decreased and TrkB level is increased (Abuhatzira et al., 2007; Deng et al., 2007).

Insulin-Like Growth Factor 1

Another factor influencing the intracellular pathways controlling synaptic strength is IGF1, which is a protein involved in growth, maturation, and neuronal development. Although CSF levels of Insulin-Like Growth Factor 1 (IGF1) have been found to be unchanged in RTT (Riikonen, 2003), both the full IGF1 molecule, and its functionally active cleavage product (1-3)IGF1 have been shown to ameliorate symptoms of the RTT pathophysiology (Tropea et al., 2009; Castro et al., 2014; Khwaja et al., 2014; O'Leary et al., 2018). IGF1 and (1-3)IGF1 administration in a RTT mouse model increases PSD95, dendritic arborization and excitatory current. Interestingly, these treatments also appear to re-establish cortical plasticity in *Mecp2* KO mice to levels observed in controls (Tropea et al., 2009; Castro et al., 2014). IGF1 signaling occurs primarily through PI3K-AKT and MAPK pathways (Fernandez and Torres-Alemán, 2012). IGF1R activates PI3K-AKT functions to increase neuronal survival (Dudek et al., 1997), while prolonged administration of IGF1 with growth hormone, determines pro-inflammatory responses via activation of MAPK (Wolters et al., 2017). IGF signaling to a lesser extent has been implicated in FXS, where correcting the low level of IGF1R was found to reduce macro-orchidism (enlarged testes) a phenotype characterizing all the adult male patients with FXS (Wise, 2017). More promising evidence comes from the use of the (1-3)IGF1 analog, NNZ-2566 (Trofinetide) as a treatment for FXS; in fact mouse models of FXS treated with NNZ-2566 showed improvements in cognitive function and hyperactivity. Also patients with FXS treated with NNZ-2566 improved in a number of clinical scoring tools (Deacon et al., 2015; Berry-Kravis et al., 2020), but further clinical tests are required to confirm the benefits of the treatment.

Both BDNF and IGF1 signals involve the activation of intracellular pathways involving the PI3K and MAPK cascades, which are related to both RTT and FXS and are involved in activity-dependent plasticity.

Cyclic Adenosine Monophosphate Response Element Binding Protein

Cyclic adenosine monophosphate (cAMP) response element binding protein is involved in transcriptional changes induced by synaptic plasticity, including increasing neuronal excitability and synapse strengthening associated to LTP induction (Caracciolo et al., 2018). Transcriptional genes expressed by CREB activation include *c-Fos*, whose protein is linked to memory and learning (Gallo et al., 2018), and the co-localization of CREB and c-Fos is associated with long term synaptic plasticity (Miyashita et al., 2018). This molecule has been found to be decreased in *Mecp2* KO mice and rectifying CREB levels can correct some of the RTT symptoms (Bu et al., 2017). The *Fmr1* gene is thought to be bound and therefore regulated by CREB (Kanellopoulos et al., 2012; Rani and Prasad, 2015), however the relationship of CREB signaling to FXS synaptic plasticity requires further investigation, especially considering the role that FMRP has in the modulation of cAMP and cGMP levels, two molecules upstream the CREB expression (Delhaye and Bardoni, 2021). It was shown that In the hippocampus, Cilostazol (an inhibitor of Phosphodiesterase 3) increases the levels of c-fos and of insulin-like growth factor 1 (IGF-1) (Zhao et al., 2010) and activates CREB in PC12 cells (Zheng and Quirion, 2006). This result suggests a link between the levels of cAMP and cGMP – both targets of PDE3 – and the levels of IGF-1. Remarkably, the inhibition of PDEs both in FXS (PDE2, PDE4, PDE4D) and in RETT (PDE4) has been shown to improve socio-cognitive deficits in animal models and in patients.

Phosphatidylinositol-3-Kinases

Phosphatidylinositol-3-kinases (PI3K) are a family of intracellular signaling molecules functioning downstream of G protein coupled receptors and tyrosine kinases.

Once activated, PI3K subsequently phosphorylates AKT which regulates cell cycle and apoptosis (Chalhoub and Baker, 2009). Further downstream of AKT phosphorylation, is the mammalian Target of Rapamycin (mTOR) whose activation

regulates nutrition, energy sensing and growth (Zoncu et al., 2011). In *Mecp2* KO mice the activation of the PI3K/AKT/mTOR pathway is reduced, while in FXS it is increased. The alterations in PI3K/AKT/mTOR level in *Mecp2* KO mice can be restored using IGF1, and treatment with PI3K antagonists rescue FXS defects (Gross et al., 2010; Ricciardi et al., 2011; Yuan et al., 2020).

Alterations of FMRP levels affect the mGluR-PI3K-AKT-mTOR cascade. In normal conditions mGluR-dependent LTD requires rapid translation of dendritic mRNA, but in *Fmr1* KO mice LTD it is enhanced and insensitive to inhibition of protein synthesis (Huber et al., 2002; Nosyreva and Huber, 2006). This insensitivity is due to the de-repression of FMRP, which causes increased basal levels of mGluR-stimulated checkpoint proteins (Thomazeau et al., 2020). Hence in FXS, mGluR-LTD is decoupled from protein synthesis/mTOR activation. Interestingly in *Fmr1* KO mice, mTOR phosphorylation is increased in embryonic neocortex and in postnatal hippocampus samples (Sharma et al., 2010; Casingal et al., 2020).

Mitogen-Activated Protein Kinase

The MAPK signaling pathway includes extracellular signal-Regulated Kinase 1 and 2 (ERK1 and ERK2), which are essential for neuronal transcriptional events, including synaptic plasticity, learning and memory (Thomas and Huganir, 2004). When *Mecp2* KO mice are treated with recombinant human IGF1, both AKT, ERK1, and ERK2 levels are increased in conjunction with the increase of the post-synaptic marker PSD95 (Castro et al., 2014). The MAPK pathway is upregulated in *Fmr1* KO mice, and is modulated by NNZ-2566 (Deacon et al., 2015), suggesting that mechanisms controlling plasticity may be potential targets of therapeutics in FXS and RTT, although the mechanisms of action of NNZ-2566 requires further investigation.

PSD95

Also at the synaptic level, MeCP2 and FMRP control the expression and localization of PSD95, which is strongly related to synaptic strength in excitatory synapses. In the hippocampus, MeCP2 controls the number of glutamatergic synapses. VGLUT1 and PSD95, which are respectively pre- and postsynaptic markers, and they are both downregulated upon loss of MeCP2 in mutant mice. Conversely, a two-fold increase of MeCP2 expression, determines an increase in density and colocalization of these two markers (Chao et al., 2007). PSD95 levels are rescued by (1-3)IGF1 to levels comparable in wild type animals (Tropea et al., 2009) achieving the same phenotype as double mutants for loss and doubling of MeCP2 (Collins et al., 2004; Chao et al., 2007). PSD-95 expression is also deregulated in *Fmr1* KO mice. FMRP binds to PSD95 mRNA *in vivo* (Todd et al., 2003; Zalfa et al., 2007), suggesting that FMRP stabilizes the PSD95 transcript, leading to adequate expression levels of PSD95 (Zalfa et al., 2007).

Bioenergetics

All energy-demanding activities, including synaptic function and plasticity, are dependent on bioenergetics, which appears to be dysfunctional in both RTT and FXS. Recent works in both FXS (Mithal and Chandel, 2020) and RTT (Neul et al., 2020) pointed at dysfunctions in mitochondria: the organelles devoted to produce the energy necessary for neuronal function. Alteration in bioenergetics has been proposed for RTT (Jin et al., 2015; Crivellari et al., 2021) and FXS (D'Antoni et al., 2019), and reflect the evolutionary need to match the cognitive function with the capacity of producing the adequate supply of energy to fulfill the requests. The link between energy metabolism and cognition has been well reviewed, and it appears clear that several brain disorders are now depending on the capacity of the organism to provide the fuel requested by the brain and to control the number

TABLE 6 | Astrocyte function in Rett syndrome and Fragile X syndrome.

Source	Region/Sample	Experiment	Findings	References
$Mecp2^{-/y}$	Hippocampal neurons (P1), cortical astrocytes (P1–P2)	Astrocyte/neuron co-culture, immune-cytochemistry	$Mecp2^{-/y}$ astrocytes negatively influence dendrite arborization	Ballas et al., 2009
$Mecp2^{Stop/y}$	Hippocampal neurons (3 months +)	Immunohistochemistry, behavioral assessment	Re-expression of *Mecp2* rescues dendrite morphology, locomotor and respiratory phenotypes	Lioy et al., 2011
$Mecp2^{tm1.1Bird}$	Primary astrocyte cultures (P1) from cerebral cortex	Expression microarray, ChIP-seq	Astrocytes express a unique gene profile incl. synaptic genes	Yasui et al., 2013
$Fmr1^{-/y}$	Hippocampal neurons, Primary astrocyte cultures (P0-P1)	Astrocyte/neuron co-culture, immune-cytochemistry	*Fmr1* astrocytes-neuron co-cultures results in abnormal increased dendritic protrusions	Jacobs and Doering, 2010
$Fmr1^{-/y}$	Conditional knockout and conditional restored astrocytes (P24–P30, P38–P45), cortical slices	Behavioral assessment, Whole cell patch clamp	Loss of FMRP: ↑Cortical activity, ↑Locomotor activity, ↓Social novelty preference and memory acquisition deficits; Corrected by *Fmr1* reactivation	Jin et al., 2021
$Fmr1^{-/y}$	iPSC from patients with FXS differentiated into astrocytes	RNA sequencing, immunocytochemistry.	↑uPA expression that alters neuronal phosphorylation of TrkB	Peteri et al., 2021

Main findings of studies reporting on astrocyte function and morphology in Rett syndrome and Fragile X syndrome. Abbreviations: Mecp2, methyl-CpG binding protein 2 gene; Fmr1, fragile X mental retardation 1 gene, FRMP, fragile X mental retardation protein; iPSC, induced pluripotent stem cell; FXS, Fragile X syndrome; uPA, urokinase plasminogen activator; TrkB tropomycin receptor kinase B.

of oxidative species, which are the natural side products of aerobic metabolism. Therefore, the ability to produce energy goes hand in hand with the capacity to control the reactive oxygen species and the possible damage created by an excess of these radicals. Considering the oxidative stress in FXS, it is interesting to underline that El Bekay et al. (2007) found that *Fmr1* KO mouse brains have higher levels of reactive oxygen species, nicotinamide adenine dinucleotide phosphate (NADPH)-oxidase activation, lipid peroxidation and protein oxidation compared to wild type mice. In the cortex of *Fmr1* KO it was also reported an increased level of metabolites that result from the attack of unsaturated lipids by the superoxide anion (Maurin et al., 2014). In normal conditions, the superoxide anion is detoxified by Sod1, the level of which is reduced in the absence of FMRP (Bechara et al., 2009), thus providing a source of oxidative stress (Maurin et al., 2014).

It is also worth mentioning that there is a two-way interaction between the systems controlling the production of energy in the cell, and the ion homeostasis (Castaldo et al., 2009), and that such interaction controls the onset and progression of neurodegeneration. These additional mechanisms should be taken into account for uncovering the underlying mechanisms in brain disorders and for designing to routes of treatment.

THE CONTRIBUTIONS OF ASTROCYTES

Considering that non-neuronal cells are involved in synaptic function and plasticity, we now discuss the contribution of astrocytes in cellular mechanisms of RTT and FXS (**Table 6**).

Astrocytes have been largely studied in RTT with a smaller body of research carried out in FXS. Astrocytes express both MeCP2 and FMRP. There is clear evidence that glial cells support normal neuronal growth and morphology, and in fact, both in RTT and FXS the co-culturing of astrocytes and neurons influence the morphology of neuronal arborization. In RTT coculturing of *Mecp2*$^{-/y}$ astrocytes with wildtype hippocampal neurons stunts dendrite arborization and cannot sustain typical cell growth. Conversely, culturing *Mecp2* KO neurons with wildtype astrocytes results in typical dendrite morphology (Ballas et al., 2009). Re-expression of *Mecp2* in astrocytes of *Mecp2* deficient mice improves locomotor and respiratory phenotypes; moreover, re-expression of *Mecp2* in astrocytes rescues mutant neuron dendritic morphology (Lioy et al., 2011). Additionally, astrocyte gene expression profiling has identified uniquely dysregulated genes because of *Mecp2* deficiency. These genes include *Cntn1*, *Syn2*, *Gabrg1*, and *Gria1*, which function at the tripartite synapse (Yasui et al., 2013). These studies suggests that MeCP2 deficiency in astrocytes contribute to the RTT phenotype.

Fragile X mental retardation protein is expressed in astrocytes and cocultures of *Fmr1* KO astrocytes with wildtype hippocampal neurons result in neurons with abnormal increased dendritic protrusions (Jacobs and Doering, 2010). While there is an increase in dendritic density, there is reduction in overall dendrite length. There is also a significant decrease in pre- and postsynaptic proteins. Interestingly, coculturing *Fmr1* KO neurons with wildtype neurons rescues the morphological abnormalities to near wildtype phenotype (Cheng et al., 2012). These results suggest that astrocytes are implicated in neuronal dendritic morphology also in FXS.

Recently, Jin and co-workers (Kang et al., 2021) provided evidence that FMRP mediates synaptic connectivity through astrocytes and therefore controls learning and behavior. By using conditional knockout (cKO) and conditional restored (cON) mice in astrocytes, they find that loss of FMRP results in cortical hyperactivity, increased locomotor activity, reduced social novelty preference and deficit of memory acquisition. Reactivation of the astrocyte *Fmr1* rescues these phenotypes (Jin et al., 2021).

Interestingly, in human FXS astrocytes generated from human induced pluripotent stem cells an increased expression of urokinase plasminogen activator (uPA), which modulates degradation of extracellular matrix, was reported. Increased uPA augmented neuronal phosphorylation of TrkB within the docking site for the phospholipase-Cγ1 (PLCγ1), indicating effects of uPA on neuronal plasticity (Peteri et al., 2021) and connecting this molecular alteration to the BDNF pathway.

CONCLUSION

In recent years it has become clear that neurodevelopmental disorders share common molecular mechanisms, and that their complex clinical presentation results from the interaction of genetic and environmental factors. Genetic studies are growing in power and are showing that genes involved in synaptic function are major risk factors for neurodevelopmental disorders, but other mechanisms, such as neuroimmunity, and mitochondrial functions are also emerging as contributors to the onset and progression of several disorders. In this context, the study of convergent and divergent mechanisms between RTT and FXS can be instructive in understanding the general biological mechanisms that underlie a variety of disorders, including those with multi-genic components. Encouraging results in therapeutic strategies for RTT (Glaze et al., 2019) and FXS (Berry-Kravis et al., 2020) confirm the perspective that some treatments can be effective for multiple conditions, and foster research that uncover overlapping mechanisms across disorders. In line with this perspective, our review suggests that the analysis of common and divergent mechanisms controlling synaptic function and plasticity can instruct new criteria for the classification of neurodevelopmental disorders, with applications to diagnosis, prognosis, and drug discovery.

AUTHOR CONTRIBUTIONS

DT, SS, and SB contributed to the initial draft of the manuscript. DT, BB, and SB revised the manuscript. All authors discussed and provided the input on the manuscript.

FUNDING

DT research is partially supported by: IRSF (3507-207417 grant), Meath Foundation (Research award 2019), Fondation

Jérôme Lejeune (DT Project#1935), and Science Foundation Ireland (SFI) under Grant Number 16/RC/3948 and co-funded under the European Regional Development Fund and by FutureNeuro industry partners. BB is funded by Agence Nationale de la Recherche ANR-20-CE16-0016 and ANR-15-IDEX-0001, Fondation Jérôme Lejeune (Project #2023). DT and BB acknowledge the Ulysses Project 2019 (Irish Research Council & Ambassade de France en Irlande).

REFERENCES

Abdala, A. P., Toward, M. A., Dutschmann, M., Bissonnette, J. M., and Paton, J. F. R. (2016). Deficiency of GABAergic synaptic inhibition in the Kolliker-Fuse area underlies respiratory dysrhythmia in a mouse model of Rett syndrome. *J. Physiol.* 594, 223–237. doi: 10.1113/JP270966

Abuhatzira, L., Makedonski, K., Kaufman, Y., Razin, A., and Shemer, R. (2007). MeCP2 deficiency in the brain decreases BDNF levels by REST/CoREST-mediated repression and increases TRKB production. *Epigenetics* 2, 214–222. doi: 10.4161/epi.2.4.5212

Amir, R. E., Van Den Veyver, I. B., Wan, M., Tran, C. Q., Francke, U., and Zoghbi, H. Y. (1999). Rett syndrome is caused by mutations in X-linked MECP2, encoding methyl- CpG-binding protein 2. *Nat. Genet.* 23, 185–188. doi: 10.1038/13810

Anastasia, A., Deinhardt, K., Chao, M. V., Will, N. E., Irmady, K., Lee, F. S., et al. (2013). Val66Met polymorphism of BDNF alters prodomain structure to induce neuronal growth cone retraction. *Nat. Commun.* 4:2490. doi: 10.1038/ncomms3490

Arbab, T., Battaglia, F. P., Pennartz, C. M. A., and Bosman, C. A. (2018). Abnormal hippocampal theta and gamma hypersynchrony produces network and spike timing disturbances in the Fmr1-KO mouse model of Fragile X syndrome. *Neurobiol. Dis.* 114, 65–73. doi: 10.1016/j.nbd.2018.02.011

Armstrong, D. D. (2005). Neuropathology of Rett syndrome. *J. Child Neurol.* 20, 747–753. doi: 10.1177/08830738050200082401

Arsenault, J., Hooper, A. W. M., Gholizadeh, S., Kong, T., Pacey, L. K., Koxhioni, E., et al. (2020). Interregulation between Fragile X Mental retardation protein and Methyl CpG Binding Protein 2 in the mouse posterior cerebral cortex. *Hum. Mol. Genet.* 29, 3744–3756.

Asaka, Y., Jugloff, D. G. M., Zhang, L., Eubanks, J. H., and Fitzsimonds, R. M. (2006). Hippocampal synaptic plasticity is impaired in the Mecp2-null mouse model of Rett syndrome. *Neurobiol. Dis.* 21, 217–227. doi: 10.1016/j.nbd.2005.07.005

Bach, S., Ryan, N. M., Guasoni, P., Corvin, A. P., El-Nemr, R. A., Khan, D., et al. (2020). Methyl - CpG - binding protein 2 mediates overlapping mechanisms across brain disorders. *Sci. Rep.* 10:22255. doi: 10.1038/s41598-020-79268-0

Bagni, C., and Zukin, R. S. (2019). A synaptic perspective of Fragile X Syndrome and autism spectrum disorders. *Neuron* 101, 1070–1088. doi: 10.1016/j.neuron.2019.02.041

Bakker, C. E., Verheij, C., Willemsen, R., van der Helm, R., Oerlemans, F., Vermey, M., et al. (1994). Fmr1 knockout mice: a model to study fragile X mental retardation. *Cell* 78, 23–33. doi: 10.1016/0092-8674(94)90569-X

Ballas, N., Lioy, D. T., Grunseich, C., and Mandel, G. (2009). Non-cell autonomous influence of MeCP2-deficient glia on neuronal dendritic morphology. *Nat. Neurosci.* 12, 311–317. doi: 10.1038/nn.2275

Banerjee, A., Miller, M. T., Li, K., Sur, M., and Kaufmann, W. E. (2019). Towards a better diagnosis and treatment of Rett syndrome: a model synaptic disorder. *Brain* 142, 239–248. doi: 10.1093/brain/awy323

Banerjee, A., Rikhye, R. V., Breton-Provencher, V., Tangb, X., Li, C., Li, K., et al. (2016). Jointly reduced inhibition and excitation underlies circuit-wide changes in cortical processing in Rett syndrome. *Proc. Natl. Acad. Sci. U.S.A.* 113, E7287–E7296. doi: 10.1073/pnas.1615330113

Baubec, T., Ivá, R., Lienert, F., and Schü Beler, D. (2013). Methylation-Dependent and -Independent Genomic Targeting Principles of the MBD Protein Family. *Cell* 153, 480–492. doi: 10.1016/j.cell.2013.03.011

Bechara, E. G., Didiot, M. C., Melko, M., Davidovic, L., Bensaid, M., Martin, P., et al. (2009). A novel function for fragile X mental retardation protein in translational activation. *PLoS Biol.* 7:e1000016. doi: 10.1371/journal.pbio.1000016

Belichenko, N. P., Belichenko, P. V., Hong, H. L., Mobley, W. C., and Francke, U. (2008). Comparative study of brain morphology in Mecp2 Mutant mouse models of Rett syndrome. *J. Comp. Neurol.* 508, 184–195. doi: 10.1002/cne.21673

Bellini, E., Pavesi, G., Barbiero, I., Bergo, A., Chandola, C., Nawaz, M. S., et al. (2014). MeCP2 post-translational modifications: A mechanism to control its involvement in synaptic plasticity and homeostasis? *Front. Cell. Neurosci.* 8:236. doi: 10.3389/fncel.2014.00236

Berry-Kravis, E., Horrigan, J. P., Tartaglia, N., Hagerman, R., Kolevzon, A., Erickson, C. A., et al. (2020). A double-blind, randomized, placebo-controlled clinical study of trofinetide in the treatment of Fragile X Syndrome. *Pediatr. Neurol.* 110, 30–41. doi: 10.1016/j.pediatrneurol.2020.04.019

Blackman, M. P., Djukic, B., Nelson, S. B., and Turrigiano, G. G. (2012). A critical and cell-autonomous role for MeCP2 in synaptic scaling up. *J. Neurosci.* 32, 13529–13536. doi: 10.1523/JNEUROSCI.3077-12.2012

Bodda, C., Tantra, M., Mollajew, R., Arunachalam, J. P., Laccone, F. A., Can, K., et al. (2013). Mild overexpression of Mecp2 in mice causes a higher susceptibility toward seizures. *Am. J. Pathol.* 183, 195–210. doi: 10.1016/j.ajpath.2013.03.019

Bostrom, C., Yau, S.-Y., Majaess, N., Vetrici, M., Gil-Mohapel, J., and Christie, B. R. (2016). Hippocampal dysfunction and cognitive impairment in Fragile-X Syndrome. *Neurosci. Biobehav. Rev.* 68, 563–574. doi: 10.1016/j.neubiorev.2016.06.033

Bu, Q., Wang, A., Hamzah, H., Waldman, A., Jiang, K., Dong, Q., et al. (2017). CREB signaling is involved in rett syndrome pathogenesis. *J. Neurosci.* 37, 3671–3685. doi: 10.1523/JNEUROSCI.3735-16.2017

Calfa, G., Li, W., Rutherford, J. M., and Pozzo-Miller, L. (2015). Excitation/Inhibition imbalance and impaired synaptic inhibition in hippocampal Area CA3 of Mecp2 Knockout Mice. *Hippocampus* 25, 159–168. doi: 10.1002/hipo.22360

Caracciolo, L., Marosi, M., Mazzitelli, J., Latifi, S., Sano, Y., Galvan, L., et al. (2018). CREB controls cortical circuit plasticity and functional recovery after stroke. *Nat. Commun.* 9:2250. doi: 10.1038/s41467-018-04445-9

Casingal, C. R., Kikkawa, T., Inada, H., Sasaki, Y., and Osumi, N. (2020). Identification of FMRP target mRNAs in the developmental brain: FMRP might coordinate Ras/MAPK, Wnt/β-catenin, and mTOR signaling during corticogenesis. *Mol. Brain* 13:167. doi: 10.1186/s13041-020-00706-1

Castagnola, S., Cazareth, J., Lebrigand, K., Jarjat, M., Magnone, V., Delhaye, S., et al. (2020). Agonist-induced functional analysis and cell sorting associated with single-cell transcriptomics characterizes cell subtypes in normal and pathological brain. *Genome Res.* 30, 1633–1642. doi: 10.1101/gr.262717.120

Castaldo, P., Cataldi, M., Magi, S., Lariccia, V., Arcangeli, S., and Amoroso, S. (2009). Role of the mitochondrial sodium/calcium exchanger in neuronal physiology and in the pathogenesis of neurological diseases. *Prog. Neurobiol.* 87, 58–79. doi: 10.1016/j.pneurobio.2008.09.017

Castrén, M. L., and Castrén, E. (2014). BDNF in fragile X syndrome. *Neuropharmacology* 76, 729–736. doi: 10.1016/j.neuropharm.2013.05.018

Castro, J., Garcia, R. I., Kwok, S., Banerjee, A., Petravicz, J., Woodson, J., et al. (2014). Functional recovery with recombinant human IGF1 treatment in a mouse model of Rett Syndrome. *Proc. Natl. Acad. Sci. U.S.A.* 111, 9941–9946. doi: 10.1073/pnas.1311685111

Chalhoub, N., and Baker, S. J. (2009). PTEN and the PI3-kinase pathway in cancer. *Annu. Rev. Pathol. Mech. Dis.* 4, 127–150. doi: 10.1146/annurev.pathol.4.110807.092311

Chang, Q., Khare, G., Dani, V., Nelson, S., and Jaenisch, R. (2006). The disease progression of Mecp2 mutant mice is affected by the level of BDNF expression. *Neuron* 49, 341–348. doi: 10.1016/j.neuron.2005.12.027

Chao, H. T., Zoghbi, H. Y., and Rosenmund, C. (2007). MeCP2 controls excitatory synaptic strength by regulating glutamatergic synapse number. *Neuron* 56, 58–65. doi: 10.1016/j.neuron.2007.08.018

Chao, H.-T. T., Chen, H., Samaco, R. C., Xue, M., Chahrour, M., Yoo, J., et al. (2010). Dysfunction in GABA signalling mediates autism-like stereotypies

and Rett syndrome phenotypes. *Nature* 468, 263–269. doi: 10.1038/nature09582

Chen, R. Z., Akbarian, S., Tudor, M., and Jaenisch, R. (2001). Deficiency of methyl-CpG binding protein-2 in CNS neurons results in a Rett-like phenotype in mice. *Nat. Genet.* 27, 327–331. doi: 10.1038/85906

Cheng, C., Sourial, M., and Doering, L. C. (2012). Astrocytes and Developmental Plasticity in Fragile X. *Neural Plast.* 2012:197491. doi: 10.1155/2012/197491

Citri, A., and Malenka, R. C. (2008). Synaptic plasticity: multiple forms, functions, and mechanisms. *Neuropsychopharmacology* 33, 18–41. doi: 10.1038/sj.npp.1301559

Collins, A. L., Levenson, J. M., Vilaythong, A. P., Richman, R., Armstrong, D. L., Noebels, J. L., et al. (2004). Mild overexpression of MeCP2 causes a progressive neurological disorder in mice. *Hum. Mol. Genet.* 13, 2679–2689. doi: 10.1093/hmg/ddh282

Comery, T. A., Harris, J. B., Willems, P. J., Oostra, B. A., Irwin, S. A., Weiler, I. J., et al. (1997). Abnormal dendritic spines in fragile X knockout mice: maturation and pruning deficits. *Proc. Natl. Acad. Sci. U.S.A.* 94, 5401–5404. doi: 10.1073/pnas.94.10.5401

Contractor, A., Klyachko, V. A., and Portera-Cailliau, C. (2015). Altered neuronal and circuit excitability in Fragile X syndrome. *Neuron* 87, 699–715. doi: 10.1016/j.neuron.2015.06.017

Cortelazzo, A., De Felice, C., Guy, J., Timperio, A. M., Zolla, L., Guerranti, R., et al. (2020). Brain protein changes in Mecp2 mouse mutant models: effects on disease progression of Mecp2 brain specific gene reactivation. *J. Proteomics* 210:103537.

Crivellari, I., Pecorelli, A., Cordone, V., Marchi, S., Pinton, P., Hayek, J., et al. (2021). Impaired mitochondrial quality control in Rett Syndrome. *Arch. Biochem. Biophys.* 700:108790. doi: 10.1016/j.abb.2021.108790

Dahlhaus, R. (2018). Of men and mice: modeling the fragile X syndrome. *Front. Mol. Neurosci.* 11:41. doi: 10.3389/fnmol.2018.00041

Dani, V. S., Chang, Q., Maffei, A., Turrigiano, G. G., Jaenisch, R., and Nelson, S. B. (2005). Reduced cortical activity due to a shift in the balance between excitation and inhibition in a mouse model of Rett Syndrome. *Proc. Natl. Acad. Sci. U.S.A.* 102, 12560–12565. doi: 10.1073/pnas.0506071102

D'Antoni, S., De Bari, L., Valenti, D., Borro, M., Bonaccorso, C. M., Simmaco, M., et al. (2019). Aberrant mitochondrial bioenergetics in the cerebral cortex of the Fmr1 knockout mouse model of fragile X syndrome. *Biol. Chem.* 401, 497–503. doi: 10.1515/hsz-2019-0221

Darnell, J. C., Van Driesche, S. J., Zhang, C., Hung, K. Y. S., Mele, A., Fraser, C. E., et al. (2011). FMRP stalls ribosomal translocation on mRNAs linked to synaptic function and autism. *Cell* 146, 247–261. doi: 10.1016/j.cell.2011.06.013

Deacon, R. M. J., Glass, L., Snape, M., Hurley, M. J., Altimiras, F. J., Biekofsky, R. R., et al. (2015). NNZ-2566, a Novel Analog of (1–3) IGF-1, as a Potential Therapeutic Agent for Fragile X Syndrome. *Neuromol. Med.* 17, 71–82. doi: 10.1007/s12017-015-8341-2

Delhaye, S., and Bardoni, B. (2021). Role of phosphodiesterases in the pathophysiology of neurodevelopmental disorders. *Mol. Psychiatry*. doi: 10.1038/s41380-020-00997-9

Deng, V., Matagne, V., Banine, F., Frerking, M., Ohliger, P., Budden, S., et al. (2007). FXYD1 is an MeCP2 target gene overexpressed in the brains of Rett syndrome patients and Mecp2-null mice. *Hum. Mol. Genet.* 16, 640–650. doi: 10.1093/hmg/ddm007

Desai, N. S., Casimiro, T. M., Gruber, S. M., and Vanderklish, P. W. (2006). Early postnatal plasticity in neocortex of Fmr1 knockout mice. *J. Neurophysiol.* 96, 1734–1745. doi: 10.1152/jn.00221.2006

Drozd, M., Bardoni, B., and Capovilla, M. (2018). Modeling fragile X syndrome in drosophila. *Front. Mol. Neurosci.* 11:124. doi: 10.3389/fnmol.2018.00124

Dudek, H., Datta, S. R., Franke, T. F., Birnbaum, M. J., Yao, R., Cooper, G. M., et al. (1997). Regulation of neuronal survival by the serine-threonine protein kinase Akt. *Science* 275, 661–665. doi: 10.1126/science.275.5300.661

Durand, S., Patrizi, A., Quast, K. B., Hachigian, L., Pavlyuk, R., Saxena, A., et al. (2012). NMDA receptor regulation prevents regression of visual cortical function in the absence of Mecp2. *Neuron* 76, 1078–1090. doi: 10.1016/j.neuron.2012.12.004

El Bekay, R., Romero-Zerbo, Y., Decara, J., Sanchez-Salido, L., Del Arco-Herrera, I., Rodríguez-De Fonseca, F., et al. (2007). Enhanced markers of oxidative stress, altered antioxidants and NADPH-oxidase activation in brains from Fragile X mental retardation 1-deficient mice, a pathological model for Fragile X syndrome. *Eur. J. Neurosci.* 26, 3169–3180. doi: 10.1111/j.1460-9568.2007.05939.x

Ezeonwuka, C., and Rastegar, M. (2014). MeCP2-related diseases and animal models. *Diseases* 2, 45–70. doi: 10.3390/diseases2010045

Farra, N., Zhang, W. B., Pasceri, P., Eubanks, J. H., Salter, M. W., and Ellis, J. (2012). Rett syndrome induced pluripotent stem cell-derived neurons reveal novel neurophysiological alterations. *Mol. Psychiatry* 17, 1261–1271. doi: 10.1038/mp.2011.180

Fernandez, A. M. M., and Torres-Alemán, I. (2012). The many faces of insulin-like peptide signalling in the brain. *Nat. Rev. Neurosci.* 13, 225–239. doi: 10.1038/nrn3209

Foltran, R. B., and Diaz, S. L. (2016). BDNF isoforms: A round trip ticket between neurogenesis and serotonin? *J. Neurochem.* 138, 204–221. doi: 10.1111/jnc.13658

Gabel, H. W., Kinde, B. Z., Stroud, H., Gilbert, C. S., Harmin, D. A., Kastan, N. R., et al. (2015). Disruption of DNA methylation-dependent long gene repression in Rett syndrome HHS Public Access. *Nature* 522, 89–93. doi: 10.1038/nature14319

Gallo, F. T., Katche, C., Morici, J. F., Medina, J. H., and Weisstaub, N. V. (2018). Immediate early genes, memory and psychiatric disorders: focus on c-Fos, Egr1 and Arc. *Front. Behav. Neurosci.* 12:79. doi: 10.3389/fnbeh.2018.00079

Gibson, J. R., Bartley, A. F., Hays, S. A., and Huber, K. M. (2008). Imbalance of neocortical excitation and inhibition and altered UP states reflect network hyperexcitability in the mouse model of fragile X syndrome. *J. Neurophysiol.* 100, 2615–2626. doi: 10.1152/jn.90752.2008

Glaze, D. G., Neul, J. L., Kaufmann, W. E., Berry-Kravis, E., Condon, S., Stoms, G., et al. (2019). Double-blind, randomized, placebo-controlled study of trofinetide in pediatric Rett syndrome. *Neurology* 92, E1912–E1925. doi: 10.1212/WNL.0000000000007316

Godfraind, J. M., Reyniers, E., De Boulle, K., D'Hooge, R., De Deyn, P. P., Bakker, C. E., et al. (1996). Long-term potentiation in the hippocampus of fragile X knockout mice. *Am. J. Med. Genet.* 64, 246–251.

Greenough, W. T., Klintsova, A. Y., Irwin, S. A., Galvez, R., Bates, K. E., and Weiler, I. J. (2001). Synaptic regulation of protein synthesis and the fragile X protein. *Proc. Natl. Acad. Sci. U.S.A.* 98, 7101–7106. doi: 10.1073/pnas.141145998

Gross, C., Berry-Kravis, E. M., and Bassell, G. J. (2012). Therapeutic strategies in fragile X syndrome: dysregulated mGluR signaling and beyond. *Neuropsychopharmacol.* 37, 178–195. doi: 10.1038/npp.2011.137

Gross, C., Nakamoto, M., Yao, X., Chan, C. B., Yim, S. Y., Ye, K., et al. (2010). Excess phosphoinositide 3-kinase subunit synthesis and activity as a novel therapeutic target in fragile X syndrome. *J. Neurosci.* 30, 10624–10638. doi: 10.1523/JNEUROSCI.0402-10.2010

Gulmez Karaca, K., Brito, D. V. C., Zeuch, B., and Oliveira, A. M. M. (2018). Adult hippocampal MeCP2 preserves the genomic responsiveness to learning required for long-term memory formation. *Neurobiol. Learn. Mem.* 149, 84–97. doi: 10.1016/j.nlm.2018.02.010

Guy, J., Hendrich, B., Holmes, M., Martin, J. E., and Bird, A. (2001). A mouse Mecp2-null mutation causes neurological symptoms that mimic Rett syndrome. *Nat. Genet.* 27, 322–326. doi: 10.1038/85899

He, C. X., and Portera-Cailliau, C. (2013). The trouble with spines in fragile X syndrome: density, maturity and plasticity. *Neuroscience* 251, 120–128. doi: 10.1016/j.neuroscience.2012.03.049

He, L.-J. J., Liu, N., Cheng, T.-L. L., Chen, X.-J. J., Li, Y.-D. D., Shu, Y.-S. S., et al. (2014). Conditional deletion of Mecp2 in parvalbumin-expressing GABAergic cells results in the absence of critical period plasticity. *Nat. Commun.* 5:5036. doi: 10.1038/ncomms6036

He, Q., Arroyo, E. D., Smukowski, S. N., Xu, J., Piochon, C., Savas, J. N., et al. (2019). Critical period inhibition of NKCC1 rectifies synapse plasticity in the somatosensory cortex and restores adult tactile response maps in fragile X mice. *Mol. Psychiatry* 24, 1732–1747. doi: 10.1038/s41380-018-0048-y

Hodges, J. L., Yu, X., Gilmore, A., Bennett, H., Tjia, M., Perna, J. F., et al. (2017). Astrocytic contributions to synaptic and learning abnormalities in a mouse model of Fragile X Syndrome. *Biol. Psychiatry* 82, 139–149. doi: 10.1016/j.biopsych.2016.08.036

Huber, K. M., Gallagher, S. M., Warren, S. T., and Bear, M. F. (2002). Altered synaptic plasticity in a mouse model of fragile X mental retardation. *Proc. Natl. Acad. Sci. U.S.A.* 99, 7746–7750. doi: 10.1073/pnas.122205699

Ifrim, M. F., Williams, K. R., and Bassell, G. J. (2015). Single-molecule imaging of PSD-95 mRNA translation in dendrites and its dysregulation in a mouse model of fragile X syndrome. *J. Neurosci.* 35, 7116–7130. doi: 10.1523/JNEUROSCI.2802-14.2015

Irwin, S. A., Galvez, R., and Greenough, W. T. (2000). Dendritic spine structural anomalies in fragile-X mental retardation syndrome. *Cereb. Cortex* 10, 1038–1044. doi: 10.1093/cercor/10.10.1038

Ito-Ishida, A., Ure, K., Chen, H., Swann, J. W., and Zoghbi, H. Y. (2015). Loss of MeCP2 in parvalbumin-and somatostatin-expressing neurons in mice leads to distinct Rett Syndrome-like Phenotypes. *Neuron* 88, 651–658. doi: 10.1016/j.neuron.2015.10.029

Jacobs, S., and Doering, L. C. (2010). Astrocytes prevent abnormal neuronal development in the fragile X mouse. *J. Neurosci.* 30, 4508–4514. doi: 10.1523/JNEUROSCI.5027-09.2010

Jin, L. W., Horiuchi, M., Wulff, H., Liu, X. B., Cortopassi, G. A., Erickson, J. D., et al. (2015). Dysregulation of Glutamine Transporter SNAT1 in Rett Syndrome Microglia: a mechanism for mitochondrial dysfunction and neurotoxicity. *J. Neurosci.* 35, 2516–2529. doi: 10.1523/JNEUROSCI.2778-14.2015

Jin, S.-X. X., Higashimori, H., Schin, C., Tamashiro, A., Men, Y., Chiang, M. S. R., et al. (2021). Astroglial FMRP modulates synaptic signaling and behavior phenotypes in FXS mouse model. *Glia* 69, 594–608. doi: 10.1002/glia.23915

Kanellopoulos, A. K., Semelidou, O., Kotini, A. G., Anezaki, M., and Skoulakis, E. M. C. (2012). Learning and memory deficits consequent to reduction of the fragile X mental retardation protein result from metabotropic glutamate receptor-mediated inhibition of cAMP signaling in *Drosophila*. *J. Neurosci.* 32, 13111–13124. doi: 10.1523/JNEUROSCI.1347-12.2012

Kang, Y., Zhou, Y., Li, Y., Han, Y., Xu, J., Niu, W., et al. (2021). A human forebrain organoid model of fragile X syndrome exhibits altered neurogenesis and highlights new treatment strategies. *Nat. Neurosci.* 24, 1377–1391. doi: 10.1038/s41593-021-00913-6

Keith, D., and El-Husseini, A. (2008). Excitation control: balancing PSD-95 function at the synapse. *Front. Mol. Neurosci.* 1:4. doi: 10.3389/neuro.02.004.2008

Khwaja, O. S. O. S., Ho, E., Barnes, K. V. K. V., O'Leary, H. M. H. M., Pereira, L. M. L. M., Finkelstein, Y., et al. (2014). Safety, pharmacokinetics, and preliminary assessment of efficacy of mecasermin (recombinant human IGF-1) for the treatment of Rett syndrome. *Proc. Natl. Acad. Sci. U.S.A.* 111, 4596–4601. doi: 10.1073/pnas.1311141111

Kishi, N., and Macklis, J. D. (2004). MECP2 is progressively expressed in post-migratory neurons and is involved in neuronal maturation rather than cell fate decisions. *Mol. Cell. Neurosci.* 27, 306–321. doi: 10.1016/j.mcn.2004.07.006

Koekkoek, S. K. E., Yamaguchi, K., Milojkovic, B. A., Dortland, B. R., Ruigrok, T. J. H., Maex, R., et al. (2005). Deletion of FMR1 in purkinje cells enhances parallel fiber LTD, enlarges spines, and attenuates cerebellar eyelid conditioning in fragile X syndrome. *Neuron* 47, 339–352. doi: 10.1016/j.neuron.2005.07.005

Kowiański, P., Lietzau, G., Czuba, E., Waśkow, M., Steliga, A., and Moryś, J. (2018). BDNF: a key factor with multipotent impact on brain signaling and synaptic plasticity. *Cell. Mol. Neurobiol.* 38, 579–593. doi: 10.1007/s10571-017-0510-4

Kulkarni, P., and Sevilimedu, A. (2020). The known unknowns: missing pieces in *in vivo* models of Fragile X Syndrome. *J. Rare Dis. Res. Treat.* 5, 1–9. doi: 10.29245/2572-9411/2020/1.1190

Lauterborn, J. C., Rex, C. S., Kramár, E., Chen, L. Y., Pandyarajan, V., Lynch, G., et al. (2007). Brain-derived neurotrophic factor rescues synaptic plasticity in a mouse model of fragile X syndrome. *J. Neurosci.* 27, 10685–10694. doi: 10.1523/JNEUROSCI.2624-07.2007

Lee, K. Y., Jewett, K. A., Chung, H. J., and Tsai, N. P. (2018). Loss of fragile X protein FMRP impairs homeostatic synaptic downscaling through tumor suppressor p53 and ubiquitin E3 ligase Nedd4-2. *Hum. Mol. Genet.* 27, 2805–2816. doi: 10.1093/hmg/ddy189

Levenga, J., de Vrij, F. M. S., Buijsen, R. A. M., Li, T., Nieuwenhuizen, I. M., Pop, A., et al. (2011). Subregion-specific dendritic spine abnormalities in the hippocampus of Fmr1 KO mice. *Neurobiol. Learn. Mem.* 95, 467–472. doi: 10.1016/j.nlm.2011.02.009

Li, W., Xu, X., and Pozzo-Miller, L. (2016). Excitatory synapses are stronger in the hippocampus of Rett syndrome mice due to altered synaptic trafficking of AMPA-type glutamate receptors. *Proc. Natl. Acad. Sci. U.S.A.* 113, E1575–E1584. doi: 10.1073/pnas.1517244113

Licznerski, P., Park, H. A., Rolyan, H., Chen, R., Mnatsakanyan, N., Miranda, P., et al. (2020). ATP Synthase c-subunit leak causes aberrant cellular metabolism in fragile X Syndrome. *Cell* 182, 1170–1185.e9. doi: 10.1016/j.cell.2020.07.008

Linda, K., Fiuza, C., and Nadif Kasri, N. (2018). The promise of induced pluripotent stem cells for neurodevelopmental disorders. *Prog. Neuropsychopharmacol. Biol. Psychiatry* 84, 382–391. doi: 10.1016/j.pnpbp.2017.11.009

Lioy, D. T., Garg, S. K., Monaghan, C. E., Raber, J., Foust, K. D., Kaspar, B. K., et al. (2011). A role for glia in the progression of Rett-syndrome. *Nature* 475, 497–500. doi: 10.1038/nature10214

Lozovaya, N., Nardou, R., Tyzio, R., Chiesa, M., Pons-Bennaceur, A., Eftekhari, S., et al. (2019). Early alterations in a mouse model of Rett syndrome: the GABA developmental shift is abolished at birth. *Sci. Rep.* 9:9276. doi: 10.1038/s41598-019-45635-9

Martin, B. S., Corbin, J. G., and Huntsman, M. M. (2014). Deficient tonic GABAergic conductance and synaptic balance in the fragile X syndrome amygdala. *J. Neurophysiol.* 112, 890–902. doi: 10.1152/jn.00597.2013

Maurin, T., and Bardoni, B. (2018). Fragile X mental retardation protein: to be or not to be a translational enhancer. *Front. Mol. Biosci.* 5:113. doi: 10.3389/fmolb.2018.00113

Maurin, T., Lebrigand, K., Castagnola, S., Paquet, A., Jarjat, M., Popa, A., et al. (2018). HITS-CLIP in various brain areas reveals new targets and new modalities of RNA binding by fragile X mental retardation protein. *Nucleic Acids Res.* 46, 6344–6355. doi: 10.1093/nar/gky267

Maurin, T., Zongaro, S., and Bardoni, B. (2014). Fragile X Syndrome: from molecular pathology to therapy. *Neurosci. Biobehav. Rev.* 46, 242–255. doi: 10.1016/j.neubiorev.2014.01.006

Maxwell, S. S., Pelka, G. J., Tam, P. P., and El-Osta, A. (2013). Chromatin context and ncRNA highlight targets of MeCP2 in brain. *RNA Biol.* 10, 1741–1757. doi: 10.4161/rna.26921

McCarthy, D. J., Chen, Y., and Smyth, G. K. (2012). Differential expression analysis of multifactor RNA-Seq experiments with respect to biological variation. *Nucleic Acids Res.* 40, 4288–4297. doi: 10.1093/nar/gks042

Mientjes, E. J., Nieuwenhuizen, I., Kirkpatrick, L., Zu, T., Hoogeveen-Westerveld, M., Severijnen, L., et al. (2006). The generation of a conditional Fmr1 knock out mouse model to study Fmrp function *in vivo*. *Neurobiol. Dis.* 21, 549–555. doi: 10.1016/j.nbd.2005.08.019

Mithal, D. S., and Chandel, N. S. (2020). Mitochondrial dysfunction in Fragile-X Syndrome: plugging the leak may save the ship. *Mol. Cell* 80, 381–383. doi: 10.1016/j.molcel.2020.10.002

Miyashita, T., Kikuchi, E., Horiuchi, J., and Saitoe, M. (2018). Long-Term Memory Engram Cells Are Established by c-Fos/CREB Transcriptional Cycling. *Cell Rep.* 25, 2716–2728. doi: 10.1016/j.celrep.2018.11.022

Moretti, P., Levenson, J. M., Battaglia, F., Atkinson, R., Teague, R., Antalffy, B., et al. (2006). Learning and memory and synaptic plasticity are impaired in a mouse model of Rett syndrome. *J. Neurosci.* 26, 319–327. doi: 10.1523/JNEUROSCI.2623-05.2006

Muddashetty, R. S., Nalavadi, V. C., Gross, C., Yao, X., Xing, L., Laur, O., et al. (2011). Reversible Inhibition of PSD-95 mRNA Translation by miR-125a, FMRP Phosphorylation, and mGluR Signaling. *Mol. Cell* 42, 673–688. doi: 10.1016/j.molcel.2011.05.006

Na, E. S., Nelson, E. D., Adachi, M., Autry, A. E., Mahgoub, M. A., Kavalali, E. T., et al. (2012). A mouse model for MeCP2 duplication syndrome: MeCP2 overexpression impairs learning and memory and synaptic transmission. *J. Neurosci.* 32, 3109–3117. doi: 10.1523/JNEUROSCI.6000-11.2012

Na, E. S., Nelson, E. D., Kavalali, E. T., and Monteggia, L. M. (2013). The impact of MeCP2 loss-or gain-of-function on synaptic plasticity. *Neuropsychopharmacology* 38, 212–219. doi: 10.1038/npp.2012.116

Nakamoto, M., Nalavadi, V., Epstein, M. P., Narayanan, U., Bassell, G. J., and Warren, S. T. (2007). Fragile X mental retardation protein deficiency leads to excessive mGluR5-dependent internalization of AMPA receptors. *Proc. Natl. Acad. Sci. U.S.A.* 104, 15537–15542. doi: 10.1073/pnas.0707484104

Nelson, E. D., Kavalali, E. T., and Monteggia, L. M. (2006). MeCP2-dependent transcriptional repression regulates excitatory neurotransmission. *Curr. Biol.* 16, 710–716. doi: 10.1016/j.cub.2006.02.062

Neul, J. L., Skinner, S. A., Annese, F., Lane, J., Heydemann, P., Jones, M., et al. (2020). Metabolic signatures differentiate Rett syndrome from unaffected siblings. *Front. Integr. Neurosci.* 14:7. doi: 10.3389/fnint.2020.00007

Nimchinsky, E. A., Oberlander, A. M., and Svoboda, K. (2001). Abnormal development of dendritic spines in FMR1 knock-out mice. *J. Neurosci.* 21, 5139–5146. doi: 10.1523/jneurosci.21-14-05139.2001

Nosyreva, E. D., and Huber, K. M. (2006). Metabotropic receptor-dependent long-term depression persists in the absence of protein synthesis in the mouse model of fragile X syndrome. *J. Neurophysiol.* 95, 3291–3295. doi: 10.1152/jn.01316.2005

O'Leary, H. M., Kaufmann, W. E., Barnes, K. V., Rakesh, K., Kapur, K., Tarquinio, D. C., et al. (2018). Placebo-controlled crossover assessment of mecasermin for the treatment of Rett syndrome. *Ann. Clin. Transl. Neurol.* 5, 323–332. doi: 10.1002/acn3.533

Paluszkiewicz, S. M., Olmos-Serrano, J. L., Corbin, J. G., and Huntsman, M. M. (2011). Impaired inhibitory control of cortical synchronization in fragile X syndrome. *J. Neurophysiol.* 106, 2264–2272. doi: 10.1152/jn.00421.2011

Paradee, W., Melikian, H. E., Rasmussen, D. L., Kenneson, A., Conn, P. J., and Warren, S. T. (1999). Fragile X mouse: strain effects of knockout phenotype and evidence suggesting deficient amygdala function. *Neuroscience* 94, 185–192. doi: 10.1016/S0306-4522(99)00285-7

Patel, A. B., Hays, S. A., Bureau, I., Huber, K. M., and Gibson, J. R. (2013). A target cell-specific role for presynaptic Fmr1 in regulating glutamate release onto neocortical fast-spiking inhibitory neurons. *J. Neurosci.* 33, 2593–2604. doi: 10.1523/JNEUROSCI.2447-12.2013

Peteri, U. K., Pitkonen, J., de Toma, I., Nieminen, O., Utami, K. H., Strandin, T. M., et al. (2021). Urokinase plasminogen activator mediates changes in human astrocytes modeling fragile X syndrome. *Glia* 69, 2947–2962. doi: 10.1002/glia.24080

Pieretti, M., Zhang, F., Fu, Y. H., Warren, S. T., Oostra, B. A., Caskey, C. T., et al. (1991). Absence of expression of the FMR-1 gene in fragile X syndrome. *Cell* 66, 817–822. doi: 10.1016/0092-8674(91)90125-I

Pietri, T., Roman, A. C., Guyon, N., Romano, S. A., Washbourne, P., Moens, C. B., et al. (2013). The first mecp2-null zebrafish model shows altered motor behaviors. *Front. Neural Circuits* 7:118. doi: 10.3389/fncir.2013.00118

Pitzianti, M. B., Palombo, A. S., Esposito, S., and Pasini, A. (2019). Rett syndrome in males: the different clinical course in two brothers with the same microduplication MECP2 Xq28. *Int. J. Environ. Res. Public Health* 16:3075. doi: 10.3390/ijerph16173075

Prieto, M., Folci, A., Poupon, G., Schiavi, S., Buzzelli, V., Pronot, M., et al. (2021). Missense mutation of Fmr1 results in impaired AMPAR-mediated plasticity and socio-cognitive deficits in mice. *Nat. Commun.* 12:1557. doi: 10.1038/s41467-021-21820-1

Qiu, Z., Sylwestrak, E. L., Lieberman, D. N., Zhang, Y., Liu, X. Y., and Ghosh, A. (2012). The rett syndrome protein MeCP2 regulates synaptic scaling. *J. Neurosci.* 32, 989–994. doi: 10.1523/JNEUROSCI.0175-11.2012

Raman, A. T., Pohodich, A. E., Wan, Y. W., Yalamanchili, H. K., Lowry, W. E., Zoghbi, H. Y., et al. (2018). Apparent bias toward long gene misregulation in MeCP2 syndromes disappears after controlling for baseline variations. *Nat. Commun.* 9:3225. doi: 10.1038/s41467-018-05627-1

Ramocki, M. B., Peters, S. U., Tavyev, Y. J., Zhang, F., Carvalho, C. M. B., Schaaf, C. P., et al. (2009). Autism and other neuropsychiatric symptoms are prevalent in individuals with MECP2 duplication syndrome. *Ann. Neurol.* 66, 771–782. doi: 10.1002/ana.21715

Ramocki, M. B., Tavyev, Y. J., and Peters, S. U. (2010). The MECP2 Duplication Syndrome. *Am. J. Med. Genet. Part A* 152A, 1079–1088. doi: 10.1002/ajmg.a.33184

Rani, A., and Prasad, S. (2015). A Special Extract of Bacopa monnieri (CDRI-08)-Restored Memory in CoCl2-Hypoxia Mimetic Mice Is Associated with Upregulation of Fmr-1 Gene Expression in Hippocampus. *Evid. Based Complement. Altern. Med.* 2015:347978. doi: 10.1155/2015/347978

Reichardt, L. F. (2006). Neurotrophin-regulated signalling pathways. *Philos. Trans. R. Soc. B Biol. Sci.* 361, 1545–1564. doi: 10.1098/rstb.2006.1894

Reichow, B., George-Puskar, A., Lutz, T., Smith, I. C., and Volkmar, F. R. (2015). Brief report: systematic review of Rett Syndrome in Males. *J. Autism Dev. Disord.* 45, 3377–3383. doi: 10.1007/s10803-015-2519-1

Ricciardi, S., Boggio, E. M., Grosso, S., Lonetti, G., Forlani, G., Stefanelli, G., et al. (2011). Reduced AKT/mTOR signaling and protein synthesis dysregulation in a Rett syndrome animal model. *Hum. Mol. Genet.* 20, 1182–1196. doi: 10.1093/hmg/ddq563

Richter, J. D., and Zhao, X. (2021). The molecular biology of FMRP: new insights into fragile X syndrome. *Nat. Rev. Neurosci.* 22, 209–222. doi: 10.1038/s41583-021-00432-0

Riikonen, R. (2003). Neurotrophic factors in the pathogenesis of Rett syndrome. *J. Child Neurol.* 18, 693–697. doi: 10.1177/08830738030180101101

Rube, H. T., Lee, W., Hejna, M., Chen, H., Yasui, D. H., Hess, J. F., et al. (2016). Sequence features accurately predict genome-wide MeCP2 binding *in vivo*. *Nat. Commun.* 7:11025. doi: 10.1038/ncomms11025

Sawicka, K., Hale, C. R., Park, C. Y., Fak, J. J., Gresack, J. E., Van Driesche, S. J., et al. (2019). FMRP has a cell-type-specific role in CA1 pyramidal neurons to regulate autism-related transcripts and circadian memory. *eLife* 8:e46919. doi: 10.7554/eLife.46919

Sceniak, M. P., Lang, M., Enomoto, A. C., James Howell, C., Hermes, D. J., Katz, D. M., et al. (2016). Mechanisms of functional hypoconnectivity in the medial prefrontal cortex of Mecp2 null mice. *Cereb. Cortex* 26, 1938–1956. doi: 10.1093/cercor/bhv002

Seese, R. R., Babayan, A. H., Katz, A. M., Cox, C. D., Lauterborn, J. C., Lynch, G., et al. (2012). LTP induction translocates cortactin at distant synapses in wild-type but not Fmr1 knock-out mice. *J. Neurosci.* 32, 7403–7413. doi: 10.1523/JNEUROSCI.0968-12.2012

Sharma, A., Hoeffer, C. A., Takayasu, Y., Miyawaki, T., McBride, S. M., Klann, E., et al. (2010). Dysregulation of mTOR signaling in fragile X syndrome. *J. Neurosci.* 30, 694–702. doi: 10.1523/JNEUROSCI.3696-09.2010

Sidorov, M. S., Auerbach, B. D., and Bear, M. F. (2013). Fragile X mental retardation protein and synaptic plasticity. *Mol. Brain* 6, 1–11. doi: 10.1186/1756-6606-6-15

Skene, P. J., Illingworth, R. S., Webb, S., Kerr, A. R. W., James, K. D., Turner, D. J., et al. (2010). Neuronal MeCP2 is expressed at near histone-octamer levels and globally alters the chromatin state. *Mol. Cell* 37, 457–468. doi: 10.1016/j.molcel.2010.01.030

Soden, M. E., and Chen, L. (2010). Fragile X protein FMRP is required for homeostatic plasticity and regulation of synaptic strength by retinoic acid. *J. Neurosci.* 30, 16910–16921. doi: 10.1523/JNEUROSCI.3660-10.2010

Sohal, V. S., and Rubenstein, J. L. R. (2019). Excitation-inhibition balance as a framework for investigating mechanisms in neuropsychiatric disorders. *Mol. Psychiatry* 24, 1248–1257. doi: 10.1038/s41380-019-0426-0

Sohal, V. S., Zhang, F., Yizhar, O., and Deisseroth, K. (2009). Parvalbumin neurons and gamma rhythms enhance cortical circuit performance. *Nature* 459, 698–702. doi: 10.1038/nature07991

Sons, M. S., Busche, N., Strenzke, N., Moser, T., Ernsberger, U., Mooren, F. C., et al. (2006). A-Neurexins are required for efficient transmitter release and synaptic homeostasis at the mouse neuromuscular junction. *Neuroscience* 138, 433–446. doi: 10.1016/j.neuroscience.2005.11.040

Suvrathan, A., and Chattarji, S. (2011). Fragile X syndrome and the amygdala. *Curr. Opin. Neurobiol.* 21, 509–515. doi: 10.1016/J.CONB.2011.04.005

Suzuki, S., Numakawa, T., Shimazu, K., Koshimizu, H., Hara, T., Hatanaka, H., et al. (2004). BDNF-induced recruitment of TrkB receptor into neuronal lipid rafts: roles in synaptic modulation. *J. Cell Biol.* 167, 1205–1215. doi: 10.1083/jcb.200404106

Takeguchi, R., Takahashi, S., Kuroda, M., Tanaka, R., Suzuki, N., Tomonoh, Y., et al. (2020). MeCP2_e2 partially compensates for lack of MeCP2_e1: a male case of Rett syndrome. *Mol. Genet. Genomic Med.* 8:e1088. doi: 10.1002/mgg3.1088

Telias, M., Mayshar, Y., Amit, A., and Ben-Yosef, D. (2015). Molecular mechanisms regulating impaired neurogenesis of Fragile X syndrome human embryonic stem cells. *Stem Cells Dev.* 24, 2353–2365. doi: 10.1089/scd.2015.0220

Thomas, G. M., and Huganir, R. L. (2004). MAPK cascade signalling and synaptic plasticity. *Nat. Rev. Neurosci.* 5, 173–183. doi: 10.1038/nrn1346

Thomazeau, A., Bosch, M., Essayan-Perez, S., Barnes, S. A., De Jesus-Cortes, H., and Bear, M. F. (2020). Dissociation of functional and structural plasticity of dendritic spines during NMDAR and mGluR-dependent long-term synaptic depression in wild-type and fragile X model mice. *Mol. Psychiatry*. doi: 10.1038/s41380-020-0821-6 [Epub ahead of print].

Tian, Y., Yang, C., Shang, S., Cai, Y., Deng, X., Zhang, J., et al. (2017). Loss of FMRP impaired hippocampal long-term plasticity and spatial learning in rats. *Front. Mol. Neurosci.* 10:269. doi: 10.3389/fnmol.2017.00269

Todd, P. K., Mack, K. J., and Malter, J. S. (2003). The fragile X mental retardation protein is required for type-I metabotropic glutamate receptor-dependent

translation of PSD-95. *Proc. Natl. Acad. Sci. U.S.A.* 100, 14374–14378. doi: 10.1073/pnas.2336265100

Tropea, D., Giacometti, E., Wilson, N. R., Beard, C., McCurry, C., Fu, D. D., et al. (2009). Partial reversal of Rett Syndrome-like symptoms in MeCP2 mutant mice. *Proc. Natl. Acad. Sci. U.S.A.* 106, 2029–2034. doi: 10.1073/pnas.0812394106

Vanhala, R., Korhonen, L., Mikelsaar, M., Lindholm, D., and Riikonen, R. (1998). Neurotrophic factors in cerebrospinal fluid and serum of patients with Rett syndrome. *J. Child Neurol.* 13, 429–433. doi: 10.1177/088307389801300903

Vaz, R., Hofmeister, W., and Lindstrand, A. (2019). Zebrafish models of neurodevelopmental disorders: limitations and benefits of current tools and techniques. *Int. J. Mol. Sci.* 20:1296. doi: 10.3390/ijms20061296

Verkerk, A. J. M. H., Pieretti, M., Sutcliffe, J. S., Fu, Y. H., Kuhl, D. P. A., Pizzuti, A., et al. (1991). Identification of a gene (FMR-1) containing a CGG repeat coincident with a breakpoint cluster region exhibiting length variation in fragile X syndrome. *Cell* 65, 905–914. doi: 10.1016/0092-8674(91)90397-H

Vicario, A., Colliva, A., Ratti, A., Davidovic, L., Baj, G., Gricman, Ł, et al. (2015). Dendritic targeting of short and long 3′ UTR BDNF mRNA is regulated by BDNF or NT-3 and distinct sets of RNA-binding proteins. *Front. Mol. Neurosci.* 8:62. doi: 10.3389/fnmol.2015.00062

Wahlstrom-Helgren, S., and Klyachko, V. A. (2015). GABAB receptor-mediated feed-forward circuit dysfunction in the mouse model of fragile X syndrome. *J. Physiol.* 593, 5009–5024. doi: 10.1113/JP271190

Wang, G., Gilbert, J., and Man, H. Y. (2012). AMPA receptor trafficking in homeostatic synaptic plasticity: functional molecules and signaling cascades. *Neural Plast.* 2012:825364. doi: 10.1155/2012/825364

Wang, H., Xu, H., Wu, L. J., Kim, S. S., Chen, T., Koga, K., et al. (2011). Identification of an adenylyl cyclase inhibitor for treating neuropathic and inflammatory pain. *Sci. Transl. Med.* 3:65ra3. doi: 10.1126/scitranslmed.3001269

Wang, L., Chang, X., She, L., Xu, D., Huang, W., and Poo, M. M. (2015). Autocrine action of BDNF on dendrite development of adult-born hippocampal neurons. *J. Neurosci.* 35, 8384–8393. doi: 10.1523/JNEUROSCI.4682-14.2015

Weiler, I. J., Irwin, S. A., Klintsova, A. Y., Spencer, C. M., Brazelton, A. D., Miyashiro, K., et al. (1997). Fragile X mental retardation protein is translated near synapses in response to neurotransmitter activation. *Proc. Natl. Acad. Sci. U.S.A.* 94, 5395–5400. doi: 10.1073/pnas.94.10.5395

Wijetunge, L. S., Angibaud, J., Frick, A., Kind, P. C., and Nägerl, U. V. (2014). Stimulated emission depletion (STED) microscopy reveals nanoscale defects in the developmental trajectory of dendritic spine morphogenesis in a mouse model of fragile X syndrome. *J. Neurosci.* 34, 6405–6412. doi: 10.1523/JNEUROSCI.5302-13.2014

Wise, T. L. (2017). Changes in insulin-like growth factor signaling alter phenotypes in Fragile X Mice. *Genes Brain Behav.* 16, 241–249. doi: 10.1111/gbb.12340

Wolters, T. L., Netea, M. G., Hermus, A. R. M., Smit, J. W. A., and Netea-Maier, R. T. (2017). IGF1 potentiates the pro-inflammatory response in human peripheral blood mononuclear cells via MAPK. *J. Mol. Endocrinol.* 59, 129–139. doi: 10.1530/JME-17-0062

Wondolowski, J., and Dickman, D. (2013). Emerging links between homeostatic synaptic plasticity and neurological disease. *Front. Cell. Neurosci.* 7:223. doi: 10.3389/FNCEL.2013.00223

Wood, L., and Shepherd, G. M. G. (2010). Synaptic circuit abnormalities of motor-frontal layer 2/3 pyramidal neurons in a mutant mouse model of Rett syndrome. *Neurobiol. Dis.* 38, 281–287. doi: 10.1016/j.nbd.2010.01.018

Wu, H., Tao, J., Chen, P. J., Shahab, A., Ge, W., Hart, R. P., et al. (2010). Genome-wide analysis reveals methyl-CpG-binding protein 2-dependent regulation of microRNAs in a mouse model of Rett syndrome. *Proc. Natl. Acad. Sci. U.S.A.* 107, 18161–18166. doi: 10.1073/pnas.1005595107

Xing, L., and Bassell, G. J. (2013). mRNA localization: an orchestration of assembly, traffic and synthesis. *Traffic* 14, 2–14. doi: 10.1111/tra.12004

Xu, X., Miller, E. C., and Pozzo-Miller, L. (2014). Dendritic spine dysgenesis in Rett syndrome. *Front. Neuroanat.* 8:97. doi: 10.3389/fnana.2014.00097

Xu, X., and Pozzo-Miller, L. (2017). EEA1 restores homeostatic synaptic plasticity in hippocampal neurons from Rett syndrome mice. *J. Physiol.* 595, 5699–5712. doi: 10.1113/JP274450

Yang, Y., Geng, Y., Jiang, D., Ning, L., Kim, H. J., Jeon, N. L., et al. (2019). Kinase pathway inhibition restores PSD95 induction in neurons lacking fragile X mental retardation protein. *Proc. Natl. Acad. Sci. U.S.A.* 116, 12007–12012. doi: 10.1073/pnas.1812056116

Yasui, D. H., Xu, H., Dunaway, K. W., LaSalle, J. M., Jin, L.-W., and Maezawa, I. (2013). MeCP2 modulates gene expression pathways in astrocytes. *Mol. Autism* 4, 1–11. doi: 10.1186/2040-2392-4-3

Yuan, Z.-F. Z. F., Mao, S. S. S.-S., Shen, J., Jiang, L. H. L.-H., Xu, L., Xu, J.-L. J. L., et al. (2020). Insulin-Like growth factor-1 down-regulates the phosphorylation of FXYD1 and rescues behavioral deficits in a mouse model of Rett syndrome. *Front. Neurosci.* 14:20. doi: 10.3389/fnins.2020.00020

Zalfa, F., Eleuteri, B., Dickson, K. S., Mercaldo, V., De Rubeis, S., Di Penta, A., et al. (2007). A new function for the Fragile X Mental Retardation Protein in the regulation of PSD-95 mRNA stability Europe PMC Funders Group. *Nat. Neurosci.* 10, 578–587. doi: 10.1038/nn1893

Zang, J. B., Nosyreva, E. D., Spencer, C. M., Volk, L. J., Musunuru, K., Zhong, R., et al. (2009). A mouse model of the human fragile X syndrome I304N mutation. *PLoS Genet.* 5:e1000758. doi: 10.1371/journal.pgen.1000758

Zhang, F., Kang, Y., Wang, M., Li, Y., Xu, T., Yang, W., et al. (2018). Fragile X mental retardation protein modulates the stability of its m6A-marked messenger RNA targets. *Hum. Mol. Genet.* 27, 3936–3950. doi: 10.1093/hmg/ddy292

Zhao, J., Harada, N., Kurihara, H., Nakagata, N., and Okajima, K. (2010). Cilostazol improves cognitive function in mice by increasing the production of insulin-like growth factor-I in the hippocampus. *Neuropharmacology* 58, 774–783. doi: 10.1016/j.neuropharm.2009.12.008

Zheng, W. H., and Quirion, R. (2006). Insulin-like growth factor-1 (IGF-1) induces the activation/phosphorylation of Akt kinase and cAMP response element-binding protein (CREB) by activating different signaling pathways in PC12 cells. *BMC Neurosci.* 7:51. doi: 10.1186/1471-2202-7-51

Zhong, X., Li, H., and Chang, Q. (2012). MeCP2 phosphorylation is required for modulating synaptic scaling through mGluR5. *J. Neurosci.* 32, 12841–12847. doi: 10.1523/JNEUROSCI.2784-12.2012

Zoncu, R., Efeyan, A., and Sabatini, D. M. (2011). MTOR: from growth signal integration to cancer, diabetes and ageing. *Nat. Rev. Mol. Cell Biol.* 12, 21–35. doi: 10.1038/nrm3025

Conflict of Interest: The authors declare that the research was conducted in the absence of any commercial or financial relationships that could be construed as a potential conflict of interest.

Publisher's Note: All claims expressed in this article are solely those of the authors and do not necessarily represent those of their affiliated organizations, or those of the publisher, the editors and the reviewers. Any product that may be evaluated in this article, or claim that may be made by its manufacturer, is not guaranteed or endorsed by the publisher.

Copyright © 2021 Bach, Shovlin, Moriarty, Bardoni and Tropea. This is an open-access article distributed under the terms of the Creative Commons Attribution License (CC BY). The use, distribution or reproduction in other forums is permitted, provided the original author(s) and the copyright owner(s) are credited and that the original publication in this journal is cited, in accordance with accepted academic practice. No use, distribution or reproduction is permitted which does not comply with these terms.

frontiers in Cellular Neuroscience

ORIGINAL RESEARCH
published: 14 December 2021
doi: 10.3389/fncel.2021.707857

Molecular Identity and Location Influence Purkinje Cell Vulnerability in Autosomal-Recessive Spastic Ataxia of Charlevoix-Saguenay Mice

Brenda Toscano Márquez[1], Anna A. Cook[1], Max Rice[1], Alexia Smileski[1], Kristen Vieira-Lomasney[1], François Charron[2], R. Anne McKinney[2] and Alanna J. Watt[1]**

[1] Department of Biology, McGill University, Montreal, QC, Canada, [2] Department of Pharmacology and Therapeutics, McGill University, Montreal, QC, Canada

OPEN ACCESS

Edited by:
Annalisa Scimemi, University at Albany, United States

Reviewed by:
Richard Hawkes, University of Calgary, Canada
Janelle M. P. Pakan, Otto von Guericke University Magdeburg, Germany

***Correspondence:**
Alanna J. Watt
alanna.watt@mcgill.ca
R. Anne McKinney
anne.mckinney@mcgill.ca

Specialty section:
This article was submitted to Cellular Neuropathology, a section of the journal Frontiers in Cellular Neuroscience

Received: *10 May 2021*
Accepted: *03 November 2021*
Published: *14 December 2021*

Citation:
Toscano Márquez B, Cook AA, Rice M, Smileski A, Vieira-Lomasney K, Charron F, McKinney RA and Watt AJ (2021) Molecular Identity and Location Influence Purkinje Cell Vulnerability in Autosomal-Recessive Spastic Ataxia of Charlevoix-Saguenay Mice. Front. Cell. Neurosci. 15:707857. doi: 10.3389/fncel.2021.707857

Patterned cell death is a common feature of many neurodegenerative diseases. In patients with autosomal-recessive spastic ataxia of Charlevoix-Saguenay (ARSACS) and mouse models of ARSACS, it has been observed that Purkinje cells in anterior cerebellar vermis are vulnerable to degeneration while those in posterior vermis are resilient. Purkinje cells are known to express certain molecules in a highly stereotyped, patterned manner across the cerebellum. One patterned molecule is zebrin, which is expressed in distinctive stripes across the cerebellar cortex. The different zones delineated by the expression pattern of zebrin and other patterned molecules have been implicated in the patterning of Purkinje cell death, raising the question of whether they contribute to cell death in ARSACS. We found that zebrin patterning appears normal prior to disease onset in *Sacs*$^{-/-}$ mice, suggesting that zebrin-positive and -negative Purkinje cell zones develop normally. We next observed that zebrin-negative Purkinje cells in anterior lobule III were preferentially susceptible to cell death, while anterior zebrin-positive cells and posterior zebrin-negative and -positive cells remained resilient even at late disease stages. The patterning of Purkinje cell innervation to the target neurons in the cerebellar nuclei (CN) showed a similar pattern of loss: neurons in the anterior CN, where inputs are predominantly zebrin-negative, displayed a loss of Purkinje cell innervation. In contrast, neurons in the posterior CN, which is innervated by both zebrin-negative and -positive puncta, had normal innervation. These results suggest that the location and the molecular identity of Purkinje cells determine their susceptibility to cell death in ARSACS.

Keywords: ataxia, mouse models, patterning, cerebellum, Purkinje cell, zebrin/Aldolase C

INTRODUCTION

Autosomal-recessive spastic ataxia of Charlevoix-Saguenay (ARSACS) is a progressive neurodegenerative disorder (Bouchard et al., 1978) caused most often by a deletion mutation in the *SACS* gene encoding the large (521 kD) protein sacsin (Engert et al., 2000) that functions as a chaperone (Parfitt et al., 2009) and regulates the cytoskeleton (Duncan et al., 2017;

Gentil et al., 2019). Mouse models of ARSACS have been developed that recapitulate key disease phenotypes, such as ataxia and progressive loss of cerebellar Purkinje cells (Girard et al., 2012; Lariviere et al., 2015, 2019). Remarkably, Purkinje cell death is patterned in human patients (Bouchard et al., 1998) and mouse models (Lariviere et al., 2015, 2019): cell death is more prominent in Purkinje cells in the anterior vermis while Purkinje cells in the posterior vermis are largely spared. The factors that cause anterior Purkinje cells to be vulnerable to changes in cellular function caused by the absence of sacsin have yet to be determined.

Patterning is a striking feature of the molecular identity of Purkinje cells. Purkinje cells express aldolase C, also known as zebrin II (zebrin), in a distinctive, striped pattern across the cerebellum that is evolutionarily conserved (Brochu et al., 1990). More recently, other molecules have been shown to be expressed in a patterned distribution across the cerebellum (Wadiche and Jahr, 2005; Apps and Hawkes, 2009; Marzban and Hawkes, 2011). How the molecular identity of neurons affects their function is not completely understood. Remarkably, however, recent evidence suggests that the molecular identity of Purkinje cells and their location within the cerebellum confer differences in both synaptic (Wadiche and Jahr, 2005; Hawkes, 2014) and firing properties (Zhou et al., 2014; Perkins et al., 2018).

The observation that many diseases show specific deficits related to molecular patterning underscores the urgency of understanding cerebellar patterning in more depth (Sarna and Hawkes, 2003). For instance, some diseases display Purkinje cell death predominantly in specific regions of the cerebellum, such as regions that are comprised of largely zebrin-negative or zebrin-positive cells (Sarna and Hawkes, 2003). One intriguing hypothesis is that diseases that share common vulnerabilities in Purkinje cells of a particular molecular identity may share pathophysiology that could be targeted by the same therapeutic interventions. It is therefore important to identify whether a neurodegenerative disease displays patterning in its cell loss and whether that patterning is associated with a specific molecular identity. We thus wanted to determine whether the patterned cell death observed in ARSACS arose from changes in specific populations of Purkinje cells that express specific molecular markers.

To shed light on whether Purkinje cells of a particular molecular identity are vulnerable to cell death, we explored whether zebrin expression is altered in a mouse model of ARSACS. We found that there were no changes in the zebrin patterning in *Sacs*$^{-/-}$ mice prior to Purkinje cell death, suggesting that the developmental sequences of patterning (Larouche and Hawkes, 2006) are unaltered in ARSACS. Interestingly, however, we found that Purkinje cell death occurs predominantly in zebrin-negative cells in the anterior vermis, even at later disease stages when Purkinje cell death is more widespread. Finally, we show that the deficit that we had previously observed in Purkinje cell synaptic innervation in the cerebellar nuclei (CN) (Ady et al., 2018) is also shaped by zebrin identity and anterior-posterior divisions. We observed that the reduction of Purkinje cell inputs onto CN neurons is only observed for zebrin-negative Purkinje cell terminals made onto cells in the anterior CN. In contrast, Purkinje cell innervation to the posterior CN, which is comprised of both zebrin-negative and -positive puncta, appears unaffected. These findings support the hypothesis that zebrin-negative Purkinje cells in the anterior vermis are uniquely susceptible to Purkinje cell death in ARSACS.

MATERIALS AND METHODS

Animals

Sacs$^{-/-}$ mice carrying a deletion of the *Sacs* gene were used as previously described (Girard et al., 2012; Lariviere et al., 2015; Ady et al., 2018). Heterozygous *Sacs*$^{+/-}$ mice were bred to obtain litter-matched *Sacs*$^{-/-}$ and wildtype (WT) mice. Roughly equal numbers of male and female mice were used in all experiments. Sex differences were tested for but not observed. Experiments were performed at postnatal day 40 (P40; $N = 4$ for WT and $N = 4$ for *Sacs*$^{-/-}$ mice), P150 ($N = 7$ for WT and $N = 8$ for *Sacs*$^{-/-}$ mice), P270 ($N = 4$ for WT and $N = 4$ for *Sacs*$^{-/-}$ mice), and P365 ($N = 4$ for WT and $N = 4$ for *Sacs*$^{-/-}$ mice). Breeding and animal procedures were approved by the McGill University Animal Care Committee and were in accordance with the rules and regulations established by the Canadian Council on Animal Care.

Tissue Preparation and Immunohistochemistry

Brain tissue from WT and *Sacs*$^{-/-}$ mice was prepared as previously described (Ady et al., 2018). In brief, mice were deeply anesthetized with 2,2,2-tribromoethanol (Avertin) via intraperitoneal injection, and tissue fixation was carried out via intracardiac perfusion. An initial flush was performed with phosphate-buffered saline (PBS, 0.1M, pH 7.4) and 5.6 μg/ml heparin salt. This was followed by perfusion with 40 ml of 4% paraformaldehyde (PFA) in phosphate buffer (PB, pH 7.4), which was also used for post-fixation storage of the extracted brains for a further 3 days at 4°C on a shaker at 70 RPM. If further storage was required, brains were stored in PBS with 0.5% sodium azide until slicing.

The cerebellum was sliced coronally using a Vibratome 3000 sectioning system (Concord, ON, Canada) to produce 100 μm thick slices. Immunohistochemistry was carried out on free-floating slices and two sections per location were used for each animal. Briefly, slices were incubated for half an hour in blocking solution (containing 1 × PBS, pH 7.4, 0.4% Triton X, 5% bovine serum albumin (BSA), and 0.05% Sodium Azide) followed by a 3-day incubation with the primary antibodies in blocking solution and 90 minutes for secondary antibodies in blocking solution. Following the final incubation, slices were washed in PBS and mounted using ProLong Gold Antifade mounting medium (ThermoFisher Scientific, Waltham, MA, United States), protected from light, and kept at 4°C. All chemicals were purchased from Millipore Sigma (Oakville, Canada) unless otherwise indicated.

Lobule immunohistochemistry: To label zebrin-positive cells, we used goat Aldolase C antibody (1:300; Catalogue number SCl-12065; Santa Cruz Biotechnology, Dallas, TX, United States) in combination with Alexa-488 conjugated anti-goat antibody

(A11055; Life Technologies, Burlington, ON, Canada). In addition, we used rabbit anti-calbindin antibody (1:500, CB-38a; Swant, Marly, Switzerland) as a Purkinje cell marker in combination with Alexa-594 conjugated anti-rabbit secondary antibody (R37119; Life Technologies). All secondary antibodies were used at 1:1,000 dilution. In a separate set of experiments to validate the use of calbindin staining to determine Purkinje cell numbers in **Supplementary Figure 1**, we performed immunohistochemistry as previously described for calbindin, followed by a counterstaining step using NeuroTrace 435/455 blue fluorescent Nissl stain (1:80; 1-hour incubation; N21479; Life Technologies).

Cerebellar nuclei immunohistochemistry: To label Purkinje cell terminal puncta in the CN, sagittal cerebellar slices were prepared and stained with rabbit anti-calbindin antibody (1:500, CB-38a, Swant) in combination with an Alexa-594 conjugated anti-rabbit secondary antibody (711-585-152, Jackson Immunoresearch, West Grove, PA, United States). To label zebrin-positive Purkinje cell puncta, mouse aldolase-C antibody (1:500, ab190368, Abcam, Toronto, Canada) was used in combination with Alexa-488 anti-mouse secondary antibody (715-545-150, Jackson Immunoresearch). CN neurons were labeled with guinea pig anti-NeuN antibody (1:500, abN90, Millipore, Burlington, MA, United States) in combination with DyLight 405 anti-guinea pig secondary antibody (1:500, 106475003, Jackson Immunoresearch). In separate experiments on additional slices from the same experimental animals, guinea pig vesicular GABA transporter (VGAT) antibody (1:200, 131 004, Synaptic Systems, Gottingen, Germany) with Alexa-488 anti-guinea pig secondary antibody (1:1000, 706-545-148, Jackson Immunoresearch) was used in conjunction with rabbit anti-calbindin antibody (Swant, as before), to label GABAergic terminals in the CN, shown in **Supplementary Figure 2**. For each animal, eight sagittal slices were collected at spaced intervals to ensure sampling across the fastigial and interposed CN. We used four WT and three *Sacs*$^{-/-}$ P90 mice. Number of cells: WT anterior = 28 cells, WT posterior = 26 cells, *Sacs*$^{-/-}$ mice anterior = 25 cells, *Sacs*$^{-/-}$ mice posterior = 46 cells.

Image Acquisition and Analysis

Zebrin stripe imaging: Images were acquired using an Axio Observer Z1 fluorescent microscope equipped with Zen blue software (Zeiss, Oberkochen, Germany) at a 20× magnification and tiled together for a whole lobule visualization. Gain and contrast were kept constant for all conditions during the imaging process. To compare across conditions, we used anatomical markers in the cerebellum to ensure that we were comparing data at the same brain location. We selected the cerebellar slices using images from the coronal view of the interactive Allen Mouse Brain atlas viewer[1] (Allen Institute of Brain Science, mouse coronal Atlas, 2011). For the analysis of the anterior lobules, we selected sections that matched images between 115 and 117; and for the posterior lobules, we selected sections that matched images between 127 and 130. We used two sections per lobule per animal. Mean fluorescence intensity and band thickness were measured using ImageJ 1.51F software. Briefly, the mean intensity was measured by tracing a box that contained both soma and dendrites of each zebrin-positive band. A similar box (size and position) was used to measure the zebrin-negative bands. To measure the thickness of the bands, a line containing only the zebrin-positive label was traced parallel to the length of the lobule, midway of the length of the dendritic tree. Complementary measurements were done in the zebrin-negative bands (refer to **Supplementary Figure 3** for illustration of analysis).

Purkinje cell counts: Images were acquired at a 20× magnification. Images were taken in one focal plane where the label of both primary antibodies was seen. In a separate set of experiments, we confirmed using a Nissl stain that calbindin gave us a good measurement of total Purkinje cell number (**Supplementary Figures 1, 3**), at an age when Purkinje cell death was observed. Thus, calbindin labeling was used to count total Purkinje cell numbers, while zebrin labeling was used to discern zebrin-positive (that were co-labeled for calbindin and zebrin) cells from zebrin-negative cells (that were labeled only for calbindin), even when Purkinje cell death was evident. We measured Purkinje cell density by measuring the number of Purkinje cells as a function of the length of the Purkinje cell layer, reporting numbers per 100 μm. The same measurement was used for zebrin-positive and zebrin-negative cells. Measurements were performed on sections that were identified using coordinates from the Allen Mouse Brain Atlas as described above. Briefly, anterior lobule III and possibly the boundary of lobule IV were identified between positions 115 and 117, and posterior lobules (lobules VIII and IX) were identified between positions 127 and 130. Total Purkinje cell length per condition was similar and is reported in **Table 1**. Representative images of the immunostaining are shown in pseudo-color.

Cerebellar nuclei imaging: Images were acquired using an LSM800 confocal microscope (Zeiss) at 1024 × 1024 resolution with a 63× objective and consistent imaging conditions and settings throughout. Images stacks of CN cells were obtained, and the cross-section of each cell at the widest point was chosen for analysis. The number of Purkinje cell synapses onto each CN cell was quantified by counting the number of calbindin-positive puncta surrounding large CN cells (>15 μm diameter). Puncta were only included in counts if they were immediately adjacent to the NeuN-positive CN cells. Puncta that were not touching the CN cell (located more than 0.5 μm away from the NeuN-positive area) were determined to not be forming a synapse with that CN cell and were not included in counts (refer to **Supplementary Figure 2** for examples). Zebrin-positive Purkinje cell synapses were identified by counting the number of the previously identified calbindin-positive puncta that were also zebrin-positive (**Supplementary Figure 2**). The number of zebrin-negative Purkinje cell synapses was then determined by subtracting the number of zebrin-positive puncta from the total number of calbindin-positive puncta. The data were then collated to show the number of zebrin-positive or zebrin-negative Purkinje cell puncta per large CN cell. All imaging was acquired and analyzed blind to condition, and images are presented in pseudo-color.

[1]https://mouse.brain-map.org/static/atlas

TABLE 1 | Animal and section number per condition.

Age	Anterior Lobule				Posterior Lobule			
	WT		*Sacs*$^{-/-}$		WT		*Sacs*$^{-/-}$	
	N animals (sections)	Total length of Purkinje cell layer analyzed (mm)	*N* animals (sections)	Total length of Purkinje cell layer analyzed (mm)	*N* animals (sections)	Total length of Purkinje cell layer analyzed (mm)	*N* animals (sections)	Total length of Purkinje cell layer analyzed (mm)
P40	4 (8)	37.19	4 (8)	38.33	4 (8)	35.54	4 (8)	37.34
P150	7 (14)	73.94	8 (16)	73.39	4 (8)	34.01	4 (8)	37.14
P270	4 (8)	37.48	4 (8)	37.99	4 (8)	38.43	4 (8)	37.94
P365	4 (8)	34.10	4 (8)	34.61	4 (8)	34.96	4 (8)	35.67

Animal number and the number of sections used for each condition are indicated for both genotypes in anterior and posterior lobules. Total Purkinje cell layer length (in mm) used in the analysis is indicated for each comparison. For each animal and lobule (anterior, posterior), two slices were selected for the analysis and one image was taken per slice.

Statistics

Comparisons were made using paired or unpaired Student's *t*-tests for normally distributed data or Mann Whitney *U* tests for when data were not normally distributed using JMP 12 (SAS, Cary, NC, United States) software. Data are represented by box and whisker plots, showing the median (horizontal line within boxes), second and third quartiles (rectangles) ± 1 SD (whiskers), or by an average ± SEM.

RESULTS

Patterning of Purkinje Cell Death in Autosomal-Recessive Spastic Ataxia of Charlevoix-Saguenay Mouse Model

The anterior-posterior differences in Purkinje cell firing properties have been associated with the expression profile of zebrin (Larouche and Hawkes, 2006): zebrin-positive cells are enriched in posterior lobules and fire at a lower frequency than zebrin-negative cells, which are enriched in anterior lobules (Xiao et al., 2014; Zhou et al., 2014). Since abnormal zebrin expression has been observed in rodent models of other forms of ataxia (Sawada et al., 2009; Sarna and Hawkes, 2011; Bailey et al., 2014; White et al., 2021), the changes in anterior-lobule firing that we previously reported (Ady et al., 2018) may likewise arise from abnormal expression of zebrin in the cerebellum in *Sacs*$^{-/-}$ mice. Conversely, intact neurotransmission from Purkinje cells to their downstream targets is required for proper zone formation in the cerebellum (White et al., 2014), and given that we have previously shown that Purkinje cells in *Sacs*$^{-/-}$ mice both fire at reduced frequencies and have deficits in their innervation of the CN (Ady et al., 2018), we wondered whether changes in Purkinje cell properties could themselves lead to disrupted zebrin patterning.

Anterior lobules (III and IV) are comprised of mostly zebrin-negative Purkinje cells, with only three thin, sagittally oriented zebrin-positive stripes in the vermis. We rationalized that if changes we observed in firing rates were due to changes in zebrin expression, they might arise either from the expansion of the width of zebrin stripes or from aberrant ectopic zebrin expression in regions that are normally zebrin-negative, which would be associated with lower Purkinje cell firing rates. We used immunohistochemistry in coronal slices from WT and *Sacs*$^{-/-}$ mice at disease onset (P40-50) to examine zebrin expression throughout anterior lobules III/IV (**Figure 1A** and **Supplementary Figure 3**). We found no significant differences in the width of zebrin-positive stripes when comparing WT and *Sacs*$^{-/-}$ cerebellum (N = 4 mice for WT and *Sacs*$^{-/-}$, 2 sections/brain analyzed; **Figure 1B**, see **Table 2** for individual *P*-values for each band). If developmental changes in zebrin patterning occurred in *Sacs*$^{-/-}$ mice, the intensity of zebrin staining in both zebrin-negative and -positive bands might be altered, since changes in molecular compartmentalization have been reported in other mice (Miyazaki et al., 2012; Bailey et al., 2014). We determined the intensity of zebrin staining in both zebrin-positive and zebrin-negative stripes in anterior lobules and found no significant differences in *Sacs*$^{-/-}$ mice compared to WT (Student's *t*-test for all comparisons other than posterior bands 2_L, 1_R, and 2_R when Mann Whitney *U* tests were performed, not significantly different; zebrin-positive bands: band 2_L: $P = 0.217$, band 1: $P = 0.075$, band 2_R: $P = 0.109$; zebrin-negative bands: band 2_L: $P = 0.10$, band 1_L: $P = 0.525$, band 1_R: $P = 0.675$, band 2_R: $P = 0.706$; **Figures 1C,D**). This suggests that the reduction in Purkinje cell firing rates that we observed in anterior lobules at P40 (Ady et al., 2018) does not arise from abnormal expression of zebrin in these cells or from changes in the developmental patterning or expression of zebrin. Previously, it has been reported that Purkinje cell death is not observed at P30 but is evident at P90 (Lariviere et al., 2015). To determine whether cell death is observed at P40, we determined the density of Purkinje cell bodies and found that no differences were observed in *Sacs*$^{-/-}$ mice compared to WT (Student's *t*-test, $P = 0.99$; **Figure 1E**). Similarly, there were no detectable differences in

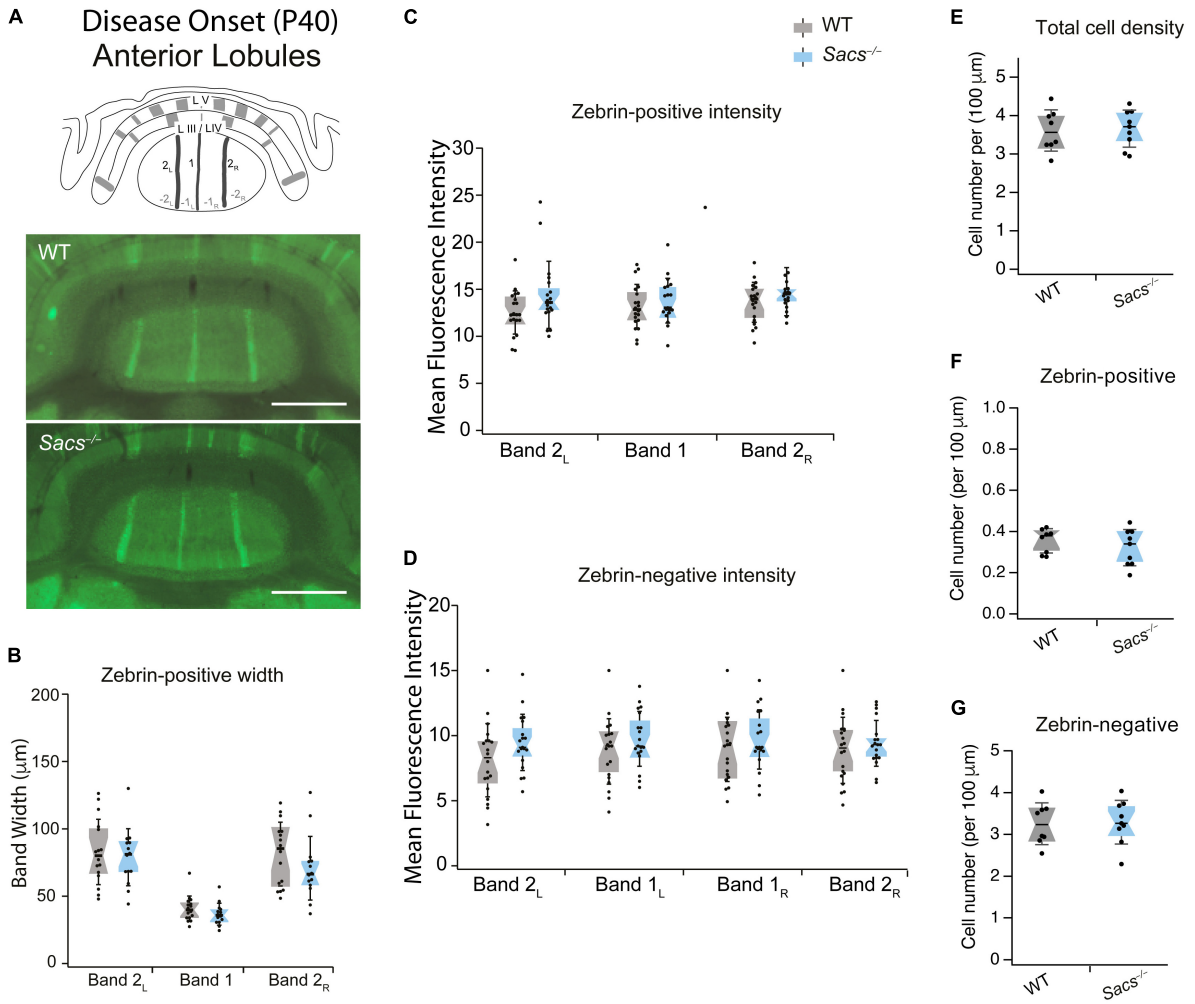

FIGURE 1 | Anterior vermis zebrin expression is unaltered in disease-onset (P40) *Sacs*$^{-/-}$mice. **(A)** Schematic (top) illustrates a coronal view of anterior lobules (L) and zebrin bands. Measurements were taken from anterior lobule III/IV at P40. Representative images show anterior zebrin expression (green) in WT (middle) and *Sacs*$^{-/-}$ mice (bottom). **(B)** The widths of the zebrin-positive bands in the anterior lobule were not significantly different in *Sacs*$^{-/-}$ cerebellum (blue) compared to WT (gray). **(C,D)** Similarly, there were no significant differences observed between the mean fluorescence intensity (arbitrary fluorescence units, a.u.) of **(C)** zebrin-positive bands **(D)** or zebrin-negative bands in WT (gray) and *Sacs*$^{-/-}$ (blue) cerebellar vermis. **(E–G)** No significant reduction was observed in the total density of Purkinje cells in anterior lobules [**(E)** shown as the number of cells per μm]. We also observed no differences in zebrin-positive **(F)** and zebrin-negative **(G)** cell densities. No significant differences were observed for any comparisons. *N* = 4 for both WT and *Sacs*$^{-/-}$ mice, two sections per animal; see **Table 2** for *P*-values; Student's *t*-test, $P > 0.05$ when no comparison is shown. Scale bar, 1 mm. WT, wildtype.

TABLE 2 | Statistics for anterior lobules.

Age	Anterior Lobule band width						
	Zebrin-positive bands			Zebrin-negative bands			
	2_L	1	2R	2_L	1_L	1_R	2_R
P40	*0.865*	*0.534*	*0.54*	*0.585*	0.609	*0.692*	*0.678*
P150	***0.022***	*0.233*	***0.0056***	0.937	*0.26*	0.164	*0.678*
P270	***0.012***	*0.271*	***0.002***	*0.269*	**0.042**	0.093	0.504
P365	***0.0009***	***0.0028***	***0.001***	0.102	**0.044**	***0.03***	0.985

P-values are indicated for all comparisons of anterior lobule bandwidths for zebrin-positive and -negative bands at all ages studied. Mann Whitney U tests were used for italicized values, while all other comparisons were performed using Student's t-tests. Statistically significant P-values are indicated in bold.

either zebrin-positive (Student's *t*-test, $P = 0.37$; **Figure 1F**) or zebrin-negative (Student's *t*-test, $P = 0.89$; **Figure 1G**) cell density.

Zebrin-positive Purkinje cells are more prominent in posterior lobules. We predicted that zebrin expression would be unchanged in posterior *Sacs*$^{-/-}$ cerebellar vermis, since we observed no Purkinje cell firing deficits (Ady et al., 2018) and no later Purkinje cell loss (Lariviere et al., 2015, 2019) in this region. To address this, we measured zebrin expression in posterior lobules VIII and IX (**Figure 2A** and **Supplementary Figure 3**) and observed no differences in zebrin band width (**Figure 2B** and **Table 3**), or zebrin intensity in either zebrin-positive (Student's *t*-test for all comparisons, not significantly different; zebrin-positive bands: band 3_L: $P = 0.878$, band 2_L: $P = 0.89$, band 1: $P = 0.543$, band 2_R: $P = 0.368$, band 3_R: $P = 0.47$; **Figure 2C**) or zebrin-negative (Student's *t*-test for all comparisons, not significantly different; zebrin-negative bands: band 2_L: $P = 0.515$, band 1_L: $P = 0.467$, band 1_R: $P = 0.43$, band 2_R: $P = 0.401$; **Figure 2D**) bands from posterior lobules in WT and *Sacs*$^{-/-}$ mice. Similarly, we observed no differences in the total cell density in posterior lobules (Student's *t*-test, $P = 0.52$; **Figure 2E**) or in the densities of zebrin-positive (Student's *t*-test, $P = 0.54$; **Figure 2F**) or zebrin-negative (Student's *t*-test, $P = 0.70$; **Figure 2G**) cells.

Although Purkinje cell death is known to occur in the predominantly zebrin-negative anterior lobules of the *Sacs*$^{-/-}$

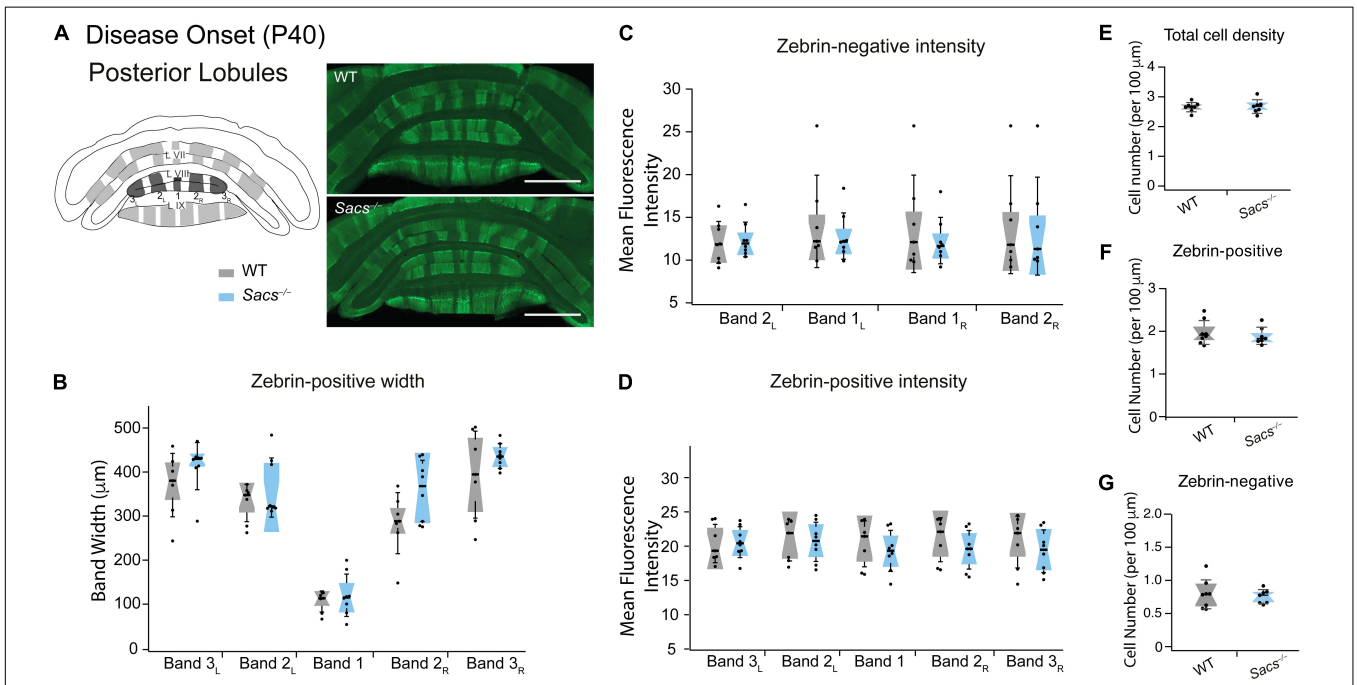

FIGURE 2 | Posterior vermis zebrin expression is unaltered in disease-onset (P40) *Sacs*$^{-/-}$mice. **(A)** Schematic (left) illustrates the coronal view of posterior lobules (L) and zebrin bands. Measurements were taken from posterior lobules VIII and IX. Sample images (right) show posterior zebrin expression in WT (top) and *Sacs*$^{-/-}$ mice (bottom). **(B)** The widths of the zebrin-positive bands in the posterior lobules were not significantly different between WT (gray) and *Sacs*$^{-/-}$ cerebellum (blue). **(C,D)** Similarly, there were no significant differences observed between the mean fluorescence intensity (arbitrary fluorescence units, a.u.) of **(C)** zebrin-positive, or **(D)** zebrin-negative bands in WT (gray) and *Sacs*$^{-/-}$ (blue) cerebellar vermis. ($N = 6$ for both WT and *Sacs*$^{-/-}$ mice. **(E–G)** There was no significant change in the total number of Purkinje cells of the posterior lobules [**(E)** the number of cells per 100 μm]. We also observed no differences in zebrin-positive **(F)** and zebrin-negative **(G)** cell densities. $N = 4$ for WT; $N = 4$ for *Sacs*$^{-/-}$, two sections per animal; see **Table 3** for *P*-values; Student's *t*-test, $P > 0.05$ when no comparison is shown. Scale bar, 1 mm.

TABLE 3 | Statistics for posterior lobules.

Age	Posterior Lobule band width								
	Zebrin-positive bands					Zebrin-negative bands			
	3_L	2_L	1	2_R	3_R	2_L	1_L	1_R	2_R
P40	0.076	0.10	0.483	0.063	0.524	*0.272*	0.786	*0.118*	*0.272*
0272P150	0.307	*0.12*	0.631	*0.155*	0.615	0.126	**0.035**	0.844	0.626
P270	*0.093*	***0.043***	0.434	*0.272*	*0.603*	0.138	0.303	0.723	0.974
P365	0.829	0.793	**0.018**	0.236	*0.603*	0.0514	0.50	0.375	0.437

P-values are indicated for all comparisons of posterior lobule bandwidths for zebrin-positive and -negative bands at all ages studied. Mann Whitney U tests were used for italicized values, while all other comparisons were performed using Student's t-tests. Statistically significant P-values are indicated in bold.

mouse cerebellum (Lariviere et al., 2015, 2019), the molecular profile of surviving neurons has not been determined in *Sacs*$^{-/-}$ mice. To ascertain this, we examined an age when Purkinje cell death is known to occur that is still relatively early during disease progression (P150; **Figure 3**). We used immunohistochemistry to label Purkinje cells with calbindin for total Purkinje cells, and zebrin to discern zebrin-positive (which are dual labeled) and zebrin-negative (which only express calbindin) cells. We

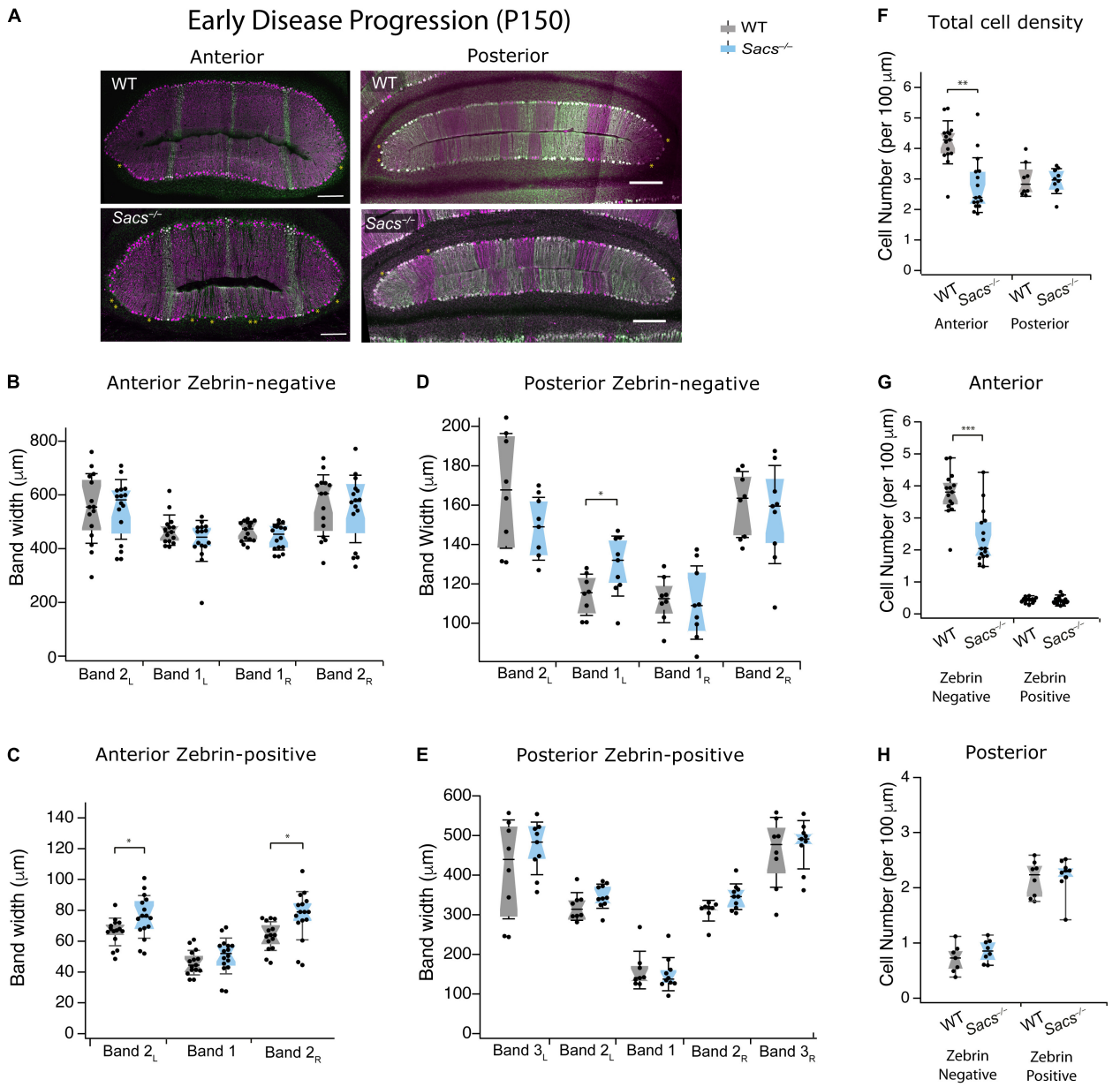

FIGURE 3 | Purkinje cell death occurs primarily in zebrin-negative cells in the anterior vermis at P150. **(A)** Representative images of anterior lobules (left) and posterior lobules (right), from WT (top) and *Sacs*$^{-/-}$ (bottom) from a P150 mouse with Purkinje cells labeled with calbindin (purple) and zebrin (green). **(B)** The widths of the zebrin-negative bands in the anterior lobule were not significantly different in *Sacs*$^{-/-}$ cerebellum (blue) compared to WT (gray). **(C)** However, the widths of two of the zebrin-positive bands in the anterior lobule were significantly higher in *Sacs*$^{-/-}$ cerebellum (blue) compared to WT (gray) ($N = 7$ for WT; $N = 8$ for *Sacs*$^{-/-}$, 2 images per animal per lobule; Mann Whitney U test $^{*}P < 0.05$). **(D)** The width of one zebrin-negative band was elevated in *Sacs*$^{-/-}$ mice compared to WT (Band 1_L). **(E)** The widths of zebrin-positive bands in posterior lobules were not significantly different in *Sacs*$^{-/-}$ cerebellum (blue) compared to WT (gray). **(F–H)** Total Purkinje cell density (number of cells per 100 µm) from anterior (left) and posterior (right) lobules were calculated. A significant reduction was observed in Purkinje cell density in the anterior (left), but not posterior (right) lobules at this age **(F)**, in line with previous reports (Lariviere et al., 2015). **(G)** We observed a significant reduction in the zebrin-negative (left) but not zebrin-positive (right) Purkinje cell density only anterior lobules in *Sacs*$^{-/-}$ mice compared to WT, while **(H)** neither were significantly affected in posterior lobules. ($N = 7$ for WT; $N = 8$ for *Sacs*$^{-/-}$, 2 sections per lobule per animal; see **Tables 2**, **3** for P-values; Student's t-test $^{*}P < 0.05$, $^{**}P < 0.005$, $P > 0.05$ when no comparison is shown, Scale bar, 200 µm.

measured the width of bands in the anterior zebrin-negative lobules and found no difference in *Sacs*$^{-/-}$ mice compared to WT (**Figure 3B** and **Table 2**). Interestingly, the width of two of the three zebrin-positive bands in the anterior lobules at P150 was slightly expanded in *Sacs*$^{-/-}$ mice compared to WT (**Figure 3C** and **Table 2**). We next measured the width of zebrin-negative (**Figure 3D** and **Table 3**) and zebrin-positive (**Figure 3E** and **Table 3**) bands in posterior lobules at P150 and found a small

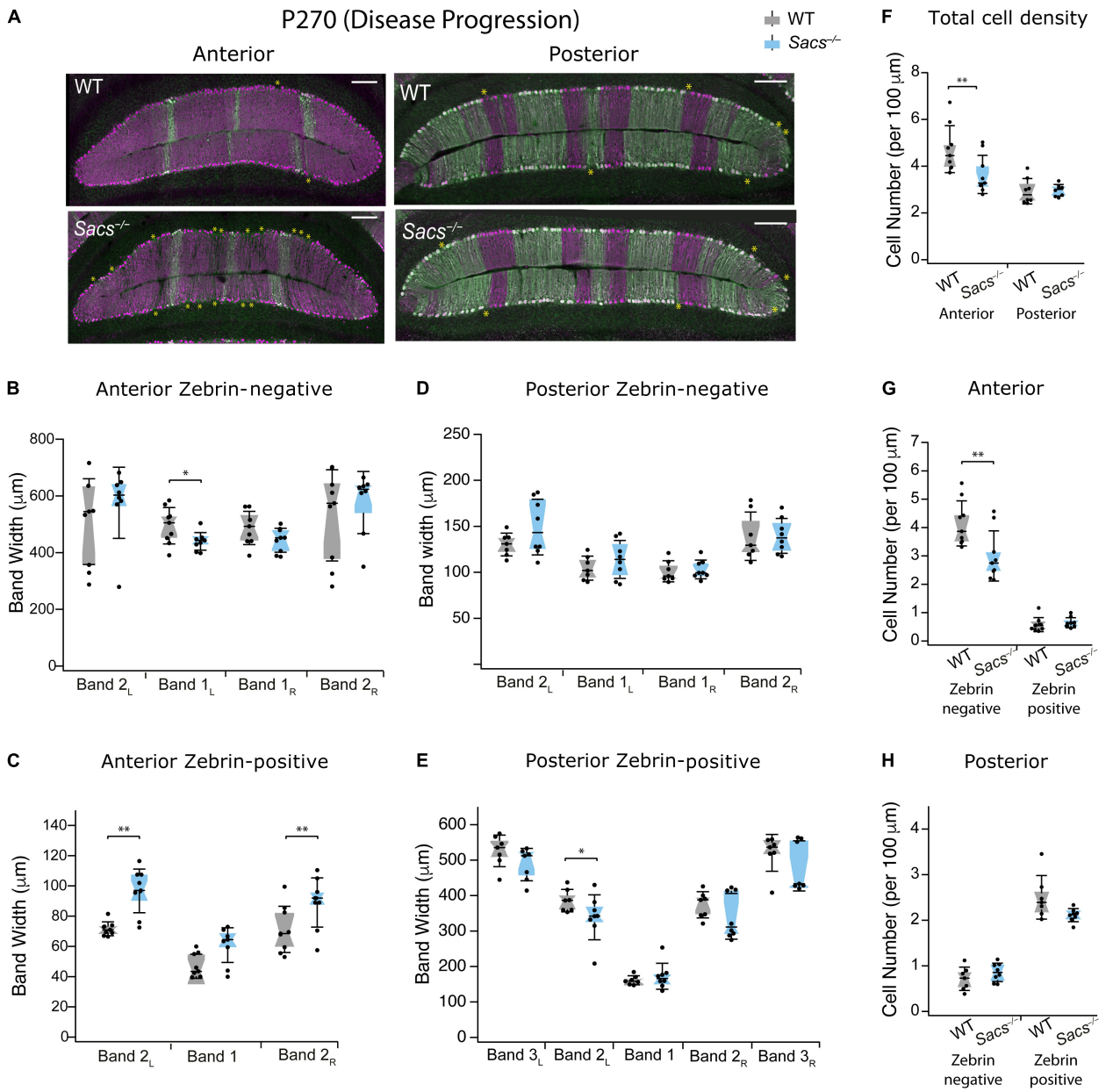

FIGURE 4 | Patterned cell death persists as the disease progresses in zebrin-negative Purkinje cells in anterior vermis in P270 mice. **(A)** Representative images of anterior lobules (left) and posterior lobules (right), from WT (top) and *Sacs*$^{-/-}$ (bottom) from a P270 mouse with Purkinje cells labeled with calbindin (purple) and zebrin (green). Asterisks indicate gaps in Purkinje cells. **(B)** The widths of three of the four zebrin-negative bands in the anterior lobule were not significantly different in *Sacs*$^{-/-}$ cerebellum (blue) compared to WT (gray) although band 1_L was moderately reduced. **(C)** The widths of two zebrin-positive bands (2_L and 2_R) in the anterior lobule were significantly increased in *Sacs*$^{-/-}$ cerebellum (blue) compared to WT (gray). **(D,E)** In posterior lobules at P365, neither **(D)** zebrin-negative nor **(E)** most of the zebrin-positive band width was affected in *Sacs*$^{-/-}$ cerebellum (blue) compared to WT (gray). **(F)** Total Purkinje cell density (cells per 100 μm) showed a significant reduction in anterior (left) but not posterior lobules (right). **(G)** In anterior lobules, this reduction was only observed in zebrin-negative (left) but not zebrin-positive (right) Purkinje cells **(H)**. However, in posterior lobules, neither zebrin-negative (left) nor zebrin-positive (right) cells showed significant differences. $N = 4$ for WT; $N = 4$ for *Sacs*$^{-/-}$, 2 sections per lobule per animal; see **Tables 2**, **3** for *P*-values; Student's *t*-test used for normally distributed and Mann Whitney *U* test used for non-normally distributed data; $^*P < 0.05$, $^{**}P < 0.005$, $P > 0.05$ if no comparison is shown. Scale bar, 200 μm.

increase in one zebrin-negative band (band 1_L; **Figure 3D** and **Table 3**), with no other statistically significant differences in *Sacs*$^{-/-}$ mice posterior bands.

To determine if changes in band width reflect changes in Purkinje cell density at P150, we next measured this in WT and *Sacs*$^{-/-}$ mice (**Figure 3F**). We found that the total density of calbindin-labeled Purkinje cell somata was reduced in anterior lobules in P150 *Sacs*$^{-/-}$ mice, consistent with previous reports (Student's *t*-test, $P < 0.001$; **Figure 3F**) (Lariviere et al., 2015). To determine whether this reduction was observed equally in zebrin-positive and -negative Purkinje cells, we then examined cells of each molecular profile separately. We observed a significant reduction in anterior lobule zebrin-negative Purkinje cells (Student's *t*-test, $P < 0.0001$; **Figure 3G**, left). Although the number of zebrin-positive cells in anterior lobules is low (**Figure 3A**, left), we did not observe any significant differences in their density in *Sacs*$^{-/-}$ mice (Student's *t*-test, $P = 0.68$; **Figure 3G**). Since cell death has not been reported in posterior lobules in *Sacs*$^{-/-}$ mice (Lariviere et al., 2015, 2019), we expected no differences in the proportion of zebrin-positive and -negative Purkinje cells there. Consistent with this, we observed that the densities of both zebrin-positive and -negative cells in posterior lobules were not significantly different in P150 *Sacs*$^{-/-}$ mice (Student's *t*-test for all measurements: $P = 0.82$ for total cell density; $P = 0.44$ for zebrin-negative cell density; and $P = 0.70$ for zebrin-positive cell density; **Figure 3H**). These results suggest that Purkinje cell death occurs primarily in zebrin-negative neurons in anterior lobules at an early stage of disease progression (P150) and that although zebrin-positive bands expand, they appear to do so to occupy the space left by the zebrin-negative cell death.

ARSACS is a progressive neurodegenerative disease, and in mouse models, increased levels of Purkinje cell death have been observed with aging (Lariviere et al., 2015, 2019). Therefore, we wondered whether advanced stages of disease progression extend cell death to include previously resilient zebrin-positive cells. To determine this, we measured zebrin-positive and -negative Purkinje cells in anterior and posterior lobules at advancing disease stages. First, we examined P270 (9 months; **Figure 4A**). We found that in anterior lobules, one zebrin-negative band was reduced, while two were unchanged (**Figure 4B** and **Table 2**) and two of the three zebrin-positive bands were wider in *Sacs*$^{-/-}$ mice (**Figure 4C** and **Table 2**), just as we observed at P150. In posterior lobules, however, there was only a small reduction observed in one zebrin-positive band (band 2_L; **Figure 4E** and **Table 3**), with no other differences were observed in the remaining zebrin-positive and zebrin-negative bands (**Figures 4D,E** and **Table 3**). Similar to our findings at P150, the total cell density was reduced in anterior but not posterior lobules in *Sacs*$^{-/-}$ mice (Student's *t*-test, $P = 0.02$; **Figure 4F**), which was reflected in a reduction in zebrin-negative, but not zebrin-positive cell density in anterior lobules (Student's *t*-test for both measurements; zebrin-negative cell density: $P = 0.01$; zebrin-positive density: $P = 0.52$; **Figure 4G**). However, no differences in total zebrin-positive or -negative cells were observed in posterior lobules (Student's *t*-test for all comparisons; total: $P = 0.13$; zebrin-negative: $P = 0.26$; zebrin-positive: $P = 0.08$; **Figure 4H**).

Finally, we examined an even more advanced stage of disease progression at 1 year (P365; **Figure 5A**) and found results similar to those at P150 and P270, but more severe. We now observed that two out of four anterior zebrin-negative bands were reduced in *Sacs*$^{-/-}$ mice compared to WT (**Figure 5B** and **Table 2**), and this was accompanied by significant increases in the band width of all three anterior zebrin-positive bands in *Sacs*$^{-/-}$ mice at P365 (**Figure 5C** and **Table 2**), suggesting that Purkinje cells become more disorganized in anterior lobules as the disease progresses. However, restructuring was predominantly observed in anterior lobules, as even at this later disease stage, posterior bandwidths appeared largely normal in *Sacs*$^{-/-}$ mice for zebrin-negative (**Figure 5D** and **Table 3**) and most zebrin-positive (**Figure 5E** and **Table 3**) bands, other than a small increase in zebrin-positive band 1 (**Figure 5E** and **Table 3**). The density of Purkinje cells in *Sacs*$^{-/-}$ mice at P365 was again only affected in anterior, but not posterior lobules (Student's *t*-test for both comparisons; anterior: $P = 0.003$; posterior: $P = 0.48$; **Figure 5F**). Similar to what we observed at earlier ages, this change appeared to arise predominantly from changes in anterior zebrin-negative, but not zebrin-positive cell density (Student's *t*-test for both comparisons; zebrin-negative cell density: $P = 0.004$; zebrin-positive cell density: $P = 0.75$; **Figure 5G**). In agreement with results from overall posterior cell density at P365 (**Figure 5F**), no change in posterior zebrin-negative and -positive cell densities was observed in *Sacs*$^{-/-}$ mice at P365 (Student's *t*-test for both comparisons, zebrin-negative cell density: $P = 0.67$; zebrin-positive cell density: $P = 0.60$; **Figure 5H**). These results agree with our hypothesis that cell death is largely limited to anterior lobules even at relatively advanced disease stages and that this is manifested by changes in cell density of zebrin-negative cells. However, although no changes in zebrin-positive numbers are observed, anterior lobules become more disorganized at P365 in *Sacs*$^{-/-}$ mice, likely because zebrin-positive bands expand into space where zebrin-negative cells have died.

Given that we have examined the progression of Purkinje cell loss in a mouse model of ARSACS over time, we wondered whether this represented change arising from aging or from disease progression. We compared the change in anterior lobule Purkinje cells across time, from P40 to P365, which allows us to normalize to WT cells, and thus graphically represent the contribution arising exclusively from disease progression. We observed a gradual decrease of Purkinje cell numbers in anterior lobules (**Figure 6A**), which was reflected in the proportion of zebrin-negative cells over time (**Figure 6B**), while the proportion of zebrin-positive cells remained remarkably similar at all ages (**Figure 6C**).

Patterned Loss of Purkinje Cell Puncta Made Onto Large Cells in the Cerebellar Nuclei

Purkinje cell death is one of the most prominent pathophysiological changes in both ARSACS brains and animal models of ARSACS, but other changes have also been observed. For instance, although the numbers of cells in the CN of the cerebellum are unaltered in *Sacs*$^{-/-}$ cerebellum,

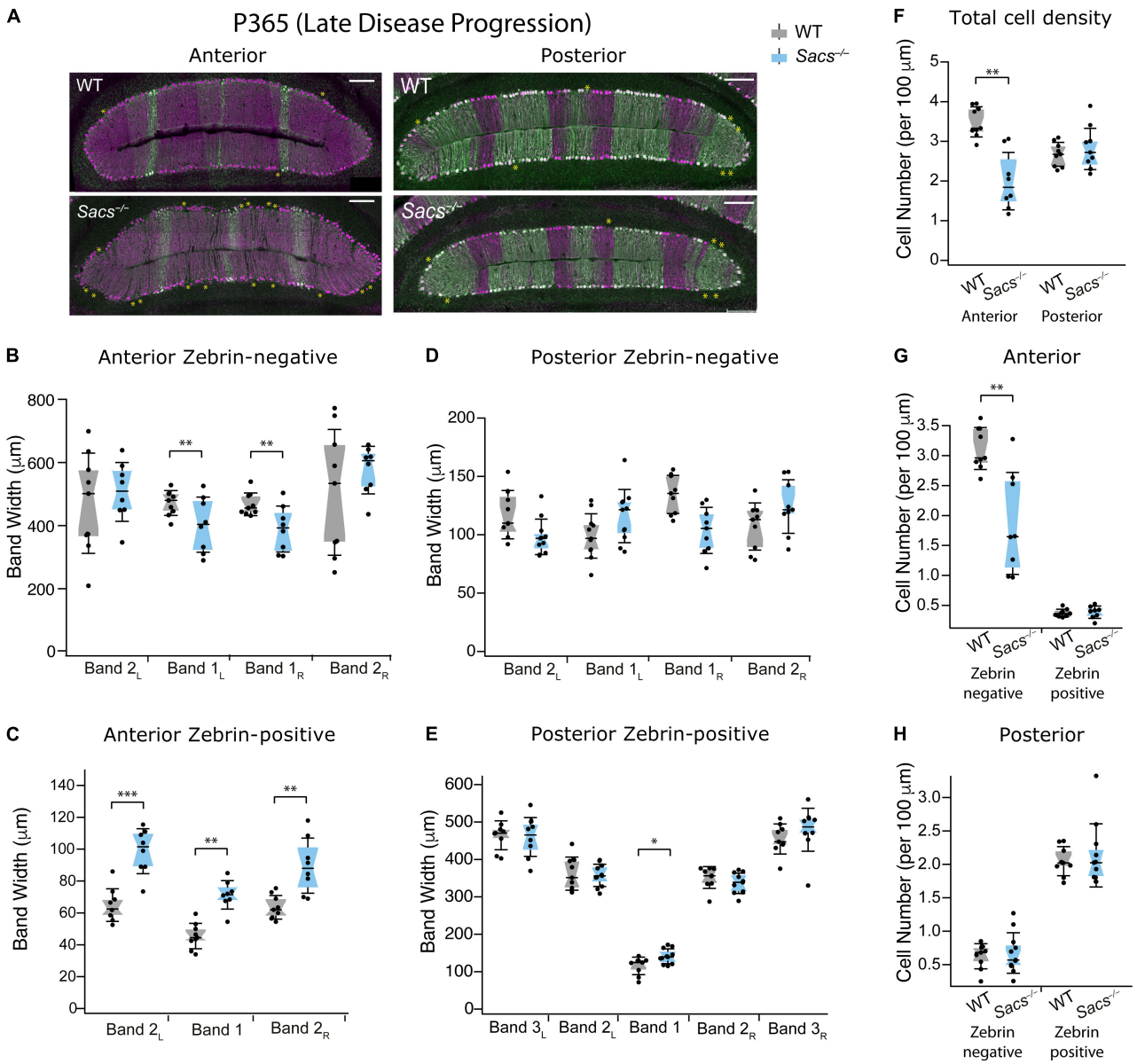

FIGURE 5 | Patterned cell death at late disease progression (P365) is restricted to zebrin-negative Purkinje cells in the anterior vermis. **(A)** Representative images of anterior lobules (left) and posterior lobules (right), from WT (top) and *Sacs*$^{-/-}$ (bottom) from a P365 mouse with Purkinje cells labeled with calbindin (purple) and zebrin (green). Asterisks indicate gaps in Purkinje cells. **(B)** The widths of zebrin-negative bands 1_L and 1_R were significantly reduced in *Sacs*$^{-/-}$ anterior cerebellum (blue) compared to WT (gray). **(C)** The widths of all 3 zebrin-positive bands in the anterior cerebellum were significantly increased in *Sacs*$^{-/-}$ (blue) compared to WT (gray). **(D,E)** However, in posterior lobules at P365, neither **(D)** zebrin-negative nor **(E)** most of zebrin-positive band width was affected in *Sacs*$^{-/-}$ cerebellum (blue) compared to WT (gray). **(F)** Total Purkinje cell density (number of cells per 100 μm) showed a significant reduction anterior (left) but not posterior lobules (right). **(G)** In anterior lobules, this reduction was only observed in zebrin-negative (left) but not zebrin-positive (right) Purkinje cells **(H)**. However, in posterior lobules, neither zebrin-negative (left) nor zebrin-positive (right) cells showed significant differences. $N = 4$ for WT; $N = 4$ for *Sacs*$^{-/-}$, 2 sections per lobule per animal; see **Tables 2**, **3** for *P*-values; Student's *t*-test used for normally distributed and Mann Whitney *U* test used for non-normally distributed data; $^*P < 0.05$, $^{**}P < 0.005$, $^{***}P < 0.001$, $P > 0.05$ if no comparison is shown. Scale bar, 200 μm.

the number of puncta, likely reflecting the number of synaptic inputs onto these cells, is reduced at the onset of disease in *Sacs*$^{-/-}$ mice (Ady et al., 2018). Changes in the innervation of target neurons in the CN will likely have a profound impact on cerebellar function. This raises the question of whether this reduction arises from changes in numbers of inputs from all Purkinje cells or whether specific subsets of Purkinje cells also show preferential changes in their innervation of the CN?

We first determined whether the decrease in the number of puncta, which we used as a proxy for the number of potential Purkinje cell terminals innervating the CN neurons, that we previously observed at disease onset (Ady et al., 2018), was

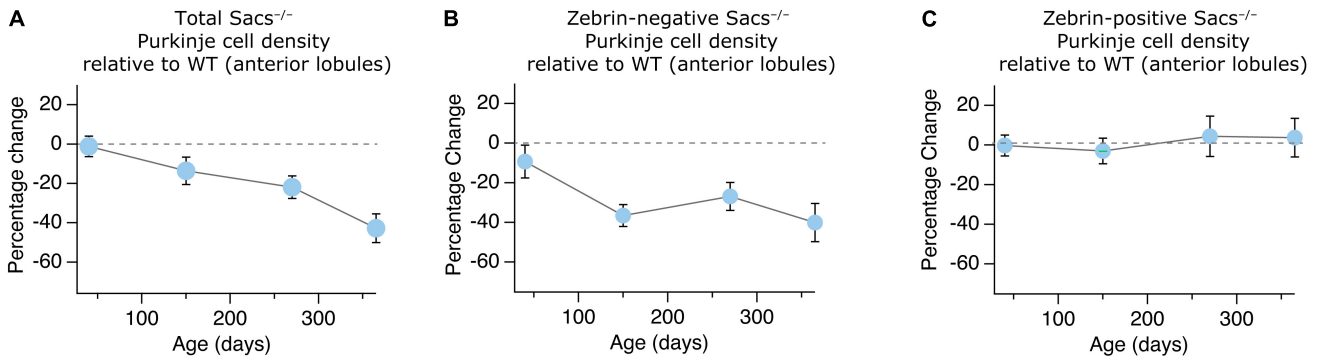

FIGURE 6 | Gradual anterior Purkinje cell loss across ages in *Sacs*$^{-/-}$ mice. **(A–C)** The proportion of Purkinje cells in anterior lobules (% change *Sacs*$^{-/-}$ relative to WT) at each age is plotted. We observed **(A)** a gradual decrease in total Purkinje cell number in anterior lobules that is similar to **(B)** the time course of loss observed in zebrin-negative cells in anterior lobules. **(C)** However, there are no proportional changes in zebrin-positive cell number across ages in *Sacs*$^{-/-}$ mice. Data are represented as averages ± SEM.

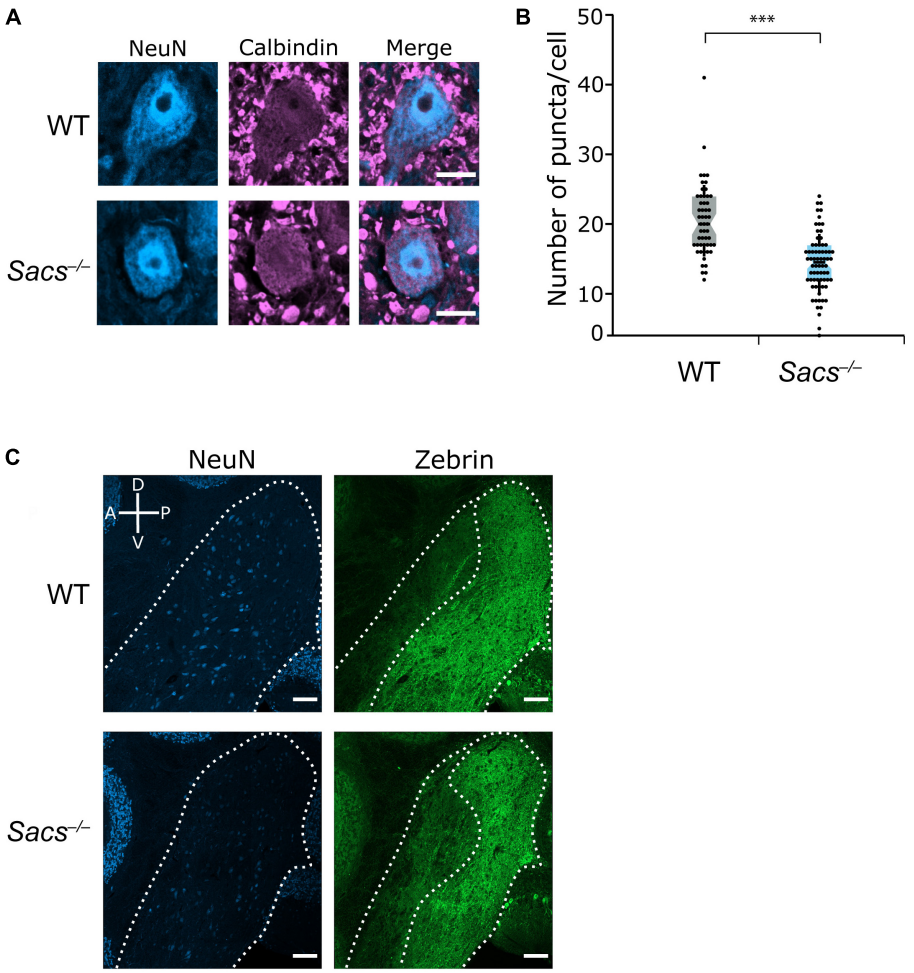

FIGURE 7 | Reduction in Purkinje cell puncta in cerebellar nuclei (CN) in *Sacs*$^{-/-}$ mice. **(A)** Representative images of large neurons (>15 μm diameter) in the CN with calbindin-positive puncta as a measure of Purkinje cell inputs. Scale bar, 10 μm. **(B)** The number of calbindin-positive puncta onto large cells in the CN is significantly lower in *Sacs*$^{-/-}$ mice, data shown per cell (Student's *t*-test, $P < 0.000001$). **(C)** Representative images show that zebrin-positive Purkinje cell innervation is predominantly restricted to the posterior half of the CN in both WT and *Sacs*$^{-/-}$ mice. The compass shows dorsal-ventral and anterior-posterior axes. Scale bar, 100 μm. ***$P < 0.0001$.

observed as the disease progressed (at P90). We measured the number of calbindin-positive Purkinje cell puncta made onto large projection neurons in the fastigial and interposed nuclei (**Figure 7A**) since these receive innervation from the vermis (Voogd and Ruigrok, 2004). We found that the number of puncta was reduced in *Sacs*$^{-/-}$ mice (Student's *t*-test; $P < 0.0001$; **Figures 7A,B**), similar to what is observed at earlier ages (Ady et al., 2018). We have previously demonstrated that in the CN of both WT and *Sacs*$^{-/-}$ mice, there is a high degree of colocalization between calbindin-positive puncta and puncta that are stained with VGAT at P40 (Ady et al., 2018). This indicates that these previously identified calbindin-positive puncta are likely functional GABAergic Purkinje cell terminals. We found a high degree of co-labeling in WT and *Sacs*$^{-/-}$ mice at P90 (**Supplementary Figure 2**). Thus, the reduction in the number of calbindin-positive puncta in the CN of ARSACS mice at P90 appears to reflect a loss of functional Purkinje cell presynaptic terminals rather than a shift in the proportion of inputs arising from Purkinje cell terminals compared to other inputs.

It has previously been described that the pattern of zebrin projections respects the anterior – posterior (or rostral – caudal) division of the CN (Hawkes and Leclerc, 1986; Sugihara, 2011), with the anterior regions of the nuclei receiving predominantly zebrin-negative input and posterior nuclei receiving predominantly zebrin-positive input (Sugihara, 2011). We observed this division in both WT and *Sacs*$^{-/-}$ mice (**Figure 7C**). Thus, to determine whether changes were made in the number of zebrin-positive or -negative puncta in the CN, we analyzed neurons with respect to their anterior – posterior location within both CN nuclei.

In anterior CN, which receives largely zebrin-negative Purkinje cell innervation, we observed a reduction in the number of zebrin-negative puncta onto large CN neurons compared to WT (WT: $N = 4$; *Sacs*$^{-/-}$ $N = 3$; Student's *t*-test, $P < 0.0001$; **Figures 8A,B**). The number of zebrin-positive Purkinje cell puncta in anterior CN was low in both WT and *Sacs*$^{-/-}$ mice and did not significantly differ between genotype (Mann Whitney *U* test, $P = 0.81$; **Figures 8A,B**), which suggests

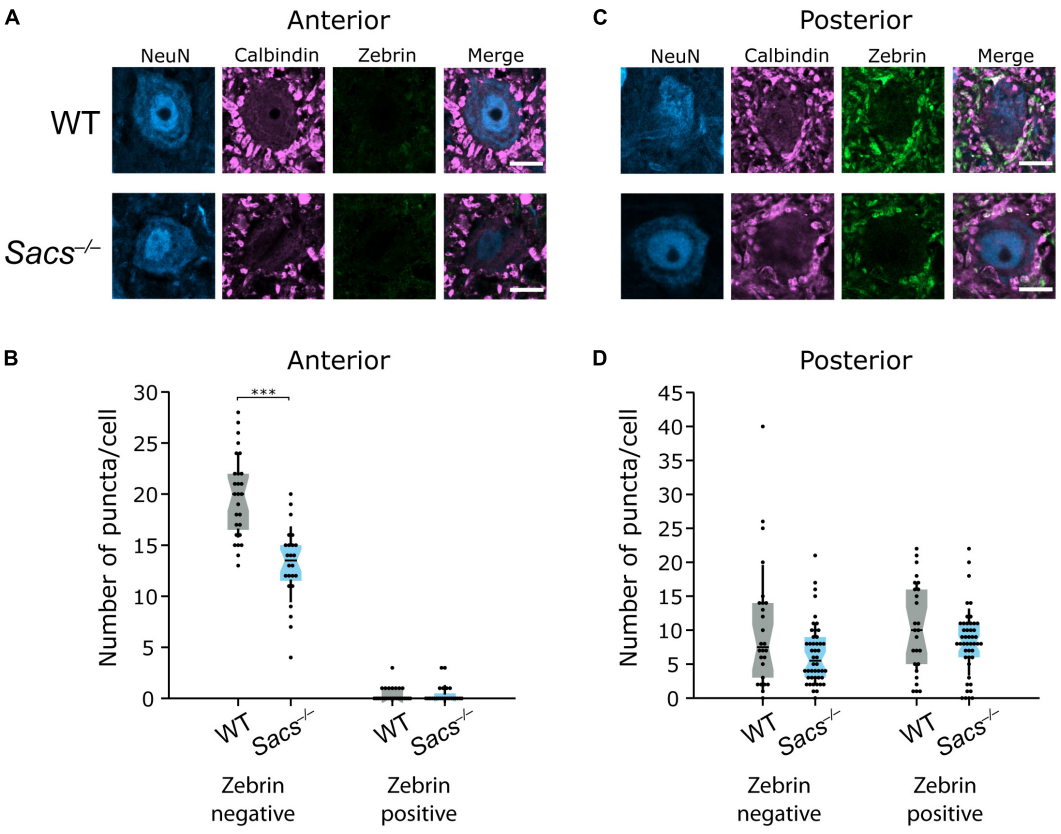

FIGURE 8 | Reduced innervation of CN neurons is restricted to anterior zebrin-negative puncta in *Sacs*$^{-/-}$ mice. **(A)** Representative images of large (>15 μm) CN neurons from the anterior interposed nucleus, with calbindin-positive puncta from Purkinje cells but minimal zebrin-positive puncta. **(B)** Anterior cells in the CN received significantly fewer zebrin-negative Purkinje cell (calbindin only) puncta in *Sacs*$^{-/-}$ mice compared to WT (left; Student's *t*-test, $P < 0.000001$). However, neither WT nor *Sacs*$^{-/-}$ anterior CN neurons received significant input from zebrin-positive Purkinje cells and there were no significant differences between them (Mann Whitney *U* test, $P = 0.81$). **(C)** Representative images of CN neurons from the posterior interposed nucleus. **(D)** Both WT and *Sacs*$^{-/-}$ CN neurons received input from both zebrin-positive and -negative puncta and there was no difference in either the numbers of zebrin-negative (left) or -positive (right) puncta between groups (zebrin-negative: Mann Whitney *U* test, $P = 0.146$, zebrin-positive: Student's *t*-test, $P = 0.163$). ***$P < 0.0001$; $P > 0.05$ when no comparison is shown. Scale bar = 10 μm.

that no major rewiring of puncta occurs from zebrin-positive cells. Interestingly, although the total number of zebrin-negative puncta made onto neurons was lower in posterior CN compared to anterior CN, there was no significant reduction in the number of zebrin-negative puncta in *Sacs*$^{-/-}$ cerebellum compared to WT (Mann Whitney *U* test, $P = 0.15$; **Figures 8C,D**). We also observed unchanged numbers of zebrin-positive Purkinje cell puncta in posterior CN in *Sacs*$^{-/-}$ mice (Student's *t*-test, $P = 0.16$; **Figures 8C,D**). These data suggest that reduction in the innervation of targets in the CN by Purkinje cell axons is predominantly arising from alterations in zebrin-negative Purkinje cells in the anterior vermis. Taken together, our results are consistent with a specific population of Purkinje cells, which do not express zebrin and reside in anterior vermis, that are uniquely vulnerable to loss of sacsin. Vulnerable cells display firing deficits (Ady et al., 2018), show reduced innervation of downstream targets (although Purkinje cells in other projection regions may also be affected in this altered innervation pattern, **Figures 8A,B**) and also are vulnerable to Purkinje cell death as the disease progresses (**Figures 3–6**).

DISCUSSION

In this study, we show that the patterned Purkinje cell death that has been previously described in *Sacs*$^{-/-}$ mice (Lariviere et al., 2015, 2019) occurs predominantly in cells in the anterior vermis that do not express the molecule zebrin, even at late disease stages. Although these cells eventually die, their development appears normal, as the zebrin patterning that arises during development appears largely unaffected in young adult mice prior to Purkinje cell death. Projections from Purkinje cells to target large neurons in the CN also show a pattern of degeneration: reduced synaptic innervation is observed only among zebrin-negative calbindin-positive puncta in anterior CN, but neither zebrin-negative nor zebrin-positive puncta appear affected in posterior CN. These findings support the hypothesis that zebrin-negative Purkinje cells residing in the anterior vermis are uniquely susceptible to cell death in ARSACS.

Patterned Purkinje cell death has been observed in several different diseases and conditions. Sarna and Hawkes suggested that four distinct patterned cell death motifs existed (Sarna and Hawkes, 2003): (1) zebrin-negative cells were uniquely susceptible to cell death, (2) zebrin-positive cells were uniquely susceptible to cell death, (3) cell death is not random, but does not respect a particular molecular profile, or (4) Purkinje cells die randomly. While zebrin-negative cells appear to be uniquely affected in *Sacs*$^{-/-}$ mice, it appears that not all zebrin-negative cells are susceptible, only those residing in anterior lobules. It is possible that in addition to the lack of zebrin expression, there are additional molecules that can be used to characterize these cells. Indeed, there exist molecules that are expressed in subsets of Purkinje cells in patterns that are more reminiscent of the patterning of degeneration we observe, such as PLCβ4 (Sarna et al., 2006), and it is likely that heterogeneity exists even within the zebrin bands that we describe. The predominantly zebrin-negative anterior-vermis degeneration observed here is reminiscent of several other forms of ataxia that show similar patterns of degeneration (Sarna and Hawkes, 2003), including SCA1 (White et al., 2021). It is possible that diseases that share similar patterns of cell degeneration may share common pathophysiological pathways (Niewiadomska-Cimicka et al., 2021), which suggests that common treatment strategies may be pursued for these disparate diseases.

Although we observe no significant differences in zebrin-positive Purkinje cells in anterior lobules since their density is low, it is reasonable to question whether anterior zebrin-positive cells do also degenerate, but their proportion is simply too small to detect. Given that we have queried zebrin-positive cell density at four different ages, and observed virtually identical results across these ages (**Figure 6C**), even while cell death increases in *Sacs*$^{-/-}$ mice overall to ∼40% of WT levels (**Figure 6A**), we feel that this is unlikely, although still possible. We do see systematic increases in the width of zebrin-positive bands as zebrin-negative cells die, suggesting that some rearrangement does occur in the Purkinje cell layer. However, the most parsimonious explanation for our data is that zebrin-positive cells are resilient to cell death in anterior lobules.

We have previously observed that CN neurons showed reduced innervation by Purkinje cell puncta in P40 *Sacs*$^{-/-}$ mice, before cell death in Purkinje cells is observed (**Figures 1**, **2**; Ady et al., 2018). Purkinje cell projections to the CN are not randomly organized, but cluster into different zones with different molecular profiles (Chung et al., 2009), and CN neurons receiving input from predominantly zebrin-negative Purkinje cells fire at higher frequencies *in vivo* than those that receive input predominantly from zebrin-positive Purkinje cells. Therefore, the preferential loss of either zebrin-negative or -positive innervation of the CN likely leads to a drastic alteration in the output of the cerebellar circuit (Beekhof et al., 2021). Notably, there is very little zebrin-positive innervation in the anterior portions of the nuclei (Hawkes and Leclerc, 1986; Sugihara, 2011). Given that firing deficits (Ady et al., 2018) and cell death are predominantly in anterior lobules (**Figures 3–5**; Lariviere et al., 2015), we wondered whether there were changes in the innervation of the CN that we had hitherto missed in *Sacs*$^{-/-}$ mice, since we had not explored the molecular profile of inputs, nor where the neurons we examined were located within the CN. We found that the innervation deficits that we had previously reported (Ady et al., 2018) arose exclusively due to a reduction in zebrin-negative innervation of anterior CN neurons, with no differences observed for neurons in posterior CN in either zebrin-negative or -positive inputs. This suggests that both zebrin identity and positional information help determine the deficits observed in *Sacs*$^{-/-}$ mice. Further molecular subdivision of zebrin-negative neurons may exist, which might shed light on pathophysiological pathways in the Purkinje cells affected in ARSACS.

We have previously reported that sacsin is expressed in cerebellar Purkinje cells (Lariviere et al., 2019), where we did not observe any visible patterning in its distribution. Our results suggest that it is a particular subset of Purkinje cells that are vulnerable to loss of sacsin in ARSACS and that these vulnerable cells, which do not express zebrin and are

located in anterior lobules in the cerebellar vermis, also are likely those that display firing deficits (Ady et al., 2018). However, it is possible that the reduced innervation from zebrin-negative puncta in anterior CN (**Figure 6**) arises from these anterior zebrin-negative Purkinje cells, although zebrin-negative Purkinje cells in other regions may contribute as well. Our data caution that it is essential to consider both the location and the molecular identity of Purkinje cells when studying the disease-causing changes in ARSACS, and likely in other cerebellar disorders since zebrin-negative cells in posterior lobules appear to be resilient. Perhaps by examining the expression pattern of several molecular markers that display unique patterned expression, we will identify a molecular characterization that uniquely identifies the susceptible population of Purkinje cells in ARSACS. Understanding the molecular characteristics that give rise to this vulnerability may contribute to understanding the pathophysiology of ARSACS.

DATA AVAILABILITY STATEMENT

The raw data supporting the conclusions of this article will be made available by the authors, without undue reservation.

ETHICS STATEMENT

The animal study was reviewed and approved by McGill University Animal Care Committee.

AUTHOR CONTRIBUTIONS

RM and AW conceived and designed the manuscript, supervised the study. BT, AC, AS, MR, KV-L, and FC performed the experiments and analyzed the data. BT, AC, RM, and AW wrote the manuscript. All the authors agreed to be accountable for the content of the study.

FUNDING

Funding was provided by the Ataxia Charlevoix-Saguenay (ARSACS) Foundation Research Grant: RM and AW; from the Canada First Research Excellence Fund (CFREF) and Fonds de recherche du Quebec (FRQ), awarded to the Healthy Brains for Healthy Lives (HBHL) initiative at McGill University: RM and AW; the Canadian Institute of Health Research Project Grant (PJT-153150): AW; a doctoral training award from the Fonds de recherche du Québec – Santé: AC; a Faculty of Science Undergraduate Research Award from McGill University: MR; and a MITACS Globalink Research Internship: AS.

ACKNOWLEDGMENTS

We thank all past and present members of the Watt and McKinney labs for helpful advice and thoughtful feedback on the project. Imaging was performed in the McGill University Advanced BioImaging Facility (ABIF), and we thank ABIF staff members for their technical support. We are grateful for the animal care and training we received from the McGill Animal Resources Centre (CMARC), and particularly for the expert help of Tanya Koch.

SUPPLEMENTARY MATERIAL

The Supplementary Material for this article can be found online at: https://www.frontiersin.org/articles/10.3389/fncel.2021.707857/full#supplementary-material

REFERENCES

Ady, V., Marquez, B. T, Nath, M., Chang, P. K., Hui, J., Cook, A. C., et al. (2018). Altered Synaptic and Intrinsic properties of cerebellar Purkinje cells in a mouse model of ARSACS. *J. Physiol.* 596, 4253–4267.

Apps, R., and Hawkes, R. (2009). Cerebellar cortical organization: a one-map hypothesis. *Nat. Rev. Neurosci.* 10, 670–681.

Bailey, K., Rahimi Balaei, M., Mannan, A., Del Bigio, M. R., and Marzban, H. (2014). Purkinje cell compartmentation in the cerebellum of the lysosomal Acid phosphatase 2 mutant mouse (nax - naked-ataxia mutant mouse). *PLoS One* 9:e94327.

Beekhof, G. C., Gornati, S. V., Canto, C. B., Libster, A. M., Schonewille, M., De Zeeuw, C. I., et al. (2021). Activity of Cerebellar Nuclei Neurons Correlates with ZebrinII Identity of Their Purkinje Cell Afferents. *Cells* 10:2686.

Bouchard, J. P., Barbeau, A., Bouchard, R., and Bouchard, R. W. (1978). Autosomal recessive spastic ataxia of Charlevoix-Saguenay. *Can J. Neurol. Sci.* 5, 61–69.

Bouchard, J. P., Richter, A., Mathieu, J., Brunet, D., Hudson, T. J., Morgan, K., et al. (1998). Autosomal recessive spastic ataxia of Charlevoix-Saguenay. *Neuromuscul. Disord.* 8, 474–479.

Brochu, G., Maler, L., and Hawkes, R. (1990). Zebrin II: a polypeptide antigen expressed selectively by Purkinje cells reveals compartments in rat and fish cerebellum. *J. Compar. Neurol.* 291, 538–552.

Chung, S. H., Marzban, H., and Hawkes, R. (2009). Compartmentation of the cerebellar nuclei of the mouse. *Neuroscience* 161, 123–138.

Duncan, E. J., Lariviere, R., Bradshaw, T. Y., Longo, F., Sgarioto, N., Hayes, M. J., et al. (2017). Altered organization of the intermediate filament cytoskeleton and relocalization of proteostasis modulators in cells lacking the ataxia protein sacsin. *Hum. Mol. Genet.* 26, 3130–3143.

Engert, J. C., Berube, P., Mercier, J., Dore, C., Lepage, P., Ge, B., et al. (2000). ARSACS a spastic ataxia common in northeastern Quebec, is caused by mutations in a new gene encoding an 11.5-kb ORF. *Nat. Genet.* 24, 120–125.

Gentil, B. J., Lai, G. T., Menade, M., Lariviere, R., Minotti, S., Gehring, K., et al. (2019). Sacsin, mutated in the ataxia ARSACS, regulates intermediate filament assembly and dynamics. *FASEB J.* 33, 2982–2994.

Girard, M., Lariviere, R., Parfitt, D. A., Deane, E. C., Gaudet, R., Nossova, N., et al. (2012). Mitochondrial dysfunction and Purkinje cell loss in autosomal recessive spastic ataxia of Charlevoix-Saguenay (ARSACS). *Proc. Natl. Acad. Sci. U S A* 109, 1661–1666.

Hawkes, R. (2014). Purkinje cell stripes and long-term depression at the parallel fiber-Purkinje cell synapse. *Front. Syst. Neurosci.* 8:41.

Hawkes, R., and Leclerc, N. (1986). Immunocytochemical demonstration of topographic ordering of Purkinje cell axon terminals in the fastigial nuclei of the rat. *J. Comparat. Neurol.* 244, 481–491.

Lariviere, R., Gaudet, R., Gentil, B. J., Girard, M., Conte, T. C., Minotti, S., et al. (2015). Sacs knockout mice present pathophysiological defects underlying autosomal recessive spastic ataxia of Charlevoix-Saguenay. *Hum. Mol. Genet.* 24, 727–739.

Lariviere, R., Sgarioto, N., Marquez, B. T., Gaudet, R., Choquet, K., McKinney, R. A., et al. (2019). Sacs R272C missense homozygous mice develop an ataxia phenotype. *Mol. Brain* 12:19.

Larouche, M., and Hawkes, R. (2006). From clusters to stripes: the developmental origins of adult cerebellar compartmentation. *Cerebellum* 5, 77–88.

Marzban, H., and Hawkes, R. (2011). On the architecture of the posterior zone of the cerebellum. *Cerebellum* 10, 422–434.

Miyazaki, T., Yamasaki, M., Hashimoto, K., Yamazaki, M., Abe, M., Usui, H., et al. (2012). Cav2.1 in cerebellar Purkinje cells regulates competitive excitatory synaptic wiring, cell survival, and cerebellar biochemical compartmentalization. *J. Neurosci.* 32, 1311–1328.

Niewiadomska-Cimicka, A., Doussau, F., Perot, J.-B., Roux, M. J., Keime, C., Hache, A., et al. (2021). SCA7 mouse cerebellar pathology reveals preferential downregulation of key Purkinje cell-identity genes and shared disease signature with SCA1 and SCA2. *J. Neurosci.* 2021, 1882–1820.

Parfitt, D. A., Michael, G. J., Vermeulen, E. G., Prodromou, N. V., Webb, T. R., Gallo, J. M., et al. (2009). The ataxia protein sacsin is a functional co-chaperone that protects against polyglutamine-expanded ataxin-1. *Hum. Mol. Genet.* 18, 1556–1565.

Perkins, E. M., Clarkson, Y. L., Suminaite, D., Lyndon, A. R., Tanaka, K., Rothstein, J. D., et al. (2018). Loss of cerebellar glutamate transporters EAAT4 and GLAST differentially affects the spontaneous firing pattern and survival of Purkinje cells. *Hum. Mol. Genet.* 27, 2614–2627.

Sarna, J. R., and Hawkes, R. (2003). Patterned Purkinje cell death in the cerebellum. *Prog. Neurobiol.* 70, 473–507.

Sarna, J. R., and Hawkes, R. (2011). Patterned Purkinje cell loss in the ataxic sticky mouse. *Eur. J. Neurosci.* 34, 79–86.

Sarna, J. R., Marzban, H., Watanabe, M., and Hawkes, R. (2006). Complementary stripes of phospholipase Cbeta3 and Cbeta4 expression by Purkinje cell subsets in the mouse cerebellum. *J. Comparat. Neurol.* 496, 303–313.

Sawada, K., Kalam Azad, A., Sakata-Haga, H., Lee, N. S., Jeong, Y. G., and Fukui, Y. (2009). Striking pattern of Purkinje cell loss in cerebellum of an ataxic mutant mouse, tottering. *Acta Neurobiol. Exp.* 69, 138–145.

Sugihara, I. (2011). Compartmentalization of the deep cerebellar nuclei based on afferent projections and aldolase C expression. *Cerebellum* 10, 449–463.

Voogd, J., and Ruigrok, T. J. (2004). The organization of the corticonuclear and olivocerebellar climbing fiber projections to the rat cerebellar vermis: the congruence of projection zones and the zebrin pattern. *J. Neurocytol.* 33, 5–21.

Wadiche, J. I., and Jahr, C. E. (2005). Patterned expression of Purkinje cell glutamate transporters controls synaptic plasticity. *Nat. Neurosci.* 8, 1329–1334.

White, J. J., Arancillo, M., Stay, T. L., George-Jones, N. A., Levy, S. L., Heck, D. H., et al. (2014). Cerebellar zonal patterning relies on Purkinje cell neurotransmission. *J. Neurosci.* 34, 8231–8245.

White, J. J., Bosman, L. W. J., Blot, F. G. C., Osorio, C., Kuppens, B. W., Krijnen, W., et al. (2021). Region-specific preservation of Purkinje cell morphology and motor behavior in the ATXN1[82Q] mouse model of spinocerebellar ataxia 1. *Brain Pathol.* 2021:e12946.

Xiao, J., Cerminara, N. L., Kotsurovskyy, Y., Aoki, H., Burroughs, A., Wise, A. K., et al. (2014). Systematic regional variations in Purkinje cell spiking patterns. *PLoS One* 9:e105633.

Zhou, H., Lin, Z., Voges, K., Ju, C., Gao, Z., Bosman, L. W., et al. (2014). Cerebellar modules operate at different frequencies. *Elife* 3:e02536.

Conflict of Interest: The authors declare that the research was conducted in the absence of any commercial or financial relationships that could be construed as a potential conflict of interest.

Publisher's Note: All claims expressed in this article are solely those of the authors and do not necessarily represent those of their affiliated organizations, or those of the publisher, the editors and the reviewers. Any product that may be evaluated in this article, or claim that may be made by its manufacturer, is not guaranteed or endorsed by the publisher.

Copyright © 2021 Toscano Márquez, Cook, Rice, Smileski, Vieira-Lomasney, Charron, McKinney and Watt. This is an open-access article distributed under the terms of the Creative Commons Attribution License (CC BY). The use, distribution or reproduction in other forums is permitted, provided the original author(s) and the copyright owner(s) are credited and that the original publication in this journal is cited, in accordance with accepted academic practice. No use, distribution or reproduction is permitted which does not comply with these terms.

frontiers in Cellular Neuroscience

ORIGINAL RESEARCH
published: 13 January 2022
doi: 10.3389/fncel.2021.803302

Neuroprogenitor Cells From Patients With TBCK Encephalopathy Suggest Deregulation of Early Secretory Vesicle Transport

*Danielle de Paula Moreira[1†], Angela May Suzuki[1†], André Luiz Teles e Silva[2], Elisa Varella-Branco[1], Maria Cecília Zorél Meneghetti[3], Gerson Shigeru Kobayashi[1], Mariana Fogo[1,2], Merari de Fátima Ramires Ferrari[4], Rafaela Regina Cardoso[4], Naila Cristina Vilaça Lourenço[1], Karina Griesi-Oliveira[1,2], Elaine Cristina Zachi[1], Débora Romeo Bertola[1,5], Karina de Souza Weinmann[1], Marcelo Andrade de Lima[3], Helena Bonciani Nader[3], Andrea Laurato Sertié[2] and Maria Rita Passos-Bueno[1]**

[1] Centro de Pesquisas Sobre o Genoma Humano e Células-Tronco, Instituto de Biociências, Universidade de São Paulo, São Paulo, Brazil, [2] Instituto de Ensino e Pesquisa Albert Einstein, Albert Einstein Hospital, São Paulo, Brazil, [3] Departamento de Bioquímica, Escola Paulista de Medicina, Universidade Federal de São Paulo, São Paulo, Brazil, [4] Departamento de Genética e Biologia Evolutiva, Instituto de Biociências, Universidade de São Paulo, São Paulo, Brazil, [5] Instituto da Criança do Hospital das Clínicas, Faculdade de Medicina da Universidade de São Paulo, São Paulo, Brazil

Biallelic pathogenic variants in TBCK cause encephaloneuropathy, infantile hypotonia with psychomotor retardation, and characteristic facies 3 (IHPRF3). The molecular mechanisms underlying its neuronal phenotype are largely unexplored. In this study, we reported two sisters, who harbored biallelic variants in TBCK and met diagnostic criteria for IHPRF3. We provided evidence that TBCK may play an important role in the early secretory pathway in neuroprogenitor cells (iNPC) differentiated from induced pluripotent stem cells (iPSC). Lack of functional TBCK protein in iNPC is associated with impaired endoplasmic reticulum-to-Golgi vesicle transport and autophagosome biogenesis, as well as altered cell cycle progression and severe impairment in the capacity of migration. Alteration in these processes, which are crucial for neurogenesis, neuronal migration, and cytoarchitecture organization, may represent an important causative mechanism of both neurodevelopmental and neurodegenerative phenotypes observed in IHPRF3. Whether reduced mechanistic target of rapamycin (mTOR) signaling is secondary to impaired TBCK function over other secretory transport regulators still needs further investigation.

Keywords: STAM, early secretory pathway, vesicle trafficking, autophagy, GM130, clathrin, mTOR, iPSC-neurodevelopmental disease modeling

OPEN ACCESS

Edited by:
Annalisa Scimemi, University at Albany, United States

Reviewed by:
Daisuke Mori, Nagoya University, Japan
Gaelle Boncompain, Institut Curie, France

****Correspondence:***
Maria Rita Passos-Bueno
passos@ib.usp.br

[†] These authors have contributed equally to this work and share first authorship

Specialty section:
This article was submitted to Cellular Neuropathology, a section of the journal Frontiers in Cellular Neuroscience

Received: *27 October 2021*
Accepted: *15 December 2021*
Published: *13 January 2022*

Citation:
Moreira DP, Suzuki AM, Silva ALT, Varella-Branco E, Meneghetti MCZ, Kobayashi GS, Fogo M, Ferrari MFR, Cardoso RR, Lourenço NCV, Griesi-Oliveira K, Zachi EC, Bertola DR, Weinmann KS, Lima MA, Nader HB, Sertié AL and Passos-Bueno MR (2022) Neuroprogenitor Cells From Patients With TBCK Encephalopathy Suggest Deregulation of Early Secretory Vesicle Transport. Front. Cell. Neurosci. 15:803302. doi: 10.3389/fncel.2021.803302

INTRODUCTION

Genomic high throughput studies in cohorts of individuals with neurodevelopmental disorders, involving autism spectrum disorder (ASD), epilepsy, and intellectual disability (ID), have recognized several novel rare genetic syndromes. Among them, biallelic pathogenic variants in TBCK (TBC1 domain containing kinase) have been shown to cause infantile hypotonia with

psychomotor retardation and characteristic-facies 3 (IHRPF3, OMIM#616900), a severe early onset encephaloneuropathy mainly characterized by developmental delay, hypotonia, and facial dysmorphisms (Bhoj et al., 2016; Chong et al., 2016; Sumathipala et al., 2019). The number of reported cases is still limited to about 40 cases, and the description of novel cases can contribute to a better characterization of the spectrum of clinical variability of this syndrome.

TBCK, a member of the TBC family of proteins, contains a predicted active TBC Rab-GAP domain, which usually functions as GAP for members of the Rab family of small GTPases (also known as small G-proteins), flanked by an N-terminal catalytically inactive kinase domain and a C-terminal rhodanese homology domain (RHOD) (Komurov et al., 2010; Gabernet-Castello et al., 2013). TBCK has been proposed to act on cell proliferation and autophagy through the mechanistic target of rapamycin (mTOR) signaling pathway in non-neural studies (Liu et al., 2013; Ortiz-González et al., 2018). However, to date, less is known about the mechanism of action of TBCK, being unknown whether disruption of mTOR signaling is a primary or secondary effect of loss of TBCK. In addition, depending on the cell type, TBCK has been associated with both tumor-promoting and tumor-suppressive function (Liu et al., 2013; Wu et al., 2014; Wu and Lu, 2021), suggesting variable regulation according to the cell type. Although biallelic loss-of-function variants in TBCK are associated with several neural clinical phenotypes, functional studies of TBCK in neural cells are still lacking.

In this study, we described two new IHPRF3-affected sibs that present autism as an additional clinical feature of the syndrome and are compound heterozygotes for loss-of-function variants in TBCK. In order to gain more insights into mechanisms of action of TBCK in neural cells and to better understand the pathophysiology of IHPRF3 syndrome, we employed neuroprogenitor cells (iNPC) derived from induced pluripotent stem cells (iPSC) from the two IHPRF3-affected sibs. Colocalization analysis of the TBCK protein with early secretory pathway markers suggests altered ER-to-Golgi vesicle transport as a possible mechanism for the impaired autophagosome biogenesis, cell cycle progression, and migration observed in cells of patients. iNPC of patients also showed decreased mTOR signaling, which may be secondary to impaired regulation of TBCK-mutated protein over other early secretory vesicle transport regulators.

MATERIALS AND METHODS

Subjects

The two affected sisters (F6331-1 and F6331-4) were ascertained after initial diagnosis of ASD and the following referral to the genetic counseling service at Centro de Estudos do Genoma Humano e Células-Tronco (CEGH-CEL), Universidade of São Paulo (USP). Patients were routinely diagnosed based on DSM-5 (American Psychiatric Association, 2013) and CARS evaluation.

Control individuals (F7007-1, F8799-1, and F10006-1; one male and two females, respectively, aged 31, 29, and 33 years) are healthy and unrelated to the affected individuals.

This study was approved by the National Ethics Committee (Comissão Nacional de Ética em Pesquisa no Brazil, Process no. CAAE43559314.0.0000.5464). Blood from all the individuals was collected after a signed written informed consent by the participants of the study or their legal representatives.

Investigation of Pathogenic Variants

DNA Extraction

Genomic DNA extraction from whole blood was performed using the QIAsymphony automated workstation, following the instructions of the manufacturer (Qiagen, United States).

Selection of Whole-Exome Sequencing and Variants

Whole-exome sequencing (WES) and bioinformatic analysis were performed at the CEGH-CEL sequencing facility. Exome capture was carried out using the TruSeq Exome Library Prep Kit (Illumina, Inc., United States) following the recommendations of the manufacturer. HiSeq 2500 sequencer (Illumina) was used for sequencing paired-end reads of approximately 100 bp × 100 bp. Reads were aligned with Burrows-Wheeler Aligner (BWA), against the hg19 reference genome (Li and Durbin, 2009). Data processing and variant calling were carried out on Picard and Genome Analysis Tool Kit (GATK) (McKenna et al., 2010). ANNOVAR (Wang et al., 2010) was used to annotate variants. Candidate pathogenic variants were filtered according to the following criteria: (a) exclusion of low-quality variants; (b) inclusion of rare variants with minor allele frequency (MAF) < 0.01 in reference databases (i.e., 1,000 Genomes Project (1000G), National Institutes of Health; 6,500 Exome Sequencing Project (6500ESP), Washington University; and ABraOM, University of São Paulo (Naslavsky et al., 2017); (c) inclusion of variants with frequency < 0.05 in internal control samples (i.e., DNA samples that were sequenced and processed in the same batch); (d) exclusion of polymorphic genes (Fajardo et al., 2012); and (e) exclusion of variants located within the last three amino acids of a protein. We prioritized homozygous or compound-heterozygous loss-of-function (LoF) variants shared between the two affected siblings. The position of the candidate LoF variant identified was manually converted to GRCh38/hg38, using the UCSC website[1].

Sanger Sequencing

Sanger sequencing of genomic DNA and cDNA was performed for the validation of the candidate variant and segregation analysis. Primers for PCR amplification and sequencing were designed on Primer-BLAST (NCBI;[2]) (**Supplementary Table 1**).

Array Comparative Genomic Hybridization and Real-Time Quantitative PCR for Copy Number Analysis

Array comparative genomic hybridization (aCGH, 180K, Agilent, United States) was performed in both patients according to the recommendations of the manufacturer. The analysis was carried out using Agilent Genomic Workbench 7.0 (Agilent Technologies, Santa Clara, CA, United States).

[1]https://genome.ucsc.edu/

[2]http://www.ncbi.nlm.nih.gov/tools/primer-blast/

Real-time quantitative PCR (RT-qPCR) of TBCK was performed to detect the predicted small deletion in the region chr4:107,071,580−107,113,380. Six primer pairs were designed on Primer-BLAST (**Supplementary Table 2**). Relative quantification was carried out by normalization to GAPDH, and quantification data were calibrated relative to a control without any known CNV in TBCK (D'haene et al., 2010).

iPSC Reprogramming

Induced pluripotent stem cells were reprogrammed from peripheral blood mononuclear cells (PBMC), using a non-viral method with non-integrating plasmids (Okita et al., 2013), which was established at HUG-CELL with minor modifications (Griesi-Oliveira et al., 2015; Miller et al., 2017). AMAXA nucleoporator (Lonza, Basel, Switzerland) was used for the transfection of plasmids containing the transcription factors OCT-4, SOX2, KLF4, L-MYC, and LIN28. Each reprogrammed cell line was cocultivated with irradiated murine embryonic fibroblasts (MEF, Millipore) in DMEM/F12 medium supplemented with 2mM GlutaMAX-I, 0.1 mM non-essential amino acids, 55 μM 2-mercaptoethanol, 30 ng/ml fibroblast growth factor (FGF-2), and 20% of knockout serum replacement (KSR, Life Technologies). iPSC colonies with typical morphology were then transferred to Matrigel (BD-Bioscience) coated plates and fed with E8 medium (Life Technologies). All iPSC colonies were tested for plasmid integration into the host genome and excluded for the presence of aneuploidies with SALSA MLPA P070 Human Telomere-5 probe mix (MRC-Holland). Cell pluripotency was evaluated through stem cell markers prior to differentiation to iNPC.

Neuroprogenitor Cells Differentiation

Differentiation of iPSC into iNPC was carried out using a protocol previously established at HUG-CELL (Griesi-Oliveira et al., 2015). In brief, iPSC were cultivated in 0.5 × NB medium (1/2 DMEM/F12: 1/2 Neurobasal media with 0.5 × N-2 supplement (100×) (Thermo Fisher Scientific) and 0.5 × B27 minus vitamin A supplement (50×) (Thermo Fisher Scientific) supplemented with Dorsomorphin, 1 μM (Tocris) for 2 days. Then, iPSC were harvested with accutase treatment, and cell clumps were manually transferred into low-attachment plates (Corning) on 0.5 × NB medium supplemented with 1 μM dorsomorphin. The next day, the medium was replaced with 0.5 × NB medium supplemented with 20 ng/ml FGF-2 and 20 ng/ml epidermal growth factor (EGF) (Thermo Fisher Scientific) and allowed to grow in suspension for 7 days. Then, the resulting embryoid bodies were lightly dissociated with accutase and plated on matrigel-coated plates, from which rosettes start to form within 4–7 days. The selected rosettes were manually collected and plated in poly-L-ornithine (10 μg/ml; Sigma) and natural mouse laminin (5 μg/ml; Invitrogen) coated plates for iNPC expansion. All iNPC were characterized through neural progenitor markers.

Except in cell cycle and BrdU incorporation assays, for which we used iNPC only from patient F6331-1, in each experiment performed in this study, we used iNPC from all individuals (patients: F6331-1 and F6331-4; and controls F7007-1, F8799-1, and F10006-1).

Neurosphere Formation (3D Model)

Notably, 25 μl drops of cell suspension containing a total of 4 × 104 iNPC (N = 5, in passage number ranging between 6 and 8) in 0.5 × NB medium containing 20 ng/ml FGF-2 and 20 ng/ml EGF were placed onto the lid of a 10-cm dish and set to rest for 48 h at 37°C and 5% CO_2. After this period, the cells aggregated into homogeneous neurosphere sizes were placed into 6-well low attachment plates in 0.5 × NB medium supplemented with 20 ng/ml FGF-2 and 20 ng/ml EGF.

Cell Culture Conditions

mTOR signaling activity and autophagy in iNPC were evaluated in normal culture condition and in the following three stress-inducing conditions: (i) absence of EGF and FGF-2 for 24 h; (ii) absence of EGF and FGF-2 and concomitant incubation with mTOR inhibitor, rapamycin (100 nM) for 24 h; and (iii) absence of EGF and FGF-2 for 24 h and subsequent addition of brefeldin A (BFA, 4 μM), which induce Golgi complex fragmentation, for 3 h.

RNA Extraction and RT-qPCR

Total RNA from all iPSC and iNPC cultures was isolated using NucleoSpin RNA II Kit (Macherey-Nagel, Thermo Fisher; Merk Millipore), and cDNA was synthesized by reverse transcription using SuperScript IV (Thermo Fisher Scientific).

Primer pairs for *TBCK*, *CLTC*, *CLTD*, *RAB5A*, *STAM1,* and *STAM2* (**Supplementary Table 3**) were designed at Primer-BLAST, while primers of pluripotency markers (*OCT3/4* and *NANOG*), neural markers (*PAX6* and *SOX1*), and housekeeping genes (*GAPDH* and *TBP*) were adopted from the literature (Ishiy et al., 2015; Miller et al., 2017). Each sample was analyzed in triplicate with the use of Fast SYBR Green PCR Master Mix (Applied Biosystems) according to the recommendations of the manufacturer. The reactions were run in a QuantStudio® 5 Real-Time PCR system (Applied Biosystems). The expression of each gene was normalized to GAPDH or TBP housekeeping gene, and the results are shown as the mean fold change of the normalized gene expression relative to a calibrator sample. For pluripotency or neural markers, another cell type with no expression of the gene tested was used as a negative control.

Cell Lysis and Western Blot

Cells were homogenized in RIPA buffer (Thermo Fisher Scientific) containing protease and phosphatase inhibitor cocktails (Sigma). Lysates were incubated on ice for 10 min and then centrifuged at 8,000 × g for 15 min at 4°C, and the supernatants of total cell lysates were collected. Protein concentrations were determined with a BCA microprotein assay kit (BioAgency). A total of 20 μg of protein from each sample were separated by sodium dodecyl sulfate-polyacrylamide gel electrophoresis (SDS-PAGE) and transferred to nitrocellulose membranes, which were blocked with 5% bovine serum albumin (BSA) for 1 h and then incubated

with primary antibodies overnight at 4°C. Detection was performed using horseradish peroxidase-coupled anti-mouse or anti-rabbit secondary antibodies (1:2,000, Cell Signaling Technology), enhanced chemiluminescence (ECL) substrate (GE Healthcare), and ImageQuant LAS-4000 (GE Healthcare). The intensity of the bands was determined by densitometry using NIH ImageJ software (Bethesda, MD, United States)[3]. The following primary antibodies were used: anti-TBCK (1:50, #sc-81865, Santa Cruz Biotechnology), anti-pRPS6240/244 (1:5,000, #5364), anti-LC3A/B (1:1,000, #12741), anti-BECN1 (1:1,000, #3738), anti-p62/SQSTM1 (1:1,000, #8025) from Cell Signaling Technology, anti-Cathepsin D (1:2,000, #ab75852), anti-Vinculin (1:5,000, #ab18058) from Abcam, and anti-βactin (1:15,000, A2228 Sigma) antibodies. All target protein levels were quantified and normalized to the corresponding β-actin or vinculin levels.

AKT/Mechanistic Target of Rapamycin Multiplex Assay

mTOR signaling activity from iNPC cultured in the absence of EGF and FGF-2 for 24 h was also assayed using the MILLIPLEX MAP® Akt/mTOR Phosphoprotein Magnetic Bead 11-Plex panel (#48-611MAG) and the MILLIPLEX MAP AKT/mTOR 11-plex panel (#48-612MAG) (Millipore) with 10 μg of total protein extracts of each sample, according to the instructions of the manufacturer.

Immunofluorescence

iPSC and iNPC grown on coverslips were fixed in 4% Paraformaldehyde (PFA), permeabilized in 0.2% Triton X-100 in Phosphate Buffered Saline (PBS) for 30 min at 4°C, and blocked for 1 h in PBS containing 5% BSA, and then incubated overnight at 4°C with primary antibodies diluted in the same blocking buffer. Primary antibodies used are as follows: anti-SOX1 (1:200, #4194S), anti-RAB7 (1:200, #9367), anti-LC3 (1:200, #3868) from Cell Signaling Technology; anti-SOX2 (1:100, #ab171380) and anti-GM130 (1:50, #ab52649) from Abcam; anti-COPII (1:200, #PA1-069A) from Thermo Fisher Scientific; anti-TBCK (1:50, #sc-81865), anti-RAB5A (1:100, #sc-309), anti-clathrin (1:200, #sc-6579), and anti-caveolin (1:200, #sc-894) from Santa Cruz Biotechnology; anti-STAM (1:200, #12434-1-AP, Proteintech). Cells for anti-LC3 labeling were fixed with methanol and proceeded with the same protocol described. Then, cells were washed 3 times with PBS and incubated with secondary antibodies conjugated with Alexa fluor 488 or Alexa fluor 680 for 1 h at room temperature. After another washing step, the cells were mounted in a Vectashield mounting medium with 4′,6-diamidino-2-phenylindole (DAPI) (1 μg/ml, Vector Labs). Samples were analyzed using a confocal laser scanning microscope, LSM800 (Zeiss), using an immersion lens (63 × /1.40 Oil). Each channel was imaged separately. The acquired fluorescent images were converted to tiff format and further processed using Fiji software. Background from all the images was subtracted using the Fiji background subtraction algorithm (rolling ball radius = 50 pixels). To quantify TBCK colocalization with Caveolin, Clathrin, RAB5A, STAM, GM130/GOLGA2, and COPII, the Manders method of correlation (MCC) was performed using ImageJ/Fiji-Coloc2 plugin. For the analysis of LC3 puncta, the binary images generated after background subtraction were filtered for particles with Feret diameter larger than 100 nm. The number of puncta was calculated by dividing the total number per number of cell nuclei labeled in a given image. Then, we calculated the mean and SD for the puncta number and puncta size (Kjos et al., 2017) of each sample.

[3]http://rsbweb.nih.gov/ij/

Cell Cycle and Cell Proliferation Analysis

A total of 5 × 105 iNPC from each sample (in similar passage number, ranging between 5 and 6) were seeded in duplicate into 6-well plates (Corning) in 0.5 × NB medium supplemented with 20 ng/ml EGF and 20 ng/ml FGF-2. The day after seeding, EGF and FGF-2 were removed from 0.5 × NB medium during 24 h for cell cycle synchronization at G0/G1 (T0) (Mazemondet et al., 2011). After this period, the medium was replaced with 0.5 × NB medium supplemented with EGF and FGF-2 to induce cell cycle progression and cell proliferation. Cells were collected at T0 (right after 24 h of EGF and FGF-2 deprivation), 24 and 40 h after growth factor supplementation (T24 and T40, respectively).

Three hours before collection of the cells, at each time point, 20 μM BrdU was added (Sigma-Aldrich). Then, iNPC were rinsed twice with PBS, harvested with trypsin incubation, and fixed in 70% EtOH overnight at −20°C. After complete fixation, cells were double-stained with propidium iodide (PI) and anti-BrdU (BrdU Monoclonal Antibody, FITC, Invitrogen), in order to ascertain the cell distribution through cell cycle stages (G0/G1, S, and G2/M) and cell proliferation, respectively. Appropriate assay controls were used in the assay (unstained sample; PI-stained- and anti-BrdU-stained-only samples), and at least 5,000 events were acquired. Data were analyzed using Guava Express PRO software (Millipore) and gated to remove debris and cell clumps.

Apoptosis Analysis

A total of 2 × 105 iNPC were seeded into a 12-well plate (Corning), in duplicate. In the following day, cells were incubated with 20 μl of CellEvent® Caspase-3/7 Green ReadyProbes Reagent (Thermo Fisher Scientific) for 1 h, at 37°C, and 5% CO_2. Then, iNPC were rinsed with PBS, fixed with 4% PFA, and the nuclei stained with Vectashield mounting medium with DAPI. Images were captured using a Nikon fluorescence microscope (Nikon Eclipse Ti-E, Nikon). The quantification of caspase marked cells was performed using ImageJ software from three different fields from each duplicate. We determined the total number of cells by DAPI nuclear staining.

Cell Migration

For radial migration assay, 25 μl drops of cell suspension containing a total of 5 × 104 iNPC (in passage number ranging between 5 and 6) in 0.5 × NB medium containing 20 ng/ml FGF-2 and 20 ng/ml EGF were placed onto the lid of a 10-cm dish and set to rest for 48 h at 37°C and 5% CO_2. After this period, the cells aggregate into homogeneous

neurosphere size. A total of 4 neurospheres per sample were then transferred to poly-L-ornithine (10 μg/ml; Sigma) and natural mouse laminin (5 μg/ml; Invitrogen) coated plates in 0.5 × NB medium containing 20 ng/ml FGF-2 and 20 ng/ml EGF. Images were captured at 4, 8, and 24 h after adhesion to the coated plates. The pictures were acquired using the EVOS Cell Imaging System (Thermo Fisher Scientific). Cell migration was analyzed using ImageJ software. For each time point, we measured the neurosphere outer edges. Cell migration was estimated by the outer diameter of neurosphere migration normalized to inner neurosphere diameter (μm) (Ge et al., 2016).

Statistical Analysis

Data were analyzed using the non-parametric unpaired two-tailed Wilcoxon-Mann-Whitney test or one-way ANOVA followed by the recommended correction test, using Graphpad 7.0 (Graphpad Software Inc., La Jolla, CA, United States). A regression *via* decision tree was used to analyze cell-cycle progression, using the R package (R Core team, 2019). For functional enrichment analysis of proteomic data, Fisher's exact test was applied. p-values < 0.05 were considered statistically significant. In the figures, statistical significances are indicated as follows: $^{*}p < 0.05$, $^{**}p < 0.01$, and $^{***}p < 0.001$. Data are expressed as mean ± SD.

RESULTS

Clinical Presentation of Patients

The two affected sisters in this study reported were born from a non-consanguineous healthy couple (**Figure 1A**) at 38 weeks of gestation *via* vaginal delivery, with normal anthropometric measurements (**Table 1**). The proband (Patient F6331-1), first evaluated at CEGH-CEL by the age of 6 years, presented with global developmental delay. At the age of 3 months, her parents noticed she had low muscle tone (e.g., she could not hold her neck and head). Later, they noticed delayed unassisted sitting (after 12 months) and walking (after 30 months), as well as delayed speech (first words after 24 months), which was limited to a few words. At the age of 3 years, she was diagnosed with autism and ID, and at the age of 7 years, she had a severe psychotic episode. Further clinical evaluation showed several dysmorphic features, prominent digit pads, metabolic abnormalities like dyslipidemia and hypothyroidism, and brain MRI at 12 years showed white matter volumetric reduction and T2 hyperintensity (**Table 1** and **Supplementary Figure 1A**). ECG and EEG were normal. At 14 years of age, she attended a special school and only said a few words and short sentences and showed inattention and lack of motivation to engage in educational activities.

The second affected sister (Patient F6331-4), first evaluated at CEGH-CEL by the age of 3 years, showed a better initial psychomotor developmental course. She sat unaided at about 6 months and could walk unassisted at about 14 months, but at around 12 months, she was diagnosed with autism and global developmental delay. She had the first seizure episode at the age of 4 years and was diagnosed with focal and generalized epilepsy at approximately 6 years of age. EEG demonstrated diffuse bilateral slow waves with multifocal epileptiform discharges. Clinical evaluation at the age of 7 years showed similar dysmorphic features to her sister F6331-1, in addition to brachydactyly of the fourth and fifth toes and hypoplastic nails. She also developed metabolic abnormalities, and an MRI of the brain at the age of 9 years showed a volumetric reduction of the white matter (**Supplementary Figure 1B**). At 10 years of age, she showed progressive weakness in her lower limbs, first noticed approximately at the age of 8 years. ECG was normal.

Biallelic Loss-of-Function Variants in TBCK Cosegregate With the Syndrome

To investigate the genomic cause of the clinical phenotypes of patients, we performed array comparative genomic hybridization (aCGH), whole-exome sequencing (WES), and subsequent site-specific quantification of genomic DNA using the RT-qPCR. WES and RT-qPCR analyses revealed that the sisters share rare LoF variants in exon 23 of the TBCK gene: a stopgain variant (NM_001163435: c.2130C > G; p.Tyr710*) and a microdeletion (NM_001163435: c.2060_2235del; p.Glu687Valfs9*) (**Figures 1B,C** and **Supplementary Figure 2**). Conventional PCR and Sanger sequencing, using either genomic DNA or cDNA isolated from iNPC validated both variants and are better described below.

cDNA sequencing revealed that the microdeletion leads to the loss of exon 23 and juxtaposition of exons 22 and 24, resulting in a predicted premature termination codon (PTC) in exon 24 (**Figures 1B,C** and **Supplementary Figure 2C**). Segregation analysis showed that the stopgain variant was inherited from their father and the microdeletion from their mother (**Supplementary Figures 2A,B**), while the unaffected sib did not inherit any of these variants. Both variants were considered pathogenic according to the American College of Medical Genetics and Genomics (ACMG) guidelines (Richards et al., 2015). No additional disrupting variants following an autosomal recessive inheritance model were identified by WES or aCGH.

Quantitative analyses showed that iNPC of patients exhibited over the twofold decrease in *TBCK* mRNA expression, both truncated alleles were transcribed (**Figures 1B,D**), and through Western blot (WB), we observed a single faint band with the same electrophoretic mobility as the wild type (WT) *TBCK* protein in controls (**Figures 1E,F**). These results show that the C-terminal variants identified in these patients cause a strong disruption in TBCK translation.

Patient-Derived Neuroprogenitor Cells Under Stress-Inducing Conditions Exhibit Downregulation of Mechanistic Target of Rapamycin Signaling Activity

To explore the neural functional consequences of the identified variants in *TBCK*, we differentiated iNPC from iPSC from the 2 IHPRF3 patients and 3 unrelated controls. All iPSC colonies were positive for pluripotency markers (*OCT3/4* and *NANOG*) (**Supplementary Figures 3A,B**), and the iNPC were positive for neural stem cell markers (*SOX1*, *SOX2,* and *PAX6*) (**Supplementary Figures 3C,E**), suggesting successful cell reprogramming and differentiation.

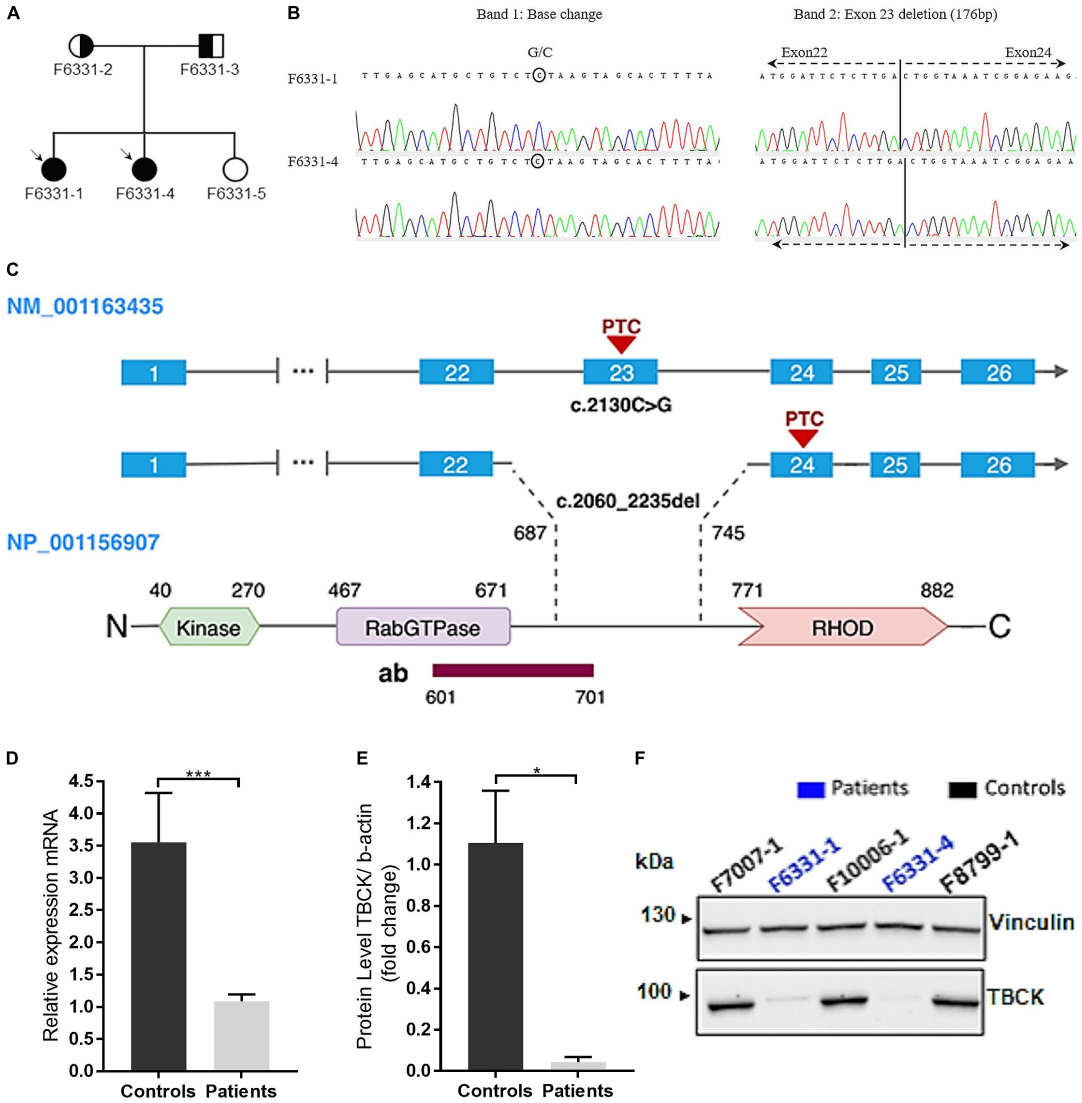

FIGURE 1 | IHPRF3 patients harboring biallelic pathogenic variants in TBCK and relative quantification of mRNA and protein expression levels in iNPC. **(A)** Pedigree of family F6331. Circle—female; square—male; symbol-filled—affected patients; symbol empty—not affected sister; circle half-filled—harbors the heterozygous microdeletion; square half-filled—harbors the heterozygous stopgain variant. **(B)** Chromatograms of the cDNA sequence show that both alleles are expressed: in the left image, a base change in Band 1 (expected base G changed to a C in reverse strand) represents the stopgain variant; and in the right image, the juxtaposition of exons 22 and 24 (excision of exon 23) in Band 2 representing the allele with the microdeletion. Bands 1 and 2 represent cDNA PCR products for TBCK in agarose gel (**Supplementary Figure 2A**). **(C)** Schematic representation of TBCK transcript and protein. The illustration shows the two mutant isoforms identified in the patients and the predicted positions on the protein. The antibody target region is also represented. The pathogenic variants create a putative premature termination codon (PTC) in exons 23 and 24, located within the C-terminal region of the protein, upstream of the RHOD domain. **(D)** TBCK mRNA expression (data from TBCK-mRNA-3 primer pair) shows reduced transcript levels in patients, compared with controls. Each biological sample had three technical replicates, and each individual was considered a biological replicate. **(E,F)** Western blot (WB) shows low levels of TBCK protein in iNPC of patients, compared with iNPC of controls, which are compatible with an autosomal recessive inheritance condition. *p-value < 0.05, ***p-value < 0.001, and n.s.—not significant. Data on graphs are shown as mean ± SD of technical replicates and biological samples. Patients: F6331-1 and F6331-4 ($N = 2$); controls: F7007-1, F8799-1, and F10006-1 ($N = 4$).

First, to investigate whether iNPC from IHPRF3 patients show abnormal mTOR signaling activity, we analyzed by Western blot the phosphorylation levels of the ribosomal protein RPS6, a downstream target of the mTORC1 signaling pathway. Phosphorylated RPS6 (p-RPS6S240/244) was quantified in iNPC grown in normal conditions (in the presence of EGF and FGF-2 growth factors) and in three stress-inducing conditions. Under normal growth conditions, we did not detect any difference in p-RPS6S240/244 levels between patient-derived and control-derived iNPC (**Figures 2A,C** and **Supplementary Figures 4A,C,D**). Intracellular stress caused by the withdrawal of EGF/FGF-2 alone significantly decreased RPS6 activation in iNPC of patients in comparison to controls (p-RPS6S240/244 protein level: patients—0.55 ± 0.11 vs. controls—0.96 ± 0.05;

TABLE 1 | Clinical characteristics of two patients with IHPRF3.

Patient	F6331-1	F6331-4
Age (year), Sex	14, F	10, F
Birth evaluation		
°Birth Weight (centile)	3,990 g (p90)	3,850 g (p50)
°Birth Length (centile)	51 cm (p75)	48 cm (p50)
°Apgar Scores (1st/5th min)	10/10	8/9
Last evaluation		
°Weight (centile)	53.5 kg (p90)	33.5 kg (p75)
°Height (centile)	164 cm ($p > 97$)	133 cm (p50)
°Head circumference (centile)	55 cm (p96)	53.5 cm ($p < 96$)
Development		
°Regression	No	yes
°Seizures	no	yes
°Speech	Few words	Non-verbal
°Neuropsychomotor development	Severe delay	Severe delay
°Cognitive	Severe delay	Severe delay
°ASD	yes	yes
°ID	yes	yes
°Hypotonia	yes	no
°Motor	Motor delay	Motor dyspraxia
EEG	No	Diffuse bilateral slow waves with multifocal epileptiform discharges
MRI	Volumetric reduction and abnormal T2 signal hyperintensity in white matter	Volumetric reduction and abnormal T2 signal hyperintensity in white matter
Facial dismorphism	Deep-set eyes, prominent nasal bridge, accentuated Cupid's bow of the upper lip, high palate, widely spaced teeth; bitemporal narrowing	Deep-set eyes, prominent nasal bridge, accentuated Cupid's bow of the upper lip, high palate, widely spaced teeth, bitemporal narrowing
Other features	Prominent digit pads	prominent digit pads, brachydactyly of the 4th and 5th toes and hypoplastic nails
Metabolic alterations	dyslipdemia and hypothyroidism	dyslipdemia and hypothyroidism

ASD, autism spectrum disorder; ID, intellectual disability; EEG, electroencephalogram; MRI, magnetic resonance imaging.

Mann–Whitney test, two-tailed, p-value = 0.0238), and the same was observed under EGF/FGF-2 withdrawal combined with treatment with mTORC1 complex inhibitor rapamycin (p-RPS6S240/244 protein level: patients—0.46 ± 0.09 vs. controls—0.73 ± 0.13; Mann–Whitney test, two-tailed, p-value = 0.0286) (**Figures 2A,B** and **Supplementary Figures 4B,C**). Conversely, inhibition of mTOR signaling through EGF/FGF-2 deprivation for 24 h and subsequent addition of BFA (which interferes with glutamine-induced lysosomal localization and activation of mTOR—Jewell et al., 2015; Meng et al., 2020) led to similar RPS6 phosphorylation in both groups (**Figure 2C** and **Supplementary Figure 4D**). Together, these results show that mTOR signaling in patient-derived iNPC is altered only under specific stress-inducing conditions and suggest that TBCK acts through an indirect mechanism over mTOR signaling.

TBCK Colocalizes With Proteins Involved in Both Endocytic and Secretory Pathways

To evaluate whether *TBCK* plays a role in intracellular vesicle transport in iNPC, we first investigated intracellular localization of TBCK through the analysis of immunocolocalization levels with several proteins involved in endocytic (caveolin, RAB5A) and/or secretory (COPII, GM130/GOLGA2) pathways, in addition to Clathrin and STAM implicated in both. In iNPC of patients and controls growing under normal culture conditions, we observed that TBCK protein was diffusely distributed in the cytosol, together with a more condensed perinuclear localization, suggesting that a fraction of TBCK-mutated protein is translated and that this protein is not retained in any particular cellular compartment in iNPC of patients (**Supplementary Figures 5A–F**). Subsequent colocalization analysis showed that WT TBCK exhibits modest colocalization with caveolin (MCC mean value: 0.32 ± 0.15) and GM130/GOLGA2 (MCC mean value: 0.37 ± 0.13) and high colocalization levels with STAM, RAB5A, COPII, and clathrin (MCC mean values: 0.76 ± 0.13, 0.74 ± 0.28, 0.79 ± 0.17, and 0.8 ± 0.13, respectively), consistent with an important role for TBCK in both endocytic and early secretory pathways (**Figures 3A–F** and **Supplementary Figures 5A–F**). Importantly, whereas a similar colocalization pattern was observed between TBCK-mutated protein and caveolin, COPII, and RAB5A (MCC mean values: 0.29 ± 0.23, 0.74 ± 0.26, and 0.67 ± 0.35, respectively) (**Figures 3A,F** and **Supplementary Figures 5A–C**), decreased colocalization was observed with clathrin (MCC mean value: 0.73 ± 0.14; $p < 0.00001$) (**Figure 3B** and **Supplementary Figure 5D**), and increased colocalization with STAM (MCC mean value: 0.83 ± 0.1; $p < 0.0001$) (**Figure 3D** and **Supplementary Figure 5E**) and GM130/GOLGA2 (MCC mean value: 0.49 ± 0.14; $p < 0.0001$) (**Figure 3C** and **Supplementary Figure 5F**).

We also examined the effect of lack of functional TBCK protein over clathrin, RAB5A, and STAM expression in iNPC grown as neurospheres (3D model system). RT-qPCR showed reduced clathrin heavy chain CLTD and STAM1 transcript levels in neurospheres of patients, compared with controls (**Figure 3G**). Interestingly, quantification of clathrin and STAM by Western blot showed a tendency to increase protein levels in patients but not statistically significant (**Figure 3H** and **Supplementary Figures 4E,F**). Together, these results suggest altered intracellular membrane trafficking along the endolysosomal and/or the early secretory pathways in patient-derived iNPC.

Patient-Derived Neuroprogenitor Cells Do Not Show Evidence for Altered Endosome Maturation Along With the Endolysosomal System

As part of the ESCRT sorting machinery, STAM together with clathrin contributes to the recognition and sorting of

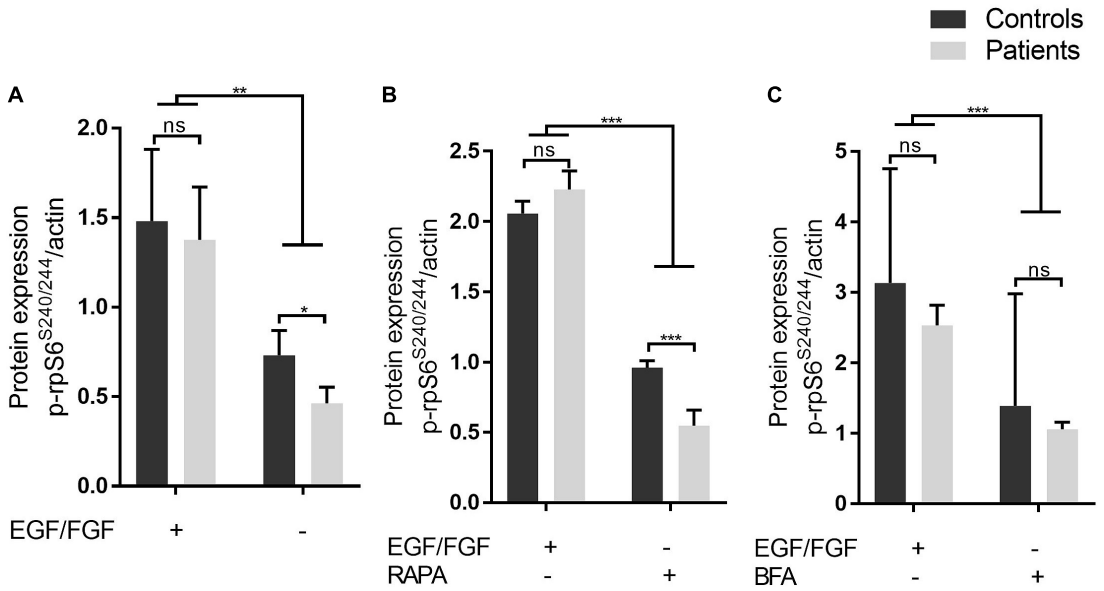

FIGURE 2 | Under stress-inducing conditions, patient-derived iNPC exhibits reduced RPS6 phosphorylation. **(A–C)** Protein level of phospho-RPS6 (residues S240-244) from iNPC cultivated under normal growth conditions and three stress-inducing conditions. iNPC without epidermal growth factor (EGF) and FGF-2 for 24 h only **(A)**, without EGF/FGF-2 and concomitant treatment with rapamycin (100 nM) for 24 h **(B)**, or without EGF/FGF-2 and subsequent treatment with brefeldin A (BFA, 4 μM) for 3 h **(C)**. **p*-value < 0.05. WB experiments were replicated twice. Data are shown as mean ± SD of technical replicates and biological samples. Patients: F6331-1 and F6331-4 (*N* = 2); controls: F7007-1, F8799-1, and F10006-1 (*N* = 3). ***p*-value < 0.01, ****p*-value < 0.001, ns - not significant.

ubiquitinated cargos at early endosomes, which mature to late endosomes prior to targeting ubiquitinated proteins for degradation at lysosomes (Vietri et al., 2020). Thus, to investigate whether altered colocalization of TBCK-mutated protein with STAM and clathrin is associated with defects in the endolysosomal system, we quantified the immunofluorescence intensities of RAB7A, a late-endosome marker. RAB7A fluorescence intensities did not differ between patients and controls (**Supplementary Figure 6**), suggesting that the expression of TBCK-mutated protein does not disrupt late endosome maturation in cells under normal growth conditions.

Lack of Functional TBCK Protein May Alter Early Secretory Pathway and Autophagosome Membrane Recruitment in Basal Autophagy

Next, we sought to verify if the patient-derived cells show impairment of the early secretory pathway. STAM has been implicated in the deubiquitination of SEC31A (component of COPII outer layer), modulating the formation of large COPII carriers that mediate the transport of macromolecules (such as procollagen) from the endoplasmic reticulum (ER)-to-Golgi (Rismanchi et al., 2009; Kawaguchi et al., 2018). Thus, we first investigated whether patient-derived iNPC present abnormal large COPII-carrier formation (> 1 μm). Measurement of the diameter of COPII puncta showed that iNPC of patients had a smaller average diameter compared with controls (average diameter of large COPII carriers—patients: 1.89 ± 1.01 μm and controls: 2.31 ± 1.23 μm; $p < 0.0001$) (**Figure 3I**) and a tendency to have less large COPII carriers per cell (**Figure 3J**).

COPII-coated vesicles have also been shown to act as templates for LC3 lipidation (conversion of cytoplasmic LC3I to membrane-bound LC3II) during autophagy, playing an important role as a membrane source for autophagosome biogenesis (Ge et al., 2014; Farhan et al., 2017; Shima et al., 2019). Thus, we also evaluated whether iNPC of patients show evidence of defective autophagosome biogenesis, by quantifying the protein levels of the autophagosome marker LC3 under normal culture condition (basal autophagy) and the three stress-inducing conditions (absence of EGF/FGF-2, and absence of EGF/FGF-2 + rapamycin or BFA). Western blot analysis of cells in all conditions showed a modest decrease in the LC3II/I ratio in iNPC of patients but not statistically significant (**Figures 4A,B** and **Supplementary Figures 4G–J**). Several other autophagy markers, including BECN1, p62/SQSTM1, and cathepsin D, did not show differences between patients and controls in the absence of EGF/FGF-2 only (**Supplementary Figure 7**). Despite the lack of statistical significance, the LC3II/I ratio always shows a trend to be decreased in iNPC of patients. Further confocal microscope analysis of LC3B under normal growth conditions showed that the number of LC3B puncta is also trended to be reduced in cells of patients, while the average diameter of LC3B puncta was significantly smaller compared with controls (LC3B average puncta diameter—patients: 528.7 ± 280.6 nm and controls: 621 ± 341.2 nm; $p < 0.001$) (**Figures 4C–E**). These results suggest altered autophagosome formation in basal autophagy in patient-derived iNPC.

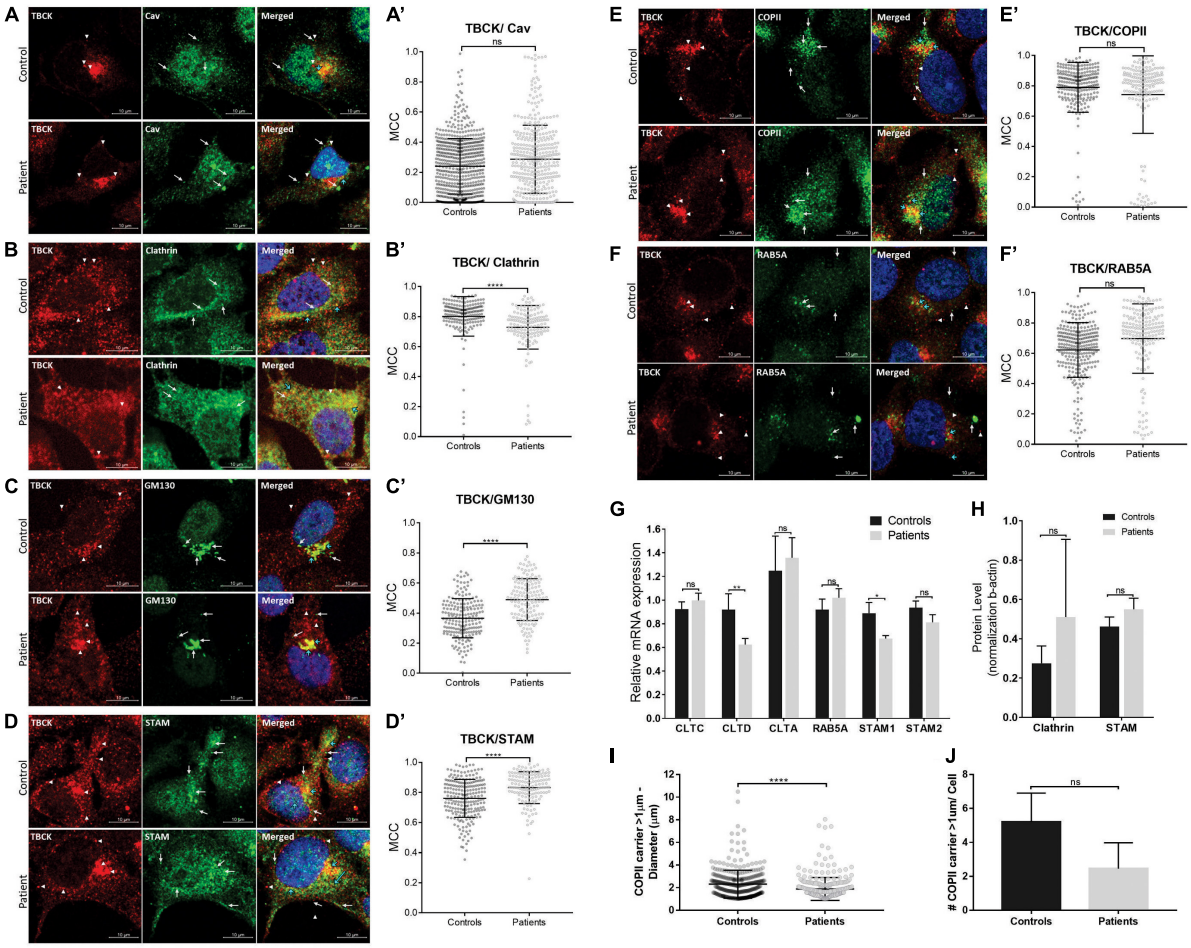

FIGURE 3 | Patient-derived iNPC show altered colocalization levels with endocytic and early secretory pathway markers. **(A–F)** Representative images of confocal microscopy of iNPC coimmunostained for endogenous TBCK and specific vesicle transport machinery components: **(A)** Caveolin (Cav), **(B)** Clathrin, **(C)** GM130/GOLGA2, **(D)** STAM, **(E)** COPII, and **(F)** RAB5A. For more detailed images, see **Supplementary Figure 5**. White arrowheads indicate TBCK dots; white arrows indicate the vesicle transport regulators indicated on each image; blue arrows indicate the colocalized dots. **(A′–F′)** Graphs of Manders coefficient colocalization (MCC) of TBCK with each target protein. Measurements were performed using ImageJ/Fiji-Coloc2 plugin. Error bars indicate SD (each dot represents the MCC in each cell; data represent the analysis of $n > 150$ cells/individual). **(G)** Relative mRNA expression of vesicle transport regulators in iNPC grown as neurospheres show reduced clathrin heavy chain CLTD and STAM1 transcript levels in neurospheres of patients, compared with neurospheres of controls. **(H)** Clathrin and STAM immunoblot densitometries reveal a tendency to increase protein levels in neurospheres of patients, compared with neurospheres of controls. **(I,J)** Analysis of large COPII carrier (>1 µm) average diameter **(I)** and number per cell **(J)**. ****p-value < 0.0001. Unpaired t-test, two-tailed. Data are shown as mean ± SD of biological replicates. 4′,6-diamidino-2-phenylindole (DAPI) (blue) marks cell nuclei. Scale bar = 10 µM. Patients: F6331-1 and F6331-4 ($N = 2$); controls: F7007-1, F8799-1, and F10006-1 ($N = 3$). *p-value < 0.05, **p-value < 0.01, ns - not significant.

Neuroprogenitor Cells Expressing TBCK-Mutated Protein Show Altered Cell Cycle Progression and Severe Impairment in the Capacity of Cell Migration

Finally, we sought to verify whether the expression of TBCK-mutated protein is associated with aberrant cell proliferation and migration in the context of neural development. Flow cytometry analysis showed a higher percentage of cells arrested at G0/G1 in patient-derived iNPC at 24 h and 40 h of recovery from the withdrawal of growth factors compared with control iNPC (p-value < 0.01) (**Figure 5A** and **Supplementary Figure 8**). Detection of S-phase cells *via* BrdU incorporation showed that BrdU-positive cells in the control population increased on average 4.5 and 6.7% after 24 h and 40 h of medium supplementation, respectively, while BrdU-positive cells in the TBCK-mutated population decreased 12.6 and 6.8% after 24 h and 40 h of medium supplementation, respectively (**Figure 5B**). These alterations were not attributed to an increase in apoptosis since activation of caspase 3/7 did not differ between patient and control cells (**Supplementary Table 4**). Taken together, these results suggest that patient-derived iNPC show reduced cell proliferation due to delayed cell cycle progression.

We also evaluated the migration rates of iNPC from IHPRF3 patients and controls by quantifying the distance of cell migration

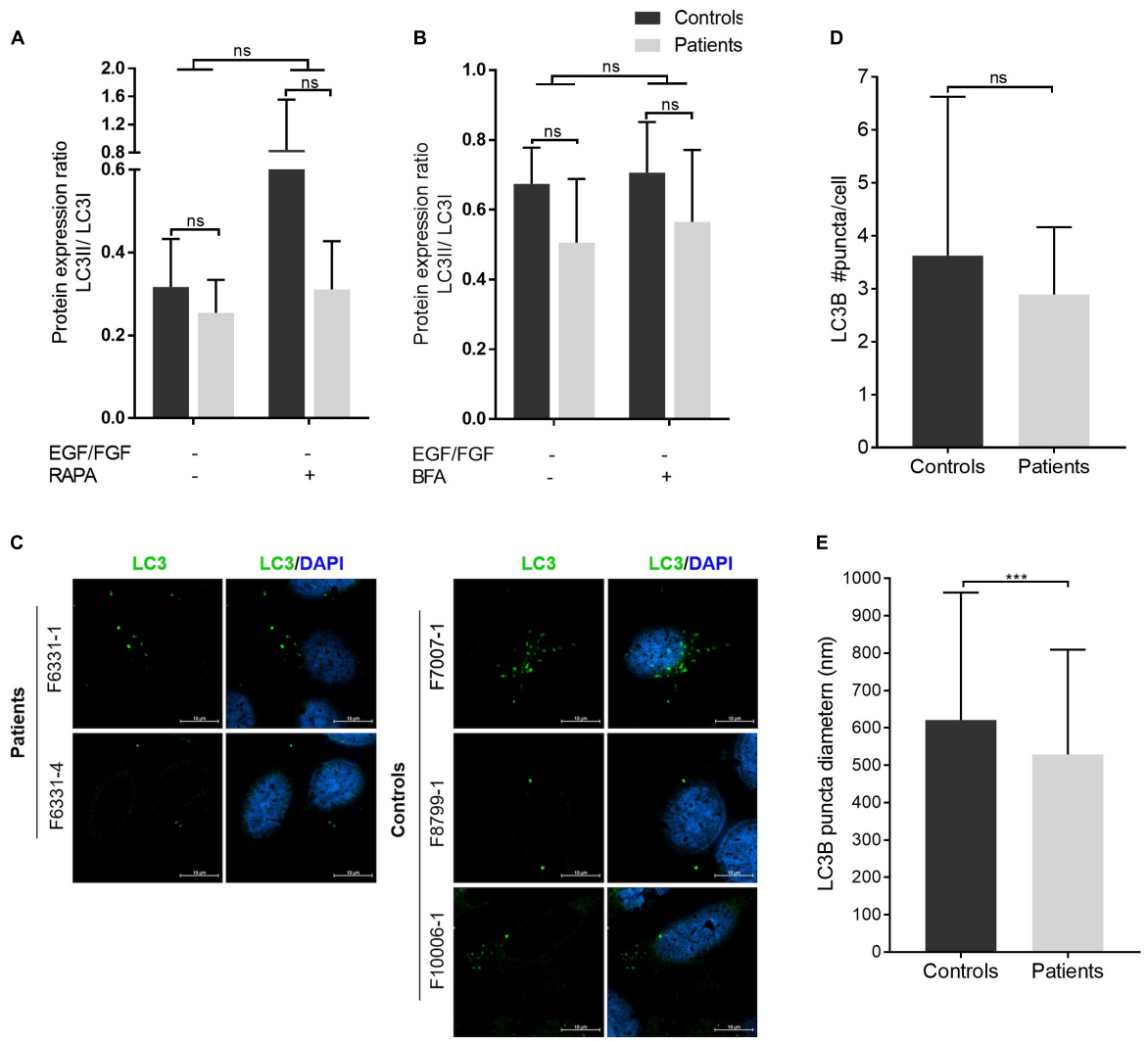

FIGURE 4 | Autophagosome biogenesis analysis: LC3B puncta diameter is reduced in patient-derived iNPC. **(A,B)** Graphs show the densitometries of immunoblots shown in **Supplementary Figure 4**. Patients are represented in gray ray bars and controls in black bars. Graphs show the LC3A-B II/I ratio from iNPC cultivated under normal growth conditions and under stress-inducing conditions: absence of EGF and fibroblast growth factor-2 (FGF-2) for 24 h and **(A)** concomitant treatment with rapamycin (100 nM) for 24 h, and **(B)** subsequent treatment with BFA (4 μM) for 3 h. β-actin was used as a loading control. Graphs are represented in arbitrary units. **(C–E)** Immunostaining analysis of endogenous LC3B by confocal microscopy. Representative images are presented in panel **(C)**; average LC3B puncta diameter (nm) in panel **(D)**; and an average number of LC3B puncta per cell in panel **(E)**. ***p-value < 0.001; n.s.—not significant. Data are shown as mean values ± SD of biological replicates. Patients: F6331-1 and F6331-4 ($N = 2$); controls: F7007-1, F8799-1, and F10006-1 ($N = 3$).

outward from the edge of neurospheres at 4, 8, and 24 h after adhesion. While iNPC from control neurospheres showed robust migration rates after 24 h, we observed that patient-derived iNPC showed dramatically reduced capacity of migration (**Figures 5C,D**).

DISCUSSION

In this study, we described two sisters who were referred to the CEGH-CEL at the age of 3 and 6 years due to suspected ASD. Detailed clinical investigation and follow-up for 7 years revealed several facial dysmorphic features and progressive muscle weakness and psychomotor developmental delay. These clinical symptoms along with the biallelic LoF variants in *TBCK* led to the diagnosis of IHPRF3 (OMIM#616900), an autosomal recessive condition with approximately 40 cases reported so far. Several cases of IHPRF3 show premature death before early adulthood. Importantly, in keeping with another patient described by Bhoj et al. (2016), we highlighted autism as an additional clinical feature of the syndrome.

Our patients are compound heterozygous for pathogenic LoF variants in *TBCK*: a stopgain variant (p.Tyr710*) in exon 23 and a microdeletion (p.Glu687Valfs9*) predicted to create a premature stop codon in exon 24 that has been

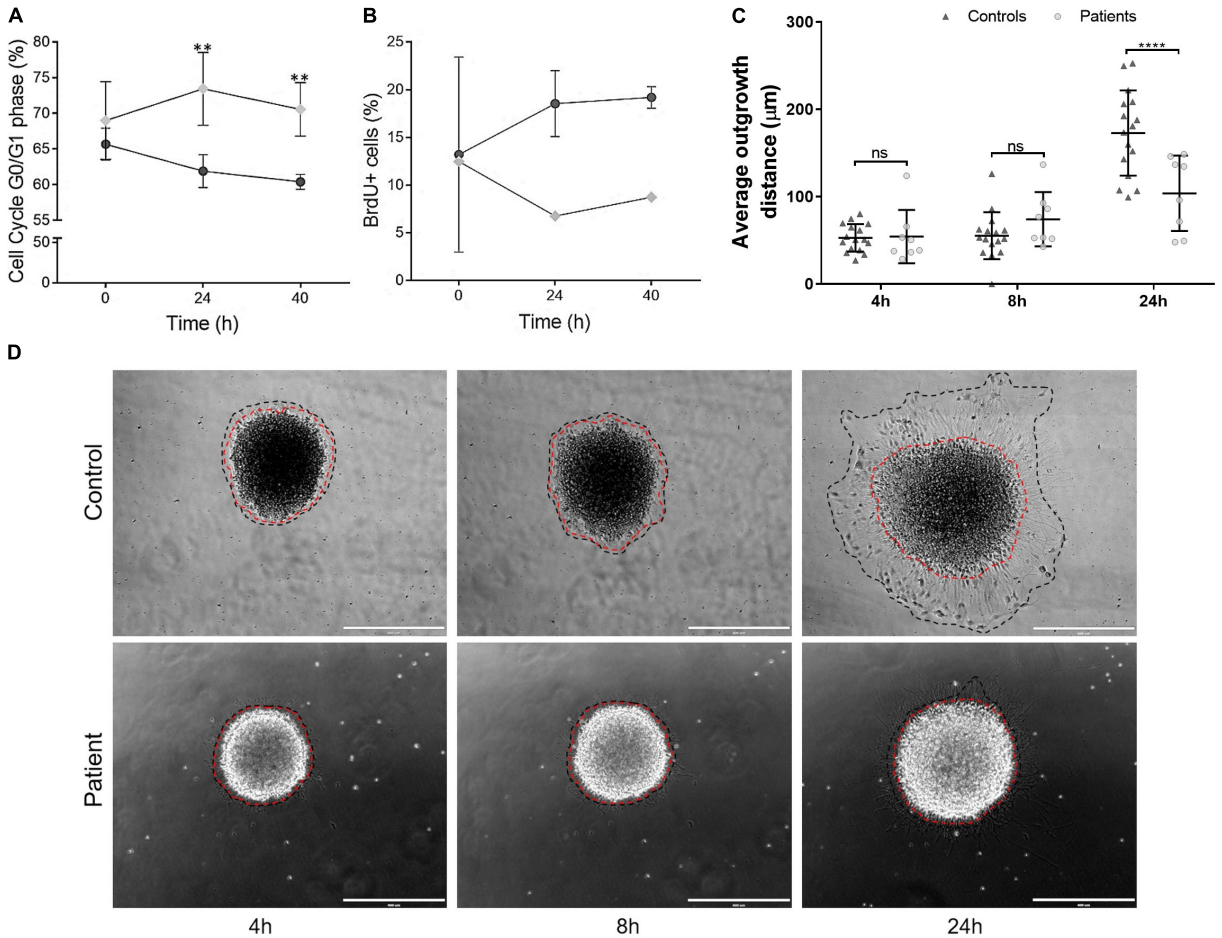

FIGURE 5 | iNPC expressing TBCK-mutated protein show altered cell cycle progression, cell proliferation, and cell migration. **(A)** G0/G1-phase analyses at three time points, showing an increased percentage of cells of patients arrested at G0/G1 cell cycle stage. Cell cycle experiments were replicated twice. **(B)** BrdU-positive cells showed that iNPC of patients had lower incorporation of BrdU. Data are shown as percentages. BrdU incorporation experiment was performed once for each sample. Patient: F6331-1; controls: F7007-1, F8799-1, and F10006-1. **(C,D)** iNPC migration from neurospheres, measured as the distance of the longest outer diameter of the cells that migrated from the neurosphere, normalized to the inner neurosphere edge. **(D)** Representative images of migration assay. Red dashed line—inner diameter; black dashed line—outer diameter. Scale bar = 400 µm. Patients: F6331-1 and F6331-4 ($N = 2$); controls: F7007-1, F8799-1, and F10006-1 ($N = 3$); Neurosphere technical replicates = 4. Data are shown as mean values ± SD of patients and control biological replicates. $^{**}p$-value < 0.01, $^{****}p$-value < 0.0001, ns - not significant.

previously identified in homozygosity in another IHPRF3 patient (Sumathipala et al., 2019). While most pathogenic variants reported in IHPRF3 patients located at the region encompassing the kinase and TBC domains (Zapata-Aldana et al., 2019), the variants in this study identified, together with two variants reported elsewhere (Bhoj et al., 2016; Sumathipala et al., 2019), located in a more distal region, downstream of the TBC domain.

The hypomorphic variants in *TBCK* in this study reported led to reduced mRNA and protein expression levels in patient-derived iNPC; however, we found a high number of TBCK-positive puncta in iNPC of patients through confocal microscope immunofluorescence labeling, with the same subcellular localization as iNPC of controls. Previous studies on fibroblasts and lymphoblastoid cells of IHPRF3 patients, harboring variant upstream of the TBC domain, also showed a drastic reduction to an absence of TBCK protein in cells of patients (Bhoj et al., 2016; Sumathipala et al., 2019). These results may suggest that TBCK in patient-derived iNPC partly escapes from both nonsense mediated-mRNA decay and protein quality control pathways (Giannandrea et al., 2013; Supek et al., 2021). Similar findings were described for odontochondrodysplasia (OCDC) (Wehrle et al., 2019). OCDC patients, who harbored hypomorphic mutations in the thyroid hormone receptor interactor 11 (TRIP11), also known as Golgi-associated microtubule-binding protein (GMAP-210), expressed different mutant isoforms of this gene, which can maintain the partial function of the wild-type isoforms. Thus, we can speculate that the clinical progression of the syndrome in our patients, which are milder than most of the patients reported so far (Beck-Wödl et al., 2018; Sumathipala et al., 2019; Zapata-Aldana et al., 2019), may possibly be due to a higher expression of mutant *TBCK*.

Neuroprogenitor cells from our patients showed reduced RPS6 phosphorylation when submitted to the withdrawal of EGF and FGF-2 growth factors either with or without rapamycin treatment, indicating reduced mTOR signaling pathway activation. Conversely, the addition of BFA, which interferes with glutamine-induced lysosomal localization and activation of mTORC1 (Jewell et al., 2015; Meng et al., 2020), to growth factor-deprived cells led to similar RPS6 phosphorylation levels between patients and controls. That is, BFA seems to have affected iNPC of controls in a more pronounced way than iNPC of patients. Previous study also demonstrated reduced mTOR signaling pathway on TBCK depleted non-neuronal cells (Liu et al., 2013; Bhoj et al., 2016; Ortiz-González et al., 2018), which could be partially rescued by leucine treatment. mTOR signaling activation by leucine depends on Rag GTPase (Lee et al., 2018), which does not seem to be dysregulated in IHPRF3 patients. In contrast, our results may suggest that TBCK plays a role in mTOR signaling through the same pathway as BFA, and preexisting disruption of this signaling in iNPC of patients makes cells of patients less sensitive to the inhibitory effect of BFA compared with controls. BFA targets the GEF of intra-Golgi vesicle transport regulator ARF1 GTPase, preventing the conversion of ARF1 from its GDP-bound state to the active GTP-bound state (Robineau et al., 2000). ARF1 activity toward mTOR signaling pathway is induced by a specific subset of amino acids, including asparagine and glutamine, with the latter being highly enriched in the NB medium (Jewell et al., 2015; Meng et al., 2020). Thus, reduced RPS6 activation in iNPC expressing TBCK-mutated protein may be due to impaired ARF1 activation making patient-derived iNPC less sensitive to an inhibitory effect of BFA.

Consistent with a role in endosomal and/or early secretory vesicle transport regulation, we showed that TBCK protein in iNPC under normal growth conditions localizes to both the endosomes (e.g., RAB5A$^+$ compartment) and the early secretory pathway (e.g., COPII vesicles). In fact, knockdown of TBCK has been suggested to affect vesicle transport at RAB5$^+$/EEA1$^+$ early endosomes in non-neural cells (Collinet et al., 2010). However, in this study, iNPC of patients did not show altered endosome maturation.

Notably, our results provide support for the interaction between TBCK and STAM, which have been predicted to act as a complex, together with HGS and RANGRF in HeLa and HEK293 cell lines (Havugimana et al., 2012). Increased colocalization of TBCK-mutated protein with STAM and GM130/GOLGA2 (a *cis*-Golgi tethering factor that facilitates ER-derived vesicle fusion) and decreased colocalization with clathrin observed in cells of patients suggest altered early secretory transport and impaired clathrin-coated vesicle-dependent post-Golgi transport of proteins. In agreement with this view, patient-derived iNPC showed a smaller average diameter of COPII carriers, suggesting impaired macromolecule transport from ER to Golgi. Consistent with early secretory defects, iNPC of our patients showed smaller LC3B puncta. Despite the lack of statistical significance, which may be due to the limited detection capability of Western blot, the average LC3II/I ratio tends to be decreased in iNPC of patients, in both basal and stress-induced autophagy. Thus, further study is needed to elucidate the autophagy regulation in iNPC with depletion of functional TBCK. Regardless, our findings support the hypothesis that TBCK acts in ER-to-Golgi vesicle trafficking and that lack of functional TBCK protein might impair both the transport of newly synthesized proteins to their destination and autophagosome biogenesis due to altered early secretory transport (**Supplementary Figure 9**). It is important to note that unlike observations by Ortiz-González et al. (2018) reduced mTOR signaling in iNPC of patients treated with the well-established autophagy inducer, rapamycin, was not associated with an increased level of autophagosome formation. This apparent contradictory data may be associated with previous suggestions that TBCK seems to present functional differences according to the cell type (Liu et al., 2013; Wu et al., 2014; Wu and Lu, 2021) and emphasize the relevance of studying neural cells to investigate the pathophysiological mechanisms of neuronal phenotypes of IHPRF3. Furthermore, the discordance between mTOR signaling activity and autophagosome formation observed in cells of our patients suggests that dysregulated mTOR signaling alone may be insufficient to account for all the clinical features of the syndrome.

Furthermore, in this study, we observed that patient-derived iNPC showed G0/G1 cell cycle arrest and delayed S-phase progression, as well as a significantly impaired capacity of migration. Impaired cell cycle progression has also been observed by Wu et al. (2014). These authors together with Liu et al. (2013) observed an overlapped localization between TBCK and α- and γ-tubulin, respectively, suggesting a potential role of TBCK on microtubule (MT) nucleation. In this context, studies have shown that Golgi apparatus can function as an important microtubule-organizing center (MTOC) in many cell types, and unlike centrosomal MTOC, it can give rise to polarized MTs important for a number of cellular processes, including Golgi reassembly after mitosis (Maia et al., 2013) and polarized transport of post-Golgi carriers that are important for cell migration (Vinogradova et al., 2009, 2012; Hurtado et al., 2011; Wu et al., 2016). In neuronal cell types, Golgi-anchored MTs have also been implicated in neurite outgrowth and branching (Oddoux et al., 2013; Yalgin et al., 2015). Thus, it is tempting to speculate that impaired activity of TBCK mutant protein over other Golgi resident vesicle transport regulators impact MT nucleation and Golgi-derived MT dependent processes that are essential for normal brain development and structural organization, such as cell division, migration, and neuronal morphogenesis (Ori-McKenney et al., 2012; Etienne-Manneville, 2013; Roccio et al., 2013; Borrell and Calegari, 2014; Maizels and Gerlitz, 2015; Garcin and Straube, 2019; Shokrollahi and Mekhail, 2021). However, we cannot rule out that the migration defect observed in the TBCK-deficient neurospheres may also be related to the altered proliferation of cells of patients. Nevertheless, impairment in these processes may further contribute to abnormal brain structures, like microcephaly and cortical atrophy presented by IHPRF3 patients.

In summary, we described a novel IHPRF3 family, adding autism as a clinical feature of this syndrome. Using iNPC from IHPRF3 patients and control individuals, we pinpointed a role for *TBCK* in regulating the early secretory pathway and suggested that the impairment in mTOR signaling and autophagosome

biogenesis observed in *TBCK*-mutated cells might be related to impaired signaling toward other early secretory transport regulators, such as RAB1A or ARF1 small GTPases. It is of note that pathogenic mutations in other members of the TBC family of proteins (*TBC1D20*, *TBC1D23*, *TBC1D24*), which also mediate intracellular membrane transport, such as endosome-to-Golgi and ER-to-Golgi trafficking or autophagy, have also been implicated in neurodevelopmental syndromes (OMIM#615663, OMIM#617695, and OMIM#220500, respectively) with high clinical overlap with IHPRF3 (Falace et al., 2014; Sidjanin et al., 2016; Ivanova et al., 2017; Shin et al., 2017; Aprile et al., 2019), reinforcing the importance of vesicle trafficking kinetics in neurodevelopment.

DATA AVAILABILITY STATEMENT

The datasets presented in this study can be found in online repositories. The names of the repository and accession numbers can be found below: https://www.ncbi.nlm.nih.gov/ (clinvarSCV002032078 and SCV002032079).

ETHICS STATEMENT

The studies involving human participants were reviewed and approved by National Ethics Committee (Comissão Nacional de Ética em Pesquisa no Brazil, Process no. CAAE43559314.0.0000.5464). Written informed consent to participate in this study was provided by the participants' legal guardian/next of kin. Written informed consent was obtained from the individual(s), and minor(s)' legal guardian/next of kin, for the publication of any potentially identifiable images or data included in this article.

AUTHOR CONTRIBUTIONS

DPM, AMS, and MP-B: conceptualization, methodology, and writing—original draft. ATS, EV-B, MF, MRF, RC, MM, NL, KG-O, EZ, DB, KW, ML, HN, GSK, and ALS: investigation. DPM, AMS, GSK, ALS, and MP-B: writing—review and editing. MP-B: funding acquisition, resources, and supervision. All authors contributed to the article and approved the submitted version.

FUNDING

The main funders of this project are Fundação de Amparo à Pesquisa do Estado de São Paulo (FAPESP/CEPID 2013/08028-1), Conselho Nacional de Desenvolvimento Científico e Tecnológico (CNPq—466651/2014-7 and 448536/2014-5), and Coordenação de Aperfeiçoamento de Pessoal de Nível Superior (CAPES).

ACKNOWLEDGMENTS

The authors would like to thank the family of patients for their contribution. They would also like to thank Luciana Amaral Haddad and Mariz Vainzof for antibody donation and comments and MSc Isabela MW Silva and MSc. Frederico Monfardini for aCGH analyses and statistical analysis instructions, respectively.

SUPPLEMENTARY MATERIAL

The Supplementary Material for this article can be found online at: https://www.frontiersin.org/articles/10.3389/fncel.2021.803302/full#supplementary-material

REFERENCES

American Psychiatric Association (2013). *Diagnostic and Statistical Manual of Mental Disorders*, 5th Edn. Arlington, VA: American Psychiatric Association.

Aprile, D., Fruscione, F., Baldassari, S., Fadda, M., Ferrante, D., and Falace, A. (2019). TBC1D24 regulates axonal outgrowth and membrane trafficking at the growth cone in rodent and human neurons. *Cell Death Differ.* 26, 2464–2478. doi: 10.1038/s41418-019-0313-x

Beck-Wödl, S., Harzer, K., Sturm, M., Buchert, R., Rieß, O., Mennel, H. D., et al. (2018). Homozygous TBC1 domain-containing kinase (TBCK) mutation causes a novel lysosomal storage disease - a new type of neuronal ceroid lipofuscinosis (CLN15)? *Acta Neuropathol. Commun.* 6:145. doi: 10.1186/s40478-018-0646-6

Bhoj, E. J., Li, D., Harr, M., Edvardson, S., Elpeleg, O., and Chisholm, E. (2016). Mutations in TBCK, encoding TBC1-domain-containing kinase, lead to a recognizable syndrome of intellectual disability and hypotonia. *Am. J. Hum. Genet.* 98, 782–788. doi: 10.1016/j.ajhg.2016.03.016

Borrell, V., and Calegari, F. (2014). Mechanisms of brain evolution: regulation of neural progenitor cell diversity and cell cycle length. *Neurosci. Res.* 86, 14–24. doi: 10.1016/j.neures.2014.04.004

Chong, J. X., Caputo, V., Phelps, I. G., Stella, L., Worgan, L., and Dempsey, J. C. (2016). Recessive inactivating mutations in TBCK, encoding a Rab GTPase-activating protein, cause severe infantile syndromic encephalopathy. *Am. J. Hum. Genet.* 98, 772–781. doi: 10.1016/j.ajhg.2016.01.016

Collinet, C., Stöter, M., Bradshaw, C. R., Samusik, N., Rink, J. C., and Kenski, D. (2010). Systems survey of endocytosis by multiparametric image analysis. *Nature* 464, 243–249. doi: 10.1038/nature08779

D'haene, B., Vandesompele, J., and Hellemans, J. (2010). Accurate and objective copy number profiling using real-time quantitative PCR. *Methods* 50, 262–270. doi: 10.1016/j.ymeth.2009.12.007

Etienne-Manneville, S. (2013). Annual review of cell and developmental biology. *Microtubules Cell Migration* 29, 471–499.

Fajardo, K. V. F., Adams, D., NISC Comparative Sequencing Program, Mason, C. E., Sincan, M., et al. (2012). Detecting false-positive signals in exome sequencing. *Hum. Mutat.* 33, 609–613. doi: 10.1002/humu.22033

Falace, A., Buhler, E., Fadda, M., Watrin, F., Lippiello, P., Pallesi-Pocachard, E., et al. (2014). TBC1D24 regulates neuronal migration and maturation through modulation of the ARF6-dependent pathway. *Proc. Natl. Acad. Sci. U S A.* 111, 2337–2342. doi: 10.1073/pnas.1316294111

Farhan, H., Kundu, M., and Ferro-Novick, S. (2017). The link between autophagy and secretion: a story of multitasking proteins. *Mol. Biol. Cell* 28, 1161–1164. doi: 10.1091/mbc.E16-11-0762

Gabernet-Castello, C., O'Reilly, A. J., Dacks, J. B., and Field, M. C. (2013). Evolution of Tre-2/Bub2/Cdc16 (TBC) Rab GTPase-activating proteins. *Mol. Biol. Cell* 24, 1574–1583. doi: 10.1091/mbc.E12-07-0557

Garcin, C., and Straube, A. (2019). Microtubules in cell migration. *Essays Biochem.* 63, 509–520.

Ge, H., Yu, A., Chen, J., Yuan, J., Yin, Y., Duanmu, W., et al. (2016). Poly-L-ornithine enhances migration of neural stem/progenitor cells via promoting α-Actinin 4 binding to actin filaments. *Sci. Rep.* 6:37681. doi: 10.1038/srep37681

Ge, L., Zhang, M., and Schekman, R. (2014). Phosphatidylinositol 3-kinase and COPII generate LC3 lipidation vesicles from the ER-Golgi intermediate compartment. *Elife* 3:e04135. doi: 10.7554/eLife.04135

Giannandrea, M., Guarnieri, F. C., Gehring, N. H., Monzani, E., Benfenati, F., Kulozik, A. E., et al. (2013). Nonsense-mediated mRNA decay and loss-of-function of the protein underlie the X-linked epilepsy associated with the W356× mutation in synapsin I. *PLoS One* 8:e67724. doi: 10.1371/journal.pone.0067724

Griesi-Oliveira, K., Acab, A., Gupta, A. R., Sunaga, D. Y., Chailangkarn, T., and Nicol, X. (2015). Modeling non-syndromic autism and the impact of TRPC6 disruption in human neurons. *Mol. Psychiatry* 20, 1350–1365. doi: 10.1038/mp.2014.141

Havugimana, P. C., Hart, G. T., Nepusz, T., Yang, H., Turinsky, A. L., and Li, Z. (2012). A census of human soluble protein complexes. *Cell* 150, 1068–1081.

Hurtado, L., Caballero, C., Gavilan, M. P., Cardenas, J., Bornens, M., and Rios, R. M. (2011). Disconnecting the Golgi ribbon from the centrosome prevents directional cell migration and ciliogenesis. *J. Cell Biol.* 193, 917–933.

Ishiy, F. A., Fanganiello, R. D., Griesi-Oliveira, K., Suzuki, A. M., Kobayashi, G. S., Morales, A. G., et al. (2015). Improvement of in vitro osteogenic potential through differentiation of induced pluripotent stem cells from human exfoliated dental tissue towards mesenchymal-like stem cells. *Stem Cells Int.* 2015:249098.

Ivanova, E. L., Mau-Them, F. T., Riazuddin, S., Kahrizi, K., Laugel, V., and Schaefer, E. (2017). Homozygous truncating variants in TBC1D23 cause pontocerebellar hypoplasia and alter cortical development. *Am. J. Hum. Genet.* 101, 428–440. doi: 10.1016/j.ajhg.2017.07.010

Jewell, J. L., Kim, Y. C., Russell, R. C., Yu, F. X., Park, H. W., Plouffe, S. W., et al. (2015). Metabolism. differential regulation of mTORC1 by leucine and glutamine. *Science* 347, 194–198. doi: 10.1126/science.1259472

Kawaguchi, K., Endo, A., Fukushima, T., Madoka, Y., Tanaka, T., and Komada, M. (2018). Ubiquitin-specific protease 8 deubiquitinates Sec31A and decreases large COPII carriers and collagen IV secretion. *Biochem. Biophys. Res. Commun.* 499, 635–641. doi: 10.1016/j.bbrc.2018.03.202

Kjos, I., Borg Distefano, M., Sætre, F., Repnik, U., Holland, P., Jones, A. T., et al. (2017). Rab7b modulates autophagic flux by interacting with Atg4B. *EMBO Rep.* 18, 1727–1739. doi: 10.15252/embr.201744069

Komurov, K., Padron, D., Cheng, T., Roth, M., Rosenblatt, K. P., and White, M. A. (2010). Comprehensive mapping of the human kinome to epidermal growth factor receptor signaling. *J. Biol. Chem.* 285, 21134–21142. doi: 10.1074/jbc.M110.137828

Lee, M., Kim, J. H., Yoon, I., Lee, C., Fallahi Sichani, M., and Kang, J. S. (2018). Coordination of the leucine-sensing Rag GTPase cycle by leucyl-tRNA synthetase in the mTORC1 signaling pathway. *Proc. Natl. Acad. Sci. USA.* 115, E5279–E5288. doi: 10.1073/pnas.1801287115

Li, H., and Durbin, R. (2009). Fast and accurate short read alignment with burrows-wheeler transform. *Bioinformatics* 25, 1754–1760. doi: 10.1093/bioinformatics/btp324

Liu, Y., Yan, X., and Zhou, T. (2013). TBCK influences cell proliferation, cell size and mTOR signaling pathway. *PLoS One* 8:e71349. doi: 10.1371/journal.pone.0071349

Maia, A. R., Zhu, X., Miller, P., Gu, G., Maiato, H., and Kaverina, I. (2013). Modulation of Golgi-associated microtubule nucleation throughout the cell cycle. *Cytoskeleton* 70, 32–43. doi: 10.1002/cm.21079

Maizels, Y., and Gerlitz, G. (2015). Shaping of interphase chromosomes by the microtubule network. *FEBS J.* 282, 3500–3524. doi: 10.1111/febs.13334

Mazemondet, O., Hubner, R., Frahm, J., Koczan, D., Bader, B. M., Weiss, D. G., et al. (2011). Quantitative and kinetic profile of Wnt/β-catenin signaling components during human neural progenitor cell differentiation. *Cell Mol. Biol. Lett.* 16, 515–538. doi: 10.2478/s11658-011-0021-0

McKenna, A., Hanna, M., Banks, E., Sivachenko, A., Cibulskis, K., and Kernytsky, A. (2010). The genome analysis toolkit: a MapReduce framework for analyzing next-generation DNA sequencing data. *Genome Res.* 20, 1297–1303. doi: 10.1101/gr.107524.110

Meng, D., Yang, Q., Wang, H., Melick, C. H., Navlani, R., Frank, A. R., et al. (2020). Glutamine and asparagine activate mTORC1 independently of Rag GTPases. *J. Biol. Chem.* 295, 2890–2899. doi: 10.1074/jbc.AC119.011578

Miller, E. E., Kobayashi, G. S., Musso, C. M., Allen, M., Ishiy, F. A. A., and de Caires, L. C. (2017). EIF4A3 deficient human iPSCs and mouse models demonstrate neural crest defects that underlie richieri-costa-pereira syndrome. *Hum. Mol. Genet.* 26, 2177–2191. doi: 10.1093/hmg/ddx078

Naslavsky, M. S., Yamamoto, G. L., de Almeida, T. F., Ezquina, S. A. M., Sunaga, D. Y., and Pho, N. (2017). Exomic variants of an elderly cohort of Brazilians in the ABraOM database. *Hum. Mutat.* 38, 751–763. doi: 10.1002/humu.23220

Oddoux, S., Zaal, K. J., Tate, V., Kenea, A., Nandkeolyar, S. A., Reid, E., et al. (2013). Microtubules that form the stationary lattice of muscle fibers are dynamic and nucleated at Golgi elements. *J. Cell Biol.* 203, 205–213. doi: 10.1083/jcb.201304063

Okita, K., Yamakawa, T., Matsumura, Y., Sato, Y., Amano, N., Watanabe, A., et al. (2013). An efficient nonviral method to generate integration-free human-induced pluripotent stem cells from cord blood and peripheral blood cells. *Stem Cells* 31, 458–466. doi: 10.1002/stem.1293

Ori-McKenney, K. M., Jan, L. Y., and Jan, Y. N. (2012). Golgi outposts shape dendrite morphology by functioning as sites of acentrosomal microtubule nucleation in neurons. *Neuron* 76, 921–930. doi: 10.1016/j.neuron.2012.10.008

Ortiz-González, X. R., Tintos-Hernández, J. A., Keller, K., Li, X., Foley, A. R., and Bharucha-Goebel, D. X. (2018). Homozygous boricua TBCK mutation causes neurodegeneration and aberrant autophagy. *Ann. Neurol.* 83, 153–165. doi: 10.1002/ana.25130

R Core team (2019). A language and environment for statistical Computing. *R Foundation for Statistical Computing, Vienna, Austria.* Avalaible online at: https://www.R-project.org/

Richards, S., Aziz, N., Bale, S., Bick, D., Das, S., and Gastier-Foster, J. (2015). Standards and guidelines for the interpretation of sequence variants: a joint consensus recommendation of the American college of medical genetics and genomics and the association for molecular pathology. *Genet. Med.* 17, 405–424. doi: 10.1038/gim.2015.30

Rismanchi, N., Puertollano, R., and Blackstone, C. (2009). STAM adaptor proteins interact with COPII complexes and function in ER-to-Golgi trafficking. *Traffic* 10, 201–217. doi: 10.1111/j.1600-0854.2008.00856.x

Robineau, S., Chabre, M., and Antonny, B. (2000). Binding site of brefeldin A at the interface between the small G protein ADP-ribosylation factor 1 (ARF1) and the nucleotide-exchange factor Sec7 domain. *Proc. Natl. Acad. Sci. USA.* 97, 9913–9918. doi: 10.1073/pnas.170290597

Roccio, M., Schmitter, D., Knobloch, M., Okawa, Y., Sage, D., and Lutolf, M. P. (2013). Predicting stem cell fate changes by differential cell cycle progression patterns. *Development* 140, 459–470. doi: 10.1242/dev.086215

Shima, T., Kirisako, H., and Nakatogawa, H. (2019). COPII vesicles contribute to autophagosomal membranes. *J. Cell Biol.* 218, 1503–1510. doi: 10.1083/jcb.201809032

Shin, J. J. H., Gillingham, A. K., Begum, F., Chadwick, J., and Munro, S. (2017). TBC1D23 is a bridging factor for endosomal vesicle capture by golgins at the trans-Golgi. *Nat. Cell Biol.* 19, 1424–1432.

Shokrollahi, M., and Mekhail, K. (2021). Interphase microtubules in nuclear organization and genome maintenance. *Trends Cell Biol.* 31, 721–731. doi: 10.1016/j.tcb.2021.03.014

Sidjanin, D. J., Park, A. K., Ronchetti, A., Martins, J., and Jackson, W. T. (2016). TBC1D20 mediates autophagy as a key regulator of autophagosome maturation. *Autophagy* 12, 1759–1775. doi: 10.1080/15548627.2016.1199300

Sumathipala, D., Strømme, P., Gilissen, C., Corominas, J., Frengen, E., and Misceo, D. (2019). TBCK encephaloneuropathy with abnormal lysosomal storage: use of a structural variant bioinformatics pipeline on whole-genome sequencing data unravels a 20-year-old clinical mystery. *Pediatr. Neurol.* 96, 74–75. doi: 10.1016/j.pediatrneurol.2019.02.001

Supek, F., Lehner, B., and Lindeboom, R. G. H. (2021). To NMD or Not To NMD: nonsense-mediated mRNA decay in cancer and other genetic diseases. *Trends Genet.* 37, 657–668. doi: 10.1016/j.tig.2020.11.002

Vietri, M., Radulovic, M., and Stenmark, H. (2020). The many functions of ESCRTs. *Nat. Rev. Mol. Cell Biol.* 21, 25–42. doi: 10.1038/s41580-019-0177-4

Vinogradova, T., Miller, P. M., and Kaverina, I. (2009). Microtubule network asymmetry in motile cells: role of Golgi-derived array. *Cell Cycle* 8, 2168–2174. doi: 10.4161/cc.8.14.9074

Vinogradova, T., Paul, R., Grimaldi, A. D., Loncarek, J., Miller, P. M., and Yampolsky, D. (2012). Concerted effort of centrosomal and golgi-derived microtubules is required for proper Golgi complex assembly but not for maintenance. *Mol. Biol. Cell* 23, 820–833. doi: 10.1091/mbc.E11-06-0550

Wang, K., Li, M., and Hakonarson, H. (2010). ANNOVAR: functional annotation of genetic variants from high-throughput sequencing data. *Nucleic Acids Res.* 38:e164. doi: 10.1093/nar/gkq603

Wehrle, A., Witkos, T. M., Unger, S., Schneider, J., Follit, J. A., and Hermann, J. (2019). Hypomorphic mutations of TRIP11 cause odontochondrodysplasia. *JCI Insight* 4:e124701. doi: 10.1172/jci.insight.124701

Wu, J., and Lu, G. (2021). Multiple functions of TBCK protein in neurodevelopment disorders and tumors. *Oncol. Lett.* 21:17.

Wu, J., de Heus, C., Liu, Q., Bouchet, B. P., Noordstra, I., Jiang, K., et al. (2016). Molecular pathway of microtubule organization at the golgi apparatus. *Dev. Cell* 39, 44–60. doi: 10.1016/j.devcel.2016.08.009

Wu, J., Li, Q., Li, Y., Lin, J., Yang, D., Zhu, G., et al. (2014). A long type of TBCK is a novel cytoplasmic and mitotic apparatus-associated protein likely suppressing cell proliferation. *J. Genet. Genom.* 41, 69–72. doi: 10.1016/j.jgg.2013.12.006

Yalgin, C., Ebrahimi, S., Delandre, C., Yoong, L. F., Akimoto, S., Tran, H., et al. (2015). Centrosomin represses dendrite branching by orienting microtubule nucleation. *Nat. Neurosci.* 18, 1437–1445. doi: 10.1038/nn.4099

Zapata-Aldana, E., Kim, D. D., Remtulla, S., Prasad, C., Nguyen, C. T., and Campbell, C. (2019). Further delineation of TBCK - infantile hypotonia with psychomotor retardation and characteristic facies type 3. *Eur. J. Med. Genet.* 62, 273–277. doi: 10.1016/j.ejmg.2018.08.004

Conflict of Interest: The authors declare that the research was conducted in the absence of any commercial or financial relationships that could be construed as a potential conflict of interest.

Publisher's Note: All claims expressed in this article are solely those of the authors and do not necessarily represent those of their affiliated organizations, or those of the publisher, the editors and the reviewers. Any product that may be evaluated in this article, or claim that may be made by its manufacturer, is not guaranteed or endorsed by the publisher.

Copyright © 2022 Moreira, Suzuki, Silva, Varella-Branco, Meneghetti, Kobayashi, Fogo, Ferrari, Cardoso, Lourenço, Griesi-Oliveira, Zachi, Bertola, Weinmann, Lima, Nader, Sertié and Passos-Bueno. This is an open-access article distributed under the terms of the Creative Commons Attribution License (CC BY). The use, distribution or reproduction in other forums is permitted, provided the original author(s) and the copyright owner(s) are credited and that the original publication in this journal is cited, in accordance with accepted academic practice. No use, distribution or reproduction is permitted which does not comply with these terms.

frontiers in Cellular Neuroscience

ORIGINAL RESEARCH
published: 18 January 2022
doi: 10.3389/fncel.2021.763423

High-Frequency Head Impact Disrupts Hippocampal Neural Ensemble Dynamics

Daniel P. Chapman[1†], Stephanie S. Sloley[1†], Adam P. Caccavano[1], Stefano Vicini[1,2‡] and Mark P. Burns[1,3‡]*

[1] Georgetown Interdisciplinary Program in Neuroscience, Georgetown University Medical Center, Washington, DC, United States, [2] Department of Pharmacology and Physiology, Georgetown University Medical Center, Washington, DC, United States, [3] Department of Neuroscience, Georgetown University Medical Center, Washington, DC, United States

We have recently shown that the cognitive impairments in a mouse model of high-frequency head impact (HFHI) are caused by chronic changes to synaptic physiology. To better understand these synaptic changes occurring after repeat head impact, we used Thy1-GcCAMP6f mice to study intracellular and intercellular calcium dynamics and neuronal ensembles in HFHI mice. We performed simultaneous calcium imaging and local field potential (LFP) recordings of the CA1 field during an early-LTP paradigm in acute hippocampal slice preparations 24 h post-impact. As previously reported, HFHI causes a decrease in early-LTP in the absence of any shift in the input-output curve. Calcium analytics revealed that HFHI hippocampal slices have similar numbers of active ROIs, however, the number of calcium transients per ROI was significantly increased in HFHI slices. Ensembles consist of coordinated activity between groups of active ROIs. We exposed the CA1 ensemble to Schaffer-collateral stimulation in an abbreviated LTP paradigm and observed novel coordinated patterns of post stimulus calcium ensemble activity. HFHI ensembles displayed qualitatively similar patterns of post-stimulus ensemble activity to shams but showed significant changes in quantitative ensemble inactivation and reactivation. Previous *in vivo* and *in vitro* reports have shown that ensemble activity frequently occurs through a similar set of ROIs firing in a repeating fashion. HFHI slices showed a decrease in such coordinated firing patterns during post stimulus ensemble activity. The present study shows that HFHI alters synaptic activity and disrupts neuronal organization of the ensemble, providing further evidence of physiological synaptic adaptation occurring in the brain after a high frequency of non-pathological head impacts.

Keywords: calcium imaging, subconcussive head impact, mouse model, brain injury–traumatic, plasticity

OPEN ACCESS

Edited by:
Annalisa Scimemi, University at Albany, United States

Reviewed by:
Omid Miry, Stanford University, United States
Rüdiger Köhling, University of Rostock, Germany

***Correspondence:**
Mark P. Burns
mpb37@georgetown.edu

[†]These authors share first authorship

[‡]These authors share senior authorship

Specialty section:
This article was submitted to Cellular Neuropathology, a section of the journal Frontiers in Cellular Neuroscience

Received: *23 August 2021*
Accepted: *21 December 2021*
Published: *18 January 2022*

Citation:
Chapman DP, Sloley SS, Caccavano AP, Vicini S and Burns MP (2022) High-Frequency Head Impact Disrupts Hippocampal Neural Ensemble Dynamics. Front. Cell. Neurosci. 15:763423. doi: 10.3389/fncel.2021.763423

INTRODUCTION

Traumatic brain injury (TBI) is one of the most common neurological disorders worldwide. The majority of TBIs (∼80%) are mild TBI with symptom resolution occurring in a matter of days to weeks (Cassidy et al., 2004; Laker, 2011; Frost et al., 2013; Voss et al., 2015; Blennow et al., 2016; Lefevre-Dognin et al., 2021). Repetitive mild TBI (rmTBI), such as those injuries seen in contact sports athletes and members of the armed forces, increases the severity and duration of symptoms (Guskiewicz et al., 2007; Greco et al., 2019). Evidence is also emerging to suggest that sub-concussive impacts such as heading a soccer ball or sustained high frequency low amplitude cranial movement seen in professional sled athletes can lead to lasting cognitive symptoms

(Colvin et al., 2009; Talavage et al., 2014; McCradden and Cusimano, 2018). The mechanism by which high frequency sub-concussive impacts can lead to lasting cognitive impairments is poorly understood.

Recently, our lab has shown that mice exposed to a high-frequency of closed head impacts (HFHI) have chronic cognitive impairments (Sloley et al., 2021). The HFHI protocol consists of five closed head impacts given in rapid succession every day for 6 days totaling thirty impacts (Main et al., 2017).

The average college football player receives 21 head impacts per week, with defensive ends receiving 41 head impacts per week (Crisco et al., 2010). To study the physiological changes that occur following head impact, we developed the HFHI mouse model of very mild impact to model the large number of human head impact exposures that occur during a single week of contact sport (Crisco et al., 2010). We recently reported that the HFHI model has very limited TBI or neurodegenerative disease pathology, and does not produce p-tau or Aβ accumulation, and no evidence of inflammation, cell death, or axonal damage outside of the optic tract (Sloley et al., 2021). Using transcriptomics, electrophysiology and pharmacology, we found that the cognitive impairments caused by HFHI are due to impaired long-term potentiation (LTP) in the CA3-CA1 synapse and reduced AMPA/NMDA ratio in CA1 pyramidal cells (Sloley et al., 2021). HFHI mice have strong transcriptomic changes in synaptic signaling and synaptic processes pathways in both the hippocampus and cortex that are present acutely, and are maintained through 1 month post-HFHI (Sloley et al., 2021). The cognitive deficits in HFHI mice can be blocked by pre-administration of memantine, an extrasynaptic NMDA antagonist, supporting the theory that the synaptic adaptations in HFHI mice are driven by short acute bursts of glutamate release at excitatory synapses. Other animal models of mild closed head impacts have demonstrated similar synaptic changes such as shifts in excitatory/inhibitory (E/I) balance in cortical areas (Witkowski et al., 2019). The HFHI model is considerably milder than other published TBI models, including the controlled cortical impact model and lateral fluid percussion models which result in widespread inflammation, cell death and lesion formation. The HFHI model is also pathologically less severe than other published mild TBI models that have associated cognitive deficits with pathologies such as axonal injury, inflammation, and p-tau pathology that are present (Laurer et al., 2001; Prins et al., 2010; Creed et al., 2011; Kane et al., 2012; Ren et al., 2013; Aungst et al., 2014; Mouzon et al., 2014).

Our previous whole cell electrophysiology experiments provide insight into synaptic adaptations on a single cell basis. However, while spatially accurate, they lack information on the integration of the patched neuron into the neuronal network. In contrast LFPs provide rapid measurements from a large population of neurons but have poor spatial localization. Neither of the techniques provide information on the coordinated activity occurring between neurons, known as an ensemble. Neuronal ensembles are understudied in the TBI field, and it is unknown how repetitive head impacts effect neuronal activity at the population level.

In this manuscript, we use Thy1-GCaMP6f transgenic mice expressing fluorescent calcium indicators to measure meso-scale neuronal activity with single cell resolution. While calcium imaging allows for higher spatial specificity, the slow indicator dynamics yield decreased temporal resolution. To observe both the spatial specificity with the temporal resolution, we combine calcium imaging simultaneously with local field potential (LFP) recordings to elucidate microcircuit changes following HFHI using methods recently developed in our lab (Caccavano et al., 2020). Combining these two methods allows for comparison of the relatively slow calcium dynamics in an ensemble specific fashion to canonical and rapid time series data from traditional electrophysiological long-term potentiation (LTP) studies.

MATERIALS AND METHODS

High Frequency Head Impact Model

All procedures were performed in accordance with protocols approved by the Georgetown University Animal Care and Use Committee. Closed head High Frequency Head Impact (HFHI) procedures were performed as previously described (Main et al., 2017; Sloley et al., 2021). Male and female, 2–3-month-old, Thy1-GcAMP6f mice were anesthetized for 3 min in 3% isoflurane in 1.5 L/min oxygen. Mice were placed in the injury device with their unrestrained head resting on a gel pad and isoflurane delivered via a nosecone for an additional minute. The 10 mm diameter Teflon tip was positioned to impact directly on the midline dorsal surface of the head with the front of the impact tip positioned immediately rostral to the eye socket and equidistance from the mouse ears. The area impacted is equivalent to the rostro-caudal length of the parietal bone, with inclusion of rostral areas of the frontal bone. The pneumatically controlled impact was delivered at an impact speed of 2.35 m/s, dwell time of 32 ms, and an impact depth of 7.5 mm. Five impacts were delivered in rapid succession per day for 6 days (totaling 30 hits). Shams received identical handling and anesthesia protocols, but no head impacts.

Slice Preparation

Acute transverse hippocampal (no preference was given along the dorso-ventral axis) slices were prepared from experimental animals 24 h following the final impact. Brain slices were prepared in NMDG and HEPES-buffered artificial cerebrospinal fluid (aCSF), as previously described (Ting et al., 2014). Briefly, mice were anesthetized in open isoflurane prior to transcardial perfusion, brain dissection, and brain slicing in 0°C NMDG solution (92 mM NMDG, 2.5 mM KCl, 1.25 mM $NaH_2PO_4{\cdot}2H_2O$, 30 mM $NaHCO_3$, 20 mM HEPES, 25 mM glucose, 10 mM sucrose, 5 mM ascorbic acid, 2 mM thiourea, 3 mM sodium pyruvate, 5 mM N-acetyl-L-cysteine, 10 mM $MgSO_4{\cdot}7H_2O$, 0.5 mM $CaCl_2{\cdot}2H_2O$, pH ∼ 7.4, osmolarity ∼ 300–310 mOsm). 350 μm thick transverse slices were prepared using a Vibratome Series 3000. Slices were bisected in the slicing chamber and immediately placed in 32°C NMDG solution for 12 min before being transferred to an incubation chamber containing room temperature carboxygenated HEPES solution (92 mM NaCl, 2.5 mM KCl, 1.25 mM $NaH_2PO_42H_2O$, 30 mM

$NaHCO_3$, 20 mM HEPES, 25 mM glucose, 5 mM ascorbic acid, 2 mM thiourea, 3 mM sodium pyruvate, 5 mM N-acetyl-L-cysteine, 2 mM $MgSO_4{\cdot}7H_2O$, 2 mM $CaCl_2{\cdot}2H_2O$, pH ∼ 7.4, osmolarity ∼ 300–310 mOsm) and were allowed to recover for at least 4 h prior to recording.

Electrophysiology

Slices were transferred to a Siskiyou PC-H perfusion chamber, anchored to the bottom of the recording chamber and submerged in circulating carboxygenated aCSF (124 mM NaCl, 3.5 mM KCl, 1.2 mM $NaH_2PO_4{\cdot}2H_2O$, 26 mM $NaHCO_3$, 10 mM glucose, 1 mM $MgCl_2{\cdot}6H_2O$, 2 mM $CaCl_2{\cdot}2H_2O$, pH ∼ 7.4, osmolarity ∼ 300–310 mOsm) at 5 mL/min. Recordings were performed with a Multiclamp 700B amplifier (Molecular Devices), digitized to 20 kHz, and low-pass filtered at 2 kHz with a computer running Clampex 11 and DigiData 1440 (Molecular Devices). One recording channel for the LFP was recorded with 0.5–1 MΩ borosilicate pipettes pulled the day of recordings and filled with aCSF and placed in stratum radiatum to measure peak amplitude of field excitatory post synaptic potentials (fEPSPs). A bipolar stimulating electrode was placed in the Schaffer Collaterals. All recording sessions consisted of 10 stimulations given 10 seconds apart. LFP sessions were kept to this short time limit so as not to risk photobleaching of the slice during simultaneous calcium imaging. Recording field potentials between imaging sessions was also not possible since the LFP signal and the calcium imaging signal needed to be time aligned for analysis and we were unable to record multiple separate imaging sessions during a single long LFP recording session. For the input/output response, stimulus pulses ranging from 0 to 90 mA were given to determine the responsiveness of each slice to increasing current pulses. The order of stimulus intensity during input/output sessions was counterbalanced so that the highest intensity stimulus responses weren't recorded in succession to avoid harming the surrounding tissue or unintentionally inducing a plasticity response (usually depression) in the slice during the input/output response. A stimulus intensity that resembled 30–50% of the maximum response was selected for the high frequency stimulation (HFS) paradigm. Another session was recorded as a baseline before the same stimulus was used in a high-frequency stimulation paradigm to elicit LTP, whereby four tetanic trains were delivered at 100 Hz, 1 s each, with an interstimulus interval of 10 s (Partridge et al., 2000; Sloley et al., 2021). Three LTP sessions were recorded; thirty seconds following HFS, 5 min post HFS, and 10 min post HFS. For LTP analysis, slices that showed depression (<1 normalized peak amplitude) in the post HFS session were excluded from analysis (5/13 sham slices, 4/13 HFHI slices).

Calcium Imaging

Ca^{2+} ensemble activity of acute slices from Thy1-GcAMP6f mice was simultaneously recorded during LFP sessions with a resonant scanning confocal laser (Thorlabs) at 488 nm. The confocal head is mounted on an Eclipse FN1 microscope (Nikon Instruments). Recordings consisted of seven-hundred and twenty 512 × 512-pixel frames captured at a sample rate of 7.5 Hz using a 40× immersion objective lens covering an area of 350 × 350 μm directly over the stratum pyramidale in the CA1 region. To avoid recording too deep in the slice such that a poor signal/noise ratio or too shallow such that too many calcium loaded cells from slicing were obtained, the z-stepper was used to ensure that each recording took place 30 ± 2 μm below the surface of the slice. Following imaging, imaging files were subject to bleach and motion correction followed by semi-automatic ROI extraction using EZCalcium. LFP and calcium imaging signals were then time matched and feature extraction was then performed (see below).

Data Analysis

Local Field Potential

Local Field Potential preprocessing was done in Clampfit 11 (pClamp, Molecular Devices). Files for the imaging experiments were trimmed around the confocal laser signal for alignment with the calcium transients. Stimulus events were detected using threshold search and stimulus start, peak, and end times were transferred to independent excel files for each session. Cursors were manually placed around the fEPSP response so that slope and maximum response were recorded and transferred to the excel file for that session.

Bleach Correction

Raw imaging files were preprocessed as previously described (Caccavano et al., 2020). Briefly, TIF files were converted to change in fluorescence normalized to baseline (ΔF/F) using custom built ImageJ (FIJI) macros. Images were imported using the Bio-Formats plugin and saved as TIF stacks. The resulting stacks were corrected for photo-bleaching using two iterations of the exponential Correct-Bleach plugin for fast and slow bleaching.

Motion Correction

Non-rigid motion correction was performed for each session using the EZCalcium package (Cantu et al., 2020). A grid size of 48 × 48 and an upsampling factor of 50 across 200 frames were used for an original template. A sliding bin size of 200 frames with a max shift of 15 pixels was used for subsequent templates for motion correction.

ROI Extraction

Somatic ROIs were automatically extracted from motion corrected TIF stacks using the Constrained FOOPSI-SPGL1 algorithm in the EZCalcium package (Cantu et al., 2020). The stacks were spatially downsampled by a factor of two with no temporal downsampling. The algorithm was initialized with a greedy search for an estimated 100 ROIs biased toward an ellipsoid shape. Estimated ROI width was 8 pixels with a merge threshold of 0.9 and a fudge factor of 0.95.

ROI Refinement

ROIs were excluded in a semiautomatic fashion using the ROI refinement tool in EZCalcium (Cantu et al., 2020). The automatic exclusion criteria were as follows: no more than 25% baseline drift over the course of 100 frames, baseline stability of 1,000, maximum 2.2 roundness, maximum 3.6 oblongness, area

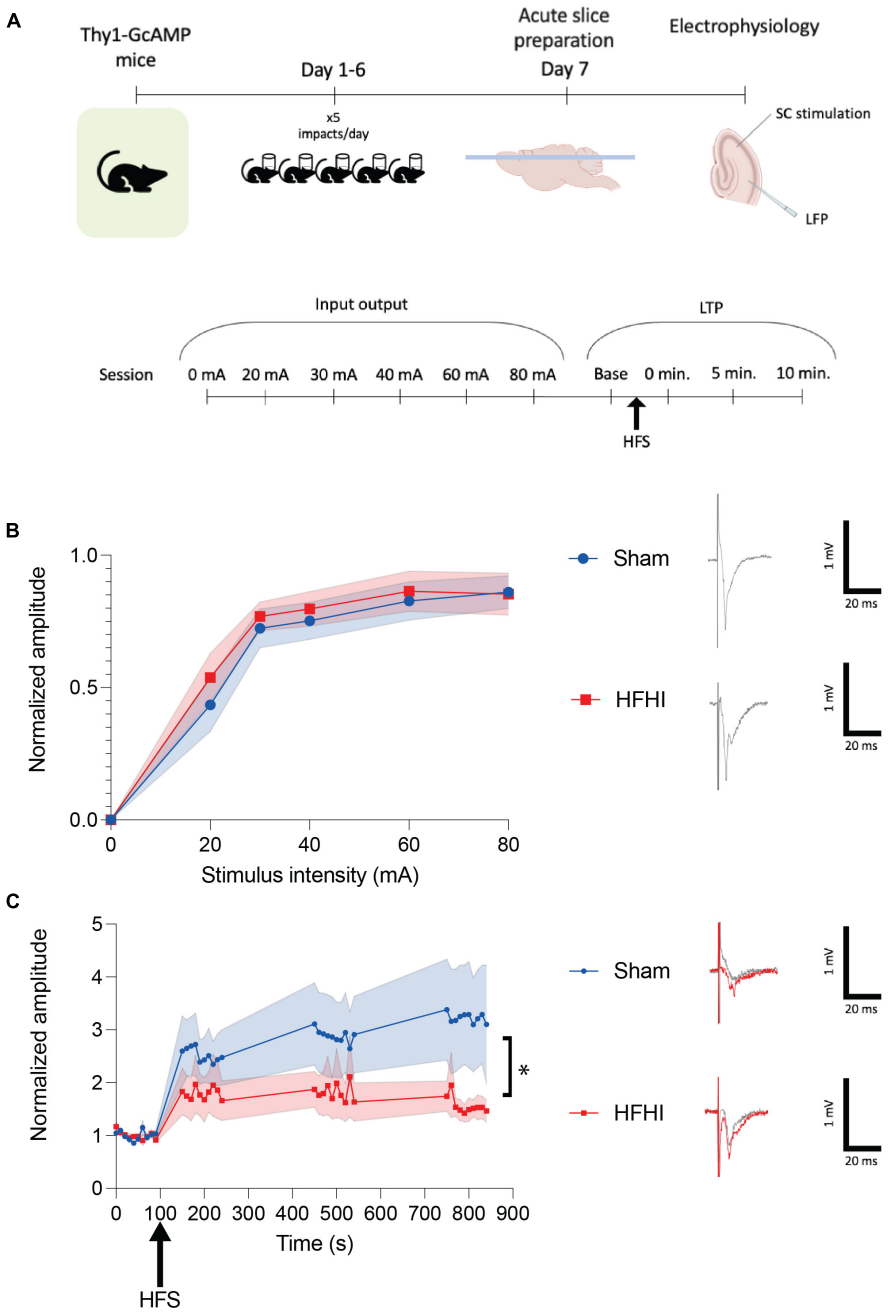

FIGURE 1 | High Frequency Head Impact (HFHI) decreases hippocampal early-LTP. **(A)** Acute slices from Thy1-GCaMP6f mice were prepared 24 h following the last day of HFHI and field recordings in the CA1 field were performed during an abbreviated LTP paradigm. **(B)** HFHI does not alter the input output response (quantified in left, example traces from 80 mA shown on right). **(C)** A significant interaction between time and group in early-LTP was seen following HFHI (quantified in left, example traces from immediately post-HFS shown on right). Shaded regions represent mean ± SEM. Mixed effects analysis, $^*p < 0.05$, $n_{Sham} = 8$, $n_{HFHI} = 9$.

between 5 and 500. Skewness and kurtosis were not assessed at this stage of processing (see below) and zero saturated frames were allowed. A blinded experimenter also manually excluded ROIs on an anatomical basis. Only ROIs in stratum pyramidale were included and ROI's with largely irregular activity such as those on the border of the field of view or near bright pixels that may have moved into or out of the ROI mask were also excluded.

Aligning Local Field Potential With ΔF/F

Calcium events from raw ΔF/F were detected as previously described using custom MATLAB scripts (Caccavano et al., 2020). Briefly, slow changes in fluorescence from further photobleaching or drifting of the imaging plane was smoothed using a moving average calculated with locally weighted regression. Baseline corrected ΔF/F traces were then interpolated from

the raw frame rate of 7.5 Hz–2 kHz and the LFP signal was downsampled from 20 to 2 kHz for post stimulus analysis. Calcium event detection was set at 4 SD above the calculated baseline with start and end times for events set at 2 SD. Baselines for each ROI was determined by an iterative algorithm of Gaussian fitting to the histogram of all data points. After calculating the baseline mean, SD, and event thresholds, features of detected events for each cell were extracted [start, peak, end, inter-event-interval (IEI), amplitude, and frequency]. To detect events occurring during spontaneous epochs and post stimulation, the interpolated calcium traces were trimmed and aligned with the downsampled LFP trace.

Calcium Threshold Normalization

Analysis and visualization of calcium time series data was done using custom MATLAB scripts. To extract ensemble activity, the data set was truncated below the 4 SD event threshold for each cell and normalized to the maximum $\Delta F/F$ for that session as previously described (Hamm et al., 2017). Briefly, on a cell-by-cell basis for each session, all values in the time series vector below the 4 SD event threshold were set to 0 and the resulting above threshold signal was divided by the maximum value for that session. This was done for two reasons: (1) calcium events are not binary and thus a relative magnitude should be assessed and (2) spurious pairwise correlations and ensemble peaks resulting from baseline noise are not indicative of true functional activity.

Shuffled Dataset

To assess the stimulus evoked ensemble activity, a bootstrapping method was used as previously described (Hamm et al., 2017). For each session, a random number was generated for each ROI to circularly shift the time series signal on a cell-by-cell basis. At each shuffling, the ensemble activity and similarity during the three post-stimulus epochs (see below) was calculated. This step was repeated 1,000 times to generate a dataset with ensemble activity at chance levels.

Ensemble Activity

To observe CA1 ensemble activity, the mean for each frame across ROI's were taken such that the resulting one-dimensional signal represented a percentage of the total active ensemble through time. This upsampled ensemble trace was aligned with the downsampled LFP to determine the periods of stimulus onsets. The continuous ensemble activity was binned into 10 s sweeps of activity between stimulus onsets. For characterization of this activity, sweeps for each session were averaged to give a clear pattern of ensemble activity for each slice and session. Due to the difference in timing of ensemble events (see below) relative to the stimulus, which we attribute to differences in placement of the stimulating electrode and position of the slice along the dorso-ventral axis, the timing of the three epochs of post-stimulus activity characterized in this paper were individually determined for each slice and session using the MATLAB "islocalmax" and "islocalmin" functions for ensemble maxima and minima respectively. ***Ensemble fraction*** during these epochs was calculated by determining the fraction of ROIs with calcium transients during a 10 ms window surrounding the local maxima and minima in the averaged ensemble sweeps for that session.

Ensemble Overlap

Overlap of ROI activity during ensemble epochs between stimulations was calculated using a Hamming distance metric between active ROIs of one epoch to the same epoch following a different stimulation. The Jaccard index and cosine similarity metric have been used in the past (Hamm et al., 2017; Caccavano et al., 2020), however, these metrics cannot account for similarity values between two zero matrices, a finding often seen during the ensemble minimum epoch and were not used for this reason.

Statistics

All statistics were done in Prism 8 (GraphPad). In total, 13 slices from 8 sham animals (5 animals with two slices) and 13 slices from 9 HFHI animals (4 animals with two slices) were recorded from. "n" values in figure legends refer to the number of slices. The n number can vary from analysis to analysis as some sessions were excluded due to slice shifting or a diminishing number of ROIs below the determined minimum of 3 during one session but valid during other sessions. Outliers were defined as those slices showing a value 1.5 times the interquartile range above or below either quartile. Due to this, a mixed effects analysis with Šídák's *post hoc* comparisons were performed on the LFP response and continuous calcium metrics (**Figures 1B,C**, **2C,D**, **3B–I**, **5A–F**, **6A–F**) throughout the paradigm. Shaded regions on line graphs indicate mean ± SEM.

Code Availability

MATLAB code for semiautomatic extraction of calcium ROIs using EZCalcium is openly accessible (Cantu et al., 2020). MATLAB functions for aligning raw calcium traces with LFP and extracting calcium events from Caccavano et al. (2020) can be found here: https://github.com/acaccavano/SWR-Analysis. Custom MATLAB software used in the present study for feature extraction and ensemble analysis can be found here: https://github.com/dpchapma/CalciumImagingAnalysis.

RESULTS

High-Frequency Head Impact Impairs Early-LTP 24 h Post-injury

To assess synaptic plasticity 24 h following HFHI, we investigated early-LTP in the CA3-CA1 circuit (**Figure 1A**). Mixed effects analysis revealed no changes to the input-output response in HFHI brain compared to sham brain (**Figure 1B**). Following 10 baseline stimulations at a stimulus intensity that was 30–50% of the maximum response a high frequency stimulation (HFS) was given (ending at time 0) and the relative field response was measured 0-, 5-, and 10-min post HFS (**Figure 1C**). We found a significant interaction between injury group and time following HFS despite between group effects not reaching significance [mixed effects analysis: Time × Group, $p = 0.0104$, $F(39, 553) = 1.633$; Group, $p = 0.1291$, $F(1, 15) = 2.580$; Time, $p = 0.0061$, $F(2.073, 29.40) = 5.987$; $n_{Sham} = 8$, $n_{HFHI} = 9$].

These results corroborate previous work from our lab showing a reduction in early-LTP in the absence of a change in the input/output curve (Sloley et al., 2021).

High Frequency Head Impact Does Not Change Number of Active ROIs

To understand the inability of the repeat head impact brain to fully potentiate, we examined calcium dynamics in the CA1 field during the early-LTP paradigm. The active constituents of the CA1 ensemble were assessed during the early-LTP paradigm by imaging the CA1 field of Thy1-GCaMP6f animals simultaneously during the CA3-CA1 LTP protocol (**Figure 2A**). To assess the number of active neurons in the CA1 field following HFHI, somatic ROIs were extracted, and raw calcium traces were aligned with the LFP signal (see section "Materials and Methods") in both groups (**Figure 2B**). Calcium transients were defined as periods of time in which the ΔF/F reached 4 SD above the baseline for each ROI. The number of ROIs with calcium transients did not differ between the groups during the input/output sessions (**Figure 2C**) or the LTP sessions (**Figure 2D**). We also quantified the number of ROIs with calcium transients across all sessions for each slice and found no difference between the groups (**Figure 2E**). This corroborates previous reports from our group that HFHI does not lead to neuron cell death. However, due to the importance of calcium following TBI, we next quantified differences in calcium transients following HFHI.

Number of Calcium Transients Are Increased in High Frequency Head Impact Slices

We next sought to understand whether the calcium event dynamics differed between groups across the stimulation paradigm. Average transient amplitude, duration, IEI, and number of transients were averaged across ROIs for each input output sessions and an abbreviated LTP paradigm (**Figure 3A**). Only active ROIs were considered and all events across the sessions were considered irrespective of each transient time relation to the stimulus onset. Event duration did not differ between the groups during the input output sessions (**Figure 3B**) and LTP sessions (**Figure 3C**). Similarly, calcium transient ΔF/F remained unchanged between the groups during both input output sessions (**Figure 3D**) and LTP sessions (**Figure 3E**). Calcium transient IEI displayed an inverse relationship with stimulus intensity in HFHI slices, but no relationship with sham slices, resulting in a significant decrease of IEI in HFHI across the input output sessions [**Figure 3F**, Mixed effects analysis: Stimulus × Group, $p = 0.2260$, $F(5, 102) = 1.4$; Group, $p = 0.0313$, $F(1, 24) = 5.234$; Stimulus, $p = 0.3399$, $F(2.660, 54.27) = 1.134$; $n_{Sham} = 13$, $n_{HFHI} = 13$]. This change in IEI, however, was not reflected during the LTP sessions (**Figure 3G**) which took place at relatively low stimulus intensities (∼20–50 mA). The number of calcium transients per ROI were significantly increased in HFHI slices during the input/output sessions [**Figure 3H**, Mixed effects analysis: Stimulus × Group, $p = 0.4038$, $F(1, 23) = 9.31$; Group, $p = 0.0057$, $F(1, 23) = 9.31$; Stimulus, $p = 0.1498$, $F(2.706, 52.50) = 1.879$; $n_{Sham} = 11$, $n_{HFHI} = 12$; Šídák's multiple comparisons test; 60 mA, $p = 0.0326$; 80 mA $p = 0.0447$] as well as during the LTP sessions [**Figure 3I**, Mixed effects analysis: Time × Group, $p = 0.9892$, $F(3, 49) = 0.03$; Group, $p = 0.0092$, $F(1, 21) = 8.241$; Time, $p = 0.8361$, $F(2.568, 41.94) = 0.2439$; $n_{Sham} = 11$, $n_{HFHI} = 12$]. These data demonstrate that individual ROIs of HFHI slices differ in the number of calcium transients, but not amplitude or duration.

High Frequency Head Impact and Sham Slices Show Coordinated Patterns of Post Stimulus Ensemble Activity

We next sought to understand how individual calcium ROIs were functionally connected during the early-LTP paradigm. Calcium imaging offers the ability to record from tens-of-thousands of neurons simultaneously to assess network changes *in vivo* (Cossart et al., 2003; Hamm et al., 2017). Ensembles are defined as groups of transiently coactive neurons and are thought to be one of the most basic units of neural computation (Buzsaki, 2010). We assessed the correlation between individual pairs of cells but found no significant relationships or differences between groups (Mean ± SEM pairwise correlations across all sessions: Sham = 0.1177 ± 0.015, HFHI = 0.1294 ± 0.010). To assess CA1 ensemble activity following HFHI, collective calcium activity was mapped across our stimulation paradigm (**Figure 4A**). Ensemble activity was calculated by averaging the normalized activity across ROIs (**Figure 4B**: example session with individual ROIs). The resultant trace (**Figure 4C**), which reflects the averaged ensemble activity across time, was time aligned with the downsampled LFP signal (**Figure 4C**: vertical lines) to assess ensemble activity in the seconds following each stimulus. We then binned the ensemble activity for each recording into 10-second inter-stimulus sweeps (9 total) and averaged ensemble activity across each sweep. Both sham and HFHI slices showed coordinated patterns of activity and we observed three distinct features (**Figures 4D–F**) numerically illustrated in the shaded regions as (1) first ensemble maximum, (2) ensemble minimum, and (3) second ensemble maximum. All three features are best illustrated from example sessions in **Figure 4D** where the first maximum (epoch 1) which usually occurred <1 s followed by the ensemble minimum (epoch 2) occurring 1–3 s following the stimulus and ending with the second ensemble maximum (epoch 3) occurring within 5 s of the stimulus. Both sham and HFHI slices displayed patterns of activity with one or all three of these patterns. Interestingly, across groups as well as individual slice ensemble patterns, the ensemble minimum (epoch 2) was the most consistent pattern of (in)activation seen and was observed in every slice in both groups at the highest stimulus intensity.

We classified slices as either having a Type A (1st maximum is greater and an ensemble inactivation, Example 4D), Type B (2nd maximum and no 1st maximum Example 4E), or Type C (no maxima, only a transient inactivation of the ensemble, Example 4F) patterns at the highest stimulus intensity recorded for that slice (**Figure 4G**). We chose the highest stimulus intensity for this classification since the consistency and magnitude of these patterns at lower stimulus intensities was reduced compared to higher intensities. Despite this fact, slices which displayed

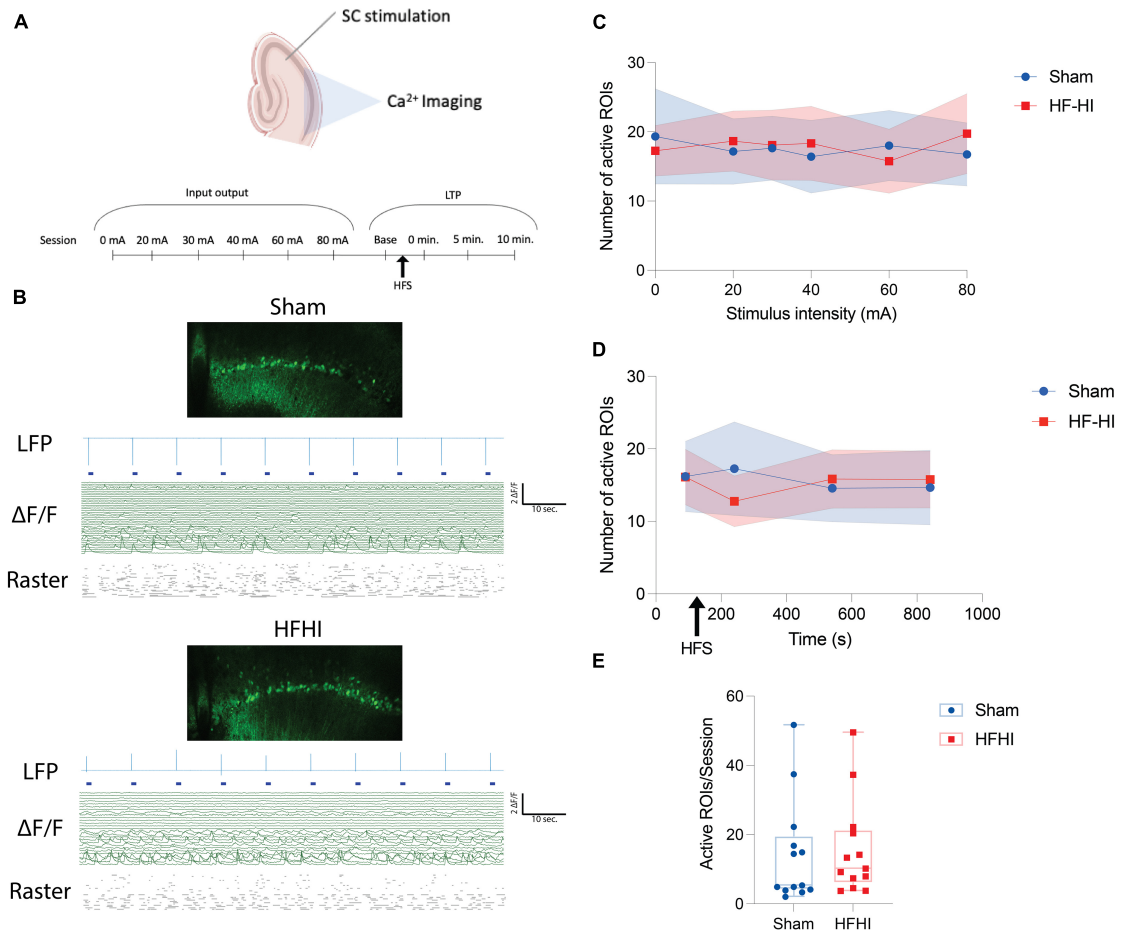

FIGURE 2 | High Frequency Head Impact (HFHI) does not alter number of ROIs with calcium activity. **(A)** Acute slices from Thy1-GcAMP6f mice were prepared 24 h following the last day of HFHI and calcium imaging of the CA1 field was performed during an abbreviated LTP paradigm. **(B)** Example confocal view, aligned LFP, raw calcium traces, and raster plot of sham (top) and HFHI (bottom) slices. **(C)** Semi-automatic ROI extraction revealed no differences in the number of ROIs with activity during the input output sessions, **(D)** LTP sessions, or **(E)** overall number of ROIs extracted per session. Shaded regions represent mean ± SEM in line graphs. n_{Sham} = 13, n_{HFHI} = 13.

a particular ensemble activity pattern at higher intensities displayed the same pattern at lower intensities as well, albeit with diminished consistency from stimulus to stimulus. Chi-squared analysis revealed no difference between the prevalence of these patterns amongst slices. The timing of each feature did not differ between groups or with stimulus intensity during the input/output sessions and time during the LTP session. These traces demonstrate a novel pattern of CA1 calcium ensemble activity following SC stimulation and show that these patterns are qualitatively unaffected by HFHI.

High Frequency Head Impact Increases CA1 Ensemble Fraction During Coordinated Activity Periods

We next sought to quantify ROI activity during the ensemble epochs in sham and HFHI slices to characterize differences in these activity patterns in the repeat head impact brain. To quantitatively assess ensemble activity following stimulus onset, we calculated the fraction of ROIs with calcium transients during 10 ms windows in the three major events described in **Figure 4** were calculated. The activity of the raw ensemble was compared to a shuffled dataset generated similar to Hamm et al. (2017). During the input/output sessions, a positive correlation was seen between stimulus intensity and the ensemble fraction during the first ensemble maximum (**Figures 4D–F**, epoch 1). Ensembles from both groups displayed a larger fraction of active ROIs compared to their shuffled datasets, however, there was no difference observed between groups (**Figure 5A**). ROI fraction during the first ensemble maximum activity was not altered by HFS and did not differ between groups but remained well above the fraction seen in the shuffled datasets (**Figure 5B**). Unsurprisingly, the ensemble fraction during the ensemble minimum (**Figures 4D–F**, epoch 2) was substantially lower than that of the first ensemble maximum and the shuffled data, however it did not differ between groups or correlate to stimulus intensity (**Figure 5C**). During the LTP sessions, a significant difference between groups was seen in the ensemble fraction

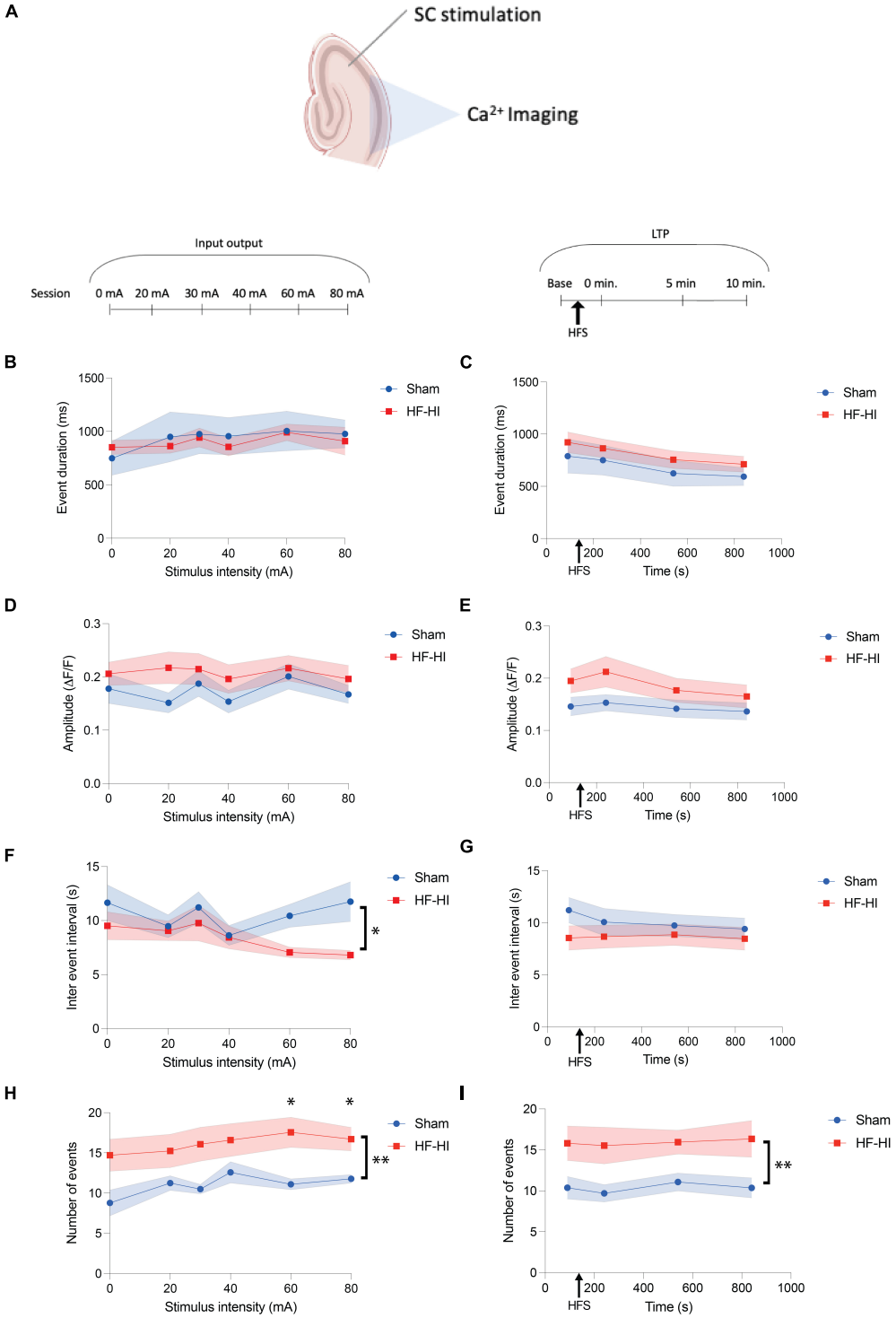

FIGURE 3 | High Frequency Head Impact (HFHI) increases the number of calcium transients but does not alter event features. **(A)** Acute slices from Thy1-GcAMP6f mice were prepared 24 h following the last day of HFHI and calcium imaging of the CA1 field was performed during an abbreviated LTP paradigm. **(B)** HFHI does not alter calcium transient duration during the input output curve or **(C)** following HFS of the Schaffer collaterals. A similar trend was seen for normalized event amplitude in the **(D)** input output sessions and **(E)** LTP sessions. **(F)** HFHI slices displayed a significant decrease in the IEI during the input output sessions, but not **(G)** the LTP sessions. The average number of calcium transients was significantly increased in HFHI slices during **(H)** the input output sessions and **(I)** the LTP sessions. Shaded regions represent mean ± SEM. With brackets: mixed effects analysis, $^{*}p < 0.05$, $^{**}p < 0.01$, **(F)** $n_{Sham} = 13$, $n_{HFHI} = 13$, **(H)** and **(I)** $n_{Sham} = 12$, $n_{HFHI} = 13$ (one sham outlier removed). Above graph in **(I)** Šídák's multiple comparisons test, $^{*}p < 0.05$, $n_{Sham} = 12$, $n_{HFHI} = 13$.

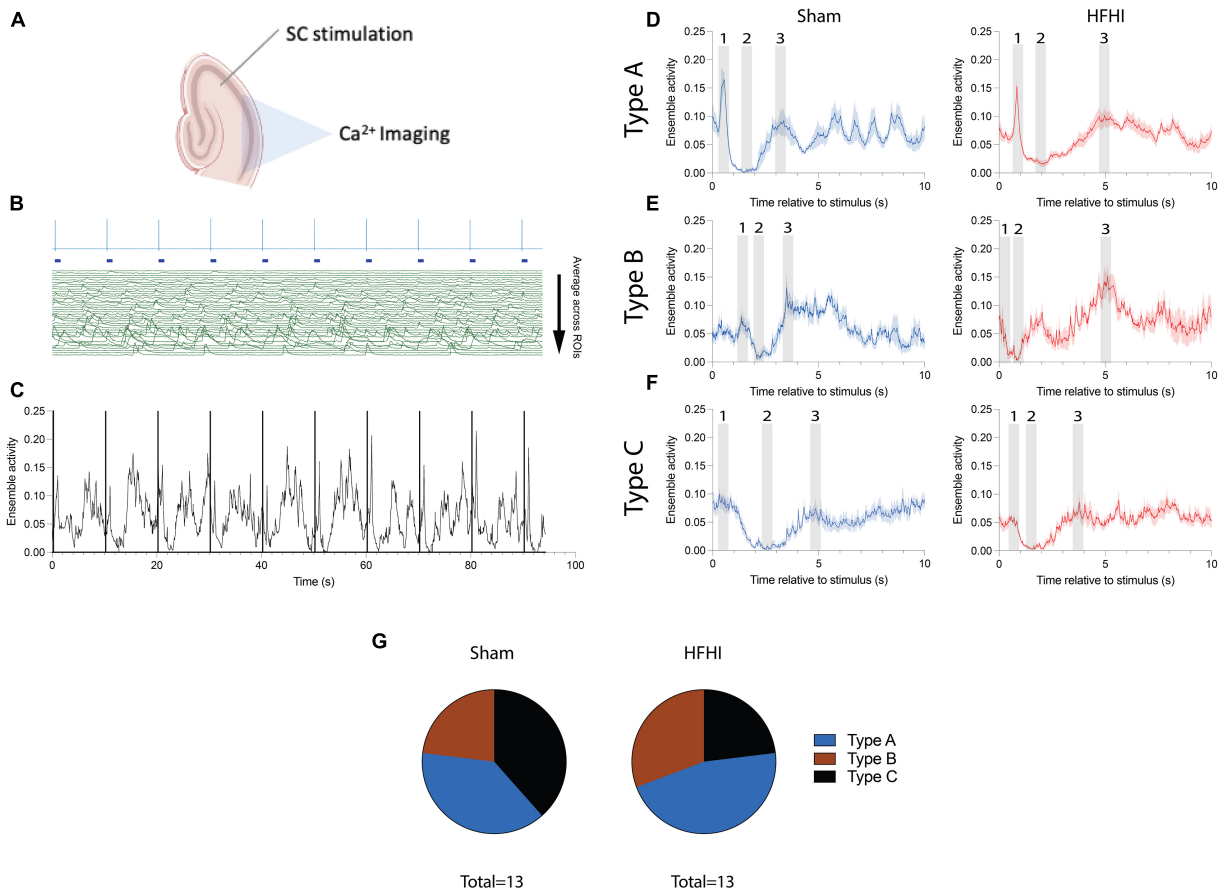

FIGURE 4 | High Frequency Head Impact (HFHI) and sham slices both display distinct ensemble activity following SC stimulation. **(A)** Acute slices from Thy1-GCaMP6f mice were prepared 24 h following the last day of HFHI and calcium imaging was performed simultaneously with LFP recordings of the CA1 field during an abbreviated LTP paradigm. **(B)** Example HFHI LFP (top, blue) aligned with raw calcium traces (bottom, green) from one recording. Ensemble activity was obtained by setting individual ROI calcium activity below threshold (4 SD above the baseline) to zero and averaging across all ROIs at each timepoint. **(C)** Example ensemble activity (black) with stimulus onset overlain (purple) for one session. Calcium ensemble activity following stimulus onset was visualized by binning ensemble activity into 10 s sweeps between stimulus onsets and averaging all the sweeps. We characterized various patterns of post-stimulus ensemble activity generally consisting of **(D)** a prominent maximum shortly <1 s after the stimulus (epoch 1), an ensemble minimum 1–3 s following stimulation (epoch 2), and a second ensemble maximum following the minimum (epoch 3) which was usually less prominent although slices from both groups displayed **(E)** more prominent second maxima or **(F)** only a transient ensemble inactivation with no maxima. **(G)** Pie charts showing distribution of patterns classified into Type A (1st maximum and ensemble minimum), Type B (2nd maximum an ensemble minimum), and Type C (ensemble minimum only). Shaded regions represent mean ± SEM across 9 sweeps in line graphs.

during the ensemble minimum with HFHI slices displaying elevated activity during this epoch compared to sham slices [**Figure 5D**, Mixed effects analysis: Time × Group, $p = 0.7627$, $F(35, 644) = 0.8189$; Group, $p = 0.0462$, $F(1, 22) = 4.465$; Time, $p = 0.3541$, $F(6.016, 110.7) = 1.122$; $n_{Sham} = 12$, $n_{HFHI} = 12$]. Lastly, assessing the second ensemble maximum (**Figures 4D–F**, epoch 3) revealed an inverse relationship between stimulus intensity and ensemble fraction in sham slices, with the ensemble fraction dropping below chance levels with increasing stimulus intensity. This did not occur in HFHI slices, which remained at chance levels throughout the paradigm. This resulted in a significant interaction between time and group with HFHI slices displaying an increased ensemble fraction [**Figure 5E**, Mixed effects analysis: Stimulus × Group, $F(5, 85) = 2.398$; Group, $p = 0.3107$, $F(1, 24) = 1.072$; Time, $p = 0.6682$, $F(2.882, 59.81) = 0.5122$; Šídák's multiple comparisons test; 60 mA, $p = 0.05$; $n_{Sham} = 13$, $n_{HFHI} = 13$]. However, there was no difference between groups during the second ensemble maximum throughout the LTP sessions, which took place at relatively low stimulus intensities (∼20–50 mA), nor did either group differ from their shuffled dataset (**Figure 5F**). We generally found an increase in number of calcium transients in HFHI slices compared to shams when assessing transients across the entire session (**Figures 3F–I**) and revealed a similar trend in the ensemble analysis during the second ensemble maximum (**Figure 5E**) and ensemble minimum (**Figure 5D**) during the input/output curve and LTP sessions, respectively. These findings illustrate an abnormality in HFHI animals in the normal calcium transient firing during specific time periods related to stimulus induced ensemble activity.

Repetitive Ensemble Firing Is Partially Diminished Following High Frequency Head Impact

Previous reports of calcium activity from various brain regions *in vivo* and *in vitro* have revealed that ensemble activations frequently occur through a similar set of ROIs firing in a repeating fashion (Cossart et al., 2003; Villette et al., 2015; Hamm et al., 2017) and plasticity events are known to alter the makeup of the ensemble *in vitro* (Yuan et al., 2011). To assess the repetitive nature of specific ROIs during the novel post-stimulus ensemble epochs described in the present study (**Figures 4D–F**), we quantified a distance metric, a comparison between the pattern of ROIs that fired or didn't fire, following each stimulation and compared them against a shuffled dataset for reference (**Figure 6**). Generally, groups did not differ in ROI set distance during the first ensemble maximum (1) during either the input/output (**Figure 6A**) or LTP sessions (**Figure 6B**). Interestingly, there was no difference in distance in the ensemble minimum epoch (2) between group, stimulus intensity during the input output sessions (**Figure 6C**), or time during the LTP sessions (**Figure 6D**), however, ensemble distance was well below that of the shuffled datasets during this epoch in both groups. Contrarily, we observed a significant increase in HFHI ensemble distance during the second ensemble maximum (3) of the input/output sessions [**Figure 6E**, Mixed effects analysis: Stimulus × Group, $p = 0.1388$, $F(4, 83) = 1.78$; Group, $p = 0.0091$, $F(1, 24) = 8.334$; Stimulus, $p = 0.8951$, $F(3.401, 70.58) = 0.2319$; $n_{Sham} = 13$, $n_{HFHI} = 13$]. Like our findings on ensemble fraction during this epoch (**Figure 5E**), we observed an inverse correlation between ensemble distance and stimulus intensity in sham mice, but not HFHI, despite starting at similar levels to both the HFHI group and shuffled datasets at the lower intensities (**Figures 5E**, **6E**). No difference was seen between group, time, or against the shuffled datasets, however, during the LTP sessions (**Figure 6F**). Collectively, this data shows an abnormality in repetitive ROI activation during patterns of ensemble activity following HFHI.

DISCUSSION

Sub-concussive impacts or sustained high frequency low amplitude cranial movement seen in high school football players, soccer players, and professional sled athletes can lead to lasting cognitive symptoms (Colvin et al., 2009; Talavage et al., 2014; McCradden and Cusimano, 2018); however, the mechanism by which these impacts can contribute to changes in brain function is poorly understood. Here we used field recordings to demonstrate that Thy1-GCaMP6f mice exposed to HFHI have reduced early-LTP, and matched calcium imaging to demonstrate that CA1 neurons have increased calcium activity and impaired ensemble dynamics.

High Frequency Head Impact Impairs Early-LTP and Increases Calcium Activity

Impaired hippocampal plasticity has been reported in several TBI models of various severity and frequency (Miyazaki et al., 1992; Albensi et al., 2000; Goldstein et al., 2012; Aungst et al., 2014; Mei et al., 2018; Tagge et al., 2018). However, the heterogenous pathologies that occur following TBI, such as neuron death, axon shearing, reduction in synapses, and synaptic adaptation can all affect plasticity. For this reason, the mechanism behind impaired LTP in other TBI models can often be difficult to dissect out due to the multi-pathology phenotypes. Contrarily, we do not observe hippocampal cell death or inflammation in the HFHI model, but instead reported isolated synaptic changes that underlies this altered plasticity (Sloley et al., 2021). In the present study we extended those results to Thy1-GCaMP6f mice exposed to sham or HFHI and found that HFHI reduced hippocampal early-LTP which occurs without measurable change in the input/output curve, similar to our previous findings in HFHI C57Bl/6 mice (Sloley et al., 2021).

We hypothesized that synaptic adaptations occur following HFHI, whereby the neurons adapt to the head impacts in a manner that is designed to protect the brain against future insult. If true, we would expect that the synaptic adaptations would act to alter the downstream events occurring in response to TBI-induced glutamate release, including changes to calcium dynamics. In this study, we report that HFHI slices have similar numbers of somatic ROIs to sham animals but show increased calcium transient frequency in these ROIs. These data contrast with previous calcium imaging done *in vivo* hyperacutely (∼1 h) following two-successive days of blast injury, which showed hypoactivity, including vastly decreased intracellular calcium activity and altered calcium event dynamics (Hansen et al., 2018). There are several experimental differences that could account for these contrasting results. The blast model is more severe, has a lower frequency of impacts, and imaging was performed at a much earlier timepoint relative to the injury when compared to our study (Hansen et al., 2018). Furthermore, the recent characterization of HFHI by our group showed a general pattern of decreased excitability in whole-cell patch clamp recordings of HFHI neurons (Sloley et al., 2021). Despite this hypoexcitability phenotype in whole cell configuration, it is possible to see increased calcium dynamics possibly originating from several sources: increased spontaneous glutamate release, decreased reuptake, disinhibition, and decreased intracellular calcium sequestration. In a single and repetitive controlled cortical impact model, a much more severe model of TBI, single cell electrophysiology and calcium imaging revealed increased baseline calcium accompanied by hyperexcitability in the input/output response in TBI groups (McDaid et al., 2021). This both corroborates and contrasts our results as we see an increase in calcium transients but no change in the input/output response in HFHI animals. Further work using pharmacological isolation is needed to understand the source of increased calcium transients seen in the present study.

The CA1 Field Shows Coordinated Patterns of Ensemble Activity Following Schaffer-Collateral Stimulation

Ensemble dynamics *in vitro* are impossible to reasonably correlate to behavior states; however, they can provide useful

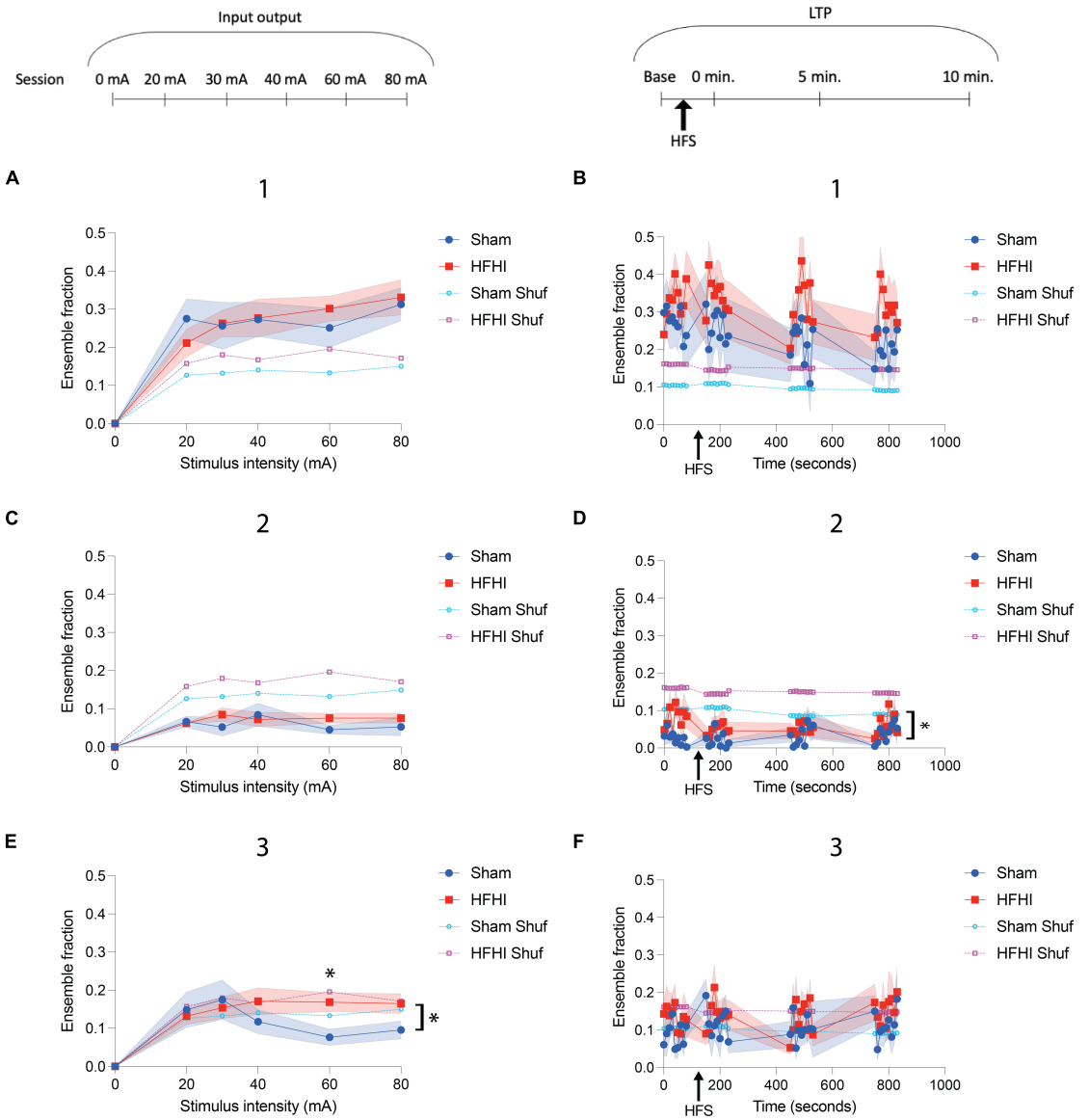

FIGURE 5 | High Frequency Head Impact (HFHI) increases ensemble size during coordinated activity periods. **(A)** HFHI and sham slices display increasing number of events during the first ensemble maximum with increasing stimulus intensity, but no differences were observed between the group. **(B)** Potentiation of the CA1 field with HFS did not alter transient frequency during the first ensemble maximum. **(C)** Calcium transient frequency during the ensemble minimum remained low for both groups throughout the input/output paradigm relative to the ensemble maxima and did not differ with stimulus intensity. **(D)** A significant difference in the fraction of ensemble with calcium transients during the ensemble minima between the groups was seen **(E)** Sham ensemble activity during the second ensemble maxima appeared to be inversely related with stimulus intensity while HFHI slices remained stable at higher stimulus intensities, leading to a significant interaction between time and group. **(F)** The activity during the second ensemble maximum was not altered by HFS and did not differ between groups. Shaded regions represent mean ± SEM. With brackets: mixed effects analysis, $^*p < 0.05$, comparing real data (non-shuffled) from each group. Above graph in E) Šídák's multiple comparisons test, $^*p = 0.05$ $n_{Sham} = 13$, $n_{HFHI} = 13$.

insight into network integrity at the meso- and micro-circuit level. In our experiment, we measured ensemble activations following stimulation by averaging across ROI activity and aligning this activity trace with the stimulus onsets. This analysis revealed a pattern of activity similar to a previous report using genetically encoded voltage indicators (GEVI) *in vitro* (Nakajima et al., 2021) but, to our knowledge, has not been previously characterized using Thy1-GCaMP6f animals. We broke the activity down into three distinct features that occurred between ∼0 and ∼5 s following stimulus onset and consisted of (1) a first ensemble maximum; a narrow (∼0.2 s) and prominent peak usually between 0 and 1 s following stimulus onset. (2) An ensemble minimum; a significant and consistent decrease in ensemble activity, often times even to 0% of the ROIs being active and lasting around 1 s. We attribute this to lateral inhibition in the CA1 field following excitation of somata in the first

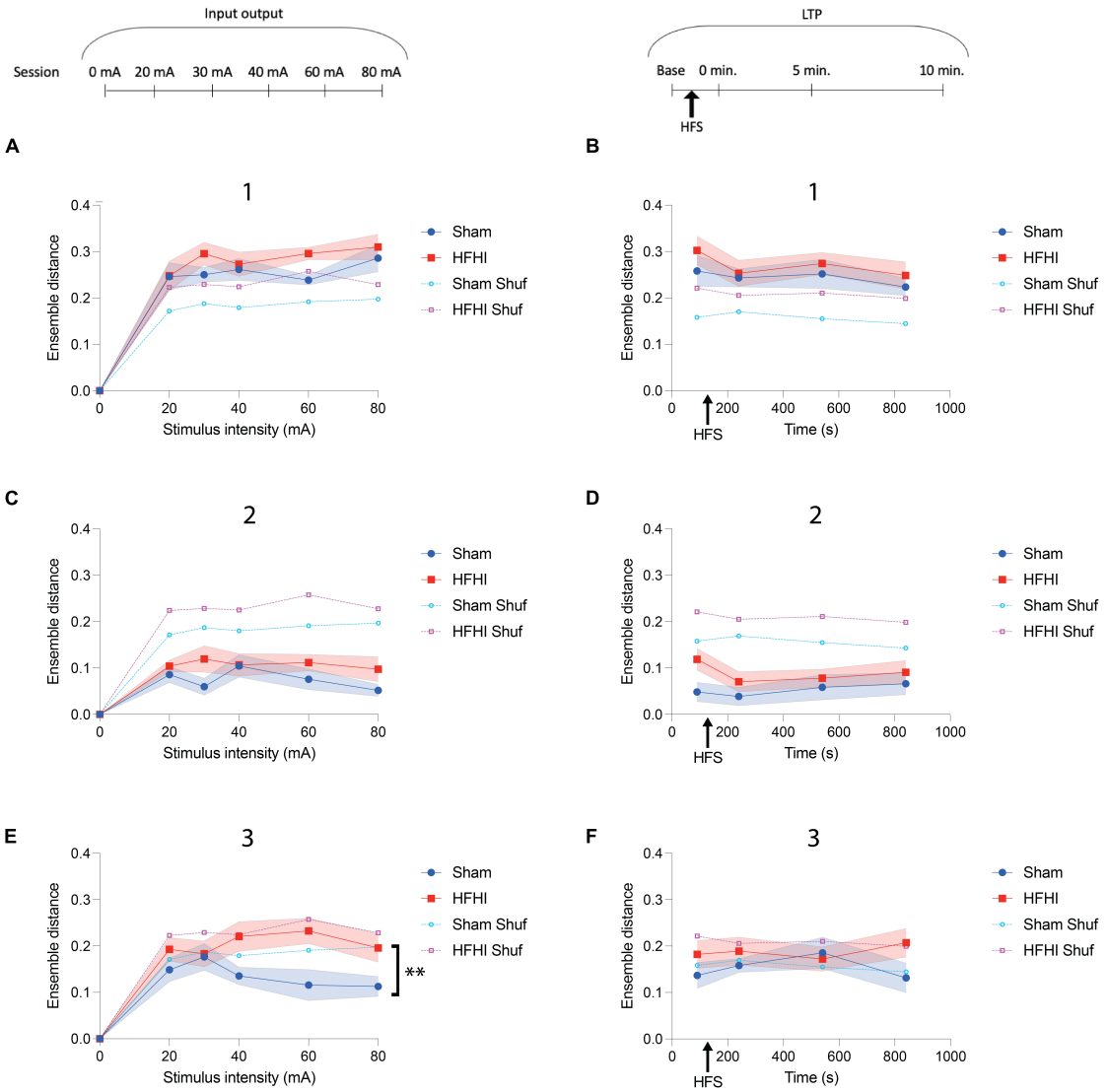

FIGURE 6 | High Frequency Head Impact (HFHI) increases post stimulus ensemble distance during second maximum. **(A)** HFHI slices displayed significantly increased ensemble distance during the first maximum during the 60 mA input output session, despite the mixed effects analysis not significantly differing between groups or **(B)** during the LTP sessions. **(C)** Ensemble distance during the minimum time range did not differ significantly between groups in the input output session, however, **(D)** during the LTP sessions HFHI displayed a trend toward increased ensemble distance. **(E)** During the second maximum, HFHI slices displayed significantly increased ensemble distance, especially at higher stimulus intensities, but **(F)** not during the LTP sessions. Mixed effects analysis, $^{**}p < 0.01$, comparing real data (non-shuffled) from each group, $n_{Sham} = 13$, $n_{HFHI} = 13$.

maximum. This hypothesis is supported by the previous study of CA1 stimulation using GEVI mice as the similar dip in activity following stimulation was sensitive to GABA blockers (Nakajima et al., 2021). This decrease in ensemble activity was the most consistent across slices, groups, and sessions. (3) A second ensemble maximum; a broader peak than the first ensemble maximum that usually was of less amplitude. This third epoch is the most variable in terms of timing and amplitude of the three epochs identified.

By combining these three features (see above) we observed one of the three patterns (type A, B, or C) in all slices and the type of pattern observed did not change across different stimulus intensities within the same slice, although some slices did not display coordinated ensemble activity at the lowest stimulus intensity of the input output curve. Some animals had multiple slices recorded from (Sham, $n = 5$; HFHI, $n = 4$ animals with two slices), some of which displayed different patterns of activation between slices of the same animal. This precludes the possibility that the type of coordinated ensemble activity observed is implicit to the animal but rather reflects slight differences in experimental parameters at the time of recording. Thus, we attribute the qualitative difference in coordinated activity patterns (Type A, B, or C) to slice level along the dorso-ventral axis and/or the exact placement of the stimulating electrode relative to the CA1 field.

While our pattern of ensemble activity reflects a mirror image of that seen reported from Nakajima et al., their report drew data from all regions of the imaging field rather than just looking at active soma in stratum pyramidale and did not look at plasticity inducing stimulations. Furthermore, the timescale for activity in the present study is significantly drawn out due to the slow indicator dynamics of GCaMP6f when compared to GEVIs. Despite these differences, ensemble activity extracted from active soma in the CA1 from Thy1-GCaMP6f mice and mined activity using GEVIs showed similar qualitative properties following stimulation. Other groups have reported similar calcium ensemble spikes in the dorsal CA1 (Xia et al., 2017) and amygdala (Corder et al., 2019) *in vivo* relating to conditional behavior paradigms as opposed to stimulation paradigms, however, none have reported the same pattern of lateral inhibition following stimulus onset.

Qualitatively, no difference was seen between sham and HFHI slices in the pattern of post-stimulus ensemble activity. These findings along with the unchanged input/output curve during the field recordings would indicate a grossly intact network architecture in the CA1 field, once again reaffirming our findings that neuron death, axon shearing, or widespread inflammation are unlikely causes of decreased learning and plasticity in HFHI.

High Frequency Head Impact Alters ROI Activation During Periods of Coordinated Ensemble Activity

We quantified the percentage of ROIs with calcium transients (ensemble fraction) during the periods described above for both the input/output and LTP sessions and compared groups against each other and a shuffled dataset. Ensemble activity from both groups during the first maximum and ensemble minimum showed an increase and decrease in ensemble activity compared to the shuffled data, respectively. During the second maximum, only the sham slices significantly deviated from the shuffled datasets at higher stimulus intensities during the input/output sessions, but not the LTP sessions, which took place at lower stimulus intensities (∼20–40 mA). When comparing the real data from both groups, we found a significant increase in HFHI slices of ensemble fraction during the ensemble minimum of the LTP sessions. This corresponds to the decreased IEI seen in HFHI slices during the input/output sessions, which was only observed at the two highest stimulus intensities, indicating that the general decrease in IEI at higher stimulus intensities can be accounted for by events occurring during the ensemble minimum.

Some authors hypothesize that white matter disruptions or neuronal degeneration following rmTBI are the cause of network disruptions (Sharp et al., 2014; Wolf and Koch, 2016; Schumm et al., 2020). However, other work done *in vivo* following a fluid percussion injury showed decreased CA1 network synchrony despite no change in firing rates or neuron cell death (Koch et al., 2020) and further *in vitro* work suggests changes to NMDA subunit density and distribution due to mechanical forces reduces network correlation (Patel et al., 2014). This is complemented by modeling work showing that altered NMDA receptor properties following TBI showed deficient spike time dependent plasticity and computational properties in injured networks compared to uninjured ones without the removal of network components (Gabrieli et al., 2021). Thus, we attribute the differences seen in ensemble fraction activity across the stimulation paradigm in HFHI to a synaptic mechanism.

There are several possible mechanisms that could explain this finding. Given that the ensemble minimum is likely due to lateral inhibition in the CA1 field (Nakajima et al., 2021), one possible mechanism to explain the observed increase in the HFHI slices is a disruption in the microcircuit between pyramidal cells and inhibitory interneurons. Given that qualitative pattern of coordinated ensemble activity can differ across slices of the same animal, but not across stimulus intensity within the same slice (see above), we believe that efficacy of lateral inhibition in the CA1 field of HFHI slices may be compromised and lead to the altered ensemble fractions seen in this study. This is in line with previous work done in a more severe model of TBI which found prominent increases in cortical E/I balance in the hours following injury, but these effects were dampened by 48 h post injury (Witkowski et al., 2019). Similarly, another report found decreased cortical inhibition in a fluid percussion model, however, this inhibition occurred at later timepoints (Hsieh et al., 2017). Changes to inhibitory neurons following HFHI have yet to be characterized, however, their prominent role in hippocampal ensemble coordination during network events such as sharp-wave ripples (Buzsaki, 1986) suggest that changes to inhibition in the CA1 microcircuit could contribute to the decreased ensemble coordination observed in the present study.

A second possible explanation is decreased glutamate reuptake at the CA3-CA1 synapse. A growing body of literature in the Alzheimer's field has pinpointed impaired glutamate reuptake as a possible source of hyperactivity seen in various models of pathology (Busche et al., 2008; Zott et al., 2019). While these studies showed hyperactivity *in vivo* and not naturally *in vitro*, a similar mechanism could explain both the increased ensemble activity during minima and rebound maxima following stimulation as well as the diminished LTP from field recordings. Lingering glutamate in the synaptic cleft can activate extrasynaptic NMDA receptors, leading to a slower and more drawn-out entry of calcium into cells, a pattern most often associated with synaptic depression. If this were true in the present study, we may have expected to see an increase in event duration. While we did not see this effect, it is possible that an extension of the event duration is present closer to the synapse at dendritic ROIs but is washed out by the time transients reach the soma.

Lastly, calcium indicators are proxy for neural activity, however, in theory not all calcium events represent neural activity. Thus, a third explanation for the general hyperactivity in both individual calcium transients and coordinated ensemble activity in HFHI slices could be due to decreased intracellular calcium sequestration mechanisms. Previous studies in a single and repetitive CCI model showed increased levels of basal calcium due to voltage-gated calcium channels but found that ryanodine receptor (RYR) calcium responses decreased with repetitive head impacts (McDaid et al., 2021), indicating that intracellular calcium is not the source of increased calcium events

we see. Our HFHI model is notably less severe than a CCI model of TBI, however, further work to pharmacologically block the intracellular RYR is necessary to understand this mechanism.

While the exact mechanism of ensemble asynchrony in the present study is currently unknown, our characterization of the HFHI model showed a persistent decrease in the AMPA/NMDA ratio as well as changes in neuronal excitability 24 h following HFHI despite no changes in input/output responses or hippocampal neuron damage (Sloley et al., 2021), indicating that the altered ensemble patterns seen in the present study are not likely due to white matter disruptions or neuron cell death, but rather alterations to excitatory and/or inhibitory synaptic function.

CONCLUSION AND LIMITATIONS

The results of this experiment show that HFHI alters CA1 calcium ensemble dynamics and provide further evidence of physiological adaptations in neurons following non-damaging head impacts. Decreased, but not fully abolished, plasticity responses and functional changes to activity in neurons are likely to contribute to behavioral deficits seen in the repeat head impact brain. The present study employed calcium imaging simultaneously with LFP recordings in the CA1 field during a plasticity paradigm. While these techniques offer the ability to simultaneously image dozens of neurons, we chose only to select somatic ROIs in stratum pyramidale. This was initially done from an empirical perspective as it is rarer to find slices that contain dendritic ROIs compared to somatic ROIs. This analysis shed light on stimulus evoked ensemble activity, however, limiting ROI extraction to soma only could potentially limit the ability of our experimental design to capture plasticity induced calcium events that may be occurring if dendritic ROIs in stratum radiatum were assessed. As such, the potentiation of the slices had little effect on the somatic calcium activity (spontaneous and stimulus evoked) observed in this study as somatic analysis only represents an integration of upstream synaptic inputs and not a direct measure of synaptic activity. Future work, likely involving pharmacological isolation, is needed to parse apart the exact mechanisms of stimulus evoked ensemble activity to determine the role of lateral inhibition and glutamate reuptake in the seconds following SC stimulation. A further limitation of this study is the inclusion of only the first ∼10 min. of the LTP response. Early-LTP is reflective of some, but not all mechanisms of plasticity in CA1 pyramidal cells and the study would be strengthened by extending the field recordings up to an hour post-tetanus. This was not done due to the large data requirements and possible photobleaching that comes with calcium imaging (see section "Materials and Methods").

DATA AVAILABILITY STATEMENT

The raw data supporting the conclusions of this article will be made available by the authors, without undue reservation.

ETHICS STATEMENT

The animal study was reviewed and approved by the Georgetown University Animal Care and Use Committee.

AUTHOR CONTRIBUTIONS

DC, SS, AC, SV, and MB conceptualized the project and contributed to the experimental design. SS and DC performed the experiments and collected the data. DC and AC wrote the code to analyze the data. DC performed the statistical analysis, wrote the manuscript, and created the figures. All authors revised, edited, and approved the submitted version of the manuscript.

FUNDING

Research reported in this publication was supported by the National Institute of Neurological Disorders and Stroke of the National Institutes of Health under award number R01NS107370.

REFERENCES

Albensi, B. C., Sullivan, P. G., Thompson, M. B., Scheff, S. W., and Mattson, M. P. (2000). Cyclosporin ameliorates traumatic brain-injury-induced alterations of hippocampal synaptic plasticity. *Exp. Neurol.* 162, 385–389. doi: 10.1006/exnr.1999.7338

Aungst, S. L., Kabadi, S. V., Thompson, S. M., Stoica, B. A., and Faden, A. I. (2014). Repeated mild traumatic brain injury causes chronic neuroinflammation, changes in hippocampal synaptic plasticity, and associated cognitive deficits. *J. Cereb. Blood Flow Metab.* 34, 1223–1232. doi: 10.1038/jcbfm.2014.75

Blennow, K., Brody, D. L., Kochanek, P. M., Levin, H., Mckee, A., Ribbers, G. M., et al. (2016). Traumatic brain injuries. *Nat. Rev. Dis. Primers* 2:16084.

Busche, M. A., Eichhoff, G., Adelsberger, H., Abramowski, D., Wiederhold, K. H., Haass, C., et al. (2008). Clusters of hyperactive neurons near amyloid plaques in a mouse model of Alzheimer's disease. *Science* 321, 1686–1689. doi: 10.1126/science.1162844

Buzsaki, G. (1986). Hippocampal sharp waves: their origin and significance. *Brain Res.* 398, 242–252. doi: 10.1016/0006-8993(86)91483-6

Buzsaki, G. (2010). Neural syntax: cell assemblies, synapsembles, and readers. *Neuron* 68, 362–385. doi: 10.1016/j.neuron.2010.09.023

Caccavano, A., Bozzelli, P. L., Forcelli, P. A., Pak, D. T. S., Wu, J. Y., Conant, K., et al. (2020). Inhibitory parvalbumin basket cell activity is selectively reduced during hippocampal sharp wave ripples in a mouse model of familial Alzheimer's disease. *J. Neurosci.* 40, 5116–5136. doi: 10.1523/JNEUROSCI.0425-20.2020

Cantu, D. A., Wang, B., Gongwer, M. W., He, C. X., Goel, A., Suresh, A., et al. (2020). EZcalcium: open-source toolbox for analysis of calcium imaging data. *Front. Neural Circuits* 14:25. doi: 10.3389/fncir.2020.00025

Cassidy, J. D., Carroll, L. J., Peloso, P. M., Borg, J., Von Holst, H., Holm, L., et al. (2004). Incidence, risk factors and prevention of mild traumatic brain injury:

results of the WHO collaborating centre task force on mild traumatic brain injury. *J. Rehabil. Med.* (43 Suppl), 28–60. doi: 10.1080/16501960410023732

Colvin, A. C., Mullen, J., Lovell, M. R., West, R. V., Collins, M. W., and Groh, M. (2009). The role of concussion history and gender in recovery from soccer-related concussion. *Am. J. Sports Med.* 37, 1699–1704. doi: 10.1177/0363546509332497

Corder, G., Ahanonu, B., Grewe, B. F., Wang, D., Schnitzer, M. J., and Scherrer, G. (2019). An amygdalar neural ensemble that encodes the unpleasantness of pain. *Science* 363, 276–281. doi: 10.1126/science.aap8586

Cossart, R., Aronov, D., and Yuste, R. (2003). Attractor dynamics of network UP states in the neocortex. *Nature* 423, 283–288. doi: 10.1038/nature01614

Creed, J. A., Dileonardi, A. M., Fox, D. P., Tessler, A. R., and Raghupathi, R. (2011). Concussive brain trauma in the mouse results in acute cognitive deficits and sustained impairment of axonal function. *J. Neurotrauma* 28, 547–563. doi: 10.1089/neu.2010.1729

Crisco, J. J., Fiore, R., Beckwith, J. G., Chu, J. J., Brolinson, P. G., Duma, S., et al. (2010). Frequency and location of head impact exposures in individual collegiate football players. *J. Athl. Train.* 45, 549–559. doi: 10.4085/1062-6050-45.6.549

Frost, R. B., Farrer, T. J., Primosch, M., and Hedges, D. W. (2013). Prevalence of traumatic brain injury in the general adult population: a meta-analysis. *Neuroepidemiology* 40, 154–159. doi: 10.1159/000343275

Gabrieli, D., Schumm, S. N., Vigilante, N. F., and Meaney, D. F. (2021). NMDA receptor alterations after mild traumatic brain injury induce deficits in memory acquisition and recall. *Neural Comput.* 33, 67–95. doi: 10.1162/neco_a_01343

Goldstein, L. E., Fisher, A. M., Tagge, C. A., Zhang, X. L., Velisek, L., Sullivan, J. A., et al. (2012). Chronic traumatic encephalopathy in blast-exposed military veterans and a blast neurotrauma mouse model. *Sci. Transl. Med.* 4:134ra160.

Greco, T., Ferguson, L., Giza, C., and Prins, M. L. (2019). Mechanisms underlying vulnerabilities after repeat mild traumatic brain injuries. *Exp. Neurol.* 317, 206–213. doi: 10.1016/j.expneurol.2019.01.012

Guskiewicz, K. M., Marshall, S. W., Bailes, J., Mccrea, M., Harding, H. P. Jr., Matthews, A., et al. (2007). Recurrent concussion and risk of depression in retired professional football players. *Med. Sci. Sports Exerc.* 39, 903–909. doi: 10.1249/mss.0b013e3180383da5

Hamm, J. P., Peterka, D. S., Gogos, J. A., and Yuste, R. (2017). Altered cortical ensembles in mouse models of schizophrenia. *Neuron* 94, 153–167.e8. doi: 10.1016/j.neuron.2017.03.019

Hansen, K. R., Dewalt, G. J., Mohammed, A. I., Tseng, H. A., Abdulkerim, M. E., Bensussen, S., et al. (2018). Mild blast injury produces acute changes in basal intracellular calcium levels and activity patterns in mouse hippocampal neurons. *J. Neurotrauma* 35, 1523–1536. doi: 10.1089/neu.2017.5029

Hsieh, T. H., Lee, H. H. C., Hameed, M. Q., Pascual-Leone, A., Hensch, T. K., and Rotenberg, A. (2017). Trajectory of parvalbumin cell impairment and loss of cortical inhibition in traumatic brain injury. *Cereb. Cortex* 27, 5509–5524. doi: 10.1093/cercor/bhw318

Kane, M. J., Angoa-Perez, M., Briggs, D. I., Viano, D. C., Kreipke, C. W., and Kuhn, D. M. (2012). A mouse model of human repetitive mild traumatic brain injury. *J. Neurosci. Methods* 203, 41–49. doi: 10.1016/j.jneumeth.2011.09.003

Koch, P. F., Cottone, C., Adam, C. D., Ulyanova, A. V., Russo, R. J., Weber, M. T., et al. (2020). Traumatic brain injury preserves firing rates but disrupts laminar oscillatory coupling and neuronal entrainment in hippocampal CA1. *eNeuro* 7:ENEURO.0495-19.2020. doi: 10.1523/ENEURO.0495-19.2020

Laker, S. R. (2011). Epidemiology of concussion and mild traumatic brain injury. *PM R* 3, S354–S358.

Laurer, H. L., Bareyre, F. M., Lee, V. M., Trojanowski, J. Q., Longhi, L., Hoover, R., et al. (2001). Mild head injury increasing the brain's vulnerability to a second concussive impact. *J. Neurosurg.* 95, 859–870. doi: 10.3171/jns.2001.95.5.0859

Lefevre-Dognin, C., Cogne, M., Perdrieau, V., Granger, A., Heslot, C., and Azouvi, P. (2021). Definition and epidemiology of mild traumatic brain injury. *Neurochirurgie* 67, 218–221. doi: 10.1016/j.neuchi.2020.02.002

Main, B. S., Sloley, S. S., Villapol, S., Zapple, D. N., and Burns, M. P. (2017). A mouse model of single and repetitive mild traumatic brain injury. *J. Vis. Exp.* 124:e55713. doi: 10.3791/55713

McCradden, M. D., and Cusimano, M. D. (2018). Concussions in sledding sports and the unrecognized "sled head": a systematic review. *Front. Neurol.* 9:772. doi: 10.3389/fneur.2018.00772

McDaid, J., Briggs, C. A., Barrington, N. M., Peterson, D. A., Kozlowski, D. A., and Stutzmann, G. E. (2021). Sustained hippocampal synaptic pathophysiology following single and repeated closed-head concussive impacts. *Front. Cell Neurosci.* 15:652721. doi: 10.3389/fncel.2021.652721

Mei, Z., Qiu, J., Alcon, S., Hashim, J., Rotenberg, A., Sun, Y., et al. (2018). Memantine improves outcomes after repetitive traumatic brain injury. *Behav. Brain Res.* 340, 195–204. doi: 10.1016/j.bbr.2017.04.017

Miyazaki, S., Katayama, Y., Lyeth, B. G., Jenkins, L. W., Dewitt, D. S., Goldberg, S. J., et al. (1992). Enduring suppression of hippocampal long-term potentiation following traumatic brain injury in rat. *Brain Res.* 585, 335–339. doi: 10.1016/0006-8993(92)91232-4

Mouzon, B. C., Bachmeier, C., Ferro, A., Ojo, J. O., Crynen, G., Acker, C. M., et al. (2014). Chronic neuropathological and neurobehavioral changes in a repetitive mild traumatic brain injury model. *Ann. Neurol.* 75, 241–254. doi: 10.1002/ana.24064

Nakajima, R., Laskaris, N., Rhee, J. K., Baker, B. J., and Kosmidis, E. K. (2021). GEVI cell-type specific labelling and a manifold learning approach provide evidence for lateral inhibition at the population level in the mouse hippocampal CA1 area. *Eur. J. Neurosci.* 53, 3019–3038. doi: 10.1111/ejn.15177

Partridge, J. G., Tang, K. C., and Lovinger, D. M. (2000). Regional and postnatal heterogeneity of activity-dependent long-term changes in synaptic efficacy in the dorsal striatum. *J. Neurophysiol.* 84, 1422–1429. doi: 10.1152/jn.2000.84.3.1422

Patel, T. P., Ventre, S. C., Geddes-Klein, D., Singh, P. K., and Meaney, D. F. (2014). Single-neuron NMDA receptor phenotype influences neuronal rewiring and reintegration following traumatic injury. *J. Neurosci.* 34, 4200–4213. doi: 10.1523/JNEUROSCI.4172-13.2014

Prins, M. L., Hales, A., Reger, M., Giza, C. C., and Hovda, D. A. (2010). Repeat traumatic brain injury in the juvenile rat is associated with increased axonal injury and cognitive impairments. *Dev. Neurosci.* 32, 510–518. doi: 10.1159/000316800

Ren, Z., Iliff, J. J., Yang, L., Yang, J., Chen, X., Chen, M. J., et al. (2013). 'Hit & run' model of closed-skull traumatic brain injury (TBI) reveals complex patterns of post-traumatic AQP4 dysregulation. *J. Cereb. Blood Flow Metab.* 33, 834–845.

Schumm, S. N., Gabrieli, D., and Meaney, D. F. (2020). Neuronal degeneration impairs rhythms between connected microcircuits. *Front. Comput. Neurosci.* 14:18. doi: 10.3389/fncom.2020.00018

Sharp, D. J., Scott, G., and Leech, R. (2014). Network dysfunction after traumatic brain injury. *Nat. Rev. Neurol.* 10, 156–166.

Sloley, S. S., Main, B. S., Winston, C. N., Harvey, A. C., Kaganovich, A., Korthas, H. T., et al. (2021). High-frequency head impact causes chronic synaptic adaptation and long-term cognitive impairment in mice. *Nat. Commun.* 12:2613. doi: 10.1038/s41467-021-22744-6

Tagge, C. A., Fisher, A. M., Minaeva, O. V., Gaudreau-Balderrama, A., Moncaster, J. A., Zhang, X. L., et al. (2018). Concussion, microvascular injury, and early tauopathy in young athletes after impact head injury and an impact concussion mouse model. *Brain* 141, 422–458. doi: 10.1093/brain/awx350

Talavage, T. M., Nauman, E. A., Breedlove, E. L., Yoruk, U., Dye, A. E., Morigaki, K. E., et al. (2014). Functionally-detected cognitive impairment in high school football players without clinically-diagnosed concussion. *J. Neurotrauma* 31, 327–338. doi: 10.1089/neu.2010.1512

Ting, J. T., Daigle, T. L., Chen, Q., and Feng, G. (2014). Acute brain slice methods for adult and aging animals: application of targeted patch clamp analysis and optogenetics. *Methods Mol. Biol.* 1183, 221–242. doi: 10.1007/978-1-4939-1096-0_14

Villette, V., Malvache, A., Tressard, T., Dupuy, N., and Cossart, R. (2015). Internally recurring hippocampal sequences as a population template of spatiotemporal information. *Neuron* 88, 357–366. doi: 10.1016/j.neuron.2015.09.052

Voss, J. D., Connolly, J., Schwab, K. A., and Scher, A. I. (2015). Update on the epidemiology of concussion/mild traumatic brain injury. *Curr. Pain Headache Rep.* 19:32. doi: 10.1007/s11916-015-0506-z

Witkowski, E. D., Gao, Y., Gavsyuk, A. F., Maor, I., Dewalt, G. J., Eldred, W. D., et al. (2019). Rapid changes in synaptic strength after mild traumatic brain injury. *Front. Cell Neurosci.* 13:166. doi: 10.3389/fncel.2019.00166

Wolf, J. A., and Koch, P. F. (2016). Disruption of network synchrony and cognitive dysfunction after traumatic brain injury. *Front. Syst. Neurosci.* 10:43. doi: 10.3389/fnsys.2016.00043

Xia, L., Nygard, S. K., Sobczak, G. G., Hourguettes, N. J., and Bruchas, M. R. (2017). Dorsal-CA1 hippocampal neuronal ensembles encode nicotine-reward contextual associations. *Cell Rep.* 19, 2143–2156. doi: 10.1016/j.celrep.2017.05.047

Yuan, Q., Isaacson, J. S., and Scanziani, M. (2011). Linking neuronal ensembles by associative synaptic plasticity. *PLoS One* 6:e20486. doi: 10.1371/journal.pone.0020486

Zott, B., Simon, M. M., Hong, W., Unger, F., Chen-Engerer, H. J., Frosch, M. P., et al. (2019). A vicious cycle of beta amyloid-dependent neuronal hyperactivation. *Science* 365, 559–565. doi: 10.1126/science.aay0198

Conflict of Interest: The authors declare that the research was conducted in the absence of any commercial or financial relationships that could be construed as a potential conflict of interest.

Publisher's Note: All claims expressed in this article are solely those of the authors and do not necessarily represent those of their affiliated organizations, or those of the publisher, the editors and the reviewers. Any product that may be evaluated in this article, or claim that may be made by its manufacturer, is not guaranteed or endorsed by the publisher.

Copyright © 2022 Chapman, Sloley, Caccavano, Vicini and Burns. This is an open-access article distributed under the terms of the Creative Commons Attribution License (CC BY). The use, distribution or reproduction in other forums is permitted, provided the original author(s) and the copyright owner(s) are credited and that the original publication in this journal is cited, in accordance with accepted academic practice. No use, distribution or reproduction is permitted which does not comply with these terms.

frontiers in Cellular Neuroscience

ORIGINAL RESEARCH
published: 21 January 2022
doi: 10.3389/fncel.2021.784045

Chronic Intermittent Hypoxia-Induced Aberrant Neural Activities in the Hippocampus of Male Rats Revealed by Long-Term *in vivo* Recording

Linhao Xu[1,2], *Qian Li*[1], *Ya Ke*[1,3]* *and Wing-Ho Yung*[1,3]*

[1] School of Biomedical Sciences, Faculty of Medicine, The Chinese University of Hong Kong, Hong Kong, Hong Kong SAR, China, [2] Department of Cardiology, Affiliated Hangzhou First People's Hospital, Zhejiang University School of Medicine, Hangzhou, China, [3] Gerald Choa Neuroscience Centre, Faculty of Medicine, The Chinese University of Hong Kong, Hong Kong, Hong Kong SAR, China

Chronic intermittent hypoxia (CIH) occurs in obstructive sleep apnea (OSA), a common sleep-disordered breathing associated with malfunctions in multiple organs including the brain. How OSA-associated CIH impacts on brain activities and functions leading to neurocognitive impairment is virtually unknown. Here, by means of *in vivo* electrophysiological recordings via chronically implanted multi-electrode arrays in male rat model of OSA, we found that both putative pyramidal neurons and putative interneurons in the hippocampal CA1 subfield were hyper-excitable during the first week of CIH treatment and followed by progressive suppression of neural firing in the longer term. Partial recovery of the neuronal activities was found after normoxia treatment but only in putative pyramidal neurons. These findings correlated well to abnormalities in dendritic spine morphogenesis of these neurons. The results reveal that hippocampal neurons respond to CIH in a complex biphasic and bidirectional manner eventually leading to suppression of firing activities. Importantly, these changes are attributed to a larger extent to impaired functions of putative interneurons than putative pyramidal neurons. Our findings therefore revealed functional and structural damages in central neurons in OSA subjects.

Keywords: chronic intermittent hypoxia, obstructive sleep apnea, *in vivo* recording, neurocognitive impairment, neural firing

OPEN ACCESS

Edited by:
Annalisa Scimemi,
University at Albany, United States

Reviewed by:
David D. Kline,
University of Missouri, United States
Rodrigo Del Rio,
Pontifical Catholic University of Chile, Chile

***Correspondence:**
Wing-Ho Yung
whyung@cuhk.edu.hk
Ya Ke
yake@cuhk.edu.hk

Specialty section:
This article was submitted to Cellular Neuropathology, a section of the journal Frontiers in Cellular Neuroscience

Received: *27 September 2021*
Accepted: *13 December 2021*
Published: *21 January 2022*

Citation:
Xu L, Li Q, Ke Y and Yung W-H (2022) Chronic Intermittent Hypoxia-Induced Aberrant Neural Activities in the Hippocampus of Male Rats Revealed by Long-Term in vivo Recording. Front. Cell. Neurosci. 15:784045. doi: 10.3389/fncel.2021.784045

INTRODUCTION

Obstructive sleep apnea (OSA), a common sleep-disordered breathing, is associated with intermittent hypoxia resulting from upper airway obstruction of structural or neural causes (Mathieu et al., 2008). The most distinct features of OSA are episodes of oxyhemoglobin desaturations, which are terminated by brief microarousals that result in sleep fragmentation and alteration in sleep pattern (Deegan and McNicholas, 1995). The impact of OSA on neurocognitive performance has been well-documented, including impairment in attention, perception, memory, executive functions and also behavioral problems in children (Ali et al., 1996; Chervin et al., 1997; Gozal, 1998; Gozal et al., 2001; Row et al., 2002).

Many of the neurocognitive deficits found in OSA are consistent with malfunctions of the temporal lobe, including the hippocampal and para-hippocampal region, and other cortical areas such as the prefrontal cortex (Beebe and Gozal, 2002; Rosenzweig et al., 2015). In the past, investigators largely relied on neuroimaging techniques, especially magnetic resonance imaging (MRI), to investigate brain changes in OSA subjects. Significant changes in the gray matter and white matter are often found in the hippocampal area in both adult and children OSA subjects (Macey et al., 2002; Morrell et al., 2010; Torelli et al., 2011; Cha et al., 2017; Song et al., 2018; Owen et al., 2019). However, how intermittent hypoxia that occurs in OSA impacts on the neurons in the hippocampus or other brain areas are far from clear.

Animal models have been indispensible in advancing our understanding of the pathophysiology of OSA. For example, studies on rodents have shown that chronic intermittent hypoxia treatment, as a model of OSA, could impair spatial memory functions of the animals to different degrees (Goldbart et al., 2003a,b; Kheirandish et al., 2005a,b; Tartar et al., 2006; Ward et al., 2009). These results are consistent with studies showing that hippocampal long-term synaptic plasticity is impaired after chronic intermittent hypoxia treatment (Payne et al., 2004; Xie et al., 2010; Xu et al., 2015). However, the key question of how episodes of hypoxia affect the activity and therefore functions of hippocampal neurons in the intact brain is still unsolved.

In this study, we performed real-time and long-term recordings from neuronal ensemble in hippocampal CA1 region of rats at single cell and population levels during and after a chronic intermittent hypoxia paradigm. We found complex effects of intermittent hypoxia on the activities of principal neurons and interneurons in CA1. In addition, we correlated these results with the effects of chronic intermittent hypoxia on morphogenesis of dendritic spines of hippocampal neurons. Our findings help identify the cellular correlates of impaired hippocampal function imposed by chronic intermittent hypoxia that occurs in OSA and possibly other related pathological conditions.

MATERIALS AND METHODS

Animals

A total of 29 six-week old male Sprague Dawley rats weighing 220–250 g were used in the experiments, including 14 control and 15 chronic intermittent hypoxia rats. The animals were housed under standard laboratory conditions, namely 12 h light/dark cycle at 22–24°C, with food and water provided *ad libitum*. The procedures of experimentation were approved by the Animal Experimentation and Ethics Committee of the Chinese University of Hong Kong.

Implantation of Microwire Electrode Recording Array

Eleven rats (five controls and six IH) were used for implanting microwire electrode. Before electrode implantation, the rats were deeply anesthetized with pentobarbital sodium salt (Sigma-Aldrich, Darmstadt, Germany) at the dosage of 50 mg/kg by intraperitoneal injection. To record multi-unit neuronal activities and local field potentials *in vivo*, a multi-channel recording array consisting of 16 stainless steel Teflon-coated microwires of 50 μm diameter, arranged in 4 x 4 and measured ∼1.1 x 1.1 mm^2 (Plexon Inc, Dallas, TX), was implanted unilaterally targeting at hippocampal CA1 region according to standard stereotaxic atlas (center position: AP, −3.5 mm, ML, −2.0 mm, DV, 2.05 mm from dura). Four stainless steel screws were firmly attached to the skull for electrode anchoring, and an additional ground wire was connected to one of them as reference. The whole electrode array was secured with dental cement.

Rat Model of Chronic Intermittent Hypoxia

After two weeks of recovery from the implantation surgery, a rat was put in a specially designed chamber (46 × 20 × 22 cm) and exposed to intermittent hypoxia environment under the control of an oxygen profiler (Oxycycler model A48XOV; Reming Bioinstruments, Redfield, NY). The hypoxia paradigm consisted of cycles of oxygen levels between 10 and 21% every 90s, i.e., 40 cycles/h, pioneered by Gozal's group which demonstrated its effectiveness decreasing pO_2 values during the hypoxic cycles (Gozal et al., 2001). This or highly similar protocol has since been widely adopted (e.g., Goldbart et al., 2003a,b; Ma et al., 2008), including in our previous works (Xie et al., 2010; Xu et al., 2015). The hypoxia treatment was given during the daytime for 8 h, from 09:00 to 17:00 while the temperature, humidity and CO_2 level inside the chamber were monitored by remote sensors. The temperature and humidity were maintained at 22–24°C and 40–50% respectively. Ambient CO_2 in the chamber was periodically monitored and maintained at 0.03% by adjusting the overall chamber basal ventilation. The hypoxia treatment was given during the daytime for 8 h, from 09:00 to 17:00 for two weeks. After 2 weeks of IH treatment, the animals were returned to normoxia condition for 1 week.

In vivo Electrophysiological Recording

Both the extracellular single-unit activities and local field potentials in the hippocampal CA1 subfield were recorded simultaneously by the 32-channel OmniPlex® system (Plexon Inc., Dallas, TX). Continuous spike signals were amplified (×2500–3000), band-pass filtered (300 Hz to 5 k Hz, 4-pole Bessel) and sampled at 40 k Hz. For the control rats, data were recorded 5 min before IH. For the IH rats, the recorded data included 5 min before IH, the first of 5 min of IH and another 5 min after 8 h IH.

In order to avoid problems associated with responses to initiation of IH, all animals, including control rats and IH rats, were put into the CIH chamber for acclimatization with the environment two days before IH experiments. In addition, at the first and second day of IH treatment, several cycles of changing oxygen were given but with the door of the chamber opened, to minimize the behavorial and physiological responses to the flushing of gas and associated sounds. Real IH and recording started after this procedure.

Spike Sorting and Long-Term Stability Analysis

Off-Line Spike Sorter (Version 3, Plexon Inc., Dallas, TX) was used for analysis of electrophysiological data by using a combination of automatic and manual sorting techniques (Li et al., 2012, 2017). A minimum waveform amplitude threshold of 3SDs higher than the noise amplitude was detected as a spike in each channel for analyzing the continuous spike trains. The first three principal components (PC) of all waveforms recorded from each channel were depicted in 3-dimensional (3D) space. Initially, individual clusters were separated by automatic clustering techniques (K-means clustering and valley seeking methods) based on the unit waveform (Li et al., 2012, 2017). Each cluster was then checked manually to ensure that the cluster boundaries were well-separated and the spike waveforms were consistent in each day. A similar waveform in each channel was considered as being generated from a single neuron only if it defined a discrete cluster in 2D/3D PC space. Each cluster was termed as a "single-unit" which was different from another. In addition, single-units had a characteristic waveform and exhibited a clearly recognizable refractory period ($\geq$1 ms) in its inter-spike interval (ISI) histogram.

The stability of units throughout the experiment was confirmed by plotting the PC1 and PC2 vs. the time stamp for each waveform. Furthermore, three different statistics were used to objectively quantify the overall separation between identified clusters in a certain channel. These evaluation indexes included the classic F, the J3 and the Davies-Bouldin (DB) validity index (Nicolelis et al., 2003). F is a parametric statistics of multivariate analysis of variance (MANOVA), J3 is a measure of the ratio of between-cluster to within-cluster scatter, and DB is a measure of the ratio of the sum of within-cluster scatter to between cluster separations. Channels with high J3 and F statistics and low DB values indicate the presence of well-separated clusters. Although none of these measures alone provided the optimal criterion for separating clusters, using them in conjunction improves the quality of unit isolation. Based on the offline sorting result, multi-unit spikes generated by both principal, pyramidal and interneurons could be recognized. Pyramidal neurons and interneurons were identified based on their waveforms and temporal firing characteristics (Csicsvari et al., 1999; Hussaini et al., 2011). In order to validity of the long-term study, the "single unit" which consistently appeared in each detection without waveform change was included for analysis while those which were separated in the first time of detection but disappeared subsequent recording days were excluded.

Golgi–Cox Staining

Golgi–Cox staining was performed using the FD Rapid GolgiStain kit (FD NeuroTechnologies) according to the instruction of the manufacturer. Neurons from the CA1 region of the hippocampus were observed under a light microscope (Zeiss Microscope Axiophot 2, USA) by an investigator blind to the treatment. 18 rats (nine control and 9 IH, three rats for each time point, including Day 1, Day 14 and Day 21) were sacrificed to assess dendritic change. Pyramidal neurons and interneurons were identified according to the location of the cell body and the morphology of dendrites (Klausberger and Somogyi, 2008). The spines, classified as stubby, mushroom or thin subtypes based on well-defined criteria (Harris et al., 1992). Three rats were used in each group, and 15 putative pyramidal neurons (54 dendrites) and 12 putative interneurons (45 dendrites) of each group were selected.

Statistical Analysis

Results are displayed as box plots, and in each box, the central mark indicates the median, and the bottom and top edges of the box indicate the 25th and 75th percentiles, respectively, while mean $\pm$ SEM are used in **Figures 2A,B**, **3A,B**, **4**. Paired Student's *t*-test was performed on the data from the same animal for two different time points except firing rates of pyramidal neurons which were analyzed by Wilcoxon's paired signed rank test. Unpaired Student's *t*-tests were used to compare between two different groups. Repeated-measures ANOVA and the Newman–Keuls *post-hoc* test were applied to compare values from the same group or more than two time points expect analyzing firing rate of pyramidal neurons which was performed by Repeated-measures ANOVA (Friedman test) and Dunn's multiple comparisons *post-hoc* test. One-way ANOVA and the Newman–Keuls *post-hoc* test were applied to compare values from the multiple groups.

RESULTS

Characterization of Neural Activities in CA1 During Prolonged *in vivo* Recordings

To mimic OSA-associated intermittent hypoxia, rats were placed in specially designed chambers and exposed to intermittent hypoxia paradigm consisting of cycling oxygen levels between 10 and 21% in 90s for 8 h (**Figure 1A**). Neural activities from hippocampal CA1 regions were recorded at specified time via prior implantation of multi-electrode arrays (**Figure 1B**; **Supplementary Figure 1A**). Extracellular action potentials originating from individual units were identified and sorted by their characteristic waveforms, and checked for their long-term stability (**Supplementary Figure 2**). Based on the duration of the spikes and their frequencies, two populations of neurons were found with properties that are consistent with the principal, pyramidal neurons (lower frequency of $<$ 5 spikes/s; spikes with broad widths with peak-to-trough width $>$ 0.3 ms) and interneurons (higher frequency of $>$ 5 spikes/s; spikes with shorter widths with peak-to-trough width $<$ 0.3 ms) reported previously (Csicsvari et al., 1999; Hussaini et al., 2011). As shown in **Figure 1B**, putative pyramidal neurons (five rats, 41 neurons in control group; six rats, 50 neurons in IH group) have relatively long spike duration of more than 0.3 ms (0.53 $\pm$ 0.01 ms in control group, 0.51 $\pm$ 0.02 ms in IH group,) and a mean firing frequency $<$5 Hz (2.43 $\pm$ 0.13 spikes/s in control group, 1.86 $\pm$ 0.16 spikes/s in IH group; 50 cells). On the other hand, putative interneurons (5 rats, 10 neurons in control group; six rats, 12 neurons in IH group) have shorter spike duration of $<$0.3 ms (0.20 $\pm$ 0.01 ms in control group; 0.21 $\pm$ 0.02 ms in IH group)

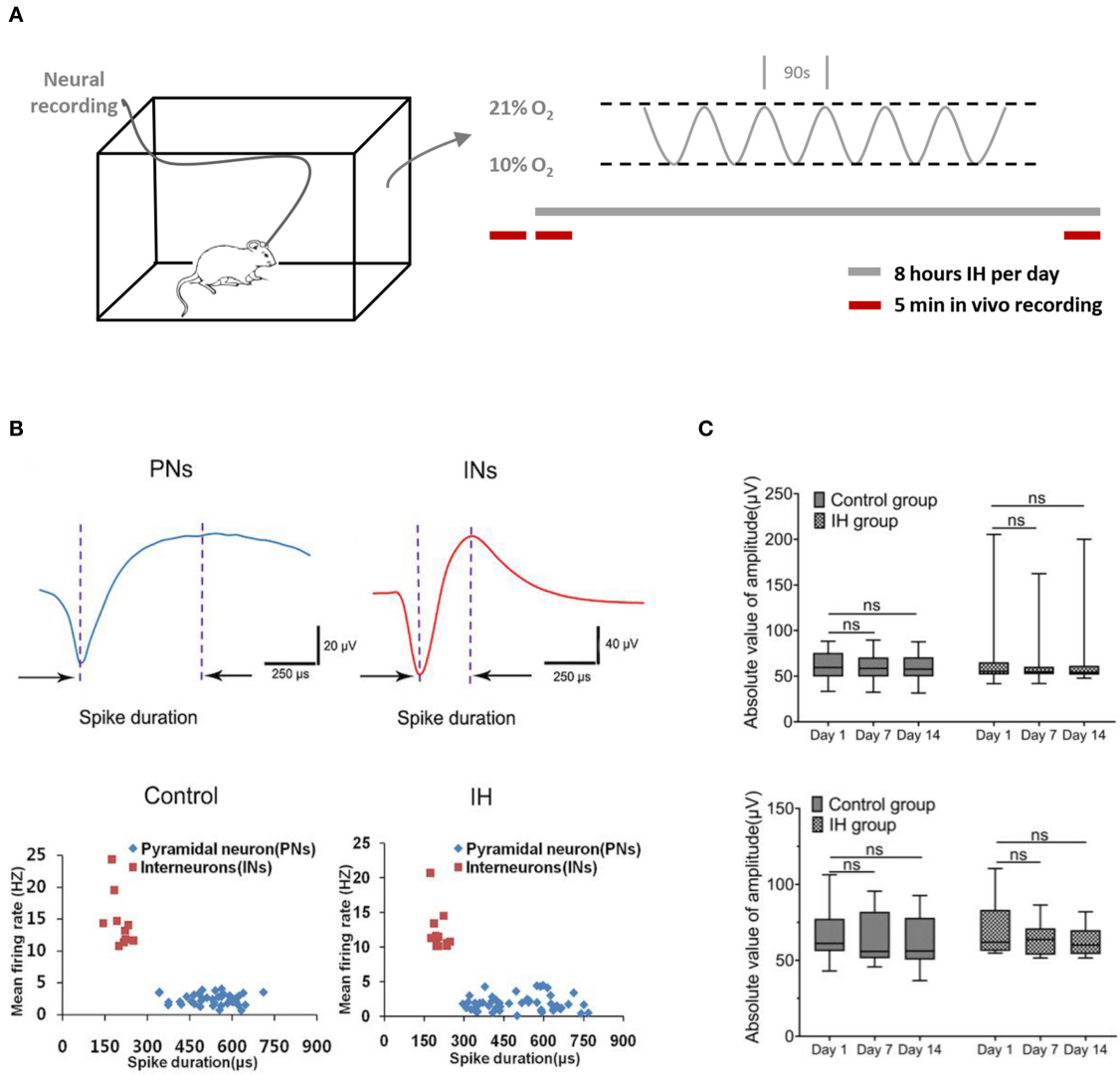

FIGURE 1 | Characterization of neural activities in hippocampl CA1 sub-field during prolonged *in vivo* recordings. **(A)** (Left) Ventilated cages that mimic typical housing conditions were used to expose the experimental rats to intermittent hypoxia paradigms while recording the neural activities from the hippocampus. (Right) The intermittent hypoxia pattern consists of cyclic oscillations of O2 between 21 and 10% within 90 s during the 8-h daylight. Five-min recording sessions was conducted which were immediately before, at the beginning and also at the end of the daily 8-hr hypoxia treatment during the entire 2-weeks study. **(B)** Recorded neurons were classified into putative pyramidal neurons (PNs) and putative interneurons (INs) based on their electrophysiological properties. (Top) Two typical single-units representing PN (blue) and IN (red) respectively. (Bottom) Scatter plots depicting the distribution of mean firing rate vs. spike width of all PNs and INs recorded from the CA1 region of hippocampus in control and intermittent hypoxia (IH) group. Compared with putative pyramidal neurons, putative interneurons exhibited spikes with shorter spike width but higher firing rates. **(C)** Repeated measure ANOVA revealed that the amplitudes of putative pyramidal neurons (top) and putative interneurons (bottom) during the 2 weeks showed no significant changes.

and a mean firing rate of more than 10 Hz (14.60 ± 1.35 spikes/s in control group; 12.15 ± 0.87 spikes/s in IH group).

To ensure the validity of our approach in elucidating the long-term effect of intermittent hypoxia on neuronal activities, we performed stringent tests for inclusion of units for analysis (see Methods; **Supplementary Figures 1**, **2**). Examples of stable single-unit recordings during the 2 weeks are shown in **Supplementary Figure 2**. In this report, data presented were obtained from 41(80.4%) and 50 (85.1%) putative pyramidal neurons, and also 10 (19.6%) and 12 (14.9%) putative interneurons, in the control and hypoxia group respectively that met our criteria of recording stability (**Supplementary Figure 1B**). As summarized in **Figure 1C**, the stability was also reflected in the stable mean amplitudes of the

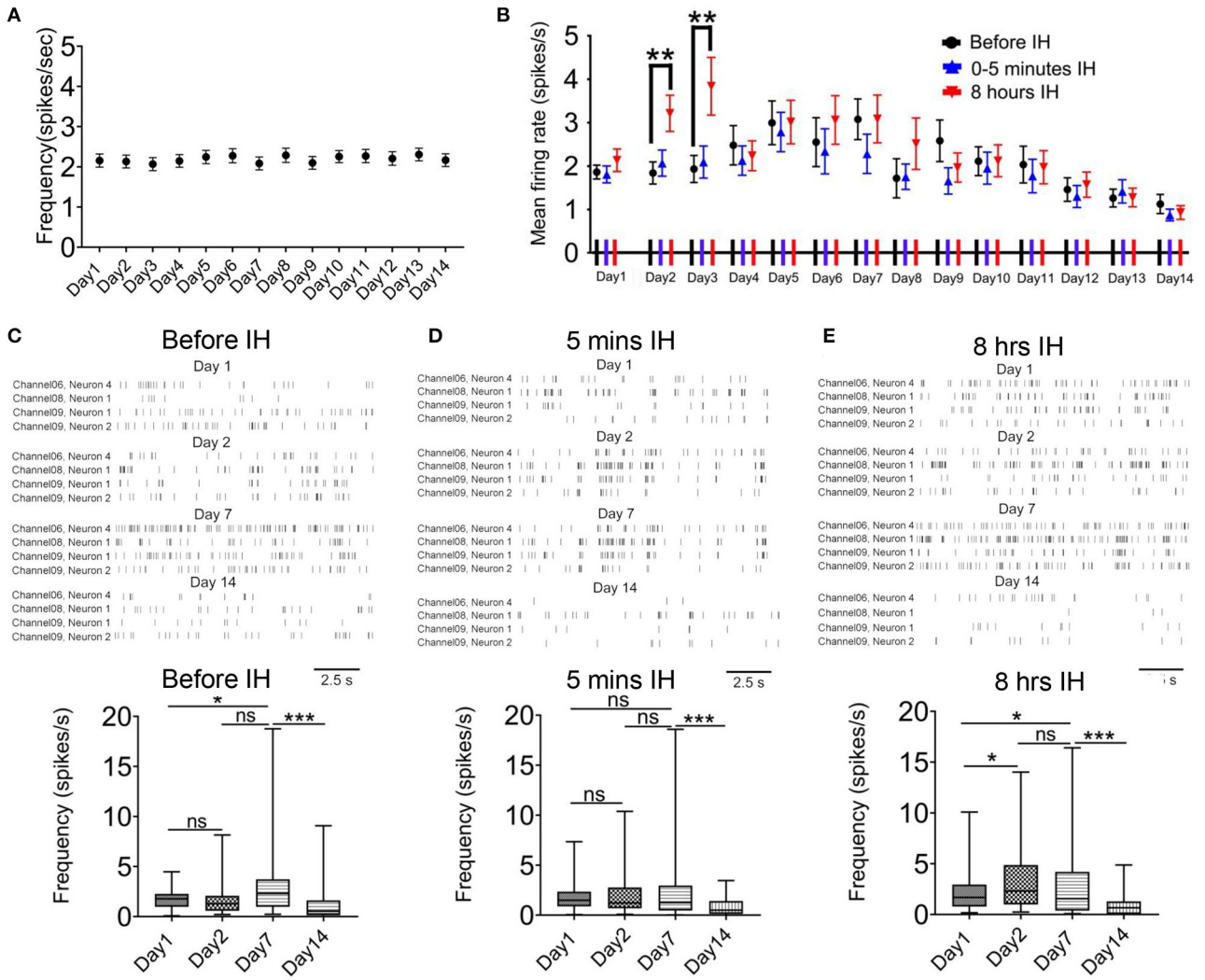

FIGURE 2 | Intermittent hypoxia (IH) exerts complex acute and long-term effects on the firing activities of CA1 putative pyramidal neurons. **(A)** Repeated measured ANOVA revealed that neuronal firing was not significantly affected in control group which was recorded at about 9:00–9:05 a.m. **(B)** Summary of the mean firing rates of putative pyramidal neurons recorded in the 3 recording sessions in each day over the 2-week period. Putative pyramidal neurons in CA1 region tended to increase their firing activities during the first week of IH treatment, particularly apparent at the late hours (at 8 h) but not early hours (at 5 min and 3 h) of daily IH paradigm. Repeated measured ANOVA revealed that neuronal firing was significantly affected in the 2nd and 3rd day. The hyper-excitability, however, was followed by gradual suppression of firing in the second week. **(C)** Typical raster plots of the CA1 putative pyramidal neurons recorded before IH on day 1, 2, 7 and 14 (up panel). Statistical results are shown on the bottom. **(D)** Typical raster plots of the CA1 putative pyramidal neurons recorded in the first 5 IH min of IH treatment on day 1, 2, 7 and 14 are shown on the up and the mean data are summarized on the bottom. **(E)** Typical raster plots of the CA1 putative pyramidal neurons recorded in the last 5 IH min of IH treatment are shown on the up and the mean data are summarized on the bottom. $^{*}P < 0.05$, $^{***}P < 0.001$.

extracellular spikes in both control and hypoxia groups in day 1, day 7 and day 14, for both putative pyramidal neurons [control group: $F_{(1.41,\ 56.46)} = 1.75$, $n = 41$, from five rats, $P = 0.19$; IH group: $F_{(1.47,72.25)} = 0.49$, $n = 50$, from six rats, $P = 0.56$; top] and putative interneurons [control group: $F_{(1,69,15.17)} = 1.40$, $n = 10$, from five rats, $P = 0.27$; IH group: $F(1,35,\ 14.81) = 4.28$, $n = 12$, from six rats, $P = 0.05$; bottom]. Therefore, we concluded that we could reliably track the activities of the recorded neurons throughout the periods studied.

Acute and Long-Term Effects of Intermittent Hypoxia on the Firing of CA1 Putative Pyramidal Neurons

We conducted 5-min recording sessions immediately before, at the beginning and also at the end of the daily 8-h hypoxia treatment during the entire 2-weeks study. This design enabled us to determine the acute as well as prolonged effects of intermittent hypoxia on neuronal excitability and population activities in the hippocampus. In addition, we

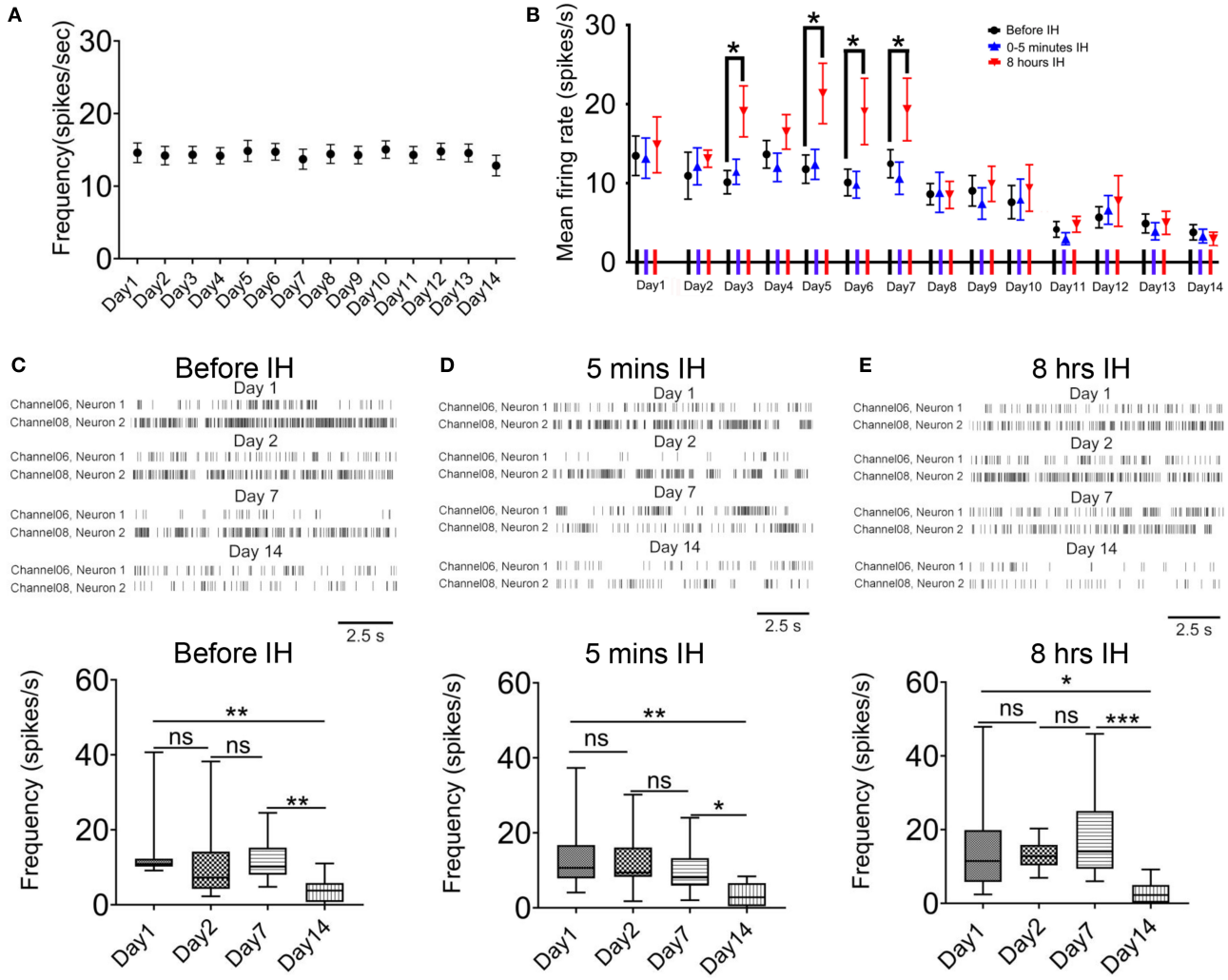

FIGURE 3 | Acute and long-term effects of intermittent hypoxia (IH) on the firing of CA1 putative interneurons. **(A)** Repeated measured ANOVA revealed that neuronal firing was not significantly affected in control group. **(B)** Summary of the mean firing rates of putative interneurons recorded in the three recording sessions in each day over the 2-week period. Apart from the significantly elevated firing of the putative interneurons after 8 h of IH treatment in some days of the first week, the major effect of the chronic intermittent hypoxia was a strong suppression of firing found in the second week of IH treatment. **(C)** The up panel shows typical raster plots of the putative interneurons recorded before IH on day 1, 2, 7 and 14. Statistical results are shown on the bottom. **(D)** Typical raster plots of the putative interneurons recorded in the first 5 IH min of IH treatment on day 1, 2, 7 and 14 are shown on the up and the mean data are summarized on the bottom. **(E)** Typical raster plots of the putative interneurons recorded in the last 5 IH mins of IH treatment on day 1, 2, 7 and 14 are shown on the up and the mean data are summarized on the bottom. $^{*}P < 0.05$, $^{**}P < 0.01$, $^{***}P < 0.001$.

could assess the sustained effects of intermittent hypoxia after the subjects had been re-exposed to normal oxygen levels, and also the accumulated effects of intermittent hypoxia over days and weeks. Control animals received the same handling procedures except the hypoxic treatments. During the recording in the daytime that corresponded to the inactive phase of the daily cycle, the animals were mainly resting and largely immobile.

We did not find any changes in the firing rate of the control animals in the morning hours (08:55–09:00) during 2-week recording (Friedman statistic = 22.08, $n = 41$, from five rats, $P = 0.05$; **Figure 2A**). In the case of intermittent hypoxia-treated group, **Figure 2B** summarizes the mean firing rates of putative pyramidal neurons in the 3 recording sessions in each day over the 2-week period. We observed a complex profile of neuronal firing, which was dependent on the time of recording (namely before, at the start, or at the end of hypoxia treatment) and also the days of treatment. First, we found that within the daily hypoxia episode, the firing of the neurons in the first 5 min of intermittent hypoxia was not affected. In contrast, in the 2nd and 3rd day, 8 h of prolonged intermittent hypoxia treatment significantly increased the firing rates of these neurons (Friedman

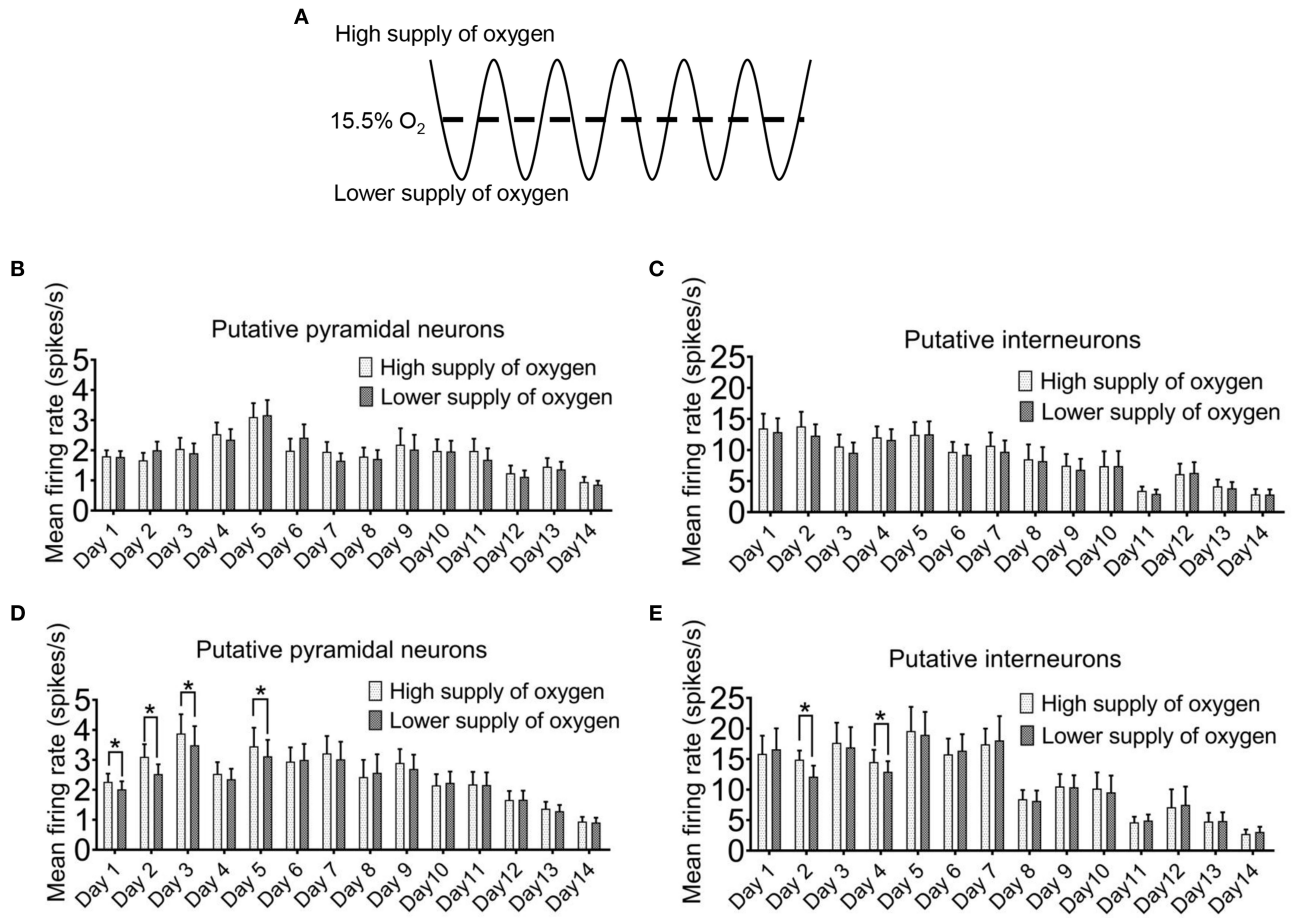

FIGURE 4 | Instantaneous firing of hippocampal neurons can be affected by the ambient oxygen level in the hypoxic cycle. **(A)** The time period during which the ambient O_2 level was above the mean (15.5%) was regarded as high supply of O_2, while the time period during which the O_2 was below the mean was designated as lower supply of O_2. In the first 5 min of intermittent hypoxia (IH), the level of oxygen supply had no clear effect on the firing of both the putative pyramidal neurons **(B)** and the putative interneurons **(C)**. However, in the last 5 min of 8 h IH treatment, both putative pyramidal neurons **(D)** and putative interneurons **(E)** tended to fire more during the period of higher oxygen supply. The data were from 50 putative pyramidal neurons and 12 putative interneurons (six rats). Wilcoxon's paired signed rank test for pyramidal neurons; Paired Student's *t*-test for interneurons; $^*P < 0.05$.

statistic = 23.08, $n = 50$, from six rats in 2nd day, $P < 0.001$; Friedman statistic = 16.59, n = 50, from six rats in 3rd day, $P < 0.001$), although no significant effect was found in the other days. This increased firing under long hours of intermittent hypoxia did not persist overnight, and the firing rates returned to baseline values the next day (**Figure 2B**), indicating that these were transient rather than sustained effects.

Regarding the prolonged, accumulative effects of daily intermittent hypoxia on the baseline firing of the neurons, a bi-phasic and bi-directional response was observed. Thus, we observed a general increase in firing of the neurons in the first week, followed by a gradual and finally significant decrease in firing activities (**Figure 2B**). Typical raster plots of the CA1 putative pyramidal neurons recorded before, during the first 5 min and the last 5 min of intermittent hypoxia on day 1, 2, 7 and 14 are shown in **Figures 2C–E**. First, it was found that the basal mean firing, that is, recordings made before the IH, was significantly increased at day 7 when compared with day 1 and then the firing rate was decreased at day 14 (**Figure 2C**). The basal firing rate before the intermittent hypoxia session on day 14 was only 60.5 % of that of day 1 (1.86 ± 0.16 spikes/s in day 1, 50 cells; 1.13 ± 0.22 spikes/s in day 14, 50 cells; $P < 0.01$). The increase in firing reached statistical significance at day 7 when compared with day 1 for recordings made before and also toward the end of the intermittent hypoxia. Second, the mean firing was significantly altered in the first 5 min IH on day 1, 2, 7 (**Figure 1D**). Finally, a clearly elevated firing could be found on day 2 and 7, but this effect was not apparent in day 14, in which the firing was significantly suppressed (**Figure 2E**).

Effects of Intermittent Hypoxia on the Firing of Putative Interneurons in CA1

We also analyzed the effects of chronic intermittent hypoxia on the interneurons in the same area. First, in the control animals,

the mean firing rate in putative interneurons did not change significantly during the 2-weeks ([$F_{(1.40,12.60)} = 0.38$, $n = 41$, $P = 0.62$]; **Figure 3A**). Second, we observed a similar but not identical response pattern of these neurons with that of putative pyramidal neurons. **Figure 3B** plots the profile of the responses of the putative interneurons to intermittent hypoxia spanning the 2 weeks. Similar to the putative pyramidal neurons, no acute changes in the firing rates of the putative interneurons were found in the first 5 min of intermittent hypoxia, regardless of the number of days of treatment. We also found that, almost throughout the first week, continuous intermittent hypoxia for 8 h increased the firing rate of putative interneurons, with respect to the beginning of the intermittent hypoxia episode of the same day (**Figure 2B**). For example, repeated measured ANOVA showed that neuronal firing was significantly affected on day 3 [$F_{(1.15,12.60)} = 4.70$, $n = 12$, from six rats, $P < 0.05$], day 5 [$F_{(1.10,12.13)} = 6.13$, $n = 12$, from six rats, $P < 0.05$] and day 6 [$F_{(1.14,12.50)} = 7.59$, $n = 12$, from six rats, $P < 0.05$].

Regarding the accumulated effects of daily intermittent hypoxia, different from the biphasic response of the putative pyramidal neurons, no upregulation of basal firing was observed but only a significant decrease in firing was found in the second week. Representative raster plots of putative interneurons at the different sampling time and days are shown in **Figures 3C–E**. First, the basal firing, that is, recordings made before the IH, was significantly decreased at day 14 when compared with day 1 (**Figure 3C**). On day 14, only 28.1% of basal firing remained, which represents a much bigger suppression in neural activities compared with that of the putative pyramidal neurons [$P < 0.01$; 13.46 ± 2.50 spikes/s in day 1, 12 cells; 3.78 ± 0.97 spikes/s in day 14, 12 cells; **Figure 2C**). Second, there was no significant difference in firing rates among day 1, 2 and 7 in the first 5 min IH but a significant reduction was found in the same period in day 14 (**Figure 3D**). Finally, when recordings were made 8 h after IH and compared among different days, only a significant reduction in firing rate was detected on day 14 by Newman-Keuls's test.

Furthermore, neuronal discharges between control and CIH rats were also compared across exposure time), which confirmed significant decrease in neuronal firing of PNs (**Supplementary Figure 3A**) and INs (**Supplementary Figure 3B**) toward the second week.

Real-Time Response of Neuronal Firing With Hypoxic Cycle

Under the condition of sleep apnea, there are cyclic changes of the oxygenation level in the circulation, and therefore oxygen supply to the brain. One question of interest is whether the level of oxygenation has a real-time impact on the activities of brain neurons. Although the level of oxygen in the vicinity of the neurons under recording cannot be measured, studying the temporal relationship between the ambient air oxygen level and the instantaneous firing rate of the neurons may provide insight into this question.

For most of the time, we did not find a clear temporal relationship between the firing rates of the neurons with the ambient oxygen level. When we compared the sampled mean

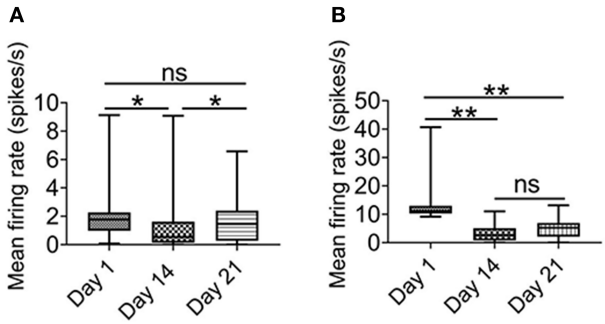

FIGURE 5 | Effect of intermittent hypoxia on CA1 putative interneurons firing is long-lasting. **(A)** Repeated measured ANOVA showed that firing activities in putative pyramidal neurons was altered on day 1 (before IH treatment), day 14 (before IH treatment) and day 21 (Friedman statistic = 20.73, n =50, from six rats, $P < 0.001$). Post Dunn's multiple comparisons showed that significant recovery in the firing activities in putative pyramidal neurons after 1 week of normoxia. **(B)** Repeated measured ANOVA showed that firing rate was different among day 1 (before IH treatment), day 14 (before IH treatment) and day 21 [$F_{(1.25,13.74)} = 11.98$, $n = 12$, from six rats, $P < 0.01$], furthermore, *post-hoc* Newman-Keuls's test showed that no recovery of firing rate of putative interneurons was found 1 week after normoxia treatment. $^{*}P < 0.05$, $^{**}P < 0.01$.

firing rates of the recorded neurons when the oxygen level was above mean level (15.5%) with those below the mean level (**Figure 4A**), no differences were detected after 5 min of intermittent hypoxia (**Figures 4B,C**). The only exception was found at the times when the overall firing rates were elevated after 8 h of intermittent hypoxia in the first week (**Figures 4D,E**). Under this condition, in both pyramidal neurons and interneurons, the mean firing rates were lower when the ambient oxygen level was below the mean, that is, when there was a relatively low supply of oxygen. The average firing rate of all pyramidal neurons recorded in the phase of relatively high oxygen level (2.27 ± 0.27 spikes/s in day 1, $n = 50$ cells; 3.10 ± 0.42 spikes/s in day 2, $n = 50$ cells; 3.88 ± 0.64 spikes/s in day 3, $n = 50$ cells; 3.45 ± 0.62 spikes/s in day 5, $n = 50$ cells) was significantly higher than that in the phase of lower oxygen level (2.02 ± 0.26 spikes/s in day 1, $n = 50$ cells ; 2.53 ± 0.32 spikes/s in day 2, $n = 50$ cells; 3.49 ± 0.63 spikes/s in day 3, $n = 50$ cells; 3.12 ± 0.54 spikes/s in day 5, $n = 50$ cells; $P < 0.05$). Although real-time pO_2 or SaO_2 values were not monitored in the freely moving rats, such cyclic changes in neuronal activities with an interval of 90s could be very obvious in some neurons (**Supplementary Figure 4**), consistent with the effect of the cyclic IH.

Long-Lasting Efforts of Intermittent Hypoxia on Putative Interneurons

One important consideration of the adverse effects of chronic intermittent hypoxia on neural activity is whether they are long lasting or readily recoverable. Thus, in our study, after two weeks of intermittent hypoxia, we allowed some animals to breathe in normoxia condition for 1 week, and tracked the progress of recovery on neuronal firing in the hippocampus at 8:55–9:00 a.m.

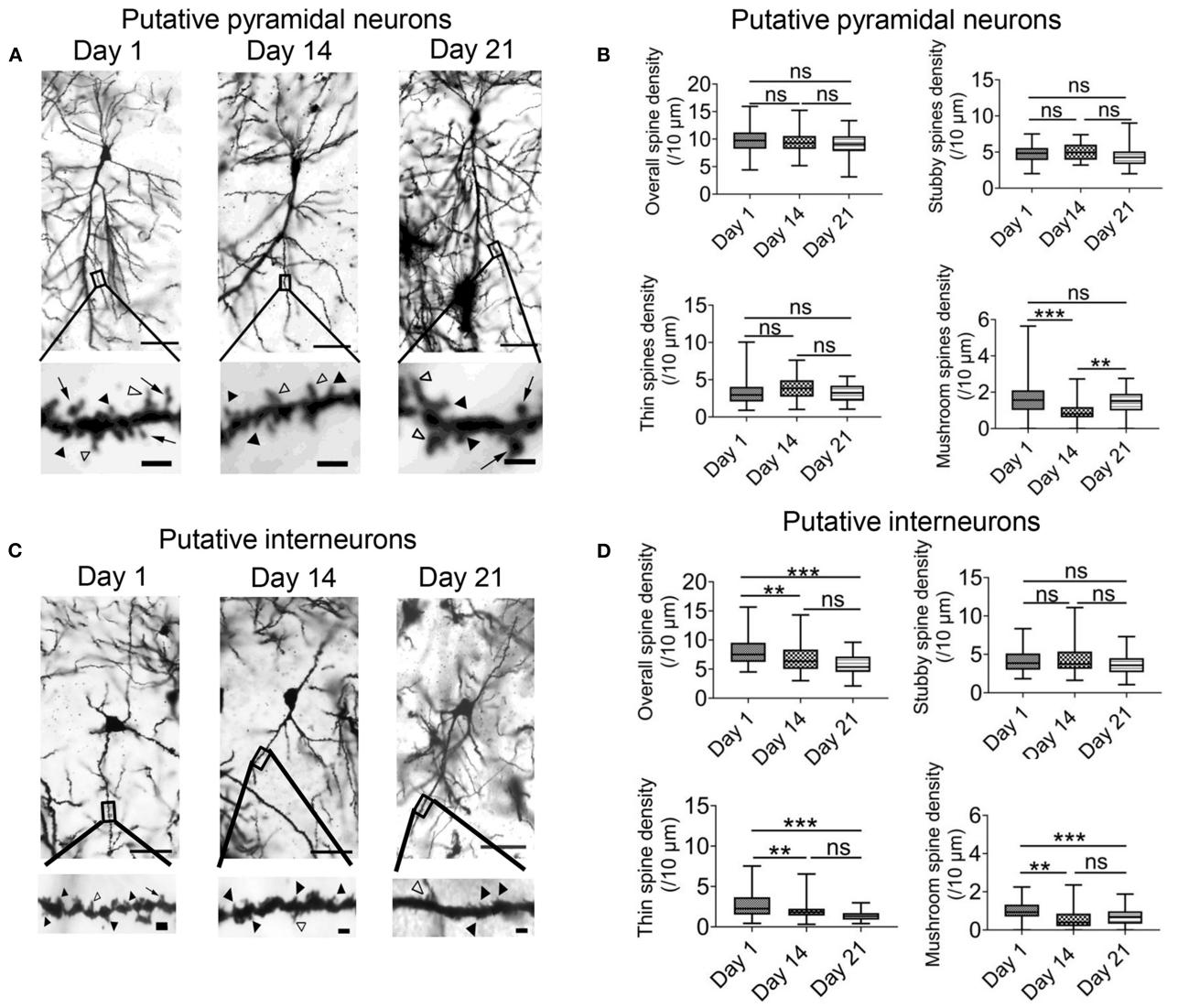

FIGURE 6 | Chronic intermittent hypoxia (IH) reduces mature spine formation of CA1 pyramidal neurons and interneurons. **(A)** Typical morphologies of individual pyramidal neurons in CA1 region revealed by Golgi staining on day 1, 14 and 21. Scale bar: 50 μm. The higher magnification pictures shown in the lower panels allowed quantification of spine density and classification of individual spines. Black arrowheads indicate stubby spines; white arrowheads indicate thin spines; arrows indicate mushroom spines Scale bar: 4 μm. **(B)** Quantification analysis from 54 dendrites revealed no significant difference between day 1, 14 and 21 in terms of overall spine density (top left), stubby spine density (top right) and thin spine density (bottom left). However, the density of the mushroom spine was significantly altered (bottom right). Meanwhile, *post-hoc* Newman-Keuls's test revealed mushroom spine density was decreased significantly in 2 weeks IH treatment, which could recover on day 21 (right panel). $^{***}P < 0.001$. **(C)** Typical morphologies of individual interneurons in CA1 region revealed by Golgi staining on day 1, 14 and 21. Scale bar: 50 μm. Higher magnification pictures are shown in the lower panels. Scale bar: 4 μm. **(D)** Quantification of data from 45 dendrites showed that there was significantly difference in the overall spine density (top left), thin spine density (bottom left) and mushroom spine (bottom right) except stubby spine density (top right). *Post-hoc* Newman-Keuls's test revealed clear reduction of overall spine density after 2 weeks of IH treatment, compared with day 1, as well as the densities of thin spine and mushroom spine. These changes were not recoverable even after 1 week of normoxia treatment, $^{**}P < 0.01$, $^{***}P < 0.001$.

As shown in **Figure 5A**, after 1 week of recovery, the firing rate of putative pyramidal neurons was largely recovered. In contrast, there was no significant recovery of the firing rate of the putative interneurons (**Figure 5B**). These results suggested that not only the putative interneurons were more sensitive to chronic intermittent hypoxia, but their activities could not be restored, at least one week later.

Correlation to Spine Morphogenesis

The previous results indicated that intermittent hypoxia could exert both transient and persistent effects on the functions of hippocampal CA1 neurons. We therefore also examined the morphology of dendritic spines in the pyramidal neurons and interneurons by the end of the 2-week hypoxia treatment as well as in the recovery phase. Based on Golgi staining, pyramidal

neurons and interneurons could be readily distinguished according to their cellular morphology as well as somatic locations (**Supplementary Figure 5**) (Klausberger and Somogyi, 2008). As demonstrated in **Figures 6A,B**, there was no significant change in the overall spine density of pyramidal neurons between day 1 group (9.72 ± 0.33 spines/10 μm, 54 dendrites) and 2 weeks intermittent hypoxia group (9.43 ± 0.28 spines/10 μm, 54 dendrites). Further analysis, however, revealed that the mushroom spine density was significantly reduced in 2 weeks intermittent hypoxia group (0.97 ± 0.09 spines/10 μm, 54 dendrites) when compared with day 1 group (1.71 ± 0.14 spines/10 μm, 54 dendrites) while no significant difference was found for the stubby and thin spines (**Figure 6B**). On the other hand, consistent with the functional data, we found that interneurons were vulnerable, as the overall density of the spines (6.83 ± 0.34 spines/10 μm, 45 dendrites), as well as mushroom spines (0.61 ± 0.09 spines/10 μm, $n = 45$) and thin spines (2.00 ± 0.16 spines/10 μm, 45 dendrites) were all decreased after 2 weeks of intermittent hypoxia treatment compared with that of day 1 group (overall spines density: 8.01 ± 0.36 spines/10 μm; mushroom spines density: 0.99 ± 0.08 spines/10 μm; thin spines density: 2.72 ± 0.26 spines/10 μm, 45 dendrites, **Figures 6C,D**).

Finally, the change in the density of the spines in pyramidal neurons was recoverable after one week of normoxia treatment (**Figure 6B**). In contrast, in the interneurons, the decrease in the overall spine density, thin spines and mushroom spines were not restored despite one week of normoxia period (**Figures 6C,D**). These results further support that alterations of neuronal activities in the hippocampus are more related to impaired function and structure of interneurons.

DISCUSSION

The nervous system has a high energy demand and is therefore particularly sensitive to oxygen supply (Jiang and Haddad, 1994; Ances et al., 2008). Although there exists in the literature a large volume of data suggesting structural and functional deficits in the hippocampus of OSA subjects and animal models (Macey et al., 2002; Morrell et al., 2010; Torelli et al., 2011; Cha et al., 2017; Song et al., 2018; Owen et al., 2019), the impact of chronic intermittent hypoxia on the excitability of hippocampal neurons is virtually an untackled question. The present attempt is the first to systematically investigate both the acute and accumulated effects of intermittent hypoxia on the neuronal firing rate of hippocampal neurons in the intact brain. In terms of individual neurons in CA1 sub-field, we found that there are intricate and multiple phases of response to intermittent hypoxia treatment. CA1 putative pyramidal neurons tended to increase their firing activities during short-term (i.e., within 1 week) exposure to daily intermittent hypoxia. During this period, an episode of intermittent hypoxia for hours also increased the sensitivity of both putative pyramidal neurons and putative interneurons to ambient oxygen levels, resulting in exaggerated and probably aberrant firing activities. These phenomena were then followed by a progressive decline in firing in the second week finally leading to strong suppression of neural activities. Recovery of the neuronal activities was evident after 1-week recovery, only for putative pyramidal neurons but not putative interneurons.

Given the known heterogeneity in response to hypoxia and the different time courses of distinct adaptive or regulatory processes (Richter et al., 1991; Bickler and Donohoe, 2002; Pena and Ramirez, 2005), our finding of a complex response to chronic intermittent hypoxia is not entirely surprising. Although the exact causes of the biphasic, bi-directional responses are unclear and are beyond the scope of the present study, one may speculate that the increase in activity during the short-term intermittent hypoxia treatment could be related to altered neurotransmission, e.g., as a consequence of enhanced glutamate release (Hansen, 1985; Vangeison and Rempe, 2009) or other factors such as increased release of brain-derived neurotrophic factor (Vermehren-Schmaedick et al., 2012), consistent with increased expression of c-fos (Ma et al., 2008; Sharpe et al., 2013). On the other hand, the decrease in excitability after a long-term exposure to daily intermittent hypoxia may reflect the cellular damages caused by elevated level of oxidative stress (Kim et al., 2013) and ER stress (Xu et al., 2015), or represents an adaptive response important for the survival of the neurons, at the cost of reduced neuronal function (Gavello et al., 2012). Meanwhile, more prolonged IH could trigger other adaptive responses such as down-regulation of Na-channels (Gu and Haddad, 2001), which could confer some advantages in preventing excessive energy expenditure**.** The impaired activities could also be contributed by changes in the density of mature spines after 2 weeks of intermittent hypoxia treatment, which were evident in both pyramidal neurons and interneurons. Despite that a causal relationship between impaired activities and density of mature spines was not investigated in the present study, it had been demonstrated that NMDA and AMPA receptor existed in mature spines which could affect neuronal activity (Duman and Li, 2012; Wang et al., 2016).

It should be noted that hemodynamic compensatory changes may influence IH-mediated neural activities alteration. For example, higher respiration rhythm and instability (Chang et al., 2013) and a significant shift of the heart rate variability power spectrum, with a predominance of the sympathetic modulation (Iturriaga et al., 2010) were observed in OSA patients. In agreement, sustained sympathoexcitation and elevated arterial pressure present in OSA patients or after exposure to IH treatment had been found (Weiss et al., 2015). However, exactly how hemodynamic changes affect the neuronal firing of the hippocampal neurons would require further investigation.

Sleep fragmentation is an important factor in behavioral and functional defects in OSA patients. But one feature of the OSA model adopted in the present study is its dissociation from the impact of sleep fragmentation, as the hypoxia was induced not by respiratory blockade but by mimicking the resulting hypoxic cycles (Gozal et al., 2001). Therefore, in this study, we showed that in the absence of clear or significant sleep fragmentation, cyclic hypoxic episodes could affect hippocampal neuronal structures and functions.

Intriguingly, we found that there were no obvious changes in the activities of CA1 neurons in the first few minutes of intermittent hypoxia. This is in sharp contrast to previous

in vitro studies which have shown that hippocampal neurons stop to generate action potentials in response to even brief period of hypoxia because of membrane depolarization or hyperpolarization affecting ion channel activities (Hansen et al., 1982; Hansen, 1985). Whether such tolerance is due to the involvement of anaerobic metabolism *in vivo* (Milton and Dawson-Scully, 2013) or is a reflection of the difference between intermittent and continuous hypoxia is not known.

Unlike the pyramidal neurons, the effect of intermittent hypoxia on interneurons has not been addressed before and thus their roles in mediating alteration of neuronal circuits in hypoxia are not known. An important finding of the present study is that, in the hippocampus, putative interneurons are more vulnerable to damage than putative pyramidal neurons in response to accumulative intermittent hypoxia. Not only that putative interneurons exhibit a much stronger suppression in neuronal firing, their activities also could not recover when the animals were allowed to breathe under normoxia for up to one week. Together, these observations implicate that dysfunctions of interneurons might contribute to a much larger extent than pyramidal neurons on neuronal circuit malfunctions under CIH.

There are several technical issues in this study that should be pointed out. Although control rats were also put into a chamber which was identical to the hypoxic chamber, no flushing of O_2/NO_2 was given to the control animals, which breathed normal O_2. It is possible that flushing of gases may have a mild effect on neuronal activities of the IH animals. For the *in vivo* recording, Teflon-coated microelectrode arrays rather than tetrodes were used to track the activity of neurons. Although this may compromise the accuracy in the identification of single units, non-tetrode microarrays had also been used successfully for chronic recordings by others (Tseng et al., 2011) as well as in our previous study (Li et al., 2017), fulfilling multiple criteria. Furthermore, in the present study, the animals were singly housed in the present study, which may have imposed some stress on them and influencing activities of hippocampal neurons (Irvine and Abraham, 2005). Also, only male rats were used in this study since it was reported that the prevalence of OSA was higher in men when compared with women (Lurie, 2011; Kang et al., 2014). Although the reason remains obscure, hormonal factor has been considered to contribute to gender difference in OSA prevalence. Further investigation is needed to determine if there is any difference in the response of the hippocampus to chronic intermittent hypoxia between male and female rats. Finally, although memory deficits would be induced by the current CIH protocol as had been demonstrated in previous works (Gozal et al., 2001; Xie et al., 2010), we had not conducted parallel measurement of memory and learning capability of the animals in the present study.

CONCLUSION

In conclusion, for the first time, our study reveals that hippocampal neurons respond to chronic intermittent hypoxia in a complex biphasic and bidirectional manner finally leading to suppression of firing activities. Notably, these changes correlate better with impaired functions of interneurons than those of pyramidal neurons.

DATA AVAILABILITY STATEMENT

The original contributions presented in the study are included in the article/**Supplementary Material**, further inquiries can be directed to the corresponding author/s.

ETHICS STATEMENT

The animal study was reviewed and approved by the Animal Experimentation and Ethics Committee of the Chinese University of Hong Kong.

AUTHOR CONTRIBUTIONS

YK and W-HY: conceptualization, resources, and supervision. LX, QL, and W-HY: methodology. LX: investigation and writing-original draft. LX and QL: formal analysis. LX, QL, YK, and W-HY: writing-review and editing. W-HY: funding acquisition. All authors contributed to the article and approved the submitted version.

FUNDING

This work was supported by a Hong Kong RGC-CRF grant C6004-17G and the Gerald Choa Neuroscience Centre, the Chinese University of Hong Kong.

SUPPLEMENTARY MATERIAL

The Supplementary Material for this article can be found online at: https://www.frontiersin.org/articles/10.3389/fncel.2021.784045/full#supplementary-material

Supplementary Figure 1 | Single-unit spike sorting and electrophysiological identification of pyramidal neurons (PNs) and INs (INs) in CA1 region of freely behaving rats. **(A)** Verification of electrode tips by post-mortem histological staining. Scale bar: 1 mm (left); 0.1 mm (right). **(B)** The number of PNs and INs included and excluded for analysis in the control group and intermittent hypoxia group.

Supplementary Figure 2 | Spike sorting and assessment of long-term stability of single-unit recordings by single microwire array over 14 days IH treatment. Example of spike sorting from single microwire array in 14 days, showing the superimposed spike waveforms of PNs and INs **(left panel)** and the inter-spike-interval histogram (ISIH, **right panel**), and the corresponding identified clusters in the PCs space (far **right panel**). Clear isolation of units from a given recording channel is indicated by high, F statistic of MANOVA (F), J3 and low Davis-Bouldin (DB) index. Scale bar : 200 μS; 58 μV.

Supplementary Figure 3 | The pyramidal neurons [PNs, **(A)**] and INs [INs, **(B)**] discharge was compared between control and CIH rats. Significant decreases in neuronal firing were found toward the second week of CIH.

Supplementary Figure 4 | A typical example showing that there were cyclic changes in firing oscillating at the same frequency of the hypoxia paradigm.

Supplementary Figure 5 | Identification of pyramidal neurons (PNs) and interneurons (INs) in Golgi staining for quantitative analysis of spine morphogenesis. In the CA1 region of the hippocampus, PNs and INs were identified by their somatic location and somatodendritic morphologies. Scale bar: 0.4 mm.

REFERENCES

Ali, N. J., Pitson, D., and Stradling, J. R. (1996). Sleep disordered breathing: effects of adenotonsillectomy on behaviour and psychological functioning. *Eur. J. Pediatr.* 155, 56–62. doi: 10.1007/BF02115629

Ances, B. M., Leontiev, O., Perthen, J. E., Liang, C., Lansing, A. E., and Buxton, R. B. (2008). Regional differences in the coupling of cerebral blood flow and oxygen metabolism changes in response to activation: implications for BOLD-fMRI. *Neuroimage* 39, 1510–1521. doi: 10.1016/j.neuroimage.2007.11.015

Beebe, D. W., and Gozal, D. (2002). Obstructive sleep apnea and the prefrontal cortex: towards a comprehensive model linking nocturnal upper airway obstruction to daytime cognitive and behavioral deficits. *J. Sleep Res.* 11, 1–16. doi: 10.1046/j.1365-2869.2002.00289.x

Bickler, P. E., and Donohoe, P. H. (2002). Adaptive responses of vertebrate neurons to hypoxia. *J. Exp. Biol.* 205(Pt 23), 3579–3586. doi: 10.1242/jeb.205.23.3579

Cha, J., Zea-Hernandez, J. A., Sin, S., Graw-Panzer, K., Shifteh, K., Isasi, C. R., et al. (2017). The effects of obstructive sleep apnea syndrome on the dentate gyrus and learning and memory in children. *J. Neurosci.* 37, 4280–4288. doi: 10.1523/JNEUROSCI.3583-16.2017

Chang, J. S., Lee, S. D., Ju, G., Kim, J. W., Ha, K., and Yoon, I. Y. (2013). Enhanced cardiorespiratory coupling in patients with obstructive sleep apnea following continuous positive airway pressure treatment. *Sleep Med.* 14, 1132–1138. doi: 10.1016/j.sleep.2013.04.024

Chervin, R. D., Dillon, J. E., Bassetti, C., Ganoczy, D. A., and Pituch, K. J. (1997). Symptoms of sleep disorders, inattention, and hyperactivity in children. *Sleep* 20, 1185–1192. doi: 10.1093/sleep/20.12.1185

Csicsvari, J., Hirase, H., Czurko, A., Mamiya, A., and Buzsaki, G. (1999). Oscillatory coupling of hippocampal pyramidal cells and interneurons in the behaving Rat. *J. Neurosci.* 19, 274–287. doi: 10.1523/JNEUROSCI.19-01-00274.1999

Deegan, P. C., and McNicholas, W. T. (1995). Pathophysiology of obstructive sleep apnoea. *Eur. Respir. J.* 8, 1161–1178. doi: 10.1183/09031936.95.08071161

Duman, R. S., and Li, N. (2012). A neurotrophic hypothesis of depression: role of synaptogenesis in the actions of NMDA receptor antagonists. *Philos. Trans. R. Soc. Lond. B Biol. Sci.* 367, 2475–2484. doi: 10.1098/rstb.2011.0357

Gavello, D., Rojo-Ruiz, J., Marcantoni, A., Franchino, C., Carbone, E., and Carabelli, V. (2012). Leptin counteracts the hypoxia-induced inhibition of spontaneously firing hippocampal neurons: a microelectrode array study. *PLoS ONE* 7:e41530. doi: 10.1371/journal.pone.0041530

Goldbart, A., Cheng, Z. J., Brittian, K. R., and Gozal, D. (2003a). Intermittent hypoxia induces time-dependent changes in the protein kinase B signaling pathway in the hippocampal CA1 region of the rat. *Neurobiol. Dis.* 14, 440–446. doi: 10.1016/j.nbd.2003.08.004

Goldbart, A., Row, B. W., Kheirandish, L., Schurr, A., Gozal, E., Guo, S. Z., et al. (2003b). Intermittent hypoxic exposure during light phase induces changes in cAMP response element binding protein activity in the rat CA1 hippocampal region: water maze performance correlates. *Neuroscience* 122, 585–590. doi: 10.1016/j.neuroscience.2003.08.054

Gozal, D. (1998). Sleep-disordered breathing and school performance in children. *Pediatrics* 102(3 Pt 1), 616–620. doi: 10.1542/peds.102.3.616

Gozal, D., Daniel, J. M., and Dohanich, G. P. (2001). Behavioral and anatomical correlates of chronic episodic hypoxia during sleep in the rat. *J. Neurosci.* 21, 2442–2450. doi: 10.1523/JNEUROSCI.21-07-02442.2001

Gu, X. Q., and Haddad, G. G. (2001). Decreased neuronal excitability in hippocampal neurons of mice exposed to cyclic hypoxia. *J. Appl. Physiol. (1985)* 91, 1245–1250. doi: 10.1152/jappl.2001.91.3.1245

Hansen, A. J. (1985). Effect of anoxia on ion distribution in the brain. *Physiol. Rev.* 65, 101–148. doi: 10.1152/physrev.1985.65.1.101

Hansen, A. J., Hounsgaard, J., and Jahnsen, H. (1982). Anoxia increases potassium conductance in hippocampal nerve cells. *Acta Physiol. Scand.* 115, 301–310. doi: 10.1111/j.1748-1716.1982.tb07082.x

Harris, K. M., Jensen, F. E., and Tsao, B. (1992). Three-dimensional structure of dendritic spines and synapses in rat hippocampus (CA1) at postnatal day 15 and adult ages: implications for the maturation of synaptic physiology and long-term potentiation. *J. Neurosci.* 12, 2685–2705. doi: 10.1523/JNEUROSCI.12-07-02685.1992

Hussaini, S. A., Kempadoo, K. A., Thuault, S. J., Siegelbaum, S. A., and Kandel, E. R. (2011). Increased size and stability of CA1 and CA3 place fields in HCN1 knockout mice. *Neuron* 72, 643–653. doi: 10.1016/j.neuron.2011.09.007

Irvine, G. I., and Abraham, W. C. (2005). Enriched environment exposure alters the input-output dynamics of synaptic transmission in area CA1 of freely moving rats. *Neurosci. Lett.* 391, 32–37. doi: 10.1016/j.neulet.2005.08.031

Iturriaga, R., Moya, E. A., and Del Rio, R. (2010). Cardiorespiratory alterations induced by intermittent hypoxia in a rat model of sleep apnea. *Adv. Exp. Med. Biol.* 669, 271–274. doi: 10.1007/978-1-4419-5692-7_55

Jiang, C., and Haddad, G. G. (1994). A direct mechanism for sensing low oxygen levels by central neurons. *Proc. Natl. Acad. Sci. U S A* 91, 7198–7201. doi: 10.1073/pnas.91.15.7198

Kang, K., Seo, J. G., Seo, S. H., Park, K. S., and Lee, H. W. (2014). Prevalence and related factors for high-risk of obstructive sleep apnea in a large korean population: results of a questionnaire-based study. *J. Clin. Neurol.* 10, 42–49. doi: 10.3988/jcn.2014.10.1.42

Kheirandish, L., Gozal, D., Pequignot, J. M., Pequignot, J., and Row, B. W. (2005a). Intermittent hypoxia during development induces long-term alterations in spatial working memory, monoamines, and dendritic branching in rat frontal cortex. *Pediatr. Res.* 58, 594–599. doi: 10.1203/01.pdr.0000176915.19287.e2

Kheirandish, L., Row, B. W., Li, R. C., Brittian, K. R., and Gozal, D. (2005b). Apolipoprotein E-deficient mice exhibit increased vulnerability to intermittent hypoxia-induced spatial learning deficits. *Sleep* 28, 1412–1417. doi: 10.1093/sleep/28.11.1412

Kim, S. M., Kim, H., Lee, J. S., Park, K. S., Jeon, G. S., Shon, J., et al. (2013). Intermittent hypoxia can aggravate motor neuronal loss and cognitive dysfunction in ALS mice. *PLoS ONE* 8:e81808. doi: 10.1371/journal.pone.0081808

Klausberger, T., and Somogyi, P. (2008). Neuronal diversity and temporal dynamics: the unity of hippocampal circuit operations. *Science* 321, 53–57. doi: 10.1126/science.1149381

Li, Q., Ke, Y., Chan, D. C., Qian, Z. M., Yung, K. K., Ko, H., et al. (2012). Therapeutic deep brain stimulation in Parkinsonian rats directly influences motor cortex. *Neuron* 76, 1030–1041. doi: 10.1016/j.neuron.2012.09.032

Li, Q., Ko, H., Qian, Z. M., Yan, L. Y. C., Chan, D. C. W., Arbuthnott, G., et al. (2017). Refinement of learned skilled movement representation in motor cortex deep output layer. *Nat. Commun.* 8:15834. doi: 10.1038/ncomms15834

Lurie, A. (2011). Obstructive sleep apnea in adults: epidemiology, clinical presentation, and treatment options. *Adv. Cardiol.* 46, 1–42. doi: 10.1159/000327660

Ma, S., Mifflin, S. W., Cunningham, J. T., and Morilak, D. A. (2008). Chronic intermittent hypoxia sensitizes acute hypothalamic-pituitary-adrenal stress reactivity and Fos induction in the rat locus coeruleus in response to subsequent immobilization stress. *Neuroscience* 154, 1639–1647. doi: 10.1016/j.neuroscience.2008.04.068

Macey, P. M., Henderson, L. A., Macey, K. E., Alger, J. R., Frysinger, R. C., Woo, M. A., et al. (2002). Brain morphology associated with obstructive sleep apnea. *Am. J. Respir. Crit. Care Med.* 166, 1382–1387. doi: 10.1164/rccm.200201-050OC

Mathieu, A., Mazza, S., Decary, A., Massicotte-Marquez, J., Petit, D., Gosselin, N., et al. (2008). Effects of obstructive sleep apnea on cognitive function: a comparison between younger and older OSAS patients. *Sleep Med.* 9, 112–120. doi: 10.1016/j.sleep.2007.03.014

Milton, S. L., and Dawson-Scully, K. (2013). Alleviating brain stress: what alternative animal models have revealed about therapeutic targets for hypoxia and anoxia. *Future Neurol.* 8, 287–301. doi: 10.2217/fnl.13.12

Morrell, M. J., Jackson, M. L., Twigg, G. L., Ghiassi, R., McRobbie, D. W., Quest, R. A., et al. (2010). Changes in brain morphology in patients with obstructive sleep apnoea. *Thorax* 65, 908–914. doi: 10.1136/thx.2009.126730

Nicolelis, M. A., Dimitrov, D., Carmena, J. M., Crist, R., Lehew, G., Kralik, J. D., et al. (2003). Chronic, multisite, multielectrode recordings in macaque monkeys. *Proc. Natl. Acad. Sci. U S A* 100, 11041–11046. doi: 10.1073/pnas.1934665100

Owen, J. E., BenediktsdOttir, B., Gislason, T., and Robinson, S. R. (2019). Neuropathological investigation of cell layer thickness and myelination in the hippocampus of people with obstructive sleep apnea. *Sleep* 42. doi: 10.1093/sleep/zsy199

Payne, R. S., Goldbart, A., Gozal, D., and Schurr, A. (2004). Effect of intermittent hypoxia on long-term potentiation in rat hippocampal slices. *Brain Res.* 1029, 195–199. doi: 10.1016/j.brainres.2004.09.045

Pena, F., and Ramirez, J. M. (2005). Hypoxia-induced changes in neuronal network properties. *Mol. Neurobiol.* 32, 251–283. doi: 10.1385/MN:32:3:251

Richter, D. W., Bischoff, A., Anders, K., Bellingham, M., and Windhorst, U. (1991). Response of the medullary respiratory network of the cat to hypoxia. *J. Physiol.* 443, 231–256. doi: 10.1113/jphysiol.1991.sp018832

Rosenzweig, I., Glasser, M., Polsek, D., Leschziner, G. D., Williams, S. C., and Morrell, M. J. (2015). Sleep apnoea and the brain: a complex relationship. *Lancet Respir. Med.* 3, 404–414. doi: 10.1016/S2213-2600(15)00090-9

Row, B. W., Kheirandish, L., Neville, J. J., and Gozal, D. (2002). Impaired spatial learning and hyperactivity in developing rats exposed to intermittent hypoxia. *Pediatr. Res.* 52, 449–453. doi: 10.1203/00006450-200209000-00024

Sharpe, A. L., Calderon, A. S., Andrade, M. A., Cunningham, J. T., Mifflin, S. W., and Toney, G. M. (2013). Chronic intermittent hypoxia increases sympathetic control of blood pressure: role of neuronal activity in the hypothalamic paraventricular nucleus. *Am. J. Physiol. Heart Circ. Physiol.* 305, H1772–1780. doi: 10.1152/ajpheart.00592.2013

Song, X., Roy, B., Kang, D. W., Aysola, R. S., Macey, P. M., Woo, M. A., et al. (2018). Altered resting-state hippocampal and caudate functional networks in patients with obstructive sleep apnea. *Brain Behav.* 8:e00994. doi: 10.1002/brb3.994

Tartar, J. L., Ward, C. P., McKenna, J. T., Thakkar, M., Arrigoni, E., McCarley, R. W., et al. (2006). Hippocampal synaptic plasticity and spatial learning are impaired in a rat model of sleep fragmentation. *Eur. J. Neurosci.* 23, 2739–2748. doi: 10.1111/j.1460-9568.2006.04808.x

Torelli, F., Moscufo, N., Garreffa, G., Placidi, F., Romigi, A., Zannino, S., et al. (2011). Cognitive profile and brain morphological changes in obstructive sleep apnea. *Neuroimage* 54, 787–793. doi: 10.1016/j.neuroimage.2010.09.065

Tseng, W. T., Yen, C. T., and Tsai, M. L. (2011). A bundled microwire array for long-term chronic single-unit recording in deep brain regions of behaving rats. *J. Neurosci. Methods* 201, 368–376. doi: 10.1016/j.jneumeth.2011.08.028

Vangeison, G., and Rempe, D. A. (2009). The Janus-faced effects of hypoxia on astrocyte function. *Neuroscientist* 15, 579–588. doi: 10.1177/1073858409332405

Vermehren-Schmaedick, A., Jenkins, V. K., Knopp, S. J., Balkowiec, A., and Bissonnette, J. M. (2012). Acute intermittent hypoxia-induced expression of brain-derived neurotrophic factor is disrupted in the brainstem of methyl-CpG-binding protein 2 null mice. *Neuroscience* 206, 1–6. doi: 10.1016/j.neuroscience.2012.01.017

Wang, T., Guan, R. L., Liu, M. C., Shen, X. F., Chen, J. Y., Zhao, M. G., et al. (2016). Lead exposure impairs hippocampus related learning and memory by altering synaptic plasticity and morphology during juvenile period. *Mol. Neurobiol.* 53, 3740–3752. doi: 10.1007/s12035-015-9312-1

Ward, C. P., McCoy, J. G., McKenna, J. T., Connolly, N. P., McCarley, R. W., and Strecker, R. E. (2009). Spatial learning and memory deficits following exposure to 24 h of sleep fragmentation or intermittent hypoxia in a rat model of obstructive sleep apnea. *Brain Res.* 1294, 128–137. doi: 10.1016/j.brainres.2009.07.064

Weiss, J. W., Tamisier, R., and Liu, Y. (2015). Sympathoexcitation and arterial hypertension associated with obstructive sleep apnea and cyclic intermittent hypoxia. *J. Appl. Physiol. (1985)* 119, 1449–1454. doi: 10.1152/japplphysiol.00315.2015

Xie, H., Leung, K. L., Chen, L., Chan, Y. S., Ng, P. C., Fok, T. F., et al. (2010). Brain-derived neurotrophic factor rescues and prevents chronic intermittent hypoxia-induced impairment of hippocampal long-term synaptic plasticity. *Neurobiol. Dis.* 40, 155–162. doi: 10.1016/j.nbd.2010.05.020

Xu, L. H., Xie, H., Shi, Z. H., Du, L. D., Wing, Y. K., Li, A. M., et al. (2015). Critical role of endoplasmic reticulum stress in chronic intermittent hypoxia-induced deficits in synaptic plasticity and long-term memory. *Antioxid. Redox Signal* 23, 695–710. doi: 10.1089/ars.2014.6122

Conflict of Interest: The authors declare that the research was conducted in the absence of any commercial or financial relationships that could be construed as a potential conflict of interest.

Publisher's Note: All claims expressed in this article are solely those of the authors and do not necessarily represent those of their affiliated organizations, or those of the publisher, the editors and the reviewers. Any product that may be evaluated in this article, or claim that may be made by its manufacturer, is not guaranteed or endorsed by the publisher.

Copyright © 2022 Xu, Li, Ke and Yung. This is an open-access article distributed under the terms of the Creative Commons Attribution License (CC BY). The use, distribution or reproduction in other forums is permitted, provided the original author(s) and the copyright owner(s) are credited and that the original publication in this journal is cited, in accordance with accepted academic practice. No use, distribution or reproduction is permitted which does not comply with these terms.

frontiers in Molecular Neuroscience

REVIEW
published: 14 March 2022
doi: 10.3389/fnmol.2022.857495

The 14-3-3 Protein Family and Schizophrenia

*Meaghan Navarrete and Yi Zhou**

Department of Biomedical Sciences, Florida State University College of Medicine, Tallahassee, FL, United States

Schizophrenia is a debilitating mental disorder that affects approximately 1% of the world population, yet the disorder is not very well understood. The genetics of schizophrenia is very heterogenous, making it hard to pinpoint specific alterations that may cause the disorder. However, there is growing evidence from human studies suggesting a link between alterations in the 14-3-3 family and schizophrenia. The 14-3-3 proteins are abundantly expressed in the brain and are involved in many important cellular processes. Knockout of 14-3-3 proteins in mice has been shown to cause molecular, structural, and behavioral alterations associated with schizophrenia. Thus, 14-3-3 animal models allow for further exploration of the relationship between 14-3-3 and schizophrenia as well as the study of schizophrenia pathology. This review considers evidence from both human and animal model studies that implicate the 14-3-3 family in schizophrenia. In addition, possible mechanisms by which alterations in 14-3-3 proteins may contribute to schizophrenia-like phenotypes such as dopaminergic, glutamatergic, and cytoskeletal dysregulations are discussed.

Keywords: 14-3-3 proteins, schizophrenia, knockout mice, animal models, human studies, genetic linkage

OPEN ACCESS

Edited by:
Daniela Tropea,
Trinity College Dublin, Ireland

Reviewed by:
Annie Andrieux,
CEA Grenoble, France
Anthony J. Baucum,
Indiana University–Purdue University Indianapolis, United States

***Correspondence:**
Yi Zhou
Yi.zhou@med.fsu.edu

Specialty section:
This article was submitted to Brain Disease Mechanisms, a section of the journal Frontiers in Molecular Neuroscience

Received: *18 January 2022*
Accepted: *17 February 2022*
Published: *14 March 2022*

Citation:
Navarrete M and Zhou Y (2022) The 14-3-3 Protein Family and Schizophrenia. Front. Mol. Neurosci. 15:857495. doi: 10.3389/fnmol.2022.857495

INTRODUCTION

Schizophrenia is a psychiatric disorder that affects both cognition and behavior. The symptoms of schizophrenia are generally grouped into positive, negative, and cognitive symptoms including hallucinations, delusions, anhedonia, and reductions in attention and memory. The onset of schizophrenia typically occurs in late adolescence to early adulthood (Jablensky, 2000). However, schizophrenia symptoms can manifest differently for each individual and can vary in severity over that individual's lifetime (Freedman, 2003). Certain genetic variations, stressful life circumstances, and altered brain structure or functions have been linked to a higher incidence of schizophrenia. Nevertheless, both the etiology and the pathology of schizophrenia remain elusive. No single gene is responsible for the development of the disorder and there are no biomarkers to aid in diagnosing patients. These limitations hinder our ability to both diagnose and properly treat schizophrenia. Antipsychotic drugs are typically prescribed to treat the symptoms of schizophrenia and have been a useful therapeutic. These drugs can help alleviate the positive symptoms, and to a lesser extent the negative symptoms of the disorder, but are ineffective in treating cognitive symptoms (Freedman, 2003). In addition, many of these drugs come with undesired side effects like movement disorders (Mentzel et al., 2017) and weight gain (Volavka et al., 2002); which can lead to inconsistent usage and reduced treatment effectiveness (Kane et al., 2013). Therefore, further investigation of the etiology and pathophysiology of schizophrenia can facilitate our understanding of this disorder and is critical for the development of more effective treatments. Several genes which show promise in helping us decipher the developmental risks and mechanisms behind schizophrenia belong to the 14-3-3 family.

The 14-3-3 family of proteins has been identified in all eukaryotic organisms (van Hemert et al., 2001). There are seven known mammalian 14-3-3 genes, each of which expresses a distinct protein isoform; beta (β), gamma (γ), epsilon (ε), zeta (ζ), eta (η), theta (θ), and sigma (σ) (Berg et al., 2003). The highest concentration of 14-3-3 proteins is found in the brain, where they encompass around 1% of the total soluble proteins (Boston et al., 1982). The crystalline structure of 14-3-3 shows that two L shaped monomers come together in a dimerized pair to form a cup-shaped structure (Liu et al., 1995). All 14-3-3 isoforms can form either hetero or homodimers (Takahashi, 2003). This allows for the binding of two regions of the same interacting protein (Berg et al., 2003) or the binding of two different ligands (Fu et al., 2000). Thus, 14-3-3 proteins have a diverse range of hundreds of binding partners. Inside the concave face of the 14-3-3 dimer, polar-charged and hydrophobic amino acids create an amphipathic groove that interacts with phosphoserine and phosphothreonine containing motifs located on its binding partners (Yaffe et al., 1997; Wang et al., 1998). Consequently, 14-3-3 can modulate the function or subcellular location of its binding partners through phosphorylation-dependent protein–protein interactions. Many cellular processes and pathways have been linked to 14-3-3 function and expression. In the nervous system, published studies have indicated the involvement of 14-3-3 proteins in intracellular signaling, cell division and differentiation, apoptosis, and ion channel function (Berg et al., 2003). In addition, both human and animal studies have implicated 14-3-3 in several neurodegenerative and psychiatric diseases, including schizophrenia (Foote and Zhou, 2012).

Several human genome-wide association studies (GWAS) have revealed a genetic link between the 14-3-3 family and schizophrenia. In addition, 14-3-3 knockout animal models have shown schizophrenia-like phenotypes, providing further evidence for this connection. This review will discuss the results of some of the genetic and animal model studies that provide evidence for the link between 14-3-3 and schizophrenia.

14-3-3 AND SCHIZOPHRENIA IN HUMAN STUDIES

Genetic linkage and proteomic studies have sought to identify gene or protein expression that may be altered in individuals who are affected by schizophrenia. However, the genetics of the disorder can be heterogeneous; no single gene nor mutation has been identified as the sole cause of schizophrenia. Nevertheless, the 14-3-3 family has been implicated in several studies of schizophrenia patients (**Table 1**). These results suggest that 14-3-3 alterations may contribute to the development of the disorder; therefore, further investigation of this relationship is warranted.

A proteomic pathway analysis revealed that changes in the hippocampus of schizophrenia patients prominently implicate 14-3-3 signaling (Schubert et al., 2015). Further, several studies have revealed that there are 14-3-3 isoform specific changes associated with schizophrenia. In an expression analysis of peripheral leukocytes of drug-naïve first-episode schizophrenia patients, there were four down and one upregulated 14-3-3 mRNA isoforms, and five downregulated protein isoforms (Qing et al., 2016). There was a positive correlation between these isoform specific expression changes and schizophrenia. In addition, there was a negative correlation between the expression of the ε, θ and ζ isoforms and the positive symptoms of schizophrenia. While in a more recent study of peripheral blood expression levels, five of the seven 14-3-3 family members showed significantly higher baseline expression and significant changes in expression in schizophrenia patients who converted to psychosis compared to those that did not convert (Demars et al., 2020). Interestingly, there also is evidence that the 14-3-3 isoform expression levels respond differentially to antipsychotic treatment (Middleton et al., 2005; Rivero et al., 2015). Together these findings suggest that each of the 14-3-3 isoforms may be involved in schizophrenia in different capacities and are worthy of individual investigation. In fact, the genetic link between schizophrenia and individual isoforms has been further studied, particularly the ε, η, and ζ isoforms.

The 14-3-3ε isoform is encoded by the YWHAE gene, which has been proposed to be a schizophrenia susceptibility gene. Gene-based analyses have shown that common variants in the YWHAE gene contribute to schizophrenia (Torrico et al., 2020). In the study of one Japanese population, the rs28365859 single nucleotide polymorphism (SNP) of the YWHAE gene showed a significant difference between schizophrenia patients and controls (Ikeda et al., 2008). The minor allele was more frequent in controls and corresponded to higher protein expression, indicating that a major allele may be a risk factor for schizophrenia. In subsequent MRI studies, the same SNP as well as several others were shown to be related to changes in the orbitofrontal sulcogyral pattern and changes in the volume of the insula, putamen, and hippocampus of schizophrenia patients, possible developmental abnormalities that could contribute to the disorder (Kido et al., 2014; Takahashi et al., 2014).

Among other chromosomal loci, susceptibility for schizophrenia has been identified at the 8p and 22q locations (Badner and Gershon, 2002). 14-3-3ζ is genetically encoded by the YWHAZ gene at the 8p23 location. In addition to being located on a susceptible locus, genetic studies have releveled associations between SNPs and ultra-rare variants of the YWHAZ gene and schizophrenia (Jia et al., 2004; Wong et al., 2005; Torrico et al., 2020). The YWHAH gene which encodes 14-3-3η is located at 22q12.3, another susceptibility locus. Interestingly, a deletion in 22q11.2 leads to 22q11.2 Deletion Syndrome and a phenotype that often includes schizophrenia (Bassett and Chow, 2008). An estimated 1% of schizophrenia patients have also been diagnosed with 22q11.2 Deletion Syndrome. The proximity of 22q11.2 to the YWHAH gene and the overlapping association with schizophrenia seems to indicate a strong genetic link between 14-3-3η and schizophrenia. In further support of this link, both SNPs and variable number tandem repeats (VNTRs) in YWHAH have been associated with schizophrenia in genetic microarray studies (Toyooka et al., 1999; Wong et al., 2003; Grover et al., 2009). In addition, several studies have shown that the 14-3-3η protein is differentially expressed in schizophrenia (Vawter et al., 2001; Altar et al., 2009; Wu et al., 2012). Thus, both YWHAZ and YWHAH genes have

TABLE 1 | 14-3-3 Human Studies.

Population/patient sample	Analysis method	Results	References
24 Drug-naïve first-episode schizophrenia patients and 24 age/gender matched control subjects	Expression analysis of peripheral leukocytes	Positive correlation between isoform specific mRNA/protein expression and schizophrenia, negative correlation between ε, θ and ζ expression and the positive symptoms of schizophrenia	Qing et al., 2016
Tissue from 10 subjects with schizophrenia and 11 matched control subjects	DNA microarray analysis of the PFC, ISH analysis and multivariate analysis of covariance	Reduced expression of the β, ζ, γ, and η isoforms in schizophrenia samples	Middleton et al., 2005
1,429 schizophrenia and 1,728 control subjects from a Japanese population	Screened for DISC1-interacting molecules, assessing a total of 25 tagging SNPs	A significant difference in the rs28365859 SNP of YWHAE between schizophrenia patients and controls that corresponded to differential protein expression	Ikeda et al., 2008
72 Schizophrenia patients and 86 healthy controls from a Japanese population	Voxel-based MRI study of the relationship between the YWHAE polymorphism rs28365859 and the OFC subtypes of the "H-shaped" sulcus	rs28365859 SNP of the YWHAE related to changes in the orbitofrontal sulcogyral pattern of schizophrenia patients	Takahashi et al., 2014
186 Control and 188 schizophrenia subjects from 11 studies	Review of proteomic investigations of the brain of schizophrenia patients	Differential expression of YWHAZ and YWHAH, which are located chromosomally close to loci that are disrupted in schizophrenia	English et al., 2011
18 Studies with 1,789 subjects total	Meta-analysis of linkage data applied to published genome scans of schizophrenia	Susceptibility for schizophrenia has been identified on 8p and 22q, YWHAZ located at 8p23, YWHAH located at 22q12.3	Badner and Gershon, 2002
A Northern Chinese population	An association study between three SNPs in the 14-3-3 family and paranoid schizophrenia	SNP rs983583 G/A in the YWHAZ gene showed significant association with paranoid schizophrenia	Jia et al., 2004
35 Schizophrenia, 35 bipolar disorder and 35 control subjects	q-PCR used to determine relative mRNA levels in dorsolateral PFC samples	No significant differences in 14-3-3 mRNA expression levels, a significant genetic association with schizophrenia and SNPS of the ζ isoform	Wong et al., 2005
118 Schizophrenia patients and 118 healthy controls	Investigated allele frequencies of a VNTR in the 5′-non-coding region of the 14-3-3η chain gene	Frequencies of the two-repeat allele were increased in the schizophrenia patients, particularly in those with onset before age 22	Toyooka et al., 1999
1,211 Subjects from 318 nuclear families	A family based genetic association test between subtypes of bipolar disorder	The rs2246704 SNP of YWHAH was associated psychotic bipolar disorder	Grover et al., 2009
18 Control and 18 schizophrenia subjects	Used cDNA to investigate gene expression patterns in several brain regions	14-3-3η differentially expressed in schizophrenia	Vawter et al., 2001
9 Schizophrenia patients and 9 non-psychiatric controls were sourced from the NSW Tissue Resource Center	Alignment of RNA-Seq data to a reference genome and assembled into transcripts for quantification of exons, splice variants and alternative promoters in postmortem superior temporal gyrus	YWHAH and YWHAE differentially expressed	Wu et al., 2012
82 subjects across 7 studies	Review	A deletion in 22q11.2 leads to 22q11.2 Deletion Syndrome, a phenotype that often includes schizophrenia	Bassett and Chow, 2008
1,140 Unrelated schizophrenia cases and 1,140 controls from the Chinese Han population	A genetic association analysis between common SNPs of YWHAE and psychiatric diseases	No association between YWHAE SNPs and schizophrenia	Liu et al., 2011
24 Schizophrenia patients and 24 controls, 308 schizophrenia patients and 135 controls	Systematic search for nucleotide variants in the coding region, 5′ and 3′ untranslated region, and in the exon-intron boundaries of YWHAH	Failed to find significant associations between YWHAH and schizophrenia	Hayakawa et al., 1998
5 cDNAs and 72 ESTs, 21,155 bp of sequence	Systematic screening of YWHAE for polymorphisms in parallel with single-stranded conformational polymorphism analysis	Failed to find significant associations between YWHAH and schizophrenia	Bell et al., 2000
235 Trios: healthy parents and their affected offspring from a Chinese Han population	A family-based genotype association analysis	Failed to find significant associations between YWHAH and schizophrenia	Duan et al., 2005

(Continued)

TABLE 1 | (Continued)

Population/patient sample	Analysis method	Results	References
583 Cases and 372 controls in the Chinese Han population	Investigated several published polymorphisms in the YWHAH gene	Failed to find significant associations between YWHAH and schizophrenia	Wang et al., 2005
52 Controls and 22 schizophrenia patient Caucasian subjects	Immunoreactivity values of cytosolic 14-3-3β and 14-3-3ζ proteins were evaluated by Western blot in the prefrontal cortex	When all schizophrenia subjects were grouped together, no differences in 14-3-3 immunoreactivity were found, but when more appropriately grouped the results did show genetic linkage	Rivero et al., 2015
Japanese sample of 72 schizophrenia patients and 86 healthy controls	Whole brain voxel-based morphometric MRI study regarding the effects of YWHAE SNPs (rs28365859, rs11655548, and rs9393) on gray matter volume	Significant genotype-by-diagnosis interaction for rs28365859 in the left insula, right putamen, and right hippocampus	Kido et al., 2014
Publicly available sequencing data for 6,135 schizophrenia and 9,090 control samples of a European population	Study of the contribution of common and rare risk variants in 14-3-3 genes using ASD and schizophrenia transcriptomic data	Common variants in YWHAE contribute to schizophrenia whereas ultra-rare variants were found enriched in schizophrenia for YWHAZ	Torrico et al., 2020
Brain tissue from 20 schizophrenia cases, 20 bipolar disorder cases, and 20 healthy controls	Used data from comprehensive difference-in-gel electrophoresis (2-D DIGE) investigations of postmortem human hippocampus for Ingenuity Pathway Analysis (IPA) of implicated protein networks and pathways	IPA most prominently implicated 14-3-3 and aryl hydrocarbon receptor signaling in schizophrenia	Schubert et al., 2015
92 young individuals at ultra-high risk for psychosis	Explored the peripheral-blood expression level of the seven YWHA genes using multiplex quantitative PCR	Converters had a significantly higher baseline expression levels for 5 YWHA family genes, and significantly different longitudinal changes in the expression of YWHAE, YWHAG, YWHAH, YWHAS, and YWAHZ	Demars et al., 2020
168 Schizophrenia probands and their families	Genetic association between schizophrenia and the 14-3-3η gene and SNAP-25 genes was analyzed	Significant association with schizophrenia for two polymorphisms in the 14-3-3η gene: a 7 bp VNTR in the 5′ non-coding region and a 3′ untranslated region SNP	Wong et al., 2003

been considered as schizophrenia risk genes because they are located chromosomally close to loci that have been genetically associated with schizophrenia (English et al., 2011).

Despite the evidence discussed above for the genetic link between 14-3-3 and schizophrenia, there are some incongruencies in the literature. One study found no association between YWHAE SNPs and schizophrenia (Liu et al., 2011). While several studies have failed to find significant associations between YWHAH and schizophrenia (Hayakawa et al., 1998; Bell et al., 2000; Duan et al., 2005; Wang et al., 2005). In recognition of these discrepancies, Rivero et al. (2015) performed a western blot analysis of schizophrenia subjects and controls. This study indicated that the outcomes of genetic and proteomic studies in schizophrenia are likely influenced by gender, postmortem delay, age, and pharmacological differences in the subjects being tested. When all schizophrenia subjects were grouped together, no differences in 14-3-3 immunoreactivity were found in comparison to controls. However, when the subjects were more appropriately grouped, the results did show genetic linkages (Rivero et al., 2015). While the symptoms, demographics, and environmental factors of schizophrenia are widely varied, it is also important to consider the genetic heterogeneity of the disorder. Therefore, studying the genetic link between just one family of proteins with schizophrenia is further complicated by the fact that over 200 genetic loci have been identified in association with schizophrenia (Legge et al., 2021), and that interaction between two or more of these loci may contribute to the development of the disorder. These data suggest that the heterogeneity of schizophrenia may contribute to mixed results in the literature, especially when there is not proper grouping or when controls are not careful case matched. Thus, it is important to consider these limitations when interpreting genetic linkage studies and their discrepancies. Taking these considerations into account in future work will help further clarify the genetic link between the 14-3-3 family and schizophrenia.

Considering the evidence that 14-3-3 protein expressions are changed in the brain of schizophrenia patients, investigation of 14-3-3 levels in the cerebrospinal fluid (CSF) may serve as a promising new direction to take in the diagnosis of schizophrenia. Although the CSF is an indirect representation of neurochemistry, changes in mRNA and protein levels of various 14-3-3 isoforms could potentially be reflected in the CSF of schizophrenia patients. The 14-3-3 family has been implicated in several other neurodegenerative, neurodevelopmental, and neuropsychiatric disorders (Foote and Zhou, 2012). In fact, CSF levels of 14-3-3 have been used as a biomarker for several of these neurological diseases (Van Everbroeck et al., 2005; Antonell et al., 2020; Figgie and Appleby, 2021; Nilsson et al., 2021) as well as

several other diseases (Neal and Yu, 2010; Zeng and Tan, 2018; Morales et al., 2012). Early diagnosis of schizophrenia is difficult, yet early treatment can often make a difference in the prognosis of disease progression and severity. The history of 14-3-3 being used as a biomarker suggests that it could potentially serve as an indicator of schizophrenia, thus further study into this diagnostic possibility is warranted.

14-3-3 ANIMAL MODELS AND SCHIZOPHRENIA

Although human studies have provided valuable insight into the link between the 14-3-3 family and schizophrenia, they do not provide sufficient information about the role of 14-3-3 in the pathogenesis of schizophrenia. In order to better understand the pathology of schizophrenia and how 14-3-3 proteins may be involved; animal models are needed. Several animal models have been used to study the 14-3-3 family in the context of schizophrenia and have provided further support for the link suggested by human studies (**Table 2**).

14-3-3ζ Knockout Mice

One isoform of particular interest in regards to animal models of schizophrenia is 14-3-3ζ. Several 14-3-3ζ knockout models exhibit schizophrenia-like phenotypes. Homozygous 14-3-3ζ knockout mice of the Sv/129 background display behavioral abnormalities including hyperactivity, impaired recognition memory, reduced anxiety, dysfunction in hippocampal-dependent memory, and altered sensorimotor gating (Cheah et al., 2012). It is important to note that 14-3-3ζ knockout in this model is prominent in the hippocampus and dentate gyrus, pointing to the role of these regions in schizophrenia-like behavior. Defects in the hippocampus that may underlie these behavioral changes were apparent before the region was fully developed. The defects included neuronal migration defects, abnormal mossy fiber navigation, and altered glutamatergic synapse formation (Cheah et al., 2012). While the glutamate system may be altered, there is also evidence that 14-3-3ζ knockout affects the dopamine system within this model. The hyperactivity of 14-3-3ζ knockout mice is rescued by clozapine administration and knockout animals are more sensitive to amphetamine administration when compared to wildtype controls (Ramshaw et al., 2013). The mechanisms of action of these drugs and their effects on 14-3-3ζ knockout animals suggest that the dopamine system may underlie some of the behavioral abnormalities in this model. In fact, 14-3-3ζ was shown to have a physical association with the dopamine transporter (DAT). Further, decreased DAT levels found as a result of 14-3-3ζ knockout also led to increased striatal dopamine (Ramshaw et al., 2013). However, clozapine administration was not able to rescue altered anxiety behavior, the structural abnormalities in spine formation, or neuronal mis-localization in 14-3-3ζ knockout mice (Jaehne et al., 2015). This result suggests that the loss of 14-3-3ζ causes changes beyond the dopamine system as well.

Although these studies provide evidence that alterations in 14-3-3ζ can lead to schizophrenia-like phenotypes, these abnormalities have not been fully recapitulated in 14-3-3ζ knockout mice from other genetic backgrounds. When backcrossed into a BALB/c background, homozygous 14-3-3ζ knockout mice can live to adulthood. However, these mice show only weak learning disability and do not differ from controls in many of the same behavioral tests that Sv/129 14-3-3ζ knockout animals display schizophrenia-like behavior (Xu et al., 2015). In addition, the dopamine system appears intact in this model, as dopamine signaling and DAT expression are unaltered in the 14-3-3ζ knockout mice. Despite the discrepancies in behavior and dopamine function, BALB/c homozygous 14-3-3ζ knockout mice do display many of the same structural abnormalities in the brain as 14-3-3ζ knockout mice from the Sv/129 background. These abnormalities included mis-localized hippocampal neurons, reduced CA3 spine density, and abhorrent mossy fiber tracts (Xu et al., 2015).

Interestingly, overexpression of 14-3-3ζ can lead to increased spine density in primary hippocampal neuron culture (Angrand et al., 2006). This is consistent with the reduction in spine density seen in 14-3-3ζ knockout mice, indicating that 14-3-3ζ positively regulates spine density. Overall there is evidence that 14-3-3ζ knockout does induce schizophrenia-like defects in mice, but these defects seem to depend on the genetic background of the animal models. Thus, the models discussed above provide further support for the importance of 14-3-3ζ to many structural processes in the brain that may underlie schizophrenia-like phenotypes when altered.

14-3-3ε Knockout Mice

Several human studies have found a link between 14-3-3ε and schizophrenia, prompting further studies in 14-3-3ε knockout animals. Homozygous knockout of 14-3-3ε is prenatally lethal in in-bred genetic backgrounds. Thus, Toyo-oka et al. (2003) examined the brains of homozygous and heterozygous 14-3-3ε knockout mice at embryonic day 18.5, prior to homozygous lethality. Both genotypes had hippocampal defects and cortical thinning, structural issues which were underscored by shortened neuronal migration and mis-localization of key proteins involved in migration processes. The lethality of homozygous knockout mice points to the increased severity of these defects with complete loss of 14-3-3ε. Additional studies of heterozygous 14-3-3ε knockout mice revealed further molecular, structural, and behavioral alterations. One such alteration seen in the hippocampal formation was significantly increased levels of VMAT2, a protein involved in the transport of monoamine neurotransmitters into neuronal vesicles (Iritani et al., 2010). Another study found that 14-3-3ε knockout mice have decreased numbers of tyrosine hydroxylase positive fibers that also exhibit altered functional structure (Sekiguchi et al., 2011). Behavioral testing of this heterozygous 14-3-3ε knockout model revealed weak deficits in working memory and moderately enhanced anxiety like behavior (Ikeda et al., 2008). However, a mixed genetic background model of 14-3-3ε knockout showed different behavioral results, including weaker motor activity, hyperactivity, visual/spatial memory defects, and unaltered anxiety-like behavior (Wachi et al., 2017). Thus, the above evidence suggests that loss of 14-3-3ε causes both structural and

TABLE 2 | 14-3-3 Animal Models.

Mouse strain/line Partial/full knockout Age studied	Behavioral changes	Molecular/synaptic/anatomical changes	References
14-3-3ζ			
SV129/14-3-3 ζGt (OST062) Lex Homozygous 5–40 weeks	Hyperactive, lowered anxiety, impaired recognition memory, defect in spatial working memory, defects in sensorimotor gating	Abnormal mossy fiber navigation and glutamatergic synapse formation, 14-3-3 binding to DISC1	Cheah et al., 2012
SV129/14-3-3 ζGt (OST062) Lex Homozygous 30, 35 weeks	Hyperactivity rescued by clozapine, hypersensitive to amphetamine	TH preserved, reduced and mis-localized DAT	Ramshaw et al., 2013
BALB/c/14-3-3 ζGt (OST062) Lex Homozygous 12 weeks, 28–35 weeks	No hyperactivity, no anxiety changes, subtle learning problems, impaired spatial memory	Mis-localized hippocampal cells with aberrant connectivity, reduced spine density, normal DA signaling	Xu et al., 2015
SV129/14-3-3 ζGt (OST062) Lex Homozygous 28–32 weeks	Clozapine affects despair behavior in KOs, anxiety-like behavior not affected by KO or clozapine, clozapine had opposing affects in KO and WT in the Y maze	Dendritic spine defects in the hippocampus and cortex, anatomical differences not rescued by clozapine	Jaehne et al., 2015
14-3-3ε			
Mixed (129/S6 and NIH Black Swiss) Heterozygous/homozygous E 18.5	/	Hippocampal defects, cortical thinning, neuronal migration defects, mis-localization of NDEL/LIS1	Toyo-oka et al., 2003
Mixed (129/S6 and NIH Black Swiss) Heterozygous 9–10 weeks	Weak defect in working memory, moderately enhanced anxiety like behavior	/	Ikeda et al., 2008
Mixed (129/S6 and NIH Black Swiss) Heterozygous 12–15 weeks	/	Increased VMAT2 expression in the hippocampus	Iritani et al., 2010
Mixed (129/S6 and NIH Black Swiss) Heterozygous 15 weeks	/	Serpentine, thin, short TH immunopositive fibers, few and sparse dendritic spine like immunopositive varices, significant decrease in TH positive fibers	Sekiguchi et al., 2011
Mixed (129SVE and C57BL/6) Heterozygous/homozygous 12–16 weeks	Hyperactivity, decreased working memory, increased sociability	/	Wachi et al., 2017
14-3-3ζ/ε			
129/SvEv Heterozygous E15.5-18.5	/	Abnormal proliferation/differentiation of neuronal progenitors in culture, increased differentiation into neurons, cortical neuronal migration defects, abnormal activity of the Rho family and its effectors	Toyo-oka et al., 2014
14-3-3γ			
129SV Heterozygous/homozygous	Normal cage behavior	Several differentially expressed proteins, normal anatomy	Steinacker et al., 2005
ICR outbred *In utero* electroporation of shRNA inhibitor E17-18.5, P3-15	/	Neuronal migration delay of cerebral pyramidal neurons, thicker/highly branched leading processes, impaired ability of the leading process to enter the MZ	Wachi et al., 2016
C57BL/6/B6; CBYwhagGt (pU-21W)266Card Heterozygous 10 weeks	Hyperactivity, depressive like behavior, sensitive to acute stress	/	Kim et al., 2019
14-3-3 FKO			
C57BL/6 Transgenic expressed inhibitor 12–24 weeks	Deficit in associative learning and memory	Defects in hippocampal LTP, reduced synaptic NMDARs	Qiao et al., 2014
C57BL/6 Transgenic expressed inhibitor 12–24 weeks	Hyperactivity, unaltered anxiety response, deficit in working memory, deficit in sensorimotor gating, social withdrawal	Cortical neurotransmission deficit, morphological alterations, reduced phospho-cofilin, increase delta catenin	Foote et al., 2015
C57BL/6 AAV delivered shRNA 12–24 weeks	Behaviors recapitulated through acute 14-3-3 inhibition in the PFC and HPC	/	Graham et al., 2019
C57BL/6 Transgenic expressed inhibitor 12–24 weeks	/	Altered neural oscillations in theta/gamma frequency ranges	Jones et al., 2021
B6.SJLSlc6a3tm 1.1 (cre) Bkmn/J B6.Cg-Tg (Camk2a-cre) T29-1Stl/J AAV delivered YFP-difopein 12–24 weeks	/	Increased activation of LS neurons is necessary for over-activation of DA neurons and psychomotor behavior induced by 14-3-3 inhibition in the dCA1	Zhang et al., 2022

behavioral abnormalities in mice that resemble those seen in schizophrenia patient populations. However, these results may be affected by the genetic background of the mouse models in use. Nonetheless, 14-3-3ε knockout models may be a valuable tool in studying the molecular, structural, and behavioral aspects of schizophrenia.

14-3-3ζ/ε Double Knockout Mice

Both 14-3-3ζ and 14-3-3ε are critical proteins when it comes to proper brain development, and there is evidence that loss of either can cause defects similar to those seen in schizophrenia patients. The underpinnings of these changes have been further elucidated through the study of a double knockout mouse model in which mice were heterozygous knockout for one isoform and homozygous knockout for the other 14-3-3 isoform ($Ywhae^{+/flox}$; $Ywhaz^{KO/KO}$ and $Ywhae^{flox/flox}$; $Ywhaz^{+/KO}$) (Toyo-oka et al., 2014). Double knockout mice displayed neuronal differentiation and migration defects as well as seizures. The same phenotypes are seen in single knockout models for these proteins but are more pronounced in double knockout animals. These results point to the critical involvement of 14-3-3ζ and 14-3-3ε proteins in the developing brain, as well as the functional redundancy between isoforms. A critical pathway through which these 14-3-3 proteins can regulate neuronal differentiation is the catenin/Rho GTPase/Limk1/cofilin signaling pathway, where 14-3-3 proteins directly interact with phosphorylated delta-catenin to promote F-actin formation. 14-3-3 double knockout mice were shown to have increased levels of delta-catenin, as well as decreased levels of beta-catenin and alphaN-catenin (Toyo-oka et al., 2014). Deletion of delta-catenin did not rescue neuronal migration abnormalities in double knockout mice; but mutants of the Ndel1 protein were able to do so, indicating that 14-3-3 proteins are also involved in a separate pathway that controls neuronal migration (Toyo-oka et al., 2014). Thus, 14-3-3 proteins are important regulators of several different pathways and the loss of one or more isoforms can detrimentally impact neural development and result in behavioral abnormality.

14-3-3γ Knockout Mice

14-3-3γ is particularly enriched in the brain and is typically expressed in the developing cortex. Reduction in the γ isoform of 14-3-3 has yielded mixed outcomes when it comes to behavioral and morphological changes. One study found no obvious behavioral alterations or histological differences in the cortex of either heterozygous or homozygous 14-3-3γ knockout mice (Steinacker et al., 2005). While in another study, depletion of 14-3-3γ through *in utero* electroporation of a specific small hairpin RNA (shRNA) resulted in a delay of neural migration and morphological abnormalities in the cortex (Wachi et al., 2016). In a study of behavior, heterozygous 14-3-3γ knockout mice were hyperactive and more sensitive to acute stress when compared to wildtype littermates, while homozygous 14-3-3γ knockout mice died before birth (Kim et al., 2019). Although there are some conflicting results, there is evidence that loss of 14-3-3γ can cause abnormalities that resemble those found in psychiatric disorders like schizophrenia.

14-3-3 Functional Knockout Mice

With the many roles of 14-3-3 proteins in neuronal processes and the genetic evidence linking the proteins to schizophrenia, our lab sought to create a mammalian model to study the synaptic and cognitive functions of the 14-3-3 protein family. Transgenic 14-3-3 functional knock-out (FKO) mice were generated through the expression of yellow fluorescent protein (YFP) fused difopein (dimeric 14-3-3 peptide inhibitor), which inhibits all isoforms of 14-3-3 from interacting with endogenous binding partners (Qiao et al., 2014). An important consideration is that 14-3-3 inhibition during embryonic development can be lethal. To avoid prenatal lethality, the transgenic expression of YFP-difopein was driven by the neuronal specific Thy-1 promotor, which is normally expressed in the perinatal period. The Thy-1 promotor created several founder mice in which the expression pattern of YFP-difopein varied but was preserved within the founder line. One of these founder lines had transgene expression that was relatively higher in the hippocampus (HPC) and the pre-frontal cortex (PFC). This line was found to display several behavioral, electrophysiological, and molecular abnormalities. During the contextual fear conditioning and passive avoidance tests, these 14-3-3FKO mice displayed significantly reduced freezing behavior and reduced latency to dark chamber, indicating impairments in associative learning and memory. Electrophysiological investigation of these mice reveled that they also exhibit defects in long-term synaptic plasticity of the hippocampus. Consistently, evidence for NMDAR dysfunction in the 14-3-3FKO line was observed, including significant reductions in the NMDAR/AMPAR ratio and in NMDAR mediated currents, as well as lowered levels of the GluN1 and GluN2a NMDA receptor subunits.

Further investigation of the 14-3-3FKO line revealed additional behavioral and synaptic defects that can be considered schizophrenia-like phenotypes. Increased activity in the open field test (OFT), decreased alteration in the Y maze test, decreased pre-pulse inhibition percentage, and decreased social interaction in the three-chamber test were observed in FKO mice vs. their wildtype (WT) littermates (Foote et al., 2015). These behavioral outcomes reveal deficits in psychomotor behavior, working memory, sensorimotor gating control, and social behavior respectively; all of which can be likened to schizophrenia-related phenotypes. In addition to these behavioral changes, whole-cell voltage-clamp recording of YFP-difopein infected cells in cortical neurons of the FKO mice show significant reductions in the frequencies of spontaneous excitatory and inhibitory post synaptic potentials, as well as alterations in miniature excitatory and inhibitory post synaptic potentials. Further, the cortical layer-5 and hippocampal CA1 pyramidal neurons of FKO mice had decreased distal apical dendrite complexity and decreased spine density when compared to cells from WT littermates. Potential molecular mechanisms of these changes may come from reduced levels of phospho-cofilin and increased levels of delta-catenin in FKO brain tissue.

The behavioral, electrophysiological, and molecular results discussed above indicate that 14-3-3 inhibition in the PFC and HPC can lead to a variety of schizophrenia-like phenotypes. However, the individual roles for each of these brain regions was not distinguishable. In order to determine if inhibition in either the PFC and/or the HPC is necessary and sufficient to induce schizophrenia-like phenotypes, 14-3-3 function was regionally restored through an adeno-associated virus (AAV) delivered shRNA that knocks down YFP-difopein (Graham et al., 2019). Delivery of the shRNA to both the PFC and the HPC lead to significant reductions in OFT locomotor activity, while delivery to one region alone did not. Interestingly, shRNA injection to the HPC alone significantly increased the GluN1 levels in 14-3-3FKO animals, but not to the level of WT littermates. This was likely due to the fact that shRNA was not able to fully inhibit the YFP-difopein transgene. Due to this incomplete inhibition and the fact that the difopein expression in FKO mice is not strictly limited to the PFC and HPC, our lab sought to investigate the effect of region specific difopein expression. A virus using the CamKIIa promotor to drive YFP-difopein expression in excitatory neurons was created to determine if 14-3-3 inhibition in the PFC and/or the HPC is sufficient to induce schizophrenia related phenotypes (Graham et al., 2019). Behavioral testing revealed that WT mice with YFP-difopein injections to the HPC alone, but not the PFC alone, exhibit significantly less freezing behavior in the contextual fear conditioning test and decreased pre-pulse inhibition. In addition, injection of YFP-difopein to both the PFC and HPC, as well as the HPC alone, lead to increased locomotor activity in the OFT, while injection to the PFC alone did not. These results indicate that 14-3-3 inhibition in the HPC is sufficient to induce schizophrenia-like behaviors. In further support of this claim is the finding that YFP-difopein injection to the HPC has a direct effect on NMDA receptor regulation, resulting in decreased GluN1, GluN2A, and PSD95 levels.

To build upon the behavioral and molecular abnormalities found in our models of 14-3-3 inhibition, our lab investigated the role of 14-3-3 proteins in neural oscillations, which are dysfunctional in schizophrenia patients (Jones et al., 2021). FKO animals exhibited a range of changes in power, coherence, and phase-amplitude coupling in both resting and task-related theta and gamma oscillations. WT animals with 14-3-3 inhibited in the HPC alone showed similar yet distinct changes in these same measures. However, 14-3-3 inhibition to the PFC alone leads to few changes in neural oscillations. Overall, our *in vivo* electrophysiological results indicated that acute 14-3-3 inhibition in the HPC largely disrupts theta oscillations and is sufficient to cause neural oscillation defects in the HPC as well as the PFC.

Interestingly, FKO mice exhibit hyperactive dopamine signaling in the ventral tegmental area (VTA) and some of their altered behavior can be attenuated with antipsychotic administration (Foote et al., 2015). Yet there is no YFP-difopein expression detected in the VTA, indicating that 14-3-3 inhibition in other brain areas has an influence on VTA dopamine signaling. Acute 14-3-3 inhibition in the dorsal HPC (dHPC) alone causes c-Fos expression in the dHPC and increased locomotor activity in the OFT that is responsive to antipsychotics (Zhang et al., 2022). This overexcitation in the dHPC is accompanied by robust c-Fos expression in the VTA, indicating a connection between 14-3-3 inhibition induced dHPC overexcitation, hyperactive dopamine signaling, and hyperlocomotion. However, the neural circuitry underlying this connection is not clear, as the dHPC does not directly communicate with the VTA. Through neural tracing techniques, we found that the lateral septum (LS), which also shows increased c-Fos activity after OFT in dHPC injected mice, has mono-synaptic connections with the dHPC (Zhang et al., 2022). Previous studies have shown that the LS also communicates with the VTA, where its connections act on GABAergic interneurons to disinhibit VTA DA neurons (Vega-Quiroga et al., 2018). We confirmed that VTA projecting LS neurons are activated following OFT in difopein injected mice. Thus, the LS appears to be both activated during 14-3-3 inhibition induced hyperlocomotion and anatomically connected with the dHPC and VTA. To further confirm the role of the LS in this neural circuitry we used chemogenetic Designer Receptors Exclusively Activated by Designer Drugs (DREADDs) to manipulate the activity of the LS in mice. Our results demonstrated that chemogenetic inhibition of the LS attenuates difopein induced hyperlocomotion as well as upregulated DA activity, while chemogenetic activation of LS projecting dHPC neurons elicits hyperlocomotion in WT mice. These results indicate that increased activity in the LS is both necessary and sufficient to induce changes in psycholocomotor behavior. Overall, our results provide evidence for a polysynaptic pathway from the dHPC to the LS to the VTA in which 14-3-3 inhibition causes an imbalance in the ratio of excitatory to inhibitory signaling that results in psychomotor behavior (Zhang et al., 2022).

Through a series of studies, our lab has created a mouse model of 14-3-3 inhibition that can be useful in the study schizophrenia related phenotypes at the behavioral, molecular, and circuitry levels. The family of 14-3-3 proteins is involved in several critical neuronal processes and has been associated with schizophrenia through genetic linkage studies. We found that transgenic expression of a 14-3-3 inhibitor in key forebrain areas results in a mouse line that displays several behavioral, electrophysiological, and molecular phenotypes which resembles those seen in schizophrenia patients. Through acute viral delivery of our inhibitor, we saw that the functional loss of 14-3-3 proteins in the hippocampus is sufficient to induce these disease-related outcomes. Using our 14-3-3 inhibited mice, we delineated a previously unknown polysynaptic circuit that connects 14-3-3 inhibition induced imbalances in neuronal signaling to changes in psychomotor behavior. Together, our work provides further evidence for the role of 14-3-3 dysfunction in schizophrenia and a tool which we can use to further explore the mechanisms of pathology in schizophrenia.

POTENTIAL MECHANISMS

Human genetic and proteomic linkage studies have provided several lines of evidence that the 14-3-3 protein family and their associated genes may be altered in schizophrenia. Because the 14-3-3 proteins mediate such a wide range of cellular and

molecular processes, any mutation to or change in expression of these proteins may contribute to abnormalities in these processes and potentially to disease states such as schizophrenia.

Several neurotransmitter systems appear to be altered in schizophrenia, including the dopamine, glutamate, and GABA systems. For many years the dopamine hypothesis and the glutamate hypothesis were separate lenses in which researchers and physicians studied and tried to treat the neuropathology of schizophrenia. More recently, it has been proposed that dysfunction in the dopamine system may be a downstream consequence of dysregulated glutamate neurotransmission in the forebrain. As the major excitatory neurotransmitter, glutamate has influence all over the brain, including in the dopamine system. However, it is unknown how the two systems could be interacting in the disease state, making it difficult to merge the two hypotheses for schizophrenia. The 14-3-3 protein family may serve as a potential link between dopamine and glutamate dysfunction in schizophrenia, as there is evidence that changes in 14-3-3 have effects in both neurotransmitter systems. Alterations in NMDA receptor (NMDAR) activity is reported in several 14-3-3 knockout models, and decreased NMDAR activity can alter the excitation and inhibition balance in neural networks and circuits (Moghaddam and Javitt, 2012). Surface expression of NMDA receptors is regulated and promoted by 14-3-3 proteins, particularly the ζ and ε isoforms, through their interactions with particular NMDAR subunits (Chen and Roche, 2009; Lee et al., 2021). This relationship is further highlighted by the finding that knockdown of the NMDAR subunit NR1 leads to synaptic reduction of 14-3-3ε (Ramsey et al., 2011; Ferris et al., 2014). Further, a recent study from our lab has elucidated a polysynaptic pathway in which 14-3-3 dysfunction in the dorsal hippocampus underlies altered psychomotor behavior mediated by dopamine in the VTA (Zhang et al., 2022). These results offer evidence on how the glutamate and dopamine systems may be linked in schizophrenia, as well as a potential role for 14-3-3 dysfunction in the mechanism of the pathology.

The 14-3-3 proteins have many binding partners and are involved in several critical molecular and cellular pathways; thus, the disruption of these proteins can have many potential impacts. One pathway affected by 14-3-3 disruption is the catenin/Rho GTPase/Limk1/cofilin signaling pathway, which plays a significant role in regulating actin cytoskeleton dynamics during brain development. Moreover, the Ndel1/Lis1/14-3-3ε complex has been proposed to be critical for neuronal migration (Foote and Zhou, 2012). Interestingly, the localization of the Ndel1/Lis1/14-3-3ε complex to axons is regulated by the schizophrenia related protein DISC1 (Taya et al., 2007). 14-3-3ε binds to the DISC1 binding region of Ndel1, maintaining its phosphorylation (Toyo-oka et al., 2003; Johnson et al., 2010), and deficiency of 14-3-3ε leads to mis-localization of Ndel1 and Lis1 (Toyo-oka et al., 2003). Additionally, 14-3-3 proteins have been shown to interact with many other cytoskeleton and dendritic spine related proteins. For example, 14-3-3ζ interacts with microtubule-associated protein/microtubule affinity-regulating kinase 3 (MARK3) (Angrand et al., 2006). The proper regulation of microtubules is necessary for neuronal migration and spine formation. In fact, knockout of microtubule associated protein 6 (MAP6) in mice results in many similar schizophrenia-like phenotypes as 14-3-3 knockout models. These include deficits in synaptic plasticity, abnormal glutamatergic signaling, and locomotor hyperactivity (Cuveillier et al., 2021). The similarities between MAP6 and 14-3-3 knockout models along with the physical interaction between 14-3-3 proteins and microtubule related proteins suggest that 14-3-3 are key players in appropriate cytoskeletal regulation. The association between 14-3-3 proteins and these specific binding partners and pathways may underlie the neuronal migration and synaptic defects observed in the 14-3-3 knockout animal models discussed above, as well as provide potential mechanistic insight into the pathogenesis of schizophrenia.

Several of these processes are critical to neurodevelopment, suggesting that any changes in 14-3-3 proteins during critical periods could potentially lead to abnormal structural and functional connections in the brain. In fact, the viability of knockout animals and the severity of their abnormalities in the brain are influenced by the timing of the 14-3-3 knockout. Similarly, the timing of the progression of schizophrenia in humans also points to the importance of these critical developmental periods. The molecular changes that underlie schizophrenia require further study to create a more holistic understanding of the disease and how 14-3-3 dependent regulatory pathways may be involved. The diverse and important roles for 14-3-3 proteins serve as promising points from which to study the mechanisms underlying the disorder.

CONCLUSION

Schizophrenia is a complicated mental disorder that greatly affects those who are diagnosed with it. The heterogeneity of the disorder makes it difficult to decipher the neurobiological basis of schizophrenia. One interesting and promising route of study in schizophrenia is the role of 14-3-3 proteins. The genetic link between 14-3-3 and schizophrenia suggests that studying schizophrenia through the 14-3-3 family can offer valuable insight to the disease. The results from 14-3-3 knockout models validate this idea and have allowed for a better understanding of the pathology of schizophrenia and how the 14-3-3 family may contribute to its progression. The 14-3-3 protein family has a wide variety of binding partners and functions, the exact mechanisms behind how alterations in 14-3-3 proteins can lead to schizophrenia-like phenotypes is not fully understood. However, some potential mechanisms include abnormal neural development and neuronal signaling following altered neurotransmitter receptor levels, mis-localized protein complexes, and interrupted cellular pathways. Future study will be needed to fully elucidate the causes of these observed phenotypes but will undoubtedly provide further understanding of the complex pathology of schizophrenia.

AUTHOR CONTRIBUTIONS

MN was responsible for drafting, writing, reviewing, and editing this manuscript. YZ was responsible for

writing, reviewing, and editing the manuscript with suggestive ideas on formatting and outlining this manuscript. Both authors contributed to the article and approved the submitted version.

FUNDING

This work was supported by the National Institutes of Health (award no. R01 MH115188 to YZ).

REFERENCES

Altar, C. A., Vawter, M. P., and Ginsberg, S. D. (2009). Target identification for CNS diseases by transcriptional profiling. *Neuropsychopharmacology* 34, 18–54. doi: 10.1038/npp.2008.172

Angrand, P. O., Segura, I., Volkel, P., Ghidelli, S., Terry, R., Brajenovic, M., et al. (2006). Transgenic mouse proteomics identifies new 14-3-3-associated proteins involved in cytoskeletal rearrangements and cell signaling. *Mol. Cell Proteomics* 5, 2211–2227. doi: 10.1074/mcp.M600147-MCP200

Antonell, A., Tort-Merino, A., Rios, J., Balasa, M., Borrego-Ecija, S., Auge, J. M., et al. (2020). Synaptic, axonal damage and inflammatory cerebrospinal fluid biomarkers in neurodegenerative dementias. *Alzheimers Dement.* 16, 262–272. doi: 10.1016/j.jalz.2019.09.001

Badner, J. A., and Gershon, E. S. (2002). Meta-analysis of whole-genome linkage scans of bipolar disorder and schizophrenia. *Mol. Psychiatry* 7, 405–411. doi: 10.1038/sj.mp.4001012

Bassett, A. S., and Chow, E. W. (2008). Schizophrenia and 22q11.2 deletion syndrome. *Curr. Psychiatry Rep.* 10, 148–157. doi: 10.1007/s11920-008-0026-1

Bell, R., Munro, J., Russ, C., Powell, J. F., Bruinvels, A., Kerwin, R. W., et al. (2000). Systematic screening of the 14-3-3 eta (eta) chain gene for polymorphic variants and case-control analysis in schizophrenia. *Am. J. Med. Genet.* 96, 736–743.

Berg, D., Holzmann, C., and Riess, O. (2003). 14-3-3 proteins in the nervous system. *Nat. Rev. Neurosci.* 4, 752–762. doi: 10.1038/nrn1197

Boston, P. F., Jackson, P., and Thompson, R. J. (1982). Human 14-3-3 protein: radioimmunoassay, tissue distribution, and cerebrospinal fluid levels in patients with neurological disorders. *J. Neurochem.* 38, 1475–1482. doi: 10.1111/j.1471-4159.1982.tb07928.x

Cheah, P. S., Ramshaw, H. S., Thomas, P. Q., Toyo-Oka, K., Xu, X., Martin, S., et al. (2012). Neurodevelopmental and neuropsychiatric behaviour defects arise from 14-3-3zeta deficiency. *Mol. Psychiatry* 17, 451–466. doi: 10.1038/mp.2011.158

Chen, B. S., and Roche, K. W. (2009). Growth factor-dependent trafficking of cerebellar NMDA receptors via protein kinase B/Akt phosphorylation of NR2C. *Neuron* 62, 471–478. doi: 10.1016/j.neuron.2009.04.015

Cuveillier, C., Boulan, B., Ravanello, C., Denarier, E., Deloulme, J. C., Gory-Faure, S., et al. (2021). Beyond neuronal microtubule stabilization: MAP6 and CRMPS. two converging stories. *Front. Mol. Neurosci.* 14:665693. doi: 10.3389/fnmol.2021.665693

Demars, F., Kebir, O., Marzo, A., Iftimovici, A., Schramm, C., Icaar Study Group, et al. (2020). Dysregulation of peripheral expression of the YWHA genes during conversion to psychosis. *Sci. Rep.* 10:9863. doi: 10.1038/s41598-020-66901-1

Duan, S., Gao, R., Xing, Q., Du, J., Liu, Z., Chen, Q., et al. (2005). A family-based association study of schizophrenia with polymorphisms at three candidate genes. *Neurosci. Lett.* 379, 32–36. doi: 10.1016/j.neulet.2004.12.040

English, J. A., Pennington, K., Dunn, M. J., and Cotter, D. R. (2011). The neuroproteomics of schizophrenia. *Biol. Psychiatry* 69, 163–172. doi: 10.1016/j.biopsych.2010.06.031

Ferris, M. J., Milenkovic, M., Liu, S., Mielnik, C. A., Beerepoot, P., John, C. E., et al. (2014). Sustained N-methyl-d-aspartate receptor hypofunction remodels the dopamine system and impairs phasic signaling. *Eur. J. Neurosci.* 40, 2255–2263. doi: 10.1111/ejn.12594

Figgie, M. P. Jr., and Appleby, B. S. (2021). Clinical use of improved diagnostic testing for detection of prion disease. *Viruses* 13:789. doi: 10.3390/v13050789

Foote, M., Qiao, H., Graham, K., Wu, Y., and Zhou, Y. (2015). Inhibition of 14-3-3 proteins leads to schizophrenia-related behavioral phenotypes and synaptic defects in mice. *Biol. Psychiatry* 78, 386–395. doi: 10.1016/j.biopsych.2015.02.015

Foote, M., and Zhou, Y. (2012). 14-3-3 proteins in neurological disorders. *Int. J. Biochem. Mol. Biol.* 3, 152–164.

Freedman, R. (2003). Schizophrenia. *N. Engl. J. Med.* 349, 1738–1749. doi: 10.1056/NEJMra035458

Fu, H., Subramanian, R. R., and Masters, S. C. (2000). 14-3-3 proteins: structure, function, and regulation. *Annu. Rev. Pharmacol. Toxicol.* 40, 617–647. doi: 10.1146/annurev.pharmtox.40.1.617

Graham, K., Zhang, J., Qiao, H., Wu, Y., and Zhou, Y. (2019). Region-specific inhibition of 14-3-3 proteins induces psychomotor behaviors in mice. *NPJ Schizophr.* 5:1. doi: 10.1038/s41537-018-0069-1

Grover, D., Verma, R., Goes, F. S., Mahon, P. L., Gershon, E. S., McMahon, F. J., et al. (2009). Family-based association of YWHAH in psychotic bipolar disorder. *Am. J. Med. Genet. B Neuropsychiatr. Genet.* 150B, 977–983. doi: 10.1002/ajmg.b.30927

Hayakawa, T., Ishiguro, H., Toru, M., Hamaguchi, H., and Arinami, T. (1998). Systematic search for mutations in the 14-3-3 eta chain gene on chromosome 22 in schizophrenics. *Psychiatr. Genet.* 8, 33–36. doi: 10.1097/00041444-199800810-00006

Ikeda, M., Hikita, T., Taya, S., Uraguchi-Asaki, J., Toyo-oka, K., Wynshaw-Boris, A., et al. (2008). Identification of YWHAE, a gene encoding 14-3-3epsilon, as a possible susceptibility gene for schizophrenia. *Hum. Mol. Genet.* 17, 3212–3222. doi: 10.1093/hmg/ddn217

Iritani, S., Sekiguchi, H., Habuchi, C., Hikita, T., Taya, S., Kaibuchi, K., et al. (2010). Immunohistochemical study of vesicle monoamine transporter 2 in the hippocampal region of genetic animal model of schizophrenia. *Synapse* 64, 948–953. doi: 10.1002/syn.20846

Jablensky, A. (2000). Epidemiology of schizophrenia: the global burden of disease and disability. *Eur. Arch. Psychiatry Clin. Neurosci.* 250, 274–285. doi: 10.1007/s004060070002

Jaehne, E. J., Ramshaw, H., Xu, X., Saleh, E., Clark, S. R., Schubert, K. O., et al. (2015). *In-vivo* administration of clozapine affects behaviour but does not reverse dendritic spine deficits in the 14-3-3zeta KO mouse model of schizophrenia-like disorders. *Pharmacol. Biochem. Behav.* 138, 1–8. doi: 10.1016/j.pbb.2015.09.006

Jia, Y., Yu, X., Zhang, B., Yuan, Y., Xu, Q., Shen, Y., et al. (2004). An association study between polymorphisms in three genes of 14-3-3 (tyrosine 3-monooxygenase/tryptophan 5-monooxygenase activation protein) family and paranoid schizophrenia in northern Chinese population. *Eur. Psychiatry* 19, 377–379. doi: 10.1016/j.eurpsy.2004.07.006

Johnson, C., Crowther, S., Stafford, M. J., Campbell, D. G., Toth, R., and MacKintosh, C. (2010). Bioinformatic and experimental survey of 14-3-3-binding sites. *Biochem. J.* 427, 69–78. doi: 10.1042/BJ20091834

Jones, Z. B., Zhang, J., Wu, Y., and Zhou, Y. (2021). Inhibition of 14-3-3 proteins alters neural oscillations in mice. *Front. Neural Circuits* 15:647856. doi: 10.3389/fncir.2021.647856

Kane, J. M., Kishimoto, T., and Correll, C. U. (2013). Non-adherence to medication in patients with psychotic disorders: epidemiology, contributing factors and management strategies. *World Psychiatry* 12, 216–226. doi: 10.1002/wps.20060

Kido, M., Nakamura, Y., Nemoto, K., Takahashi, T., Aleksic, B., Furuichi, A., et al. (2014). The polymorphism of YWHAE, a gene encoding 14-3-3epsilon, and brain morphology in schizophrenia: a voxel-based morphometric study. *PLoS One* 9:e103571. doi: 10.1371/journal.pone.0103571

Kim, D. E., Cho, C. H., Sim, K. M., Kwon, O., Hwang, E. M., Kim, H. W., et al. (2019). 14-3-3Gamma haploinsufficient mice display hyperactive and stress-sensitive behaviors. *Exp. Neurobiol.* 28, 43–53. doi: 10.5607/en.2019.28.1.43

Lee, G. S., Zhang, J., Wu, Y., and Zhou, Y. (2021). 14-3-3 proteins promote synaptic localization of N-methyl d-aspartate receptors (NMDARs) in mouse hippocampal and cortical neurons. *PLoS One* 16:e0261791. doi: 10.1371/journal.pone.0261791

Legge, S. E., Santoro, M. L., Periyasamy, S., Okewole, A., Arsalan, A., and Kowalec, K. (2021). Genetic architecture of schizophrenia: a review of major advancements. *Psychol. Med.* 51, 2168–2177. doi: 10.1017/S0033291720005334

Liu, D., Bienkowska, J., Petosa, C., Collier, R. J., Fu, H., and Liddington, R. (1995). Crystal structure of the zeta isoform of the 14-3-3 protein. *Nature* 376, 191–194. doi: 10.1038/376191a0

Liu, J., Zhou, G., Ji, W., Li, J., Li, T., Wang, T., et al. (2011). No association of the YWHAE gene with schizophrenia, major depressive disorder or bipolar disorder in the Han Chinese population. *Behav. Genet.* 41, 557–564. doi: 10.1007/s10519-010-9426-1

Mentzel, T. Q., Lieverse, R., Bloemen, O., Viechtbauer, W., van Harten, P. N., and Risk Genetic and Investigators Outcome of Psychosis. (2017). High incidence and prevalence of drug-related movement disorders in young patients with psychotic disorders. *J. Clin. Psychopharmacol.* 37, 231–238. doi: 10.1097/JCP.0000000000000666

Middleton, F. A., Peng, L., Lewis, D. A., Levitt, P., and Mirnics, K. (2005). Altered expression of 14-3-3 genes in the prefrontal cortex of subjects with schizophrenia. *Neuropsychopharmacology* 30, 974–983. doi: 10.1038/sj.npp.1300674

Moghaddam, B., and Javitt, D. (2012). From revolution to evolution: the glutamate hypothesis of schizophrenia and its implication for treatment. *Neuropsychopharmacology* 37, 4–15. doi: 10.1038/npp.2011.181

Morales, D., Skoulakis, E. C., and Acevedo, S. F. (2012). 14-3-3s are potential biomarkers for HIV-related neurodegeneration. *J. Neurovirol.* 18, 341–353. doi: 10.1007/s13365-012-0121-2

Neal, C. L., and Yu, D. (2010). 14-3-3zeta as a prognostic marker and therapeutic target for cancer. *Expert Opin. Ther. Targets* 14, 1343–1354. doi: 10.1517/14728222.2010.531011

Nilsson, J., Gobom, J., Sjodin, S., Brinkmalm, G., Ashton, N. J., Svensson, J., et al. (2021). Cerebrospinal fluid biomarker panel for synaptic dysfunction in Alzheimer's disease. *Alzheimers Dement.* 13:e12179. doi: 10.1002/dad2.12179

Qiao, H., Foote, M., Graham, K., Wu, Y., and Zhou, Y. (2014). 14-3-3 proteins are required for hippocampal long-term potentiation and associative learning and memory. *J. Neurosci.* 34, 4801–4808. doi: 10.1523/JNEUROSCI.4393-13.2014

Qing, Y., Sun, L., Yang, C., Jiang, J., Yang, X., Hu, X., et al. (2016). Dysregulated 14-3-3 Family in peripheral blood leukocytes of patients with schizophrenia. *Sci. Rep.* 6:23791. doi: 10.1038/srep23791

Ramsey, A. J., Milenkovic, M., Oliveira, A. F., Escobedo-Lozoya, Y., Seshadri, S., Salahpour, A., et al. (2011). Impaired NMDA receptor transmission alters striatal synapses and DISC1 protein in an age-dependent manner. *Proc. Natl. Acad. Sci. U.S.A.* 108, 5795–5800. doi: 10.1073/pnas.1012621108

Ramshaw, H., Xu, X., Jaehne, E. J., McCarthy, P., Greenberg, Z., Saleh, E., et al. (2013). Locomotor hyperactivity in 14-3-3zeta KO mice is associated with dopamine transporter dysfunction. *Transl. Psychiatry* 3:e327. doi: 10.1038/tp.2013.99

Rivero, G., Gabilondo, A. M., Garcia-Sevilla, J. A., La Harpe, R., Morentin, B., and Meana, J. J. (2015). Up-regulated 14-3-3beta and 14-3-3zeta proteins in prefrontal cortex of subjects with schizophrenia: effect of psychotropic treatment. *Schizophr. Res.* 161, 446–451. doi: 10.1016/j.schres.2014.12.014

Schubert, K. O., Focking, M., and Cotter, D. R. (2015). Proteomic pathway analysis of the hippocampus in schizophrenia and bipolar affective disorder implicates 14-3-3 signaling, aryl hydrocarbon receptor signaling, and glucose metabolism: potential roles in GABAergic interneuron pathology. *Schizophr. Res.* 167, 64–72. doi: 10.1016/j.schres.2015.02.002

Sekiguchi, H., Iritani, S., Habuchi, C., Torii, Y., Kuroda, K., Kaibuchi, K., et al. (2011). Impairment of the tyrosine hydroxylase neuronal network in the orbitofrontal cortex of a genetically modified mouse model of schizophrenia. *Brain Res.* 1392, 47–53. doi: 10.1016/j.brainres.2011.03.058

Steinacker, P., Schwarz, P., Reim, K., Brechlin, P., Jahn, O., Kratzin, H., et al. (2005). Unchanged survival rates of 14-3-3gamma knockout mice after inoculation with pathological prion protein. *Mol. Cell Biol.* 25, 1339–1346. doi: 10.1128/MCB.25.4.1339-1346.2005

Takahashi, T., Nakamura, Y., Nakamura, Y., Aleksic, B., Takayanagi, Y., Furuichi, A., et al. (2014). The polymorphism of YWHAE, a gene encoding 14-3-3epsilon, and orbitofrontal sulcogyral pattern in patients with schizophrenia and healthy subjects. *Prog. Neuropsychopharmacol. Biol. Psychiatry* 51, 166–171. doi: 10.1016/j.pnpbp.2014.02.005

Takahashi, Y. (2003). The 14-3-3 proteins: gene, gene expression, and function. *Neurochem. Res.* 28, 1265–1273. doi: 10.1023/a:1024296932670

Taya, S., Shinoda, T., Tsuboi, D., Asaki, J., Nagai, K., Hikita, T., et al. (2007). DISC1 regulates the transport of the NUDEL/LIS1/14-3-3epsilon complex through kinesin-1. *J. Neurosci.* 27, 15–26. doi: 10.1523/JNEUROSCI.3826-06.2006

Torrico, B., Anton-Galindo, E., Fernandez-Castillo, N., Rojo-Francas, E., Ghorbani, S., Pineda-Cirera, L., et al. (2020). Involvement of the 14-3-3 gene family in autism spectrum disorder and schizophrenia: genetics, transcriptomics and functional analyses. *J. Clin. Med.* 9:1851. doi: 10.3390/jcm9061851

Toyooka, K., Muratake, T., Tanaka, T., Igarashi, S., Watanabe, H., Takeuchi, H., et al. (1999). 14-3-3 protein eta chain gene (YWHAH) polymorphism and its genetic association with schizophrenia. *Am. J. Med. Genet.* 88, 164–167. doi: 10.1002/(sici)1096-8628(19990416)88:2<164::aid-ajmg13>3.0.co;2-3

Toyo-oka, K., Shionoya, A., Gambello, M. J., Cardoso, C., Leventer, R., Ward, H. L., et al. (2003). 14-3-3Epsilon is important for neuronal migration by binding to NUDEL: a molecular explanation for Miller-Dieker syndrome. *Nat. Genet.* 34, 274–285. doi: 10.1038/ng1169

Toyo-oka, K., Wachi, T., Hunt, R. F., Baraban, S. C., Taya, S., Ramshaw, H., et al. (2014). 14-3-3epsilon and zeta regulate neurogenesis and differentiation of neuronal progenitor cells in the developing brain. *J. Neurosci.* 34, 12168–12181. doi: 10.1523/JNEUROSCI.2513-13.2014

Van Everbroeck, B., Boons, J., and Cras, P. (2005). Cerebrospinal fluid biomarkers in Creutzfeldt-Jakob disease. *Clin. Neurol. Neurosurg.* 107, 355–360. doi: 10.1016/j.clineuro.2004.12.002

van Hemert, M. J., Steensma, H. Y., and van Heusden, G. P. (2001). 14-3-3 proteins: key regulators of cell division, signalling and apoptosis. *Bioessays* 23, 936–946. doi: 10.1002/bies.1134

Vawter, M. P., Barrett, T., Cheadle, C., Sokolov, B. P., Wood, W. H. III, Donovan, D. M., et al. (2001). Application of cDNA microarrays to examine gene expression differences in schizophrenia. *Brain Res. Bull.* 55, 641–650. doi: 10.1016/s0361-9230(01)00522-6

Vega-Quiroga, I., Yarur, H. E., and Gysling, K. (2018). Lateral septum stimulation disinhibits dopaminergic neurons in the antero-ventral region of the ventral tegmental area: role of GABA-A alpha 1 receptors. *Neuropharmacology* 128, 76–85. doi: 10.1016/j.neuropharm.2017.09.034

Volavka, J., Czobor, P., Sheitman, B., Lindenmayer, J. P., Citrome, L., McEvoy, J. P., et al. (2002). Clozapine, olanzapine, risperidone, and haloperidol in the treatment of patients with chronic schizophrenia and schizoaffective disorder. *Am. J. Psychiatry* 159, 255–262. doi: 10.1176/appi.ajp.159.2.255

Wachi, T., Cornell, B., Marshall, C., Zhukarev, V., Baas, P. W., and Toyo-oka, K. (2016). Ablation of the 14-3-3gamma protein results in neuronal migration delay and morphological defects in the developing cerebral cortex. *Dev. Neurobiol.* 76, 600–614. doi: 10.1002/dneu.22335

Wachi, T., Cornell, B., and Toyo-Oka, K. (2017). Complete ablation of the 14-3-3epsilon protein results in multiple defects in neuropsychiatric behaviors. *Behav. Brain Res.* 319, 31–36. doi: 10.1016/j.bbr.2016.11.016

Wang, H., Zhang, L., Liddington, R., and Fu, H. (1998). Mutations in the hydrophobic surface of an amphipathic groove of 14-3-3zeta disrupt its interaction with Raf-1 kinase. *J. Biol. Chem.* 273, 16297–16304. doi: 10.1074/jbc.273.26.16297

Wang, H. S., Duan, S. W., Xing, Q. H., Du, J., Li, X. W., Xu, Y. F., et al. (2005). [Association study between NPY and YWHAH gene polymorphisms and schizophrenia]. *Yi Chuan Xue Bao* 32, 1235–1240.

Wong, A. H., Likhodi, O., Trakalo, J., Yusuf, M., Sinha, A., Pato, C. N., et al. (2005). Genetic and post-mortem mRNA analysis of the 14-3-3 genes that encode phosphoserine/threonine-binding regulatory proteins in schizophrenia and bipolar disorder. *Schizophr. Res.* 78, 137–146. doi: 10.1016/j.schres.2005.06.009

Wong, A. H., Macciardi, F., Klempan, T., Kawczynski, W., Barr, C. L., Lakatoo, S., et al. (2003). Identification of candidate genes for psychosis in rat models, and possible association between schizophrenia and the 14-3-3eta gene. *Mol. Psychiatry* 8, 156–166. doi: 10.1038/sj.mp.4001237

Wu, J. Q., Wang, X., Beveridge, N. J., Tooney, P. A., Scott, R. J., Carr, V. J., et al. (2012). Transcriptome sequencing revealed significant alteration of cortical

promoter usage and splicing in schizophrenia. *PLoS One* 7:e36351. doi: 10.1371/journal.pone.0036351

Xu, X., Jaehne, E. J., Greenberg, Z., McCarthy, P., Saleh, E., Parish, C. L., et al. (2015). 14-3-3zeta deficient mice in the BALB/c background display behavioural and anatomical defects associated with neurodevelopmental disorders. *Sci. Rep.* 5:12434. doi: 10.1038/srep12434

Yaffe, M. B., Rittinger, K., Volinia, S., Caron, P. R., Aitken, A., Leffers, H., et al. (1997). The structural basis for 14-3-3:phosphopeptide binding specificity. *Cell* 91, 961–971. doi: 10.1016/s0092-8674(00)80487-0

Zeng, T., and Tan, L. (2018). 14-3-3eta protein: a promising biomarker for rheumatoid arthritis. *Biomark. Med.* 12, 917–925. doi: 10.2217/bmm-2017-0385

Zhang, J., Navarrete, M., Wu, Y., and Zhou, Y. (2022). 14-3-3 Dysfunction in dorsal hippocampus CA1 (dCA1) induces psychomotor behavior via a dCA1-Lateral septum-ventral tegmental area pathway. *Front. Mol. Neurosci.* 15:817227. doi: 10.3389/fnmol.2022.817227

Conflict of Interest: The authors declare that the research was conducted in the absence of any commercial or financial relationships that could be construed as a potential conflict of interest.

Publisher's Note: All claims expressed in this article are solely those of the authors and do not necessarily represent those of their affiliated organizations, or those of the publisher, the editors and the reviewers. Any product that may be evaluated in this article, or claim that may be made by its manufacturer, is not guaranteed or endorsed by the publisher.

Copyright © 2022 Navarrete and Zhou. This is an open-access article distributed under the terms of the Creative Commons Attribution License (CC BY). The use, distribution or reproduction in other forums is permitted, provided the original author(s) and the copyright owner(s) are credited and that the original publication in this journal is cited, in accordance with accepted academic practice. No use, distribution or reproduction is permitted which does not comply with these terms.

frontiers in Cellular Neuroscience

REVIEW
published: 24 March 2022
doi: 10.3389/fncel.2022.820378

RNA N6-Methyladenosine Modifications and Its Roles in Alzheimer's Disease

Runjiao Zhang[1,2], *Yizhou Zhang*[1,2,3], *Fangzhen Guo*[1,2], *Sha Li*[1,2,3]* *and Huixian Cui*[1,2,3]*

[1] Department of Anatomy, Hebei Medical University, Shijiazhuang, China, [2] Neuroscience Research Center, Hebei Medical University, Shijiazhuang, China, [3] Hebei Key Laboratory of Neurodegenerative Disease Mechanism, Shijiazhuang, China

The importance of epitranscriptomics in regulating gene expression has received widespread attention. Recently, RNA methylation modifications, particularly N6-methyladenosine (m^6A), have received marked attention. m^6A, the most common and abundant type of eukaryotic methylation modification in RNAs, is a dynamic reversible modification that regulates nuclear splicing, stability, translation, and subcellular localization of RNAs. These processes are involved in the occurrence and development of many diseases. An increasing number of studies have focused on the role of m^6A modification in Alzheimer's disease, which is the most common neurodegenerative disease. This review focuses on the general features, mechanisms, and functions of m^6A methylation modification and its role in Alzheimer's disease.

Keywords: Alzheimer's disease, demethylase, methyltransferase, methylation-binding protein, memory disorder, N6-methyladenosine

OPEN ACCESS

Edited by:
Daniela Tropea,
Trinity College Dublin, Ireland

Reviewed by:
Francesco Rusconi,
University of Milan, Italy
Brandon Walters,
University of Toronto Mississauga, Canada

***Correspondence:**
Sha Li
lisha@hebmu.edu.cn
Huixian Cui
cuihx@hebmu.edu.cn

Specialty section:
This article was submitted to Cellular Neuropathology, a section of the journal Frontiers in Cellular Neuroscience

Received: *12 January 2022*
Accepted: *28 February 2022*
Published: *24 March 2022*

Citation:
Zhang R, Zhang Y, Guo F, Li S and Cui H (2022) RNA N6-Methyladenosine Modifications and Its Roles in Alzheimer's Disease. Front. Cell. Neurosci. 16:820378. doi: 10.3389/fncel.2022.820378

INTRODUCTION

Epitranscriptomics, i.e., chemical modification used for RNA regulation, has recently emerged as a highly investigated subfield of neuroscience. In the early 1970s, RNA methylation modifications were discovered (Desrosiers et al., 1974). These include N6-methyladenosine (m^6A), N1-methyladenosine (m^1A), N6, 2-O-dimethyladenosine (m^6Am), 5-methylcytosine (m^5C), 5-hydroxymethylcytosine (5hmC), and 7-methylguanine (m^7G) (Chen et al., 2016). Among them, m^6A is the most common and abundant type of eukaryotic methylation modification in RNAs, including mRNAs, long non-coding RNAs (lncRNAs), circular RNAs (circRNAs), microRNAs (miRNAs), rRNAs, tRNAs, and small nuclear RNAs (snRNAs) (Yue et al., 2015; Du et al., 2018; Shi et al., 2019). The adenine in the RRACH sequence (R = adenine or guanine, and H = cytosine, adenine, or uracil) is usually the site of m^6A modification (**Figure 1**; Deng et al., 2018). In mammals, m^6A methylation modification is widely distributed in many tissues, particularly in the brain (Meyer and Jaffrey, 2014). The abundance of m^6A and its emerging role as an important post-transcriptional regulator in the mammalian brain has gained wide attention in the field of neuroepigenetics (Chang et al., 2017).

Alzheimer's disease (AD), the most frequently and commonly diagnosed dementia, is an increasing global health concern with a notable impact on human health (Guo et al., 2020). Despite significant advances in our understanding of AD pathogenesis and the definition of the disease since the first case reported by Alzheimer (1907), there are still no disease-modifying treatments (Pakavathkumar et al., 2017). Altered m^6A-methylation has been considered associated with AD

FIGURE 1 | The canonical RRACH motif. R, adenine or guanine; H, cytosine, adenine, or uracil.

as many players in the m^{6}A pathway have been implicated as critical factors in neuronal function (Shafik et al., 2021).

In this review, we will focus on the general features, functions, and adjustability of m^{6}A methylation modifications and their role in AD.

RNA N6-METHYLADENOSINE METHYLATION MODIFICATION PROTEIN

The m^{6}A modification of RNA has been proven to be reversible, as it is bidirectionally regulated by m^{6}A methyltransferase and demethylase, which work with RNA m^{6}A methylation-binding protein to regulate the fate of RNAs (Knuckles and Bühler, 2018; Widagdo and Anggono, 2018). These proteins have served as valuable tools for investigating the cellular and physiological roles of m^{6}A methylation modification in the brain.

N6-Methyladenosine Methyltransferase

The m^{6}A methyltransferases, also known as "Writers" in RNA m^{6}A methylation modification, catalyze the transfer of a methyl group from S-adenosyl methionine (SAM) to adenine nucleotides of RNA substrates. Some "Writers," including methyltransferases such as 3/14 (METTL3/14), Wilms' tumor 1-associating protein (WTAP), KIAA1429, and RNA-binding motifs protein 15/15B (RBM15/15B), form the core components of m^{6}A methyltransferase, which work together to catalyze methylation of RNA substrates (Liu et al., 2020). In addition, zinc finger CCCH-type containing 13 (ZC3H13) and E3 ubiquitin-protein ligase Hakai (HAKAI) are also components of this complex. Moreover, recent studies have found that methyltransferase-like 16 (METTL16) can catalyze the methylation of target RNAs alone, without relying on the above m^{6}A methyltransferase complexes (Pendleton et al., 2017).

METTL3 (**Figures 2**, **3A**) is the best-known m^{6}A methyltransferase. It is identified as a SAM-binding component in the complex and has its own catalytic ability. Unlike METTL3, METTL14 (**Figures 2**, **3B**) does not bind to the SAM domain performing its own m^{6}A methyltransferase catalytic ability but plays a key role in substrate identification. Biochemical and structural studies have revealed that METTL3 and METTL14 form a heterodimer (**Figure 3C**; Wang et al., 2016) that has a higher methylation activity than METTL3 alone (Liu et al., 2014; Wang et al., 2017). WTAP (**Figures 2**, **3D**) is a regulatory subunit of the complex that interacts with METTL3 and METTL14 and localizes the METTL3-METTL14 complex to the nucleus (Ping et al., 2014; Schwartz et al., 2014). KIAA1429 (**Figures 2**, **3E**) can mediate preferential mRNA methylation in 3'UTR and near stop codon and is also known as vir-like m^{6}A methyltransferase-associated (VIRMA), whose N-terminus has the ability to recruit the METTL3/METTL14/WTAP complex (Yue et al., 2018). RBM15/15B (**Figures 2**, **3F,G**) was three- to four-fold higher at the RRACH sequence site than at the non-methylation site. Knockdown of RBM15/15B decreases m^{6}A levels in cellular mRNA (Knuckles et al., 2018). ZC3H13 (**Figures 2**, **3H**) and HAKAI (**Figures 2**, **3I**) are also components of the methyltransferase complex. ZC3H13 anchors the complex to the nucleus (Wen et al., 2018), and HAKAI regulates m^{6}A levels in *Arabidopsis* (Růžička et al., 2017). Additionally, METTL16 (**Figures 1**, **3J**; Doxtader et al., 2018) is also known as RNA m^{6}A methyltransferase, an enzyme that maintains SAM homeostasis (Shima et al., 2017; Warda et al., 2017; Aoyama et al., 2020). METTL16 does not form complexes with other m^{6}A methyltransferases, and has a distinct set of targets for m^{6}A modification, including the 3′-untranslated region (UTR) of MAT2A mRNA and U6 snRNA.

N6-methyladenosine methyltransferases are mainly localized in the nucleus (Ping et al., 2014), which is consistent with the m^{6}A-binding site found in nascent pre-mRNAs or pri-miRNAs (Ping et al., 2014; Ke et al., 2017; Slobodin et al., 2017). Interestingly, METTL3 catalyzes the methylation of mature mRNAs and has a non-methylating function in the cytoplasm (Lin et al., 2019; Liu et al., 2020). Lin et al. (2016) found that METTL3 was associated with ribosomes and promoted mRNA translation in the cytoplasm. Additionally, METTL16 functions independently of m^{6}A methylation. In SAM-limiting conditions, METTL16 occupancy of a hairpin (hp1) in the MAT2A 3′-UTR induces splicing of the MAT2A-retained intron, which controls the production of SAM (Pendleton et al., 2017). Thus, while m^{6}A methyltransferases generally affect RNA processing through m^{6}A "Readers," direct contributions of methyltransferases to RNA metabolism should not be overlooked (Pendleton et al., 2017; Doxtader et al., 2018).

N6-Methyladenosine Demethylase

The m^{6}A demethylases, also known as "Erasers" in RNA m^{6}A methylation modification, catalyze the demethylation of RNA substrates modified by m6A. In eukaryotes, fat mass and obesity-associated protein (FTO) and AlkB homolog 5 (ALKBH5) were both found to be demethylases. These enzymes belong to the AlkB family of the dioxygenase superfamily and have a similar catalytic core, although they prefer different substrates and are expressed in different organs (Gerken et al., 2007; Zheng et al., 2013; Zou et al., 2016; Liu et al., 2020).

Fat mass and obesity (**Figures 2**, **3K**; Han et al., 2010), also known as AlkB homolog 9 (ALKBH9), was the first discovered RNA m^{6}A demethylase. FTO is mainly detected in the nucleus, similarly to the m^{6}A methyltransferase (Jia et al., 2011). Its long stem-loop domain at the C-terminus enables substrate RNA demethylation (Jia et al., 2011; Bartosovic et al., 2017). However, Hess et al. (2013) only found 5,000

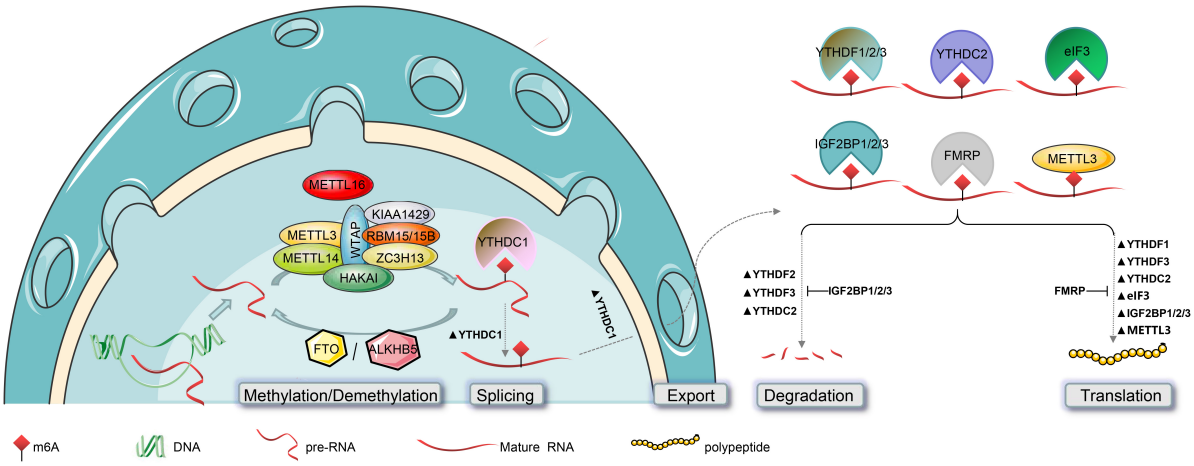

FIGURE 2 | Post-transcriptional modification of RNA by m^{6}A and its functions. The biogenesis of m^{6}A in the mammalian nucleus is catalyzed by the methyltransferase complex (composed of METTL3, METTL14, WTAP, KIAA1429, RBM15/15B, ZC3H13, and HAKAI) or METTL16, and is reversed by m^{6}A-demethylase (FTO or ALKBH5). The functional effects of m^{6}A on RNAs can affect their nuclear splicing, nuclear export, stability, and translation efficiency. This is mediated by m^{6}A "Readers," such as YTHDC1 in the nucleus, and YTHDF1/2/3, YTHDC2, eIF3, IGF2BP1/2/3, and FMRP in the cytoplasm. Notably, in addition to catalyzing m^{6}A methylation, METTL3 also directly promotes RNA translation.

new m^{6}A peaks in FTO-knockout mice, compared with 42,000 peaks in the control samples. These data indicated that FTO does not globally target all m6A-modified mRNAs, or which seems to imply that another m^{6}A "Eraser," ALKHB5, compensates for the lack of FTO. ALKBH5 (**Figures 2**, **3L**) is similar to FTO and is also a Fe^{2+} and α-Ketoglutaric acid-dependent non-heme oxygenase (Zheng et al., 2013; Feng et al., 2014).

RNA N6-Methyladenosine Methylation-Binding Protein

The m^{6}A binding proteins, also known as "Readers," in RNA m^{6}A methylation modification, specifically bind to the m^{6}A methylation region, weakening the homologous binding to RNA reading proteins, and altering the secondary structure of RNA to alter protein–RNA interaction (Li et al., 2019). This function is widely implicated in the stability, translation, alternative splicing, and subcellular targeting of specific RNAs by recruiting or repelling some RNA-binding proteins (RBPs) or by altering the secondary structure of targeted RNAs (Adhikari et al., 2016; Wu et al., 2017; Widagdo and Anggono, 2018). Many "Readers," including YTH domain-containing RNA-binding protein (YTP), fragile X mental retardation protein (FMRP), heterogeneous nuclear ribonucleoprotein (HNRNP), eukaryotic initiation factor 3 (eIF3), insulin-like growth factor 2 mRNA-binding protein (IGF2BP), and proline-rich coiled-coil 2A (PRRC2A), have already been identified.

YTH domain-containing RNA-binding protein includes YTH domain-containing family protein 1/2/3 (YTHDF1/2/3) (**Figures 2**, **3M–O**; Li et al., 2014, 2020; Xu et al., 2015) and YTH domain-containing protein 1/2 (YTHDC1/2) (**Figures 2**, **3P,Q**; Ma et al., 2019; Li Y. et al., 2021). Their YTH domains are capable of combining with the m^{6}A RRACH sites to mediate RNA-specific binding, while their proline/glutamine/asparagine-enriched (P/Q/N-rich) domains regulate the subcellular localization of target RNA (Liao et al., 2018; Patil et al., 2018). YTHDF1/2/3 and YTHDC2 play specific roles in the cytoplasm, and YTHDC1 plays a role in the nucleus. It is generally considered that YTHDF1 enhances mRNA translation by promoting ribosome occupancy and interacting with initiation factors, YTHDF2 promotes mRNA degradation by localizing m^{6}A-modified RNA to mRNA decay sites, and YTHDF3 enhances translation along with YTHDF1 and promotes degradation along with YTHDF2 in the cytoplasm (Wang et al., 2014; Li A. et al., 2017; Shi et al., 2017, 2018). However, Zaccara and Jaffrey (2020) showed that YTHDF1/2/3 co-regulated mRNA degradation rather than promoting mRNA translation in HeLa cells. Similar to YTHDF3, YTHDC2 in the cytoplasm accelerates degradation of the modified mRNA and enhances the translation of the corresponding protein by recognizing m^{6}A (Hsu et al., 2017). Additionally, YTHDC1 regulates m^{6}A-dependent mRNA splicing by recruiting splicing factors and mediates the nuclear export of m^{6}A methylated mRNAs by interacting with the nuclear export adaptor protein SRSF3 (Xu et al., 2014; Xiao et al., 2016; Roundtree et al., 2017). Briefly, YTHDF1/2/3 and YTHDC2 promote the metabolism of m^{6}A-modified mRNAs, but YTHDC1 regulates their splicing (**Figure 2**; Wang et al., 2014; Xiao et al., 2016; Hsu et al., 2017; Li A. et al., 2017; Shi et al., 2017, 2018; Zaccara and Jaffrey, 2020).

Fragile X mental retardation protein, an RBP (**Figures 2**, **3R**; Myrick et al., 2015), negatively regulates the translation of mRNAs by interacting with m^{6}A sites and then recruits RNA-induced silencing complexes and some miRNAs to arrest ribosomal elongation (Darnell et al., 2011; Suhl et al., 2014; Richter et al., 2015; Arguello et al., 2017; Chang et al., 2017).

Heterogeneous nuclear ribonucleoprotein is a group of RBPs that includes nearly 30 proteins, named A1 to U, which can

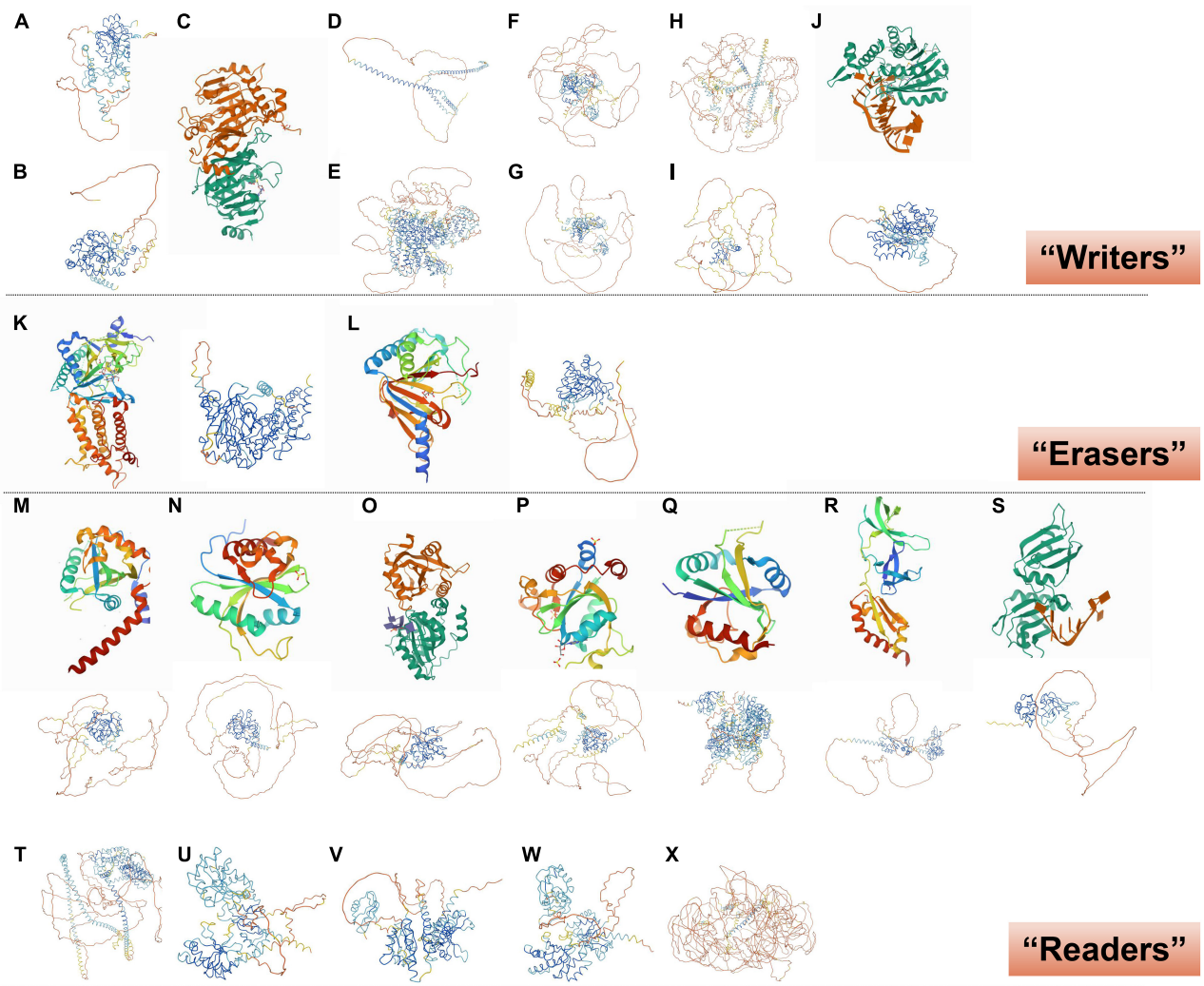

FIGURE 3 | Crystal structure of RNA m^{6}A methylation-modification enzymes. **(A)** METTL3 and **(B)** METTL14, predicted from "AlphaFold." **(C)** SAM-bound METTL3-METTL14 complex (Wang et al., 2016). **(D)** WTAP, **(E)** KIAA1429, **(F)** RBM15, **(G)** RBM15B, **(H)** ZC3H13, and **(I)** HAKAI, predicted from "AlphaFold." **(J)** Human METTL16 catalytic domain in complex with MAT2A 3'-UTR hairpin 6 (Upper; Doxtader et al., 2018); METTL16, predicted from "AlphaFold" (Lower). **(K)** FTO reveals the basis for its substrate specificity (Left; Han et al., 2010); FTO, predicted from "AlphaFold" (Right). **(L)** Human ALKBH5 in complex with citrate and acetate (Left; Feng et al., 2014); ALKBH5, predicted from "AlphaFold" (Right). **(M)** YTHDF1 YTH domain (Upper; Xu et al., 2015); YTHDF1, predicted from "AlphaFold" (Lower). **(N)** YTH-YTHDF2 in the free state (Upper; Li et al., 2014); YTHDF2, predicted from "AlphaFold" (Lower). **(O)** YTHDF3 YTH domain in complex with m^{6}A RNA (Upper; Li et al., 2020); YTHDF3, predicted from "AlphaFold" (Lower). **(P)** YTHDC1 with m^{6}A (Upper; Li Y. et al., 2021); YTHDC1, predicted from "AlphaFold" (Lower). **(Q)** Human YTHDC2 YTH domain (Upper; Ma et al., 2019); YTHDC2, predicted from "AlphaFold" (Lower). **(R)** N-terminal domain of FMRP (Upper; Myrick et al., 2015); FMRP, predicted from "AlphaFold" (Lower). **(S)** HNRNPA2B1 in complex with RNA (Upper; Wu et al., 2018); HNRNPA2B1, predicted from "AlphaFold" (Lower). **(T)** Eif3, **(U)** IGF2BP1, **(V)** IGF2BP2, **(W)** IGF2BP3, and **(X)** PRRC2A, predicted from "AlphaFold."

interact with each other to form a complex. The most studied heterogeneous nuclear ribonucleoprotein A2/B1 (HNRNPA2B1) (**Figure 3S**; Wu et al., 2018) binds directly to a set of nuclear transcripts with m^{6}A marks, and activates downstream variable shear events of partial genes (Alarcón et al., 2015; Geissler et al., 2016).

The eIF3 protein (**Figures 2**, **3T**) facilitates the translation of mRNA by binding to the m^{6}A sites of mRNA 5′-UTRs directly. In addition, IGF2BP, including IGF2BP1/2/3 (**Figures 2**, **3U–W**), promotes mRNA stability and translation by recognizing the GG (m^{6}A) C sequence (Huang et al., 2018). PRRC2A (**Figure 3X**) stabilizes mRNA expression by binding to the consensus GGACU motif in the coding sequence (CDS) region of mRNA in an m^{6}A-dependent manner (Wu et al., 2019).

ADJUSTABILITY OF RNA N6-METHYLADENOSINE METHYLATION

The dynamic nature of chemical modifications is an essential feature of functionality in the nervous system (Widagdo and Anggono, 2018). RNA m^{6}A methylation, as the most abundant

internal RNA modification, contributes markedly to this. Not surprisingly, RNA m^{6}A methylation is precisely regulated.

Activity-Dependent Regulation of N6-Methyladenosine

Previous studies have demonstrated that cellular m^{6}A levels are dynamically regulated in response to hypoxia, heat shock, and ultraviolet irradiation in cells (Dominissini et al., 2012; Meyer et al., 2015; Zhou et al., 2015; Zhang et al., 2016; Xiang et al., 2017; Lu et al., 2019). In the mammalian central nervous system, stimulus-dependent regulation of m^{6}A has recently been shown to occur in response to behavioral training, cell microenvironment changes, and nerve injury (Widagdo et al., 2016; Engel et al., 2018; Shi et al., 2018; Weng et al., 2018; Zhang et al., 2018).

KCl is used to activate neurons by increasing membrane potentials in cells and opening voltage-gated calcium ion channels in cell membranes (Rosen et al., 1994; Lakk et al., 2017). m^{6}A methylation of RNAs is upregulated following administration of KCl to primary neuronal cultures (Widagdo et al., 2016). Behavioral training is another way to stimulate neurons. Widagdo et al. (2016) discovered that the percentage of m^{6}A-occupancies RNAs increased significantly in the medial prefrontal cortex after cued fear conditioning. A similar increase in the levels of m^{6}A methylation was also observed in the dorsal hippocampus following contextual fear conditioning (Walters et al., 2017). Interestingly, activity-dependent m^{6}A RNA modification has been found to occur in many immediate early genes and synaptic plasticity-related transcripts (Widagdo et al., 2016; Shi et al., 2018; Zhang et al., 2018). However, acute restraint-stress reduced global m^{6}A levels in the mouse prefrontal cortex (Engel et al., 2018), which requires further investigation.

Tissue, Cellular/Subcellular, and Site-Specific Regulation of N6-Methyladenosine

More intriguingly, dynamic adjustability of m^{6}A has been demonstrated in different brain regions, such as the prefrontal cortex, hippocampus, and amygdala (Widagdo et al., 2016; Walters et al., 2017; Engel et al., 2018). Shafik et al. (2021) revealed that this tissue specificity was most pronounced in the hypothalamus.

As different brain areas include different types of cells, it is reasonable to speculate that RNA m^{6}A methylation may have cellular and subcellular specificity. Although the transcriptomic profiles of m^{6}A in neuronal subpopulations have yet to be established, bioinformatics analysis showed RNA m^{6}A methylation-enrichment in genes specific to neuronal subtypes (Chang et al., 2017), which implies a particular bias for m^{6}A toward RNAs in neurons rather than in glial cells. Furthermore, the m^{6}A-modified transcripts were widespread in a position distal from the neuronal cell body, indicating an interesting mode of m^{6}A regulation outside of the nucleus. Indeed, some immunocytochemical assays and biochemical subcellular fractionation tests have revealed that some m^{6}A "Writers" (METTL3, METTL14, METTL16), "Erasers" (FTO, ALKBH5), and "Readers" (YTHDF1/2/3) are present in the extra-somatic regions of neurons (Gershoni-Emek et al., 2016; Merkurjev et al., 2018; Yu et al., 2018; Nance et al., 2020). This localization of m^{6}A "Writers" and "Erasers" in the extra-somatic regions may expedite the dynamic regulation efficiency of neurons (Widagdo and Anggono, 2018) in response to changes in the extracellular milieu, although most of the work may still be done in the soma. The localization of m^{6}A in axons and its role in axonal growth has also been studied (Yu et al., 2018). An axonal elongation factor, Gap-43, was found to be an mRNA target of m^{6}A. The local translation of Gap-43 was negatively modulated by m^{6}A methylation and could be regulated by FTO in axons (Yu et al., 2018). In addition, the function of m^{6}A has been observed in the synapses. In the pre-and postsynaptic compartments of neuron, most of the m^{6}A target genes fell into the Gene Ontology functional terms "cell junction" and "synapse," as well as surface receptor pathways, all of which maintain the functionality and integrity of synapses (Merkurjev et al., 2018).

Furthermore, the sites of m^{6}A modification were found to be non-randomly distributed within genes (94.8%), where the proportions of CDS, UTRs, and introns were 50.9%, 41.9%, and 2.0%, respectively (**Figure 4A**; Meyer et al., 2012; Deng et al., 2018). Although the frequency of the RRACU sequence in last exons was the same as that in other exons (**Figure 4B**), m^{6}A was found to be enriched within the last exons of a gene (**Figures 4C,D**; Ke et al., 2015).

Developmental Stage-Specific Regulation of N6-Methyladenosine

Studies of m^{6}A modifications have highlighted the need to maintain transcriptomic dynamics during neurodevelopment. The expression pattern of m^{6}A indeed differs across various developmental phases (Meyer et al., 2012; Yoon et al., 2017). Shafik et al. (2021) also found that m6A exerted a critical function in both early and late brain development in a spatio-temporal fashion.

Prenatally, m^{6}A modification is markedly increased throughout brain development (Meyer et al., 2012). Changing the m^{6}A methylation modification by interfering with the expression levels of m^{6}A "Writers" or "Erasers" leads to defects in brain development. The loss of m^{6}A in embryonic neuronal progenitor cells by conditionally deleting METTL14 in embryonic mouse braiTablens resulted in delayed differentiation and prolonged cell cycle progression, extending cortical neurogenesis into the postnatal stages (Yoon et al., 2017). An abnormal increase of m^{6}A by knocking out FTO caused cerebellar shrinkage and impaired spatial learning and memory (Li L. et al., 2017), which might be due to the increase in m^{6}A promoting the decomposition of mRNAs encoding proteins with known functions in neuronal differentiation, stem cells, and the cell cycle (Yoon et al., 2017).

Postnatally, the function of m^{6}A in neurogenesis was first uncovered in FTO-knockout mice (Li L. et al., 2017). Loss of FTO in FTO-knockout mice resulted in decreased proliferation and differentiation and reduced numbers of adult neural stem cells. In addition to the aforementioned central nervous system, loss of FTO in FTO-knockout mice also led to a shorter

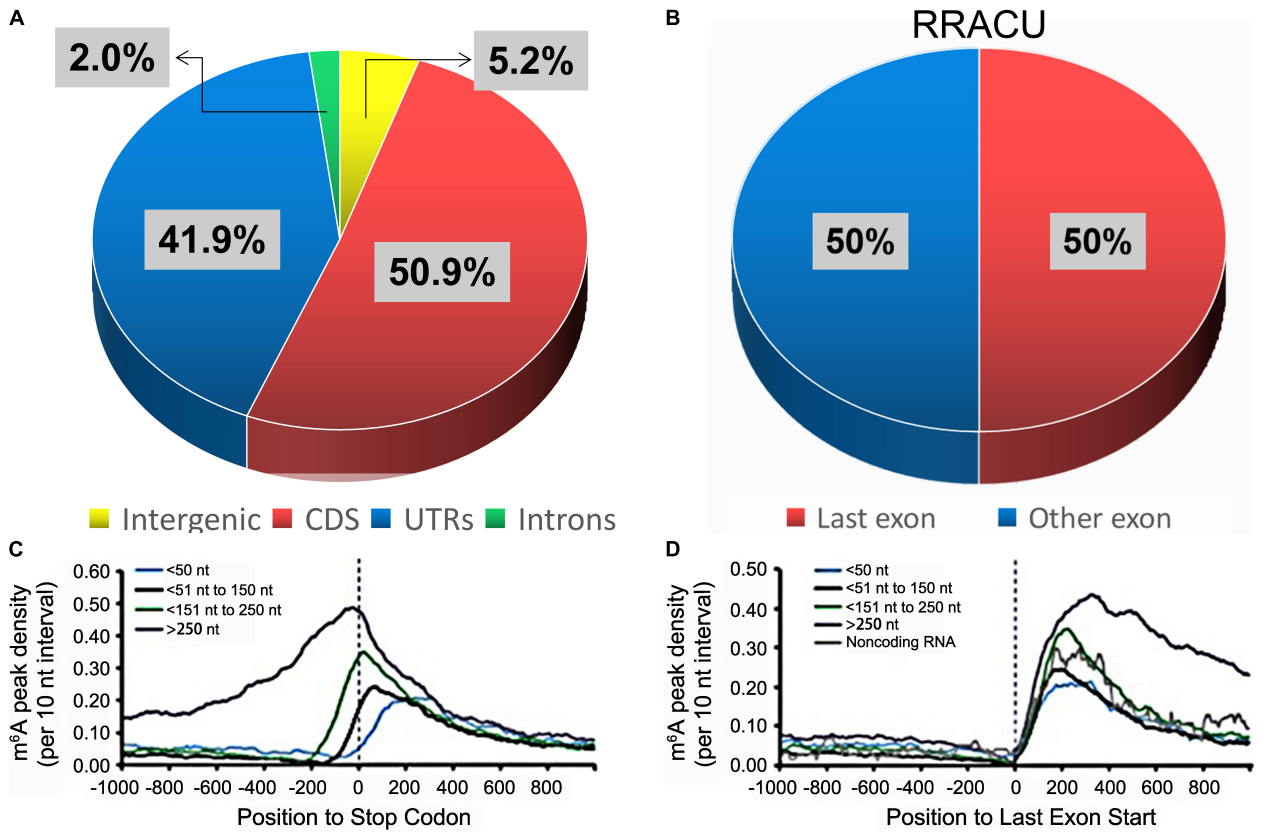

FIGURE 4 | The distributions of m^{6}A peaks. **(A)** The percentage of m^{6}A peaks within distinct RNA sequence types. **(B)** The relative proportions of RRACU motifs in the last exon and other exons, with 100% representing all RRACU sequences in mRNA (Ke et al., 2015). **(C,D)** In the last exon, m^{6}A density increased sharply (Ke et al., 2015). mRNAs were grouped according to their stop codon locations relative to the start of the last exon **(D)**.

axonal length in mouse dorsal root ganglia neurons (Widagdo and Anggono, 2018). Taken together, these results suggest that balanced m^{6}A modification plays a significant role in the establishment and development of the mammalian central and peripheral nervous systems.

MicroRNA Regulation of N6-Methyladenosine-Related Enzymes

MicroRNAs, which are approximately 22-nucleotide single-strand sequences, are a group of important post-transcriptional regulators in eukaryotes, which affect RNA m^{6}A methylation by targeting m^{6}A "Writers," "Erasers," and "Readers" in terms of both their functions and expression. It has been reported that manipulation of some miRNA sequences or their expression altered m^{6}A methylation modification levels by regulating the binding of METTL3 to some mRNAs containing miRNA-binding sites (Chen et al., 2015). In addition, miR-33a, which targets the METTL3 3′-UTR, suppressed cell proliferation (Liu et al., 2020). miRNA-421-3p targeting the "Reader" YTHDF1 inhibited p65 mRNA translation to prevent inflammatory responses in cerebral ischemia/reperfusion injury (Zheng et al., 2020). miR-145 restrained the expression of YTHDF2 by targeting YTHDF2 mRNA, thus inhibiting cell proliferation. miR-744-5p targeting the "Reader" hnRNPC promoted ovarian cancer cell death (Chen et al., 2020).

RNA N6-METHYLADENOSINE METHYLATION IN ALZHEIMER'S DISEASE

Miao et al. (2020) observed that the frequency percentage of m^{6}A in genes was positively correlated with the length and number of exons (**Figures 5A,B**) but negatively correlated with GC content and gene distance to the adjacent gene (**Figures 5C,D**), which implies that RNA m^{6}A methylation is not random and disordered. Several recent reports have started to uncover the functional significance of m^{6}A regulation in *de novo* RNA transcripts, including nuclear splicing, stability, translation, and subcellular localization, suggesting that m^{6}A serves as a regulator to fine-tune many diseases precisely over time (Li et al., 2019). Indeed, m^{6}A has been identified as a conserved epitranscriptomic modification in many neurodegenerative diseases, such as AD (Hess et al., 2013; Engel and Chen, 2018; Shafik et al., 2021).

Just as m^{6}A methylation, AD has tissue, cellular/subcellular, and site-specificity, associated with environment and

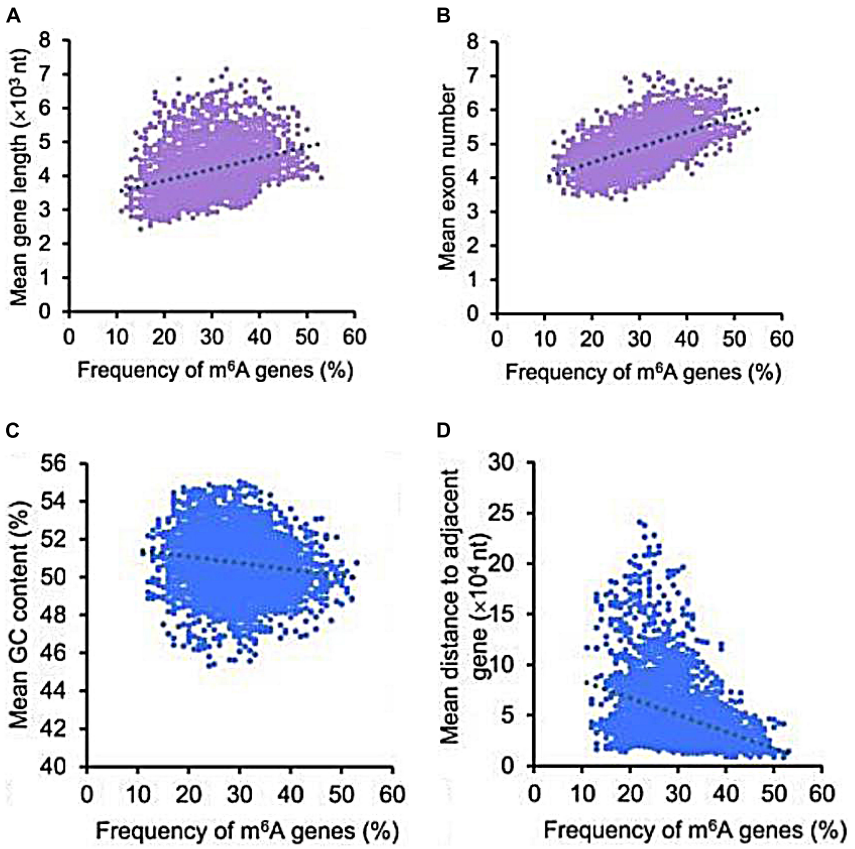

FIGURE 5 | The correlation of m^{6}A genes with multiple gene features. The frequency percentage of m^{6}A genes was positively correlated with the length **(A)** and number of exons **(B)**, but was negatively correlated with GC content **(C)** and gene distance to the adjacent gene **(D)** (Miao et al., 2020).

neurodevelopment and regulated by miRNAs. The progressive degeneration of hippocampal neurons is the main feature of AD. Mutations in the APP, PS1, and PS2 genes are considered the main causes of familial AD (Popugaeva et al., 2018). Environmental stimulation, such as infections, trauma, and radiofrequency radiation (Dasdag et al., 2020), is thought to induce sporadic AD. Neurodevelopment-related signaling pathways, such as Notch/Wnt/Reelin intracellular signaling pathways, may represent a novel approach to the regulation of neurodegenerative processes in AD (Grilli et al., 2003). In addition, the above-mentioned miRNAs that regulate m^{6}A are also considered to be involved in the pathogenesis of AD. Jaouen and Gascon (2016) described miR-33 function modulating ATP-binding cassette transporter A1 (ABCA1) and interfering with Aβ plaque formation through cholesterol metabolism regulation. Peña-Bautista et al. (2021) found hsa-miR-421 showed a positive correlation with some detected lipids (FA (16:0), FA (20:2), FA (18:2), FA (20:4), FA (20:3), FA (18:0), FA (14:0)) in AD plasma samples. Docosahexaenoic acids (DHA) are known to be beneficial in AD. miR-33a and miR-145 are regulated by DHA, and this regulation becomes disrupted in AD (Chiang, 2021).

RNA m^{6}A methylation has been considered to be an important epigenetic marker associated with AD disturbances, including mitochondrial dysfunction, neuroinflammatory response, oxidative stress, neurotoxic substance deposition, and memory deficits. Here, we will introduce them to AD one by one in the following.

N6-Methyladenosine and Mitochondrial Dysfunction of Alzheimer's Disease

The central nervous system requires approximately 20% of the body's total basal oxygen consumption to support neuronal energy expenditure. Mitochondria are organelles that are responsible for energy production. Therefore, neurons are damaged by mitochondrial deficiency. Mitochondrial dysfunction was observed in the brains of AD patients, even before the appearance of neurofibrillary tangles and senile plaques (Lim et al., 2020).

Some m^{6}A-related enzymes have been shown to affect mitochondrial function. The physiological role of METTL3 in mitochondria is under debate. Shi et al. (2021) considered that METTL3 preserved mitochondrial function in Down syndrome by reducing the expression of nuclear receptor-interacting protein 1 (NRIP1), a crucial gene in the regulation of the mitochondrial pathway. But Zhang et al. (2021) demonstrated that METTL3 and YTHDF2 cooperatively promoted mitochondrial dysfunction and inflammatory

response during oxLDL-induced inflammation in monocytes. In addition, the demethylase FTO inhibitor MO-I-500 was found to ameliorate astrocyte mitochondrial dysfunction in streptozotocin-induced AD cell models (Cockova et al., 2021).

N6-Methyladenosine and Neuroinflammatory Response of Alzheimer's Disease

An excessive neuroinflammatory response is harmful for the brain. Growing evidence shows that neuroinflammation is directly implicated in AD processes (Amor et al., 2014). Microglia are the main effectors in the neuroinflammatory process. Once overactivated, microglia may release proinflammatory cytokines and accelerate neurodegeneration.

Li Q. et al. (2021) identified a distinct m^{6}A epitranscriptome in microglia. They found that m^{6}A served as a novel and essential regulator of the anti-inflammatory and proinflammatory responses of microglia. An *in silico* analysis of immunoprecipitated methylated RNAs with microarrays also demonstrated that m^{6}A methylation was increased in major inflammatory pathways (Chokkalla et al., 2019), indicating that RNA m^{6}A methylation is closely related to neuroinflammation. Indeed, METTL3 was found to promote lipopolysaccharide (LPS)-induced neuroinflammation through the TRAF6/NF-κB pathway (Wen et al., 2020). LPS-induced neuroinflammation was considered might impair the efficient readout of neuronal genetic information and might contribute to a progressive disruption in the readout of genetic information in the AD brain (Zhao et al., 2017). The METTL3 knockdown was found to inhibit the inflammatory response by regulating the variable splicing of MyD88 (Feng et al., 2018).

N6-Methyladenosine and Oxidative Stress of Alzheimer's Disease

Oxidative stress plays a crucial role in AD pathogenesis. The brain is more vulnerable to oxidative stress than other organs, and most of the components of neurons (proteins, lipids, and nucleic acids) can be oxidized in AD (Bonda et al., 2010).

It has been reported that m^{6}A modification is affected by oxidative stress. The arsenic exposure hypothesis for AD provides a parsimonious testable hypothesis for the development and progression of this devastating disease to some degree (Gong and O'Bryant, 2010). Arsenite-induced oxidative stress possibly increases the levels of RNA m^{6}A methylation by regulating m^{6}A "Writers" or "Erasers," particularly promoting METTL14 and WTAP expression (Zhao et al., 2019). Additionally, m^{6}A modification is important in the regulation of oxidative stress. The m^{6}A-binding protein YTHDF1/3 was found to promote stress granule formation (Fu and Zhuang, 2020). Although associations *per se* cannot prove cause-effect relationships, the development of pathological stress granules has been implicated in the onset and progression of AD (Ash et al., 2014). The m^{6}A methyltransferase METTL3 was reported to attenuate oxidative stress and cell apoptosis in colistin-induced kidney injury by activating the antioxidant Keap1/Nrf2 pathway (Wang et al., 2019). The reduced neuronal m^{6}A modification in the hippocampus caused by METTL3 knockdown led to extensive synaptic loss and neuronal death along with multiple AD-related cellular alterations, including oxidative stress and aberrant cell cycle events *in vivo* (Zhao et al., 2021).

N6-Methyladenosine and Pathologic Hallmark of Alzheimer's Disease

Accumulation of insoluble neurotoxic aggregates, including extracellular amyloid (A)β plaques and intracellular tau neurofibrillary tangles, represents a major pathological hallmark of AD. Their accumulation leads to neuronal degeneration, synaptic dysfunction, and ultimately, dementia (Lane et al., 2018).

N6-Methyladenosine and Aβ Plaques

Folic acid, a water-soluble B vitamin, reduces the production of Aβ and slows the progression of AD by involving in generating S-adenosylmethionine (SAM), potentially enhancing the levels of RNA m^{6}A methylation (Li et al., 2015; Li N. et al., 2021), implying that RNA m^{6}A methylation may be involved in Aβ metabolism. Interestingly, Aβ treatment was found to have significantly reduced METTL3 and postsynaptic density-95 (PSD-95) expression in rat primary cortical neurons. On the contrary, METTL3 overexpression was found to rescue Aβ-induced synaptic PSD-95 loss *in vitro*. Importantly, METTL3 overexpression rescued synaptic damage and cognitive impairment in Aβ-induced AD mice. In addition, the demethylase FTO was reported to alleviate Aβ-induced cell degeneration via the PKA/CREB signaling pathway (Hu et al., 2020). In addition to targeting Aβ, m^{6}A methylation also altered the expression levels of Aβ production-related proteins, such as Aβ precursor protein (APP) and the β-site APP-cleaving enzyme (BACE1) (Kolisnyk et al., 2017; Edens et al., 2019). The m^{6}A "Reader" FMRP was found to regulate the local protein synthesis of neuronal synapses and change the nuclear output of m^{6}A-dependent mRNA by regulating APP mRNA translation (Chang et al., 2017; Edens et al., 2019). The downregulation of the "Reader" HNRNPA2B1 was shown to promote abnormal splicing of BACE1 (Kolisnyk et al., 2017).

N6-Methyladenosine and Tau Neurofibrillary Tangles

In human postmortem AD samples, Huang et al. (2020) observed METTL3 accumulation in the insoluble fractions, which correlated positively with levels of insoluble tau neurofibrillary tangles. This was accompanied by an increased level and redistribution of METTL3 expression in the AD hippocampus, likely representing aberrant misfolding and/or aggregation of METTL3, perhaps similar to the frequent aggregation of misfolded proteins in AD (Huang et al., 2020). In the brain of an AD mouse model, upregulated FTO was also observed to activate the phosphorylation of tau and accelerate the pathological hallmarks of AD in an mTOR-dependent manner (Li et al., 2018). In the *Drosophila* AD model, which specifically expresses the human tau gene with the R406W mutation in the eye, found that the loss of m^{6}A by loss of METTL3, METTL14 or YTHDF enhanced tau toxicity and had more severe locomotive defects (Shafik et al., 2021).

N6-Methyladenosine and Memory Disorder in Alzheimer's Disease

Learning and memory impairments are the most important clinical symptoms of AD. Synaptic plasticity, that is, the adjustability of synaptic morphology and strength, is considered to be the basis of learning and memory. It is worth noting that short- and long-term memory requires multiple layers of regulation, from protein modifications at the synapse to RNA synthesis *de novo* in the nucleus (Cai et al., 2016; Holtmaat and Caroni, 2016; Karunakaran et al., 2016). The stability and translation of RNA transcripts have been shown to depend on m^6A modification (Yue et al., 2015), which is strongly biased to neuronal genes and functions (Meyer et al., 2012; Schwartz et al., 2014). Thus, it is perhaps unsurprising that RNA m^6A methylation modifications have been implicated in neural plasticity, thereby affecting learning and memory.

N6-Methyladenosine Methyltransferase and Memory Disorders

Increased m^6A levels in adult neurons have been found to promote the transcriptome response to synaptic plasticity (Engel et al., 2018; Leighton et al., 2018). In contrast, reducing the m^6A peaks in cellular mRNAs by knocking out some m^6A methyltransferases, such as METTL3, METTL14, METTL16, WTAP, RBM15/15B, and HAKAI may result in memory disorders (Ping et al., 2014; Schwartz et al., 2014; Růžička et al., 2017; Knuckles et al., 2018; Zhang et al., 2018; Shafik et al., 2021). The most studied m^6A "Writer," METTL3, has been shown to have a direct effect on the regulation of hippocampal-dependent memory formation. The overexpression of METTL3 in the dorsal hippocampus of wildtype mice was found to enhance long-term memory consolidation significantly (Zhang et al., 2018; **Table 1**), whereas the knockout of METTL3 in the forebrain was found to inhibit memory consolidation, which could be restored by adequate training (Zhang et al., 2018; Zhao et al., 2021). METTL14-mediated RNA m^6A modification is also critical for epitranscriptomic regulation of learning. The deletion of METTL14 was observed to reduce striatal m^6A levels, increase neuronal excitability, and severely impair striatal-mediated learning-related behavior (**Table 1**; Koranda et al., 2018).

N6-Methyladenosine Demethylase and Memory Disorders

Precise RNA m^6A modification is necessary for memory formation, thereby implicating m^6A demethylase concurs with memory regulation. Despite being ubiquitously expressed, FTO, the best characterized "Eraser," is enriched in the nuclei and dendrites, and near dendritic spines of mouse dorsal hippocampal CA1 neurons (McTaggart et al., 2011). The expression of FTO protein decreased shortly after a situational fear reflex, which implies that FTO typically limits memory formation (**Table 1**; Walters et al., 2017). Indeed, knocking out FTO in the prefrontal cortex of mice was found to enhance fear memory consolidation, with m^6A modification on several fear-related genes significantly increased (Li L. et al., 2017; Engel et al., 2018). However, a gene variant of FTO was found to be a possible risk factor for AD (**Table 1**; Ho et al., 2010; Keller et al., 2011; Reitz et al., 2012). A prospective cohort study by Keller et al. (2011) suggested that the FTO AA-genotype had a higher risk for AD compared to TT-carriers. Reitz et al. (2012) used 1,877 Caucasian cases and controls from the NIA-LOAD study and 1,093 Caribbean Hispanics to further explore the association of FTO with AD. They found that genetic variation in Introns 1 and 2 of the FTO gene may contribute to AD risk (Reitz et al., 2012). The aforementioned studies suggested that maintaining a low and basic expression level of FTO in AD might be necessary for precise RNA m^6A modification.

RNA N6-Methyladenosine Methylation-Binding Protein and Memory Disorders

N6-methyladenosine methylation-binding proteins also make marked contributions to memory storage. Interrupting m^6A-mediated function via knockdown of m^6A "Readers" in

TABLE 1 | The function of RNA N6-methyladenosine methylation modification enzyme in learning and memory.

Types	Name	Roles	References
Methyltransferase "Writers"	METTL3	Enhance the long-term memory consolidation by promoting m^6A methylation.	Zhang et al., 2018; Huang et al., 2020
	METTL14	Mediated RNA m^6A modification is critical for striatum function and epitranscriptomic regulation of learning.	Koranda et al., 2018
Demethylase "Erasers"	FTO	Limit memory formation by inhibiting m^6A methylation; A gene variant of FTO has been found to be a risk factor in AD.	Ho et al., 2010; Keller et al., 2011; McTaggart et al., 2011; Reitz et al., 2012; Li L. et al., 2017; Walters et al., 2017; Engel et al., 2018
Methylation binding protein "Readers"	YTHDF1	Enhance memory formation by promoting translation process of target transcripts in a way of neuronal stimulating dependence.	Shi et al., 2018
	YTHDF3	Increase dendritic spine density and promote synaptic transmission.	Merkurjev et al., 2018
	FMRP	Regulates the translation of some functional synaptic proteins	Huber et al., 2002
	HNRNPA2B1	The selective loss in entorhinal cortex leads to aberrant alternative splicing and dendritic loss.	Berson et al., 2012
	PRRC2A	Control the specification and myelination of oligodendrocyte and improve cognitive deficits.	Wu et al., 2019

hippocampal neurons resulted in synaptic dysfunction, including immature spine morphology, and destroyed excitatory synaptic transmission, accompanied by decreased clusters of PSD-95 and reduced surface expression of the AMPA receptor subunit GluA1 (Merkurjev et al., 2018).

YTHDF1 is mainly expressed in the hippocampus and promotes the translation of target transcripts through neuronal stimulation. YTHDF1-knockout mice showed impaired learning and memory, reduced synaptic transmission, and decreased long-term potentiation (**Table 1**; Shi et al., 2018). Interestingly, these phenotypes were similar to those obtained with METTL3 depletion (Shi et al., 2018), suggesting "Readers" and "Writers" can, to some extent, phenocopy each other in the brain. In YTHDF3-knockdown neurons, excessive dendritic filopodia in place of mature spines were observed, and a decreased percentage of spines containing a PSD-95 cluster and surface GluA1 expression was observed (**Table 1**; Merkurjev et al., 2018). In addition, FMRP was found to regulate the translation of some functional synaptic proteins (**Table 1**; Huber et al., 2002). The absence of FMRP in Fragile-X Syndrome causes excessive and persistent protein synthesis in dendrites, leading to an excess number of dendritic spines and synaptic dysfunction (Bassell and Warren, 2008; Richter et al., 2015). HNRNP was found to be relatively highly expressed in brains with a high metabolism. The selective loss of HNRNPA2B1 in the entorhinal cortex led to aberrant alternative splicing and dendritic loss (**Table 1**; Berson et al., 2012). PRRC2A has been shown to control the specifications and myelination of oligodendrocytes. PRRC2A-knockout mice showed cognitive deficits (**Table 1**; Wu et al., 2019).

CONCLUSION AND OUTLOOK

RNA m^6A methylation, which is abundant in the mammalian brain, is a significant epitranscriptomic modification. m^6A has a wide range of effects on AD and can be precisely regulated. The emergence of cross-talk between m^6A "Writers," "Erasers," and "Readers" makes it more complicated. The most appropriate example is METTL3. METTL3 is a key component of the m^6A methyltransferase complex, with its eminent methyltransferase activity, but has also been reported to function as an m^6A "Reader." Studies have reported that METTL3 directly promotes the translation of several m^6A-modified mRNAs, such as the Hippo pathway effector TAZ and the epidermal growth factor receptor, by interacting with translation initiation machinery, independent of its methyltransferase and downstream m^6A "Reader" activity (Lin et al., 2016). Hence, METTL3 might be both an m^6A "Writer" that methylates mRNA along with other members of the methyltransferase complex, by identifying unmethylated mRNA, and an m^6A "Reader" that enhances mRNA translation alone, by identifying methylated mRNA. The second pertinent example is METTL16, which interacts with MAT2A hairpins to regulate MAT2A through two mechanisms: reducing mRNA stability in SAM-sufficient conditions and promoting pre-mRNA splicing in SAM-limiting conditions. The former relies on METTL16 recognition of methylated MAT2A pre-mRNA. As the sites of m^6A on MAT2A pre-mRNA are occupied, METTL16 is quickly separated from MAT2A pre-mRNA, increases retention of the last intron in MAT2A pre-mRNA, and reduces its stability. However, in SAM-limiting conditions, METTL16 binds to unmethylated MAT2A pre-mRNA to promote the splicing of MAT2A pre-mRNA by recruiting the cleavage factor I_m complex (CFIm), and finally increases the expression of MAT2A mature mRNA (Scarborough et al., 2021). In brief, the effects of METTL3 and METTL16 likely reflect the typical "Writer—Reader" paradigm. More importantly, their effects are precisely regulated. The activity of METTL3 is controlled by post-translational modifications, such as SUMOylation (Liu et al., 2020), and METTL16 is regulated by intracellular SAM levels, which makes the regulatory network extremely intricate.

In addition, differences in experimental conditions and animal models increase discrepancies in research results. Some studies have shown a reduction in m^6A modification in AD (Shafik et al., 2021) and Parkinson's disease models (Chen et al., 2019). However, Han et al. (2020) found that m^6A methylation was elevated in the cortex and hippocampus of an AD model. The variation tendency of METTL3 and FTO in AD brain were also contradictory between the studies by Han et al. (2020), Shafik et al. (2021). Shafik et al. (2021) found METTL3 was downregulated and FTO was upregulated, which was in contrast to the study by Han et al. (2020) These discrepancies might be due to differences in the animal models employed. 9-month-old APP/PS1 mice and 6-month-old mice were used by Han et al. (2020), Shafik et al. (2021), respectively. Given that Shafik et al. also observed significantly more m6A sites as age increases during the aging process in both mouse and human brain areas, we speculate the increase in m6A methylation in that the study of Han et al. (2020) may be more likely to be compensatory and early changes in AD. But, of course, more comprehensive experiments are required to elucidate the changes of RNA m^6A methylation modification in the various stages of AD.

AUTHOR CONTRIBUTIONS

RZ contributed to the design of the review and drafted the manuscript. YZ and FG contributed to revision of the manuscript. SL and HC contributed to the design of the review and critical revision of the manuscript and had primary responsibility for the final content. All authors contributed to the article and approved the submitted version.

FUNDING

This work was supported by the National Natural Science Foundation of China (82171582 and 91849134) and the Science and Technology Research Project of Higher Education Institutions in Hebei Province (ZD2020105).

REFERENCES

Adhikari, S., Xiao, W., Zhao, Y. L., and Yang, Y. G. (2016). m(6)A: signaling for mRNA splicing. *RNA Biol.* 13, 756–759. doi: 10.1080/15476286.2016.1201628

Alarcón, C. R., Goodarzi, H., Lee, H., Liu, X., Tavazoie, S., and Tavazoie, S. F. (2015). HNRNPA2B1 Is a Mediator of m(6)A-Dependent Nuclear RNA Processing Events. *Cell* 162, 1299–1308. doi: 10.1016/j.cell.2015.08.011

Alzheimer, A. (1907). Uber eine eigenartige Erkrankung der Hirnride. *Allg. Z. Psychiatr.* 64, 146–148.

Amor, S., Peferoen, L. A., Vogel, D. Y., Breur, M., van der Valk, P., Baker, D., et al. (2014). Inflammation in neurodegenerative diseases–an update. *Immunology* 142, 151–166. doi: 10.1111/imm.12233

Aoyama, T., Yamashita, S., and Tomita, K. (2020). Mechanistic insights into m^{6}A modification of U6 snRNA by human METTL16. *Nucleic Acids Res.* 48, 5157–5168. doi: 10.1093/nar/gkaa227

Arguello, A., DeLiberto, A., and Kleiner, R. (2017). RNA Chemical Proteomics Reveals the N-Methyladenosine (mA)-Regulated Protein-RNA Interactome. *J. Am. Chem. Soc.* 139, 17249–17252. doi: 10.1021/jacs.7b09213

Ash, P. E., Vanderweyde, T. E., Youmans, K. L., Apicco, D. J., and Wolozin, B. (2014). Pathological stress granules in Alzheimer's disease. *Brain Res.* 1584, 52–58. doi: 10.1016/j.brainres.2014.05.052

Bartosovic, M., Molares, H., Gregorova, P., Hrossova, D., Kudla, G., and Vanacova, S. (2017). N6-methyladenosine demethylase FTO targets pre-mRNAs and regulates alternative splicing and 3'-end processing. *Nucleic Acids Res.* 45, 11356–11370. doi: 10.1093/nar/gkx778

Bassell, G. J., and Warren, S. T. (2008). Fragile X syndrome: loss of local mRNA regulation alters synaptic development and function. *Neuron* 60, 201–214. doi: 10.1016/j.neuron.2008.10.004

Berson, A., Barbash, S., Shaltiel, G., Goll, Y., Hanin, G., Greenberg, D. S., et al. (2012). Cholinergic-associated loss of hnRNP-A/B in Alzheimer's disease impairs cortical splicing and cognitive function in mice. *EMBO Mol. Med.* 4, 730–742. doi: 10.1002/emmm.201100995

Bonda, D. J., Wang, X., Perry, G., Nunomura, A., Tabaton, M., Zhu, X., et al. (2010). Oxidative stress in Alzheimer disease: a possibility for prevention. *Neuropharmacology* 59, 290–294. doi: 10.1016/j.neuropharm.2010.04.005

Cai, D. J., Aharoni, D., Shuman, T., Shobe, J., Biane, J., Song, W., et al. (2016). A shared neural ensemble links distinct contextual memories encoded close in time. *Nature* 534, 115–118. doi: 10.1038/nature17955

Chang, M., Lv, H., Zhang, W., Ma, C., He, X., Zhao, S., et al. (2017). Region-specific RNA m^{6}A methylation represents a new layer of control in the gene regulatory network in the mouse brain. *Open Biol.* 7:170166. doi: 10.1098/rsob.170166

Chen, K., Zhao, B. S., and He, C. (2016). Nucleic Acid Modifications in Regulation of Gene Expression. *Cell Chem. Biol.* 23, 74–85. doi: 10.1016/j.chembiol.2015.11.007

Chen, T., Hao, Y. J., Zhang, Y., Li, M. M., Wang, M., Han, W., et al. (2015). m(6)A RNA methylation is regulated by microRNAs and promotes reprogramming to pluripotency. *Cell Stem Cell* 16, 289–301. doi: 10.1016/j.stem.2015.01.016

Chen, X., Yu, C., Guo, M., Zheng, X., Ali, S., Huang, H., et al. (2019). Down-Regulation of m^{6}A mRNA Methylation Is Involved in Dopaminergic Neuronal Death. *ACS Chem. Neurosci.* 10, 2355–2363. doi: 10.1021/acschemneuro.8b00657

Chen, Y., Lin, Y., Shu, Y., He, J., and Gao, W. (2020). Interaction between N-methyladenosine (mA) modification and noncoding RNAs in cancer. *Mol. Cancer* 19:94. doi: 10.1186/s12943-020-01207-4

Chiang, V. S. C. (2021). MicroRNAs as Potential Regulators of Docosahexaenoic Acid Benefits in Alzheimer's Disease. *Arch. Neurol. Neurol. Disord.* 4:125. doi: 10.1179/1476830515Y.0000000014

Chokkalla, A. K., Mehta, S. L., Kim, T., Chelluboina, B., Kim, J., and Vemuganti, R. (2019). Transient Focal Ischemia Significantly Alters the m(6)A Epitranscriptomic Tagging of RNAs in the Brain. *Stroke* 50, 2912–2921. doi: 10.1161/strokeaha.119.026433

Cockova, Z., Honc, O., Telensky, P., Olsen, M. J., and Novotny, J. (2021). Streptozotocin-Induced Astrocyte Mitochondrial Dysfunction Is Ameliorated by FTO Inhibitor MO-I-500. *ACS Chem. Neurosci.* 12, 3818–3828. doi: 10.1021/acschemneuro.1c00063

Darnell, J., Van Driesche, S., Zhang, C., Hung, K., Mele, A., Fraser, C., et al. (2011). FMRP stalls ribosomal translocation on mRNAs linked to synaptic function and autism. *Cell* 146, 247–261. doi: 10.1016/j.cell.2011.06.013

Dasdag, O., Adalier, N., and Dasdag, S. (2020). Electromagnetic radiation and alzheimer's disease. *Biotechnol. Biotechnol. Equip.* 34, 1087–1094.

Deng, X., Su, R., Weng, H., Huang, H., Li, Z., and Chen, J. (2018). RNA N(6)-methyladenosine modification in cancers: current status and perspectives. *Cell Res.* 28, 507–517. doi: 10.1038/s41422-018-0034-6

Desrosiers, R., Friderici, K., and Rottman, F. (1974). Identification of methylated nucleosides in messenger RNA from Novikoff hepatoma cells. *Proc. Natl. Acad. Sci. U. S. A.* 71, 3971–3975. doi: 10.1073/pnas.71.10.3971

Dominissini, D., Moshitch-Moshkovitz, S., Schwartz, S., Salmon-Divon, M., Ungar, L., Osenberg, S., et al. (2012). Topology of the human and mouse m^{6}A RNA methylomes revealed by m^{6}A-seq. *Nature* 485, 201–206. doi: 10.1038/nature11112

Doxtader, K. A., Wang, P., Scarborough, A. M., Seo, D., Conrad, N. K., and Nam, Y. (2018). Structural Basis for Regulation of METTL16, an S-Adenosylmethionine Homeostasis Factor. *Mol. Cell* 71, 1001–1011.e4. doi: 10.1016/j.molcel.2018.07.025

Du, Y., Hou, G., Zhang, H., Dou, J., He, J., Guo, Y., et al. (2018). SUMOylation of the m^{6}A-RNA methyltransferase METTL3 modulates its function. *Nucleic Acids Res.* 46, 5195–5208. doi: 10.1093/nar/gky156

Edens, B. M., Vissers, C., Su, J., Arumugam, S., Xu, Z., Shi, H., et al. (2019). FMRP Modulates Neural Differentiation through m(6)A-Dependent mRNA Nuclear Export. *Cell Rep.* 28, 845–854.e5. doi: 10.1016/j.celrep.2019.06.072

Engel, M., and Chen, A. (2018). The emerging role of mRNA methylation in normal and pathological behavior. *Genes Brain Behav.* 17:e12428. doi: 10.1111/gbb.12428

Engel, M., Eggert, C., Kaplick, P. M., Eder, M., Röh, S., Tietze, L., et al. (2018). The Role of m(6)A/m-RNA Methylation in Stress Response Regulation. *Neuron* 99, 389–403.e9. doi: 10.1016/j.neuron.2018.07.009

Feng, C., Liu, Y., Wang, G., Deng, Z., Zhang, Q., Wu, W., et al. (2014). Crystal structures of the human RNA demethylase Alkbh5 reveal basis for substrate recognition. *J. Biol. Chem.* 289, 11571–11583. doi: 10.1074/jbc.M113.546168

Feng, Z., Li, Q., Meng, R., Yi, B., and Xu, Q. (2018). METTL3 regulates alternative splicing of MyD88 upon the lipopolysaccharide-induced inflammatory response in human dental pulp cells. *J. Cell. Mol. Med.* 22, 2558–2568. doi: 10.1111/jcmm.13491

Fu, Y., and Zhuang, X. (2020). mA-binding YTHDF proteins promote stress granule formation. *Nat. Chem. Biol.* 16, 955–963. doi: 10.1038/s41589-020-0524-y

Geissler, R., Simkin, A., Floss, D., Patel, R., Fogarty, E., Scheller, J., et al. (2016). A widespread sequence-specific mRNA decay pathway mediated by hnRNPs A1 and A2/B1. *Genes Dev.* 30, 1070–1085. doi: 10.1101/gad.277392.116

Gerken, T., Girard, C., Tung, Y., Webby, C., Saudek, V., Hewitson, K., et al. (2007). The obesity-associated FTO gene encodes a 2-oxoglutarate-dependent nucleic acid demethylase. *Science* 318, 1469–1472. doi: 10.1126/science.1151710

Gershoni-Emek, N., Mazza, A., Chein, M., Gradus-Pery, T., Xiang, X., Li, K. W., et al. (2016). Proteomic Analysis of Dynein-Interacting Proteins in Amyotrophic Lateral Sclerosis Synaptosomes Reveals Alterations in the RNA-Binding Protein Staufen1. *Mol. Cell. Proteom.* 15, 506–522. doi: 10.1074/mcp.M115.049965

Gong, G., and O'Bryant, S. E. (2010). The arsenic exposure hypothesis for Alzheimer disease. *Alzheimer Dis. Assoc. Disord.* 24, 311–316. doi: 10.1097/WAD.0b013e3181d71bc7

Grilli, M., Toninelli, G. F., Uberti, D., Spano, P., and Memo, M. (2003). Alzheimer's disease linking neurodegeneration with neurodevelopment. *Funct. Neurol.* 18, 145–148.

Guo, T., Zhang, D., Zeng, Y., Huang, T. Y., Xu, H., and Zhao, Y. (2020). Molecular and cellular mechanisms underlying the pathogenesis of Alzheimer's disease. *Mol. Neurodegener.* 15:40. doi: 10.1186/s13024-020-00391-7

Han, M., Liu, Z., Xu, Y., Liu, X., Wang, D., Li, F., et al. (2020). Abnormality of m^{6}A mRNA Methylation Is Involved in Alzheimer's Disease. *Front. Neurosci.* 14:98. doi: 10.3389/fnins.2020.00098

Han, Z., Niu, T., Chang, J., Lei, X., Zhao, M., Wang, Q., et al. (2010). Crystal structure of the FTO protein reveals basis for its substrate specificity. *Nature* 464, 1205–1209. doi: 10.1038/nature08921

Hess, M., Hess, S., Meyer, K., Verhagen, L., Koch, L., Brönneke, H., et al. (2013). The fat mass and obesity associated gene (Fto) regulates activity of the dopaminergic midbrain circuitry. *Nat. Neurosci.* 16, 1042–1048. doi: 10.1038/nn.3449

Ho, A. J., Stein, J. L., Hua, X., Lee, S., Hibar, D. P., Leow, A. D., et al. (2010). A commonly carried allele of the obesity-related FTO gene is associated with reduced brain volume in the healthy elderly. *Proc. Natl. Acad. Sci. U. S. A.* 107, 8404–8409. doi: 10.1073/pnas.0910878107

Holtmaat, A., and Caroni, P. (2016). Functional and structural underpinnings of neuronal assembly formation in learning. *Nat. Neurosci.* 19, 1553–1562. doi: 10.1038/nn.4418

Hsu, P., Zhu, Y., Ma, H., Guo, Y., Shi, X., Liu, Y., et al. (2017). Ythdc2 is an N-methyladenosine binding protein that regulates mammalian spermatogenesis. *Cell Res.* 27, 1115–1127. doi: 10.1038/cr.2017.99

Hu, Y., Chen, J., Sun, J., Wang, Y., Huang, P., Feng, J., et al. (2020). FTO alleviates Aβ1-40 induced retinal pigment epithelium degeneration via PKA/CREB signaling pathway. *Res. Square* [Preprint] doi: 10.21203/rs.3.rs-30549/v1

Huang, H., Camats-Perna, J., Medeiros, R., Anggono, V., and Widagdo, J. (2020). Altered Expression of the m^{6}A Methyltransferase METTL3 in Alzheimer's Disease. *eNeuro* 7:ENEURO.0125-20.2020. doi: 10.1523/eneuro.0125-20.2020

Huang, H., Weng, H., Sun, W., Qin, X., Shi, H., Wu, H., et al. (2018). Recognition of RNA N(6)-methyladenosine by IGF2BP proteins enhances mRNA stability and translation. *Nat. Cell Biol.* 20, 285–295. doi: 10.1038/s41556-018-0045-z

Huber, K. M., Gallagher, S. M., Warren, S. T., and Bear, M. F. (2002). Altered synaptic plasticity in a mouse model of fragile X mental retardation. *Proc. Natl. Acad. Sci. U. S. A.* 99, 7746–7750. doi: 10.1073/pnas.122205699

Jaouen, F., and Gascon, E. (2016). Understanding the Role of miR-33 in Brain Lipid Metabolism: implications for Alzheimer's Disease. *J. Neurosci.* 36, 2558–2560. doi: 10.1523/JNEUROSCI.4571-15.2016

Jia, G., Fu, Y., Zhao, X., Dai, Q., Zheng, G., Yang, Y., et al. (2011). N6-methyladenosine in nuclear RNA is a major substrate of the obesity-associated FTO. *Nat. Chem. Biol.* 7, 885–887. doi: 10.1038/nchembio.687

Karunakaran, S., Chowdhury, A., Donato, F., Quairiaux, C., Michel, C. M., and Caroni, P. (2016). PV plasticity sustained through D1/5 dopamine signaling required for long-term memory consolidation. *Nat. Neurosci.* 19, 454–464. doi: 10.1038/nn.4231

Ke, S., Alemu, E. A., Mertens, C., Gantman, E. C., Fak, J. J., Mele, A., et al. (2015). A majority of m^{6}A residues are in the last exons, allowing the potential for 3' UTR regulation. *Genes Dev.* 29, 2037–2053. doi: 10.1101/gad.269415.115

Ke, S., Pandya-Jones, A., Saito, Y., Fak, J. J., Vågbø, C. B., Geula, S., et al. (2017). m(6)A mRNA modifications are deposited in nascent pre-mRNA and are not required for splicing but do specify cytoplasmic turnover. *Genes Dev.* 31, 990–1006. doi: 10.1101/gad.301036.117

Keller, L., Xu, W., Wang, H. X., Winblad, B., Fratiglioni, L., and Graff, C. (2011). The obesity related gene, FTO, interacts with APOE, and is associated with Alzheimer's disease risk: a prospective cohort study. *J. Alzheimers Dis.* 23, 461–469. doi: 10.3233/jad-2010-101068

Knuckles, P., and Bühler, M. (2018). Adenosine methylation as a molecular imprint defining the fate of RNA. *FEBS Lett.* 592, 2845–2859. doi: 10.1002/1873-3468.13107

Knuckles, P., Lence, T., Haussmann, I., Jacob, D., Kreim, N., Carl, S., et al. (2018). Zc3h13/Flacc is required for adenosine methylation by bridging the mRNA-binding factor Rbm15/Spenito to the mA machinery component Wtap/Fl(2)d. *Genes Dev.* 32, 415–429. doi: 10.1101/gad.309146.117

Kolisnyk, B., Al-Onaizi, M., Soreq, L., Barbash, S., Bekenstein, U., Haberman, N., et al. (2017). Cholinergic Surveillance over Hippocampal RNA Metabolism and Alzheimer's-Like Pathology. *Cereb. Cortex* 27, 3553–3567. doi: 10.1093/cercor/bhw177

Koranda, J., Dore, L., Shi, H., Patel, M., Vaasjo, L., Rao, M., et al. (2018). Mettl14 Is Essential for Epitranscriptomic Regulation of Striatal Function and Learning. *Neuron* 99, 283.e–292.e. doi: 10.1016/j.neuron.2018.06.007

Lakk, M., Yarishkin, O., Baumann, J. M., Iuso, A., and Križaj, D. (2017). Cholesterol regulates polymodal sensory transduction in Müller glia. *Glia* 65, 2038–2050. doi: 10.1002/glia.23213

Lane, C. A., Hardy, J., and Schott, J. M. (2018). Alzheimer's disease. *Eur. J. Neurol.* 25, 59–70. doi: 10.1111/ene.13439

Leighton, L., Ke, K., Zajaczkowski, E., Edmunds, J., Spitale, R., and Bredy, T. (2018). Experience-dependent neural plasticity, learning, and memory in the era of epitranscriptomics. *Genes Brain Behav.* 17:e12426. doi: 10.1111/gbb.12426

Li, A., Chen, Y. S., Ping, X. L., Yang, X., Xiao, W., Yang, Y., et al. (2017). Cytoplasmic m(6)A reader YTHDF3 promotes mRNA translation. *Cell Res.* 27, 444–447. doi: 10.1038/cr.2017.10

Li, L., Zang, L., Zhang, F., Chen, J., Shen, H., Shu, L., et al. (2017). Fat mass and obesity-associated (FTO) protein regulates adult neurogenesis. *Hum. Mol. Genet.* 26, 2398–2411. doi: 10.1093/hmg/ddx128

Li, F., Zhao, D., Wu, J., and Shi, Y. (2014). Structure of the YTH domain of human YTHDF2 in complex with an m(6)A mononucleotide reveals an aromatic cage for m(6)A recognition. *Cell Res.* 24, 1490–1492. doi: 10.1038/cr.2014.153

Li, H., Ren, Y., Mao, K., Hua, F., Yang, Y., Wei, N., et al. (2018). FTO is involved in Alzheimer's disease by targeting TSC1-mTOR-Tau signaling. *Biochem. Biophys. Res. Commun.* 498, 234–239. doi: 10.1016/j.bbrc.2018.02.201

Li, J., Yang, X., Qi, Z., Sang, Y., Liu, Y., Xu, B., et al. (2019). The role of mRNA mA methylation in the nervous system. *Cell Biosci.* 9:66. doi: 10.1186/s13578-019-0330-y

Li, N., Zhang, D., Cao, S., Qiao, M., Zhang, P., Zhao, Q., et al. (2021). The effects of folic acid on RNA m^{6}A methylation in hippocampus as well as learning and memory ability of rats with acute lead exposure. *J. Funct. Foods* 76:104276. doi: 10.1016/j.jff.2020.104276

Li, Y., Bedi, R. K., Wiedmer, L., Sun, X., Huang, D., and Caflisch, A. (2021). Atomistic and Thermodynamic Analysis of N6-Methyladenosine (m(6)A) Recognition by the Reader Domain of YTHDC1. *J. Chem. Theory Comput.* 17, 1240–1249. doi: 10.1021/acs.jctc.0c01136

Li, Q., Wen, S., Ye, W., Zhao, S., and Liu, X. (2021). The potential roles of m(6)A modification in regulating the inflammatory response in microglia. *J. Neuroinflammation* 18:149. doi: 10.1186/s12974-021-02205-z

Li, W., Jiang, M., Zhao, S., Liu, H., Zhang, X., Wilson, J. X., et al. (2015). Folic Acid Inhibits Amyloid β-Peptide Production through Modulating DNA Methyltransferase Activity in N2a-APP Cells. *Int. J. Mol. Sci.* 16, 25002–25013. doi: 10.3390/ijms161025002

Li, Y., Bedi, R. K., Moroz-Omori, E. V., and Caflisch, A. (2020). Structural and Dynamic Insights into Redundant Function of YTHDF Proteins. *J. Chem. Inf. Model.* 60, 5932–5935. doi: 10.1021/acs.jcim.0c01029

Liao, S., Sun, H., and Xu, C. (2018). YTH Domain: a Family of N(6)-methyladenosine (m(6)A) Readers. *Genomics Proteomics Bioinformatics* 16, 99–107. doi: 10.1016/j.gpb.2018.04.002

Lim, J. W., Lee, J., and Pae, A. N. (2020). Mitochondrial dysfunction and Alzheimer's disease: prospects for therapeutic intervention. *BMB Rep.* 53, 47–55. doi: 10.5483/BMBRep.2020.53.1.279

Lin, S., Choe, J., Du, P., Triboulet, R., and Gregory, R. I. (2016). The m(6)A Methyltransferase METTL3 Promotes Translation in Human Cancer Cells. *Mol. Cell* 62, 335–345. doi: 10.1016/j.molcel.2016.03.021

Lin, S., Liu, J., Jiang, W., Wang, P., Sun, C., Wang, X., et al. (2019). METTL3 Promotes the Proliferation and Mobility of Gastric Cancer Cells. *Open Med.* 14, 25–31. doi: 10.1515/med-2019-0005

Liu, J., Yue, Y., Han, D., Wang, X., Fu, Y., Zhang, L., et al. (2014). A METTL3-METTL14 complex mediates mammalian nuclear RNA N6-adenosine methylation. *Nat. Chem. Biol.* 10, 93–95. doi: 10.1038/nchembio.1432

Liu, S., Zhuo, L., Wang, J., Zhang, Q., Li, Q., Li, G., et al. (2020). METTL3 plays multiple functions in biological processes. *Am. J. Cancer Res.* 10, 1631–1646.

Lu, Z., Ma, Y., Li, Q., Liu, E., Jin, M., Zhang, L., et al. (2019). The role of N(6)-methyladenosine RNA methylation in the heat stress response of sheep (Ovis aries). *Cell Stress Chaperon.* 24, 333–342. doi: 10.1007/s12192-018-00965-x

Ma, C., Liao, S., and Zhu, Z. (2019). Crystal structure of human YTHDC2 YTH domain. *Biochem. Biophys. Res. Commun.* 518, 678–684. doi: 10.1016/j.bbrc.2019.08.107

McTaggart, J., Lee, S., Iberl, M., Church, C., Cox, R., and Ashcroft, F. (2011). FTO is expressed in neurones throughout the brain and its expression is unaltered by fasting. *PLoS One* 6:e27968. doi: 10.1371/journal.pone.0027968

Merkurjev, D., Hong, W. T., Iida, K., Oomoto, I., Goldie, B. J., Yamaguti, H., et al. (2018). Synaptic N(6)-methyladenosine (m(6)A) epitranscriptome reveals functional partitioning of localized transcripts. *Nat. Neurosci.* 21, 1004–1014. doi: 10.1038/s41593-018-0173-6

Meyer, K., Saletore, Y., Zumbo, P., Elemento, O., Mason, C., and Jaffrey, S. (2012). Comprehensive analysis of mRNA methylation reveals enrichment in 3' UTRs and near stop codons. *Cell* 149, 1635–1646. doi: 10.1016/j.cell.2012.05.003

Meyer, K. D., and Jaffrey, S. R. (2014). The dynamic epitranscriptome: N6-methyladenosine and gene expression control. *Nat. Rev. Mol. Cell Biol.* 15, 313–326. doi: 10.1038/nrm3785

Meyer, K. D., Patil, D. P., Zhou, J., Zinoviev, A., Skabkin, M. A., Elemento, O., et al. (2015). 5' UTR m(6)A Promotes Cap-Independent Translation. *Cell* 163, 999–1010. doi: 10.1016/j.cell.2015.10.012

Miao, Z., Zhang, T., Qi, Y., Song, J., Han, Z., and Ma, C. (2020). Evolution of the RNA N (6)-Methyladenosine Methylome Mediated by Genomic Duplication. *Plant Physiol.* 182, 345–360. doi: 10.1104/pp.19.00323

Myrick, L. K., Hashimoto, H., Cheng, X., and Warren, S. T. (2015). Human FMRP contains an integral tandem Agenet (Tudor) and KH motif in the amino terminal domain. *Hum. Mol. Genet.* 24, 1733–1740. doi: 10.1093/hmg/ddu586

Nance, D. J., Satterwhite, E. R., Bhaskar, B., Misra, S., Carraway, K. R., and Mansfield, K. D. (2020). Characterization of METTL16 as a cytoplasmic RNA binding protein. *PLoS One* 15:e0227647. doi: 10.1371/journal.pone.0227647

Pakavathkumar, P., Noël, A., Lecrux, C., Tubeleviciute-Aydin, A., Hamel, E., Ahlfors, J. E., et al. (2017). Caspase vinyl sulfone small molecule inhibitors prevent axonal degeneration in human neurons and reverse cognitive impairment in Caspase-6-overexpressing mice. *Mol. Neurodegener.* 12:22. doi: 10.1186/s13024-017-0166-z

Patil, D. P., Pickering, B. F., and Jaffrey, S. R. (2018). Reading m(6)A in the Transcriptome: m(6)A-Binding Proteins. *Trends Cell Biol.* 28, 113–127. doi: 10.1016/j.tcb.2017.10.001

Peña-Bautista, C., Álvarez-Sánchez, L., Cañada-Martínez, A. J., Baquero, M., and Cháfer-Pericás, C. (2021). Epigenomics and Lipidomics Integration in Alzheimer Disease: pathways Involved in Early Stages. *Biomedicines* 9:1812. doi: 10.3390/biomedicines9121812

Pendleton, K. E., Chen, B., Liu, K., Hunter, O. V., Xie, Y., Tu, B. P., et al. (2017). The U6 snRNA m(6)A Methyltransferase METTL16 Regulates SAM Synthetase Intron Retention. *Cell* 169, 824–835.e14. doi: 10.1016/j.cell.2017.05.003

Ping, X., Sun, B., Wang, L., Xiao, W., Yang, X., Wang, W., et al. (2014). Mammalian WTAP is a regulatory subunit of the RNA N6-methyladenosine methyltransferase. *Cell Res.* 24, 177–189. doi: 10.1038/cr.2014.3

Popugaeva, E., Pchitskaya, E., and Bezprozvanny, I. (2018). Dysregulation of Intracellular Calcium Signaling in Alzheimer's Disease. *Antioxid. Redox Signal.* 29, 1176–1188. doi: 10.1089/ars.2018.7506

Reitz, C., Tosto, G., Mayeux, R., Luchsinger, J. A., NIA-LOAD/NCRAD Family Study Group, and Alzheimer's Disease Neuroimaging Initiative (2012). Genetic variants in the Fat and Obesity Associated (FTO) gene and risk of Alzheimer's disease. *PLoS One* 7:e50354. doi: 10.1371/journal.pone.0050354

Richter, J. D., Bassell, G. J., and Klann, E. (2015). Dysregulation and restoration of translational homeostasis in fragile X syndrome. *Nat. Rev. Neurosci.* 16, 595–605. doi: 10.1038/nrn4001

Rosen, L. B., Ginty, D. D., Weber, M. J., and Greenberg, M. E. (1994). Membrane depolarization and calcium influx stimulate MEK and MAP kinase via activation of Ras. *Neuron* 12, 1207–1221. doi: 10.1016/0896-6273(94)90438-3

Roundtree, I. A., Luo, G. Z., Zhang, Z., Wang, X., Zhou, T., Cui, Y., et al. (2017). YTHDC1 mediates nuclear export of N(6)-methyladenosine methylated mRNAs. *Elife* 6:e31311. doi: 10.7554/eLife.31311

Růžička, K., Zhang, M., Campilho, A., Bodi, Z., Kashif, M., Saleh, M., et al. (2017). Identification of factors required for m(6) A mRNA methylation in Arabidopsis reveals a role for the conserved E3 ubiquitin ligase HAKAI. *New Phytol.* 215, 157–172. doi: 10.1111/nph.14586

Scarborough, A., Flaherty, J., Hunter, O., Liu, K., Kumar, A., Xing, C., et al. (2021). SAM homeostasis is regulated by CFI-mediated splicing of MAT2A. *Elife* 10:e64930. doi: 10.7554/eLife.64930

Schwartz, S., Mumbach, M., Jovanovic, M., Wang, T., Maciag, K., Bushkin, G., et al. (2014). Perturbation of m^{6}A writers reveals two distinct classes of mRNA methylation at internal and 5' sites. *Cell Rep.* 8, 284–296. doi: 10.1016/j.celrep.2014.05.048

Shafik, A. M., Zhang, F., Guo, Z., Dai, Q., Pajdzik, K., Li, Y., et al. (2021). N6-methyladenosine dynamics in neurodevelopment and aging, and its potential role in Alzheimer's disease. *Genome Biol.* 22:17. doi: 10.1186/s13059-020-02249-z

Shi, H., Wang, X., Lu, Z., Zhao, B. S., Ma, H., Hsu, P. J., et al. (2017). YTHDF3 facilitates translation and decay of N(6)-methyladenosine-modified RNA. *Cell Res.* 27, 315–328. doi: 10.1038/cr.2017.15

Shi, H., Wei, J., and He, C. (2019). Where, When, and How: context-Dependent Functions of RNA Methylation Writers, Readers, and Erasers. *Mol. Cell* 74, 640–650. doi: 10.1016/j.molcel.2019.04.025

Shi, H., Zhang, X., Weng, Y. L., Lu, Z., Liu, Y., Lu, Z., et al. (2018). m(6)A facilitates hippocampus-dependent learning and memory through YTHDF1. *Nature* 563, 249–253. doi: 10.1038/s41586-018-0666-1

Shi, W., Yang, F., Dai, R., Sun, Y., Chu, Y., Liao, S., et al. (2021). METTL3-Mediated N6-Methyladenosine Modification Is Involved in the Dysregulation of NRIP1 Expression in Down Syndrome. *Front. Cell. Dev. Biol.* 9:621374. doi: 10.3389/fcell.2021.621374

Shima, H., Matsumoto, M., Ishigami, Y., Ebina, M., Muto, A., Sato, Y., et al. (2017). S-Adenosylmethionine Synthesis Is Regulated by Selective N-Adenosine Methylation and mRNA Degradation Involving METTL16 and YTHDC1. *Cell Rep.* 21, 3354–3363. doi: 10.1016/j.celrep.2017.11.092

Slobodin, B., Han, R., Calderone, V., Vrielink, J., Loayza-Puch, F., Elkon, R., et al. (2017). Transcription Impacts the Efficiency of mRNA Translation via Co-transcriptional N6-adenosine Methylation. *Cell* 169, 326–337.e12. doi: 10.1016/j.cell.2017.03.031

Suhl, J., Chopra, P., Anderson, B., Bassell, G., and Warren, S. (2014). Analysis of FMRP mRNA target datasets reveals highly associated mRNAs mediated by G-quadruplex structures formed via clustered WGGA sequences. *Hum. Mol. Genet.* 23, 5479–5491. doi: 10.1093/hmg/ddu272

Walters, B., Mercaldo, V., Gillon, C., Yip, M., Neve, R., Boyce, F., et al. (2017). The Role of The RNA Demethylase FTO (Fat Mass and Obesity-Associated) and mRNA Methylation in Hippocampal Memory Formation. *Neuropsychopharmacology* 42, 1502–1510. doi: 10.1038/npp.2017.31

Wang, J., Ishfaq, M., Xu, L., Xia, C., Chen, C., and Li, J. (2019). METTL3/mA/miRNA-873-5p Attenuated Oxidative Stress and Apoptosis in Colistin-Induced Kidney Injury by Modulating Keap1/Nrf2 Pathway. *Front. Pharmacol.* 10:517. doi: 10.3389/fphar.2019.00517

Wang, X., Feng, J., Xue, Y., Guan, Z., Zhang, D., Liu, Z., et al. (2016). Structural basis of N(6)-adenosine methylation by the METTL3-METTL14 complex. *Nature* 534, 575–578. doi: 10.1038/nature18298

Wang, X., Feng, J., Xue, Y., Guan, Z., Zhang, D., Liu, Z., et al. (2017). Corrigendum: structural basis of N-adenosine methylation by the METTL3-METTL14 complex. *Nature* 542:260. doi: 10.1038/nature21073

Wang, X., Lu, Z., Gomez, A., Hon, G. C., Yue, Y., Han, D., et al. (2014). N6-methyladenosine-dependent regulation of messenger RNA stability. *Nature* 505, 117–120. doi: 10.1038/nature12730

Warda, A., Kretschmer, J., Hackert, P., Lenz, C., Urlaub, H., Höbartner, C., et al. (2017). NHuman METTL16 is a -methyladenosine (mA) methyltransferase that targets pre-mRNAs and various non-coding RNAs. *EMBO Rep.* 18, 2004–2014. doi: 10.15252/embr.201744940

Wen, J., Lv, R., Ma, H., Shen, H., He, C., Wang, J., et al. (2018). Zc3h13 Regulates Nuclear RNA mA Methylation and Mouse Embryonic Stem Cell Self-Renewal. *Mol. Cell* 69, 1028–1038.e6. doi: 10.1016/j.molcel.2018.02.015

Wen, L., Sun, W., Xia, D., Wang, Y., Li, J., and Yang, S. (2020). The m^{6}A methyltransferase METTL3 promotes LPS-induced microglia inflammation through TRAF6/NF-κB pathway. *Neuroreport* doi: 10.1097/wnr.0000000000001550 [Epub Online ahead of print].

Weng, Y., Wang, X., An, R., Cassin, J., Vissers, C., Liu, Y., et al. (2018). Epitranscriptomic mA Regulation of Axon Regeneration in the Adult Mammalian Nervous System. *Neuron* 97, 313–325.e6. doi: 10.1016/j.neuron.2017.12.036

Widagdo, J., and Anggono, V. (2018). The m^{6}A-epitranscriptomic signature in neurobiology: from neurodevelopment to brain plasticity. *J. Neurochem.* 147, 137–152. doi: 10.1111/jnc.14481

Widagdo, J., Zhao, Q. Y., Kempen, M. J., Tan, M. C., Ratnu, V. S., Wei, W., et al. (2016). Experience-Dependent Accumulation of N6-Methyladenosine in the Prefrontal Cortex Is Associated with Memory Processes in Mice. *J. Neurosci.* 36, 6771–6777. doi: 10.1523/jneurosci.4053-15.2016

Wu, B., Li, L., Huang, Y., Ma, J., and Min, J. (2017). Readers, writers and erasers of N(6)-methylated adenosine modification. *Curr. Opin. Struct. Biol.* 47, 67–76. doi: 10.1016/j.sbi.2017.05.011

Wu, B., Su, S., Patil, D. P., Liu, H., Gan, J., Jaffrey, S. R., et al. (2018). Molecular basis for the specific and multivariant recognitions of RNA substrates by human hnRNP A2/B1. *Nat. Commun.* 9:420. doi: 10.1038/s41467-017-02770-z

Wu, R., Li, A., Sun, B., Sun, J. G., Zhang, J., Zhang, T., et al. (2019). A novel m(6)A reader Prrc2a controls oligodendroglial specification and myelination. *Cell Res.* 29, 23–41. doi: 10.1038/s41422-018-0113-8

Xiang, Y., Laurent, B., Hsu, C. H., Nachtergaele, S., Lu, Z., Sheng, W., et al. (2017). RNA m(6)A methylation regulates the ultraviolet-induced DNA damage response. *Nature* 543, 573–576. doi: 10.1038/nature21671

Xiao, W., Adhikari, S., Dahal, U., Chen, Y. S., Hao, Y. J., Sun, B. F., et al. (2016). Nuclear m(6)A Reader YTHDC1 Regulates mRNA Splicing. *Mol. Cell* 61, 507–519. doi: 10.1016/j.molcel.2016.01.012

Xu, C., Liu, K., Ahmed, H., Loppnau, P., Schapira, M., and Min, J. (2015). Structural Basis for the Discriminative Recognition of N6-Methyladenosine RNA by the Human YT521-B Homology Domain Family of Proteins. *J. Biol. Chem.* 290, 24902–24913. doi: 10.1074/jbc.M115.680389

Xu, C., Wang, X., Liu, K., Roundtree, I. A., Tempel, W., Li, Y., et al. (2014). Structural basis for selective binding of m^6A RNA by the YTHDC1 YTH domain. *Nat. Chem. Biol.* 10, 927–929. doi: 10.1038/nchembio.1654

Yoon, K. J., Ringeling, F. R., Vissers, C., Jacob, F., Pokrass, M., Jimenez-Cyrus, D., et al. (2017). Temporal Control of Mammalian Cortical Neurogenesis by m(6)A Methylation. *Cell* 171, 877–889.e17. doi: 10.1016/j.cell.2017.09.003

Yu, J., Chen, M., Huang, H., Zhu, J., Song, H., Zhu, J., et al. (2018). Dynamic m^6A modification regulates local translation of mRNA in axons. *Nucleic Acids Res.* 46, 1412–1423. doi: 10.1093/nar/gkx1182

Yue, Y., Liu, J., Cui, X., Cao, J., Luo, G., Zhang, Z., et al. (2018). VIRMA mediates preferential mA mRNA methylation in 3′UTR and near stop codon and associates with alternative polyadenylation. *Cell Discov.* 4:10. doi: 10.1038/s41421-018-0019-0

Yue, Y., Liu, J., and He, C. (2015). RNA N6-methyladenosine methylation in post-transcriptional gene expression regulation. *Genes Dev.* 29, 1343–1355. doi: 10.1101/gad.262766.115

Zaccara, S., and Jaffrey, S. R. (2020). A Unified Model for the Function of YTHDF Proteins in Regulating m(6)A-Modified mRNA. *Cell* 181, 1582–1595.e18. doi: 10.1016/j.cell.2020.05.012

Zhang, C., Samanta, D., Lu, H., Bullen, J. W., Zhang, H., Chen, I., et al. (2016). Hypoxia induces the breast cancer stem cell phenotype by HIF-dependent and ALKBH5-mediated m6A-demethylation of NANOG mRNA. *Proc. Natl. Acad. Sci. U. S. A.* 113, E2047–E2056. doi: 10.1073/pnas.1602883113

Zhang, X., Li, X., Jia, H., An, G., and Ni, J. (2021). The m6A methyltransferase METTL3 modifies PGC-1α mRNA promoting mitochondrial dysfunction and oxLDL-induced inflammation in monocytes. *J. Biol. Chem.* 297:101058. doi: 10.1016/j.jbc.2021.101058

Zhang, Z., Wang, M., Xie, D., Huang, Z., Zhang, L., Yang, Y., et al. (2018). METTL3-mediated N(6)-methyladenosine mRNA modification enhances long-term memory consolidation. *Cell Res.* 28, 1050–1061. doi: 10.1038/s41422-018-0092-9

Zhao, F., Xu, Y., Gao, S., Qin, L., Austria, Q., Siedlak, S. L., et al. (2021). METTL3-dependent RNA m6A dysregulation contributes to neurodegeneration in Alzheimer's disease through aberrant cell cycle events. *Mol. Neurodegener.* 16:70. doi: 10.1186/s13024-021-00484-x

Zhao, T., Li, X., Sun, D., and Zhang, Z. (2019). Oxidative stress: one potential factor for arsenite-induced increase of N(6)-methyladenosine in human keratinocytes. *Environ. Toxicol. Pharmacol.* 69, 95–103. doi: 10.1016/j.etap.2019.04.005

Zhao, Y., Cong, L., and Lukiw, W. J. (2017). Lipopolysaccharide (LPS) Accumulates in Neocortical Neurons of Alzheimer's Disease (AD) Brain and Impairs Transcription in Human Neuronal-Glial Primary Co-cultures. *Front. Aging Neurosci.* 9:407. doi: 10.3389/fnagi.2017.00407

Zheng, G., Dahl, J., Niu, Y., Fedorcsak, P., Huang, C., Li, C., et al. (2013). ALKBH5 is a mammalian RNA demethylase that impacts RNA metabolism and mouse fertility. *Mol. Cell* 49, 18–29. doi: 10.1016/j.molcel.2012.10.015

Zheng, L., Tang, X., Lu, M., Sun, S., Xie, S., Cai, J., et al. (2020). microRNA-421-3p prevents inflammatory response in cerebral ischemia/reperfusion injury through targeting m^6A Reader YTHDF1 to inhibit p65 mRNA translation. *Int. Immunopharmacol.* 88:106937. doi: 10.1016/j.intimp.2020.106937

Zhou, J., Wan, J., Gao, X., Zhang, X., Jaffrey, S. R., and Qian, S. B. (2015). Dynamic m(6)A mRNA methylation directs translational control of heat shock response. *Nature* 526, 591–594. doi: 10.1038/nature15377

Zou, S., Toh, J., Wong, K., Gao, Y., Hong, W., and Woon, E. (2016). N(6)-Methyladenosine: a conformational marker that regulates the substrate specificity of human demethylases FTO and ALKBH5. *Sci. Rep.* 6:25677. doi: 10.1038/srep25677

Conflict of Interest: The authors declare that the research was conducted in the absence of any commercial or financial relationships that could be construed as a potential conflict of interest.

Publisher's Note: All claims expressed in this article are solely those of the authors and do not necessarily represent those of their affiliated organizations, or those of the publisher, the editors and the reviewers. Any product that may be evaluated in this article, or claim that may be made by its manufacturer, is not guaranteed or endorsed by the publisher.

Copyright © 2022 Zhang, Zhang, Guo, Li and Cui. This is an open-access article distributed under the terms of the Creative Commons Attribution License (CC BY). The use, distribution or reproduction in other forums is permitted, provided the original author(s) and the copyright owner(s) are credited and that the original publication in this journal is cited, in accordance with accepted academic practice. No use, distribution or reproduction is permitted which does not comply with these terms.

Advantages of publishing in Frontiers

OPEN ACCESS
Articles are free to read for greatest visibility and readership

FAST PUBLICATION
Around 90 days from submission to decision

HIGH QUALITY PEER-REVIEW
Rigorous, collaborative, and constructive peer-review

TRANSPARENT PEER-REVIEW
Editors and reviewers acknowledged by name on published articles

Frontiers
Avenue du Tribunal-Fédéral 34
1005 Lausanne | Switzerland

Visit us: www.frontiersin.org
Contact us: frontiersin.org/about/contact

REPRODUCIBILITY OF RESEARCH
Support open data and methods to enhance research reproducibility

DIGITAL PUBLISHING
Articles designed for optimal readership across devices

FOLLOW US
@frontiersin

IMPACT METRICS
Advanced article metrics track visibility across digital media

EXTENSIVE PROMOTION
Marketing and promotion of impactful research

LOOP RESEARCH NETWORK
Our network increases your article's readership